

**Some pages of this thesis may have been removed for copyright restrictions.**

If you have discovered material in Aston Research Explorer which is unlawful e.g. breaches copyright, (either yours or that of a third party) or any other law, including but not limited to those relating to patent, trademark, confidentiality, data protection, obscenity, defamation, libel, then please read our [Takedown policy](#) and contact the service immediately (openaccess@aston.ac.uk)

Construction of a model for the design of a rotary  
kiln for slow pyrolysis of biomass – GreenCarbon project

Jorge López Ordovás

Doctor of Philosophy

Aston University

June 2020

©Jorge López Ordovás, 2020

Jorge López Ordovás asserts his moral right to be identified as the author of this thesis

This copy of the thesis has been supplied on condition that anyone who consults it is understood to recognise that its copyright belongs to its author and that no quotation from the thesis and no information derived from it may be published without appropriate permission or acknowledgement



# Construction of a model for the design of a rotary kiln for slow pyrolysis of biomass – GreenCarbon project

Jorge López Ordovás

Doctor of Philosophy

Aston University

June 2020

## Summary

Biomass pyrolysis is one of the most promising renewable energy technologies. This research aims to create a model which automatically designs a biomass slow pyrolysis reactor from the user inputs and provides mechanical specifications, kinetic properties and process parameters. From literature, the rotary kiln was identified as the most promising slow pyrolysis technology.

This research divides the complex reactor design into three main parts, related to the transformation of the feedstock into the product: bed of solids, heat transfer and kinetics. The three aspects were integrated, and the reactor divided into physically identical slices for more straightforward implementation and to overcome model divergences.

- The **bed of solids** defines and describes the behaviour of the solids inside the reactor mathematically. The length of the reactor must be calculated, and the contact areas to transfer heat from the wall (heat source).
- **Heat transfer** is critical within pyrolysis. The model must ensure that all the particles reach the target temperature. The heat is indirectly transmitted to the solids and gases through conduction, convection and radiation.
- Pyrolysis **kinetics** are challenging due to the complex mixture of substances in the feedstock and products. Isoconversional methods are used to estimate the value of the pre-exponential factor and activation energy for the conversion of each feedstock into the products. Additionally, the reaction orders are optimised through an innovative method that compares the error between different values.

The result is a thorough methodology and comprehensive model for the design of a rotary kiln. This methodology included assumptions to achieve a compromise between accuracy, computational time and power. The finished model allows users to investigate custom reactor designs, as they can specify key variables such as feedstock and scale. It is a very powerful tool that can be used in industry or by potential investors to obtain a first approximation of the dimensions of a pyrolysis reactor. For research, it provides a robust methodology for the design of slow pyrolysis rotary kilns. It is acknowledged that the reactor model is not perfect, and some parts could be improved, but it provides a valuable step forward in the development of slow pyrolysis reactor design.

*Keywords: slow pyrolysis, rotary kiln, char, modelling, heat transfer, kinetics*

This project has received funding from the European Union's Horizon 2020 research and innovation programme under the Marie Skłodowska-Curie grant agreement No 721991

*Para ti, abuela Carmen, por cuidarme siempre tanto,*

*ojalá hubieras visto esto.*

*Siempre serás eterna, nunca te olvidaré.*

## Acknowledgement

Sin lugar a dudas, las primeras líneas son para mi familia. Este ha sido el proyecto más largo de mi vida y me han ayudado todo lo que han podido y más, cuando yo mismo no podía, ellos estaban ahí para hacerme mi vida más sencilla. Por eso el primer agradecimiento es para mis padres María del Carmen y Mariano, y mis hermanos Diego y María, y al resto de mi familia por todo su apoyo.

Abuela, gracias por todo lo que hiciste siempre por mí, podría llenar hojas enteras de lo maravillosa que fuiste, la mejor del mundo. Viste cómo empecé esto, ojalá estuvieses aquí para poder ver el final. Nada habría sido posible sin ti ni todo el amor que incondicionalmente me diste. Te echo de menos cada día desde que te fuiste. Eres eterna, porque las maravillas duran para siempre, todo esto sólo puede ir dedicado a ti.

This adventure started on 6<sup>th</sup> March 2017 when I received the e-mail from Prof. Tony Bridgwater to confirm I was the candidate selected for the position ESR 3 in GreenCarbon project at Aston. I could not imagine what a huge change on my life this e-mail would produce. I would like to acknowledge Dr. Yang Yang for all the help the first months, to make my life in a new country as easy as possible, and Prof. Tony Bridgwater, for his advice during the project.

My supervisor Dr. Katie Chong deserves all the best, her patience, support, encouragement were unbelievable. Being supervised by her makes the PhD life much easier and I don't want to imagine how this time at Aston would have been without her as my supervisor. A big thanks to the best supervisor anybody could have.

I want to express my gratitude to everyone from industry and other projects I met and kindly helped to improve my work, especially to BRISK2 project and CENER, and my previous employers from DHL, CIRCE, SAICA and Enagas.

The other ESR at Aston University, Filipe Rego, who was very supportive in all moments. We spend a lot of time together and his help was a key to make it all way to the end, muito obrigado Filipe! I also want to say thanks to the others ESRs from the GreenCarbon project, it was such a good experience to be part of it. Thanks for all the trips and amazing moments. I want to acknowledge all my colleagues from EBRI, everyone who shared some time with me and support me through this whole journey, you added much value to this experience and I learned a lot from everyone. Special thanks to the other PhD students who were with me most of my time in EBRI: Costanza, Filipe, Tom, Joe, Regina, Moe and Chris.

Many thanks to all my friends from Spain and Birmingham. I owe a lot to many of you, for your endless support and encouragement. Dr. Costanza, I really appreciate everything we lived, I would not change any single moment. Sandra, Noelia, Birmingham no habría sido lo mismo sin vosotras. En momentos diferentes me disteis toda la comprensión que necesité. To my Erasmus family, Fátima and Janire. To my other friends who are always there to help me to stand up and believe on myself, and everyone who helped me to become who I am. En especial a Mariona, que sabe como hacer de cualquier momento y lugar algo especial, y apoyar incondicionalmente.

Per últim, a tu, Revoltosa, que vas arribar del no-res per convertir-te en el meu tot. Gràcies per tant, per estimar-me, per estimar-me tan bé, per alegrar-me els dies i fer que tots els problemes deixin d'existir quan estàs aprop, per entendre'm, escoltar-me, deixar-me ser (al teu costat) i per tant més.... No tinc paraules per tot això, pero sé que arribar fins aquí no hagués set possible sense tu. Saps? *Llavors rius i se'm passen tots els mals.*

*"Show must go on!"*

*"Shown täytyy jatkaa!"*

## Table of contents

|  |           |
|--|-----------|
| Summary .....  | 3         |
| Acknowledgement .....  | 5         |
| Table of contents .....  | 6         |
| List of figures .....  | 11        |
| List of tables .....   | 13        |
| List of equations .....  | 14        |
| List of reactions .....  | 18        |
| Nomenclature .....   | 19        |
| <b>1 Introduction .....</b>                                    | <b>21</b> |
| 1.1 Biomass .....  | 21        |
| <b>1.1.1 Biomass composition .....</b>                         | <b>22</b> |
| 1.1.1.1 Cellulose .....  | 22        |
| 1.1.1.2 Hemicellulose .....                                    | 22        |
| 1.1.1.3 Lignin .....   | 23        |
| 1.1.1.4 Extractives and inorganic components .....             | 23        |
| <b>1.1.2 Biomass applications and processing .....</b>         | <b>24</b> |
| 1.2 Pyrolysis .....  | 24        |
| <b>1.2.1 Slow pyrolysis .....</b>                              | <b>28</b> |
| <b>1.2.2 Char .....</b>  | <b>29</b> |
| <b>1.2.3 Effect of parameters on pyrolysis .....</b>           | <b>30</b> |
| 1.3 GreenCarbon Project .....                                  | 32        |
| <b>1.3.1 WP4 - Pyrolysis Routes for dry feedstocks .....</b>   | <b>34</b> |
| 1.4 Thesis objectives and structure .....                      | 35        |
| <b>1.4.1 Objectives .....</b>                                  | <b>35</b> |
| <b>1.4.2 Structure .....</b>                                   | <b>37</b> |
| 1.5 References .....   | 40        |
| <b>2 Reactor selection .....</b>                               | <b>45</b> |
| 2.1 Pyrolysis reactors in the industry .....                   | 45        |
| <b>2.1.1 Batch processes .....</b>                             | <b>45</b> |
| <b>2.1.2 Semi-continuous processes .....</b>                   | <b>47</b> |
| 2.1.2.1 Tunnel retort .....                                    | 47        |
| 2.1.2.2 Shelf reactor .....                                    | 48        |
| 2.1.2.3 Twin retort .....                                      | 48        |
| <b>2.1.3 Continuous processes .....</b>                        | <b>49</b> |
| 2.1.3.1 Big particles .....                                    | 49        |
| 2.1.3.1.1 Lambiotte .....                                      | 49        |
| 2.1.3.1.2 Reichert .....                                       | 50        |
| 2.1.3.1.3 Lurgi .....  | 51        |
| 2.1.3.2 Small particles .....                                  | 52        |
| 2.1.3.2.1 Badger-Stafford process .....                        | 52        |
| 2.1.3.2.2 Herreshoff multiple-hearth furnace .....             | 52        |
| 2.1.3.2.3 Moving agitated bed .....                            | 53        |
| 2.1.3.2.4 Paddle pyrolysis kiln .....                          | 54        |
| 2.1.3.2.5 Screw reactor .....                                  | 55        |
| 2.1.3.2.6 Rotary kiln .....                                    | 55        |
| 2.2 Information available .....                                | 56        |
| 2.3 Selection criteria .....                                   | 60        |
| <b>2.3.1 Results .....</b>                                     | <b>62</b> |
| 2.4 Pyrolysis reactor design .....                             | 63        |
| 2.4.1.1 Challenges for the design of a pyrolysis reactor ..... | 63        |

|              |  |            |
|--------------|--|------------|
| 2.4.1.2      | <i>Singularities of the rotary kiln</i> .....                        | 64         |
| 2.5          | References .....   | 64         |
| <b>3</b>     | <b>The bed of solids submodel</b> .....                              | <b>68</b>  |
| 3.1          | Bed of solids behaviour.....   | 68         |
| <b>3.1.1</b> | <b>The motion of the bed of solids</b> .....                         | <b>68</b>  |
| 3.1.1.1      | <i>Parameters to determine the motion of the bed of solids</i> ..... | 69         |
| 3.1.1.2      | <i>Classification of motions of the bed of solids</i> .....          | 70         |
| 3.1.1.3      | <i>The target bed of solids motion</i> .....                         | 72         |
| 3.2          | Length of the reactor .....  | 72         |
| <b>3.2.1</b> | <b>Sensitivity analysis</b> .....                                    | <b>75</b>  |
| 3.3          | Contact areas .....  | 76         |
| <b>3.3.1</b> | <b>The special case of conductive heat flow</b> .....                | <b>80</b>  |
| 3.4          | Solid residence time.....  | 84         |
| 3.5          | Voidage and porosity .....   | 85         |
| <b>3.5.1</b> | <b>Shape and particle size</b> .....                                 | <b>86</b>  |
| 3.6          | Attachment of the flights .....                                      | 87         |
| 3.7          | References .....   | 87         |
| <b>4</b>     | <b>Heat transfer model</b> .....                                     | <b>90</b>  |
| 4.1          | Introduction .....   | 90         |
| 4.2          | Conduction .....   | 90         |
| <b>4.2.1</b> | <b>Variable area</b> .....   | <b>91</b>  |
| <b>4.2.2</b> | <b>Methodology</b> .....   | <b>93</b>  |
| <b>4.2.3</b> | <b>Effect of particle size</b> .....                                 | <b>93</b>  |
| 4.3          | Convection .....   | 94         |
| <b>4.3.1</b> | <b>Convective heat transfer coefficient</b> .....                    | <b>95</b>  |
| 4.3.1.1.1    | <i>Types of flow</i> .....   | 96         |
| 4.3.1.1.2    | <i>Gas coefficient</i> .....   | 97         |
| 4.3.1.1.3    | <i>Bed of solids coefficient</i> .....                               | 99         |
| 4.4          | Radiation .....  | 100        |
| <b>4.4.1</b> | <b>View factor</b> .....   | <b>101</b> |
| 4.5          | Approach for the model.....  | 105        |
| <b>4.5.1</b> | <b>Overall description of the model</b> .....                        | <b>106</b> |
| 4.6          | References .....   | 108        |
| <b>5</b>     | <b>Kinetic model</b> .....   | <b>110</b> |
| 5.1          | Introduction .....   | 110        |
| <b>5.1.1</b> | <b>Mechanisms suggested</b> .....                                    | <b>111</b> |
| 5.2          | Approach.....  | 113        |
| <b>5.2.1</b> | <b>Isothermal</b> .....  | <b>114</b> |
| <b>5.2.2</b> | <b>Isoconversional</b> .....   | <b>119</b> |
| <b>5.2.3</b> | <b>The approach employed in this project</b> .....                   | <b>121</b> |
| 5.2.3.1      | <i>Kissinger</i> .....   | 121        |
| 5.2.3.2      | <i>KAS (Kissinger-Akahira-Sunose)</i> .....                          | 122        |
| 5.2.3.3      | <i>FWO (Flynn-Wall-Ozawa)</i> .....                                  | 122        |
| 5.2.3.4      | <i>Friedman</i> .....  | 123        |
| 5.3          | Methodology.....   | 123        |
| <b>5.3.1</b> | <b>Experimental results</b> .....                                    | <b>124</b> |
| <b>5.3.2</b> | <b>Suggested mechanism</b> .....                                     | <b>127</b> |
| <b>5.3.3</b> | <b>Data treatment</b> .....  | <b>128</b> |
| 5.4          | Results.....   | 133        |
| 5.5          | Model adjustment.....  | 138        |
| 5.6          | Analysis of the vapours .....  | 146        |



|           |   |            |
|-----------|---|------------|
| 5.7       | Product distribution .....                          | 151        |
| 5.8       | Reaction heat .....                                 | 154        |
| 5.9       | References .....                                    | 155        |
| <b>6</b>  | <b>Additional design features.....</b>              | <b>160</b> |
| 6.1       | Feedstocks.....                                     | 160        |
| 6.1.1.1   | RDF.....  | 160        |
| 6.1.1.2   | Wheat Straw .....                                   | 161        |
| 6.1.1.3   | Woodchips .....                                     | 162        |
| 6.1.2     | Repose Angle .....                                  | 163        |
| 6.2       | Flights design and effect .....                     | 164        |
| 6.2.1     | Types of flights.....                               | 165        |
| 6.2.2     | Design of a flight .....                            | 166        |
| 6.2.3     | Analysis .....                                      | 167        |
| 6.2.4     | Influence on the other models .....                 | 170        |
| 6.3       | Heating method .....                                | 171        |
| 6.3.1     | Configuration.....                                  | 172        |
| 6.3.1.1   | Co-current .....                                    | 172        |
| 6.3.1.2   | Counter-current.....                                | 173        |
| 6.3.1.3   | Cross-flow.....                                     | 174        |
| 6.3.2     | Heat source.....                                    | 174        |
| 6.3.2.1   | Approach within this project.....                   | 174        |
| 6.4       | References .....                                    | 176        |
| <b>7</b>  | <b>Model integration .....</b>                      | <b>179</b> |
| 7.1       | Introduction .....                                  | 179        |
| 7.2       | Bed of solids .....                                 | 181        |
| 7.2.1     | Bed motion .....                                    | 182        |
| 7.2.2     | Length of the bed of solids .....                   | 182        |
| 7.2.3     | Contact areas.....                                  | 183        |
| 7.2.4     | Residence time .....                                | 184        |
| 7.3       | Heat transfer .....                                 | 184        |
| 7.3.1     | Heat flows .....                                    | 185        |
| 7.3.1.1   | Conduction .....                                    | 185        |
| 7.3.1.2   | Convection.....                                     | 186        |
| 7.3.1.3   | Radiation.....                                      | 186        |
| 7.3.2     | Approach .....                                      | 187        |
| 7.3.2.1   | Troubleshooting .....                               | 191        |
| 7.3.2.1.1 | Convergence .....                                   | 191        |
| 7.3.2.1.2 | Heat source .....                                   | 193        |
| 7.3.2.1.3 | Flow of combustion gases.....                       | 194        |
| 7.3.2.1.4 | Flow of carrier gas.....                            | 196        |
| 7.3.2.1.5 | Particle size .....                                 | 197        |
| 7.4       | Kinetic model .....                                 | 197        |
| 7.5       | Integration of the submodels .....                  | 199        |
| 7.5.1     | Target conversion .....                             | 200        |
| 7.5.2     | Convergence and consistency .....                   | 201        |
| 7.5.3     | Boundary condition and initialising the model ..... | 202        |
| 7.6       | Outputs .....                                       | 204        |
| 7.7       | Adaptability to other processes .....               | 205        |
| 7.8       | References .....                                    | 205        |
| <b>8</b>  | <b>Industrial application .....</b>                 | <b>207</b> |
| 8.1       | Knowledge from the industrial experience.....       | 207        |

|             |   |            |
|-------------|---|------------|
| 8.2         | Pre- and Post-treatment processes .....                     | 208        |
| 8.2.1       | <b>Pre-treatment</b> .....                                  | <b>208</b> |
| 8.2.1.1     | <i>Physical pre-treatment</i> .....                         | 209        |
| 8.2.1.2     | <i>Thermal pre-treatment</i> .....                          | 210        |
| 8.2.1.3     | <i>Chemical pre-treatment</i> .....                         | 211        |
| 8.2.1.4     | <i>Biological pre-treatment</i> .....                       | 211        |
| 8.2.2       | <b>Post-treatment</b> .....                                 | <b>212</b> |
| 8.2.2.1     | <i>Char</i> .....   | 212        |
| 8.2.2.2     | <i>Pyrolysis oils</i> .....                                 | 213        |
| 8.2.2.3     | <i>Permanent gases</i> .....                                | 213        |
| 8.3         | References .....  | 214        |
| 9           | <b>Results and discussion</b> .....                         | <b>217</b> |
| 9.1         | Scenario analysis .....                                     | 217        |
| 9.2         | User interfaces .....                                       | 219        |
| 9.3         | Validation of the model .....                               | 221        |
| 9.3.1       | <b>Stein Pyrolysis Ltd.</b> .....                           | <b>222</b> |
| 9.3.2       | <b>Auto validation with the model</b> .....                 | <b>222</b> |
| 9.3.3       | <b>Validation outcomes</b> .....                            | <b>223</b> |
| 9.4         | Case study .....  | 223        |
| 9.5         | Limitations.....  | 226        |
| 9.6         | References .....  | 227        |
| 10          | <b>Conclusions</b> .....                                    | <b>228</b> |
| 11          | <b>Next steps and future implementation</b> .....           | <b>230</b> |
| 11.1        | Validation .....  | 230        |
| 11.2        | Model improvements .....                                    | 230        |
| 11.2.1      | <b>Flow of nitrogen</b> .....                               | <b>230</b> |
| 11.2.2      | <b>Vapours inside the reactor</b> .....                     | <b>230</b> |
| 11.2.3      | <b>CFD modelling</b> .....                                  | <b>230</b> |
| 11.2.4      | <b>Voidage</b> .....  | <b>231</b> |
| 11.2.5      | <b>The behaviour of the solids</b> .....                    | <b>231</b> |
| 11.2.6      | <b>Flights design</b> .....                                 | <b>231</b> |
| 11.2.7      | <b>Heat losses</b> .....                                    | <b>231</b> |
| 11.2.8      | <b>Product distribution</b> .....                           | <b>232</b> |
| 11.2.9      | <b>Product properties</b> .....                             | <b>232</b> |
| 11.2.10     | <b>Simulation time</b> .....                                | <b>232</b> |
| 11.2.11     | <b>Optimisation</b> .....                                   | <b>232</b> |
| 11.2.12     | <b>Adaptability to other thermochemical processes</b> ..... | <b>232</b> |
| 11.3        | Future implementation.....                                  | 233        |
| 11.4        | Dissemination.....  | 233        |
| 11.5        | References .....  | 234        |
| 12          | <b>Appendices</b> .....                                     | <b>235</b> |
| Appendix A. | <b>Mathematical design of a flight</b> .....                | <b>235</b> |
| Appendix B. | <b>Mechanical features</b> .....                            | <b>238</b> |
| B.1.        | Sealing.....  | 238        |
| B.1.1.      | <b>Leaf Seals</b> .....                                     | <b>239</b> |
| B.1.2.      | <b>Clipper Split</b> .....                                  | <b>239</b> |
| B.1.3.      | <b>Oil</b> .....  | <b>240</b> |
| B.1.4.      | <b>Flexilip</b> .....                                       | <b>240</b> |
| B.1.5.      | <b>ProTech</b> .....  | <b>241</b> |
| B.1.6.      | <b>V-shaped</b> .....                                       | <b>241</b> |
| B.2.        | Bearings.....   | 242        |

|                    |   |            |
|--------------------|---|------------|
| B.2.1.             | Ball-bearing .....                              | 242        |
| B.2.2.             | Straight roller bearings .....                  | 243        |
| B.2.3.             | Helical roller .....                            | 243        |
| B.2.4.             | Spherical-roller thrust bearing .....           | 243        |
| B.2.5.             | Needle bearing .....                            | 243        |
| B.2.6.             | Tapered roller bearing .....                    | 243        |
| B.3.               | Drive assembly .....                            | 244        |
| B.3.1.             | Chain & Sprocket .....                          | 244        |
| B.4.               | Gear Drive .....                                | 244        |
| B.4.1.             | Friction Drive .....                            | 245        |
| B.4.2.             | Direct Drive .....                              | 245        |
| B.5.               | Construction materials.....                     | 246        |
| B.5.1.             | Refractory.....                                 | 246        |
| B.5.2.             | Carbon steel .....                              | 247        |
| B.5.3.             | Low-Alloy steels.....                           | 247        |
| B.5.4.             | Stainless Steel.....                            | 247        |
| B.6.               | Other mechanical elements.....                  | 248        |
| B.7.               | Measure and Control of process parameters ..... | 248        |
| B.7.1.             | FEECO .....                                     | 248        |
| B.7.2.             | University of Edinburgh .....                   | 249        |
| B.7.3.             | Torr®Coal.....                                  | 249        |
| B.7.4.             | CENER.....                                      | 249        |
| B.8.               | Transport of material .....                     | 250        |
| B.9.               | Feeding and collection .....                    | 251        |
| B.10.              | Piping.....                                     | 251        |
| B.10.1.            | Flanges .....                                   | 252        |
| B.10.2.            | Bellows.....                                    | 252        |
| B.11.              | References .....                                | 253        |
| <b>Appendix C.</b> | <b>Industrial experience .....</b>              | <b>255</b> |
| C.1.               | Torr®Coal.....                                  | 255        |
| C.1.1.             | Business driving forces.....                    | 255        |
| C.1.2.             | Facilities.....                                 | 255        |
| C.1.3.             | Torrefaction market.....                        | 258        |
| C.2.               | CENER.....                                      | 258        |
| C.2.1.             | Facilities.....                                 | 259        |
| C.2.2.             | AWL.....  | 261        |
| C.2.3.             | Experimental Design .....                       | 262        |
| C.2.4.             | Experiments.....                                | 264        |
| C.3.               | Secondment in BPP .....                         | 265        |
| C.3.1.             | Veolia .....                                    | 265        |
| C.3.2.             | Stein Pyrolysis Ltd. ....                       | 269        |
| C.3.3.             | AJAX Equipment Ltd.....                         | 271        |
| C.4.               | References .....                                | 272        |

## List of figures

|  |     |
|--|-----|
| Figure 1.1: Cellulose structure, from [11].....  | 22  |
| Figure 1.2: Monomers for hemicellulose, from [11].....   | 23  |
| Figure 1.3: Lignin structure, from [11] .....  | 23  |
| Figure 1.4: Biomass processing, adapted from[27] .....   | 24  |
| Figure 1.5: Scheme of the pyrolysis process.....   | 26  |
| Figure 1.6: Typical product distribution from different types of pyrolysis .....   | 28  |
| Figure 1.7: Overlap of conditions between slow pyrolysis and other thermochemical processes .....                        | 29  |
| Figure 1.8: Char, biochar and charcoal .....   | 29  |
| Figure 1.9: Product distribution of wheat straw pyrolysis at different temperatures (adapted from [73])<br>.....         | 31  |
| Figure 1.10: Scheme of the GreenCarbon project .....   | 34  |
| Figure 1.11: Scheme of the model.....  | 36  |
| Figure 1.12: Scheme of the research project.....   | 38  |
| Figure 2.1: Feedstock steps .....  | 45  |
| Figure 2.2: Missouri kiln .....  | 46  |
| Figure 2.3: Tunnel retort .....  | 48  |
| Figure 2.4: Twin retort scheme .....   | 49  |
| Figure 2.5: Lambiotte retort.....  | 50  |
| Figure 2.6: Reichert system .....  | 51  |
| Figure 2.7: Lurgi reactor.....   | 52  |
| Figure 2.8: Herreshoff multiple-hearth furnace .....   | 53  |
| Figure 2.9: Moving Agitated Bed .....  | 54  |
| Figure 2.10: Paddle pyrolysis kiln .....   | 54  |
| Figure 2.11: Screw reactor .....   | 55  |
| Figure 2.12: Rotary kiln .....   | 56  |
| Figure 2.13: Results of the weighted classification .....  | 63  |
| Figure 2.14: Representation of the correlation between bed of solids, heat transfer and kinetics in the<br>process ..... | 64  |
| Figure 3.1: Transverse motions for the bed of solids .....   | 70  |
| Figure 3.2: Sensitivity Analysis of the length of the bed of solids .....  | 75  |
| Figure 3.3: Cross-sectional area of the reactor .....  | 77  |
| Figure 3.4: H/R ratio vs filling degree .....  | 78  |
| Figure 3.5: Bed of solids scheme inside the reactor.....   | 78  |
| Figure 3.6: Relation height, length and modified length .....  | 79  |
| Figure 3.7: Gas-solid area shape (Top view) .....  | 79  |
| Figure 3.8: Contact areas in the kiln .....  | 80  |
| Figure 3.9: Area/ (Radius x Length) vs Filling degree.....   | 81  |
| Figure 3.10: variation of freeboard area towards the wall.....   | 82  |
| Figure 3.11: Feedstock in chips shape .....  | 86  |
| Figure 3.12: Feedstock in pellet shape .....   | 86  |
| Figure 4.1: Heat flow from the combustion gases to the reactor .....   | 92  |
| Figure 4.2: Maximum- minimum dimension of a sphere .....   | 94  |
| Figure 4.3: Maximum-minimum dimension of a cylinder .....  | 94  |
| Figure 4.4: Velocity profile of the gases in a pipe .....  | 95  |
| Figure 4.5: View factor geometry between two surfaces, adapted from [4].....   | 102 |
| Figure 4.6: Plane surface.....   | 103 |
| Figure 4.7: Convex surface .....   | 103 |
| Figure 4.8: Concave surface .....  | 103 |
| Figure 4.9: concentric spheres .....   | 104 |
| Figure 4.10: Temperature profile in counter-current reactor .....  | 106 |

|   |     |
|---|-----|
| Figure 4.11: Temperature profile in co-current reactor .....  | 106 |
| Figure 4.12: Scheme of the information for each slice.....  | 107 |
| Figure 4.13: Heat transfer process for each slice.....  | 107 |
| Figure 5.1: Weight loss curves of wood for different sample temperatures (From Branca and Di Blasi [51]).....   | 115 |
| Figure 5.2: Logarithm of the volatile mass fraction as a function of time (From Branca and Di Blasi [51]) ..... | 115 |
| Figure 5.3: Dimensionless solid mass fraction vs time, from [51].....   | 118 |
| Figure 5.4: Isoconversional methods .....   | 120 |
| Figure 5.5: Mettler Toledo TGA/DSC 2 STARe System.....  | 124 |
| Figure 5.6: TGA crucibles with wheat straw, woodchips and RDF.....  | 124 |
| Figure 5.7: TGA and DTG of Woodchips.....   | 125 |
| Figure 5.8: TGA and DTG of Wheat Straw.....   | 126 |
| Figure 5.9: TGA and DTG of RDF .....  | 126 |
| Figure 5.10: Kissinger method for woodchips.....  | 131 |
| Figure 5.11: KAS method for woodchips .....   | 132 |
| Figure 5.12: FWO method for Woodchips.....  | 132 |
| Figure 5.13: Friedman method for Woodchips .....  | 133 |
| Figure 5.14: Activation energy for woodchips .....  | 135 |
| Figure 5.15: Logarithm of the pre-exponential factor for woodchips.....   | 135 |
| Figure 5.16: Activation Energy for Wheat Straw .....  | 136 |
| Figure 5.17: Logarithm of the pre-exponential factor for Wheat Straw.....                                       | 136 |
| Figure 5.18: Activation energy for RDF .....  | 137 |
| Figure 5.19: Logarithm of the pre-exponential factor for RDF.....   | 137 |
| Figure 5.20: comparison Woodchips experimental-model .....  | 139 |
| Figure 5.21: comparison Wheat Straw experimental-model.....   | 139 |
| Figure 5.22: comparison RDF experimental-model.....   | 140 |
| Figure 5.23: Optimum experimental-model for woodchips.....  | 143 |
| Figure 5.24: Optimum experimental-model for wheat straw .....   | 143 |
| Figure 5.25: Optimum experimental-model for RDF.....  | 144 |
| Figure 5.26: Activation energy for Woodchips every 5% conversion .....  | 145 |
| Figure 5.27: Pre-exponential factor for Woodchips every 5% conversion .....                                     | 146 |
| Figure 5.28: Mass spectrum for Ethane (from [85]).....  | 147 |
| Figure 5.29: Mass spectrum for Hydrogen (from [85]) .....   | 147 |
| Figure 5.30: MS example for Signal 44 .....   | 149 |
| Figure 5.31: Char yield within the temperature range.....   | 151 |
| Figure 5.32: Product yields variation with temperature .....  | 153 |
| Figure 5.33: Recalculated yields for pyrolysis vapours.....   | 153 |
| Figure 6.1: Repose angle experiments for wheat straw.....   | 164 |
| Figure 6.2: Scheme of the flight .....  | 166 |
| Figure 6.3: Calculation of the volume of feedstock in the flight .....  | 166 |
| Figure 6.4: Sensitivity analysis of $R_0$ .....   | 169 |
| Figure 6.5: Sensitivity analysis for the design of the flights.....   | 170 |
| Figure 6.6: Schematic representation of the temperature profile of a co-current reactor.....                    | 173 |
| Figure 6.7: Schematic representation of the temperature profile of a counter-current reactor .....              | 173 |
| Figure 7.1: Structure of bed of solids submodel.....  | 181 |
| Figure 7.2: Structure of the heat transfer submodel.....  | 184 |
| Figure 7.3: Variation of the calorific value of the gases with temperature .....                                | 191 |
| Figure 7.4: tracking of temperatures on step after evaporation .....  | 193 |
| Figure 7.5: Square temperature difference.....  | 193 |
| Figure 7.6: temperature profile and heat flow proportions on counter-current configuration.....                 | 195 |

|  |     |
|--|-----|
| Figure 7.7: temperature profile and heat flows proportions on co-current configuration ..... | 196 |
| Figure 7.8: Variation of final temperature and conversion with flow of combustion gases..... | 199 |
| Figure 7.9: Sensitivity Analysis for the conversion .....                                    | 200 |
| Figure 7.10: Radius and combustion gases flow dependency with solids input .....             | 203 |
| Figure 7.11: Graph from outputs .....  | 204 |
| Figure 9.1: Inputs interface .....   | 220 |
| Figure 9.2: Interface during simulation.....   | 220 |
| Figure 9.3: Interface when the simulation is completed.....                                  | 221 |
| Figure 9.4: Outputs interface validation .....   | 221 |
| Figure 9.5: Radius and Length of the case study.....   | 224 |
| Figure 9.6: kiln angle and conversion of the case study .....                                | 225 |
| Figure 9.7: Convergence of the case study.....   | 225 |
| Figure 12.1: Leaf sealing from [1] .....   | 239 |
| Figure 12.2: Clipper split sealing, from [3] .....   | 240 |
| Figure 12.3: oil sealing, from [3] .....   | 240 |
| Figure 12.4: Flexilip sealing [3].....   | 241 |
| Figure 12.5: ProTech sealing [3].....  | 241 |
| Figure 12.6: V-shaped sealing [3].....   | 242 |
| Figure 12.7: ball bearing scheme, from [6] .....   | 243 |
| Figure 12.8: Chain & Sprocket, from [9].....   | 244 |
| Figure 12.9: Gear and pinion schemes, from [10].....   | 245 |
| Figure 12.10: Friction Drive mechanism, from [13] .....                                      | 245 |
| Figure 12.11: screw transport mechanism from CENER [24] .....                                | 251 |
| Figure 12.12: Basket conveyor from CENER [24] .....  | 251 |
| Figure 12.13: bellow joint, from [29] .....  | 253 |
| Figure 12.14: Scheme of the plant .....  | 255 |
| Figure 12.15: View of Google maps of Torr®Coal Production Centre .....                       | 256 |
| Figure 12.16: Smoking area .....   | 258 |
| Figure 12.17: Flow diagram of the process in CENER .....                                     | 259 |
| Figure 12.18: Biomass Dryer .....  | 260 |
| Figure 12.19: Scheme of the torrefier .....  | 261 |
| Figure 12.20: Scheme of the model used in CENER.....   | 263 |
| Figure 12.21: Process flowsheet for waste wood processing.....                               | 266 |
| Figure 12.22: Process flowsheet for commercial waste processing.....                         | 267 |
| Figure 12.23: Plant flow diagram of the waste streams.....                                   | 268 |

## List of tables

|  |     |
|--|-----|
| Table 1.1: characteristics and product distribution from the different types of pyrolysis .....    | 27  |
| Table 1.2: Project consortium .....  | 33  |
| Table 2.1: Gathered information from the reactors .....  | 58  |
| Table 2.2: Gathered information from the reactors (continuation).....                              | 59  |
| Table 2.3: Weighted classification of reactors.....  | 62  |
| Table 3.1: Conditions for each motion of the bed of solids.....                                    | 72  |
| Table 3.2: Approximation of the integral in 10 and 20 steps with three different methods .....     | 74  |
| Table 3.3: Standard values for the sensitivity analysis .....                                      | 76  |
| Table 3.4: Voidage coefficients .....  | 87  |
| Table 5.1: Classification of pyrolysis mechanisms .....  | 111 |
| Table 5.2: Integral mechanisms and mechanistic terms for the most common reaction mechanisms ..... | 120 |
| Table 5.3: Initial weights of samples for TGA.....   | 124 |

|   |     |
|---|-----|
| Table 5.4: calculation for each of the samples (Woodchips 2.5 K/min).....                   | 130 |
| Table 5.5: Output of the three samples of Woodchips at 2.5 K/min .....                      | 130 |
| Table 5.6: Gather of the values for Woodchips.....  | 131 |
| Table 5.7: Slope and Y-axis interception for woodchips.....                                 | 133 |
| Table 5.8: Results for Woodchips at reaction order 1.....                                   | 133 |
| Table 5.9: Results for Wheat Straw at reaction order 1.....                                 | 134 |
| Table 5.10: Results for RDF at reaction order 1 and single-step mechanism .....             | 134 |
| Table 5.11: Total error for first reaction order.....                                       | 140 |
| Table 5.12: Error for second reaction order .....   | 141 |
| Table 5.13: Optimum values for the different feedstocks.....                                | 142 |
| Table 5.14: Error for optimum reaction orders .....   | 142 |
| Table 5.15: Kinetic parameters for Woodchips every 5% conversion .....                      | 145 |
| Table 5.16: Channels in the MS per component .....  | 148 |
| Table 5.17: Gas yields for lignocellulosic biomass .....                                    | 150 |
| Table 5.18: Gas yields for RDF.....   | 150 |
| Table 5.19: Coefficients for the char yield of each feedstock.....                          | 152 |
| Table 6.1: Proximate and ultimate analysis of four samples of RDF feedstock .....           | 161 |
| Table 6.2: Proximate and ultimate analysis of five samples of wheat straw feedstock .....   | 162 |
| Table 6.3: typical composition for hardwood and softwood [20, 26].....                      | 162 |
| Table 6.4: Proximate and ultimate analysis of five samples of woodchips feedstock .....     | 163 |
| Table 6.5: results of repose angle experiments .....  | 164 |
| Table 6.6: Examples of configurations of flights .....                                      | 166 |
| Table 6.7: Standard values for the sensitivity analysis for the design of the flights ..... | 167 |
| Table 6.8: Standard values for the study of the angle between coordinates .....             | 168 |
| Table 6.9: Standard values for the radius of the flights .....                              | 169 |
| Table 7.1: Initial conditions .....   | 199 |
| Table 9.1: Table for Scenario analysis.....   | 217 |
| Table 9.2: Relation radius and flow of combustion gases with biomass capacity.....          | 223 |
| Table 9.3: evolution of flow of combustion gases with solids temperature .....              | 223 |
| Table 9.4: Case study .....   | 223 |
| Table 12.1: Definition of the segments of the flight .....                                  | 235 |
| Table 12.2: Coordinates of the points .....   | 235 |
| Table 12.3: Experimental Design Table.....  | 264 |
| Table 12.4: Results of the experiments.....   | 265 |

## List of equations

|  |    |
|--|----|
| Equation 3.1: Froude number .....                                  | 69 |
| Equation 3.2: Saeman's model.....                                  | 73 |
| Equation 3.3: re-arranged Saeman's model equation .....            | 73 |
| Equation 3.4: Auxiliary equations for the integration methods..... | 73 |
| Equation 3.5: Midpoint Rule expression .....                       | 74 |
| Equation 3.6: Calculation method by the Trapezoidal Rule .....     | 74 |
| Equation 3.7: Simpson's Rule .....                                 | 74 |
| Equation 3.8: calculation of angle $\phi$ .....                    | 77 |
| Equation 3.9: Area of the triangle.....                            | 77 |
| Equation 3.10: Area of the circular sector .....                   | 77 |
| Equation 3.11: Area of the bed of solids .....                     | 77 |
| Equation 3.12: Definition of filling degree .....                  | 77 |
| Equation 3.13: ratio H/R as a function of the filling degree ..... | 78 |
| Equation 3.14: Equation to calculate the freeboard line .....      | 79 |

|  |     |
|--|-----|
| Equation 3.15: angle with arctangent .....   | 79  |
| Equation 3.16: angle with arcsine.....   | 79  |
| Equation 3.17: angle with Pythagoras theorem .....   | 79  |
| Equation 3.18: Calculation of Gas-Solid area.....  | 79  |
| Equation 3.19: Length of contact bed of solids-wall.....   | 80  |
| Equation 3.20: Area wall-bed of solids .....   | 80  |
| Equation 3.21: Area wall-gas .....   | 80  |
| Equation 3.22: Wall-solid area as a function of the filling degree.....                                  | 81  |
| Equation 3.23: Wall-gas area as a function of the filling degree.....                                    | 81  |
| Equation 3.24: Solid-Gas area as a function of the filling degree.....                                   | 81  |
| Equation 3.25: integral of the area between wall-bed of solids .....                                     | 82  |
| Equation 3.26: integral of the area between wall-gases .....   | 82  |
| Equation 3.27: lineal dependency of the area between the gas and the solids and the filling degree ..... | 83  |
| Equation 3.28: Dependency of Area gas-solid on the height.....   | 83  |
| Equation 3.29: Integral of the gas-solid area with height .....  | 83  |
| Equation 3.30: Method employed when the initial and final filling degrees are higher than 0.5 .....      | 84  |
| Equation 3.31: Calculation of integral term for the third scenario .....                                 | 84  |
| Equation 3.32: usual formula to calculate the residence time of reagents in a reactor.....               | 84  |
| Equation 3.33: Mean Excursion Time (MET).....  | 85  |
| Equation 3.34: Effect of voidage in conductive heat flow for Gas-Solid .....                             | 85  |
| Equation 3.35: Effect of voidage in conductive heat flow for Wall-Solid.....                             | 85  |
| Equation 3.36: Volumetric flow for the bed of solids.....  | 87  |
| Equation 4.1: Fourier's law of heat conduction on direction n .....                                      | 91  |
| Equation 4.2: Transient heat transfer .....  | 91  |
| Equation 4.3: Conductive heat transfer with variable area .....  | 92  |
| Equation 4.4: Heat flow diffusion .....  | 92  |
| Equation 4.5: Convective heat flow .....   | 95  |
| Equation 4.6: convective coefficient in no-slip condition .....  | 96  |
| Equation 4.7: Nusselt number.....  | 96  |
| Equation 4.8: Reynolds number .....  | 98  |
| Equation 4.9: Prandtl number.....  | 98  |
| Equation 4.10: Velocity of a fluid in a pipe .....   | 99  |
| Equation 4.11: hydraulic diameter.....   | 99  |
| Equation 4.12: Gnielinski correlation .....  | 99  |
| Equation 4.13: factor friction depending on the value of the Reynolds number .....                       | 99  |
| Equation 4.14: Peclet number.....  | 100 |
| Equation 4.15: Nusselt number for the bed of solids .....  | 100 |
| Equation 4.16: Nusselt number in the function of Peclet value .....                                      | 100 |
| Equation 4.17: Blackbody emissive power.....   | 101 |
| Equation 4.18: Stefan-Boltzmann constant .....   | 101 |
| Equation 4.19: Emissive power of a small body.....   | 101 |
| Equation 4.20: Radiative heat transfer between two black bodies .....                                    | 101 |
| Equation 4.21: Heat transfer between two grey, diffuse and opaque surfaces .....                         | 101 |
| Equation 4.22: view factor definition.....   | 102 |
| Equation 4.23: View factor from surface 1 to surface 2 .....   | 103 |
| Equation 4.24: Reciprocity relation.....   | 103 |
| Equation 4.25: Summation rule .....  | 103 |
| Equation 4.26: Superposition rule.....   | 103 |
| Equation 4.27: View factor of plane surface.....   | 103 |
| Equation 4.28: view factor of a convex surface .....   | 103 |
| Equation 4.29: View factor of a concave surface.....   | 103 |



|   |     |
|---|-----|
| Equation 4.30: View factor of concentric spheres.....                             | 104 |
| Equation 4.31: view factor from the wall to the gas and bed of solids .....       | 104 |
| Equation 4.32: view factor from the gas to the wall and bed of solids .....       | 104 |
| Equation 4.33: View factor wall-gas .....   | 105 |
| Equation 4.34: View factor wall-solid .....                                       | 105 |
| Equation 4.35: View factor gas-solid .....  | 105 |
| Equation 4.36: Overall heat transfer coefficient.....                             | 105 |
| Equation 4.37: Heat flow by log mean temperature difference .....                 | 105 |
| Equation 4.38: Definition of thermal resistance .....                             | 106 |
| Equation 4.39: Radiative thermal resistance .....                                 | 106 |
| Equation 4.40: Variation of temperature with heat absorbed .....                  | 108 |
| Equation 5.1: Reaction rate of the feedstock.....                                 | 116 |
| Equation 5.2: Reaction rate of the intermediate compound .....                    | 116 |
| Equation 5.3: Reaction rate for the primary volatiles.....                        | 116 |
| Equation 5.4: Reaction rate for the secondary volatiles .....                     | 116 |
| Equation 5.5: Reaction rate for the char.....                                     | 116 |
| Equation 5.6: definition of $k_1$ .....   | 116 |
| Equation 5.7: definition of $k_2$ .....   | 116 |
| Equation 5.8: Arrhenius equation for the kinetic constant .....                   | 116 |
| Equation 5.9: Weight of feedstock with time .....                                 | 117 |
| Equation 5.10: Primary volatiles production.....                                  | 117 |
| Equation 5.11: Production of the intermediate product.....                        | 117 |
| Equation 5.12: Secondary volatiles production.....                                | 117 |
| Equation 5.13: Char production with time.....                                     | 117 |
| Equation 5.14: Solid residual.....  | 117 |
| Equation 5.15: Final mass of primary volatiles .....                              | 117 |
| Equation 5.16: Final mass of secondary volatiles .....                            | 117 |
| Equation 5.17: Final mass of char .....   | 117 |
| Equation 5.18: Mass of primary volatiles .....                                    | 117 |
| Equation 5.19: Final mass of primary volatiles .....                              | 117 |
| Equation 5.20: Mass of secondary volatiles.....                                   | 117 |
| Equation 5.21: Final mass of secondary volatiles .....                            | 117 |
| Equation 5.22: Dimensionless solid weight for step I.....                         | 117 |
| Equation 5.23: Dimensionless solid weight for step II.....                        | 118 |
| Equation 5.24: Expression for solid decomposition .....                           | 119 |
| Equation 5.25: Definition of conversion .....                                     | 119 |
| Equation 5.26: mechanistic term .....   | 119 |
| Equation 5.27: Heating rate.....  | 119 |
| Equation 5.28: Combination heating rate with the general expression .....         | 119 |
| Equation 5.29: Variation of conversion with Temperature.....                      | 119 |
| Equation 5.30: Integral function .....  | 119 |
| Equation 5.31: Kissinger linear equation .....                                    | 121 |
| Equation 5.32: Transformed Coats-Redfern temperature integral approximation ..... | 122 |
| Equation 5.33: Doyle's approximation .....  | 122 |
| Equation 5.34: KAS expression .....   | 122 |
| Equation 5.35: Doyle's approximation for FWO .....                                | 122 |
| Equation 5.36: FWO expression .....   | 123 |
| Equation 5.37: Friedman expression.....   | 123 |
| Equation 5.38: Normalised weight.....   | 125 |
| Equation 5.39: Conversion formula.....  | 129 |
| Equation 5.40: Variation of conversion with time .....                            | 129 |

|   |     |
|---|-----|
| Equation 5.41: Variation of conversion with temperature .....                                 | 129 |
| Equation 5.42: Final conversion for reaction order 1.....                                     | 138 |
| Equation 5.43: Total error Model-Experimental .....   | 140 |
| Equation 5.44: Final conversion when reaction order is different from 1.....                  | 141 |
| Equation 5.45: Signal 2 from MS.....  | 148 |
| Equation 5.46: Signal 14 from MS.....   | 148 |
| Equation 5.47: Signal 15 from MS.....   | 148 |
| Equation 5.48: Signal 18 from MS.....   | 148 |
| Equation 5.49: Signal 26 from MS.....   | 148 |
| Equation 5.50: Signal 27 from MS.....   | 148 |
| Equation 5.51: Signal 28 from MS.....   | 148 |
| Equation 5.52: Signal 30 from MS.....   | 148 |
| Equation 5.53: Signal 44 from MS.....   | 148 |
| Equation 5.54: Calculation of char yield at each temperature .....                            | 151 |
| Equation 5.55: Char yield for RDF .....   | 152 |
| Equation 5.56: Yield of pyrolysis oil with temperature .....                                  | 153 |
| Equation 5.57: Yield of permanent gas with temperature.....                                   | 153 |
| Equation 6.1: repose angle .....  | 164 |
| Equation 6.2: Dynamic angle of repose definition .....  | 167 |
| Equation 6.3: Surface of the flight wall-solid .....  | 171 |
| Equation 6.4: Surface of the flight wall-gas.....   | 171 |
| Equation 6.5: heat of reaction .....  | 175 |
| Equation 6.6: Heat from the combustion of permanent gases.....                                | 175 |
| Equation 7.1: Froude number .....   | 182 |
| Equation 7.2: re-organised Saeman's model .....   | 182 |
| Equation 7.3: Wall-solid area as a function of the filling degree.....                        | 183 |
| Equation 7.4: Wall-gas area as a function of the filling degree.....                          | 183 |
| Equation 7.5: Solid-Gas area as a function of the filling degree.....                         | 183 |
| Equation 7.6: Integral of gas-solid area with height .....                                    | 184 |
| Equation 7.7: Mean Excursion Time.....  | 184 |
| Equation 7.8: Conductive heat transfer with variable area .....                               | 185 |
| Equation 7.9: Modified contact area wall-bed of solids .....                                  | 185 |
| Equation 7.10: Modified contact area wall-gases .....   | 185 |
| Equation 7.11: Modified contact area gases-bed of solids.....                                 | 185 |
| Equation 7.12: Convective heat flow .....   | 186 |
| Equation 7.13: Modified area wall- solids for convective heat flow.....                       | 186 |
| Equation 7.14: Heat transfer between two grey, diffuse and opaque surfaces .....              | 187 |
| Equation 7.15: heat transferred to the bed of solids .....                                    | 188 |
| Equation 7.16: Heat transferred to the gases inside the reactor.....                          | 188 |
| Equation 7.17: Heat transferred from the wall.....  | 188 |
| Equation 7.18: Energy balance for the combustion gases in co-current configuration.....       | 188 |
| Equation 7.19: Energy balance for the combustion gases in counter-current configuration ..... | 188 |
| Equation 7.20: Energy balance for the bed of solids.....                                      | 189 |
| Equation 7.21: Energy balance for the gases inside the reactor.....                           | 190 |
| Equation 7.22: mass fraction of gases .....   | 190 |
| Equation 7.23: Calorific value of the mixture of gases .....                                  | 190 |
| Equation 7.24: Limit of variation of temperature .....  | 191 |
| Equation 7.25: conversion out with first reaction order .....                                 | 198 |
| Equation 7.26: conversion out with reaction order different from one .....                    | 198 |
| Equation 7.27: variation of conversion with the time.....                                     | 198 |
| Equation 7.28: Initial radius.....  | 203 |

|  |            |
|--|------------|
| <i>Equation 7.29: initial combustion gases flow .....</i>  | <i>203</i> |
| <i>Equation 12.1: AWL equation .....</i>                   | <i>262</i> |
| <i>Equation 12.2: Solid yield equation.....</i>            | <i>262</i> |
| <i>Equation 12.3: Di Blasi and Lanzetta mechanism.....</i> | <i>262</i> |

### List of reactions

|  |            |
|--|------------|
| <i>Reaction 5.1: Broido and Nelson model.....</i>                                | <i>111</i> |
| <i>Reaction 5.2: Suuberg and co-workers model .....</i>                          | <i>111</i> |
| <i>Reaction 5.3: Cooley and Antal model .....</i>                                | <i>112</i> |
| <i>Reaction 5.4: Broido and Shafizadeh (B-S) model.....</i>                      | <i>112</i> |
| <i>Reaction 5.5: Koufopoulos model .....</i>                                     | <i>112</i> |
| <i>Reaction 5.6: Modified Broido and Shafizadeh model.....</i>                   | <i>112</i> |
| <i>Reaction 5.7: Babler mechanism.....</i>                                       | <i>113</i> |
| <i>Reaction 5.8: Papari mechanism.....</i>                                       | <i>113</i> |
| <i>Reaction 5.9: Di Blasi mechanism .....</i>                                    | <i>116</i> |
| <i>Reaction 5.10: Mechanism suggested for the lignocellulosic feedstock.....</i> | <i>127</i> |
| <i>Reaction 5.11: Suggested mechanism for pyrolysis of RDF .....</i>             | <i>128</i> |
| <i>Reaction 5.12: New mechanism for the lignocellulosic feedstock .....</i>      | <i>128</i> |
| <i>Reaction 5.13: New mechanism for RDF.....</i>                                 | <i>128</i> |

## Nomenclature

| Symbol            | Description                              | Units                |
|-------------------|--|----------------------|
| A                 | Area                                     | m <sup>2</sup>       |
| A, k <sub>0</sub> | Pre-exponential factor                   | min <sup>-1</sup>    |
| A <sub>c</sub>    | Contact area                             | m                    |
| A <sub>g</sub>    | Contact area of gases inside the reactor | m <sup>2</sup>       |
| A <sub>g-s</sub>  | Contact area - gases and solids          | m <sup>2</sup>       |
| A <sub>s</sub>    | Contact area - bed of solids             | m <sup>2</sup>       |
| A <sub>w</sub>    | Contact area - wall                      | m <sup>2</sup>       |
| A <sub>w-g</sub>  | Contact area - wall and gases            | m <sup>2</sup>       |
| A <sub>w-s</sub>  | Contact area - wall and solids           | m <sup>2</sup>       |
| C <sub>p</sub>    | Heat capacity                            | J/ (kg K)            |
| D <sub>h</sub>    | Hydraulic diameter                       | m                    |
| E <sub>a</sub>    | Activation Energy                        | kJ/mol               |
| E <sub>b</sub>    | Energy emission                          | W                    |
| f                 | Filling degree                           | -                    |
| f                 | Friction factor                          | -                    |
| F <sub>12</sub>   | View factor of surface, 1 over 2         | -                    |
| Fr                | Froude number                            | -                    |
| g                 | Gravity                                  | m/s <sup>2</sup>     |
| H                 | Height of the bed of solids              | m                    |
| h                 | Convective coefficient                   | W/(m <sup>2</sup> K) |
| HHV               | High heating value                       | MJ/kg                |
| k                 | Conductivity                             | W/(m K)              |
| k                 | kinetic constant                         | min <sup>-1</sup>    |
| L                 | Length of the reactor                    | m                    |
| $\dot{m}$         | Mass flow                                | kg/s                 |
| M, m              | Mass sample                              | mg                   |
| MET               | Mean Excursion Time                      | min                  |
| n                 | Step number or number of steps           | -                    |
| p                 | Perimeter                                | m                    |
| Pe                | Peclett number                           | -                    |
| Pr                | Prandtl number                           | -                    |
| Q                 | Volumetric flow of solids                | m <sup>3</sup> /s    |
| Q                 | Heat flow                                | W                    |
| R                 | Kiln radius                              | m                    |
| R                 | Universal gas constant                   | J/ (mol K)           |
| Re                | Reynolds number                          | -                    |
| R <sub>f</sub> '' | Fouling factor                           | -                    |
| R <sub>i</sub>    | Thermal resistance                       | K/W                  |

|                 |                                      |                                     |
|-----------------|--------------------------------------|-------------------------------------|
| T               | Temperature                          | K or °C                             |
| t               | Time                                 | s                                   |
| $T_{\infty}$    | Ambient temperature                  | K                                   |
| u               | Solids velocity                      | m/s                                 |
| U               | Global heat transfer coefficient     | W/K                                 |
| V               | Volume                               | m <sup>3</sup>                      |
| z               | Position in the reactor              | m                                   |
| $\alpha$        | Conversion                           | -                                   |
| $\beta$         | Angle of the bed of solids           | rad                                 |
| $\beta$         | Heating rate                         | K/min                               |
| $\Delta T_{lm}$ | Log mean temperature difference      | K                                   |
| $\epsilon$      | Emissivity                           | -                                   |
| $\theta, \phi$  | Angle of repose                      | rad                                 |
| $\mu$           | Viscosity                            | kg/(m s)                            |
| $\mu_w$         | Wall friction coefficient            | -                                   |
| $\mu_{w,c}$     | Critical wall friction coefficient   | -                                   |
| $\rho$          | Density                              | kg/m <sup>3</sup>                   |
| $\sigma$        | Stefan-Boltzmann constant            | W/ (m <sup>2</sup> K <sup>4</sup> ) |
| $\tau_R$        | Residence time                       | s                                   |
| $\varphi$       | Auxiliary angle for area calculation | rad                                 |
| $\omega$        | Rotational speed                     | rad/s                               |

# 1 Introduction

## 1.1 Biomass

Currently, the world faces several problems, mostly related to reducing dependence on fossil fuels and seeking renewable sources to supply the ever-increasing energy demand. The management and utilisation of the waste and residues of population and industry create difficulties, where landfilling is no longer an option, due to the shortage of space and the polluting degradation of biomass [1-4].

The problems concerning fossil fuels and climate change are widely known. Worldwide energy demand increases every year, and it is crucial to reduce the dependence on non-renewable energy sources [5]. Some of the potential sources of energy which have been investigated are solar, geothermal, tidal and biomass utilisation; there are others in development such as ocean thermal gradient, wave and marine current energy [6]. The production of energy from biomass is known as bioenergy, and it has significant potential in the short- and medium-term. The main advantages of biomass compared to other sources are its versatility and storability. Furthermore, biomass is unique because it acts as a source of fixed carbon from which fuel and consumer products can be produced [5].

According to the United Nations Framework Convention on Climate Change (UNFCCC) [7], biomass is defined as *“Non-fossilized and biodegradable organic material originated from plants, animals and micro-organisms. This shall also include products, by-products, residues and waste from agriculture, forestry and related industries as well as the non-fossilized and biodegradable organic fractions of industrial and municipal wastes”*.

Biomass is not an entirely renewable source if not sustainably produced and has some disadvantages. From its definition, biomass accounts for a large variety of materials and feedstocks. This variety means that the properties and composition are very variable. The energy and mass densities are low compared to other fuels which affect long-distance transportation, limiting its utilisation. The relatively high moisture content increases the costs, and its fibrous nature increases the energy requirement for grinding the biomass, which may have very heterogeneous shape distribution otherwise [5, 6, 8].

Plants are one of the sources of biomass which could compete with food production. Their increasing use to produce biofuels could lead to food shortages and price rises, besides the impact on public health and the ethical debate. To avoid the food vs fuel debate, the most promising solution is to use harvesting residues from agriculture and forestry exclusively. Other sources are energy crops such as switchgrass, hybrid poplar, salix or miscanthus, characterised by fast-growing rate, higher energy content, and the capability to grow in low-quality agricultural land. It is essential that land used to cultivate crops was not previously used to produce food to avoid further political and ethical issues [9-12].

In the recent past, the usage and valorisation of residues were limited to combustion, which produced additional greenhouse gases emissions. Currently, utilisation focuses on the production of biofuels and energy through processes such as pyrolysis or gasification and further production of chemicals from the products. Some characteristic components of lignocellulosic biomass are present in the waste, which makes waste another source of fixed carbon. To improve the quality of the feedstock, MSW (Municipal Solid Waste) is usually upgraded to RDF (Refused Derived Fuel) through the removal of the non-combustible materials. The non-combustible components include ferrous and non-ferrous metals, glass and the plastic fraction that can be recycled [4, 13-17].

### 1.1.1 Biomass composition

Biomass accounts for a range of materials, whose common feature is the source of fixed carbon, from the organic carbon in the biomass structure [18, 19]. These structural components are cellulose, hemicellulose, lignin and other additives, whose fractions vary between feedstocks. Each component does not refer to a specific molecule, but a range of components classed under these headings [9].

#### 1.1.1.1 Cellulose

Cellulose is a naturally abundant organic polymer, mainly found in the plant cell wall and is represented in Figure 1.1 (from [11]). The internal structure of cellulose is not entirely homogeneous, because there are two structures; crystalline and semi-crystalline. The crystalline structure is highly ordered, composed of very long fibrils. The molecules ( $\beta$ -glucopyranoside) are linked through 1-4- $\beta$ -glycosidic bonds. These molecules and bonds form 3-dimensional crystals, each of which are linked through different bonds. One dimension is linked through covalent bonds along the cellulose chains; another uses hydrogen bonds which hold the chains together as sheets, and the last uses Van Der Waals bonds which bridge the cellulose sheets in fibril form. The crystal structure and intra- and intermolecular hydrogen bonds provide mechanical strength and chemical stability, especially to hydrolysis [11, 20].

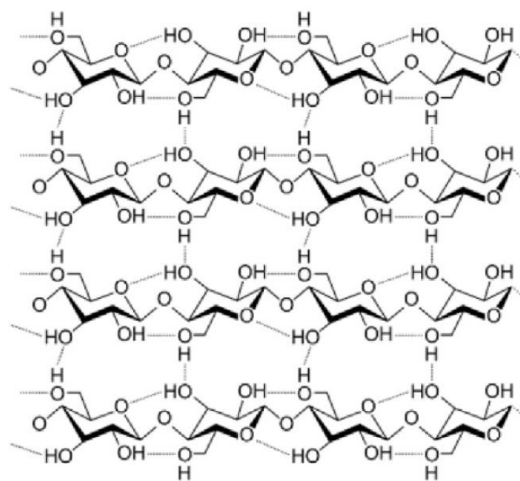


Figure 1.1: Cellulose structure, from [11]

#### 1.1.1.2 Hemicellulose

Hemicellulose surrounds the cellulose and acts as the joint between cellulose and lignin. Hemicellulose is more heterogeneous than cellulose and is composed of a group of polysaccharides. Monomers of the polysaccharides are glucose, galactose, mannose, xylose, arabinose and glucuronic acid (represented in Figure 1.2 from [11]). Hemicellulose acts as a structural element with a larger amount of monomers in each molecule, measured through the degree of polymerisation [21]. This makes the structure more amorphous with lower physical strength that is hydrolysable by acids, bases and hemicellulose enzymes [11].

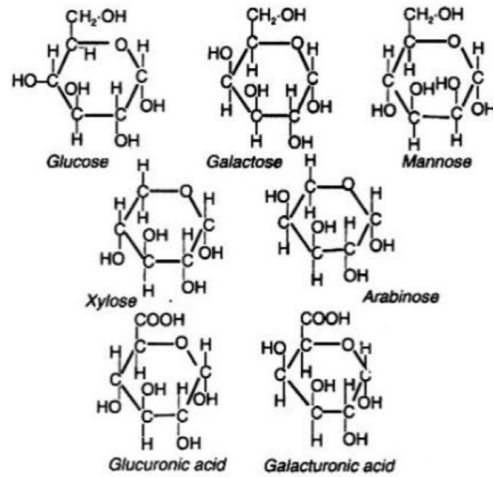


Figure 1.2: Monomers for hemicellulose, from [11]

### 1.1.1.3 Lignin

Lignin is the third significant component of biomass, which provides stiffness to the cell walls and holds the polysaccharides fibres together. It is represented by a three-dimensional and cross-linked phenolic polymer which combines phenylpropane units with hydroxyl- and methoxy-compounds. Mainly, the phenylpropane units are monomers like guaiacyl, syringyl and p-hydroxyphenol [20]. The cellulose fibres are coated with hemicellulose and the empty spaces between are filled with lignin, binding both components. In softwood, the predominant component is guaiacyl, whereas sinapyl is most predominant in hardwood [11]. One example of a lignin polymer is represented in Figure 1.3, from [11].

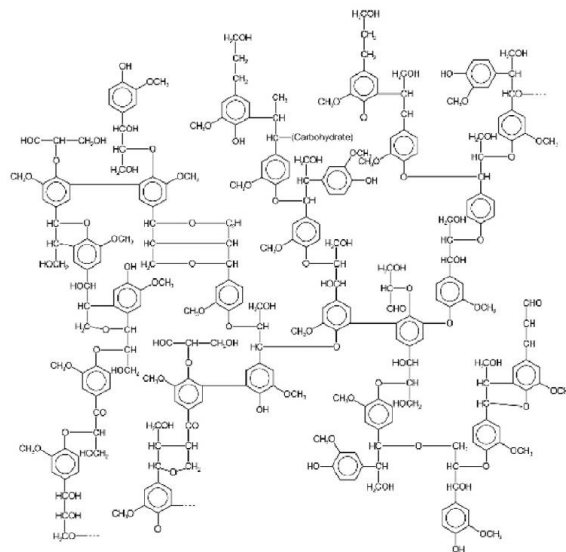


Figure 1.3: Lignin structure, from [11]

### 1.1.1.4 Extractives and inorganic components

Biomass can contain constituents besides the three main components (cellulose, hemicellulose and lignin) that are divided into extractives and inorganic components. Extractives are the organic low-molecular-weight substances within biomass [20]. This definition includes alkaloids, oils, fats, glycosides, gums, mucilage, pectins, phenolic compounds, proteins, resins, saponins, sugars, starches, terpenes and waxes. They can be separated with polar solvents such as alcohol or water, and



other non-polar solvents such as hexane or toluene. Their function is to protect the biomass from microbial and insect attacks [11, 20].

The inorganics are known as ash because it is defined as the remaining sample after complete combustion. Ash mainly consists of potassium, calcium, sodium, silicon, phosphorus and chlorine components. The percentage of ash within the biomass depends on the type and origin of the feedstock. As an example of the variability within the feedstocks, the average inorganic content in softwood is 2 wt.%, and 15 wt.% for hardwood [11]. If the origin is municipal solid waste, some sulphur or chlorine can be found, even after treatment into refused derived fuel. The composition and fraction of components of RDF are variable depending on the origin of the RDF, although a high inert content (around 12 wt.% on average) is a common characteristic [22].

### 1.1.2 Biomass applications and processing

The broad range of components that constitutes biomass makes it a very versatile feedstock. There are many potential processing options and applications for the products.

One of the uses of biomass is the manufacturing of furniture and as a construction material, for which it can be mixed with plastics [23]. Biomass is also widely known for being a food source for people and animals, like straw in farms [24].

In industry, biomass has the potential to produce many products such as fertilisers, biofuels, syngas, heat and electricity. The final product depends on the available feedstock; accounting from energy crops to organic waste or residues from agricultural activities or bioprocesses. The conversion technology plays a vital role, and there are three main pathways: catalytic, biological, and thermochemical conversion. Catalytic conversion of biomass consists of the use of a catalyst to transform the biomass into chemicals and biofuels. The biological conversion uses microorganisms for the conversion, and the thermochemical route uses temperature to convert the biomass into energy and products [25, 26]. A scheme for the conversion of biomass and the potential products are represented in Figure 1.4, adapted from [27].

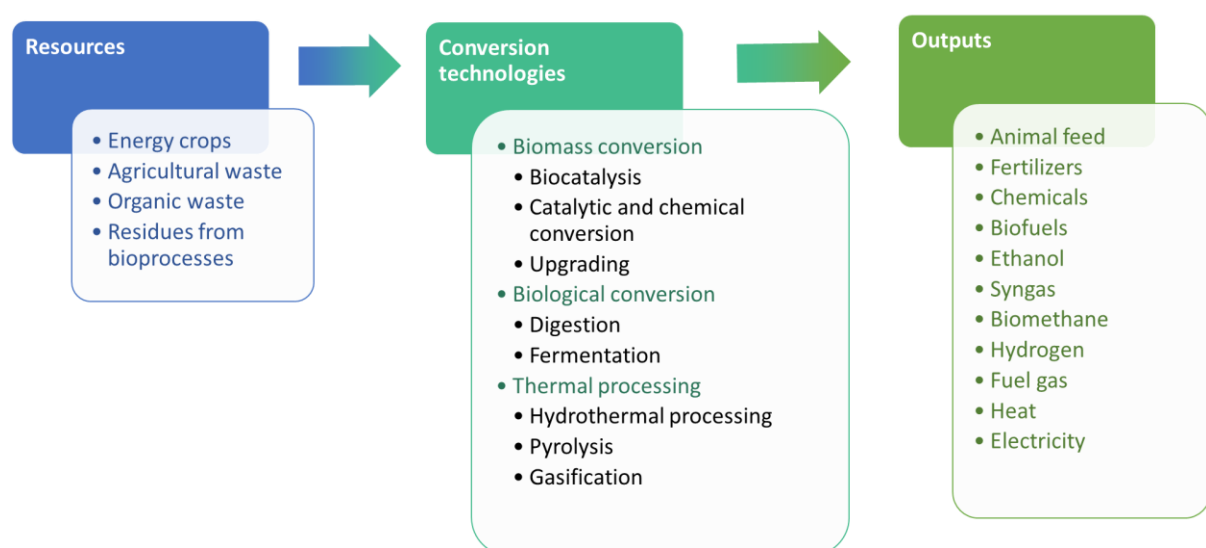


Figure 1.4: Biomass processing, adapted from [27]

## 1.2 Pyrolysis

This study focuses on the thermochemical route to produce a carbonaceous solid product. The main thermochemical processes that have been developed to industrial-scale are gasification,

combustion and pyrolysis [9, 28, 29]. There are other technologies at development stage like hydrothermal carbonisation (HTC) or torrefaction [30]. They are excluded from this research due to the low level of implementation at an industrial scale. The flexibility of the technology is another crucial aspect to consider due to the variability of feedstock properties. The possibility of scaling down the technology is an essential consideration because logistics is a source of high costs in biomass processing plants. For this reason, it may be better to consider several smaller plants, rather than a large-scale centralised plant [9].

Combustion has been widely studied [31-33] and is a very flexible technology in terms of feedstock, but it is not suitable to scale down for profitable and efficient performance. One of the main drawbacks is the emissions of carbon dioxide and carbon monoxide, which significantly contribute to the greenhouse effect.

Gasification runs effectively at a lower scale but is very specific to the feedstock type, so offers less flexibility. Even when the equipment is designed for a specific feedstock, the particle size should remain homogeneous with the particle size design for successful performance [29, 34, 35].

Overall, pyrolysis is more feedstock flexible, especially in slow pyrolysis batch systems, characterised by a straightforward and feedstock-flexible operation. Furthermore, pyrolysis can perform successfully at low scale. Although it has been implemented at industrial scale, further study is needed [36].

Pyrolysis is the thermochemical degradation of the feedstock or raw material in the absence of an oxidising agent like oxygen. This process transforms the feedstock into three products: permanent gas, pyrolysis oil and char. In this work, the term *vapours* refer to the pyrolysis oil/condensable fraction and permanent gases/ gas together in the gaseous form. Representation of pyrolysis is found in Figure 1.5 [9].

The permanent gases are those that do not condensate within the process, even with cooling. The gas is composed of low-molecular-weight non-condensable gases such as hydrogen (H<sub>2</sub>), carbon dioxide (CO<sub>2</sub>), carbon monoxide (CO), methane (CH<sub>4</sub>) and ethylene (C<sub>2</sub>H<sub>4</sub>). The composition of the gas is not fixed. It varies with the feedstock (particle size, moisture content) and the process parameters (type of pyrolysis and reactor, process temperature or solids and vapours residence time) [9]. The gas is mainly used to provide energy for pyrolysis and other parts of the system such as the dryer. In fast pyrolysis, the gases can be used to support the fluidisation of the bed in Fluidised Bed Reactors (FBR) [11]. Rarely, the permanent gases could potentially be the target product of pyrolysis to be integrated into the grid for the production of energy and heating [37].

The liquid product is called pyrolysis oil, with alternative names of bio-oil, bio-crude oil or pyroligneous liquor [38]. According to the standard ASTM D 7544-12 [39], the term bio-oil should be employed exclusively when it is the product of fast pyrolysis. Pyrolysis oil is a dark brown, free-flowing liquid, whose composition is a complex mixture of oxygenated compounds. It is the condensable fraction of the vapours released during pyrolysis of biomass. Depending on the conditions and composition, it may separate into two phases, aqueous and organic.

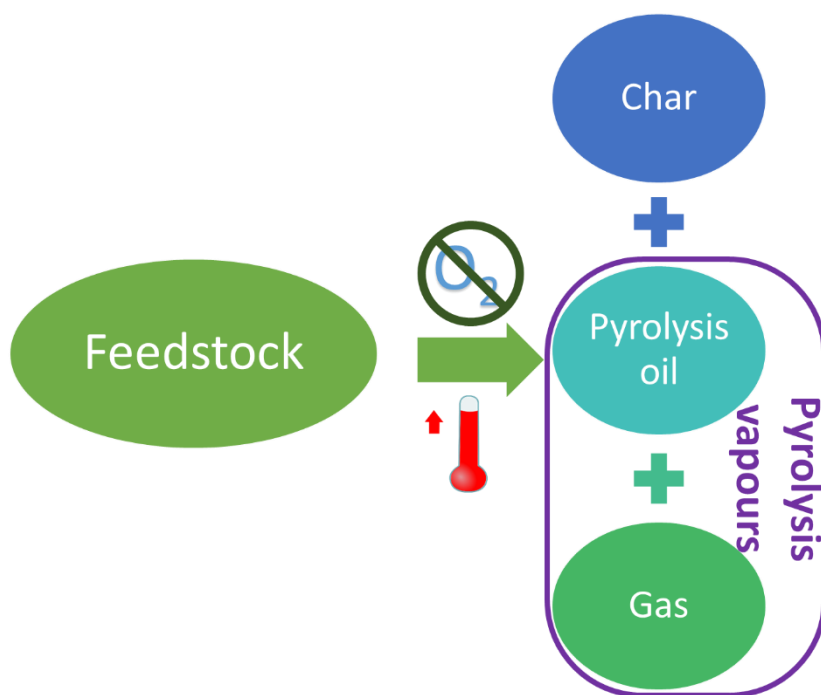


Figure 1.5: Scheme of the pyrolysis process

The dense organic fraction contains a complex mixture of heavy compounds, is dark brown and translucent. The aqueous phase is the lighter fraction containing moisture from pyrolysis and the feedstock. This phase includes components that are partially dissolved and is a transparent phase with a light yellow/brown colour. In terms of handling, storage, transportation and utilisation, pyrolysis oil has a strategic value due to its similarity to petroleum-based oil. The carbon distribution from a solution of the organic fraction with n-pentane is similar to diesel fuel [40, 41]. The compounds present in pyrolysis oil are phenol derivatives, furan, some acids and esters, and some traces of lighter hydrocarbons [42]. In research, the compounds are classified into seven categories: carboxylic acids, phenolic compounds, esters, nitrogenised compounds, hydrocarbons, alcohols and carbonyl compounds. The fraction of each of these categories depends on the feedstock and the conditions at which pyrolysis was performed [40, 43].

Pyrolysis oil is a source of chemicals and fuels due to the mixture of compounds and has a higher energy density than the original biomass. The increased energy density is caused by the lower oxygen content of the product, which makes the substance suitable for some thermal applications such as the production of steam and electricity [40]. In some industrial burners, pyrolysis oil is blended with ethanol to improve its quality [43]. Some of the chemicals that can be produced from the pyrolysis oil are polyphenols to produce resins with formaldehyde, calcium and/or magnesium acetate. These chemicals are employed to produce de-icers and fertilisers, and a range of flavouring and essence in the food industry [40].

Char is the solid product of pyrolysis. Char has been produced since ancient times, used for thousands of years for the production of heat and energy. It is a porous substance, rich in carbon content and chemically and biologically stable. Char is used mainly for soil amendment and energy production [9], although further research is carried out for its application as catalyst support, gas absorption and liquid adsorption [44]. Furthermore, char is a method of carbon sequestration [45]. All aspects related to char are further described in Section 1.2.1.

Pyrolysis is the thermochemical degradation of biomass in the absence of oxygen and can be divided into three different types: fast, intermediate and slow. Some of the differential aspects are temperature, the heating rate of the feedstock or residence time of gases and solids in the reactor. Each type of pyrolysis has different characteristics and reactor configurations; the product properties and yields are different for each. The limits are not fully defined, as there is some overlap in literature [9]. Table 1.1 summarises the aqueous and organic fractions into pyrolysis oil and describes the main features of each pyrolysis type, and Figure 1.6 represent the product yields (dry basis) [9, 46].

- **Fast pyrolysis:** the feedstock converts rapidly into products and the vapours are removed as fast as possible (often in less than a second) to avoid contact between vapours and char, which would produce further cracking of the vapours. The heating rates for fast pyrolysis are extremely high ( $10^2$ - $10^4$  °C/min). Fast pyrolysis requires high heating rates, and it is enhanced by the processing of small particles. The range of operating temperatures for fast pyrolysis varies across literature var. Basu [9] states a temperature range of 450-600°C, whereas the range should be around 500 °C according to Dhyani and Bhaskar [11] and FAO [1] states that the range is 450-650 °C. The target product in fast pyrolysis is pyrolysis oil, whose maximum yield of around 75 wt.% is found at a temperature around 550 °C [47-49]. The char and the gas are considered as by-products with respective yields of approximately 12 and 13 wt.%. Some of the companies using fast pyrolysis systems are BTG (The Netherlands), PyTec (Germany) and Metso (Finland) [46, 50].
- **Intermediate pyrolysis:** this type of pyrolysis includes aspects of fast and slow pyrolysis, using moderate heating rates (30-100 °C/min) and mild temperatures, whose normal range is 300-500 °C. The residence time of the vapours is 10-30 seconds. The typical products yields are 50 wt.% pyrolysis oil, 15 wt.% permanent gases and 25 wt.% char. Intermediate pyrolysis aims to produce pyrolysis oil using larger particle sizes than fast pyrolysis [22].
- **Slow pyrolysis:** slow pyrolysis has the lowest heating rates (<30°C/min) and longer solid and vapour residence time. Industrial processes such as Lurgi and Reichert have a residence time longer than 10 hours [51]. The temperature range for slow pyrolysis is not fully defined, and the values vary across the literature. Basu [9] and Apaydin-Varol et al. [52] consider that the range for slow pyrolysis is 250-400 °C although Park et al. [53] consider a broader range, 300-700 °C [4, 9, 47, 52]. The target product is char (see 1.2.1) although product yield is not very high (around 30 wt.%) and industrial processes are challenging to find in the literature [54].

Table 1.1: characteristics and product distribution from the different types of pyrolysis

|                        | Main Product | Heating Rate [°C/min] | Residence Time | Peak Temperature [°C] | Char yield [wt.%] | Pyrolysis oil yield [wt.%] | Gas yield [wt.%] |
|------------------------|--------------|-----------------------|----------------|-----------------------|-------------------|----------------------------|------------------|
| Slow Pyrolysis         | Char         | <30                   | <1 second      | 450-600               | 35                | 30                         | 35               |
| Intermediate Pyrolysis | Bio-oil      | 30-100                | 10-30 seconds  | 300-500               | 25                | 50                         | 25               |
| Fast Pyrolysis         | Bio-oil      | 102-104               | min-hours      | 250-400               | 13                | 75                         | 12               |

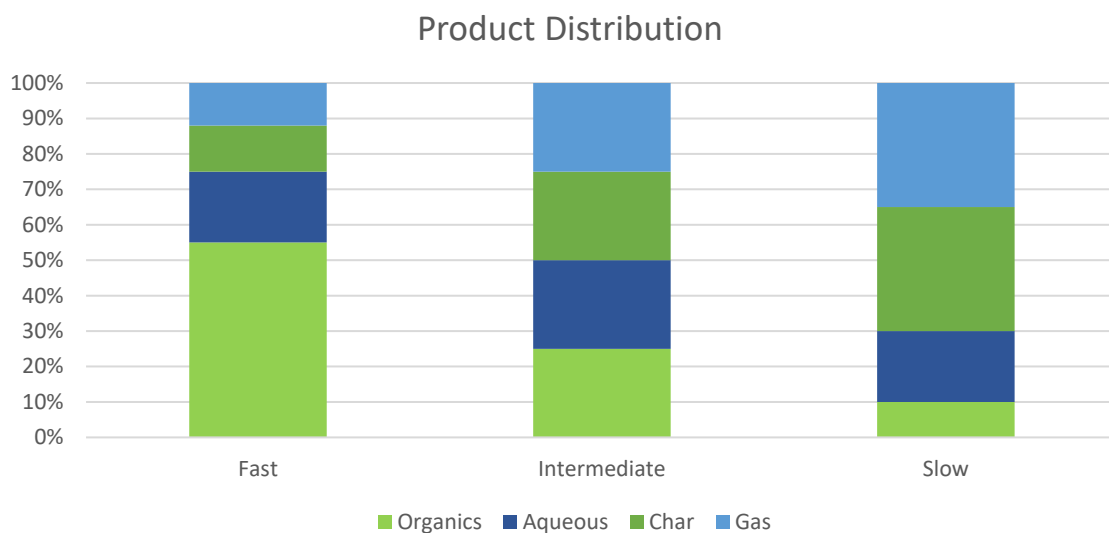


Figure 1.6: Typical product distribution from different types of pyrolysis

### 1.2.1 Slow pyrolysis

This research is part of the European project GreenCarbon (see 1.3) whose main aim is the production and upgrading of char from biomass. From the three types of pyrolysis, the only mode focusing on the production of char is slow pyrolysis and therefore is the most suitable option for this study.

According to the definition of slow pyrolysis, low temperature is an essential factor for the production of char. The use of low temperatures to degrade the feedstock can lead to confusion of slow pyrolysis with other processes such as carbonisation and torrefaction.

Torrefaction is thermochemical degradation which concentrates the energy of the feedstock through the removal of moisture and the partial degradation of hemicellulose and, to a lesser extent, cellulose. It increases the energy content of the feedstock through the removal of the light volatiles, reducing the mass of the feedstock and producing torrefied biomass. It is used as a pre-treatment step to improve the energy density of the biomass, improve the grindability and give more chemical and biological stability [55]. The limits of the temperature ranges where torrefaction occurs depend on the literature and individual research. Sadaka and Negi [56] proposes a range of 200-315 °C; Arias et al. [5] suggested the range 220-300 °C; The range addressed in Basu [9] is 200-300°C and Kolokolova et al. established a range of 200-350 °C.

The main difference between torrefaction and slow pyrolysis is found in the product yields and the characteristics of the solid products. The solid yields for torrefaction are usually very high (around 80 wt.%) when the temperature is around 225 °C (see Section C.2) compared to 30wt.% solid product yield in slow pyrolysis. In slow pyrolysis, the solid product is black, whereas, in torrefaction, the product is dark brown due to the partial instead of total degradation of the feedstock [5, 56]. The other term with which pyrolysis can be confused is carbonisation, which is the process to make carbon, in any of its forms [9, 55]. Figure 1.7 presents a scheme to explain the three terms and the possible overlap of conditions.

Slow pyrolysis is considered as a technique for carbon production, although there are some alternative methods for the production of carbon such as the other types of pyrolysis, gasification or HTC. This does not apply to torrefaction, where the solid product is torrefied biomass, different from

char and carbon. The figure aims to show that in literature, the conditions of slow pyrolysis and torrefaction overlap and it is not clear whether the process is slow pyrolysis or torrefaction until the final product is obtained and characterised. In terms of product characterisation, the torrefied product has partially degraded hemicellulose, and the light volatiles have been removed. The char from slow pyrolysis has all the volatiles removed plus further degradation of cellulose and lignin [9, 55].

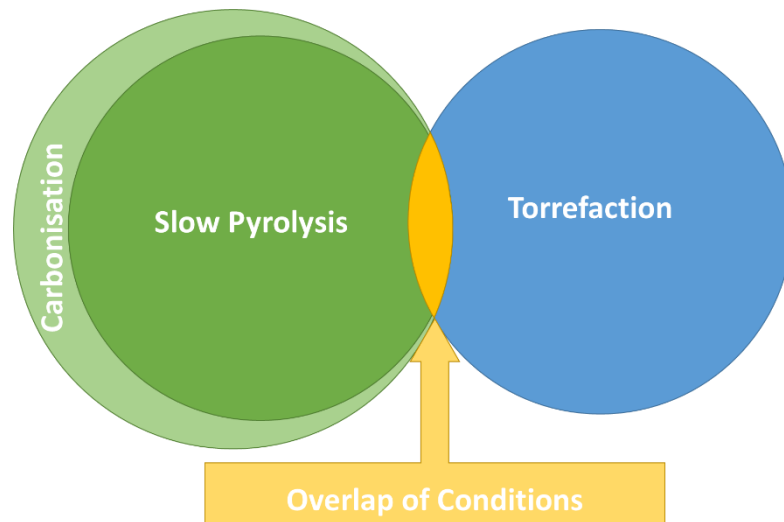


Figure 1.7: Overlap of conditions between slow pyrolysis and other thermochemical processes

### 1.2.2 Char

Char is the target product in slow pyrolysis, produced from a source of fixed carbon such as biomass. It is a porous substance, rich in carbon content (around 85 wt.%) with biological and chemical stability. In this research, the term char is used to refer to the product of slow pyrolysis. Among the literature, other terms such as biochar and charcoal are found. The difference between the terms is that biochar is produced specifically for soil amendment in agricultural and environmental applications [45]. Charcoal is mainly produced from animal or vegetal residues and is a source of heat, adsorbent material and reducing agent in metallurgical industries [1, 45, 57-61]. In the literature, both terms are found and, sometimes, they are interchangeable. Antal and Grønli [47, 51, 62] use the term charcoal, while other authors like Manyà [45, 63, 64], García-Pérez [54, 65] or the company CARBOFEX [66, 67] use the term biochar. In this study the term char includes the terms biochar and charcoal as represented in Figure 1.8.

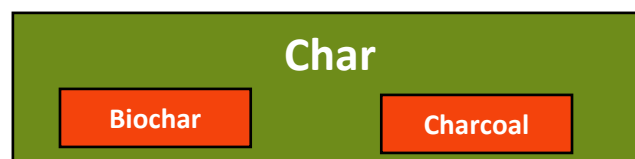


Figure 1.8: Char, biochar and charcoal

Several properties are used to define char: internal surface area, hardness, compressive strength, bulk and particle densities, pore volume distribution, calorific value, electrical resistivity or reactivity. All properties are influenced by the process parameters (temperature, residence time of solids and gases), feedstock, type of reactor, although there is an agreement that temperature is the most influential parameter [9, 47]. The target property depends on the final use; for instance, the calorific value will be significant if the char is to be used for energy production. The surface area would be more important if the final use were as an adsorbent, absorbent or for the production of activated carbon [68].

Char is an appealing product for the GreenCarbon project due to its wide range of applications [9, 47], which include:

- Energy industry for the production of electricity
- Barbeque fuel
- The production of carbon disulphide, sodium cyanide and carbide
- Used in the smelting and sintering of iron ores or the purification of nonferrous metals in the metallurgical industry
- It can be used in water and gas purification, for solvent recovery and wastewater treatment due to the high surface area
- Soil amendment and carbon sequestration
- One of the novel uses is on the medical industry for adsorption of poison
- Cosmetics, as part of scrub or toothpaste

Currently, some of the uses are as smokeless fuel and feedstock for barbeques, and the desired property is high heating value [1, 59] (generally within a range of 23-35 MJ/kg [9, 69, 70]). Raw biomass has a lower calorific value of around 20 MJ/kg [71].

Another use of carbonaceous materials is as a sorbent for organic and inorganic pollutants in soil and water. It can be used for gas separation and wastewater treatment, although it usually needs activation, to increase microporosity and surface area. An acceptable surface area for the production of activated carbon would be 500-3000 m<sup>2</sup>/g with pore volumes 0.5-1.5 cm<sup>3</sup>/g and sizes 0.3-20 nm. Some methods for carbon activation could be physical activation with steam or chemical activation with phosphoric acid [72]. Char is sometimes considered for soil amendment because some the groups containing oxygen such as carboxyl, hydroxyl or phenolic compounds could bind soil contaminants [61].

In the metallurgical industry, char is a substitute for conventional coke for metal extraction. Oxygen is combined with carbon when it is heated with metallic ores, allowing an easy extraction, but it needs compressive strength and high fracture resistance [9].

Researchers are becoming increasingly interested in using char to sequester carbon. When there are agricultural residues, the carbon is released to the atmosphere as methane or carbon dioxide, produced by natural degradation. With the production of char from this waste, a fraction of the carbon which was meant to be released to the atmosphere remains in the earth [9, 45].

### 1.2.3 Effect of parameters on pyrolysis

Pyrolysis is a very complicated process, and any small change in the process influences the performance, product distribution and product quality. Depending on the end-use of the char, it is crucial to customise the operational parameters to find the optimum product quality. For this reason, it is essential to understand the effect of pyrolysis parameters on the process. Pyrolysis parameters include the reaction temperature, pyrolysis atmosphere, feedstock, particle size, pressure, the residence time of solids and vapours or possible pre-treatment steps, among others.

- **Reaction temperature:** is the most critical process parameter because it has the most significant influence on the products. Pyrolysis oil yield is maximum within the temperature range 500-550 °C. If the reaction temperature is higher than 600 °C, most of the feedstock is converted into gas. As a general rule, the higher the temperature, the lower the char yield [45]. Figure 1.9 (adapted from [73]) shows the influence of pyrolysis temperature on the product distribution for wheat straw. The temperature also affects the char characteristics. The density and water sorption

capacity increase with temperature, as do micro-pore volume, reactivity [74, 75] and fixed carbon yield [45, 76]. Production is reduced (lower char yield) as are electrical resistivity and hydrogen and oxygen to carbon ratios [77, 78].

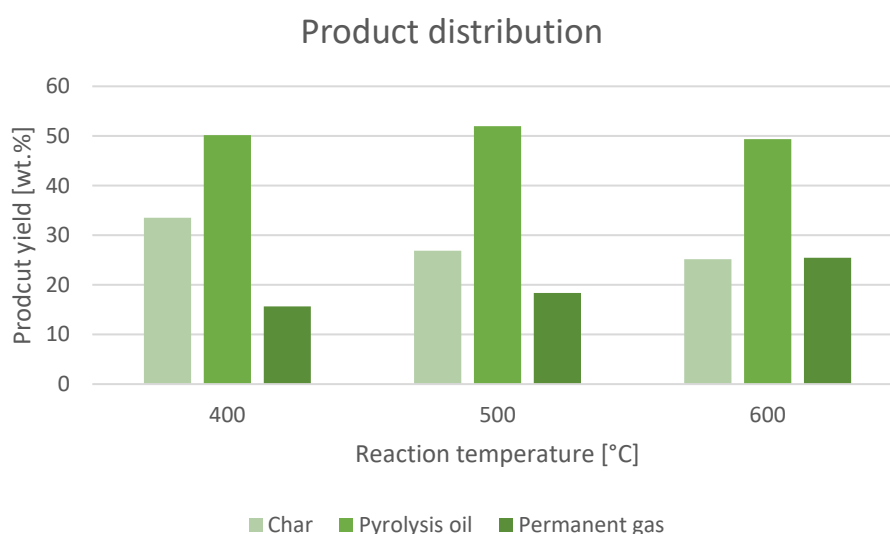


Figure 1.9: Product distribution of wheat straw pyrolysis at different temperatures (adapted from [73])

- Heating rate:** it is one of the factors which determine the type of pyrolysis. The range of heating rates is vast, it could be as low as 0.5 °C/min for slow pyrolysis up to 10,000 °C/min in fast pyrolysis, and the upper limit for slow pyrolysis is usually 30 °C/min [79]. The heating rate affects the quality of the char. A higher heating rate makes the char lighter and more friable with lower heating rates producing harder, well cured and higher carbon content chars [47, 80].
- Reaction atmosphere:** the main characteristic of the reaction atmosphere is the absence of an oxidising agent for the degradation of the feedstock. It is usually achieved with an inert nitrogen atmosphere [9]. Although different gases have been studied, such as Zhang et al. [81] who analysed different atmospheres and the influence on product distribution. The research concluded that a methane atmosphere provides higher pyrolysis oil yields, unlike carbon monoxide atmosphere, which reduces the amount of pyrolysis oil. This pyrolysis oil has an increased heating value with a carbon dioxide atmosphere. Besides this study, one of the alternatives is to use the atmosphere created by the pyrolysis vapours. In this case, the secondary cracking of the vapours is favoured, and the char yield is enhanced [2].
- Vapour residence time:** the vapour residence time is minimised in fast pyrolysis to avoid secondary cracking of the vapours that would increase the char and gas formation [9]. The method to control the residence time is the flow of inert gas. A longer vapour residence time inside the reactor would increase the char and permanent gas yields [2].
- Solid residence time:** the solid residence time mainly affects the char properties. With higher residence time, the char releases volatiles, which modifies and transforms the structure and morphology [82]. Parameters such as the rotational speed, feeding rate or the internal configuration are amended to control the solid residence time [83, 84].
- Ash content:** the term ash is very broad and mainly refers to the presence of inorganics within the biomass [9]. It is known that the presence of inorganic components such as potassium enhances the secondary cracking of the pyrolysis vapours [46] leading to lower yields of pyrolysis oils and higher yields of char and permanent gas. Ash content of 3 wt.% (dry basis) or above usually leads to phase separation of the pyrolysis oils [85].



- **Feedstock composition:** the feedstock has a significant influence on the process and the products in several ways. The content of cellulose and hemicellulose contributes to increasing the pyrolysis oil yield because they provide the volatiles released during pyrolysis. In contrast, higher lignin content enhances the production of char. The extractives and inorganic content play a key role because their presence can have a catalytic effect on secondary cracking and char-forming reactions [2, 45]. As a rough idea of the influence of the feedstock, the char from hardwood is dense and resists breakage, burning clean and slowly. The char from softwood is softer, friable and burns quickly, due to a higher amount of volatiles in the feedstock [47, 86].
- **Feedstock particle size:** as discussed in Section 4.2.3, smaller particle size is critical to enhance heat and mass transfer in pyrolysis. Small particle size promotes the production of pyrolysis oil, while the char yield and secondary cracking increase with bigger particles [46, 82].
- **Pre-treatment:** there are many different feedstock pre-treatment methods available (see Section 8.2 for further details). If the pre-treatment includes heating, it can concentrate the energy and release the light volatiles. In turn, this increases the char yield when the temperature reached in pre-treatment is higher than 200 °C with processes such as torrefaction [87]. Another option as a pre-treatment step is to wash the feedstock to partially remove the ash content, whose presence in the char reduces the heating value [47].
- **Moisture content:** this characteristic mainly affects the energy demand, but is critical for the required residence time in the reactor [83]. It can be a limiting parameter, such as in Lambiotte process where the optimum moisture content is 10 wt.% and below 20 wt.% [1]. Antal and Grønli [47] and Manyà [45] stated that wet cellulose breaks down more slowly than dry cellulose. Cetin et al. [88] concluded that the surface of the char is more similar to graphite at lower moisture content.
- **Pressure:** pressure is an interesting parameter to study due to the difficulty of increasing the pressure in a pyrolysis reactor. According to Manyà [45], char yields are minimised in a vacuum, probably due to hindering of secondary cracking of vapours because of rapid extraction of any vapour produced. With higher pressure, the time taken by the vapours to exit the solids increase, enhancing the secondary char production, increasing the char yield and its content of fixed carbon, studied in depth by Greco et al. [63]. In terms of char properties, the internal surface decreases with pressurised pyrolysis, according to Cetin et al. [88]. A possibility for this reduction in the internal surface could be the condensation of vapours on the char through secondary cracking. The secondary cracking would occur because pressure would increase the contact time between vapours and the char. The condensation of the vapours could reduce the pore size or block the pores altogether [45].

### 1.3 GreenCarbon Project

This research is part of the European project GreenCarbon. It is a Marie Skłodowska-Curie Action - Innovative Training Networks (MSCA-ITN), where a joint study between different organisations (academia and industry) is conducted. The full project title is *Advanced Carbon Materials from Biowaste: Sustainable Pathways to Drive Innovative Green Technologies*. The consortium is formed of several universities and companies, shown in Table 1.2. This consortium aims to develop new scientific knowledge, capability, technology and commercial products for carbon derived from biomass, as well as to improve the usage of carbon base materials in Europe [89].

Table 1.2: Project consortium

| Academia                               |                | Industry  |                |
|--|----------------|---|----------------|
| University of Zaragoza                 | Spain          | Fraunhofer Gesellschaft Zur Foerderung Der Angewandten Forschung E.V. | Germany        |
| University of Ghent                    | Belgium        | Deutsches Biomasseforschungszentrum Gemeinnutzige GmbH (DBFZ)         | Germany        |
| Aston University                       | United Kingdom | Viridor Waste Management Limited                                      | United Kingdom |
| Stockholm University                   | Sweden         | Biokol Sverige AB   | Sweden         |
| University of Hohenheim                | Germany        | Surface Measurements Systems Limited                                  | United Kingdom |
| University of Edinburgh                | United Kingdom | PYREG GmbH  | Germany        |
| Queen Mary University of London (QMUL) | United Kingdom | Biomass Power Projects Ltd. (BPP)                                     | United Kingdom |
|  |                | Freeland Horticulture Ltd.  | United Kingdom |

The research program covers the treatment of the feedstock, processing, post-treatment of carbons and the application and final use. To achieve this, the objectives of the research programme are [44, 90]:

- Development of customised thermochemical processes (pyrolysis and hydrothermal carbonisation) for the production of tailor-made carbons.
- Development of novel low-cost carbon materials from biomass-derived carbons.
- Usage of the novel carbon materials in heterogeneous catalysis so as for the removal of pollutants in advanced applications.
- Analysis of the use of biomass-derived carbons for solid amendment and carbon dioxide capture and sequestration.
- Study and strengthen the synergies between the production and application of carbons, to close the bioeconomy loop for the circular economy, and stimulate the links of the bioeconomy sector with industrial partners from companies working on energy, waste management, advanced material manufacturing and other areas involved.

To achieve the objectives, the project is divided into the following work packages (WPs) and tasks [44]. The sequence of the project and the interrelationships are shown in Figure 1.10.

- **Work Package 1 – Network Management**
- **Work Package 2 – Early-Stage Researcher Career Development**
- **Work Package 3 – Transfer of Technology and Knowledge**
- **Work Package 4 – Pyrolysis Routes for Dry Feedstocks**
  - Selection of dry waste biomass feedstock
  - Setting the most appropriate slow pyrolysis process conditions
  - Continuous intermediate pyrolysis
  - Fast pyrolysis and its integration with bio-oil production
  - Comprehensive pyrolysis/carbonisation model.
- **Work Package 5 – HTC Conversion Routes for Wet Feedstocks**
  - Selection of wet waste biomass feedstocks

- Setting the most appropriate HTC process conditions
- Hydrothermal carbonisation and its integration with pyrolysis.
- **Work Package 6 – Refining of BCs (biomass-derived carbons) and Advanced Applications:**
  - Development of low-cost BC-derived adsorbents for CO<sub>2</sub> capture
  - Development of low-cost BC-derived adsorbents for biogas desulphurisation
  - Development of novel metal/BC-supported catalysts for hydrogen production
  - Development of novel magnetic catalysts for 5-HMF synthesis
- **Work Package 7 – Sequential Biochar Systems:**
  - Characterisation of BCs and BC-derived materials with the view of their final land use
  - Opportunities for sequential uses of biochar

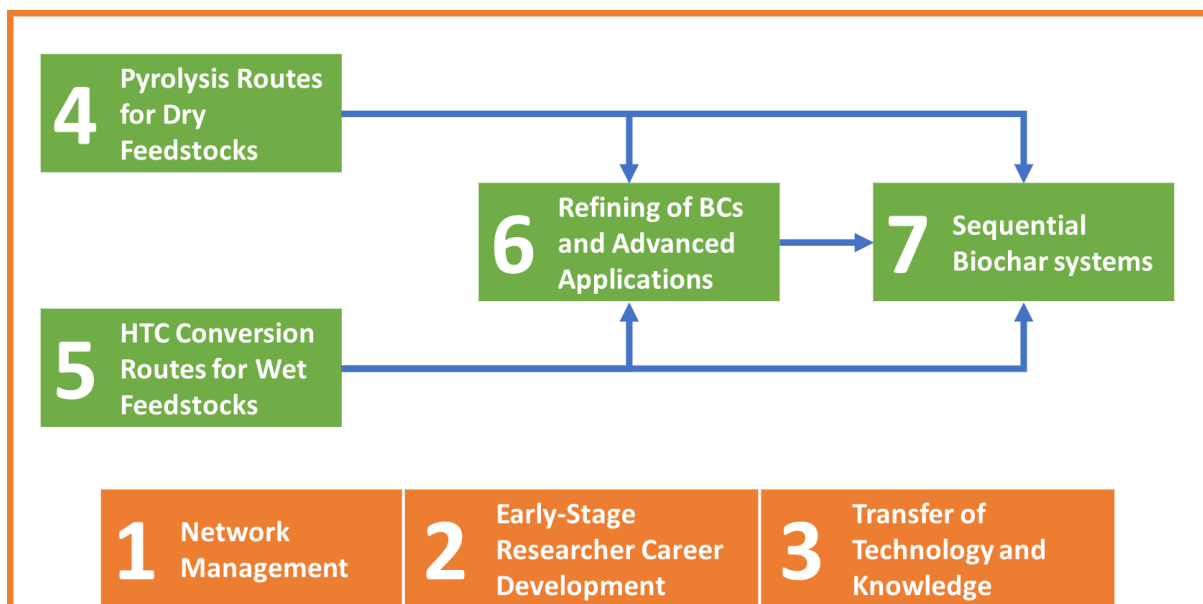


Figure 1.10: Scheme of the GreenCarbon project

### 1.3.1 WP4 - Pyrolysis Routes for dry feedstocks

This research falls under Work Package 4 (WP4), where pyrolysis is used to process biomass for the production of biomass-derived carbons. The five tasks cover topics from the selection of the process to a final model for pyrolysis based on experiments.

During the *Selection of dry waste biomass feedstock*, only waste biomass was considered. This project does not contemplate the use of purpose-grown biomass. Waste biomass is more feasible due to the lack of economic value, but it does not compete with food. Within the project, the objective is to avoid any modification in the current infrastructure and use waste biomass exclusively, which is currently landfilled or combusted. The origin of the suggested feedstocks is agricultural and dry forestry residues. The selected feedstocks were wheat straw, woodchips and RDF [44].

Typically, biomass refers to woody or grass-like material called lignocellulosic biomass, composed of cellulose, hemicellulose, lignin and extractives. Waste (MSW and RDF) is typically excluded in this definition because it is composed of materials such as paper and board, plastic, yard wastes, plastic films, textiles and food remnants [11, 91]. Nevertheless, waste is a source of fixed carbon and can be stored, transported and processed similarly to biomass. It fits with the general definition of biomass in “*non-fossilized and biodegradable organic fractions of industrial and municipal wastes*”. Furthermore, it is also a sustainable feedstock because it reduces the emissions of greenhouse gases [7]. The use of waste for pyrolysis adds value to the feedstock and gives another

valuable source of fixed carbon to transform into valuable products [9, 45]. The main challenge is the application of the biochar because it can contain a small amount of chlorine or sulphur from the waste [11, 22].

The next three tasks are: *Setting the most appropriate slow pyrolysis process conditions*; *Continuous intermediate pyrolysis* and *Fast pyrolysis and its integration with bio-oil production*, with a different scope for each. The slow pyrolysis study focused on the process under moderate pressure (1-3 MPa) to broaden the information available. The expected result is char with higher porosity, micro- and macro-porous structured material. The study on intermediate pyrolysis aimed to extend the contact between the condensable vapours and the carbon product to enhance the secondary cracking of the vapours for a well-balanced product yields. Finally, the study on fast pyrolysis aimed at a significant simultaneous production of char and bio-oil, ensuring a sufficient bio-oil quality for selected applications [44].

The last task of the WP (*Comprehensive pyrolysis/carbonisation model*) includes the development of a single-particle and reactor model for pyrolysis. This model should integrate reaction kinetics and heat and mass transfer using Eulerian-Lagrangian approach, through computational fluid dynamics (CFD) and discrete element methods (DEM), which will integrate all data from the previous tasks of the WP. The model is meant to predict the composition of the vapour phase, and properties of the carbon obtained such as elemental composition, ash and fixed-carbon contents, oxygen- and hydrogen- to-carbon ratios, porosity and particle size when the set of feedstock and process properties and parameters are given [44].

## 1.4 Thesis objectives and structure

### 1.4.1 Objectives

Despite a large amount of information about pyrolysis, the information about slow pyrolysis reactors at industrial scale is scarce [1, 51, 54, 65], and most of the knowledge for the design of reactors is found within industry with restricted access.

The main aim of this project was to study the design of a pyrolysis reactor. The study begins with a critical analysis of the different char production methods followed by the construction of a pyrolysis reactor model. After the reactor is selected and the model constructed, it will simulate the reactor with inputs provided by the user to provide all the mechanical specifications explained below. The model scheme is shown in Figure 1.11. The resulting research can be used by any stakeholder interested in the production of char to help to understand the aspects that should be considered in reactor design. It provides accurate specifications about the size of the reactor and the energy requirement, as well as parameters such as temperature or conversion profile. The creation of the model is thoroughly explained in this thesis.

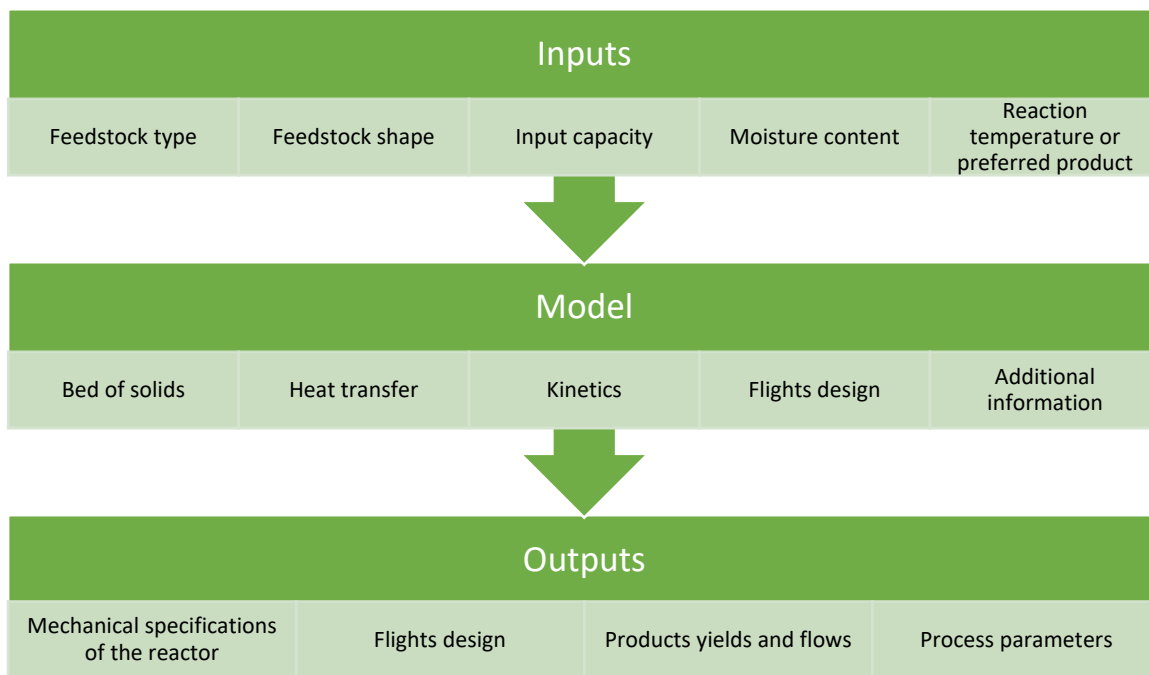


Figure 1.11: Scheme of the model

The inputs of the model are:

- **Type of feedstock:** there is a choice between the three types of raw material from the GreenCarbon project. As mentioned in Section 1.3.1, the feedstock for which the reactor is designed is one of the following: Refused Derived Fuel (RDF), woodchips and wheat straw.
- **Feedstock shape:** the shape of the feedstock is included in the model to define the particle size. The two given options are pellets and chips, accordingly to the feedstocks provided in GreenCarbon.
- **Input capacity:** the amount of raw material per hour is a crucial parameter to design the reactor and its size. The input is quantified in dry tonnes per hour.
- **Moisture content:** the moisture content of the raw material is vital from an energy point of view, it provides a crucial piece of information to estimate the energy demand of the system. The input should be introduced as a weight percentage (wt.%).
- **Targeted product/temperature:** the reaction temperature is crucial for the estimation of the amount of heat needed and the estimation of the product distribution and flows. The target product should be introduced in °C. In case there is a preferred product, the model will have correlations to calculate the optimum temperature for maximum production of that specific product (char, pyrolysis oil or gas).

The inputs are processed, and the model is integrated to provide the user with a solution for biomass pyrolysis. The bed of solids, heat transfer and kinetics are extensively described in separate chapters. The additional design features describe other aspects, such as the sealing of the reactor or other aspects that influence the design of the reactor. Once this data is processed through the model, it provides different outputs which are classified as follows:

- **Mechanical specifications of the reactor:** The results in this category contain the length, diameter of the inner reactor and the angle it is tilted. The construction materials and the sealing, feeding and collection methods are reviewed within this work.

- **Flights design:** the use of flights is very common to enhance heat transfer. The study of the influence is described, and the best solution is implemented. The flights' description and the number of flights in the reactor are provided.
- **Products yields and flows:** the products are the main output of the real reactor. The yield on a dry basis and mass flow on a wet basis for each product are calculated.
- **Process parameters:** this last category includes all parameters related to the characterisation of the process. The residence time of the solids and the vapours, and the rotational speed is presented. The initial and final temperature of the combustion gases, which acts as the heat source, is presented together with flowrate. The profile temperature of combustion gases, gases inside the reactor and solids is calculated. The voidage of the bed of solids is indicated. There is an estimation of heat provided by the wall compared to the combustion of the permanent gases. This aims to demonstrate the amount of heat needed to heat the reactor compared to the heat that can be obtained from the combustion of the permanent gases. There are checks to measure the consistency of the simulations to see how robust the model is for that set of conditions.

Other studies for the development of a pyrolysis reactor have been completed [92-97]. In most, a model was created for a specific reactor which had been built or for a specific set of inputs. This project is more complicated than previous works in the literature. The model can design a reactor automatically, once the inputs are given, providing additional user flexibility not observed in previous models. The methodology provides an innovative solution to the modelling of a slow pyrolysis reactor under a broader set of conditions.

#### 1.4.2 Structure

As a computer-based model, there are several integrated submodels. All the submodels are connected as represented in Figure 1.12. Each of the three main submodels (bed of solids, heat transfer and kinetics) is described in an individual chapter. There are other chapters which explain how they are integrated, the performance of the model and provide additional design information.

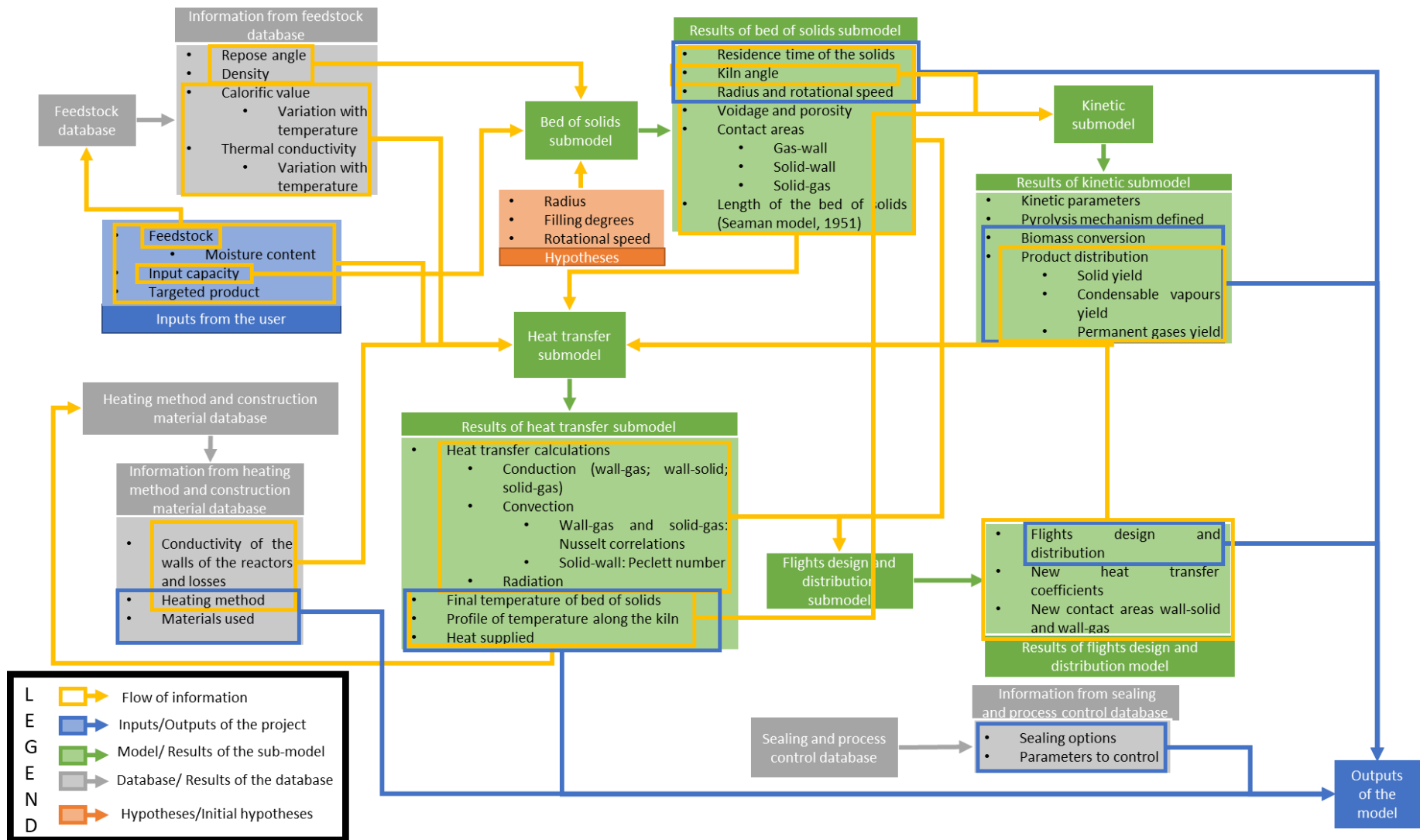


Figure 1.12: Scheme of the research project

The first step for the design of a pyrolysis reactor is to select a reactor type. With that purpose, the first chapter of the research is Chapter 2. Within this chapter, the main slow pyrolysis reactors are described and critically analysed. A classification based on different criteria is used to choose the most promising reactor for slow pyrolysis, which will be used in this study.

Chapter 3 details the behaviour of biomass solids and the different options for motion. The influence of different parameters on the length of the bed of solids is studied and the feedstock residence time calculated. There is a detailed explanation of calculations used to calculate reactor area consisting of the area of the wall, of the gas and the bed of solids as well as the contact areas between the wall and the bed of solids, the wall and the gas, and the gas and bed of solids.

The heat transfer model is described in Chapter 4. Three heat transfer methods take place within the reactor. Each method had to be carefully studied because the geometry is very complex, and parameters to calculate the conductive, convective and radiative heat flows have to be analysed in detail to find the best calculation route.

A key part of any reactor design is the reaction rate and its dependency on temperature. The study to calculate the conversion of the biomass is explained in Chapter 5. The three main parameters for each reaction step are the pre-exponential factor, the activation energy and the reaction order. The possibility of a multi-step reaction is discussed, plus the reason to have more than a one-step reaction (if applicable) and the parameters for each step. These parameters were calculated through thermogravimetric analysis (TGA), which was used to estimate the char yield. Results from other Green Carbon researchers (ESR2- Filipe Rego) are included in this model to estimate the yield of pyrolysis oil and permanent gases accurately.

Chapter 6 contains all the additional information of the reactor which has not been previously described. The feedstocks employed are described and the repose angle characteristic calculated. Furthermore, the design of the flights is analysed here, and the final implementation thoroughly explained through sensitivity analysis to find the most critical parameters on the design of the flights. The integration of the model is extensively described in Chapter 7. This chapter broadly describes how each calculation step was performed and the reason behind every decision. The final section of this chapter describes how to calculate model reliability and robustness, and how it could be adapted to other technologies such as drying or torrefaction.

During this research, a significant amount of time was spent in industry. The knowledge acquired is described in Chapter 8. This chapter contains valuable information transferred from industry to academia. Combining the knowledge of industry and literature, several options for feedstock pre-treatment and post-treatment of any of the products are described.

The output of this research is the model itself. To test the model, several sets of conditions are performed and tested. The results of the tests are shown in Chapter 9. These results help to detect potential improvements and boundary conditions. The results are discussed and analysed in detail.

Finally, Chapter 10 addresses the main conclusions of this research and highlights all the knowledge transferred from industry to academia.

The model is not perfect, and it has some parts which could be improved. Chapter 11 addresses the main points where this model could be developed further, related to the assumptions taken along the project and explained when taken. Lastly, it addresses the main parts that should be considered before a full scale-up.



Some aspects and options which are overlooked continuously in the design of reactors are described in Appendix B. These aspects include the sealing, bearings and drive. All the industrial visits addressed are described in detail in Appendix C.

## 1.5 References

1. *Industrial charcoal production, TCP/CRO/3101 (A) development of a sustainable charcoal industry*. 2008, Food and Agriculture Organization of the United Nations (FAO): Zagreb, Croatia.
2. Kan, T., V. Strezov, and T.J. Evans, *Lignocellulosic biomass pyrolysis: A review of product properties and effects of pyrolysis parameters*. *Renewable and Sustainable Energy Reviews*, 2016. **57**: p. 1126-1140.
3. Li, A.M., et al., *Experimental studies on municipal solid waste pyrolysis in a laboratory-scale rotary kiln*. *Energy*, 1999. **24**(3): p. 209-218.
4. Chen, D., et al., *Pyrolysis technologies for municipal solid waste: a review*. *Waste Manag*, 2014. **34**(12): p. 2466-86.
5. Arias, B., et al., *Influence of torrefaction on the grindability and reactivity of woody biomass*. *Fuel Processing Technology*, 2008. **89**(2): p. 169-175.
6. Niu, Y., et al., *Biomass torrefaction: properties, applications, challenges, and economy*. *Renewable and Sustainable Energy Reviews*, 2019. **115**: p. 109395.
7. UNFCCC, *Clarifications of definition of biomass and consideration of changes in carbon pools due to a CDM project activity, EB-20*. 2005.
8. Mohd Rashid, S.R., et al., *Modelling Anhydrous Weight Loss of Torrefied Wood Sawdust*. *Energy Procedia*, 2017. **138**: p. 319-324.
9. Basu, P., *Biomass gasification, pyrolysis, and torrefaction: practical design and theory*. 2013: London, UK : Elsevier : Academic Press, 2013. Second edition.
10. Chong, K.J., *A methodology for the generation and evaluation of biorefinery process chains, in order to identify the most promising biorefineries for the EU*, in *European Bioenergy Research Institute (EBRI). Chemical Engineering & Applied Chemistry (CEAC). School of Engineering and Applied Science (EAS)*. 2011, Aston University: Birmingham.
11. Dhyani, V. and T. Bhaskar, *A comprehensive review on the pyrolysis of lignocellulosic biomass*. *Renewable Energy*, 2017.
12. Naik, S.N., et al., *Production of first and second generation biofuels: A comprehensive review*. *Renewable and Sustainable Energy Reviews*, 2010. **14**(2): p. 578-597.
13. Manyà, J.J., et al., *Pyrolysis and char reactivity of a poor-quality refuse-derived fuel (RDF) from municipal solid waste*. *Fuel Processing Technology*, 2015. **140**(Supplement C): p. 276-284.
14. He, M., et al., *Syngas production from pyrolysis of municipal solid waste (MSW) with dolomite as downstream catalysts*. *Journal of Analytical and Applied Pyrolysis*, 2010. **87**(2): p. 181-187.
15. Reddy, P.J., *Energy Recovery from Municipal Solid Waste by Thermal Conversion Technologies*. 2016: CRC Press. 238.
16. Hornung, A., *Processing Municipal Solid Waste (MSW) and biomass/residual streams using Thermo Catalytic Reforming (TCR) technology*, S. Technologies, Editor. 2016, Fraunhofer Institute for Environmental, Safety and Energy Technology UMSICHT.
17. Sfakiotakis, S. and D. Vamvuka, *Study of co-pyrolysis of olive kernel with waste biomass using TGA/DTG/MS*. *Thermochimica Acta*, 2018. **670**: p. 44-54.
18. Bridgwater, A.V., *Aspects to consider in the design of a rotary kiln*, J. López-Ordovás, Editor. 2019, Aston University: Energy and Bioproducts Research Institute (EBRI).
19. Rego, F., et al., *Fast determination of lignocellulosic composition of poplar biomass by thermogravimetry*. *Biomass and Bioenergy*, 2019. **122**: p. 375-380.
20. Yliniemi, J., *Lignocellulosic raw materials I*, in *477103A: Bioproduct Technology*. 2014, Fibre and Particle Engineering Laboratory: Oulun Yliopisto.

21. Dimzon, I.K.D., J. Ebert, and T.P. Knepper, *The interaction of chitosan and olive oil: Effects of degree of deacetylation and degree of polymerization*. Carbohydrate Polymers, 2013. **92**(1): p. 564-570.
22. Yang, Y., *Energy Production from Biomass and Waste Derived Intermediate Pyrolysis Oils*, in *European Bioenergy Research Institute (EBRI)*. 2014, Aston University: Birmingham. p. 185.
23. Kirkbride-McElroy, A. *Adding Value to Wheat Straw*. [cited 2018 9th March 2018]; Available from: <http://biomassmagazine.com/articles/1367/adding-value-to-wheat-straw>.
24. Klee G., G., *The wheat straw as an important component of the servings for steers*, in *IPA Quilamapu*. 1983, INIA.
25. Gerssen-Gondelach, S.J., et al., *Competing uses of biomass: Assessment and comparison of the performance of bio-based heat, power, fuels and materials*. Renewable and Sustainable Energy Reviews, 2014. **40**: p. 964-998.
26. Liu, B. and Z. Zhang, *Catalytic Conversion of Biomass into Chemicals and Fuels over Magnetic Catalysts*. ACS Catalysis, 2016. **6**(1): p. 326-338.
27. Thornley, P., *Closing Remarks*, in *Integration of Chemical, Biochemical and Thermal Processes*, S.B.H.A.D. Network, Editor. 2018: Priory Rooms, Birmingham.
28. IUPAC, *Compendium of Chemical Terminology*. 2nd ed. 1997, Oxford: Blackwell Scientific Publications.
29. Volpe, R., et al., *Assessment of olive wastes as energy source: pyrolysis, torrefaction and the key role of H loss in thermal breakdown*. Energy, 2015. **82**: p. 119-127.
30. Remón, J., et al., *Production of bio-fuels and chemicals by microwave-assisted, catalytic, hydrothermal liquefaction (MAC-HTL) of a mixture of pine and spruce biomass*. Green Chemistry, 2019. **21**(2): p. 284-299.
31. Van Loo, S. and J. Koppejan, *The handbook of biomass combustion and co-firing*. 2007: London ; Sterling, VA : Earthscan, 2007.
32. Quaak, P., H. Knoef, and H.E. Stassen, *Energy from biomass : a review of combustion and gasification technologies*. Energy series. 1999: World Bank.
33. Nunes, L.J.R., J.C.O. Matias, and J.P.S. Catalão, *Biomass combustion systems: A review on the physical and chemical properties of the ashes*. Renewable and Sustainable Energy Reviews, 2016. **53**: p. 235-242.
34. Volpe, R., et al., *Evolution of chars during slow pyrolysis of citrus waste*. Fuel Processing Technology, 2017. **158**: p. 255-263.
35. Volpe, R., *Pyrolysis and gasification studies of biomass thermal decomposition*, in *GreenCarbon Research School 3*. 2017: Queen Mary University of London.
36. Roy, P. and G. Dias, *Prospects for pyrolysis technologies in the bioenergy sector: A review*. Renewable and Sustainable Energy Reviews, 2017. **77**: p. 59-69.
37. Day, C., *Basic project configuration for pyrolysis to syngas at 700 degrees in a rotary retort*, in *Research interests - the full scale projects issues - keyword summary*, B.P.P. Ltd, Editor. 2017, Aston University: Aston University.
38. Lehto, J., et al., *Review of fuel oil quality and combustion of fast pyrolysis bio-oils from lignocellulosic biomass*. Applied Energy, 2014. **116**: p. 178-190.
39. ASTM, *Standard Specification for Pyrolysis Liquid Biofuel*, in *D7544-12*. 2017, ASTM International: West Conshohocken, PA.
40. Yorgun, S., S. Şensöz, and Ö.M. Koçkar, *Characterization of the pyrolysis oil produced in the slow pyrolysis of sunflower-extracted bagasse*. Biomass and Bioenergy, 2001. **20**(2): p. 141-148.
41. Laird, D.A., et al., *Review of the pyrolysis platform for coproducing bio-oil and biochar*. Biofuels, Bioproducts and Biorefining, 2009. **3**(5): p. 547-562.
42. Acikgoz, C. and O.M. Kockar, *Characterization of slow pyrolysis oil obtained from linseed (*Linum usitatissimum L.*)*. Journal of Analytical and Applied Pyrolysis, 2009. **85**(1): p. 151-154.
43. Sokoto, M.A., et al., *Slow pyrolysis of Defatted Seeds Cakes of African star apple and silk cotton for production of bio-oil*. Renewable Energy, 2020. **146**: p. 1710-1716.

44. GreenCarbon-ETN. *Advanced Carbon Materials from Biowaste: Sustainable Pathways to Drive Innovative Green Technologies*. 2017 2nd November 2018 9th April 2017]; Available from: <http://greencarbon-etn.eu/>.
45. Manyà, J.J., *Pyrolysis for Biochar Purposes: A Review to Establish Current Knowledge Gaps and Research Needs*. *Environmental Science & Technology*, 2012. **46**(15): p. 7939-7954.
46. Bridgwater, A.V., *Review of fast pyrolysis of biomass and product upgrading*. *Biomass and Bioenergy*, 2012. **38**(Supplement C): p. 68-94.
47. Antal, M.J. and M. Grønli, *The Art, Science, and Technology of Charcoal Production*. *Industrial & Engineering Chemistry Research*, 2003. **42**(8): p. 1619-1640.
48. Bridgwater, A.V., *Fast pyrolysis of biomass : a handbook*. 1999: Newbury : CPL Press, ©1999.
49. Bridgwater, T. and S. A. Bridge, *A Review of Biomass Pyrolysis and Pyrolysis Technologies*, in *Biomass Pyrolysis Liquids Upgrading and Utilization*, Springer, Editor. 1991, Springer: New York. p. 11-92.
50. Chong, K., *Fast Pyrolysis of Biomass*, in *GreenCarbon Research School*, GreenCarbon, Editor. 2017, European Bioenergy Research Institute (EBRI), Aston University: University of Ghent.
51. Grønli, M., et al., *The Science and Technology of Charcoal Production*. 2005, PyNe Subject Group.
52. Apaydin-Varol, E., E. Pütün, and A.E. Pütün, *Slow pyrolysis of pistachio shell*. *Fuel*, 2007. **86**(12-13): p. 1892-1899.
53. Park, J., et al., *Slow pyrolysis of rice straw: analysis of products properties, carbon and energy yields*. *Bioresour Technol*, 2014. **155**: p. 63-70.
54. Garcia-Nunez, J.A., et al., *Historical Developments of Pyrolysis Reactors: A Review*. *Energy & Fuels*, 2017. **31**(6): p. 5751-5775.
55. Kolokolova, O., et al. *Torrefaction and Pyrolysis of biomass waste in continuous reactors*. in *13th International Conference on Environmental Science and Technology*. 2013. Athens: Global Nest, Secretariat.
56. Sadaka, S. and S. Negi, *Improvements of Biomass Physical and Thermochemical Characteristics via Torrefaction Process*. Vol. 28. 2009. 427-434.
57. Lehmann, J. and S. Joseph, *Biochar for environmental management : science and technology*. 2009, London; Sterling, VA: Earthscan.
58. *The charcoal transition: greening the charcoal value chain to mitigate climate change and improve local livelihoods*, in *The Charcoal Transition*, J. Van Dam, Editor. 2017, Food and Agriculture Organization of the United Nations (FAO): Rome.
59. *Industrial Charcoal Making*. FAO Forestry Paper: No. 63. 1985, Rome Bernan Press(PA) 1985.: Food and Agriculture Organization of the United Nations (FAO).
60. Antal, M.J., et al., *High-Yield Biomass Charcoal*. *Energy & Fuels*, 1996. **10**(3): p. 652-658.
61. Ahmad, M., et al., *Biochar as a sorbent for contaminant management in soil and water: a review*. *Chemosphere*, 2014. **99**: p. 19-33.
62. Antal, M.J., et al., *Attainment of the Theoretical Yield of Carbon from Biomass*. *Industrial & Engineering Chemistry Research*, 2000. **39**(11): p. 4024-4031.
63. Greco, G., et al., *Evolution of the mass-loss rate during atmospheric and pressurized slow pyrolysis of wheat straw in a bench-scale reactor*. *Journal of Analytical and Applied Pyrolysis*, 2018. **136**: p. 18-26.
64. Di Stasi, C., et al., *Physically activated wheat straw-derived biochar for biomass pyrolysis vapors upgrading with high resistance against coke deactivation*. *Fuel*, 2019. **255**: p. 115807.
65. Garcia-Perez, M., T. Lewis, and C.E. Kruger, *Methods for Producing Biochar and Advanced Biofuels in Washington State Part 1: Literature Review of Pyrolysis Reactors*, in *Ecology Publication*. 2011, Washington State University: Pullman, WA. p. 137 pp.
66. OY, C., *CARBOFEX OY- Sustainable Industrial Production of Biochar*, in *WASTE TO VALUABLES*, C. OY, Editor. 2017, CARBOFEX OY: Hiedranranta, Tampere, Finland.

67. Tukiainen, S., *Method for producing carbon briquettes from organic matter*, in ESPACENET, P. OY, Editor. 2011: Finland.
68. Lohri, C.R., et al., *Char fuel production in developing countries – A review of urban biowaste carbonization*. Renewable and Sustainable Energy Reviews, 2016. **59**: p. 1514-1530.
69. Diebold, J. and T. Bridgwater, *Overview of Fast Pyrolysis of Biomass for the Production of Liquid Fuels*. 1997. 5-23.
70. Waqas, M., et al., *Development of biochar as fuel and catalyst in energy recovery technologies*. Journal of Cleaner Production, 2018. **188**: p. 477-488.
71. Olszewski, M., et al., *Techno-Economics of Biocarbon Production Processes under Norwegian Conditions*. Energy & Fuels, 2017. **31**(12): p. 14338-14356.
72. Hedin, N., *Activated Carbons*, in *GreenCarbon Research School 2*. 2017: Universitet Stockholm.
73. Rego, F., *Intermediate pyrolysis of biomass in a pilot scale continuous screw reactor*, in *EBRI (Energy and Bioproducts Research Institute)*. Forthcoming, Aston University: Aston University.
74. Baldock, J.A. and R.J. Smernik, *Chemical composition and bioavailability of thermally altered Pinus resinosa (Red pine) wood*. Organic Geochemistry, 2002. **33**(9): p. 1093-1109.
75. Nguyen, B.T., et al., *Temperature Sensitivity of Black Carbon Decomposition and Oxidation*. Environmental Science & Technology, 2010. **44**(9): p. 3324-3331.
76. Ronsse, F., et al., *Production and characterization of slow pyrolysis biochar: Influence of feedstock type and pyrolysis conditions*. Vol. 5. 2013. 104-115.
77. Bhatia, S.K., R.K. Bhatia, and Y.-H. Yang, *An overview of microdiesel — A sustainable future source of renewable energy*. Renewable and Sustainable Energy Reviews, 2017. **79**(Supplement C): p. 1078-1090.
78. Foley, G., *Charcoal making in developing countries*. 1986: Earthscan, International Institute for Environment and Development.
79. Manyà, J.J., *Pressurized slow pyrolysis to improve the carbonization efficiency*, G. project, Editor. 2017: Ghent.
80. Violette, M., *Memoire sur les Charbons de Bois*. Annales de chimie et de physique. 1853.
81. Zhang, H., et al., *Biomass fast pyrolysis in a fluidized bed reactor under N<sub>2</sub>, CO<sub>2</sub>, CO, CH<sub>4</sub> and H<sub>2</sub> atmospheres*. Bioresource Technology, 2011. **102**(5): p. 4258-4264.
82. Newalkar, G., et al., *Effect of Temperature, Pressure, and Residence Time on Pyrolysis of Pine in an Entrained Flow Reactor*. Energy & Fuels, 2014. **28**(8): p. 5144-5157.
83. Stein, P., *Rotary kiln design methodology*, J. López-Ordovás, Editor. 2019: EBRI, Aston University, Birmingham, United Kingdom.
84. Day, C., *Description of an industrial rotary kiln*, J. López-Ordovás, Editor. 2019: EBRI, Aston University.
85. Lin, X., et al., *Effects of alkali and alkaline earth metals on the co-pyrolysis of cellulose and high density polyethylene using TGA and Py-GC/MS*. Fuel Processing Technology, 2019. **191**: p. 71-78.
86. Wenzl, H.F.J., *V - Further Destructive Processing of Wood*, in *The Chemical Technology of Wood*. 1970, Academic Press. p. 253-300.
87. López-Ordovás, J., et al., *Integrated rotary kiln pilot-scale plant for beechwood torrefaction*. Forthcoming.
88. Cetin, E., et al., *Influence of pyrolysis conditions on the structure and gasification reactivity of biomass chars*. Fuel, 2004. **83**(16): p. 2139-2150.
89. *Description of GreenCarbon project in CORDIS*. 2020 17th February 2020 [cited 2020 7th April 2020]; Available from: <https://cordis.europa.eu/project/id/721991>.
90. Manyà, J.J., *Advanced Carbon Materials from Biomass: an Overview*. 2019: Zenodo.
91. Haykiri-Acma, H., G. Kurt, and S. Yaman, *Properties of Biochars Obtained from RDF by Carbonization: Influences of Devolatilization Severity*. Waste and Biomass Valorization, 2017. **8**(3): p. 539-547.

92. Babler, M.U., et al., *Modelling and pilot plant runs of slow biomass pyrolysis in a rotary kiln*. Applied Energy, 2017. **207**: p. 123-133.
93. Phounglamcheik, A., *Modeling of a Rotary Drum Pyrolyzer*. 2015. p. 82.
94. Aguiar, B., et al., *THE MODELLING AND DYNAMIC SIMULATION OF A LIME KILN*, in *17 International Chemical Recovery Conference - ICRC 2017, 2017, Halifax (NS)*. 2017: Halifax, Canada.
95. Codignole Luz, F., et al., *Pyrolysis in screw reactors: a 1-D numerical tool*, in *72nd Conference of the Italian Thermal Machines Engineering Association*,. 2017, Energy Procedia: Lecce Italy. p. 683-689.
96. Martins, M., L. Oliveira, and A. Franca, *Modeling and simulation of limestone calcination in rotary kilns - Part 2: Industrial rotary kiln*. ZKG International, 2002. **55**: p. 74-83.
97. Martins, M., L. Oliveira, and A. Franca, *Modelling and simulation of limestone calcination in rotary kilns, Part 1: Pilot kiln*. Vol. 55. 2002. 76-87.

## 2 Reactor selection

The main objective of this research is the creation of a model which calculates the main specifications of a slow pyrolysis reactor based on user inputs. Each reactor is designed differently based on the characteristics and the target product. To describe the different industrial processes, it is necessary to classify the current technologies. Some articles [1, 2] divide the slow pyrolysis processes based on the heating method: internal, external and with recirculated gases. However, other articles classify the process based on the operation mode [3-6] whose main types are batch, semi-continuous and continuous processes.

Despite different modes of operation (batch, semi-continuous and continuous), the solid material always follows the same steps (see Figure 2.1), which means that the raw material and solid product undergo the same thermal stress independently of the reactor type. The first step is **feeding** the biomass, which removes the air before entering the reactor. The **drying** step usually takes place within the reactor, if no pre-drying is required or there is any moisture content left. The feedstock then undergoes the **pyrolysis** step where it is transformed into the products. The products are **cooled** and then **collected** at the end of the process [4, 7]. More pre- and post-treatment options are addressed in Chapter 8.



Figure 2.1: Feedstock steps

Consequently, the very first step in this research project is to determine which pyrolysis reactor to use. Therefore, it is necessary to review and analyse the current options for char production used within industry, establish the decision criterion and determine which technology is the most promising option.

### 2.1 Pyrolysis reactors in the industry

Char is one of the most ancient fuels and was mainly used for heating and metal extraction before coal became popular [7]. Since then, the processes to produce char have been improved although there is no preferred reactor across the literature. The criteria to classify the slow pyrolysis reactors vary depending on the influence or weight of each feature [6]. Reactors to produce char are classified in the current study by the operation mode as continuous, batch and semi-continuous based on the biomass feed procedure. For continuous operation, the feedstock is introduced to the reactor continuously. For batch processes a batch of raw material is fed to the reactor, the temperature is raised and, after the reaction and cooling time, the product is collected. Semi-continuous processes refer to those working continuously, where there are no waiting times, but the feeding occurs in batches. It can be argued whether some processes are continuous or semi-continuous. Semi-continuous processes refer to those that use exact volumetric amounts of feedstock separately (reactors, wagons) and each batch is processed separately to the others.

#### 2.1.1 Batch processes

Batch processes are the most straightforward technology and have been used for centuries to produce char. Some authors [8, 9] consider that the term slow pyrolysis can refer to this type of process exclusively and the semi- and continuous processes would not be included in the slow pyrolysis technologies.

The biomass is loaded into the reactor, which is usually a rectangular concrete kiln, like the Missouri kiln from Figure 2.2 or simply a traditional mound kiln with the biomass stack covered with earth. The feedstock is partially burned to increase the temperature through internal heating. The time required to complete the process and collect the products is very long, and it can take up to 25 days of operation, with a char yield within a range 5-20 wt.%. The cooling of the system is a problem for shorter operational times because the product cannot be removed before the product cool down, and a new batch of biomass cannot be added.

In the design of the kiln, they require an opening to load the feedstock and discharge the product. There are chimneys to remove the pyrolysis vapours if desired which are sealed during cooling to avoid air entering the reactor and producing ignition of the char. Part of the feedstock is burnt off, but the heat from pyrolysis is not recovered, which makes this type of process very inefficient. Operation of these systems usually requires considerable manual operation.

Other types of batch processes are the Brazilian or Argentinian kiln [10]. These kilns are not limited in volume although an average size range of the kilns would be 4-350 m<sup>3</sup>. The optimum size for the production of char is 180 m<sup>3</sup> because it is a good compromise between the production of char and the homogeneity of the product. Despite their inefficiency, the system can cope with a wide range of feedstocks plus having very low investment and operational costs [1, 2, 4, 6].

Although it is the oldest known technology for char production, with low efficiency, this type of batch kilns are still commercially available due to their ease of operation and low cost. Batch kilns are considered as the most promising solution for pyrolysis in developing countries due to simplicity and low investment [6]. Its use is not restricted only to developing countries, but some industrialised countries such as the United States still commercialise this technology. For instance, Horner Charcoal Company in Taneyville (USA) uses a set of Missouri kilns [4]. Another example of the use of this technology is the company Biocarbo Ind. Com. Ltd. in the Brazilian state of Minas Gerais [3]. The estimated lifetime of this technology is approximately five years [9].

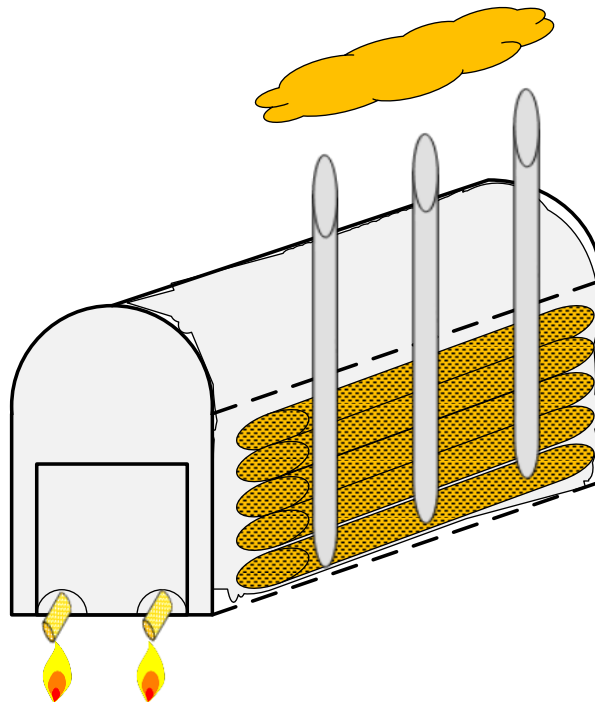


Figure 2.2: Missouri kiln

### 2.1.2 Semi-continuous processes

Due to the nature of pyrolysis and its interaction with biomass during the process, it is very challenging to produce char continuously. One of the alternatives is the use of semi-continuous processes, characterised by the feed of the raw material and discharge at the end of the process in batches. At the same time, the reactor keeps operating at the target temperature. Compared to the batch processes, this operating procedure allows the processes to have higher capacities of char production, with a range of 900-6,000 annual tonnes. Similar to the batch processes, the processes offer excellent feedstock flexibility, and the char yields are enhanced (20-30 wt.%) because feedstock is not partially burnt off. The processes described below allow partial recovery of the energy used to provide part of the energy required for the process. This is achieved through the collection and combustion of the pyrolysis vapours in the corresponding chamber. The main drawbacks are the long processing times (25-35 hours) per batch and the manual loading of the feedstock [2].

#### 2.1.2.1 Tunnel retort

In the tunnel retort (Figure 2.3), the feedstock is loaded into several wagons that travel through several sealed chambers. Each wagon carries 5-12 m<sup>3</sup> of feedstock. The first chamber is used to dry the biomass, where the moisture content of the feedstock is reduced before moving ahead towards the carbonisation chamber where the feedstock is transformed into char through pyrolysis. The final chamber, before the collection of the product, is the cooling chamber. The whole reactor with the drying and pyrolysis chambers has a length of 8-9 m and a diameter of approximately 2.5 m. The cooling tunnel has a length of 17 m and has up to four wagons to conduct gradual cooling along because cooling is the slowest process. The cooling chamber is longer because cooling is slower than the other processes. The cycle of each wagon varies from 25 to 35 hours [3].

The walls of the chambers are made of perforated steel, which allows the collection of the vapours produced in the process to move them to a combustion chamber. This combustion chamber burns the gases from the process and divides the products in three flows, two of which are used in pyrolysis while the last one is used to provide energy to the drying chamber. After the whole process, the char is collected and the wagons reused with fresh feedstock for the process [4].

This technology is used in plants in Milazzo and Mortera in Italy, each of which produces 6,000 tonnes per year of char [4]. The highest char yield obtained with this technology was 36 wt.% although the average is 20-30 wt.% [5]. This process is auto-sufficient from an energetic point of view and can cope with moisture contents up to 50 wt.% [2]. This technology has the disadvantage of needing manual loading and discharge of the wagons, which translates in higher operating costs compared to other technologies such as twin retort (2.1.2.3), besides the long cycle of each wagon. This process is commercialized by Impiant Trattamento Biomasse with plants in Milazzo and Mortera (Italy), Belišće (Hungary) and Alterna Biocarbon in Prince George (Canada) [2-4].



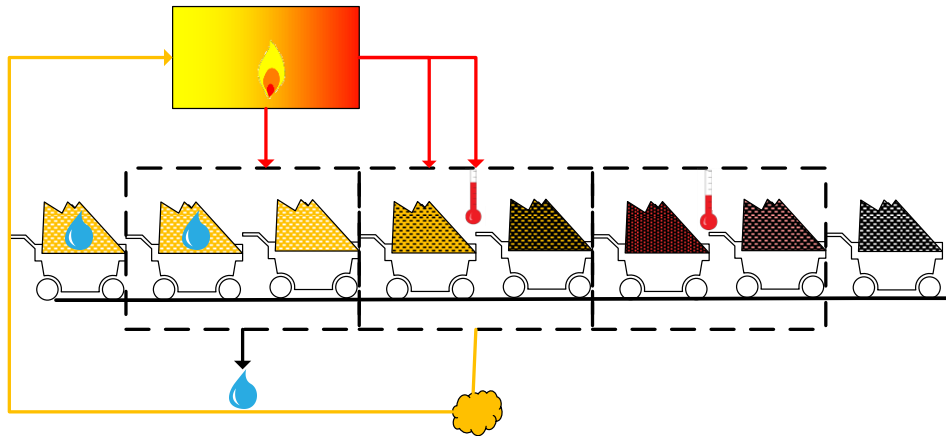


Figure 2.3: Tunnel retort

### 2.1.2.2 Shelf reactor

The shelf reactor uses the same principle as the Tunnel retort (2.1.2.1) but uses shelves instead of wagons. The system has three chambers in total, one for drying, one for carbonisation and a separate one for cooling. As an advantage, it does not need to operate at full capacity to achieve effective performance. The loading and discharge are completed manually with intermittent operation. It is not a very popular system within the available technologies because the efficiency is similar to the tunnel retort, and the particle size needs to be smaller to fit in the shelves [3, 5].

### 2.1.2.3 Twin retort

This process uses two retorts, one of which is loaded with the feedstock and heated to the pyrolysis temperature. Meanwhile, the second retort is isolated from the heating source to cool down and collect the previously produced char, which is replaced by fresh feedstock. The pyrolysis vapours from one retort are burnt in a combustion chamber to provide energy for other retort. The time required per vessel is approximately within a range of 8-12 hours [2].

The typical scheme of a twin retort is found in Figure 2.4. In industry, several variations are aiming to increase the production of char and the optimisation of the process, although the principle is the same. For instance, JCKB International (France) connects four reactors instead of two. The average volume of each reactor is between 4.5 and 16.5 m<sup>3</sup> and the time needed highly depends on the cooling ratios, but on average, it takes 22 hours for the whole process. Roughly, it takes 1 hour to charge and another hour to discharge the retort, the pyrolysis takes 6-8 hours and the remaining 14-15 hours are dedicated to cooling before the collection of the char. The production depends on the number of vessels used, where 12 retorts can produce 2,500-7,000 tonnes of char per year with a char yield between 22 and 32 wt.%. For maximum production, the 24-hour operation of 12 vessels and 3 workers per shift would be needed. It is a straightforward technology that allows flexibility, although the control of the process is very challenging, and the residence time needed very long. Some companies using this technology are Carbon Group (The Netherlands), Green Coal (Estonia) and Carbon France (France) [2, 3].

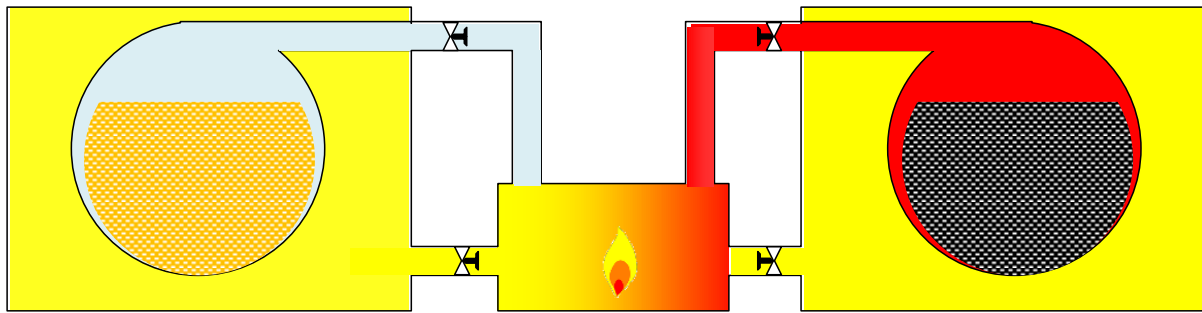


Figure 2.4: Twin retort scheme

### 2.1.3 Continuous processes

The main characteristic of the continuous processes is continuous feeding, discharge and operation. The capital cost is higher with the need for external sources of energy, and the systems are typically not portable. Some of the advantages are higher char yields and quality than discontinuous processes. There is a potential to recover by-products for higher utilisation and valorisation of the feedstock [4, 5].

Within the continuous processes, there are two categories based on the particle size of the feedstock. The processes Lambiotte, Reichert and Lurgi use big particles, understanding big particles as logs or branches without much need of pre-treatment for size reduction. The other processes, including agitated moving bed, paddle pyrolysis kiln, Herreshoff multiple-hearth furnace, screw reactor and rotary kiln use a smaller particle size (i.e. 20 mm), related to the need of reducing the particle size of the feedstock to chips or pellets. Overall, the particle size is a requirement of the process. The technologies using large pieces of biomass cannot be fed with small particles because they could pack tightly and hinder the circulation of the gases used to increase the temperature of the solid. Conversely, the reactors designed to deal with small particles are restricted to big particles due to heat transfer restrictions, and the biomass would not be fully processed [3].

#### 2.1.3.1 Big particles

This category includes Lambiotte, Reichert and Lurgi process. Overall, the gases from a combustion chamber or produced from pyrolysis flow through the solids to increase the temperature. Small particles would pack tightly and hinder the circulation of the gases. Instead, big particles allow the gases to flow through smoothly to increase the temperature of the feedstock. That is why there is a requirement for big particles in this type of reactors [3].

##### 2.1.3.1.1 Lambiotte

The Lambiotte technology is represented in Figure 2.5, consisting of a vertical retort, divided into different chambers and connected by valves. There is a lock-hopper in the upper part to feed the biomass and prevent gases from escaping. The feedstock moves slowly downwards with a counter-current flow of hot gas which dries the raw material. The gas used to dry the biomass comes from the carbonisation hearth, located below. This carbonisation chamber uses the resulting gases from the combustion of the pyrolysis gases in an external combustion chamber to increase the reactor temperature to conduct pyrolysis. When the raw material is converted to char, it moves to another chamber where cooling gas is used to decrease the temperature before it is collected [2, 4].

Since the feedstock enters into the system, it takes 11 hours until the char is collected at the bottom. Most of the drying of the feedstock occurs inside the reactor, but one of the requirements of the Lambiotte process is a moisture content below 25 wt.% for stable operation. Lambiotte process has two variants for the whole process, SIFIC and CISR, whose main difference is the treatment of the

pyrolysis vapours. The SIFIC variant takes the vapours through post-treatment to obtain commercial components such as acetic acid before burning the remaining vapours. Part of the resulting gases from combustion is re-injected into the retort to provide energy for pyrolysis. The other fraction is cooled and used at the bottom to reduce the temperature of the char. Another disadvantage is the corrosion by acetic acid because of gradient temperatures in the reactor, although this problem can be solved through the use of stainless steel [11]. The CISR variant does not treat the vapours from pyrolysis, and it only burns them to provide energy to the process. The SIFIC configuration is more effective because it obtains other by-products besides the char [2, 4].

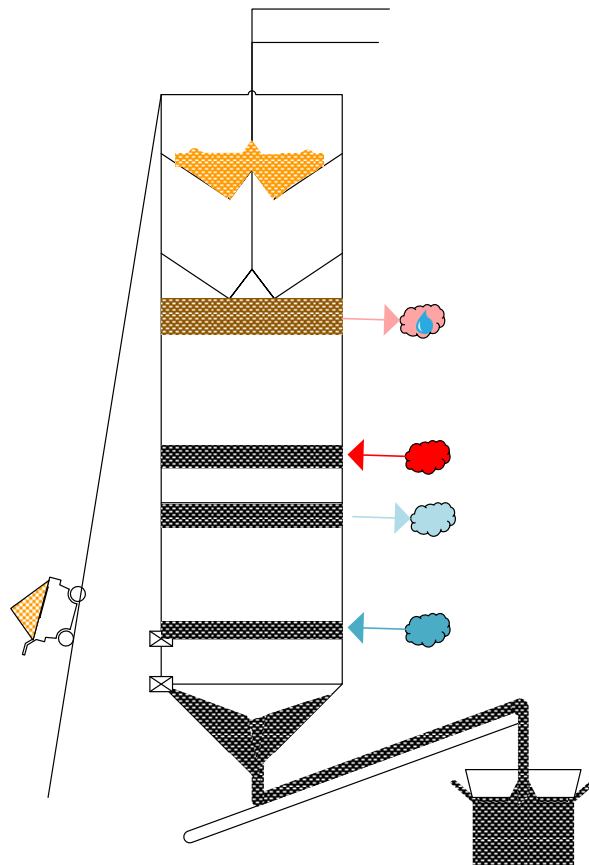


Figure 2.5: Lambiotte retort

This process relies on a high level of automation, and the vapours can be used for cogeneration. The yield of char and quality is higher than other processes, with a char yield around 32 wt.%. One of the restrictions of the process is the moisture content, which may limit the flexibility of the feedstock and may require the use of an additional feedstock to start the process. The largest plant using this technology was located in Prémery (France) [4] and used to produce 25,000 tonnes of char per year, although it was closed in 2002 due to economic problems. There are other operational plants in Europe and Russia [3, 5].

#### 2.1.3.1.2 Reichert

The Reichert retort is a conical top and brick-lined bottom, represented in Figure 2.6. A conveyor feeds the reactor from the top and closes the reactor when the reactor is full. Simultaneously, another valve opens to let the gases go into the reactor to start the pyrolysis process. This valve is located at the top where gases enter to start the process and travel slowly to the bottom. Before moving the char to the cooling bunker, pyrolysis vapours are removed to pass through a cooler and a scrubber and separate the condensable and non-condensable fraction. The non-condensable

fraction is heated to the pyrolysis temperature (450-550°C) and recirculated to the reactor as rinse gas [2].

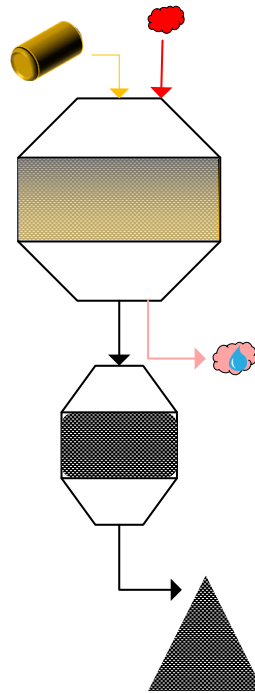


Figure 2.6: Reichert system

There is a plant in Bodenfelde (Germany), whose original name was Degussa and changed to Chemiviron Carbon and, later, ProFagus. The annual production of char is 24,000 tonnes from 70,000 tonnes of beechwood, which makes a yield of approximately 34 wt.% [4].

#### 2.1.3.1.3 Lurgi

The concept of the Lurgi reactor (Figure 2.7) is similar to Lambiotte. It consists of a reactor divided into upper pyrolysis and a lower cooling zone. The gas within the system comes from the combustion of the pyrolysis vapours with air in an external combustion chamber. One-third of the resulting gases are reinjected in the pyrolysis zone in the middle of the retort to flow upwards after conditioning to the pyrolysis temperature for the process (500-700 °C). To reinject the gases in the cooling zone, the gases are cooled by injection of water and are reintroduced at the bottom of the reactor [2].

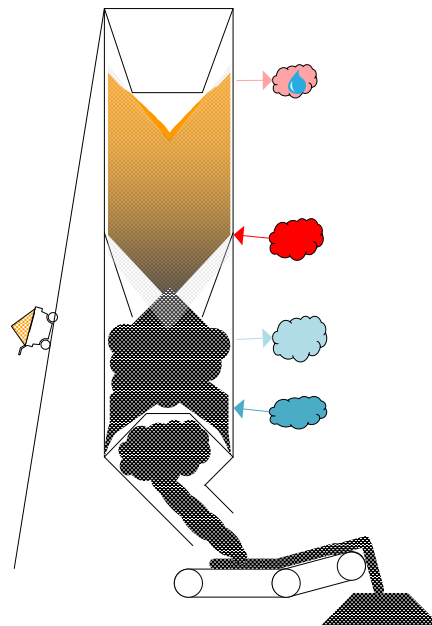


Figure 2.7: Lurgi reactor

The Silicon Metal Complex (SIMCOA) in Bunbury (Australia) produces 27,000 tonnes of char per year using this technology. The char yield of this process is 30-40 wt.% [2].

### 2.1.3.2 Small particles

Reactors for pyrolysis of small particles are usually heated externally. Heat is transferred to the solids through contact with the wall or through the flow of gases. These technologies usually take advantage of the residence time of the feedstock to increase the temperature of the feedstock and conduct pyrolysis until it is converted into char.

#### 2.1.3.2.1 Badger-Stafford process

Excluding batch processes (2.1.1) which have been used for centuries, the Badger-Stafford process is one of the oldest technologies to produce char found in the literature. It was extensively used in the 30s with a 3-meter-diameter reactor and a length of 12 meters. The wall is made of firebrick, diatomaceous earth and insulating brick. Similar to other technologies, the valves at the feeding and discharge controlled the flow rate of solids. The heat source was the heat of pyrolysis to increase the temperature to the target, 515 °C. One of the main drawbacks of this technology is the low heat transfer efficiency because the temperature near the wall was around 225 °C [12]. , the char yield is very low (20 °wt.%), and every fortnight this process had to shut down to burn the tar produced (10 wt.%). These are some of the reasons why the technology is no longer operating in any plant [4, 13].

#### 2.1.3.2.2 Herreshoff multiple-hearth furnace

As seen in Figure 2.8, the reactor consists of a vertical kiln made of a refractory-lined steel shell with several plates or circular hearths (4-10 hearths). There is a rotating shaft in the middle with attached arms on each hearth. The arms have ploughs to move the biomass across each hearth, produced by the rotational speed of the shaft (1-2 rpm). The biomass goes through all the hearths and falls to the next hearth from the centre or the side. In each of the chambers, there are combustion air blowers or ports which supply hot gases to the system to increase the temperature up to 500-600 °C (target temperature). At the same time, the biomass is agitated with the ploughs [3, 5].

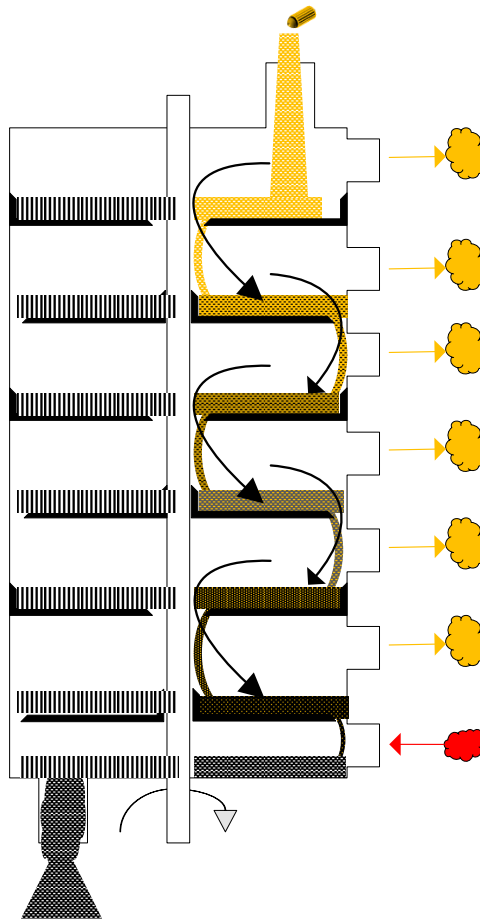


Figure 2.8: Herreshoff multiple-hearth furnace

The patent of this process belongs to R.D. Pike from 1921, and it was a system proposed for large capacity units, with one-tonne production and four tonnes processing per hour of char and biomass, respectively. It was a common system in the 1980s with more than 16 furnaces of this type in the United States. It is an efficient system and flexible in the feedstock, using fine-grained materials. The char needs briquetting to be commercially valuable, and the capital cost of that application can be high. One of the uses is as waste treatment. NESA commercialises large pyrolysis units for waste treatment, and BIG Char from Black is Green Pty. Ltd. commercialises a mobile reactor that produces briquettes of char using this technology [3, 5]. Current research [14] uses the same basis for the design of new pyrolysis units.

#### 2.1.3.2.3 Moving agitated bed

The moving agitated bed moves the biomass on a heated horizontal surface with a conveyor (see Figure 2.9). The heat source employed is usually molten salts such as potassium nitrate, sodium nitrate and sodium nitrite. Pyrovac used this technology as part of a vacuum pyrolysis unit, and the yields of pyrolysis oil were over 50 wt.%. NewEarth is commercialising one of these systems. Compared to the other technologies, this small, and the size is comparable to the height of the fixed bed in a laboratory (cm-scale). In the pilot plant in Saguanay Quebec (Canada) with a capacity of 3 tonnes per hour of biomass, there were undisclosed problems with the condensation towers [3, 5].

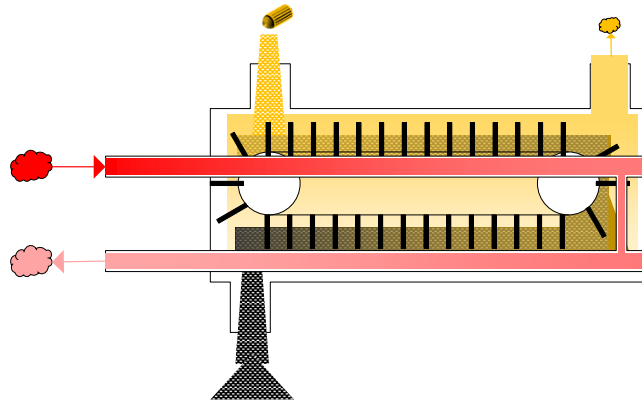


Figure 2.9: Moving Agitated Bed

There is an analogy to fast pyrolysis for this system. There is a specific technology called ablative pyrolysis where the biomass is pushed against a hot surface to degrade the biomass and obtain pyrolysis oil. It would be similar to pushing a portion of butter against a hot pan and it melts [7, 15, 16]. This system uses the same basis, the biomass is located on a hot surface, and the gravity is the force pushing the biomass against the surface. It could be argued whether this technology is fast or slow pyrolysis due to the similarity to a well-known fast pyrolysis technology. It has been included in this work because of the lower heating rate.

#### 2.1.3.2.4 Paddle pyrolysis kiln

This technology is represented in Figure 2.10 and consists of a horizontal vessel with an internal mechanism that moves and mixes the biomass. The mechanism consists of a group of paddles which increases the heat transfer and mixes the biomass. The mixing serves to generate a homogeneous product, reduce temperature gradients in the solids and control the residence time. It is used by BEST Energies and is one of the parts of the design Choren [17]. Due to the system for mixing, it is very flexible on the yield, and it is used to produce char and energy simultaneously. One of the characteristics is that the systems can be portable or stationary, and there is not a preferred option [3, 5].

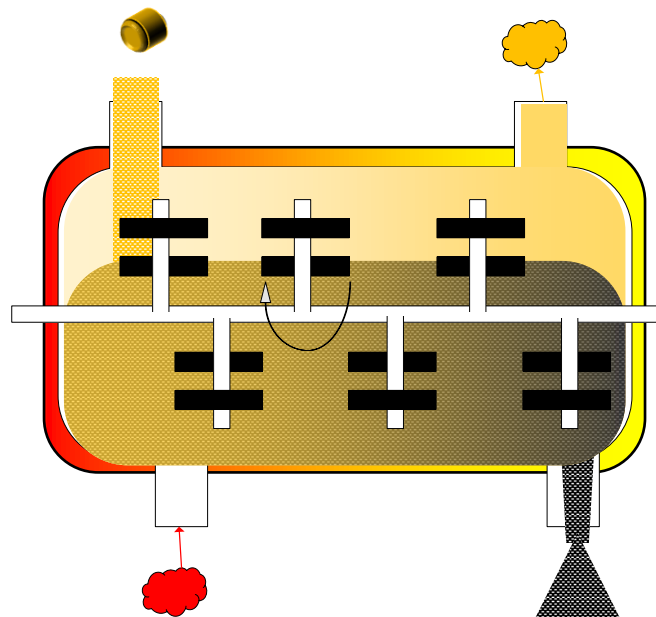


Figure 2.10: Paddle pyrolysis kiln

#### 2.1.3.2.5 Screw reactor

This type of reactor is composed of a rotating screw inside a horizontal tubular reactor, an alternative name for this technology is auger reactor [18]. The systems usually consist of a single or twin-screw design. The Energy and Bioproducts Research Institute (EBRI) in the United Kingdom has a unique screw reactor with two horizontal counter-rotating co-axial screws which aim to study the influence of the residence time of the char produced on the quality of pyrolysis oils [19]. The rotation of the screw moves the biomass along the reactor while it is heated and pyrolysed, represented in Figure 2.11 [6]. The residence time of this technology is controlled through the rotational speed of the screw. A heat carrier can be added to make the product distribution more similar to a fast pyrolysis system [15]. This heat carrier is usually sand or metal balls bearings heated to operating temperatures, which results in higher heat transfer and pyrolysis oil yields [20]. This is used by Marconi [21] and other researchers [20, 22] which uses pre-heated metal balls in the Haloclean® BioEnergy system. Due to this characteristic, some of the designs using screw reactors aim to produce pyrolysis oil, whereas the target products are usually char and heat [3, 5].

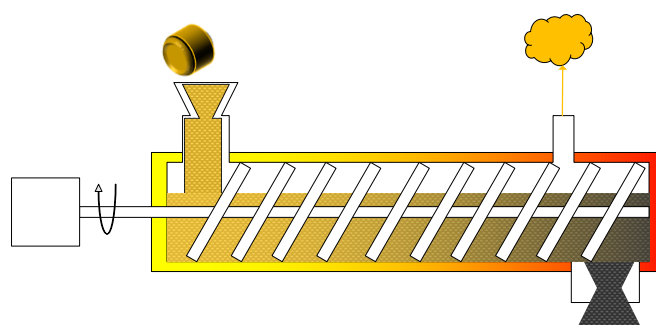


Figure 2.11: Screw reactor

The range of char yields is 17-30 wt.% and the pyrolysis oil 48-62 wt.%, although the water content is generally high (30-55 wt.%) compared to the oils from fast pyrolysis technologies, whose water content in oils is around 25 wt.% [23]. It is one of the most commonly used technologies, and some companies such as ABRI-Tech commercialises systems that process 1 tonne per day of biomass [5]. Others such as Renewable Oil International, Biogreen, Advanced Bio-refinery and Forschungszentrum Karlsruhe (FZK) focus the designs on producing pyrolysis oils and char whereas others such as International Tech Corporation, eGenesis and Agri-tech design the auger reactor to produce char and heat. Some of the advantages are the simplicity of construction and operation, the capacity to handle a wide variety of feedstocks with high char yields. Some of the issues of this system are the efficiency of the heat transfer, which limits the capacity to process biomass [3], and scale-up from experimental to industrial scale is still very challenging [20].

#### 2.1.3.2.6 Rotary kiln

Figure 2.12 is a scheme of a rotary kiln, consisting of a slightly tilted rotating cylindrical shell heated externally to increase the temperature of the solids within the reactor through the wall, which is heated externally [24]. The radius and rotational speed determine the mixing inside the reactor, which is one of the key aspects of the design [25]. The rotational speed and the angle the reactor is tilted control the residence time of the feedstock in the system, which usually takes less than an hour, significantly lower to other technologies [3, 6, 24]. This type of technology is common in industries such as cement [26-28], drying [29-35] or for novel processes like torrefaction [36, 37]. There is significant expertise in rotary kilns, although design aspects vary, such as internal heating through calcination in the cement industry [24]. From all the expertise, there is a common factor, which is the use of internal surfaces attached to the rotating wall to enhance the heat transfer. These internal



surfaces are called flights, fins or baffles, and they aim to increase surface area and heat transfer by conduction. An additional advantage of the fins is the capacity to lift the biomass, inducing movement within the bed and showering it over the bed of solids, creating an increase in the convection [3].

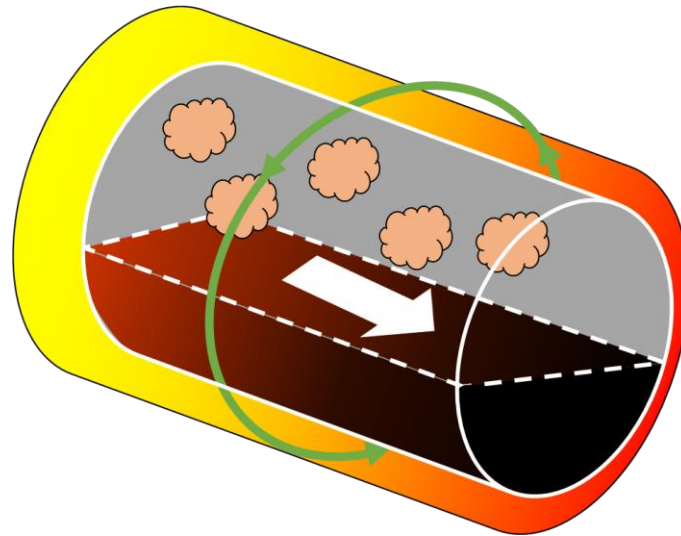


Figure 2.12: Rotary kiln

One of the main advantages highlighted by Garcia-Nunez et al. [5] is the good balance between the pyrolysis oil yields (37-62 wt.%) and char (19-38 wt.%). This system is scarce in research for pyrolysis [38-41], and it is more common in industry [42-45], although the information is limited. It is widely used for tires, sewage sludge, MSW and plastics. Some of the examples in industry are the plant in Burgau-Unterknöringen which produces 2.2MW, or VEW Energie AG Westfalen in Hamm-Uentrop, which processes 100,000 tonnes per year of biomass, both located in Germany. Despite having lower pyrolysis oil yields and more char, Amaron invented a technology with multiple high-intensity burners on a rotary kiln which optimised the heat transfer and made the yields very similar to those obtained in fast pyrolysis [3, 5]. Currently, there is a project (RE-DIRECT [46]) where a rotary kiln is being designed for the processing of unused biomass to produce char, to process 20,000 tonnes of waste biomass per year [46].

## 2.2 Information available

From all the reactors, there is a wide variety of technologies available to produce char. Each reactor has its strengths and weaknesses, singularities and standard points. Table 2.1 shows all the reactor data gathered from the literature, although some pieces of information are still missing. There are different categories to classify the data, which are described as follows:

- **Reactor size:** some characteristics such as the most typical dimensions of the reactor are included, the reactor position (horizontal, vertical or inclined), the volume and the capacity and/or production. It is important to correlate the size with the biomass input and production.
- **Process conditions:** in this category, the typical raw material is mentioned, and the possible pre-treatment needed. Some process parameters such as the temperature, pressure, operating method, residence time and the yields are addressed.
- **Heat transfer:** one of the challenges (2.4.1.1) of the slow pyrolysis reactors are the efficiency of the heat transfer, and the heating method, the ignition method and the heating rate achieved are issued within this category.

- **Economics and construction:** the materials used and its portability are important for the reactor. It refers to the automation in the loading of feedstock and discharge of products, and compare the initial investment needed and operating costs per annual ton of char produced.

Table 2.1: Gathered information from the reactors

| Criteria                             | Reichert Process                           | Lurgi                                   | Lambiotte Process                            | Waggon Retort                             | Twin Retort                             | Shelf Reactor                           | Herreshoff Multiple-Hearth Furnace      | Rotary Kiln              | Auger Reactor                           | Moving Agitated Bed                     | Paddle Pyrolysis Kiln                   |
|--------------------------------------|--|---|--|---|---|---|---|--------------------------|---|---|---|
| 1. Technical Aspects                 |  |   |  |   |   |   |   |                          |   |   |   |
| 1.1. Reactor Size                    |  |   |  |   |   |   |   |                          |   |   |   |
| 1.1.1. Dimensions                    | Large                                      | Large                                   | Large  | Small-Large                               | Small                                   | Small                                   | Large                                   | Small                    | Small                                   | Medium/large                            | Small                                   |
| 1.1.2. Position                      | Vertical                                   | Vertical                                | Vertical                                     | Horizontal                                | Horizontal/<br>Vertical                 | Horizontal/<br>Vertical                 | Vertical                                | Horizontal               | Horizontal                              | Horizontal/<br>vertical                 | Horizontal                              |
| 1.1.3. Reactor Volume [m3]           | 100  |   | 600  | 12  | 5-16.5                                  | na                                      |   |                          |   |   |   |
| 1.1.4. Size [m]                      | Height: 8.5<br>Diameter: 5                 | Height: 27<br>Diameter: 3               | Height: 16.3-18.4<br>Diameter: 3-4.3         | Length:8-9<br>Diameter: 2.5               | 0.3x0.3x0.1                             |   |   |                          |   | Height: few cm                          |   |
| 1.1.5. Capacity [t/h]                | 8.7  | 3.4-6.2                                 | 0.4-2.5                                      | 2.1                                       | 1.1                                     |   | 1-12.5                                  | 1.2-12                   | <2.1                                    | 3.0-3.5                                 |   |
| 1.1.6. Production [t/h]              | 3  | 1.6-1.7                                 | 0.25-3                                       | 0.75                                      | 0.3-0.9                                 |   | 1.9-2.75                                | 0.36-3.6                 | <0.36                                   |   |   |
| 1.2. Process conditions              |  |   |  |   |   |   |   |                          |   |   |   |
| 1.2.1. Raw material                  | Beech wood                                 |   | Oak wood                                     |   | Softwood/<br>Hardwood                   |   |   |                          |   |   |   |
| 1.2.2. Material Shape                | Cordwood                                   | Coorwood                                | Coordwood                                    | Cordwood                                  | Cordwood/chips                          | Chips                                   | Chips/ Fine<br>particles                | Chips/ Fine<br>particles | Chips/Fine<br>Particles                 | Chips/ Fine<br>particles                | Chips                                   |
| 1.2.3. Particle Size                 | Length 30-35 cm.<br>Thickness 10-15<br>cm. |   | 35 cm length<br>10 cm thickness              | 1-1.2 m length<br>0.08-0.12 m<br>Diameter |   |   |   |                          |   |   |   |
| 1.2.4. Temperature [°C]              | 450-550                                    | 550-700                                 | 547-560                                      |   | 580                                     |   |   | 500                      |   |   |   |
| 1.2.5. Pressure                      | Atmospheric                                | Atmospheric                             | Atmospheric                                  | Atmospheric                               | Atmospheric                             | Atmospheric                             | Atmospheric                             | Atmospheric              | Atmospheric                             | Atmospheric                             | Atmospheric                             |
| 1.2.6. Pretreatment needed           | None<br>Max. Moisture<br>25%               | 30% maximum<br>moisture content         | Pre-dried<br>30% maximum<br>moisture content | Drying<br>25% moisture<br>maximum         | None                                    | Pre-dried                               | Ground in<br>chips/fine<br>particles    | Ground into chips        | None                                    | Pre-dried                               | None                                    |
| 1.2.7. Feeding method                | Batches                                    | Batches                                 | Batches                                      | 5-7 m3 batches                            | 5-16.5 m3 batches                       | Shelves                                 | Continuous                              | Continuous               | Continuous                              | Continuous                              | Continuous                              |
| 1.2.8. Process Control               | Direct<br>measurement                      | Direct<br>measurement of<br>temperature | Direct<br>measurement of<br>temperature      | Direct<br>measurement of<br>temperature   | Direct<br>measurement of<br>temperature | Direct<br>measurement of<br>temperature | Direct<br>measurement of<br>temperature | Direct<br>measurement    | Direct<br>measurement of<br>temperature | Direct<br>measurement of<br>temperature | Direct<br>measurement of<br>temperature |
| 1.2.9. Cycle Time [h]                | 16-20                                      |   | 11   | 25-35                                     | 22-36                                   |   |   |                          |   |   |   |
| 1.2.10. Targeted product             | Biochar                                    | Biochar and<br>pyrolysis oil            | Biochar and<br>pyrolysis oil                 | Biochar and<br>pyrolysis oil              | Biochar, pyrolysis<br>oil and gases     | Biochar and<br>pyrolysis oil            | Biochar                                 | Biochar/heat             | Biochar/pyrolysis<br>oil/gases          | Biochar/ pyrolysis<br>oil               | Biochar                                 |
| 1.2.11. Average Gas yield [wt.%]     |  |   |  | 20-30                                     |   |   |   |                          | 18-35                                   |   |   |
| 1.2.12. Average Bio-oil yield [wt.%] |  |   |  | 30-50                                     |   |   |   | 37-62                    | 48-62                                   | >50                                     |   |
| 1.2.13. Average Char yield [wt.%]    | 33-38                                      | 30-40                                   | 30-35  | 30-38                                     | 22-33                                   |   | 25-30                                   | 19-38                    | 17-30                                   |   |   |

Table 2.2: Gathered information from the reactors (continuation)

| Criteria                             | Reichert Process              | Lurgi                                   | Lambiotte Process                       | Waggon Retort   | Twin Retort                            | Shelf Reactor          | Herreshoff Multiple-Hearth Furnace   | Rotary Kiln  | Auger Reactor   | Moving Agitated Bed                      | Paddle Pyrolysis Kiln |
|--------------------------------------|-------------------------------|---|---|---|--|------------------------|--|--|---|--|-----------------------|
| 1.3. Heat transfer                   |                               |   |   |   |  |                        |  |  |   |  |                       |
| 1.3.1. Heating method                | Direct contact with hot gases | Contact with heat gases                 | Contact with heat gases                 | Indirect heat   | Indirect Heat through the walls        | Indirect heat          | Contact with hot gases<br>Combustion of pyrolysis gases and/or auxiliary gases | Contact with hot gases<br>Combustion of auxiliary fuels and direct or indirect contact of combustion gases | Direct contact with hot gases/<br>Use of a hot heat carrier/ Indirect heating | Indirect heating (sometime molten salts) | Indirect heating      |
| 1.3.2. Charge ignition method        | N/A                           | Hot gases generated in an external oven | Hot gases generated in an external oven | Heating with an external volatiles combustion chamber | External heat and volatiles combustion | Direct measurement     | Volatile external combustion chamber to produce hot gases                      | External heating and volatile combustion   | Heating with an external combustion chamber                                   | External oven                            | External heater       |
| 1.3.3. Heat transfer rate achieved   | Slow Pyrolysis                | Slow pyrolysis                          | Slow pyrolysis                          | Slow Pyrolysis  | Slow Pyrolysis                         | Slow or Fast Pyrolysis | Typically slow pyrolysis (could be used for fast pyrolysis)                    | Slow or potentially fast pyrolysis   | Slow or fast pyrolysis  | Fast/slow                                | Slow pyrolysis        |
| 2. Economics and Construction        |                               |   |   |   |  |                        |  |  |   |  |                       |
| 2.1. Construction                    |                               |   |   |   |  |                        |  |  |   |  |                       |
| 2.1.1. Materials                     | Metal                         | Metal                                   | Metal                                   | Steel<br>High Temperature Steel                       | Steel/iron/brick                       | Metal                  | Metal/<br>Steel Vessel and piping components                                   | Steel  | Metal   | Metal                                    | Metal                 |
| 2.1.2. Portability                   | Stationary                    | Stationary                              | Stationary                              | Stationary  | Stationary                             | Stationary             | Stationary   | Stationary   | Stationary or portable  | Stationary                               | Stationary            |
| 2.1.3. Loading and discharge methods | Mechanical                    | Mechanical                              | Mechanical                              | Waggons use   | Manual                                 | Manual/<br>mechanical  | Mechanical   | Mechanical   | Mechanical  | Mechanical                               | Mechanical            |
| 2.2. Economics                       |                               |   |   |   |  |                        |  |  |   |  |                       |
| 2.2.1. CAPEX [pound/annual char ton] |                               | 1.15                                    | 60-62.5                                 |   | 120-175                                |                        |  |  | 68.5  |  |                       |
| 2.2.2. OPEX [pound/ char ton]        |                               | 280                                     | 315                                     |   | 332                                    |                        |  |  |   |  |                       |

## 2.3 Selection criteria

From Table 2.1, the wide variety of characteristics within the slow pyrolysis technologies can be reviewed. The whole set of characteristics do not have the same role and importance in the choice of a reactor, and it depends on the current social, political and economic situation of the country where the reactor is potentially going to be built. Lohri et al. [6, 47] gave an excellent example of the choice for a developing country. The article reviews different slow pyrolysis technologies and establishes criteria for the construction of a pyrolysis reactor in a country without a robust economy to support it. In the case of the current research, the technologies and criteria are considered for a developed country like the United Kingdom, where Aston University is based. As an example, the initial investment will not be as critical as in the other article, and the focus is more on the efficiency of the process.

To classify these technologies, each characteristic is graded from 1 to 5 for a particular reactor, and a weight from 1 to 5 is assigned to each feature. A grade 1 in a characteristic for a specific reactor means that is not appropriate for the process, especially compared to the others. If the value of the weight is 1, it means that its importance is low compared to the others. A grade 5 in a characteristic means that it is ideal and, in case of a weight 5, the characteristic is vital. The criteria for each characteristic and the weight are described as follows:

- **Capacity:** The capacity of biomass processing is a crucial aspect in a plant because it determines the amount of biomass input, and the maximum char production, key aspect for its feasibility. With that purpose, the maximum capacity of each technology found in industry has been divided by the maximum capacity to process biomass within all technologies, which is 10 tonnes per hour, corresponding to Herreshoff Multiple-Hearth Furnace. Overall, most of the technologies can be scaled down to lab-scale. Some problems may appear on the scale up to industrial capacities (tonnes per hour). Criteria with a value of 1 mean that maximum production of that technology was lower than 1 tonne per hour or there was a lack of values in the literature about real production. When the production is higher than 1 tonne per hour, the number used for the classification is the division of the capacity of that technology by the maximum (represented by the Herreshoff Multiple-Hearth Furnace). The technology should be better able to deal with a wide range of capacities found in industry. The weight attributed to the capacity is 5 because it is a crucial aspect for the feasibility of the plant. Ideally, the technology should be able to deal with large capacities (3 dry tonnes per hour) but also lower scale (100 kilograms per hour), with the possibility to work outside of this range.
- **Material size and uniformity:** one of the key aspects is to obtain a homogenous char and efficient heat transfer, whose production has been controlled and the properties are stable. This is mainly achieved by small particles. In systems dealing with larger particles, the bed of solids and particles are more heterogeneous, and it is more likely to have temperature gradients within. It is not a crucial aspect because the design can be amended to try to solve this problem or a pre-treatment step can solve the heterogeneous behaviour, so the weight is 2.
- **Pre-treatment (moisture):** the moisture content applies to the flexibility of the reactor. Drying is one of the more heat-demanding processes as it is explained in Section 8.2. A reactor can be previously designed for some feedstocks with higher moisture content, although some of the technologies have an established moisture limit. If there is no moisture limit, the weight is 5, and it decreases down to 1 where no moisture is allowed. Since it is such an energy-demanding step, the weight is 4.
- **Pre-treatment (Size):** the reduction of the particle size is a standard procedure for a more uniform biomass particle size. This step has to be done through the grinding, and it would increase the

operational cost of the whole process. The reactors which do not need size reduction are graded with 5 and the ones needing a reduction in the particle size are graded with 1, although it is not such a crucial aspect, attributing a grade of 3.

- **Feeding method:** the continuous feeding of the reactor allows the reactor to achieve continuous operation and to be as automatic as possible. Since there are only two feeding methods, the grades have to be 1 or 5, assigned to manual and automatic methods, respectively. If the reactor is fed in batches directly to the reactor, the grade is 1. If the biomass is fed to the system and the reactor automatically feeds, the grade is 5. This characteristic is vital to make the process as efficient and as continuous as possible and, consequently, the weight is 4.
- **Cycle time:** the cycle time is the process that takes since the biomass is introduced in the system until the actual product (char) can be collected. This time is very variable across the literature. Logically, the shorter time to produce char is preferred because it will mean higher char production rates. The technologies whose cycle time is shorter than a day but still involves several hours have a grade of 2. Finally, the technologies whose time is approximately an hour have a grade of 5. The weight is only 1 because, despite the preference of shorter residence time, it is not a crucial aspect as long as the capacity is high enough, which can be enhanced by a bigger reactor.
- **Targeted product:** The main product from slow pyrolysis is char, so the focus of the technology must be char production. This aspect can be modified with the process parameters such as residence time or temperature. It is important to evaluate the adequacy of the technology. All the processes focus on char, but if the process focuses on co-production of char with one of the by-products, the grade is 5 because a higher portion of initial material is utilised. If the only purpose is to make char, the grade is 1. The weight is 3 because this aspect can increase efficiency and profitability, and reduce the production of waste, but it is not a crucial parameter.
- **Average char yield (wt.%):** This characteristic evaluates the percentage of raw material which is transformed into char. Overall, it can be modified with the process conditions. The higher it is as a predetermined fixture, the better. A char yield of 30 wt.% is a grade 1 because it is the minimum in all reactors. Since the highest value is 40 wt.%, it is assigned to value 5. It is a crucial parameter because it shows the efficiency of the technology towards char, and it has a weight of 5.
- **Heating method:** it is impossible to evaluate the efficiency of the heat transfer for every single reactor type. For that reason, the criteria account for the heating methods within each technology. If there is only one heating method, the technology will be graded with 1; For instance, the batch reactors are only heated externally by the combustion gases through the wall. On the other side, with further actions such as mechanical movement which enhance the heat transfer and may create other heating methods such as convection, the grade is 5.
- **Loading and discharge method:** the importance of the automation of the process has been explained previously. The technologies where the loading or discharge are manual are graded with 1. When the feeding and discharge methods are automatic have a value of 5.
- **CAPEX:** the CAPEX measures the initial investment needed for the construction of the plant. The pounds per annual tonne of char is the parameter used in this case to make the values more comparable; otherwise the cost a plant which produces 20,000 tonnes of char would be compared to another one producing only 2,000. The information in the literature about this aspect is limited, and it has been graded according to available data. In this case, the higher CAPEX, the lower grade given. Up to £70 per ton of char is graded 5 and, if the CAPEX is higher than that, it is 1. This polarised evaluation is due to the lack of numbers and the fact that, overall, the terms used for CAPEX are low or high [2].

The final grade of each technology is obtained by multiplying the grade of each technology by the weight of each characteristic and summing them.

### 2.3.1 Results

The results, according to the Selection criteria, are represented in Table 2.3. The final classification, where each aspect and its weight are combined, is shown in Figure 2.13.

Table 2.3: Weighted classification of reactors

| Criteria                       | Reichert Process | Lurgi | Lambiotte Process | Waggon Retort | Twin Retort | Shelf Furnace | Herreshoff Multiple-Hearth Furnace | Rotary Drums | Auger Reactor | Moving Agitated | Paddle Pyrolysis | Weight |
|--------------------------------|------------------|-------|-------------------|---------------|-------------|---------------|------------------------------------|--------------|---------------|-----------------|------------------|--------|
| Capacity [t/h]                 | 3.7              | 2.8   | 1.5               | 1.4           | 1           | 1             | 5                                  | 4.8          | 1.4           | 1.9             | 1                | 5      |
| Material size                  | 1                | 1     | 1                 | 1             | 1           | 1             | 5                                  | 5            | 5             | 5               | 5                | 2      |
| Pretreatment needed (moisture) | 2                | 2     | 3                 | 2             | 5           | 1             | 5                                  | 5            | 5             | 1               | 5                | 4      |
| Pretreatment needed (size)     | 5                | 5     | 5                 | 5             | 1           | 1             | 1                                  | 1            | 1             | 1               | 1                | 3      |
| Feeding method                 | 5                | 5     | 5                 | 1             | 1           | 1             | 5                                  | 5            | 5             | 5               | 5                | 4      |
| Cycle Time [h]                 | 2                | 2     | 2                 | 1             | 1           | 1             | 5                                  | 5            | 5             | 5               | 5                | 1      |
| Targeted product               | 1                | 5     | 5                 | 5             | 5           | 5             | 5                                  | 5            | 5             | 5               | 1                | 3      |
| Average Char yield             | 4.1              | 5     | 3                 | 4.1           | 2.1         | 1             | 1                                  | 4.1          | 1             | 1               | 1                | 5      |
| Heating method                 | 1                | 1     | 1                 | 1             | 1           | 1             | 5                                  | 5            | 5             | 1               | 5                | 4      |
| Loading and discharge methods  | 5                | 5     | 5                 | 5             | 5           | 1             | 5                                  | 5            | 5             | 5               | 5                | 1      |
| CAPEX [pound/annual char ton]  | 5                | 5     | 5                 | 1             | 1           | 1             | 1                                  | 1            | 5             | 1               | 1                | 2      |
| Result                         | 108              | 120   | 108               | 83.5          | 72          | 46            | 130                                | 145          | 120           | 82.5            | 98               |        |

According to the table and the graph, the most promising technology for the production of char in the field of slow pyrolysis was the rotary kiln (145), followed by Herreshoff multiple-hearth furnace (130) and the Lurgi and auger reactor systems (120). The basics for the design of the reactor are the same in terms of mass and heat transfer, feedstock and construction materials. Rotary kilns have challenging issues with sealing due to its rotational movement and its internal configuration. Other reactors pose different challenges such as the heat transfer for the auger, control of the process for the Missouri kiln or the paddle kiln with the design of the flights [48-50].

## Results

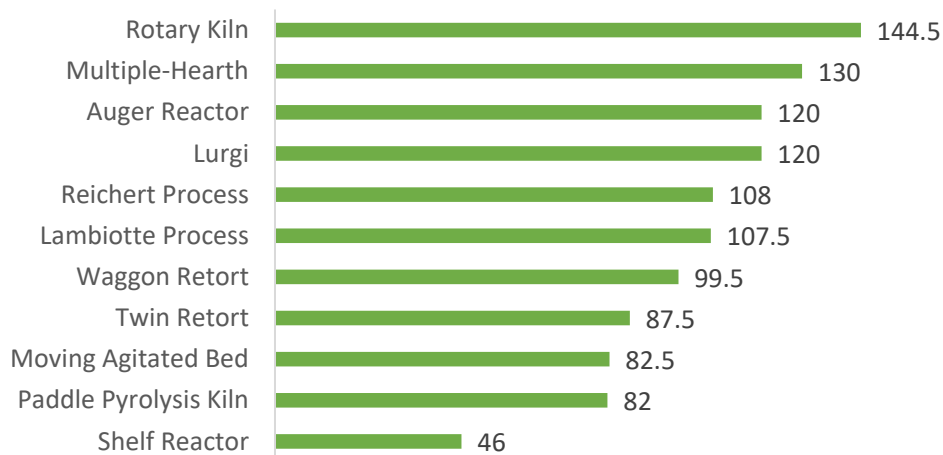


Figure 2.13: Results of the weighted classification

## 2.4 Pyrolysis reactor design

There are many challenges in the design of a pyrolysis reactor. Challenges related to the processing of biomass, the behaviour of the bed of solids or the kinetic parameters associated with the feedstock are common for all pyrolysis reactors (2.4.1.1). Additionally, the singularities of the rotary kiln have to be considered for its design (2.4.1.2). The singularities are associated with the rotation of the kiln and include the rotational method and sealing.

### 2.4.1.1 Challenges for the design of a pyrolysis reactor

One of the challenges in designing a pyrolysis reactor is the number of different reactions which take place during pyrolysis, each with a reaction constant, activation energy, and reaction order. Peters et al. [51] published a study where 149 individual reactions were simulated to obtain an excellent kinetic model for pyrolysis. It is mentioned that the model is not completed and some reactions such as the secondary reactions of condensable vapours and char are not taken into account. To have a whole set of reliable pyrolysis reactions, thousands of reactions, from which some are still unknown, should be defined. In literature, it is more common to find pyrolysis mechanisms and kinetic parameters adjusted to fit the real behaviour of the feedstock through pyrolysis, which could be analysed in TGA. Some of the pyrolysis studies and mechanisms are Broido and Nelson [52], Bradbury et al. [53], Shafizadeh et al. [54-56] or Di Blasi and Lanzetta [57]. The method to determine the kinetics for slow pyrolysis is described in Chapter 5.

Besides the determination of the kinetics and reactions, heat transfer is a critical aspect of the design of any pyrolysis reactor. A widespread practice in slow pyrolysis is the use of relatively high temperatures (in a range 300-700°C) [7, 8, 41, 58]. Most of the studies [8, 25, 59-61] use reactors which are heated indirectly, and the control of the temperature is crucial to get reliable results, and this is a consequence of an efficient heat transfer. Within the industrial process, it is usual to find the recirculation of the gases coming from the combustion of the non-condensable fraction around the reactor to transfer its heat to the feedstock. It is essential to achieve an efficient heat transfer because the reaction temperature is one of the most influential parameters. It profoundly affects product distribution, and the properties of the products, such as water sorption capacity, micro-pore volume [62, 63] or fixed carbon content [64]. With the wall at a higher temperature than the solids and gases inside the reactor, three heat transfer methods take place: conduction, convection and radiation. The



bed of solids is heated by the wall by conduction, but since the wall is rotating and the solids are moving forward, there is convection. Furthermore, the uncovered portion of the wall by solids is radiating energy because of a higher temperature than solid. Finally, the gas and the solid move and interact, exchanging heat. Further explanation is given in Chapter 4.

#### 2.4.1.2 Singularities of the rotary kiln

Figure 2.12 gives an idea of the complexity in reactor design and the need to divide the task into smaller parts. Firstly, the height of the bed of solids is not constant along the reactor. This fact will influence the contact areas and heat transfer. The behaviour of the solids needs characterisation and definition along the reactor and in the model. The heat transfer model helps with the temperature profile along with the kiln, for the bed of solids, the gases, the wall and the combustion gases, which provide the heat source. The model is influenced by the flights designed for the reactor, which mainly increase the contact area between the wall and the bed of solids and enhance the heat transfer. The temperature profile from the heat transfer model provides the kinetic model with the data needed for the conversion at each point along the length of the reactor.

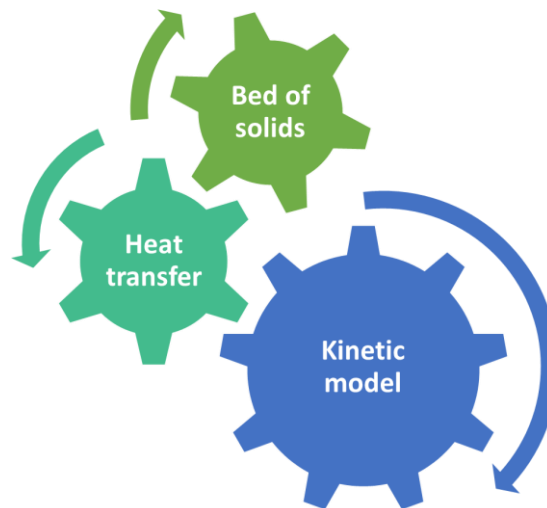


Figure 2.14: Representation of the correlation between bed of solids, heat transfer and kinetics in the process

These three parts (bed of solids, heat transfer and kinetics), represented in Figure 2.14, and are the main parts of the rotary kiln model. Although there are additional considerations taken into account for the complete design of the reactor; feedstock characteristics that are not measured in the laboratory, such as thermal conductivity or density, are obtained from literature and are crucial for the calculations. The reactor needs adequate seals to avoid air entering or the release of pyrolysis gases. Another critical point is the construction materials used for the reactor, which impacts thermal expansion.

## 2.5 References

1. Antal, M.J. and M. Grønli, *The Art, Science, and Technology of Charcoal Production*. Industrial & Engineering Chemistry Research, 2003. **42**(8): p. 1619-1640.
2. Grønli, M., et al., *The Science and Technology of Charcoal Production*. 2005, PyNe Subject Group.
3. Garcia-Perez, M., T. Lewis, and C.E. Kruger, *Methods for Producing Biochar and Advanced Biofuels in Washington State Part 1: Literature Review of Pyrolysis Reactors*, in *Ecology Publication*. 2011, Washington State University: Pullman, WA. p. 137 pp.
4. *Industrial charcoal production, TCP/CRO/3101 (A) development of a sustainable charcoal industry*. 2008, Food and Agriculture Organization of the United Nations (FAO): Zagreb, Croatia.

5. Garcia-Nunez, J.A., et al., *Historical Developments of Pyrolysis Reactors: A Review*. Energy & Fuels, 2017. **31**(6): p. 5751-5775.
6. Lohri, C.R., et al., *Char fuel production in developing countries – A review of urban biowaste carbonization*. Renewable and Sustainable Energy Reviews, 2016. **59**: p. 1514-1530.
7. Basu, P., *Biomass gasification, pyrolysis, and torrefaction: practical design and theory*. 2013: London, UK : Elsevier : Academic Press, 2013. Second edition.
8. Apaydin-Varol, E., E. Pütün, and A.E. Pütün, *Slow pyrolysis of pistachio shell*. Fuel, 2007. **86**(12-13): p. 1892-1899.
9. Fabian Stenzel, S.B., *Biochar training for environmental sustainability and development, in Biochar production*, S.a.E.T.U. Fraunhofer Institute for environmental, Editor. 2014: Santiago de Compostela, Spain.
10. *Simple Technologies for Charcoal Making*. Forestry Paper, ed. FAO. Vol. 41. 1983, Rome (Italy): Forestry Department.
11. Stassen, H.E., *Current Issues in Charcoal Production and Use*, in *Biomass Power for the World*, C.P.T.F. Group, Editor. 2015, Pan Stanford Publishing: New York. p. 760.
12. Nelson, W.G., *Waste-wood Utilization by the Badger-Stafford Process1 the ford Wood-Distillation Plant at Iron Mountain*. Industrial & Engineering Chemistry, 1930. **22**(4): p. 312-315.
13. Emrich, W., *Handbook of Charcoal Making: the Traditional and Industrial Methods*. Solar energy R & D in the European Community. Series E, Energy from biomass, ed. E.f. Biomass. Vol. 7. 1985: Springer-Science+Business Media, B. V.
14. Lotfy, M.R., *DISPOSITIF DE PRODUCTION DE CHARBON VERT A USAGE AGRICOLE*, in *HAUTIER IP; 20 Avenue Fontvieille MC-98000 Monaco*, MC, M.R. Lotfy, Editor. 2015: France.
15. Bridgwater, A.V., *Review of fast pyrolysis of biomass and product upgrading*. Biomass and Bioenergy, 2012. **38**(Supplement C): p. 68-94.
16. Radlein, D. and A. Quignard, *A short historical review of fast pyrolysis of biomass*. Oil & Gas Science and Technology - Revue d'IFP Energies nouvelles, 2013. **68**(4): p. 765-783.
17. Meier, D., *PYROLYSIS Activities in Germany*, in *IEA Bioenergy Task 34 - Pyrolysis*, H. Institute of Wood Technology and Wood Biology (HTB), Germany, Editor. 2009: Sheraton Chicago Hotels & Towers.
18. Rego, F., et al., *Chapter 2: Pyrolysis of biomass and wastes in a continuous screw reactor for char production*, in *Advanced Carbon Materials from Biomass: an Overview*. 2019, Zenodo.
19. Yang, Y., et al., *Intermediate pyrolysis of biomass energy pellets for producing sustainable liquid, gaseous and solid fuels*. Bioresour Technol, 2014. **169**: p. 794-9.
20. Brassard, P., S. Godbout, and V. Raghavan, *Pyrolysis in auger reactors for biochar and bio-oil production: A review*. Biosystems Engineering, 2017. **161**: p. 80-92.
21. *Pyrolysis Liquid for Power Generation*, in *Haloclean® BioEnergy*, S. Marconi, Editor. 2007, PyNE; IEA Bioenergy.
22. Hornung, A., *Processing Municipal Solid Waste (MSW) and biomass/residual streams using Thermo Catalytic Reforming (TCR) technology*, S. Technologies, Editor. 2016, Fraunhofer Institute for Environmental, Safet and Energy Technology UMSICHT.
23. Bridgwater, A.V., *Upgrading biomass fast pyrolysis liquids*. Environmental Progress & Sustainable Energy, 2012. **31**(2): p. 261-268.
24. Boateng, A.A., *Rotary kilns: transport phenomena and transport processes*. 2008: Amsterdam ; Boston : Elsevier/Butterworth-Heinemann, ©2008.
25. Fantozzi, F., et al., *Rotary Kiln Slow Pyrolysis for Syngas and Char Production From Biomass and Waste—Part I: Working Envelope of the Reactor*. Vol. 129. 2007. 901-907.
26. Ziatabari, J., A. Fatehi, and M.T.H. Beheshti. *Cement rotary kiln control: A supervised adaptive model predictive approach*. in *2008 Annual IEEE India Conference*. 2008.
27. Ngako, S., et al., *Numerical investigation of bed depth height, axial velocity and mean residence time of inert particles in steady state industrial cement rotary kiln: Case of Figuil Plant in Cameroon*. Powder Technology, 2015. **271**: p. 221-227.

28. *Wireless Technology Improves Cement Rotary Kiln Temperature Readings*, Honeywell, Editor. 2008, 2008 Honeywell International Inc.: Automatic & Control Solutions; Process Solutions; Honeywell; 2500 W. Union hills Dr.; Phoenix, AZ 85027.
29. Krokida, M., D. Marinos-Kouris, and A. Mujumdar, *7 Rotary Drying*. 2006.
30. Baker, C.G.J., *The design of flights in cascading rotary dryers*. *Drying Technology*, 1988. **6**(4): p. 631-653.
31. Revol, D., C.L. Briens, and J.M. Chabagno, *The design of flights in rotary dryers*. *Powder Technology*, 2001. **121**(2): p. 230-238.
32. van 't Land, C.M., *Drying in the Process Industry*. 2011: Wiley.
33. Lisboa, M., et al., *A study of particle motion in rotary dryer*. *Brazilian Journal of Chemical Engineering*, 2007. **24**(3): p. 365-374.
34. *The Rotary Dryer Handbook*. 2019: FEECO International.
35. *Rotary Dryer Sizing & Design*. 2015, FEECO International.
36. Hagenbeek, R., *Visit to a torrefaction production centre*, J. López-Ordovás, Editor. 2018, Torr-Coal: Dilsen-Stokkem, Belgium.
37. López-Ordovás, J., et al., *Torrefaction of beechwood in a pilot-scale rotary kiln*. *Applied Energy*, Forthcoming.
38. Li, A.M., et al., *Experimental studies on municipal solid waste pyrolysis in a laboratory-scale rotary kiln*. *Energy*, 1999. **24**(3): p. 209-218.
39. Li, A.M., et al., *Pyrolysis of solid waste in a rotary kiln: influence of final pyrolysis temperature on the pyrolysis products*. *Journal of Analytical and Applied Pyrolysis*, 1999. **50**(2): p. 149-162.
40. Mašek, O., et al., *Consistency of biochar properties over time and production scales: A characterisation of standard materials*. *Journal of Analytical and Applied Pyrolysis*, 2018. **132**: p. 200-210.
41. Babler, M.U., et al., *Modelling and pilot plant runs of slow biomass pyrolysis in a rotary kiln*. *Applied Energy*, 2017. **207**: p. 123-133.
42. *The Rotary Kiln Handbook*. 2019: FEECO International.
43. Ebbenis, A. and C. Carlson, *Rotary kiln process optimisation*. 2019, FEECO International.
44. Gerlach, D., *Connect smarter today's*, in *DGE Thermolysis, Plant Type MIDI*, M. Engineering, Editor., The Adecco group.
45. *Green-Charcoal*, in *Innovation Towards Sustainable Development*. 2004, Pro Natura International: Paris.
46. Steber, M. *RE-DIRECT*. 2018 [cited 2018 5th April 2018]; Available from: <http://re-direct-nwe.eu/>.
47. Duku, M.H., S. Gu, and E.B. Hagan, *Biochar production potential in Ghana—A review*. *Renewable and Sustainable Energy Reviews*, 2011. **15**(8): p. 3539-3551.
48. Stein, P., *Rotary kiln design methodology*, J. López-Ordovás, Editor. 2019: EBRI, Aston University, Birmingham, United Kingdom.
49. Day, C., *Description of an industrial rotary kiln*, J. López-Ordovás, Editor. 2019: EBRI, Aston University.
50. Bridgwater, A.V., *Aspects to consider in the design of a rotary kiln*, J. López-Ordovás, Editor. 2019, Aston University: Energy and Bioproducts Research Institute (EBRI).
51. Peters, J.F., D. Iribarren, and J. Dufour, *Predictive pyrolysis process modelling in Aspen Plus*. 2014.
52. Broido, A. and M. A. Nelson, *Char yield on pyrolysis of cellulose*. Vol. 24. 1975. 263-268.
53. Bradbury, A.G.W., Y. Sakai, and F. Shafizadeh, *A kinetic model for pyrolysis of cellulose*. *Journal of Applied Polymer Science*, 1979. **23**(11): p. 3271-3280.
54. Shafizadeh, F., G.D. McGinnis, and C.W. Philpot, *Thermal degradation of xylan and related model compounds*. *Carbohydrate Research*, 1972. **25**(1): p. 23-33.
55. Shafizadeh, F. and P.P.S. Chin, *Thermal Deterioration of Wood*, in *Wood Technology: Chemical Aspects*. 1977, AMERICAN CHEMICAL SOCIETY. p. 57-81.

56. Shafizadeh, F., et al., *Production of Levoglucosan and Glucose from Pyrolysis of Cellulosic Materials*. Vol. 23. 1979. 3525-3539.
57. Di Blasi, C. and M. Lanzetta, *Intrinsic kinetics of isothermal xylan degradation in inert atmosphere*. Journal of Analytical and Applied Pyrolysis, 1997. **40-41**: p. 287-303.
58. Park, J., et al., *Slow pyrolysis of rice straw: analysis of products properties, carbon and energy yields*. Bioresour Technol, 2014. **155**: p. 63-70.
59. Codignole Luz, F., et al., *Pyrolysis in screw reactors: a 1-D numerical tool*, in *72nd Conference of the Italian Thermal Machines Engineering Association*,. 2017, Energy Procedia: Lecce Italy. p. 683-689.
60. Tomasi Morgano, M., et al., *Screw pyrolysis with integrated sequential hot gas filtration*. Journal of Analytical and Applied Pyrolysis, 2015. **113**: p. 216-224.
61. Yu, Y., et al., *Pyrolysis of Rice Husk and Corn Stalk in Auger Reactor. 1. Characterization of Char and Gas at Various Temperatures*. Energy & Fuels, 2016. **30**(12): p. 10568-10574.
62. Baldock, J.A. and R.J. Smernik, *Chemical composition and bioavailability of thermally altered Pinus resinosa (Red pine) wood*. Organic Geochemistry, 2002. **33**(9): p. 1093-1109.
63. Nguyen, B.T., et al., *Temperature Sensitivity of Black Carbon Decomposition and Oxidation*. Environmental Science & Technology, 2010. **44**(9): p. 3324-3331.
64. Ronsse, F., et al., *Production and characterization of slow pyrolysis biochar: Influence of feedstock type and pyrolysis conditions*. Vol. 5. 2013. 104-115.

### 3 The bed of solids submodel

The bed of solids submodel determines and describes the behaviour of the solids within the reactor. The objective of this submodel is to calculate the areas for which there are interaction and contact between the gas, bed of solids and reactor wall. The information calculated in this chapter is based on for a rotary kiln without internal flights, whose main driving force is gravity and the slight inclination of the reactor. Section 3.6 addresses how flights affect the current model. This submodel needs several inputs:

- **Kiln angle:** the rotary kiln is not horizontal, which helps the solids to move forward through the reactor. Usually, this angle is within a range of 1-4° [1]. Its influence on other parameters is described in Section 3.2.1.
- **Solids input capacity:** the capacity is a key input to determine characteristics such as the radius, and has a direct effect on residence time, reactor length and contact areas.
- **Feedstock:** is the raw material to undergo pyrolysis (wheat straw, RDF or wood pellets). Some aspects of the feedstock are needed to estimate its behaviour and calculate the outputs of this model. The two main parameters used for the bed of solids submodel are the repose angle and the density.

This model relies on different initial values, which are estimated for a first approximation, and subsequently optimised to achieve higher accuracy through iterations:

- **Radius:** in this part of the model, the radius is the radius of the inner kiln, where the bed of solids and non-condensable gases are contained.
- **Initial and final filling degree:** the filling degree is the fraction of cross-sectional area occupied by the bed of solids, the same concept as used by Fantozzi et al. [2]. The filling degree evolves along the reactor, and the initial and final values are different.

#### 3.1 Bed of solids behaviour

Operations which involve solids processing are not easy to model. Each type of solid has many characteristics that make it unique (such as density or repose angle, among others), and for this reason, there is no single way to treat all solids. Analyses can define up to 32 variables to study the solid and its flow [3], with different significance. Some of the most common are the size, shape, density or thickness of particle.

In the case of the bed of solids in a rotary kiln, there are several aspects to consider. The solids should flow smoothly, like a liquid would do and only in one direction [4]. The movement of solids is not entirely unpredictable but is subject to numerous different equations and restrictions. For instance, one of the first parameters to calculate is the length of the reactor, because as the solids move forward, the height of the solids slowly decreases.

Besides these considerations observed at macro-scale, the heat transfer can be enhanced by specific parameters of the bed of solids like rotational speed or radius, in a similar way to a fluidised bed reactor when the gas flow is high enough to reach the minimum fluidization velocity [5]. In the case of a rotary kiln, the movement of the solids is more restricted, leading to different behaviours known as *motions* [6].

##### 3.1.1 The motion of the bed of solids

The rotary kiln has two dispersion mechanisms. The first is in an axial direction, which is usually determined by an axial mixing coefficient, which is considered negligible in this study similar to other examples in literature [2, 7, 8], and the transverse direction. The axial component helps with the

overall convection and the movement of the bed of solids along the reactor, making the solids move forward. The transverse component acts at micro-scale, describing the interaction between the particles. The axial coefficient mainly affects the residence time and can be calculated very accurately [6, 9]. The transverse term affects other processes such as material mixing, the heat transfer and the reaction rate. Simultaneously, all these processes are interconnected; the mixing affects the heterogeneous composition of the bed of solids, which impacts the heat transfer and its efficiency, but at the same time, may create temperature gradients. The same principle can be applied to physical and chemical reactions [6, 9].

*Assumption 1: There is no axial mixing in this study*

The term motion is used to classify the bed of solids behaviour within the reactor. There is not a proper definition in the literature, but it can be described as the behaviour of the bed of solids under certain conditions. Motion is influenced by the radius, the rotational speed, the height of the bed of solids, the feeding rate [10], the filling degree, and the repose angle. These parameters then depend on many parameters such as moisture content, bulk density, fragility or material consistency [11].

### 3.1.1.1 Parameters to determine the motion of the bed of solids

One of the first documents where the motion of a bed of solids was described was on Henein (1980) [12]. There are three main parameters to define the motion of the bed of solids: Fill ratio, Froude number and the minimum shear wedge. These parameters are the same as those used in more recent papers [2, 9, 13, 14], with different names: Filling degree, Froude number and wall friction coefficient.

The filling degree [ $f$ ] represents the portion of the reactor that is filled with solids. This fraction can consider the amount of solids in relation of the volume of the reactor, or it can be defined as a fraction of the cross-sectional area. Herz et al. [14] use the volumetric fraction for the filling degree. In contrast to that, Mellmann [9], Fantozzi et al. [2] and Boateng [6] use the definition of the cross-sectional area. For this study, the fraction of the cross-sectional area filled with solids will be used. The main reason is that this is the more common terminology used within the literature, but because it seems more reasonable to analyse the cross-sectional area for the motion of the solid due to the filling degree variation in the reactor.

The dimensionless number Froude (Equation 3.1) represents a balance between the centrifugal, inertial, and the gravitational forces [12, 15]. It is used to specify the rotational speed in rotary kilns [9]. At an equal fraction of critical speed or peripheral critical speed, the bed behaviour would be expected to be equal. This feature makes it an essential element for the scale-up of rotating reactors [12]. In the drying industry, it is common to reach values within the range  $5 \times 10^{-4}$  and  $2 \times 10^{-2}$  although sometimes higher values such as  $6 \times 10^{-2}$  are achieved. It is a method to control the residence time, which decreases when the Froude number increases, following a power trend [15]. It is calculated from the rotational speed ( $\omega$ ), gravity ( $g$ ) and the radius of the kiln ( $R$ ).

$$Fr = \frac{\omega^2 \left[ \frac{rad}{s} \right]^2 \cdot R[m]}{g \left[ \frac{m}{s^2} \right]}$$

Equation 3.1: Froude number

The wall friction coefficient [ $\mu_w$ ] is essential to consider that the solids partially adhere to the wall, which helps to move the bed. Consequently, the wall friction needs a lower value than the critical value of the wall itself to move forward [2, 9]. Typically, refractory materials have enough roughness

to prevent slipping of the bed of solids [9]. The friction is caused by gravity and centrifugal force and is measured with the momentum of the particle. According to Mellmann [9] and Fantozzi et al. [2], the filling degree, the Froude number, the height of the bed of solids, the radius of the reactor and the dynamic angle of repose of the feedstock influences this result.

One of the assumptions of the model is a higher wall friction coefficient than the critical wall friction coefficient  $[\mu_{w,c}]$ , due to the impossibility of measuring the materials experimentally and the positive results in the literature with the characterisation of the feedstocks used within this project [2].

*Assumption 2: The wall friction coefficient is higher than the critical wall friction coefficient, and a portion of the bed of solids adheres to the wall*

### 3.1.1.2 Classification of motions of the bed of solids

In the literature, there are six different types of motions, represented in Figure 3.1, adapted from [6].

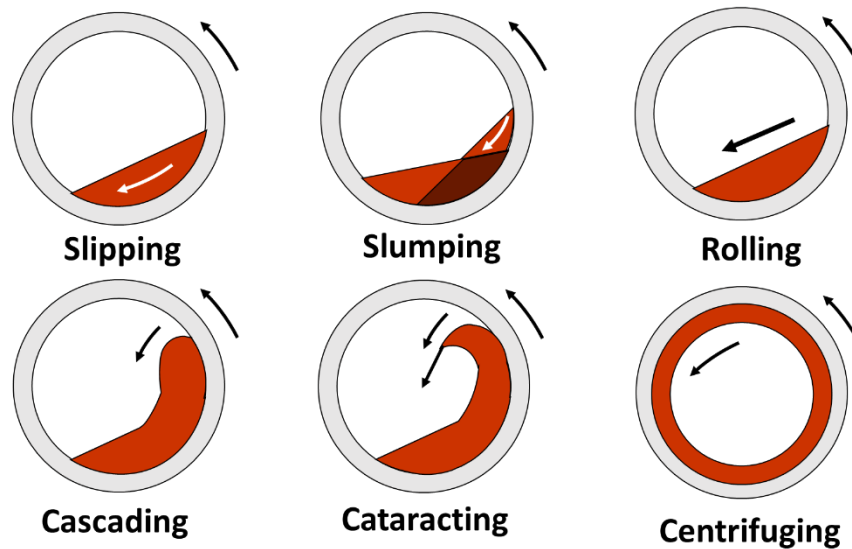


Figure 3.1: Transverse motions for the bed of solids, adapted from [6]

The classification into six different motions is used by Boateng [6] and Henein [12] from lower to higher rotational speed. Mellmann [9] defined a new motion between slipping and slumping and grouped all seven motions within three categories (slipping, cascading and cataracting). There is no apparent use for slipping and centrifuging in industry and cataracting is often used for ball milling. Slumping, rolling and cascading motion is used for rotary dryers and coolers, rotary reactors and mixing equipment.

**Slipping motion** takes place when the solids move with the bed until reaching an inclination similar to the repose angle when it slips against the cylinder wall and moves to lower repose angle. This process is repeated like the oscillatory movement of a pendulum, with a certain frequency and amplitude. The bed rotates with the reactor wall and slips when the maximum inclination is reached [12]. Ronco [16] suggested that during slipping motion, the solids rise at a slower speed than the rotational speed, due to the solids acting as bearings between the bed and the wall itself, and the solids move slowly down when they reach the upper part. This process is transient until it reaches the adequate upper and lower extremities when the process becomes stationary. The restrictions for slipping motion are [9]:

$$0 < Fr < 10^{-4} \quad f < 0.1 \quad \mu_w < \mu_{w,c}$$

During **slumping motion**, the reactor rotates at a low speed with little relative motion between the solids and the wall. The inclination of the bed increases until it reaches the static angle of repose, when a portion of the solids detaches from the bulk and falls from the cylinder wall, slumping towards the lower part of the bed of solids. This process repeats until the angle between the solids at the bottom, and the top reaches an equilibrium, called the shear angle, which usually has a value of 12-15° at a rotational speed of 1-2 rpm [12]. When moving in the same direction as the wall, these solids have a fixed circular trajectory whose centre is the axis of rotation of the cylinder so, consequently, no mixing takes place in the bed as the inclination increases. The solids change the circular trajectory position when slumping, and there is some mixing, but it is negligible [17]. The motion is achieved through the following criteria [9]:

$$10^{-5} < Fr < 10^{-3} \quad f < 0.1 \quad \mu_w > \mu_{w,c}$$

**Rolling motion** appears at higher rotational velocities. The main feature is a continuous movement of a layer of solids on the surface of the bed of solids, fed with solids from the bed which reach the upper part supported by the rotation of the cylinder. The rest of the particles remain below the moving layer. All particles from the bed are continuously moving in fixed trajectories. The bed has a constant angle of inclination with an apparently flat surface [12]. To obtain this motion, the conditions to be accomplished are [9]:

$$10^{-4} < Fr < 10^{-2} \quad f > 0.1 \quad \mu_w > \mu_{w,c}$$

Increasing the rotational speed from the rolling motion produces a **cascading motion**. The solids are dragged slightly by the wall, increasing the maximum height achieved and the equilibrium angle. The trajectories of the particles are still fixed, but the solid surface is not flat. Some studies [12] give slightly different descriptions of rolling and cascading motions. While within the rolling motion, the bed has a fixed shape, cascading is more difficult to describe. If the criteria are analysed, there is some overlap in the Froude number within the range  $[10^{-2}-10^{-3}]$ , so it is advised that the behaviour is very similar:

$$10^{-3} < Fr < 10^{-1} \quad f > 0.1 \quad \mu_w > \mu_{w,c}$$

**Cataracting motion** occurs when the rotational speed increases more. The particles reach a greater height than before and a higher velocity. The particle then separates from the bed of solids and falls to the bottom of the reactor. To obtain this motion, the conditions to achieve are [9]:

$$0.1 < Fr < 1 \quad f > 0.1 \quad \mu_w > \mu_{w,c}$$

The last motion is **centrifuging motion**, where the velocity is so high that the wall always drags the particles, so the centrifugal force is larger than the weight of the bed of solids, so it does not fall. The particle reaches the path where its trajectory is the same as the wall of the cylinder. The particles only move in circular fixed trajectories with the same centre as the reactor. It is the only motion which requires a minimum filling degree of 0.2 because the bed of solids covers the whole wall. The criteria to define this motion is [9]:

$$1 \leq Fr \quad f > 0.2 \quad \mu_w > \mu_{w,c}$$

All the conditions for the types of motion are summarised in Table 3.1:



Table 3.1: Conditions for each motion of the bed of solids

|              | Fr[-]                              | f[-] | $\mu_{w,c}$ [-] |
|--------------|------------------------------------|------|-----------------|
| Slipping     | 0-10 <sup>-4</sup>                 | <0.1 | < $\mu_{w,c}$   |
| Slumping     | 10 <sup>-5</sup> -10 <sup>-3</sup> | <0.1 | > $\mu_{w,c}$   |
| Rolling      | 10 <sup>-4</sup> -10 <sup>-2</sup> | >0.1 | > $\mu_{w,c}$   |
| Cascading    | 10 <sup>-3</sup> -10 <sup>-1</sup> | >0.1 | > $\mu_{w,c}$   |
| Cataracting  | 0.1-1                              | >0.1 | > $\mu_{w,c}$   |
| Centrifuging | ≤1                                 | >0.2 | > $\mu_{w,c}$   |

### 3.1.1.3 The target bed of solids motion

To define the target motion for the bed of solids submodel, it is necessary to understand its role within the model. The motion can cause beneficial temperature gradients within the bed, and maintain constant properties of the solids. Another essential aspect to consider is the portion of the wall that is covered by the solids as this is where heat transfer occurs in indirectly heated rotary kilns.

Slipping motion is barely used in industry because the solids have a very narrow movement range and mostly remain in the same place, with a lack of mixing. In slumping motion, the material is not homogeneous, plus there is not a clear trajectory for the solids to follow. Within the literature, rolling motion is the most widely used [2, 9, 15] as it makes the material more homogeneous due to the continuous movement and mixing while covering a significant portion of the wall. Cascading differs slightly from rolling with inevitable overlap, and it is characterised by further drag of the solids by the wall and a higher portion of the wall covered without solids showering over the bed. The shape of the bed of solids in cascading motion is not straight, and many assumptions should be made for the calculation of the contact areas.

From the drawings in literature [6, 9] and Figure 3.1, cascading motion covers at least half of the wall surface, with surfaces not fully defined and some particles jumping from the solids, which makes the material more homogeneous because it is continuously mixing. This motion is not perfect, and one drawback is that these particles can potentially crush the feedstock within the bed of solids. Finally, the centrifuging motion covers the whole wall and would be the best choice if this was the only criterion. The particle always remains in the same place, and circular layers are created, causing temperature and property gradients, which can produce a heterogeneous product.

According to this analysis, the most feasible motion to study within the model is **rolling motion**, which has a balance between mixing, with a portion of the wall covered and maintaining the solid bulk physical properties. Additionally, it is the method recommended among literature within the drying industry and for materials processing [6, 9, 13, 15]. To deal with the range where rolling motion is found, the Froude number value will be taken as constant with a value of 10<sup>-3</sup>, as the logarithmic midpoint of the limits.

## 3.2 Length of the reactor

As described in the Contact areas section (3.3) and previously in the description of the bed of solids (3.1.1), two of the parameters to describe the solids in the rotary kiln are the initial and the final

filling degree, which has limits for the different motions. This filling degree (and consequently its height) does not develop arbitrarily for the bed of solids, and there are equations to model it.

Babler et al. [18] use the Saeman model [19] to describe the flow of solids inside the reactor. To apply the model, the reactor should operate with a rolling motion and granular flow of the solid. Granular flow is characterised by two-phase flow, with the particles and interstitial fluid. It is associated with the deformation of bulk solids such as coal, grains, powders or sand, defining its movement through fluid mechanics, plasticity theory, soil mechanics and rheology [6]. These aspects are considered in the Saeman model where the solids rotate with the drum, and granular solids occur on the surface. It is, at first sight, a simple expression but it is capable of describing the solid flow, even with particles with an irregular shape, rough surfaces or cohesive powdery particles. There are two main assumptions for this model to work; the rolling motion of the bed of solids and a constant volumetric flow rate along the kiln axis. This last assumption is more complicated because of particle shrinkage. If we consider that shrinkage occurs perpendicular to the biomass fibres, the volumetric flow variation is less significant. Equation 3.2 is the Saeman's model which describes the bed height along the kiln axis.

$$\frac{dH[m]}{dz[m]} = -\frac{3 \cdot \tan \theta [rads]}{4 \cdot \pi \cdot \omega [rad/s]} \cdot Q \left[ \frac{m^3}{s} \right] \cdot [R^2[m] - (R[m] - H[m])^2]^{-\frac{3}{2}} + \frac{\tan \beta [rads]}{\cos \theta [rads]}$$

Equation 3.2: Saeman's model

If Equation 3.2 is rearranged to give the height on one side and the variation of length on the other, Equation 3.3 can be used to calculate the length of the bed of solids when the initial and final filling degree (and consequently height) of the bed of solids are known.

$$\int_0^{Length} dz = \int_{H_i}^{H_f} \frac{dH}{-\frac{3 \cdot \tan \theta}{4 \cdot \pi \cdot \omega} \cdot Q \cdot [R^2 - (R - H)^2]^{-\frac{3}{2}} + \frac{\tan \beta}{\cos \theta}}$$

Equation 3.3: re-arranged Saeman's model equation

The right side of the equation is not a direct integral that can be solved, so an approximation is used to estimate the value. Matlab software was used to solve the integral at the beginning of the process and for the Sensitivity Analysis (3.2.1). Since the model is configured in Excel, it needs automation to work by itself and be able to adjust and calculate parameters automatically, including the reactor length.

There are three main approximation methods found in the literature: Midpoint, Trapezoidal Rule and Simpson's Rule [20-23]. For the following methods,  $b$  and  $a$  represent limits between which the integral of function  $f(x)$  is completed. The letter  $n$  stands for the number of steps by which the function is divided, and the letter  $i$  is the corresponding step number. The following equations are the tools employed by the three studied procedures.

$$\Delta x = \frac{b - a}{n} \qquad x_i = a + i \cdot \Delta x \qquad \bar{x}_i = \frac{1}{2} \cdot (x_{i-1} + x_i)$$

Equation 3.4: Auxiliary equations for the integration methods

- **Midpoint Rule:** this method uses the Riemann sum to calculate the value of the integral by calculating its value on each of  $n$  midpoints and multiplying its sum by the variation of the variable. The equation of this method is Equation 3.5.

$$\int_a^b f(x) \cdot dx \approx \sum_{i=1}^n f(\bar{x}_i) \cdot \Delta x = \Delta x \cdot [f(\bar{x}_1) + f(\bar{x}_2) + \dots + f(\bar{x}_{n-1}) + f(\bar{x}_n)]$$

Equation 3.5: Midpoint Rule expression

- **Trapezoidal Rule:** the method bases its calculation on the analogy of the area under the curve. It calculates the area of  $n$  trapezoids under the curve; the higher the number of trapezoids, the more accurate the model. Equation 3.6 shows the steps to approximate the value of the integral with this method.

$$\int_a^b f(x) \cdot dx \approx \frac{\Delta x}{2} \cdot [f(x_0) + 2 \cdot f(x_1) + 2 \cdot f(x_2) + \dots + 2 \cdot f(x_{n-2}) + 2 \cdot f(x_{n-1}) + f(x_n)]$$

Equation 3.6: Calculation method by the Trapezoidal Rule

- **Simpson's Rule:** similar to the trapezoidal rule but using parabolas instead of trapezoids to approximate the function. The function changes slightly as shown in Equation 3.7

$$\int_a^b f(x) \cdot dx \approx \frac{\Delta x}{3} \cdot [f(x_0) + 4 \cdot f(x_1) + 2 \cdot f(x_2) + \dots + 2 \cdot f(x_{n-2}) + 4 \cdot f(x_{n-1}) + f(x_n)]$$

Equation 3.7: Simpson's Rule

The three methods were initially applied to a 10-step procedure. The higher the number of steps, the more accurate the calculation but, the more challenging to implement and the more computer processing power required. The idea was to study how the number of steps affected the calculation of the integral and how significant was the difference between methods and between the number of steps employed, to find the most suitable way to calculate the integral.

Applying the three methods (Equation 3.5, Equation 3.6 and Equation 3.7) with ten steps, the variation in the results is lower than 5 mm over more than 25 m of reactor length, which was the final result for the given conditions. In statistical terms, the standard deviation was slightly higher than 0.8 mm or, as a percentage, 0.003%. The number of steps was doubled to calculate the integral and study the impact of the number of steps in more detail. The results did not vary significantly with this increment of steps. The absolute difference between the results using 10 and 20 steps was lower than  $5 \times 10^{-4}$  m, which in percentage terms is 0.0016%. Simultaneously, the standard deviation among the methods is 0.2 mm or 0.0008%. Due to the small variability in the results from 10 to 20 steps, further study was not considered. An average between the three methods is an accurate solution for the reactor length when using either 10 or 20 steps. The results are shown in Table 3.2, where  $n$  is the number of steps employed, and the length is shown in meters.

Table 3.2: Approximation of the integral in 10 and 20 steps with three different methods

|           | n=10     | n=20     |
|-----------|----------|----------|
| Midpoint  | 26.76669 | 26.76719 |
| Trapezoid | 26.76868 | 26.76768 |
| Simpson   | 26.76736 | 26.76735 |
| Average   | 26.76758 | 26.76741 |

### 3.2.1 Sensitivity analysis

The formula to determine the length of the bed of solids is complex, and it can result in non-valid results such as negative values. A sensitivity analysis was conducted to assess how the different parameters affect the length. The sensitivity analysis was performed with a set of carefully defined values to deduce what parameters are more influential.

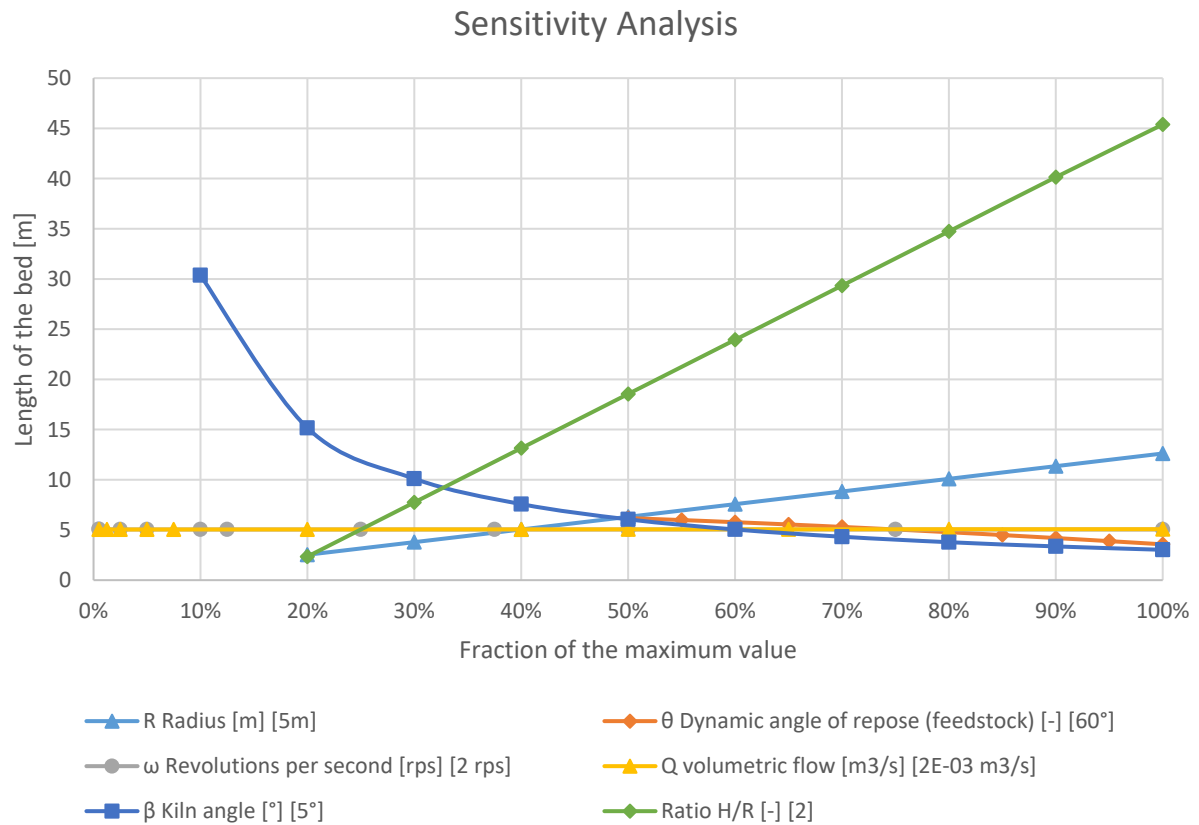


Figure 3.2: Sensitivity Analysis of the length of the bed of solids

Figure 3.2 shows the results of the sensitivity analysis. The Y-axis is the length of the bed of solids when Seaman's model is applied (Equation 3.2), on the X-axis, the normalised value of the parameters is represented. It is the percentage of the maximum value of each parameter, and this maximum value is shown in the legend within square brackets. For instance, the maximum value for the radius is 5 meters, and the first point at 20% corresponds to a value of 1 m radius (20% of 5m).

The ratio H/R is equivalent to the filling degree, and only the initial value was changed; the final filling degree was kept to 0.1 to stay at the limit of rolling motion and is equivalent to a ratio 0.313. The standard values for the experiments are shown in Table 3.3.

Table 3.3: Standard values for the sensitivity analysis

| Radius     | Dynamic repose angle | Rotational Speed | Solids volumetric flow |
|------------|----------------------|------------------|------------------------|
| [m]        | [°]                  | [rps]            | [m <sup>3</sup> /s]    |
| 2          | 45                   | 0.25             | 10 <sup>-4</sup>       |
| Kiln Angle | Initial ratio H/R    | Final ration H/R |                        |
| [°]        | [-]                  | [-]              |                        |
| 3          | 0.5                  | 0.313            |                        |

From Figure 3.2, the significant influence of the initial filling degree, the kiln angle and the radius is observed. The volumetric flow and the rotational speed do not have a strong influence on the length of the bed of solids, which only changes by 1%. The initial filling degree profoundly affects the length, because a very high initial filling degree will require more length to achieve the final value of 10%. Conversely, the kiln angle influences in the opposite way, the lower the angle, the longer the reactor; the solids are less affected by gravity to fall with a lower slope and need more length to reach a lower filling degree. The fact that a higher angle of repose decreases the length is due to the angle formed by the bed of solids, plus the sharp fall and slope of the solids. Finally, with a larger radius, the reactor is more extended because the variation of the height is broader, and a more extended segment is needed for the fall.

### 3.3 Contact areas

The main outputs of the bed of solids model, besides the length of the bed (3.2) and the residence time of the solids (3.4), are the three contact areas within the system:

- Gases inside the reactor- Bed of solids
- Gases inside the reactor- Reactor wall
- Bed of solids- Reactor wall

The final filling degree of the bed of solids has a lower limit of 10% to maintain rolling motion (3.1.1.3). According to Boateng [6], the initial filling degree should not be too high to achieve more heat transfer through radiation (Section 4.4). With this in mind, and due to its small influence on final conversion (Section 7.5.1), the initial filling degree is established as 15%.

With the repose angle of the feedstock (Section 6.1.2), solids input, filling degrees, kiln angle and the initial length, the areas can be calculated. To begin, the height and the angle of the bed of solids (Figure 3.3) is needed. The area of the bed of solids is the area of the circular sector (Equation 3.10) when the area of the triangle (Equation 3.9) is subtracted (Equation 3.11). This is easily related to the filling degree, which is the cross-sectional area occupied by the bed of solids [2, 6] defined by Equation 3.12.

Using the definition of cosine, we can calculate the angle  $\varphi$  (Equation 3.8), which represents the angle of the bed from the axis of the inner kiln, and the area of the white triangle as shown in Equation 3.9. The area of the circular sector (white triangle + bed of solids) is calculated using Equation 3.10.

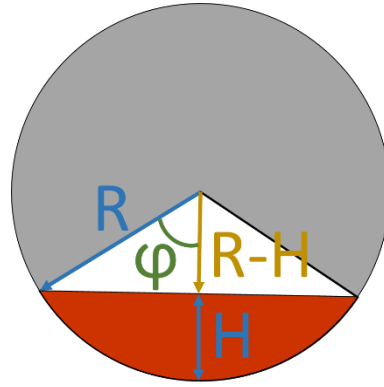


Figure 3.3: Cross-sectional area of the reactor

$$\cos \varphi = \frac{R - H}{R} = 1 - \frac{H}{R} \Rightarrow \varphi = \arccos \left( 1 - \frac{H}{R} \right)$$

Equation 3.8: calculation of angle  $\varphi$

$$A_{\text{white triangle}} = 2 \cdot \frac{\text{base} \cdot \text{height}}{2} = R \cdot (R - H) \cdot \sin(\varphi)$$

Equation 3.9: Area of the triangle

$$A_{\text{circular sector}} = \pi \cdot R^2 \cdot \frac{2 \cdot \varphi}{360}$$

Equation 3.10: Area of the circular sector

$$A_{\text{bed of solids}} = A_{\text{circular sector}} - A_{\text{triangle}} = \pi \cdot R^2 \cdot \frac{2 \cdot \varphi}{360} - R \cdot (R - H) \cdot \sin(\varphi)$$

Equation 3.11: Area of the bed of solids

$$\begin{aligned} f = \frac{A_{\text{bed of solids}}}{A_{\text{reactor}}} &= \frac{\pi \cdot R^2 \cdot \frac{2 \cdot \varphi}{360} - R \cdot (R - H) \cdot \sin(\varphi)}{\pi \cdot R^2} \\ &= \frac{2 \cdot \arccos \left( 1 - \frac{H}{R} \right)}{360} - \frac{\left( 1 - \frac{H}{R} \right) \cdot \sin \left[ \arccos \left( 1 - \frac{H}{R} \right) \right]}{\pi} \end{aligned}$$

Equation 3.12: Definition of filling degree

This equation shows that the filling degree only depends on the factor  $\left( 1 - \frac{H}{R} \right)$ . The different factors can be calculated for each filling degree. It is not a direct correlation, but for each filling degree, the ratio H/R is adjusted using the solver tool in Microsoft Excel. The ratio H/R is plotted in Figure 3.4 against each filling degree (with a 5% increase) to show the correlation and calculate the height as a function of filling degree.

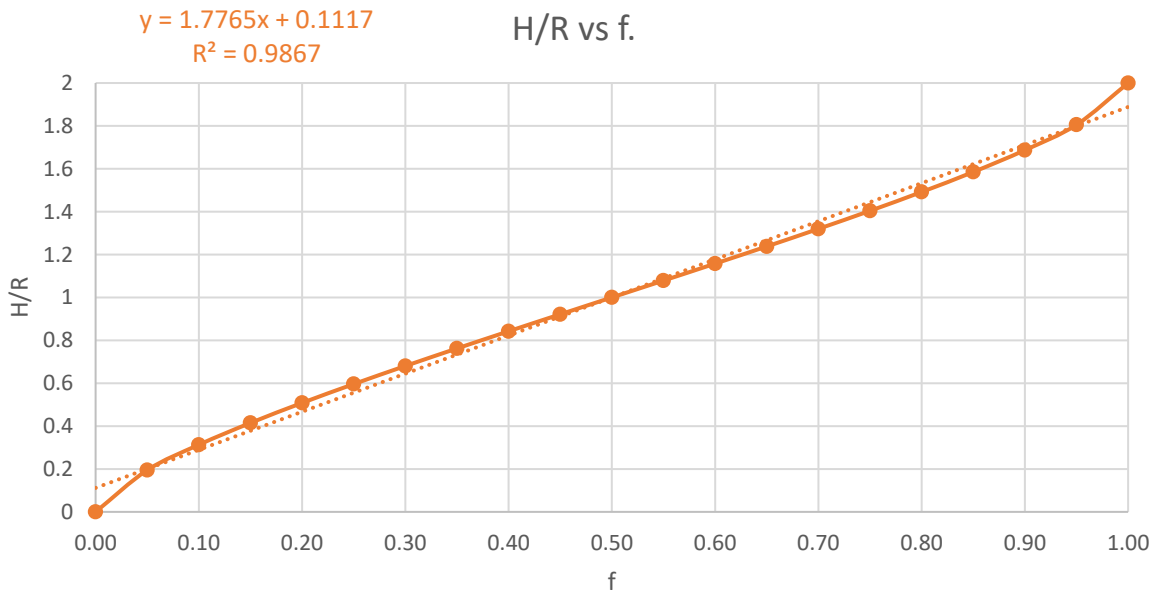


Figure 3.4: H/R ratio vs filling degree

The graph shows a clear linear relationship between the ratio H/R and the filling degree. The Y-axis has a maximum value of 2 because when the reactor is filled, the height is equivalent to the diameter. The correlation can be easily adjusted to a linear expression (Equation 3.13) with a regression higher than 98%. In a more detailed study evaluating the filling degree every 5% variation, the equation within the range [5%-95%] has a regression of 99.67% (compared to the 98.67% for the whole range) and is shown in Equation 3.13 (range 5-95%).

$$\frac{H}{R} = 1.698 \cdot f + 0.151$$

Equation 3.13: ratio H/R as a function of the filling degree

The height can now be easily calculated from the filling degree and the radius. Another critical and challenging value to derive is the length of the line that separates the bed of solids and the gases. The whole surface which contacts the solids and the gas is called “freeboard”. It is coloured in orange in Figure 3.5, but first, a method to calculate the freeboard line (in yellow) should be obtained for each position of the reactor. The green lines are the initial and final freeboard. The term “modified length” refers to the length when the inclination of the bed of solids is taken into account, it is the  $Length^*$  term in Figure 3.6 and is the blue line in Figure 3.5. It exists because the initial and final heights of the bed of solids are different, if the height were constant along the reactor,  $Length^*$  would be equivalent to Length.

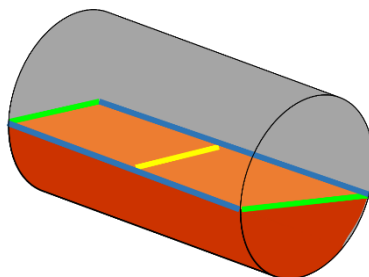


Figure 3.5: Bed of solids scheme inside the reactor

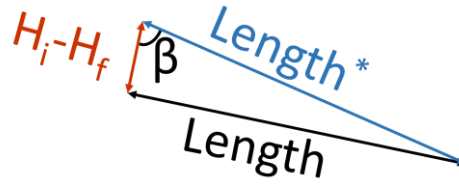


Figure 3.6: Relation height, length and modified length

The yellow line for the freeboard is calculated with Equation 3.14. The angle  $\beta$  represents the angle of the bed of solids, and there are different ways to calculate it with Equation 3.15, Equation 3.16 and Equation 3.17.

$$\text{freeboard line} = 2 \cdot R \cdot \text{sen}(\varphi)$$

Equation 3.14: Equation to calculate the freeboard line

$$\beta = \arctan\left(\frac{\text{Length}}{H_i - H_f}\right)$$

Equation 3.15: angle with arctangent

$$\beta = \arcsin\left(\frac{\text{Length}}{\text{Length}^*}\right)$$

Equation 3.16: angle with arcsine

$$\text{Length}^* = \sqrt{\text{Length}^2 + (H_i - H_f)^2}$$

Equation 3.17: angle with Pythagoras theorem

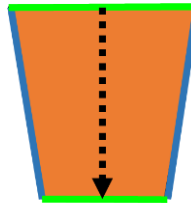


Figure 3.7: Gas-solid area shape (Top view)

Figure 3.7 shows the top view for the bed of solids in the reactor when the initial filling degree is bigger than the final value, and both are lower than 0.5. The dotted arrow represents the direction of the solids flow and has the value of  $\text{Length}^*$ . It is a representation of the bed of solids inside the kiln with typical filling degrees having a value around 0.1 and 0.2. This area is calculated with Equation 3.18, whose terms are previously defined and calculated. This formula is similar to the area of a trapezoid because it is the most similar shape when it comes to the gas-solid area.

$$\text{Area}_{\text{gas-solid}} = \left(\frac{\text{free board line}_{\text{initial}} + \text{free board line}_{\text{final}}}{2}\right) \cdot \text{Length}^*$$

Equation 3.18: Calculation of Gas-Solid area

A more straightforward method is used to calculate the contact areas wall-gas and wall-solids. First, it is necessary to calculate the portion of the wall covered by the solids (brown surface in Figure 3.8). The length of the wall covered by the bed of solids at each position of the reactor varies with the filling degree, and it affects the angle  $\varphi$ . This length is calculated with Equation 3.19. If the variation of height is linear, the contact area between the bed of solids and the wall is calculated with Equation 3.20.



$$\text{Wall covered length} = 2 \cdot \pi \cdot R \cdot \frac{2 \cdot \varphi}{360}$$

Equation 3.19: Length of contact bed of solids-wall

$$\text{Area}_{\text{wall-bed of solids}} = \frac{(\text{Wall covered length}_{\text{initial}} + \text{Wall covered length}_{\text{final}})}{2} \cdot \text{Length}$$

Equation 3.20: Area wall-bed of solids

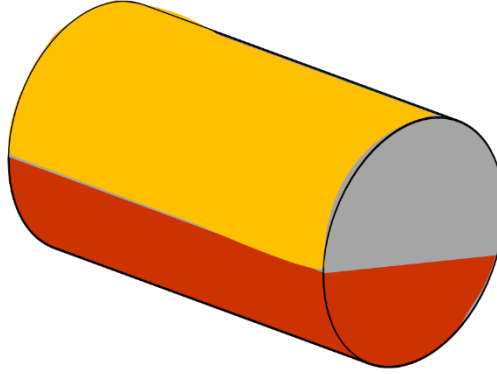


Figure 3.8: Contact areas in the kiln

The last area to calculate is the area between the wall and the gas (coloured in yellow in Figure 3.8). It is calculated by subtracting the area of the solids from the total area of the reactor (Equation 3.21).

$$\text{Area}_{\text{wall-gas}} = 2 \cdot \pi \cdot R \cdot \text{Length} - \text{Area}_{\text{wall-bed of solids}}$$

Equation 3.21: Area wall-gas

### 3.3.1 The special case of conductive heat flow

Within the heat transfer model, the conductive heat transfer (Section 4.2) is used to calculate the term  $\int_{x_1}^{x_2} \frac{dx}{A(x)}$  which appears as the denominator in Equation 4.3, and each area depends on the particular system studied. Since this term is related to the areas, it is calculated within the bed of solids model. It is found that the area is directly proportional to the radius and the length, so the area term was divided by  $R \cdot L$ . The term  $\frac{A}{R \cdot L}$  is plotted against each filling degree, and the result is shown in Figure 3.9.

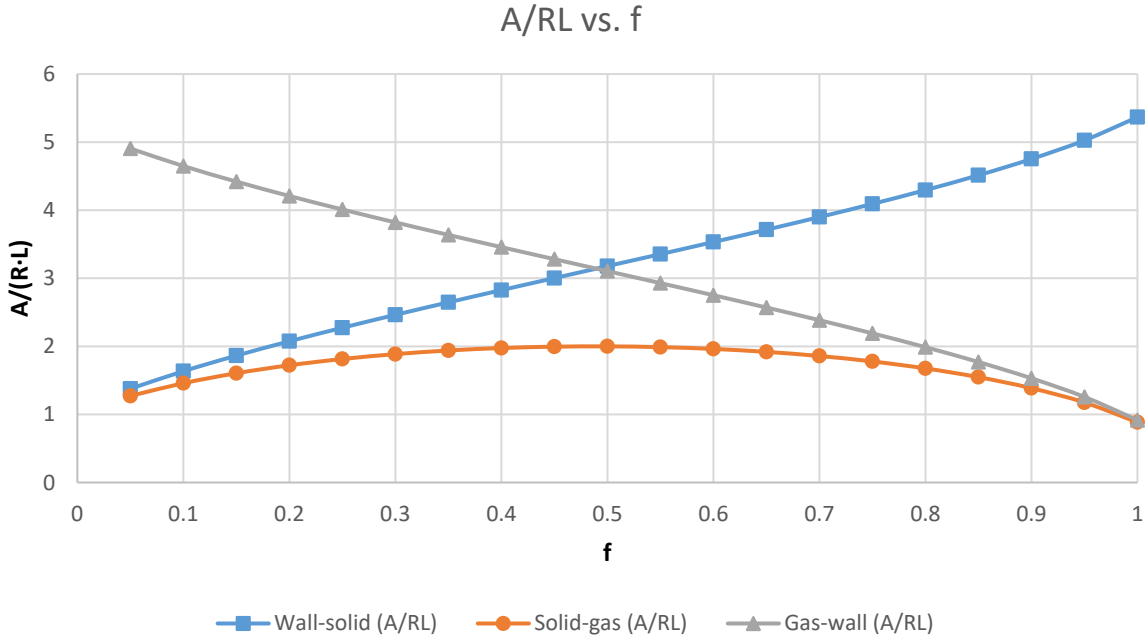


Figure 3.9: Area/ (Radius x Length) vs Filling degree

The term  $\frac{A}{R \cdot L}$  is directly correlated to the filling degree with a linear equation with regression values higher than 99% for the interaction wall-bed of solids (Equation 3.22) and wall-gas (Equation 3.23) with regressions of 99.25% for both. The gas-bed of solids area is represented by a second-degree equation (Equation 3.24).

$$\left(\frac{A}{R \cdot L}\right)_{W-S} = 3.91 \cdot f + 1.24$$

$$\left(\frac{A}{R \cdot L}\right)_{W-G} = -3.91 \cdot f + 5.04$$

Equation 3.22: Wall-solid area as a function of the filling degree    Equation 3.23: Wall-gas area as a function of the filling degree

$$\left(\frac{A}{R \cdot L}\right)_{S-G} = -3.95 \cdot f^2 + 3.83 \cdot f + 1.10$$

Equation 3.24: Solid-Gas area as a function of the filling degree

These calculations aim to find a simple way to solve the term  $\int_{x_1}^{x_2} \frac{dx}{A(x)}$  for conduction, required to calculate the conductive heat flow. There are two different cases: from the wall towards the gas and the bed of solids, based on the radius, and contact between the bed of solids and gas, which ultimately depends on height.

The heat transferred from the wall to the bed and gases inside the reactor is dependent on the portion of the wall covered by solids, which varies with the filling degree and bed height, shown by Figure 3.4 and Equation 3.13. The heat flow is transported radially from the walls, and the direction is towards the centre of the reactor. Since heat is transferred from the wall towards the bed and gases, a good approximation is to make the heat flow dependant on the radius. It is essential to know how much heat is transferred to the surface of the bed of solids, in case there is no temperature driving force or if the heat capacity of the gases is too low. As a result, the expression is integrated between the radius  $[R]$  (as the starting point) and the height of the bed  $[H]$ , all represented by Equation 3.25.

$$\int_R^H \frac{dR}{A_{wall-solids}(R)} = \int_R^H \frac{dR}{(3.91 \cdot f_{av} + 1.24) \cdot L \cdot R} = \frac{\ln\left(\frac{H}{R}\right)}{(3.91 \cdot f_{av} + 1.24) \cdot L}$$

Equation 3.25: integral of the area between wall-bed of solids

For the heat transfer model, the reactor is divided into slices (Section 4.5.1). The filling degree ( $f_{av}$ ) in the equation is the average. Implementing the variation would be very complicated, and the result will not change significantly.

$$\int_R^H \frac{dR}{A_{wall-gas}(R)} = \int_R^H \frac{dR}{2\pi \cdot L \cdot R - (3.91 \cdot f_{av} + 1.24) \cdot L \cdot R} = \frac{\ln\left(\frac{H}{R}\right)}{(2\pi - 3.91 \cdot f_{av} + 1.24) \cdot L}$$

Equation 3.26: integral of the area between wall-gases

For the contact area between the gas and the solids, it is more complicated. Firstly, the area varies with the height of the bed of solids, and it does not correlate to a linear expression but a second-degree equation. The direction is radial but starts with a flat surface as the contact area (freeboard area between the gases inside the reactor and the bed of solids). If Figure 3.10 represents the whole reactor, it is seen how the freeboard surface reduces when the colour changes from the initial state (yellow) to the final (brown).

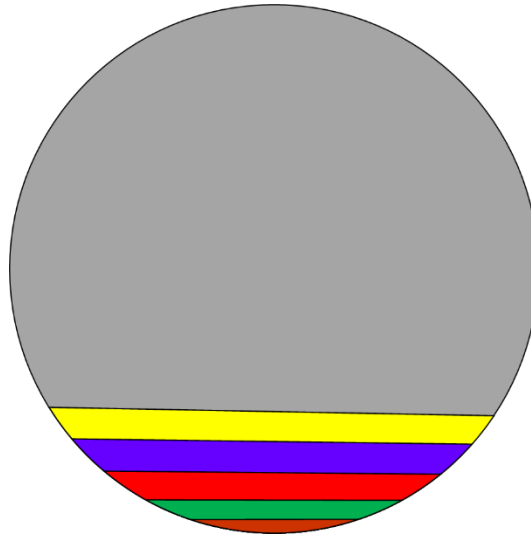


Figure 3.10: variation of freeboard area towards the wall

As a consequence, the calculation method is different despite having the same direction, because the initial shape is different. The use of a second-degree equation for the calculation of the integral would make the process much more complicated. Therefore, another approach was employed. A minimum filling degree of 0.1 is desired (as explained on 3.1.1.3) to maintain a rolling motion within the bed. As a consequence, the initial filling degree is unlikely to be higher than 0.2 [24] to have a significant percentage of heat transferred by radiation, as discussed in [6]. The main issue with the area being described by a second-degree equation as a function of the filling degree is the maximum achieved when the filling degree is 0.5. Instead of using the whole range, the area will be divided into two parts due to its symmetrical behaviour.

The calculation of coefficients (slope and intercept) together with the regression were completed for several ranges. All ranges started at a filling degree of 0.1 up to different limits, varying

from 0.15 to 1. The regression coefficient varied from 100% when the filling degree is up to 0.15 (because it was adjusted by only two points), down to 0.01% when the filling degree is up to 0.9. For the range of the filling degree 0.1-0.4, the regression value was slightly higher than 90%. This range will be used to calculate the areas in the final model. Its corresponding expression which correlates the filling degree with the area is shown in Equation 3.27.

$$\left(\frac{A}{R \cdot L}\right)_{S-G} = 1.70 \cdot f + 1.35$$

Equation 3.27: lineal dependency of the area between the gas and the solids and the filling degree

With this expression, it is possible to obtain the dependence of area on the height of the bed of solids, equalising the filling degree. The letters m and n in Equation 3.28 are the slope and intercept respectively. The subscripts correspond to the expressions related to H (height of the bed of solids from Equation 3.13) and A (area in Equation 3.27). The integral term is solved with Equation 3.29 for calculation of conductive heat flow between the gas inside the reactor and the bed of solids. In Equation 3.29, there are two types of Radius (**R**, R). The **R** in bold are those which appear due to being the limits of the integral. Those not in bold are the radius used to calculate the area and is constant in the integral.

$$\begin{aligned} \frac{A_{g-s}}{R \cdot L} = m_A \cdot f + n_A \rightarrow f = \frac{\frac{A_{g-s}}{R \cdot L} - n_A}{m_A} & \left\{ \begin{aligned} \frac{A_{g-s}}{R \cdot L} - n_A = \frac{H}{R} - n_H \rightarrow \frac{A_{g-s}}{R \cdot L} = \frac{H}{R} - n_H \cdot m_A + n_A \\ \frac{H}{R} = m_H \cdot f + n_H \rightarrow f = \frac{\frac{H}{R} - n_H}{m_H} \end{aligned} \right. \\ \rightarrow A_{g-s} = H \cdot \underbrace{\frac{m_A}{m_H}}_{C_1} \cdot L + \underbrace{\left(n_A - n_H \cdot \frac{m_A}{m_H}\right)}_{C_2} \cdot R \cdot L \rightarrow A = H \cdot C_1 + C_2 \end{aligned}$$

Equation 3.28: Dependency of Area gas-solid on the height

$$\int_H^R \frac{dH}{A_{gas-solids}(H)} = \int_H^R \frac{dH}{H \cdot C_1 + C_2} = \frac{\ln\left(\frac{R \cdot C_1 + C_2}{H \cdot C_1 + C_2}\right)}{C_1} = \frac{\ln\left(\frac{R \cdot \frac{m_A}{m_H} \cdot L + \left(n_A - n_H \cdot \frac{m_A}{m_H}\right) \cdot R \cdot L}{H \cdot \frac{m_A}{m_H} \cdot L + \left(n_A - n_H \cdot \frac{m_A}{m_H}\right) \cdot R \cdot L}\right)}{\frac{m_A}{m_H} \cdot L}$$

Equation 3.29: Integral of the gas-solid area with height

There are some circumstances which should be considered due to the range of filling degrees used. The height employed for the calculation is the average (between the initial and final) for each slice (extensively explained on Section 4.5.1). For each slice, the integral term has to be calculated to find the conductive heat flow. To calculate the integral term, three different scenarios are possible depending on the value of the filling degree:

- When the *initial and final filling degrees are lower than 0.5*, Equation 3.29 is applied.

- When *both filling degrees are greater than 0.5*, Equation 3.30 is applied. There have to be two steps to calculate the integral term. Firstly a term between the radius and the centre of the reactor (with a value of 0). Secondly from the centre of the reactor to the height of the bed of solids. The “height of the gases” is calculated, and this quantity is subtracted to double the term integrated between the radius and the centre. Instead of calculating the integral term for the solids, the approach is calculating the integral term for the whole reactor subtract the corresponding term of the gases to calculate the integral term of the solids.

$$\int_H^R \frac{dH}{A_{gas-solids}(H)} = \int_H^0 \frac{dH}{A_{gas-solids}(H)} + \int_0^R \frac{dH}{A_{gas-solids}(H)} = 2 \cdot \int_0^R \frac{dH}{A_{gas-solids}(H)} - \int_R^{R-H} \frac{dH}{A_{gas-solids}(H)}$$

Equation 3.30: Method employed when the initial and final filling degrees are higher than 0.5

- In the case that the *initial filling degree is greater than 0.5 and the final lower than 0.5*. The filling degree and height of the bed decreases along the length of the reactor. To calculate this scenario, the average value is used between the integral term for the initial height in Equation 3.30 and the final height from Equation 3.29. The result is shown in Equation 3.31.

$$\int_H^R \frac{dH}{A_{gas-solids}(H)} = \frac{\left( \overbrace{\int_{H_i}^0 \frac{dH}{A_{gas-solids}(H)} + \int_0^R \frac{dH}{A_{gas-solids}(H)}}^{H_i} + \overbrace{\int_{H_f}^R \frac{dH}{A_{gas-solids}(H)}}^{H_f} \right)}{2}$$

Equation 3.31: Calculation of integral term for the third scenario

The conductive heat flow in a rotary kiln becomes complex due to the variable area. The difficulty in establishing expressions that explain the variable area correlated to the height of the bed of solids makes the calculation of the conductive heat transfer difficult. These small deviations from reality do not have a significant impact on the model because, as will be shown in Section 7.3.2.1.3, the conductive heat flow only accounts for 1% of the total heat transferred within the rotary kiln.

### 3.4 Solid residence time

The residence time in the reactor is usually calculated by dividing the volume by the solid volumetric flow, as represented in Equation 3.32 [25]. The residence time of the solids is influenced by the angle of the kiln and the speed of rotation. The variation of temperature and composition of the gas varies the physical properties. Subsequently, it affects the residence time of the solids. Some other factors affecting the residence time include the generation of gases within the bed, the flights, the diameter of the kiln, particle size and distribution, and the solids mass flow [12].

$$\tau_R [s] = \frac{V_{bed\ of\ solids}}{\dot{Q}_{bed\ of\ solids}} \left[ \frac{m^3}{m^3/s} \right]$$

Equation 3.32: usual formula to calculate the residence time of reagents in a reactor

Fantozzi et al. [2] studied a term called the Mean Excursion Time (MET), which is defined as the average time a particle needs to pass through the reactor. It would be equivalent to the time that a particle stays in the reactor, which is the residence time. The MET is the method to calculate the residence time within this work and is represented in Equation 3.33.

$$MET [min] = \tau_R = \frac{L[m] \cdot \theta[rad]}{2 \cdot \pi \cdot \left( \omega[rpm] \cdot \frac{1}{2 \cdot \pi} \left[ \frac{rad}{revolutions} \right] \right) \cdot (\tan \alpha + \cos \theta \cdot \tan \beta) \cdot (\cos \beta)^2}$$

Equation 3.33: Mean Excursion Time (MET)

This formula is influenced by the length ( $L$ ), the repose angle of the solids ( $\vartheta$ ), rotational speed ( $\omega$ ), kiln angle ( $\alpha$ ) and the angle of the bed of solids ( $\beta$ ). It is preferred over others, such as that proposed by Boateng [6] because it can be “easily” calculated and the values are consistent. It is simple but accurate enough to be compared to others which require much deeper calculations or oversimplified alternatives such as Equation 3.32.

### 3.5 Voidage and porosity

Within the reactor, the bed of solids is not made of solid raw material. It is a porous bed of solids, whose density is defined as the bulk density. Other scientific fields such as mass transfer are affected by a similar issue when the material is porous. To make the value of the diffusion coefficient more realistic, it is modified with two parameters. Firstly, the tortuosity factor accounts for the path the molecule travels and the varying cross-sections of the pores, and it corrects possible tiny orifices. The second factor is the free cross-section, which is identical to the fractional void volume or voidage. It is defined as the average cross-section not covered by solids in a surface parallel to the face, this direction and the one the material diffusing follows does not necessarily have to match [26, 27]. These two parameters are valid for a porous material. It is required to find other similar parameters to apply to the bed of solids to take account of this as the bed is not a solid block, with no air gaps.

In this thesis, the terms porosity and voidage refer to the bed of solids. It is logical to think that the voidage and porosity will be highly influenced by the particle size because a bed of powdery material such as sand will not be as porous as big packed cubes of sand inside the reactor. To take into account the voidage, a coefficient is established within the model and is implemented in the term for conduction  $\int_{x_1}^{x_2} \frac{dx}{A(x)}$ . Equation 3.34 and Equation 3.35 shows how the coefficient is applied to the systems Gas-Solid and Wall-Solid

$$\int_H^R \frac{dR}{A(R)_{Gas-Solids} \cdot (1 + voidage)}$$

Equation 3.34: Effect of voidage in conductive heat flow for Gas-Solid

$$\int_R^H \frac{dR}{A(R)_{Wall-Solids} \cdot (1 - voidage)}$$

Equation 3.35: Effect of voidage in conductive heat flow for Wall-Solid

In the case of the contact area Gas-Solid, the voidage has a positive effect on the area because the interstitial space between the particles is filled with the gases inside the reactor, increasing the contact surface. For the contact area between the wall and the bed of solids, the voidage coefficient reduces the area in which the solid and the wall are in contact, and conductive heat flow is induced.

Additionally, the voidage could be considered further in the heat transferred by convection from the Gas-Solid interaction, taking into account that gas flows through the bed of solids. However, the bed of solids matrix is very complex and should consider the portion of the gases within the matrix, creating temperature gradients within the gas. There will be a difference in gas velocity for gas travelling through the bed, versus gas travelling through the headspace. To avoid gradients of

temperature and velocity and to simplify the model, voidage is not considered for the convective heat flow.

*Assumption 3: The voidage mainly has an impact on the conductive heat flows where the solid interacts with the gas and the wall. The convective and radiative heat flows are not affected by the voidage.*

### 3.5.1 Shape and particle size

It has been previously mentioned that voidage is highly influenced by the particle size and shape. This section analyses the impact and the methods implemented in the bed of solids model to account for particle shape and size. The model is designed to deal with three different feedstocks with two different shapes: chips (Figure 3.11) and pellets (Figure 3.12).



Figure 3.11: Feedstock in chips shape




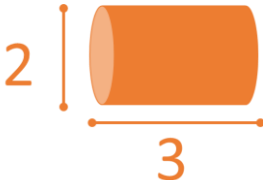
Figure 3.12: Feedstock in pellet shape

The initial approach included a full correlation with particle size and shape with the voidage. The lack of voidage and/or porosity data based on the shape and particle size made this objective too challenging for this study. There is a lack of data in the literature regarding values of voidage and the approximations found by [28] were for tiny cylinders, with even less information about chips.

A voidage estimation included in the heat flow equations, as part of the bed of solids model. This coefficient gains importance for the conductive heat transfer, whose heat flow is around 1% of the total heat transferred. Even if this porosity multiplied the conductive heat transfer, it would not be more significant in the model than 5% (Section 7.3.2.1.3).

Therefore, instead of calculating the voidage for every particle size and shape, a voidage coefficient is associated with each general shape. The value chosen is linked to particle size from the literature, establishing one of the boundary conditions of the model. The values of the voidage coefficients and the size and shape of particles are shown in Table 3.4.

Table 3.4: Voidage coefficients

| Shape [-] | Size [mm]   | Voidage [-] | Source |
|-----------|---|-------------|--------|
| Chips     |  | 57%         | [18]   |
| Pellets   |  | 40%         | [28]   |

*Assumption 4: The particle size of the feedstock is the same as the one from literature sources and is defined by the shape*

### 3.6 Attachment of the flights

The information within this chapter accounts for a single rotary kiln configuration without flights. As described later in Section 6.2, the flights were not successfully designed within this submodel work for a variety of reasons.

If flights were included, the assumption would be that the velocity of the solids affected by the flights is the same as the bed of solids. For the definition of the length of the bed and the areas, a new parameter would be defined. This new parameter would be a dimensionless number which indicates the average portion of solids which is on the flights or showering. This new parameter would have a constant value along the reactor, assuming the same portion of solids is on the flights.

Once defined, it would influence the length of the bed because the volumetric flow would not be identical to the input capacity of biomass. The portion of solids on the flights should be subtracted, as shown in Equation 3.36. Regarding the contact areas, the flights provide extra area for conduction and radiation between the wall and the other components inside the reactor. In addition, the solids showering along the reactor provide extra area for conduction and convection between the gases and the solids. The filling degrees remain unvaried and should not change. Consequently, the methodology could be similar to the one used in this chapter with the variation of the extra areas provided by the flights, which would depend on the flight design, and it is one of the recommendations for future research addressed in Section 11.2.

$$Q_{Bed\ of\ solids} = Q_{Biomass\ input} \cdot (1 - Ratio_{Biomass\ on\ flights-input})$$

Equation 3.36: Volumetric flow for the bed of solids

### 3.7 References

1. Boateng, A.A. and P.V. Barr, *A thermal model for the rotary kiln including heat transfer within the bed*. International Journal of Heat and Mass Transfer, 1995. **39**(10): p. 2131-2147.
2. Fantozzi, F., et al., *Rotary Kiln Slow Pyrolysis for Syngas and Char Production From Biomass and Waste—Part I: Working Envelope of the Reactor*. Vol. 129. 2007. 901-907.
3. *Advanced Particle Analysis*, Microtrac, Editor. 2019, FEECO International.



4. Kunii, D. and T. Chisaki, *2 - Movement of Solids in Rotary Cylinder*, in *Rotary Reactor Engineering*, D. Kunii and T. Chisaki, Editors. 2008, Elsevier: Amsterdam. p. 11-25.
5. Kunii, D. and O. Levenspiel, *Fluidization Engineering* 2nd Edition ed. 1991, Boston: Butterworth-Heinemann.
6. Boateng, A.A., *Rotary kilns: transport phenomena and transport processes*. 2008: Amsterdam ; Boston : Elsevier/Butterworth-Heinemann, ©2008.
7. Funcia-Muguerza, I., *Presentation of CENER*, J. López-Ordovás, Editor. 2018, CENER: CENER, Aoiz, Spain.
8. Maione, R., *Modélisation d'un système de pyrogazéification de la biomasse*. 2017.
9. Mellmann, J., *The transverse motion of solids in rotating cylinders—forms of motion and transition behavior*. *Powder Technology*, 2001. **118**(3): p. 251-270.
10. Le Capitaine, S. and C. Carlson, *Rotary Dryer Flights Increase Efficiency of Heat Transfer*. 2019, FEECO International.
11. *Rotary Dryer Sizing & Design*. 2015, FEECO International.
12. Henein, H., *Bed behaviour in rotary cylinders with applications to rotary kilns*, in *Applied Science, Faculty of Materials Engineering*. 1980, University of British Columbia: Vancouver: University of British Columbia Library.
13. Ngako, S., et al., *Numerical investigation of bed depth height, axial velocity and mean residence time of inert particles in steady state industrial cement rotary kiln: Case of Figuil Plant in Cameroon*. *Powder Technology*, 2015. **271**: p. 221-227.
14. Herz, F., E. Specht, and A. Abdelwahab, *Modeling and Validation of the Siderite Decomposition in a Rotary Kiln*. *Energy Procedia*, 2017. **120**: p. 524-531.
15. Hellou, M., et al., *Theoretical description of the motion of a particle in rotary dryer*. *The Canadian Journal of Chemical Engineering*, 2019. **97**(1): p. 103-114.
16. Ronco, J.J., *Technology of Operations and Processes in the Chemical Industry*. *Química Industrial*, 1960. **6**(1): p. 20-23.
17. Henein, H., J.K. Brimacombe, and A.P. Watkinson, *Experimental-study of transverse bed motion in rotary kilns*. *Metallurgical Transactions B-Process Metallurgy*, 1983. **14**(2): p. 191-205.
18. Babler, M.U., et al., *Modelling and pilot plant runs of slow biomass pyrolysis in a rotary kiln*. *Applied Energy*, 2017. **207**: p. 123-133.
19. Saeman, W.C., *Passage of Solid through Rotary Kiln*. *Chemical Engineering Progress*, 1951. **47**(10): p. 508-514.
20. Burden, R.L., J.D. Faires, and A.M. Burden, *Numerical analysis*. Tenth edition. ed. 2016: Cengage Learning.
21. Rao, G.S., *Numerical analysis*. Rev. 3rd ed. ed. 2006: New Age International (P) Limited, Publishers.
22. Iyengar, S.R.K. and R.K. Jain, *Numerical methods*. 2009: New Age International (P) Limited, Publishers.
23. Jain, M.K., *Numerical methods: problems and solutions*. 2nd ed. ed. 2004: New Age International (P) Limited, Publishers.
24. Boateng, A.A., *Additional information for the design of rotary kilns*, J. López-Ordovás, Editor. 2019.
25. Santamaría Ramiro, J.M., et al., *Ingeniería de reactores*. *Ciencias Químicas, Ingeniería Química* 3. 2002, Madrid: Síntesis, D. L.
26. Sherwood, T.K., R.L. Pigford, and C.R. Wilke, *Mass transfer*. (3rd ed.) / (by) Thomas K. Sherwood, Robert L. Pigford, Charles R. Wilke. ed. McGraw-Hill Chemical Engineering Series. 1976: McGraw-Hill.
27. Hines, A.L. and R.N. Maddox, *Mass transfer : fundamentals and applications*. 1984: Prentice-Hall.

28. Rolland, M., et al., *Predicting average void fraction and void fraction uncertainty in fixed beds of poly-lobed particles*. *Industrial and engineering chemistry research*, 2019. **58**(9): p. 3902-3911.

## 4 Heat transfer model

### 4.1 Introduction

Pyrolysis is a thermochemical process where the feedstock is heated to the reaction temperature in the absence of an oxidising agent. The temperature varies depending on the type of pyrolysis, reactor configuration, the aim of the process and target product. Among the existing challenges to develop pyrolysis further, heat transfer is the most significant [1]. The three main aspects to consider for the design of a pyrolysis reactor are the behaviour of the bed of solids, the heat transfer and the kinetics of the process. Heat transfer occupies a crucial position within the model because at steady-state, every particle should reach the target temperature of the process.

Rotary type reactors (rotary kiln and rotary dryer) use conduction, convection and radiation to increase the temperature of the raw material. Conduction occurs when there are two materials in contact at different temperatures. Convection involves a fluid (gas or liquid) in movement, in contact with the solid, between which there is a heat flow due to the temperature difference. The last heat transfer method is radiation; this differs from the others because it does not need direct contact. Radiation occurs through electromagnetic waves, produced by the material because its temperature is higher than 0 K [2].

### 4.2 Conduction

Conduction occurs when more energetic particles (with higher temperature) of a substance are transferred to an adjacent substance with a lower energy level, due to the interaction between them. It means that the two substances have to be in direct contact to exchange this energy. Heat is transferred in fluids because of the collisions and diffusion of molecules, whereas for solids it is the vibration of molecules that causes the transfer. The parameters affecting the conduction rate are the geometry, thickness of the system, the material through which it occurs, steady-state and temperature difference [3].

Conductive heat transfer can occur in any direction, so the problems for heat transfer can be one-, two- or three-dimensional. The variation of temperature in different directions is the reason for the temperature gradients in a system. The more dimensions used, the more accurate the calculations are, but the more complex. The temperature of the material needs the coordinates (which can be rectangular, cylindrical or spherical) and the time if the system is not steady-state to define the temperature of a specific position at a specific time [3].

In a material, the variation of temperature is usually negligible in at least one direction, so the problems are usually simplified to two-dimensional. The interactive systems occasionally are one-dimensional, but only if the temperature varies in one direction and the temperature difference in the other two directions is negligible. Some examples can easily be found for 1-D heat transfer systems, such as the heat transfer through the window or from a hot water pipe to the atmosphere. In both cases, the heat transfer occurs mainly in one direction, to the surface of the glass and radially, respectively [3].

As stated previously, the conductive heat transfer is affected proportionally by the temperature difference and the area, and inversely proportional to the distance in that direction. The most common expression to calculate the conductive heat flow is Fourier's law of heat conduction (Equation 4.1). In this equation,  $k$  is the thermal conductivity of the material measured in  $W/(m \cdot K)$ , that quantifies the capacity of the material to conduct heat,  $\partial T/\partial n$  is the temperature gradient in the direction  $n$  with units  $K/m$ . Finally, the parameter  $A$  is the area through which the heat flow travels (measured in  $m^2$ ). To calculate the temperature accurately at a position within the system, Equation

4.1 should be extended to three dimensions, and the total heat transfer would be the summation of the three dimensions [3].

$$Q_n^{cond}[W] = -k \left[ \frac{W}{m \cdot K} \right] \cdot A[m^2] \cdot \frac{\partial T}{\partial n} \left[ \frac{K}{m} \right]$$

Equation 4.1: Fourier's law of heat conduction on direction  $n$

This equation only considers the conductivity, area, and the gradients of temperature and position. It is defined by an assumption of steady-state conditions, so the properties do not change with time. To consider time within the calculations, heat flows into the body during a differential of time have to be equal to the increase in energy of the body during that fraction of time, usually measured by the increase of temperature.

In Equation 4.2, the summation of all heat flows produces a variation in the temperature, which varies with time, with  $m$  as the mass whose temperature changes and  $c_p$  as the heat capacity, defined as the amount of energy needed to increase the temperature per unit of mass. The heat flows considered in the summation are for three directions, and in each direction alternative heat transfer methods such as convection or radiation should be considered. This summation of heat flows during a period  $dt$  should be equivalent to the increase of the temperature [3].

$$\left( \sum_{n=0}^{x,y,z} Q_n \right) [W] \cdot dt[s] = m[kg] \cdot c_p \left[ \frac{J}{kg \cdot K} \right] \cdot dT[K]$$

Equation 4.2: Transient heat transfer

With this expression, there are four coordinates to cope with: the directions,  $x$ ,  $y$ ,  $z$  and time,  $t$ . To deal with the variation of properties in the direction of the solids flow ( $z$ ), the reactor models are usually divided into slices, all physically identical. A more detailed description can be found in Sections 4.5.1 and 7.3.2.

Most of the problems encountered in the field of heat transfer are because it is theoretically transient with varying conditions and properties. Thus, problems are usually considered as steady-state, because they are easier to analyse, and it is an adequate approximation to reality. The most common approach is to use the worst-case scenario. For instance, when a heater for a room is sized, it is designed to perform and solve the maximum rate of heat loss, under the worst conditions. In that way, the heater can keep the room warm under the worst conditions and, consequently, under any conditions [3], although it will be oversized.

*Assumption 5: The heat transfer model uses the steady-state approach for each of the slices and the whole reactor.*

#### 4.2.1 Variable area

Figure 4.1 represents the direction of heat flow (red arrows) within the reactor. The combustion gases around the reactor (represented by the yellow ring) transfer heat to the gases inside the kiln (grey) and the bed of solids (brown). There is some heat exchange between the bed of solids and the gases inside the kiln when there is a temperatures difference.

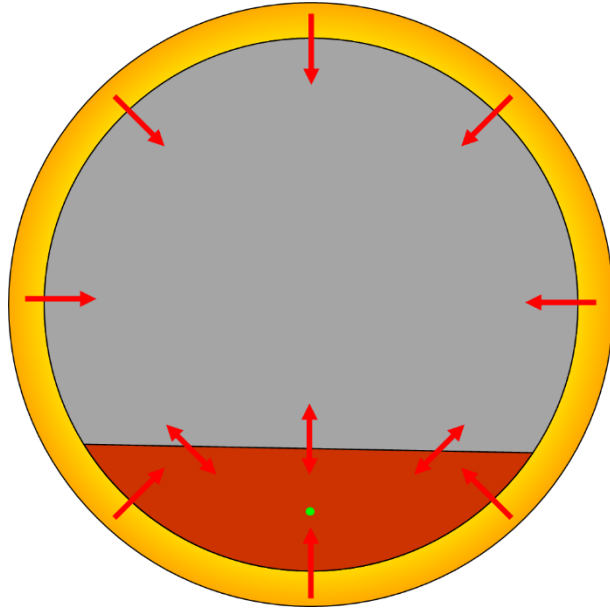


Figure 4.1: Heat flow from the combustion gases to the reactor

In a standard case where the material inside the kiln is fully mixed, or there is only one type of material, cylindrical coordinates to describe the kiln would be the most suitable solution. This case is more complicated because the heat transfer is not divided by radius, but height, so the limits of the two dimensions through which heat is transferred are variable. The cylindrical coordinates do not seem to be a suitable approach in this case. Instead, it is assumed that heat is transferred to the surface of the bed by conduction in a single direction with a variable area. The method to calculate the variable area is explained in Sections 3.3.1. Heat transferred by conduction with variable area can be calculated using Equation 4.3 [4].

$$Q_x^{cond} [W] = \frac{\lambda \left[ \frac{W}{m \cdot K} \right] \cdot (T_1 - T_2) [K]}{\int_{x_1}^{x_2} \frac{dx}{A(x)} \left[ \frac{m}{m^2} \right]}$$

Equation 4.3: Conductive heat transfer with variable area

In this equation, the higher temperature is found at  $x_1$ , and the conductive heat flow to  $x_2$  is studied through a material with conductivity  $\lambda$ , transferring heat in the direction  $x$  through an area  $A$  that changes between the two points. Equation 4.4 is used to solve the temperature at a particular point in the bed of solids [4]. The kiln is divided into slices over the length of the reactor (dimension  $z$ ), and the temperature in each slice is considered constant. This method is explained further in Sections 4.5.1 and 7.3.2.

$$\frac{\partial^2 T}{\partial x^2} + \frac{\partial^2 T}{\partial y^2} + \frac{\partial^2 T}{\partial z^2} = 0$$

Equation 4.4: Heat flow diffusion

Once one of the dimensions has been removed from Equation 4.4, there are still two dimensions ( $x$  and  $y$ ) to analyse and calculate. The critical point to achieve the final temperature is the centre of the bed of solids. The centre is the furthest point from the freeboard (contact area gases-bed of solids) and the wall of the reactor. An example of the furthest point is represented in Figure 4.1 by a green point. Heat flow is mainly directed towards heating the centre because once this point

achieves the target temperature, it guarantees that the rest of the bed of solids has reached that temperature.

The simplification of Equation 4.4 into Equation 4.3 lies in the assumption that heat flow in one direction is much larger than others, in a way that the variation of temperature in one dimension is much more significant [4]. Practically, it implies that the heat from the gases inside the solid is only transferred to the centre because further than that is heated by the wall instead. The same principle applies to the heat transferred from the wall to the bed of solids towards the centre. Another fact to consider is the nature of the division into slices (Sections 4.5.1 and 7.3.2). Despite the different heat flow and different directions towards the bed, the temperature gradients will be considered negligible for two reasons. Firstly, the slices into which the reactor is divided are considered as CSTR reactors, which are known for good-mixing [5]. Secondly, the rolling motion used (Section 3.1.1.3) makes the bed of solids more homogeneous, hindering temperature gradients.

#### 4.2.2 Methodology

The equation employed to calculate the heat transferred by conduction is Equation 4.3. It is important to consider that the three substances exchange heat between themselves, so the heat transferred through conduction has to be calculated for the interaction wall- gases, wall- bed of solids and gases-bed of solids. The major challenge of the conductive heat flow is the calculation of the denominator of the equation. The method to calculate  $\int_{x_2}^{x_1} \frac{dx}{A(x)}$  is explained in Section 3.3.1. Once this term is applied to each step, Equation 4.3 is applied with conductivity of the material receiving the heat flow and the contact area with the other material.

#### 4.2.3 Effect of particle size

In the bed of solids chapter, the influence of particle size and shape is addressed, and its effect on that specific submodel is explained (Section 3.5.1) – in particular, information about the voidage. Two of the parameters which affect the voidage are the shape and size of the particles. This model associates a particle shape (chosen by the user) to particle size and voidage of the bed.

In terms of heat transfer, the main aim is that the furthest particle from the heat source reaches the pyrolysis temperature and achieves the target conversion. This point is defined by the maximum-minimum dimension (MMD) of each particle. The MMD is the shortest distance from the surface to the centre of the particle, which is defined as the furthest point from the surface [6]. There are two examples to help understand this concept. Figure 4.2 shows the MMD for a sphere, whose furthest point is the centre of the sphere (represented by a blue circle). In this case, the MMD is achievable from any point of the surface because it is a perfect sphere. In the case of the cylinder in Figure 4.3, the centre is in the middle of the height, at a perpendicular distance from the wall.

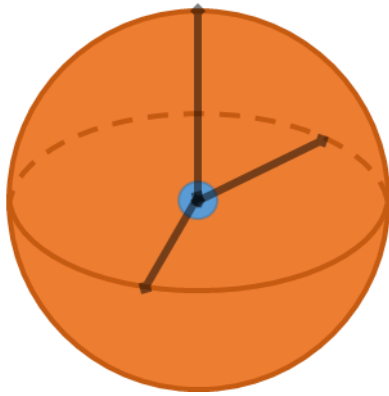


Figure 4.2: Maximum- minimum dimension of a sphere

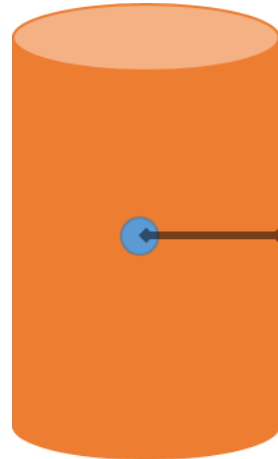


Figure 4.3: Maximum-minimum dimension of a cylinder

The aim of the reactor is for the centre of each particle to reach the operating temperature and target conversion. If the model ensures that the heat reaches any distance equivalent to the MMD inside the particle and reaches the target temperature, this guarantees that the centre will also reach the target. This type of calculation requires temperature gradients within the particle, and the use of Computational Fluid Dynamics (CFD). The advantage of this approach would be a more accurate model. Nevertheless, a significant problem would be the necessary computational power for the study for a single particle in so many different situations (100 different steps at each simulation with hundreds of particles each), and the assumptions that all particles behave in the same way which would be a thesis itself. Instead, the approach is to assume a lack of temperature gradients within the particles and the bed of solids, assuming equilibrium is achieved. It leads to a higher level of inbuilt error but makes the work achievable and available for any computer without the need for specialist CFD software.

*Assumption 6: There are no temperature gradients within a particle nor the bed of solids*

*Assumption 7: For the calculation of the temperature, the system is considered stationary, and equilibrium is reached*

### 4.3 Convection

Convection is the transfer of energy between two materials when at least one of them is in motion. It is typically applied to a fluid transferring energy to a solid, through its contact surface. Like conduction, it requires contact between two materials at different temperatures. This movement combines the effect of conduction and macroscopic fluid motion to transfer the heat. The motion of one of the materials enhances the heat transfer but makes the calculation of the heat transfer coefficients more complex [3, 7]. The total heat transferred is the sum of energy transport by random intrinsic motion and the bulk motion of the material. Convection accounts for both types of motion, whereas the term advection refers exclusively to the macroscopic movement, the bulk motion of the material [8]. Some examples of convection would be blowing on a hot piece of food to cool it down, taking a shower in winter to warm up, hot air balloons or boiling water, where the heat is transferred faster due to the motion of the moving fluid [2, 3].

Since convection implies movement and trajectories of particles and fluids, the presence of surfaces in the trajectory of a fluid affects its flow. The results of all experiments in the field indicated that a moving fluid stops at the surface, and the velocity relative to the surface becomes zero. Due to viscous effects, the fluid in contact with the wall sticks in an effect called the no-slip condition. This layer on the surface slows the adjacent fluid, which slows the next one, which slows its adjacent layer, creating a velocity profile (See Figure 4.4, adapted from [3]). The region where the variation of velocity is significant is called the boundary layer. If the surface is moving, the fluid acquires the same velocity as the surface. The fluid on the surface has no velocity with respect to the surface and the surface drag; the force that is exerted on a surface in the flow direction. When the fluid at the surface has no velocity, the heat is transferred by pure conduction. The variation of energy in the layer adjacent to the solid is convected away as a result of fluid motion [3].

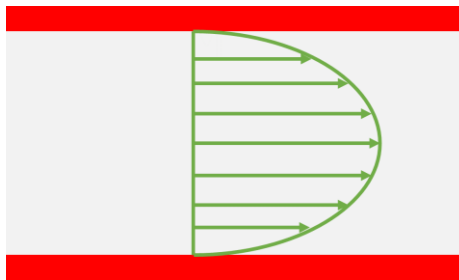


Figure 4.4: Velocity profile of the gases in a pipe

There are several types of convection, depending on how the motion of the fluid is produced. When the motion is produced by external means (wind, pump, fan or compressor), it is called **forced convection**. The other method to induce motion occurs naturally, like the difference of density and/or gravity, and receives the name of **natural convection** or, very rarely, **free convection** [3]. Natural convection seems complicated, but it is found more commonly than expected, for instance, to cool down food that has just been cooked or heated. The air around the food increases in temperature and decreases in density, producing motion and transferring the heat away by natural convection. Another example is when boiling water, the bubbles created at the bottom move upwards to surface.

Convective heat transfer is represented by Newton's law of cooling, in Equation 4.5. The convective heat flow is proportional to the convective coefficient  $h$ , the surface  $A_s$  through which convection occurs, and the temperature difference between the surface  $T_s$  and the medium  $T_\infty$ . The challenge for the convective heat flow is to calculate the convective coefficient, which is not a property of the fluid or the solid, but a combination of both and is dependent on the conditions where the heat is transferred [3].

$$Q^{conv}[W] = h \left[ \frac{W}{m^2 \cdot K} \right] \cdot A_s[m^2] \cdot (T_s - T_\infty)[K]$$

Equation 4.5: Convective heat flow

#### 4.3.1 Convective heat transfer coefficient

According to Equation 4.5 and conceptually, the convective heat transfer coefficient is defined as the rate of heat transfer between the materials per unit surface area and temperature difference. According to the no-slip condition, it could be calculated with Equation 4.6 when the fluid direction is parallel to the surface. Furthermore, the coefficient would vary along the flow direction. The most common practice is to use an average or mean coefficient.



$$h = \frac{-k_{fluid} \left( \frac{\partial T}{\partial y} \right)_{y=0}}{T_s - T_\infty}$$

Equation 4.6: convective coefficient in no-slip condition

The most common practice to calculate this coefficient is to use dimensionless numbers when governing equations and its variables are combined. This case is usually solved with the dimensionless Nusselt number  $Nu$ , which correlates the thermal conductivity of the fluid  $k$ ,  $h$  as the convective coefficient and  $D_h$  as the hydraulic diameter (See Equation 4.11). The Nusselt number represented in Equation 4.7 shows how the convection increases the heat transfer over conduction. The higher the Nusselt number, the more significant the convection, and the lesser effect of conduction within the system. If the number reaches 1, the heat transfer is by pure conduction [3].

$$Nu = \frac{h \left[ \frac{W}{m^2 \cdot K} \right] \cdot D_h [m]}{k \left[ \frac{W}{m \cdot K} \right]}$$

Equation 4.7: Nusselt number

#### 4.3.1.1.1 Types of flow

The convective heat transfer coefficient depends significantly on the fluid because it is highly influenced by fluid mechanics. The wide variety of fluids creates the need for classification depending on the working system and region, and the inherent properties [3]:

- **Viscous versus Inviscid Regions of Flow:** viscosity is the resistance of a liquid to move and flow, due to friction between the liquid layers, the cohesive forces between molecules in liquids and molecular collisions in gases. A zero viscosity does not exist, but the viscosity forces are negligible in some flow regions compared to others such as inertial or pressure and can simplify the calculus. Conversely, when the forces are significant, the frictional effects are significant [3].
- **Internal versus External Flow:** the coefficient and methods to calculate the convective heat transfer changes depending on the flow being confined in material or flowing over a surface. When the fluid flows through a pipe or duct, it is considered internal flow because it is surrounded by a solid material and the viscous forces have a very significant effect. Conversely, it is considered external flow when the fluid is free to flow over a surface such as a plate, wire or a pipe. In this case, there are only viscous effects in layers near the solid surfaces. A mixture of both flows would be a river where water flows in a channel with a free surface on the top. This type of flow receives the name of open-channel flow and applies to partially filled pipes [3]. The layout significantly affects other parameters such as the limits for laminar or turbulent flow [3].
- **Compressible versus Incompressible flow:** the compressibility of a fluid depends on how the density changes. When the density does not change, a fluid is classified as incompressible, the density of every portion of fluid remains unchanged if the pressure changes. The most common rule is to consider liquids incompressible. For instance, the variation of the density of water is only 1% when pressure is increased from 1 to 210 atmospheres. This variation is achieved in the air when pressure varies by 0.01 atm, in which case the flow is compressible. Despite the difference, gas is considered incompressible overall if the variation of temperature and/or pressure is lower than 5%. The density and its variation affect the calculation of some dimensionless numbers such as Reynolds number [3].

- **Laminar versus Turbulent Flow:** these are two regimes of flow. When the flow is highly ordered with smooth layers of fluid, it is referred to as laminar flow. The more viscous and the less velocity the fluid possesses, the more laminar it is. When the fluid is more chaotic and moves less smoothly, it is referred to as turbulent, attributed to low viscous fluids at high velocity. It is mostly defined by the dimensionless Reynolds number, whose value defines if the fluid is in the turbulent or laminar region, and it changes when it is internal or external flow. There is a range where it is not defined because it alternates between laminar and turbulent flow, in which case it is called the transitional regime.  
A good example is the smoke of a cigarette, which rises smoothly during the first centimetres but fluctuates randomly later [3]. Water flowing from a tap behaves similarly because when the flow is low (but enough to have a continuous flow), it is possible to look through because it flows smoothly. When the flow is increased, it becomes more disordered, and you cannot look through.
- **Natural versus Forced Flow:** as deduced from the name, natural flow occurs when the fluid moves from natural effects such as density difference, produced by, for instance, a temperature gradient. A flow whose motion is caused by external forces (a pump or a fan, for example) is forced flow and usually driven towards a surface [3]. It is directly connected to the classification of natural and forced convection.
- **Steady versus Unsteady Flow:** this characteristic is related to the change of properties in a certain point of the fluid with time. When there is any change in fluid properties with time, it is understood as unsteady, contrary to constant properties of the fluid, attributed to a steady flow. The other terms commonly used to describe the change of properties with time are *uniform* for steady, and *transient* or *periodic* for transient. However, they cannot be used in fluid mechanics because they have different meanings. Uniform implies invariability on a location instead of a whole region, which is more of interest. The term transient is a specific term used for flows which are developing, and periodic refers to flow oscillating steadily within unsteady regions [3].
- **One, Two and Three Dimensional Flows:** the number of dimensions is a key aspect to consider for the analysis of the flow and the simplicity of the calculations. A fluid involves three-dimensional geometry, and the velocity may vary in all three dimensions, which can be measured and calculated in rectangular or cylindrical coordinates. Depending on the velocity of each, some may be negligible in comparison to the others, so as the error if omitted. The dimensions are not always necessarily rectangular ( $x, y, z$ ), but might be cylindrical too ( $r, \theta, z$ ), sometimes leading to a more straightforward solution. For instance, if analysed in cylindrical coordinates, a fully developed flow varies in the radial ( $r$ ) direction but is constant for the other directions [3].

#### 4.3.1.2 Gas coefficient

From all the types of flows, it is necessary to define the flow rate of gases inside and outside the kiln to calculate the heat transfer. Some characteristics can be defined, and others depend on the specific position along the reactor. It is important to note that the reactor is divided into slices and, for each slice; the properties will be recalculated, in agreement with temperatures and flows as explained in Sections 4.5.1 and 7.3.2. Within this project, the characteristics of the gases are as follows:

- **Viscosity:** the viscosity is one of the properties correlated for each gas and, since each of the flows is a mixture of different gases, the viscosity is a key parameter to consider for the calculations.

- **Internal flow:** the gases are found inside the kiln and are considered as internal flow, which profoundly influences the limits for the laminar or turbulent flow. When the flow is external, the regime is laminar until it reaches a value of around  $10^5$  where it becomes turbulent, with the transition regime in between. The limit for the turbulent regime varies depending on the source, but overall  $10^5$  is the minimum value [3, 8-10]. In contrast, the limits for the internal flow are different and much lower. Mostly, the upper limit for laminar flow is 2,300, and 10,000 is the lower limit for turbulent flow. The transition regime is established within a range of 2,300-10,000. Contrary to external flow, the internal flow depends on characteristics of the pipe such as surface roughness and pipe vibration, and the fluctuation of the flow. The importance of considering internal or external flow is crucial to calculate if the flow is laminar or turbulent and, consequently, the Nusselt value and the convective heat transfer coefficient.
- **Compressible:** the density of the gases are considered variable along the entire reactor but constant within each reactor slice. Keeping a constant density is not realistic in this case because the gases vary in composition, and temperature, which significantly influences the density. For instance, the density of nitrogen at 0 °C is 2 kg/m<sup>3</sup>, and it is reduced to less than 1 kg/m<sup>3</sup> at 300 °C [3], lower than the minimum temperature that can be considered for pyrolysis.
- **Laminar or turbulent regime:** This characteristic will be defined for each step depending on the value of the Reynolds number.
- **Forced flow:** convection occurs due to forced flow within the kiln and over the bed of solids.
- **Steady flow:** the flow and its properties are assumed as steady-state to simplify the calculations, so there is no variation of properties with time.
- **One Dimensional Flow:** the properties vary along the reactor for each reactor slice, and the properties within each are constant.

After the definition of the flow, Reynolds (Equation 4.8) and Prandtl (Equation 4.9) dimensionless numbers for the specific conditions of each step are calculated. The Reynolds number is the result of the division of inertial and viscous forces where the dynamic viscosity ( $\mu$ ) and the density ( $\rho$ ) represent the viscous forces. The hydraulic diameter ( $D_h$ ) and velocity ( $u$ ) represent the inertial force. The Prandtl number is the result of the division of the momentum and thermal diffusivities. The parameters that define this number are the dynamic viscosity, conductivity ( $\lambda$ ) and the heat capacity at constant pressure ( $C_p$ ) [4].

$$Re_D[-] = \frac{\rho \left[ \frac{kg}{m^3} \right] \cdot u \left[ \frac{m}{s} \right] \cdot D_h [m]}{\mu \left[ \frac{kg}{m \cdot s} \right]} \quad Pr[-] = \frac{\mu \left[ \frac{kg}{m \cdot s} \right] \cdot C_p \left[ \frac{J}{kg \cdot K} \right]}{\lambda \left[ \frac{W}{m \cdot K} \right]}$$

Equation 4.8: Reynolds number

Equation 4.9: Prandtl number

In the previous dimensionless numbers, some parameters need further clarification such as the velocity and hydraulic diameter. In Figure 4.4, the velocity profile of a fluid in a pipe was represented. Ideally, a different Reynolds number for each value of the velocity should be calculated, yet this is not feasible due to the complex integration of all values for each step. Instead, a constant velocity is calculated for each step using Equation 4.10, where  $\dot{m}$  is the mass flow,  $\rho$  is the density, and  $A$  is the cross-sectional area through which the fluid moves. The other parameter that needs further explanation is the hydraulic diameter, defined by Equation 4.11. The term  $A_c$  is the cross-sectional area of the tube and  $p$  is the wetted perimeter [3], where the two materials exchanging heat connect. In the case where a pipe is full of gas, the wet parameter refers to the entire wall; In the case of a rotary kiln, the perimeter is different if the heat exchange is considered towards the wall or the bed of solids.

*Assumption 8: The velocity of the fluid is constant through the cross-section*

$$u \left[ \frac{m}{s} \right] = \frac{\dot{m} \left[ \frac{kg}{s} \right]}{A[m^2] \cdot \rho \left[ \frac{kg}{m^3} \right]} \quad D_h[m] = \frac{4 \cdot A_c[m^2]}{p[m]}$$

Equation 4.10: Velocity of a fluid in a pipe

Equation 4.11: hydraulic diameter

The rest of the parameters ( $\rho$ ,  $\mu$ ,  $\lambda$  and  $C_p$ ) are empirical values from the literature [3]. The values for individual components (carbon dioxide, carbon monoxide, methane, hydrogen, steam and nitrogen) [3] flows in the model is calculated from the temperature and the composition.

Once the Reynolds and Prandtl number have been calculated, different correlations can be used to find the Nusselt number. Only two correlations were utilised in the model to cover the three regimes, to keep it as simple as possible. When the flow is laminar ( $Re_D < 2,300$ ), the Nusselt can be approximated to 3.66 according to [4, 11, 12]. The correlation of Gnielinski (Equation 4.12) [13, 14] is valid when Reynolds number is located in a range  $[2,300 - 5 \times 10^6]$  and the Prandtl number within  $[0.5 - 2,000]$ . We will suppose that the values of the Reynolds and the Prandtl are within limits when the regime is not laminar. In the case of the Reynolds, the values are around 2300, and 0.7 for the Prandtl. There is no danger of surpassing the upper limit of the Reynolds nor Prandtl. The only problematic situation would appear when the Prandtl is lower than 0.5 and the Reynolds higher than 2,300. In that particular case, which is very rare, the Gnielinski correlation can also be used, although one of the conditions is not achieved because overall, the Prandtl limit is 0.7 or 0.5 [4]. From the Nusselt number obtained, the convective coefficient of heat transfer is calculated with Equation 4.7.

$$Nu_D = 3.66 \quad Nu_D = \frac{\left(\frac{f}{8}\right) \cdot (Re_D - 1000) \cdot Pr}{1.07 + 12.7 \cdot \left(\frac{f}{8}\right)^{0.5} \cdot (Pr^{2/3} - 1)}$$

Equation 4.12: Gnielinski correlation and requirements

$$Re_D < 2300 \quad 2300 \leq Re_D \leq 5 \cdot 10^6$$

$$0.5 \leq Pr \leq 2000$$

In the Gnielinski correlation (Equation 4.12), the parameter  $f$  stands for the friction factor of the kiln. It will be assumed that the kiln has no roughness, and the friction factor is calculated through Equation 4.13 from the Moody diagram [3], depending on the value of the Reynolds number.

$$Re_D < 2300 \quad 10^4 < Re_D \leq 2 \cdot 10^4 \quad 2 \cdot 10^4 \leq Re_D$$

$$f = 64/Re_D \quad f = 0.316 \cdot Re_D^{-1/4} \quad f = 0.184 \cdot Re_D^{-1/5}$$

Equation 4.13: factor friction depending on the value of the Reynolds number

*Assumption 9: The material of the rotary kiln is smooth and has no roughness, so the friction factor exclusively depends on the Moody Diagram*

#### 4.3.1.3 Bed of solids coefficient

Ideally, the same equations could be applied to the bed of solids and the gases to calculate the heat transferred by convection. In contrast to the gases, the bed of solids do not have the viscosity

as one of the characteristics. Therefore, neither the Prandtl nor Reynolds numbers can be calculated for the solids. This has a significant impact on the methodology to calculate the convective heat transfer because there is no alternative to calculate the convective heat transfer coefficient.

Boateng [15] used the Peclet number instead to find a dimensionless number to correlate with convective heat transfer. The formula to calculate the Peclet number is Equation 4.14, and it shows how similar or different the advection and conduction are [4]. After a very complex demonstration, Boateng found a method to calculate the Nusselt number correlated to the Peclet, as shown in Equation 4.15. Due to its complexity, the denominator is reduced to 1 when the Peclet number acquires high values (higher than  $10^4$ ) [15]. This could lead to a gap in the model if the Peclet number does not reach the value. For that, Boateng [15] highlighted the importance of the correlation of Tscheng and Watkinson [16] who found an expression which correlates the Peclet with the Nusselt if the Peclet number is lower. The ranges and formulas are shown in Equation 4.16. After calculating the Nusselt number, the procedure is the same as for gases. The Nusselt number (Equation 4.7) is employed to calculate the convective coefficient, and Equation 4.5 is employed for the heat flow.

$$Pe = Re_D \cdot Pr = \frac{\rho \cdot u \cdot D_h}{\mu} \cdot \frac{\mu \cdot C_p}{\lambda} = \frac{\rho \cdot u \cdot D_h \cdot C_p}{\lambda}$$

Equation 4.14: Peclet number

$$Nu = \frac{2 \cdot \sqrt{2 \cdot Pe}}{1 + \sum_{j=1}^{\infty} \left[ \left( \frac{B_j(\xi)}{\pi \cdot a_1} \right) \cdot \left( 1 - e^{-\frac{j^2 \cdot \pi \cdot \xi^2}{2 \cdot a_2^2 \cdot Pe}} \right) \right]}$$

Equation 4.15: Nusselt number for the bed of solids

$$Nu = 11.6 \cdot Pe^{0.3} \quad Nu = 2 \cdot \sqrt{2 \cdot Pe}$$

$$Pe \leq 10^4 \quad Pe > 10^4$$

Equation 4.16: Nusselt number in the function of Peclet value

#### 4.4 Radiation

The radiative heat transfer is the last, and probably the most complex heat transfer method. Unlike the other two methods (conduction and convection), radiative heat transfer does not need direct contact between the two materials exchanging heat. Radiation can occur between two bodies separated by a colder medium. One of the best examples to explain radiative heat transfer is the use of a fireplace to warm up the house in winter or the Earth heated by the sun. It does not occur through direct conduction or convection, but radiation, with a warming sensation without being in direct contact [3].

The key for understanding radiation is the electromagnetic waves or electromagnetic radiation, which are the variable electric currents or accelerated charges, which raise the electric and magnetic field, producing changes in molecular and atomic electronic configurations, which emit energy [3]. All the electromagnetic waves fall in a spectrum with a wavelength range of  $10^{-9}$ - $10^{10}$   $\mu\text{m}$  and the waves it includes are radio or TV waves, microwaves, infrared, visible, ultraviolet, x-rays, cosmic rays or gamma rays; all cause thermal radiation. Among all types of thermal radiation, the waves of interest for this work have a wavelength spectrum of 0.1-100  $\mu\text{m}$ , and the radiation is produced by the energy transition of molecules, atoms, and electrons of a substance. A macroscopic measurement of these transitions is the temperature, and the rate of radiative emission increases with increasing temperature [3].

All bodies with a temperature higher than absolute zero emit radiation because the particles are always in motion, so are being absorbed or transmitted through the whole volume, which means that radiation is a volumetric phenomenon, but it is reduced to surface phenomenon for nontransparent solids (opaque), such as metals, wood, rocks and unlike glass or windows. In the case of opaque solids, the inner regions do emit radiation, but it does not reach the surface. From this, it is fathomed that different bodies emit different amounts of radiation per unit of surface. To make materials comparable, the blackbody is defined as the perfect emitter and absorber of radiation, whose radiation energy emitted is on Equation 4.17 where  $\sigma$  is the Stefan-Boltzmann constant and  $T$  is the temperature in K [3].

$$E_b(T) = \sigma \cdot T^4 \qquad \sigma = 5.670 \cdot 10^{-8} \left[ \frac{W}{m^2 \cdot K^4} \right]$$

Equation 4.17: Blackbody emissive power

Equation 4.18: Stefan-Boltzmann constant

To compare the energy any surface emits to a blackbody at a specific temperature, the parameter emissivity ( $\varepsilon$ ) is defined. This parameter has a value between 0 and 1 and shows how similar the emitting surface is to the blackbody. Equation 4.17 is modified to Equation 4.19, which accounts for the emissivity power of a small body [3].

$$E(T) = \varepsilon \cdot \sigma \cdot T^4$$

Equation 4.19: Emissive power of a small body

For this project, the essential data is the amount of heat transferred by radiation, which is calculated by the subtraction of the radiation leaving surface 2 that strikes surface 1 by the radiation leaving surface 1 that strikes surface 2. This radiation is measured with the temperature, and when both surfaces are considered black bodies, Equation 4.20 is applied. The parameter  $F$  is the view factor and is explained in 4.4.1 [3].

$$Q_{1 \rightarrow 2}^{rad} = A_1 \cdot E_{b1} \cdot F_{1 \rightarrow 2} - A_2 \cdot E_{b2} \cdot F_{2 \rightarrow 1} = A_1 \cdot F_{1 \rightarrow 2} \cdot \sigma \cdot (T_1^4 - T_2^4)$$

Equation 4.20: Radiative heat transfer between two black bodies

The last studied case is applied to ideal systems where the surfaces exchanging heat are blackbodies. For a more realistic approach, the surfaces exchanging heat are treated as grey surfaces, with an emissivity characteristic ( $\varepsilon_x$ ) associated with each of them. Simultaneously, the view factor needs consideration. Consequently, the resulting equation is not a simple combination of Equation 4.19 and Equation 4.20. Instead, the system should be treated as a network with different resistances, two linked to the surface and its emissivity, and another associated to the view factor, similarly to an electrical circuit where the current flowing goes through several resistances. The resulting method to calculate the heat exchanged between two surfaces through radiation is Equation 4.21 [3, 4].

$$Q_{1 \rightarrow 2}^{rad} [W] = \frac{\sigma \left[ \frac{W}{m^2 \cdot K^4} \right] \cdot (T_1^4 - T_2^4) [K^4]}{\frac{1 - \varepsilon_1 [-]}{A_1 [m^2] \cdot \varepsilon_1 [-]} + \frac{1}{A_1 [m^2] \cdot F_{12} [-]} + \frac{1 - \varepsilon_2 [-]}{A_2 [m^2] \cdot \varepsilon_2 [-]}}$$

Equation 4.21: Heat transfer between two grey, diffuse and opaque surfaces

#### 4.4.1 View factor

Any body emits radiation from its entire surface, which does not necessarily mean that the heat is fully transferred by radiation to the colder surface. For instance, a fireplace in a living room can

be emitting its radiative energy to the chimney, two people, the sofa and the table simultaneously, with different intensities and strength. The view factor is a necessary parameter that accounts for orientation of the surfaces in radiative heat transfer. It represents the fraction of radiation that leaves the emitting surface and reaches the receiving surface. This parameter does not consider the surface properties and the temperatures, it is purely geometric. Depending on the source, it can be called the shape factor, configuration factor or angle factor [3].

The view factor is generally represented by the letter F and two subscripts, which represent the origin of the radiation and the target surface. For instance, the view factor  $F_{12}$  is an abbreviation of  $F_{1 \rightarrow 2}$ . This view factor represents the fraction of radiation from surface 1, which reaches the surface 2 [3].

Figure 4.5 depicts all parameters needed to calculate the view factor from surface 1 towards surface 2. The differential surfaces  $dA_1$  and  $dA_2$  belong to  $A_1$  and  $A_2$ , respectively, and are separated by a distance  $r$ . The angle between the surface and each of its normal ( $n$ ) vector is represented by the angle  $\theta$ . The parameter  $d\omega_{21}$  is the subtended angle of  $dA_2$  when it is viewed by  $dA_1$  [3].

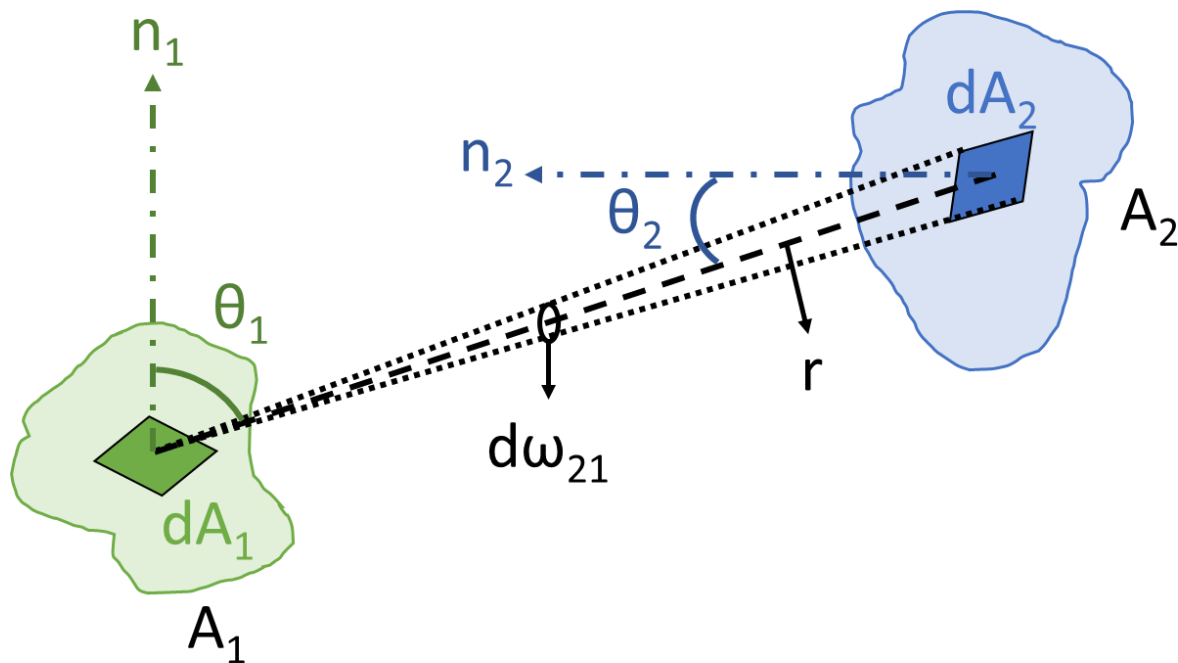


Figure 4.5: View factor geometry between two surfaces, adapted from [4]

Equation 4.22 is the formula to calculate the view factor between the two differential areas. The parameter  $J$  represents the radiosity, which is the total amount of radiation leaving a surface; and the parameter  $I$  is the intensity of the radiation. It is the fraction of the heat emitted by the surface 1 that reaches the surface 2, and it is calculated using the parameters from Figure 4.5. Equation 4.23 extrapolates the differentials of the area to the whole surface of systems 1 and 2, giving expression to calculate the absolute view factor [3].

$$dF_{dA_1 \rightarrow dA_2} = \frac{Q_{dA_1 \rightarrow dA_2}}{Q_{dA_1}} = \frac{I_1 \cdot \cos \theta_1 \cdot dA_1 \cdot d\omega_{21}}{J_1 \cdot dA_1} = \frac{I_1 \cdot \cos \theta_1 \cdot dA_1 \cdot \frac{dA_2 \cdot \cos \theta_2}{r^2}}{\pi \cdot I_1 \cdot dA_1} = \frac{\cos \theta_1 \cdot \cos \theta_2}{\pi \cdot r^2} \cdot dA_2$$

Equation 4.22: view factor definition

$$F_{dA_1 \rightarrow A_2} = \int_{A_2} \frac{\cos \theta_1 \cdot \cos \theta_2}{\pi \cdot r^2} \cdot dA_2 \rightarrow F_{A_1 \rightarrow A_2} = F_{A_1 A_2} = \frac{1}{A_1} \int_{A_1} \int_{A_2} \frac{\cos \theta_1 \cdot \cos \theta_2}{\pi \cdot r^2} \cdot dA_2 \cdot dA_1$$

Equation 4.23: View factor from surface 1 to surface 2

The complexity of Equation 4.23 to calculate the view factor is evident. There are some properties and characteristics of the view factor that helps with its calculation. Firstly, the reciprocity relation from Equation 4.24 correlates the view factor between surfaces with different areas, a useful expression once the surfaces and one of the view factors are known. The summation rule shows that the sum of all view factors from the surface  $i$  is 1, which means that all radiation has to reach a surface. This is closely connected to the superposition rule in Equation 4.26, which explains that the view factor towards two surfaces together is equivalent to the sum of both view factors. From Figure 4.6 and Figure 4.7 and their respective expressions Equation 4.27 and Equation 4.28, we see the flat and convex surfaces do not transfer heat within by radiation. Conversely, a concave surface like the one in Figure 4.8 does radiate heat over itself according to Equation 4.29. The understanding of Equation 4.30 from Figure 4.9, which represents concentric spheres is crucial for this research [3].

$$A_1 \cdot F_{12} = A_2 \cdot F_{21}$$

Equation 4.24: Reciprocity relation

$$\sum_{j=1}^N F_{i \rightarrow j} = 1$$

Equation 4.25: Summation rule

$$F_{1 \rightarrow (2,3)} = F_{1 \rightarrow 2} + F_{1 \rightarrow 3}$$

Equation 4.26: Superposition rule

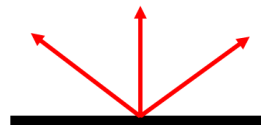


Figure 4.6: Plane surface

$$F_{1 \rightarrow 1} = 0$$

Equation 4.27: View factor of plane surface

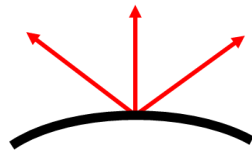


Figure 4.7: Convex surface

$$F_{1 \rightarrow 1} = 0$$

Equation 4.28: view factor of a convex surface

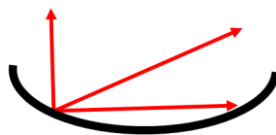
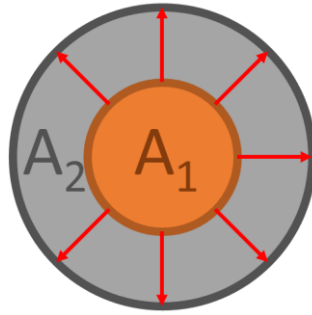


Figure 4.8: Concave surface

$$F_{1 \rightarrow 1} \neq 0$$

Equation 4.29: View factor of a concave surface





$$F_{1 \rightarrow 2} = 1$$

Equation 4.30: View factor of concentric spheres

Figure 4.9: concentric spheres

There are expressions for some standard geometries in the literature [3, 4, 8, 17] such as aligned parallel rectangles, coaxial parallel disk, perpendicular rectangles with a standard edge or parallel, perpendicular or inclined plates, or infinite plane with a row of cylinders. In most, graphs are varying the configuration or correlation of parameters like widths or lengths of the interacting surfaces.

*Assumption 10: The wall of the kiln does not radiate itself; all the radiative heat is transferred to the bed of solids and gases inside the reactor*

In the literature, the existing geometries for which the view factor is calculated are minimal, and none are equivalent to the system studied within this work. The rotary kiln is unique because it implies an interaction between three systems (bed of solids, gases inside the reactor and wall), two of which cannot be found in the literature due to their shape. In the definition of view factors within this work, the letter *G* refers to the gases inside the reactor, *S* to the bed of solids and *W* to the wall. The calculation of the integral in Equation 4.23 is not feasible because it should be calculated several times for the design of different reactors, and each time the new function and values of parameters to integrate would be different. As explained in Sections 4.5.1 and 7.3.2, the model is divided into slices and parameters are re-calculated many times for each slice. The necessary view factors within the model are the  $F_{WG}$ ,  $F_{WS}$  (because the wall will emit radiation and heat the bed of solids and gases) and  $F_{GS}$ . It is assumed that all radiation from the wall is received by the gas and solids, as shown in Equation 4.31. Similarly, all the heat radiated by the gas is received by the wall and the solids in Equation 4.32. The view factor is not defined for the bed of solids because, in principle, the bed of solids is always the coldest of the three systems. The other two view factors where the bed of solids emits radiation can be calculated with Equation 4.24 applied to Equation 4.31 and Equation 4.32.

$$F_{W \rightarrow (G,S)} = 1 = F_{W \rightarrow G} + F_{W \rightarrow S} \quad F_{G \rightarrow (W,S)} = 1 = F_{G \rightarrow W} + F_{G \rightarrow S}$$

Equation 4.31: view factor from the wall to the gas and bed of solids

Equation 4.32: view factor from the gas to the wall and bed of solids

To reach a valid and realistic approximation for the view factors, they were analysed and calculated using different approaches and methods. The main output was the high dependency of the factor on the surfaces involved, and the complexity of the remaining parameters like the angle of the distances. To obtain an estimation similar to the real value of the view factor, the receiving surface is divided by the sum of all potential receiving surfaces. For instance, in the case of the view factor of the wall to the gas, the wall emits radiative heat to the solid and the gas. The view factor is the division of the area of gas and the areas of gases and solids, as shown in Equation 4.33. The view factors of the wall to the bed of solids and from the gas to the bed of solids are in Equation 4.34 and Equation 4.35.

$$F_{WG} = \frac{A_G}{A_G + A_S}$$

$$F_{WS} = \frac{A_S}{A_G + A_S}$$

$$F_{GS} = \frac{A_S}{A_W + A_S}$$

Equation 4.33: View factor wall-gas

Equation 4.34: View factor wall-solid

Equation 4.35: View factor gas-solid

## 4.5 Approach for the model

The main aim of the heat transfer model is to define the temperature of each component at the end of the length of the reactor. The components within the system are the solid feedstock, the gases inside the reactor in the inner shell, and flow of combustion gases around this shell as a source of heat. This methodology agrees with the procedure used with heat exchangers, defined as a piece of equipment where there is heat exchange between two materials at different temperatures indirectly, through a wall that separates them [8].

This definition is very similar to the process of a rotary kiln. Instead of having two fluids involved, the flow of combustion gases heats the inner shell, where the solid feedstock and the gases from pyrolysis are located. It is similar to a shell-and-tube heat exchanger with one shell and tube pass, and only one tube. If the efficiency is taken as 100%, the heat transfer follows the overall heat transfer coefficient, expressed as  $U$  on Equation 4.36 [8].

$$\frac{1}{U \left[ \frac{W}{m^2 \cdot K} \right] \cdot A [m^2]} = \frac{1}{(U \cdot A)_c} = \frac{1}{(U \cdot A)_h} = \frac{1}{\left( h \left[ \frac{W}{m^2 \cdot K} \right] \cdot A [m^2] \right)_c} + \frac{R''_{f,c} \left[ \frac{m^2 \cdot K}{W} \right]}{(A)_c [m^2]} + R_w \left[ \frac{K}{W} \right] + \frac{R''_{f,h}}{(A)_h} + \frac{1}{(h \cdot A)_h}$$

Equation 4.36: Overall heat transfer coefficient

The subscripts  $c$  and  $h$  refer to the cold and hot fluids, respectively. The term  $R_w$  represents the conduction resistance, with a different method depending on the shape (plane wall, cylindrical wall or others). The terms  $R''_{f,c}$  and  $R''_{f,h}$  are called fouling factors for the cold and hot fluid, respectively. The fouling factor accounts for inefficiencies caused by the impurities of the fluids, rust and scale formation or other potential sources of reduced efficiency. For instance, there might be some reaction between the wall and the gases or solids. The deposition of materials on the wall could significantly decrease the heat transfer between the hot and cold fluid. The  $h$  accounts for the convective heat transfer coefficient. Consequently, the expression for the overall heat transfer coefficient accounts for all resistances and the fouling of the equipment. This expression is used to calculate the exit temperature of one of the fluids when the others are defined through Equation 4.38 with the log mean temperature difference ( $\Delta T_{lm}$ ). The  $\Delta T_1$  and  $\Delta T_2$  are explained in Figure 4.10, and Figure 4.11 where the red line is the hot fluid and the blue is the cold fluid, and they represent the profile temperature for counter-current and co-current configuration [8].

$$Q = U \left[ \frac{W}{m^2 \cdot K} \right] \cdot A [m^2] \cdot \Delta T_{lm} [K] = U \cdot A \cdot \frac{\Delta T_2 - \Delta T_1}{\ln \left( \frac{\Delta T_2}{\Delta T_1} \right)}$$

Equation 4.37: Heat flow by log mean temperature difference

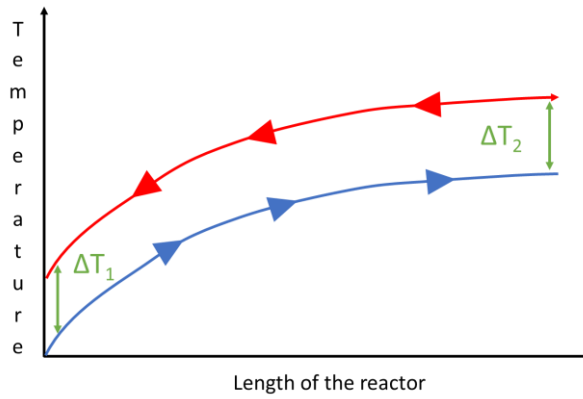


Figure 4.10: Temperature profile in counter-current reactor

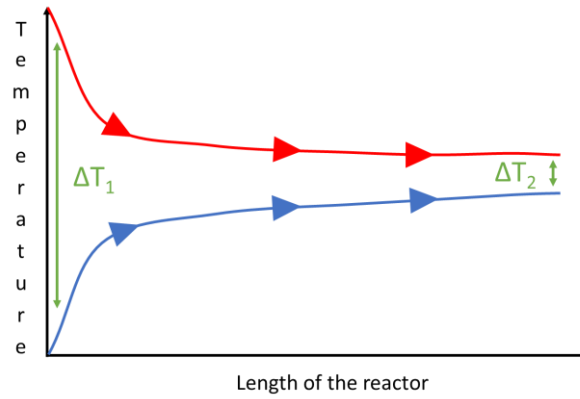


Figure 4.11: Temperature profile in co-current reactor

It is seen that the method to calculate the heat flow between the fluids or the exit temperature of fluid once the other parameters are defined is relatively easy. The overall heat transfer coefficient should account for the resistances of the three heat transfer methods (conduction, convection and radiation), where resistance is defined in Equation 4.38 [8]. When this equation is taken into account to calculate the overall heat transfer coefficient (Equation 4.36) is the summation of several resistances.

$$R_i = \frac{T_h - T_c}{Q_i}$$

Equation 4.38: Definition of thermal resistance

The advantages of this method are its simplicity to calculate the exit temperatures or the heat needed, and the fact that resistances do not depend on the temperature. There are several drawbacks by which this method is not used within this work. Firstly, this method does not account for the radiative heat transfer method, whose resistance is shown in Equation 4.39, according to [8]. This equation makes the resistance and the overall heat transfer coefficient dependent on temperatures. The overall heat transfer coefficient accounts for the complexity of transfer heat between two fluids. However, it ignores other aspects such as the evaporation of the moisture content, the heat of reaction, varying mass when there is chemical reactions or the change of properties along the reactor.

$$R_{rad} = \frac{1}{A \cdot \varepsilon \cdot \sigma \cdot (T_c + T_h) \cdot (T_c^2 + T_h^2)}$$

Equation 4.39: Radiative thermal resistance

#### 4.5.1 Overall description of the model

The model needs to take into account all heat transfer methods and the temperature-dependent properties of the materials along the reactor, such as density or thermal conductivity. These properties change with temperature and along the reactor. The mass flow of solids and gases inside the reactor changes along the reactor due to the degradation of biomass through pyrolysis and its consequent transformation into char, pyrolysis gas and vapours. The method employed to model this complex reactor is dividing the reactor into slices (also called steps), with the same thickness and physically identical, where the outputs of each are the inputs for the next slice. Each of these slices is modelled as a CSTR (Continuous Stirred Tank Reactor). Figure 4.12 describes the inputs and the outputs for each slice.

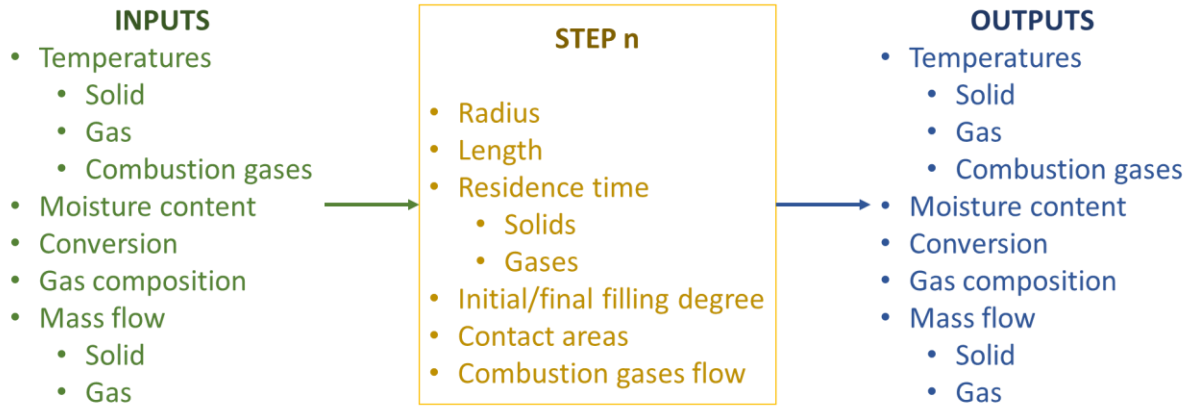


Figure 4.12: Scheme of the information for each slice

Each slice receives the temperature and the flow of the solids, gases inside the reactor and the combustion gases. It receives the remaining moisture content of the solids (if applicable) and, if the reaction has started, conversion of the solid and composition of gases inside the reactor, which should be a mixture of the carrier gas and pyrolysis gases. In the heat transfer submodel, the final temperatures are calculated, taking into account the radius of the reactor and residence time of the solids, contact areas and the initial temperatures.

The process the heat transfer submodel follows is represented in Figure 4.13. From the previous slices, we have the input temperatures, the submodel of the bed of solids (Chapter 3) provides the contact areas and the kinetic submodel (Chapter 5) coupled with the heat transfer and inputs to the model give the information about flows of gases, solids and its composition.

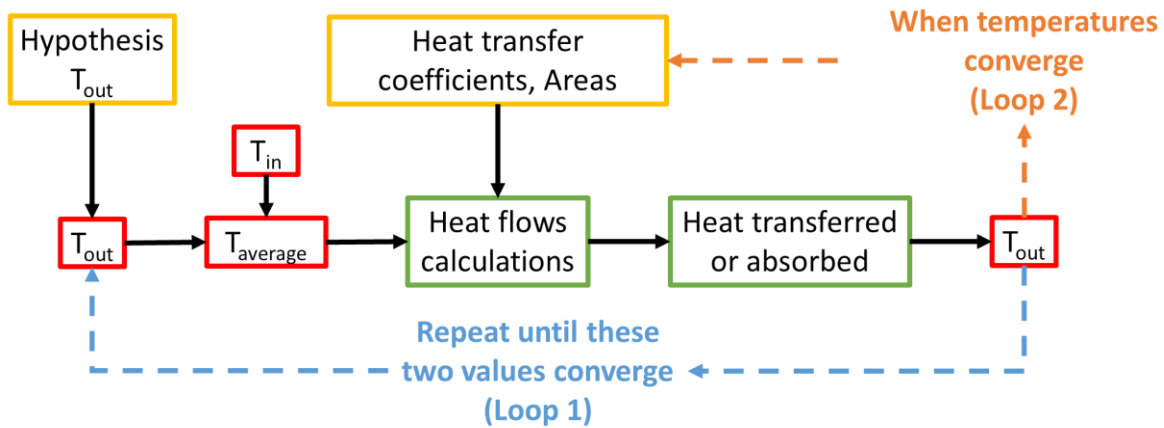


Figure 4.13: Heat transfer process for each slice

To start, the first series of temperature values are suggested for the gas, bed of solids and wall as final temperature. These values are 1 °C higher than the entrance for the gas and the bed of solids and 1 °C lower than the entrance value for the wall. The wall temperature is attributed to the combustion gases flowing around the inner kiln and acting as the heat source with a counter-current configuration. One of the assumptions is the lack of gradient through the wall from the combustion gases to the inner wall.

*Assumption 11: There is no temperature gradient through the wall of the kiln.*

With the first estimation of the exit temperatures of each component, the average temperatures are estimated, and the heat flows by conduction (Equation 4.3), convection (Equation 4.5) and radiation (Equation 4.21) are calculated. Equation 4.40 is then employed to find the exit temperature. With this exit temperature, the average temperature and the heat flows could be different, and the process is repeated using the new exit temperatures until they converge, which means that from one iteration to another the final temperature does not change. This is Loop 1 from Figure 4.13, which results in new converging temperatures for the three components.

Once calculated, the viscosity and density of the gases are re-calculated, and the temperature is recalculated to see the effect of this variation on the final temperature. This part is attributed to the second loop, corresponding to the effects of some temperature-dependent properties, especially the ones for the gases inside the reactor and the combustion gases (Figure 4.13). Once the properties change on the second loop, the first loop needs recalculation until it converges again. The calculation of a step is finished once the first and second loop converge simultaneously, which happens when the properties are recalculated and the difference is minimal. The resulting temperature is the same as before.

Equation 4.40 is general, and it has to be amended for each specific component to include other aspects that affect the heat demand, for instance, moisture content, the heat of reaction or variation of mass flow is considered for the bed of solids. Likewise, the flow of gases inside the reactor accounts for variable mass flow and different gas temperature and flow mixing. A good example is represented when the feedstock is partially converted into pyrolysis gases. These pyrolysis gases are released and mixed with the previous gas flow, which is probably at a different temperature and with a different flow. The resulting mixture should account for temperature and properties of both gas currents with a different contribution of each gas stream to the final one, depending on the flow and temperature. This is a brief introduction to the whole integrated model; a more detailed description of the model is found in Section 7.3.2, where Equation 4.40 is explained for each component.

$$\sum_{i=0}^{cond,conv,rad} Q_j^i [W] = \dot{m}_j \left[ \frac{kg}{s} \right] \cdot C_{p_j} \left[ \frac{J}{kg \cdot K} \right] \cdot (T_{out} - T_{in})_j [K]$$

Equation 4.40: Variation of temperature with heat absorbed

## 4.6 References

1. Bridgwater, A.V., *Review of fast pyrolysis of biomass and product upgrading*. Biomass and Bioenergy, 2012. **38**(Supplement C): p. 68-94.
2. Le Capitaine, S. and C. Carlson, *Principles of heat transfer as Applied to Rotary Dryers, Rotary Kilns and Rotary Coolers*. 2019, FEECO International.
3. Çengel, Y.A., A.J. Ghajar, and M. Kanoglu, *Heat and mass transfer: fundamentals & applications*. 2015: New York, N.Y.: McGraw-Hill Education, ©2015. 5th ed. in SI units.
4. Marín Herrero, J.M., C. Monne Bailo, and J. Uche Marcuello, *Transferencia de calor*. 2007: Zaragoza : Kronos, 2007. 2ª ed.
5. Levenspiel, O., *Chemical reaction engineering*. 3rd ed. ed. 1999: Wiley.
6. Bridgwater, A.V., *Maximum minimum dimension of a particle*, J. López-Ordovás, Editor. 2019, Aston University: EBRI.
7. Le Guen, L., et al., *Heat convection and radiation in flighted rotary kilns: A minimal model*. The Canadian Journal of Chemical Engineering, 2017. **95**(1): p. 100-110.
8. Incropera, F.P., *Fundamentals of heat and mass transfer*. 2007: Hoboken, NJ : John Wiley, ©2007. 6th ed. / Frank P. Incropera ... [et al.].

9. Ghiaasiaan, S.M., *Convective heat and mass transfer. [electronic resource]*. 2011: Cambridge ; New York : Cambridge University Press, 2011.
10. Ghoshdastidar, P.S., *Heat transfer. [electronic resource]*. 2012: New Delhi : Oxford University Press, 2012. Second edition.
11. Fahien, R.W., *Fundamentals of Transport Phenomena*. 1983, New York: McGraw-Hill.
12. Cornwell, K., *Transferencia de calor*. 1981, México: Editorial Limusa S.A. De C.V.
13. Gnielinski, V., *Neue Gleichungen für den Wärme- und den Stoffübergang in turbulent durchströmten Rohren und Kanälen*. Forschung im Ingenieurwesen A, 1975. **41**(1): p. 8-16.
14. Gnielinski, V., *New equations for heat and mass transfer in the turbulent flow in pipes and channels*. NASA STI/Recon Technical Report A, 1975. **41**: p. 8-16.
15. Boateng, A.A., *Rotary kilns: transport phenomena and transport processes*. 2008: Amsterdam ; Boston : Elsevier/Butterworth-Heinemann, ©2008.
16. Tscheng, S.H. and A.P. Watkinson, *Convective heat transfer in a rotary kiln*. The Canadian Journal of Chemical Engineering, 1979. **57**(4): p. 433-443.
17. Holman, J.P., *Heat transfer*. 10th ed., International ed. ed. McGraw-Hill series in mechanical engineering. 2010: McGraw-Hill.

## 5 Kinetic model

### 5.1 Introduction

The kinetics play a vital role in the design and performance of any reactor, which involves a chemical reaction. The kinetic studies aim to calculate the reaction order, pre-exponential factor and activation energy for each step of a reaction mechanism. To understand the complexity of a kinetic model for pyrolysis, it is necessary to mention that the liquid product (pyrolysis oil) is a mixture of more than 300 different chemical compounds [1]. Some of the reasons for this complex mixture are the range of substances within lignocellulosic biomass: cellulose, hemicellulose and lignin [2, 3]. The complexity of the products highlights the associated complexity with the reaction kinetics.

A comprehensive model to simulate the kinetics of pyrolysis was created by Peters et al. [4] for fast pyrolysis. The group of reactions considered did not take into account the possible secondary cracking by the condensable vapours to the char. Peters et al. [5] tried to have a reliable set of reactions without being too complicated, for the compilation of the model and the understanding of the reader. Despite trying to have a comprehensive model without many equations, there were 149 chemical reactions to model the pyrolysis process with each of the components and products. His model was validated with successful results [6] although it could be only used for fast pyrolysis, and it should be expanded if slow or intermediate pyrolysis were used.

For a first approximation, Basu [7] establishes several steps during pyrolysis relating to incremental temperature increase. Some of the stages overlap, for the interaction between cellulose, hemicellulose and lignin and their broad range of decomposition temperatures:

- **Drying:** in the majority of reactions, the biomass is not completely dry, and there is some remaining moisture content in the biomass which is evaporated before pyrolysis starts. Feedstock moisture content is a critical parameter in the overall energy demand and the need for an external source of energy for the reactor. When the feedstock moisture content is high, lignin can be melted with a high decomposition range [7]. This last effect is called steam bending, and this property is utilised in furniture manufacture [8].
- **Initial stage:** this stage takes place after the biomass is moisture free and before reaching 300 °C. The low weight volatile matter such as CO and CO<sub>2</sub> is released, and any remaining water vapour is evaporated. If the targeted process is torrefaction, this would be the last step.
- **Intermediate stage:** this stage refers mainly to the primary pyrolysis, which takes place within the range 200-600 °C. It is characterised by the decomposition of large molecules into char and condensable and non-condensable vapours.
- **Final stage:** when the temperature is higher than 300 °C, the volatiles start cracking and the production of non-condensable vapours and char increase. The main characteristic of this stage is the transformation of condensable vapours into a gas at high temperatures, and into char at lower temperatures [9, 10].

This first approximation from Basu [7] does not study every single component from the feedstock and the product but uses a “black-box” approach. This approach consists of studying the parameters for the conversion of feedstock into the products, taking into account all processes together [7]. This approach can be used for a specific feedstock with one step design [11] or with multiple steps for a group of feedstock [12]. Other authors studied the decomposition of a single component of the biomass, such as cellulose [13] or lignin [14].

In an extensive review about pyrolysis reaction mechanisms, Anca-Couce [15] analysed the state of the art of pyrolysis kinetics. The conclusions state the need to have more detailed reaction

schemes, reaction pathways and products for the secondary cracking reactions. The only conclusion regarding the mechanism of pyrolysis is the existence of a primary pyrolysis process, whose intermediate liquid compound may react further in secondary cracking reactions.

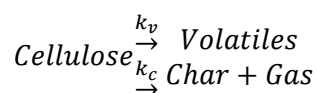
### 5.1.1 Mechanisms suggested

Despite a large number of papers studying the mechanisms of pyrolysis, there is no definitive mechanism or pathway to describe the pyrolysis of biomass; among the classification of pyrolysis mechanisms [16-18], Patwardhan [17] classified them into three different categories represented in Table 5.1.

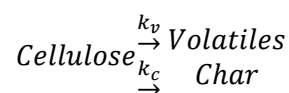
Table 5.1: Classification of pyrolysis mechanisms, adapted from [17]

| Category  | Reaction models  |
|---|--|
| Single-step with multiple competitive reactions   | Broido and Nelson [19], and Suuberg and co-workers [20,21] |
| Single first-order irreversible reaction          | Cooley and Antal [23]                                      |
| Two-step process, primary and secondary reactions | Broido and Shafizadeh [24], and Koufopoulos [26]           |

The first comprises the mechanisms that describe the process in a single step, but with multiple competitive reactions within. This category includes the models from Broido and Nelson [19] and the model proposed by Milosavljevic et al. [20, 21]. The model from Broido and Nelson [19] was proposed for the degradation of cellulose, which shows a preference towards the formation of char and low molecular weight volatiles if the temperature is lower than 250°C. This tendency changes when 280°C is surpassed because tar formation becomes significant. Milosavljevic et al. [20, 21] introduced the innovation of studying the pyrolysis of cellulose with different heating rates from low heating rates of 0.1 °C/min up to 60°C/min. This resulted in a variation of the activation energy at around 320 °C from 218 kJ/mol to 140 kJ/mol. This effect was attributed to two competitive reactions in a single step; an endothermic reaction for the formation of tar favoured by higher heating rates due to the volatilisation, with an energy demand of 538 J/g of volatiles. At low heating rates, the exothermic reaction of char was favoured, releasing 2000 J/g of char formed.



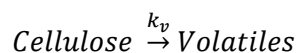
Reaction 5.1: Broido and Nelson model



Reaction 5.2: Suuberg and co-workers model

The second category of models includes the mechanisms where the expression for the thermal decomposition is a single first-order irreversible reaction. In a preliminary study, Mok and Antal [22] observed the large particle size used in the previous experiments and predicted the existence of heat and mass transfer processes. After the experiments with a TGA and DSC, it was observed that small sample size and high gas flow rates minimised the amount of char produced, and the reaction was endothermic. In examples of larger particle sizes and low flow rates, the char yield increased, and the reaction was exothermic. To continue with this study, Cooley and Antal [23] conducted a study of the cellulose pyrolysis kinetics minimising any mass or heat transfer process which could potentially affect the decomposition. According to the results, a first-order reaction fitted the results with the activation energy for the pyrolysis of ash-free cellulose of 193 kJ/mol.





Reaction 5.3: Cooley and Antal model

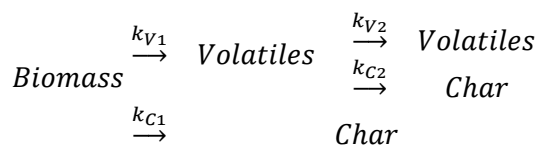
The last category includes the kinetic models where there are two steps, which account for the primary and secondary reactions. The first model belonging to this category appeared a few years after Broido and Nelson [19] released theirs. This mechanism was modified by Shafizadeh and renamed as the Broido and Shafizadeh (B-S) model (Reaction 5.4) [24, 25], which proposed an initial step with depolymerisation to produce a compound called *active cellulose*, an anhydrous fragment of the original cellulose.

The active cellulose degraded through single-step reactions into volatiles and char. In this case, the volatiles referred to both condensable and non-condensable vapours. It is debatable if this mechanism should be in this category because it does not technically have two steps for reactions, but only one - because the first one is activation. Shafizadeh et al. [24] modified the original B-S mechanism to produce the modified Broido and Shafizadeh model (Reaction 5.4). This modified model had a new first step with three competitive reactions for the production of the three primary products (condensable vapours, char and gases). The condensable vapours decompose to obtain gas and char.

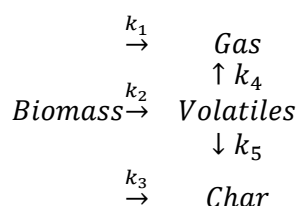
The last model analysed within the work of Partwardhan [17] is that produced by Koufopoulos et al. (Reaction 5.5) [26], which produces in the first step, volatiles and char. The volatile compounds react with the char to produce secondary volatiles and char. Recent models such as those developed by Di Blasi et al. [14, 27, 28] or Fantozzi et al. [29] are based on the modified Broido and Shafizadeh model [24], or the work from Gómez [12] where the model from Suuberg [20, 21] and coworkers was used to determine the kinetics of different feedstocks.



Reaction 5.4: Broido and Shafizadeh (B-S) model



Reaction 5.5: Koufopoulos model

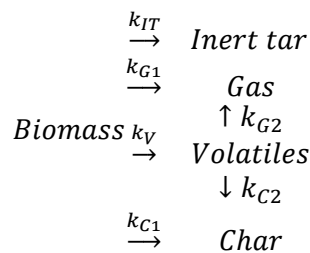


Reaction 5.6: Modified Broido and Shafizadeh model

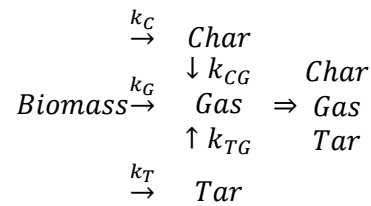
In this categorisation, there is a missing mechanism - the instances with single-step reaction orders and variable reaction orders. In section 5.2, the methods to calculate the kinetic parameters will be explained. One of these uses a single reaction step for the decomposition of the feedstock, but when the reaction order is different to 1, such as in the work of Cortés and Bridgwater [11], none of the mechanisms describes the results. A broader classification would be needed to include this mechanism, single irreversible reaction with any reaction order.

Further mechanisms fall out of the classifications described above. The mechanism studied by Babler et al. [30] is very similar to the modified B-S, with the difference of having a portion of inert tar that remains until the end, which would be equivalent to the pyrolysis liquid (Reaction 5.7). In the

model of Neves et al. [31], the mechanism is similar to water as an extra component, which remains independent until the end with part of the tar converted to water. Finally, the mechanism from Papari et al. [32] is similar to the modified B-S. The main difference is that both char and tar contribute to the gas instead of further cracking of tars into char and gas.



Reaction 5.7: Babler mechanism



Reaction 5.8: Papari mechanism

Within the review of the kinetics of pyrolysis, Anca-Couce [15] studied other mechanisms. The mechanism from Piskorz et al. [33] included an activation step, which happened at the same time as the initial production of char and gas. The second step was more specific and aimed at the formation of hydroxyacetaldehyde and levoglucosan in two competitive reactions. Instead of using a general equation, this model was aimed at the kinetics of specific products and did not connect each component with the general product. The same occurs with the mechanism proposed by Banyasz et al. [34, 35], which includes a third step from the two last products to produce hydroxyacetaldehyde, formaldehyde and more levoglucosan. Furthermore, there is the model suggested by Costa et al. [36], which accounts for nine different reactions where all the four products and the feedstock interact together.

Finally, at the limit of the “black-box”, we can find two models whose main difference is the inclusion in the RAC model [37] of the secondary cracking reactions - one of the main weaknesses of the model from Ranzi et al. [38]. It is very complicated if it is compared to the other models. In these two models, pyrolysis of feedstock is calculated as the superposition of pyrolysis of each component. The volatiles produced are represented by twenty species; one fragmentation reaction has 10 different species as products, and each of the components has a different mechanism and number of steps. This complexity makes the models more accurate but more difficult to integrate for the design of a model for a pyrolysis reactor and less feasible for this project. As a consequence, the model employed within this PhD project accounts for each feedstock as a whole instead of considering it as the superposition of cellulose, hemicellulose, lignin and others such as inorganic content or plastics in the case of lignocellulosic biomass and RDF, respectively.

## 5.2 Approach

The kinetic submodel is a fundamental and crucial part of the model created for this PhD project. It has to approximate the real behaviour of the different feedstocks. The kinetic model aims to simulate the chemical behaviour of the feedstock and its variation with the temperature. The parameters to simulate are the reaction steps, the reaction order, pre-exponential factor and activation energy. The production of vapours inside the reactor and the product distribution are also included.

The “black-box” approach is a suitable method for this project to model the behaviour of the feedstock through pyrolysis because the results tend to fit the behaviour from the experiments accurately. A more complicated approach such as the mechanism from Razi and Anca-Couce et al. [37, 38] or the reactions list from Peters et al. [4] which would be more time-demanding and not feasible for the scope of this project. This study is conducted for each feedstock specified by the project,

instead of for each biomass component because the composition of cellulose, hemicellulose and lignin is not fixed [39-41]. The proportions within the feedstock change from source to source, even if the feedstock has the same name [7, 40, 41]. Furthermore, one of the feedstocks is RDF, which is well-known for its variability in composition because of its municipal waste origin, and the type and proportion of plastics vary significantly among all types of RDF [42-46].

Instead of defining a mechanism and adapting the data from experiments to that mechanism, the procedure will be the opposite, similar to other studies, which conducted experiments and found the mechanism based on results [11, 42, 47, 48]. The data will be analysed, and the mechanism will be defined based on these results. Among many studies about pyrolysis kinetic with a simplistic approach, there are two main types approaches in the literature to fit pyrolysis behaviour: isothermal [14, 19, 26, 49-52] and isoconversional [11, 24, 25, 42, 48, 53-58]. These approaches can be extrapolated to other thermochemical processes such as combustion, as demonstrated by Álvarez et al. [59] when the isoconversional approach is used to analyse combustion or by Henrich et al. [49] and Savage et al. [60, 61] using the isothermal approach for combustion and hydrothermal liquefaction, respectively. These two approaches are described in the following sections.

### 5.2.1 Isothermal

The isothermal method analyses the degradation of the feedstock in a chamber or reactor where the temperature remains constant. There is a preceding step where the temperature of the chamber has to be increased to the target for pyrolysis, and it can be completed in two different ways [14]:

- Firstly, very low heating rates (1.5-2.5 °C/min) can be used to raise the temperature. This is an excellent approach to avoid gradients within the particle. However, the weight loss is not negligible, and an important fraction of the weight loss may have occurred during this heating step [14].
- The other option is to place the sample in a reactor or chamber that has been previously pre-heated. It is a more realistic approach because the heating rates are more similar to those in an industrial reactor. Nevertheless, the samples are very likely to suffer from heat transfer limitations and have intra-particle temperature gradients [14].

Branca and Di Blasi [51] chose a heating rate of 1000 °C/min to achieve a final temperature of 300-435 °C; Di Blasi [14] used heating rates of 27-36°C/min to reach final temperatures of 270-340 °C; The works from Koufopoulos et al. [26] and Bradbury et al. [50] used unknown heating rates for the dynamic step and final temperatures of 300-600 °C and 259-341 °C, respectively.

The reaction rates increase with temperature, and the final solid char yields decrease. This is deduced from the representation of the remaining sample weight divided by the initial mass of feedstock when plotted against the time at different temperatures (from Figure 5.1). The letter  $Y$  represents the current weight of the sample divided by the initial weight, which results in a dimensionless number, the letter  $t$  is the time measured in seconds. The heating rate employed in the experiments is 1000 K/min [51].



*Figure 5.1: Weight loss curves of wood for different sample temperatures (From Branca and Di Blasi [51])*

For this method, the number of steps is determined by the change in the slope when the logarithm of the difference of the normalised weight of the sample minus the normalised weight of the sample at the end of the experiment. The method was explained by Di Blasi [14] but also applied by Branca and Di Blasi [51] and shown in Figure 5.2. The meaning of the letters are explained below:

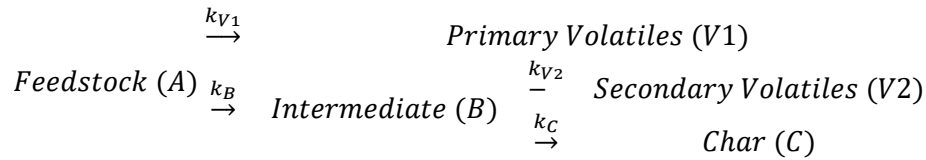
- $Y$ : weight fraction of the sample, division of the actual weight by the initial mass [-]
- $Y_{C\infty}$ : weight fraction of the sample at the end of the experiment [-]
- $T_r$ : reaction temperature [K]
- $t$ : reaction time [s]



*Figure 5.2: Logarithm of the volatile mass fraction as a function of time (From Branca and Di Blasi [51])*

From this figure, the lines are not straight, and there is a change in the gradient. According to Di Blasi [14], the slope changes when the reaction goes from one step to another. In this case, the mechanism employed is the modified Broido and Shafizadeh, explained previously in Reaction 5.6.

The model used by Di Blasi was represented by the following equations, constants and terms:



Reaction 5.9: Di Blasi mechanism

In this mechanism, the initial feedstock is degraded into primary volatiles and the intermediate products. This intermediate product has the char and secondary volatiles from thermal decomposition. The terms primary and secondary volatiles refer to its source. The origin of primary volatiles is the feedstock, and the origin of the secondary volatiles is the intermediate compound. The following equations are deduced:

$$\frac{dM_A}{dt} = -k_1 \cdot M_A$$

Equation 5.1: Reaction rate of the feedstock

$$\frac{dM_B}{dt} = k_B \cdot M_A - k_2 \cdot M_B$$

Equation 5.2: Reaction rate of the intermediate compound

$$\frac{dM_{V1}}{dt} = k_{V1} \cdot M_A$$

Equation 5.3: Reaction rate for the primary volatiles

$$\frac{dM_{V2}}{dt} = k_{V2} \cdot M_B$$

Equation 5.4: Reaction rate for the secondary volatiles

$$\frac{dM_C}{dt} = k_C \cdot M_B$$

Equation 5.5: Reaction rate for the char

The terms  $k_1$  and  $k_2$  are not defined in the scheme because it includes two kinetic constants:

$$k_1 = k_B + k_{V1}$$

Equation 5.6: definition of  $k_1$

$$k_2 = k_C + k_{V2}$$

Equation 5.7: definition of  $k_2$

All the reaction constants are supposed to follow the Arrhenius equation for any of the components:

$$k_i = A_i \cdot e^{\left(\frac{-E_{ai}}{R \cdot T}\right)}$$

Equation 5.8: Arrhenius equation for the kinetic constant

The initial and final weights of each component are defined below as the boundary conditions to solve the equations:

$$M_A(0) = W(0) = M_0$$

$$M_B(0) = M_{V1}(0) = M_{V2}(0) = M_C(0) = 0$$

$$M_{V1}(\infty) = M_{V1\infty}$$

$$M_{V2}(\infty) = M_{V2\infty}$$

$$M_C(\infty) = M_{C\infty}$$

$$W_{C\infty} = M_{C\infty}$$

Integrating the equations with the conditions, the following expressions are obtained to define the weight of each component at a time ( $t$ ):

$$M_A = M_0 \cdot e^{-k_1 \cdot t} \quad M_{V1} = \frac{M_0 \cdot k_{V1}}{k_1} \cdot (1 - e^{-k_1 \cdot t}) \quad M_B = \frac{M_0 \cdot k_B}{k_1 - k_2} \cdot (e^{-k_2 \cdot t} - e^{-k_1 \cdot t})$$

Equation 5.9: Weight of feedstock with time

Equation 5.10: Primary volatiles production

Equation 5.11: Production of the intermediate product

$$M_{V2} = \frac{M_0 \cdot k_B \cdot k_{V2}}{(k_1 - k_2) \cdot k_1 \cdot k_2} \cdot (k_1 - k_2 - k_1 \cdot e^{-k_2 \cdot t} + k_2 \cdot e^{-k_1 \cdot t})$$

Equation 5.12: Secondary volatiles production

$$M_C = \frac{M_0 \cdot k_B \cdot k_C}{(k_1 - k_2) \cdot k_1 \cdot k_2} \cdot (k_1 - k_2 - k_1 \cdot e^{-k_2 \cdot t} + k_2 \cdot e^{-k_1 \cdot t})$$

Equation 5.13: Char production with time

The residual solid mass is defined with the letter  $W$ , and it is the sum of the three mass components: feedstock, intermediate product and char:

$$W = M_A + M_B + M_C$$

Equation 5.14: Solid residual

The final product yields are calculated when the time is significant, and it is assumed that the mass of components remains constant with infinite time:

$$M_{V1\infty} = \frac{k_{V1} \cdot M_0}{k_1}$$

Equation 5.15: Final mass of primary volatiles

$$M_{V2\infty} = \frac{k_{V2} \cdot k_B \cdot M_0}{(k_1 - k_2)}$$

Equation 5.16: Final mass of secondary volatiles

$$M_{C\infty} = \frac{k_C \cdot k_B \cdot M_0}{k_2 \cdot k_1}$$

Equation 5.17: Final mass of char

In Figure 5.2, there is a change in the slope, which indicates the point where there is a transition between the first and second step. This time is defined as the demarcation time ( $t^*$ ), and it is the moment when the concentration of the intermediate product B is maximum ( $M_{B^*}$ ). At this point, the first stage has been completed, and the only active reaction is the second stage. From this definition, there is a new method to define the total mass of primary and second volatiles production:

$$M_{V1} = M_0 - W$$

Equation 5.18: Mass of primary volatiles

$$M_{V1\infty} = M_0 - M_{B^*}$$

Equation 5.19: Final mass of primary volatiles

$$M_{V2} = M_{B^*} - W$$

Equation 5.20: Mass of secondary volatiles

$$M_{V2\infty} = M_{B^*} - M_{C\infty}$$

Equation 5.21: Final mass of secondary volatiles

Combining Equation 5.10, Equation 5.15, Equation 5.18 and Equation 5.19, the dimensionless mass fraction ( $P_1$ ) is obtained for the first step. This parameter represents the remaining fraction of primary volatiles to be converted.

$$\ln \left( 1 - \frac{M_0 - W}{M_0 - M_{B^*}} \right) = \ln(P_1) = k_1 \cdot t$$

Equation 5.22: Dimensionless solid weight for step I

The combination of Equation 5.4, Equation 5.19 and Equation 5.20 gives the dimensionless solid weight of step II ( $P_2$ ). Similarly to  $P_1$ ,  $P_2$  shows the remaining fraction of secondary volatiles to be converted.

$$\ln\left(1 - \frac{M_{B^*} - W}{M_{B^*} - M_{C\infty}}\right) = \ln(P_2) = k_2 \cdot (t - t^*)$$

Equation 5.23: Dimensionless solid weight for step II

The logarithm of dimensionless solid weights ( $P_1$  and  $P_2$ ) are plotted against the time to obtain the kinetic constants. An example of this representation is Figure 5.3, taken from Branca and Di Blasi [51]. The slope of each line is the kinetic constant at that temperature, so the kinetic constants  $k_1$  and  $k_2$  and their respective activation energies and pre-exponential factors can be calculated in this step.



Figure 5.3: Dimensionless solid mass fraction vs time, from [51]

Given the value of  $k_1$  and  $k_2$ , the final volatile value  $V_{1\infty}$  and  $V_{2\infty}$ , and the Equation 5.6, Equation 5.7, Equation 5.15 and Equation 5.16; the values of the remaining kinetic constants ( $k_{V1}$ ,  $k_{V2}$ ,  $k_B$  and  $k_C$ ) are solved.

In a reactor, the biomass is introduced in a chamber where temperatures are high, and it is exposed to high heating rates and large temperature differences. The isothermal method tries to analyse the behaviour of a sample of biomass under similar conditions, using high heating rates at the beginning to achieve the reaction temperature as soon as possible. Ideally, the sample should be placed in a chamber where the temperature is already at the reaction temperature [14].

This main advantage of this method results in a disadvantage because the kinetics of the reaction are not the only process studied. Within the bed of solids and the particle, there are some mass and heat transfer limitations. The heat flow to the particle can be high, and its thermal conductivity might not be high enough to transfer all that heat, which could result in a temperature gradient within the particle. A mass transfer limitation would be ignoring the time it takes for the gases to be released from the particle [14].

## 5.2.2 Isoconversional

The decomposition of feedstock is generally expressed in Equation 5.24. This expression shows that the variation of conversion ( $\alpha$ ) with time depends on the rate constant and a function of the conversion. The conversion is defined in Equation 5.25 and is the difference between the initial mass ( $m_0$ ) and mass at a certain time ( $m_t$ ) divided by the difference of the initial mass with the final mass when the experiments finish ( $m_\infty$ ). The kinetic constant follows an Arrhenius expression, represented in Equation 5.8. The function that describes the dependency on conversion can be defined as Equation 5.26 when it is referred to as a pure kinetic expression [11, 42, 55, 58].

$$\frac{d\alpha}{dt} = k \cdot f(\alpha)$$

Equation 5.24: Expression for solid decomposition

$$\alpha = \frac{m_0 - m_t}{m_0 - m_\infty}$$

Equation 5.25: Definition of conversion

$$f(\alpha) = (1 - \alpha)^n$$

Equation 5.26: mechanistic term

The iso-conversional methods study the decomposition of the feedstock in a range of temperatures. The increase in temperature is defined by a constant heating rate for each of the experiments. The heating rate is defined by the letter  $\beta$  as in Equation 5.27. If the heating rate and the general conversion definition are combined, Equation 5.28 is obtained.

$$\beta = \frac{dT}{dt}$$

Equation 5.27: Heating rate

$$\frac{d\alpha}{dt} \cdot \frac{dT}{dT} = \frac{d\alpha}{dT} \cdot \frac{dT}{dt} = \frac{d\alpha}{dT} \cdot \beta$$

Equation 5.28: Combination heating rate with the general expression

Combining Equation 5.24, Equation 5.8 and Equation 5.28, the dependency of conversion with temperature can be calculated as shown in Equation 5.29. It can be recombined to calculate the integral function  $g(\alpha)$  according to Equation 5.30.

$$\frac{d\alpha}{dT} = \frac{A}{\beta} \cdot e\left(-\frac{E_a}{R \cdot T}\right) \cdot f(\alpha)$$

Equation 5.29: Variation of conversion with Temperature

$$g(\alpha) = \int_0^\alpha \frac{d\alpha}{f(\alpha)} = \frac{A}{\beta} \int_0^T e\left(-\frac{E_a}{R \cdot T}\right) \cdot dT$$

Equation 5.30: Integral function

The function  $g(\alpha)$  changes its expression depending on the reaction mechanism. The most common mechanisms are summarised in Table 5.2 [11, 62].



Table 5.2: Integral mechanisms and mechanistic terms for the most common reaction mechanisms

| Reaction Mechanism                | $g(\alpha)$                                   |
|-----------------------------------|---|
| Chemical reaction models          |   |
| 1 <sup>st</sup> order             | $-\ln(1 - \alpha)$                            |
| Reaction order $N \neq 1$         | $[(1 - \alpha)^{1-N} - 1] / (N - 1)$          |
| Diffusion controlled models       |   |
| 1D transport-plane                | $\alpha^2$                                    |
| 2D transport                      | $\alpha + (1 - \alpha) \cdot \ln(1 - \alpha)$ |
| 3D transport-spherical            | $[1 - (1 - \alpha)^{1/3}]^2$                  |
| 3D transport                      | $[(1 + \alpha)^{1/3} - 1]^2$                  |
| Phase boundary reaction models    |   |
| 2D, shrinking cylinder            | $1 - (1 - \alpha)^{1/2}$                      |
| 3D, contraction of sphere         | $1 - (1 - \alpha)^{1/3}$                      |
| Nucleation reaction models        |   |
| $N=1, 1.5, 2, 3$ (Avrami-Erofeev) | $[-\ln(1 - \alpha)]^{1/N}$                    |
| Power law                         | $\alpha^{1/N}$                                |

After the definition of the integral function of the reaction mechanism, different methods can be applied to obtain the activation energy and pre-exponential factor. A selection is represented in Figure 5.4 (adapted from [1]). The two different categories of methods (model-fitting and model-free) describe whether there is a pre-established mechanism for the reaction to fit. In the case of model-fitting methods, the model has been defined previously, and the kinetic parameters are calculated to adapt the results. The most common model-fitting method is Coats and Redfern [63] for the calculation of kinetic parameters [42, 58].

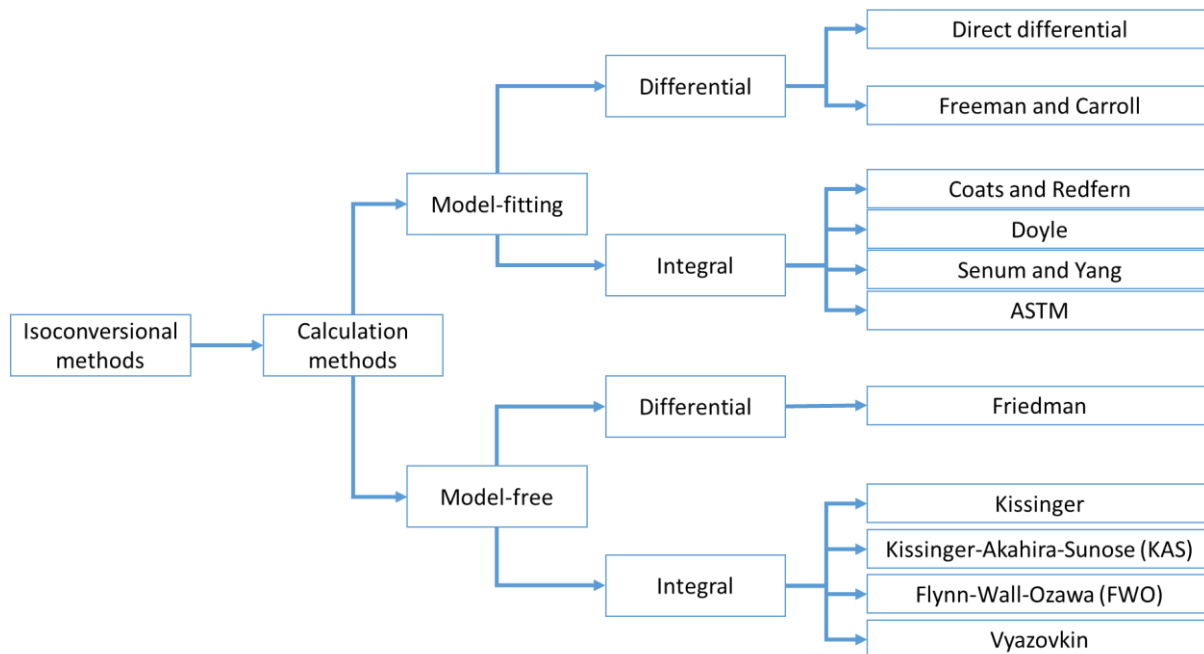


Figure 5.4: Isoconversional methods

The isoconversional methods obtain the values for activation energy and pre-exponential factor from a study where several samples of a feedstock are heated under different heating rates.

These heating rates are kept low to avoid heat transfer limitations. There is no apparent limit reported within the literature for a maximum heating rate where heat transfer limits the process significantly. Çepelioğullar et al. [42] used a maximum heating rate of 50°C/min, Cortés and Bridgwater [11] and Olszewski et al. [58] used 40°C/min without any apparent heat transfer limitations. The crucial advantage of this method is the range of temperatures used. Heat transfer issues are avoided through low heating rates. The main drawback from this process is that the heating rates are usually low (1-10 °C/min), and these heating rates are lower than the ones achieved in real chemical reactors used for slow pyrolysis, so the behaviour is not as realistic as in the isothermal approach [14].

### 5.2.3 The approach employed in this project

This project aims to create a model that can predict the mechanical and process specifications of a reactor from user-specified inputs. One of the user inputs is either the final temperature or the target product (which is correlated to the final temperature of the solids).

This approach allows the study of a broad temperature range. The parameters studied are those associated with the degradation of the biomass and the reaction rate, which are the pre-exponential factor, activation energy and reaction order for each reaction step. However, the temperature within the reactor does not stay constant, but the wall temperature keeps changing until the end of the reactor length. These factors make the isoconversional method more suitable for the study due to the temperature change, the kinetic parameters and a broader change of temperature.

This work does not aim to fit any model to the data in advance. It will be defined from the experiments and the results from the thermogravimetric analysis. With that principle, the model-fitting methods are not applicable in this study, and the focus is on the model-free methods. The model-free methods use mathematical approximations to calculate the activation energy without defining the reaction model [1]. The isoconversional method will be the object of study, and the model will be determined after calculating the activation energy that is required for the pre-exponential factor [11]. Additionally, this work aims to use linear methods to adjust the kinetic expressions, whereas Vyazovkin [64] uses a non-linear approach to calculate the activation energy and pre-exponential factor. The kinetic methods to be used within this work are Kissinger, Kissinger-Akahira-Sunose (KAS), Flynn-Wall-Ozawa (FWO) and Friedman.

#### 5.2.3.1 Kissinger

From the four methods, Kissinger is a bit different from the others. It calculates activation energy and the pre-exponential factor, which is independent of the conversion. The parameters are estimated when the value decomposition rate is maximum. The equation describing the method is Equation 5.31:

$$\ln\left(\frac{\beta}{T_m^2}\right) = \ln\left(\frac{A \cdot R}{E_a}\right) - \frac{E_a}{R} \cdot \frac{1}{T_m}$$

Equation 5.31: Kissinger linear equation

The parameter  $T_m$  is the temperature where the variation of the conversion with temperature  $\left\{\frac{d\alpha}{dT}\right\}$  is maximum. The logarithm of the heating rate divided by the temperature  $\left\{\ln\left(\frac{\beta}{T_m^2}\right)\right\}$  is plotted against the inverse of the temperature  $\left\{\frac{1}{T_m}\right\}$ . The gradient of the graph is the negative value of the activation energy divided by the universal gas constant  $\left\{-\frac{E_a}{R}\right\}$ . The y-axis intercept is the logarithm of the pre-exponential factor multiplied by the universal constant gases and divided by the activation energy  $\left\{\ln\left(\frac{A \cdot R}{E_a}\right)\right\}$  [56, 62].

### 5.2.3.2 KAS (Kissinger-Akahira-Sunose)

The Coats-Redfern temperature integral approximation (Equation 5.32) can be transformed into an expression used for isoconversional calculations:

$$\ln\left(\frac{\beta}{T_{ai}^2}\right) = \ln\left(\frac{A \cdot R}{E_a \cdot g(\alpha)} \cdot \left(1 - \frac{2 \cdot R \cdot T}{E_a}\right)\right) - \frac{E_a}{R} \cdot \frac{1}{T_{ai}}$$

Equation 5.32: Transformed Coats-Redfern temperature integral approximation

This method uses  $1 \gg \frac{2 \cdot R \cdot T}{E_a}$  to simplify the expression, and bases its estimation on Doyle's approximation (Equation 5.33), which can be employed when the conversion is within the range  $0.2 < \alpha < 0.6$ . Applying these two considerations, the KAS expression is obtained (Equation 5.34). This linear expression plots the logarithm of the heating rate divided by the squared temperature at which each conversion is achieved  $\left\{\ln\left(\frac{\beta}{T_{ai}^2}\right)\right\}$  against the inverse of that temperature  $\left\{\frac{1}{T_{ai}}\right\}$ . The slope is the negative value of the activation energy divided by the universal gas constant  $\left\{-\frac{E_a}{R}\right\}$  and the y-axis intercept is the logarithm of the pre-exponential factor multiplied by the universal gas constant divided by the activation energy and the integral function  $\left\{\ln\left(\frac{A \cdot R}{E_a \cdot g(\alpha)}\right)\right\}$  [42, 62].

$$\left[p\left(\frac{E_a}{R \cdot T}\right)\right] \sim \left(e^{-\frac{E_a}{R \cdot T}}\right) / \left(\frac{E_a}{R \cdot T}\right)^2$$

Equation 5.33: Doyle's approximation

$$\ln\left(\frac{\beta}{T_{ai}^2}\right) = \ln\left(\frac{A \cdot R}{E_a \cdot g(\alpha)}\right) - \frac{E_a}{R} \cdot \frac{1}{T_{ai}}$$

Equation 5.34: KAS expression

This method uses an oversimplified temperature integral. It assumes constant activation energy from the beginning of the reaction to the conversion degree of interest and, consequently, some significant error may appear on the activation energy [48].

### 5.2.3.3 FWO (Flynn-Wall-Ozawa)

The FWO method uses another Doyle's approximation (Equation 5.35), which is only valid if  $20 < \frac{E_a}{R \cdot T} < 60$  [62]:

$$\ln\left[p\left(\frac{E_a}{R \cdot T}\right)\right] \sim -5.331 - 1.052 \frac{E_a}{R \cdot T}$$

Equation 5.35: Doyle's approximation for FWO

When this approximation is replaced in Equation 5.30 and rearranged, the expression for FWO approximation becomes Equation 5.36. The logarithm of the heating rate  $\{\ln(\beta)\}$  is plotted against the inverse of the temperature at which each conversion is achieved  $\left\{\frac{1}{T}\right\}$ . The activation energy is calculated from the slope  $\left\{-1.052 \frac{E_a}{R}\right\}$  and the pre-exponential factor is obtained from the y-intercept which has a logarithm of the pre-exponential factor multiplied by the activation energy and divided by the universal gas constant and the integral mechanistic term and a factor from Doyle's approximation  $\left\{\ln\left(\frac{A \cdot E_a}{R \cdot g(\alpha)}\right) - 5.331\right\}$  [1, 11, 42].

$$\ln(\beta) = \ln\left(\frac{A \cdot E_a}{R \cdot g(\alpha)}\right) - 5.331 - 1.052 \frac{E_a}{R} \cdot \frac{1}{T}$$

Equation 5.36: FWO expression

Similarly to the KAS method (5.2.3.2), it comes from an oversimplified temperature integral approximation, derived from the beginning of the reaction to the target conversion degree. The errors in the calculation of the activation energy  $\{E_a\}$  might be significant [48]. Furthermore, the coefficients from Doyle's approximation vary within the literature [65, 66], the differences are observed in Cortés and Bridgwater [11] and Çepelioğullar et al. [42] with different values from Cai et al. [48] and Bryant [62]. According to Lyon [65], the coefficients used within this work are the most commonly used.

#### 5.2.3.4 Friedman

The primary assumption of this method is that the decomposition process depends only on the rate of mass loss, and it is not influenced by the temperature. As a consequence,  $f(\alpha)$  is supposed to be constant. The Friedman method is the only differential method studied and its expression is obtained, taking logarithms at both sides of Equation 5.29, resulting in the Friedman expression, on Equation 5.37 [1, 11].

$$\ln\left(\beta \cdot \frac{d\alpha}{dT}\right) = \ln\left(\frac{d\alpha}{dt}\right) = \ln(f(\alpha) \cdot A) - \frac{E_a}{R} \cdot \frac{1}{T}$$

Equation 5.37: Friedman expression

The logarithm of the variation of the conversion with time  $\left\{\ln\left(\frac{d\alpha}{dt}\right)\right\}$  or the logarithm of the variation of the conversion with temperature multiplied by the heating rate  $\left\{\ln\left(\beta \cdot \frac{d\alpha}{dT}\right)\right\}$  against the inverse of the temperature  $\left\{\frac{1}{T}\right\}$  at which the values of conversion of the mechanistic term  $\{f(\alpha)\}$  are obtained. The slope is the negative value of the activation energy divided by the universal gas constant  $\left\{-\frac{E_a}{R}\right\}$  and the y-axis intercept is the logarithm of the mechanistic term multiplied by the pre-exponential factor  $\{\ln(f(\alpha) \cdot A)\}$ . The reaction order is taken into account in the mechanistic term to estimate the dependency on the conversion [42, 62], according to Cai et al. [48], the results are usually accurate, and it is not limited to a linear variation of the heating rate. It requires derivative conversion data, which can lead to numerical instability and "noise".

## 5.3 Methodology

As observed in previous studies of pyrolysis kinetics [11, 42, 48, 58], the ThermoGravimetric Analysis (TGA) was used to study the behaviour of the different feedstocks and calculate the main parameters. The equipment used was a Mettler Toledo TGA/DSC 2 STARe System (Figure 5.5), connected to a continuous nitrogen flow of 60 ml/min as a carrier gas and to make the atmosphere inert. This high carrier gas flow removes the pyrolysis vapours rapidly and leads to a first assumption. The origin and characteristics of the feedstocks used in this study are described in Section 6.1.

*Assumption 12: Pyrolysis vapours are quickly removed from the sample, and there is no study of the secondary cracking*

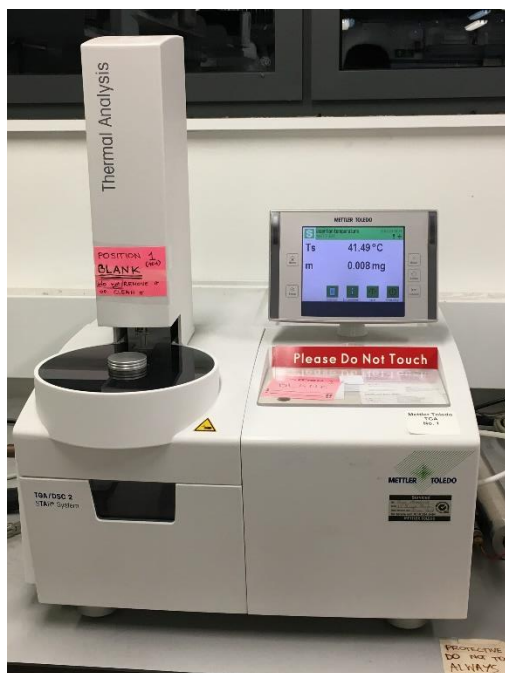


Figure 5.5: Mettler Toledo TGA/DSC 2 STARe System



Figure 5.6: TGA crucibles with wheat straw, woodchips and RDF

The sample is placed in a TGA crucible (Figure 5.6). The crucibles are heated from an initial temperature of 40 °C to 900 °C. The main objective is to avoid any heat or mass transfer limitations within the sample and, consequently, the heating rates should be as low as possible. For that reason, the chosen heating rates are 1, 2.5 and 5 °C/min. For each of the three feedstock and heating rates, the experiment was repeated three times. The initial weight of each sample is represented in Table 5.3.

Table 5.3: Initial weights of samples for TGA

| Samples weight [mg] | 1 K/min |         |         | 2.5 K/min |         |         | 5 K/min |         |         |
|---------------------|---------|---------|---------|-----------|---------|---------|---------|---------|---------|
|                     | 1       | 2       | 3       | 1         | 2       | 3       | 1       | 2       | 3       |
| RDF                 | 27.2036 | 21.776  | 30.1817 | 24.5897   | 29.4005 | 29.7797 | 29.7407 | 29.9886 | 33.6635 |
| Wheat straw         | 23.3203 | 30.5112 | 24.7454 | 25.6552   | 31.2084 | 27.0633 | 33.4002 | 33.8884 | 29.2034 |
| Woodchips           | 13.8105 | 16.5742 | 19.8462 | 15.6173   | 22.9924 | 15.3945 | 23.7163 | 23.5543 | 22.2843 |

The continuous flow of the carrier gas could result in a buoyancy effect, where the mass increases with time instead of undergoing a mass loss. This effect depends on sample volume and the density of carrier gas [67] and has to be subtracted from the actual sample. To check this, an empty crucible is run to see the mass variation, which ideally should be 0 and the results are amended with these runs afterwards.

*Assumption 13: The buoyancy effect of the carrier gas on the empty crucibles is equivalent when they have samples*

### 5.3.1 Experimental results

As a result, the TGA gave the time, sample temperature and remaining mass of the sample without the crucible weight. The buoyancy effect was subtracted from this data to obtain real data. The variation of mass with time is calculated to obtain the DTG (Derivative ThermoGravimetry) curve. The DTG curve is the derivative of the TGA curve, which is equivalent to the variation of weight with

time. Alternatively, it can be expressed as the variation of weight with temperature because time and temperature are fully correlated through the heating rate. The normalised mass and DTG curve of each sample is represented in Figure 5.7, Figure 5.8 and Figure 5.9. A colour scheme is used throughout the chapter to represent the different heating rates. The colour code for the heating rates and their curves are 1 °C/min, 2.5 °C/min and 5 °C/min. The normalised weight on the Y-axis is calculated using Equation 5.38. In this equation,  $W_t$  is the weight of the sample at each time,  $W_0$  is the initial weight (at 120 °C to ensure dried biomass) and  $W_\infty$  is the weight at the end of the experiment.

$$\text{Weight [wt. \%]} = \frac{W_t - W_\infty}{W_0 - W_\infty}$$

Equation 5.38: Normalised weight

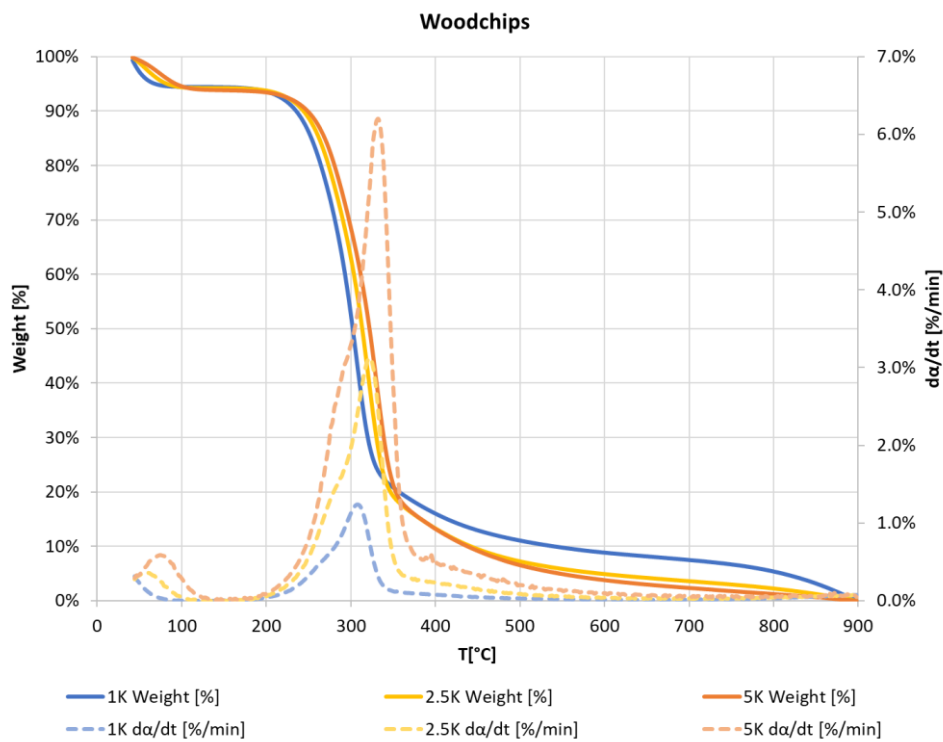


Figure 5.7: Thermogravimetric Analysis and Derivative Thermogravimetry of Woodchips

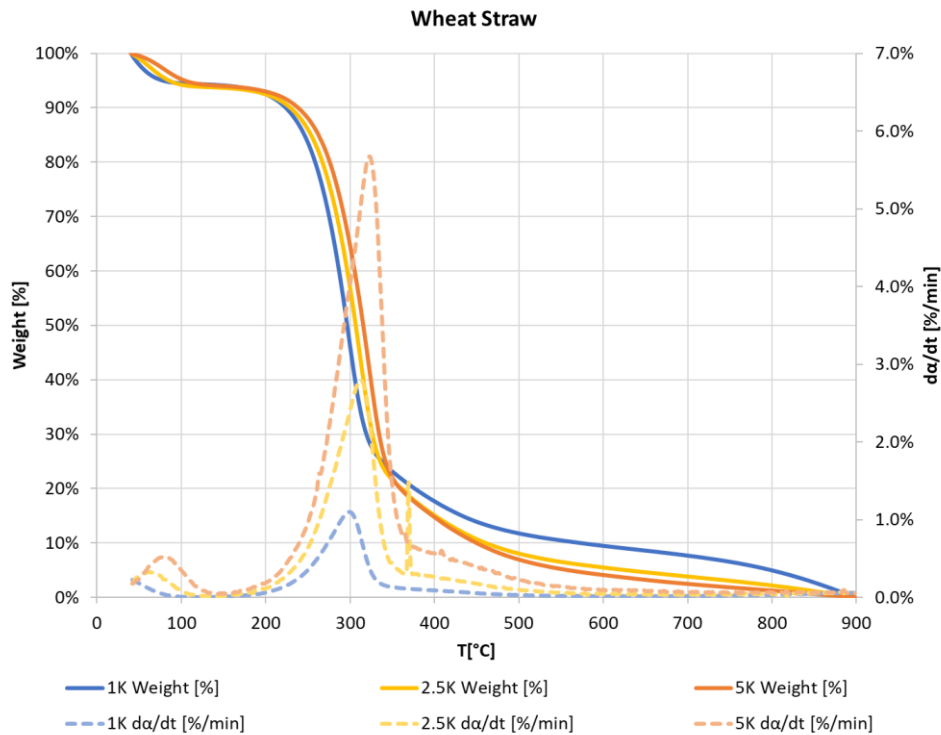


Figure 5.8: Thermogravimetric Analysis and Derivative Thermogravimetry of Wheat Straw

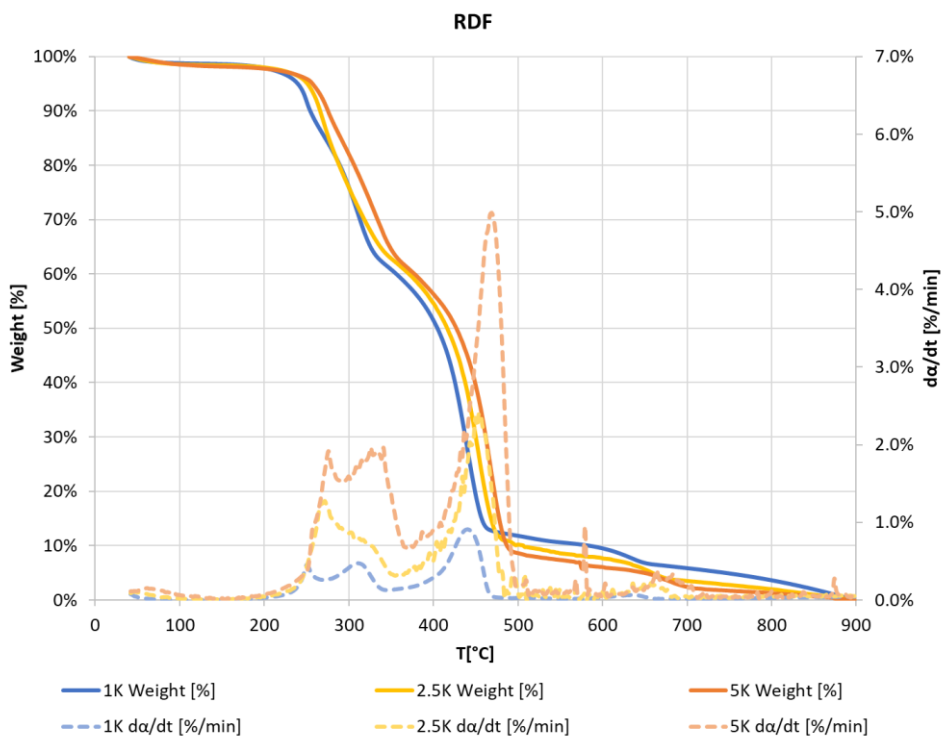


Figure 5.9: Thermogravimetric Analysis and Derivative Thermogravimetry of RDF

In all three cases, there is an initial fall in weight at around 100°C that can be observed in the DTG in peak form. This drop comes from the evaporation of moisture in the sample. In addition to the peak which appears for the lignocellulosic samples of woodchips and wheat straw (Figure 5.7 and Figure 5.8), there is an extra peak in Figure 5.9 for the RDF sample. The first peak is usually associated

with the simultaneous degradation of cellulose and hemicellulose. This data agrees with literature where the temperature ranges for cellulose and hemicellulose are 225-375°C and 200-375°C, respectively [42, 68, 69]. Once both components have degraded, there is still some mass loss with temperature. This mass loss remains until the end of the experiment (900°C), and it is associated with the degradation of lignin, whose degradation range is 200-725 °C [68, 70]. These curves are similar to previous studies in literature, with a peak for the moisture content at 100 °C, one or two peaks for the degradation of the cellulose and/or hemicellulose, and a gradual fall at the end when lignin degrades [11, 42, 55, 58].

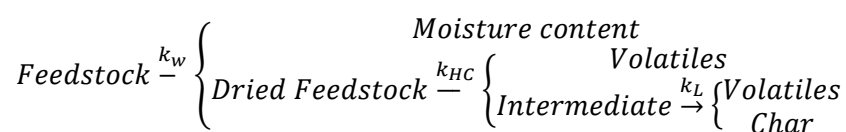
After the moisture evaporation, the TGA graph for RDF (Figure 5.9) has a drop starting at 250 °C. It is noticeable that the DTG for RDF differs from the lignocellulosic materials, whose peaks are narrower. This is associated with cellulose and hemicellulose but can be partially attributed to the degradation of some plastics or a higher portion of hemicellulose than in lignocellulosic biomass. Both cases would explain the first peak at a lower temperature. The initial degradation of plastics would add a peak that did not exist for the other feedstocks, and a higher proportion of hemicellulose would agree with its lower decomposition temperature mentioned previously. The full degradation of plastics is indicated by the second prominent peak at 450 °C. According to literature, the degradation of plastics occurs within a range of 400-475°C [42, 69]. The final part of the experiment is similar to wheat straw and woodchips because there is a continuous mass loss without any significant peak.

The influence of the heating rates on the DTG curves is recognised; the higher the heating rate, the higher value for the curves. This is caused by the TGA, which gives the data at certain temperatures, and the variation of time between two consecutive temperatures is less at higher heating rates. With a lower variation of time between measurements, the DTG term  $\frac{dW}{dt}$  where  $dW$  is the differential of weight during the differential of time ( $dt$ ) increases and gives higher values to the DTG curve.

### 5.3.2 Suggested mechanism

The mechanism is a crucial part of the study because it determines the reaction path followed by each feedstock and the accuracy of the model results. It is an iterative process between the results from the TGA and the possibilities the methods offer. According to the TGA and DTG curves of the woodchips and wheat straw (Figure 5.7 and Figure 5.8), there should be three steps in the reaction when moisture content is considered. The first step is the water evaporation at an approximate temperature of 100 °C; followed by a pyrolysis step for cellulose and hemicellulose, these are the most significant peaks in the DTG curves. Finally, there should be a step for the decomposition of the lignin.

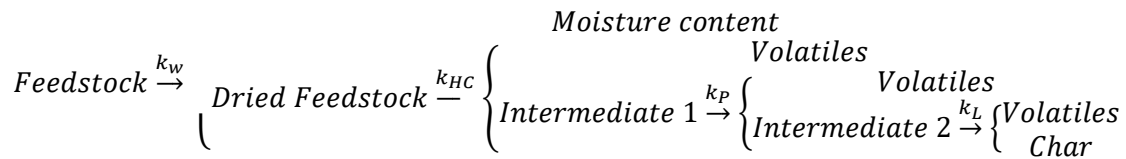
The suggested mechanism is represented on Reaction 5.10, where the letters  $k$  represent the different kinetic constants, and each subscript refers to the decomposing fraction. The process would start with the evaporation of moisture content ( $k_w$ ), the decomposition of cellulose and hemicellulose takes place afterwards ( $k_{HC}$ ), and it finishes with the decomposition of lignin ( $k_L$ ). According to the TGA and DTG curves, there should be a value for each of them. The term *volatiles* is used to define the vapours released from the sample, condensable and non-condensable. Further research about its similarity and an approximate value is given in Section 5.6.



Reaction 5.10: Mechanism suggested for the lignocellulosic feedstock



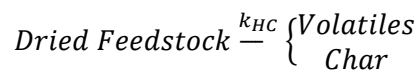
The mechanism for the RDF would be very similar, but with another intermediate step for the decomposition of plastics. In this intermediate step, the constant is  $k_p$  (Reaction 5.11).



Reaction 5.11: Suggested mechanism for pyrolysis of RDF

As explained in Sections 5.3.3 and 5.4, the conversion values have been taken into account from a temperature where the moisture content has been removed, and the calculation of  $k_w$  is considered as a rapid process, which happens when the solid achieves the evaporation temperature. The analysis methods for the kinetics of pyrolysis do not work for high conversion values (above 80% conversion). According to the TGA curves (Figure 5.7, Figure 5.8 and Figure 5.9), the lignin decomposition starts at 80% conversion for lignocellulosic feedstock and 90% for RDF. These values are too high to be analysed by the methods because results at such high conversion values cannot be calculated. In addition to negative activation energies, some negative pre-exponential factors are calculated from the methods, which would mean that the reaction does not take place due to negative velocity (5.4).

The consequence is a change in the suggested mechanisms (Reaction 5.10 and Reaction 5.11) to those proposed by Reaction 5.12 and Reaction 5.13. The terminology is the same as used before, but the kinetic constants for moisture content and lignin decomposition have been removed.



Reaction 5.12: New mechanism for the lignocellulosic feedstock



Reaction 5.13: New mechanism for RDF

### 5.3.3 Data treatment

The TGA gives for each of the samples 5 columns of data. These columns are measured at the same temperatures, the time at which this temperature is achieved is shown in a different column and changes when heating rate varies:

- **Index:** is the time of the experiment, it is measured in seconds, and it is the number of seconds after the sample was placed in the TGA at a temperature of 40°C.
- **Abscissa:** It is identical to the Index column, providing the time since the experiment started.
- **Ts:** is the actual temperature of the sample measured in degrees. The objective of having low heating rates to achieve a very similar temperature to **Tr**.
- **Tr:** refers to the temperature in the oven in degrees.
- **Value:** is the final column and represents the remaining weight of the sample. The initial weight has been introduced to the device, so the weight of the crucible is already subtracted.

As mentioned before (section 5.3), there is a blank run for each heating rate with an empty crucible to measure the buoyancy effect [67]. The first action is to subtract the weight of the blank run (which should be 0). The next step was to find out the conversion ( $\alpha$ ) at each data point, calculated as observed in Equation 5.39.

$$\alpha = \frac{W_0 - W_t}{W_0 - W_\infty}$$

Equation 5.39: Conversion formula

This formula is typically used with the initial weight ( $W_0$ ). Since the main aim of the study was to find the kinetics of pyrolysis (and avoid other processes such as evaporation), this initial weight was not taken at 40°C when the experiments start but at a temperature where the moisture content has been evaporated. The main aim was to avoid the first fall in the TGA/DTG curves, so the initial weight was selected around 120°C, where a flat zone between the end of evaporation and beginning of pyrolysis is observed. This point is defined by a very low  $\frac{d\alpha}{dt}$ , with orders of magnitude of  $10^{-5}$ , low compared to data when peaks appear with magnitude orders of  $10^{-2}$ . The column  $\frac{d\alpha}{dt}$  is calculated through differences as it is shown in Equation 5.40.

$$\frac{d\alpha}{dt} = \frac{\Delta\alpha}{\Delta t} = \frac{\alpha_n - \alpha_{n-1}}{t_n - t_{n-1}}$$

Equation 5.40: Variation of conversion with time

This calculation approach leads to one assumption for the whole model; the lack of effect of the moisture content on the kinetic constants, and it is only considered for the energy consumption and the profile temperature in the heat transfer model.

*Assumption 14: Moisture content does not influence the value of the kinetic constants nor the final yields of products and the evaporation is instantaneous*

The calculation path depends on the method to calculate the activation energy and pre-exponential factor. It is different for Kissinger and for the others. If the Kissinger method is applied (5.2.3.1), there is a requirement to know the temperature at which the reaction rate is maximum, called  $T_m$ . With that purpose, an extra column with the variation of conversion with temperature (Equation 5.41) was added.

$$\frac{d\alpha}{dT} = \frac{\Delta\alpha}{\Delta T} = \frac{\alpha_n - \alpha_{n-1}}{T_n - T_{n-1}}$$

Equation 5.41: Variation of conversion with temperature

Once this temperature is known, the inverse of this temperature  $\left(\frac{1}{T_m}\right)$  is found. The logarithm of the heating rate divided by the square of the temperature is obtained  $\ln\left(\frac{\beta}{T_m^2}\right)$ .

The other methods require the detection of the temperature at which the new conversion values are achieved. The analysed values for conversion were 10%, 20%, 30%, 40%, 50%, 60%, 70%, 80% and 90%. Four extra columns are needed to calculate the parameters through the other three methods. The common X-axis value is the inverse of the temperature at which each conversion is achieved  $\left(\frac{1}{T}\right)$ . For the Y-axis, the following parameters are calculated:  $\ln\left(\frac{\beta}{T^2}\right)$  for KAS,  $\ln(\beta)$  for FWO and  $\ln\left(\frac{d\alpha}{dt}\right)$  for Friedman.

All of these parameters are calculated for each sample of each feedstock at each heating rate. An example of the calculations for each sample is shown in Table 5.4 for Woodchips at a heating rate of 2.5 K/min. The standard deviation of these values is under 5%. Each feedstock at each heating rate has a conversion output for each of the three methods which depends on the conversion value and values for the Kissinger method (see Table 5.5 for Woodchips with a heating rate of 2.5 K/min).

Table 5.4: calculation for each of the samples (Woodchips 2.5 K/min)

|     | Test1    |           |          |          |          | Test2    |           |          |          |          | Test3    |           |          |          |          |
|-----|----------|-----------|----------|----------|----------|----------|-----------|----------|----------|----------|----------|-----------|----------|----------|----------|
|     | 1/T      | Kissinger | KAS      | FWO      | Friedman | 1/T      | Kissinger | KAS      | FWO      | Friedman | 1/T      | Kissinger | KAS      | FWO      | Friedman |
| 10% | 0.001865 | 13.69245  | -11.6524 | 0.916445 | -4.61767 | 0.001858 | 13.69926  | -11.661  | 0.915983 | -4.55896 | 0.001865 | 13.69245  | -11.6524 | 0.916445 | -4.6252  |
| 20% | 0.0018   | 1/Tm      | -11.7239 | 0.916445 | -4.15387 | 0.0018   | 1/Tm      | -11.7239 | 0.916445 | -4.17155 | 0.0018   | 1/Tm      | -11.7239 | 0.916445 | -4.15573 |
| 30% | 0.001752 | 0.001682  | -11.7782 | 0.915983 | -3.8981  | 0.001752 | 0.001676  | -11.7782 | 0.915983 | -3.93972 | 0.001752 | 0.001682  | -11.7782 | 0.915983 | -3.91764 |
| 40% | 0.001719 |           | -11.8154 | 0.916445 | -3.62354 | 0.001719 |           | -11.8154 | 0.916445 | -3.66478 | 0.001719 |           | -11.8154 | 0.916445 | -3.64393 |
| 50% | 0.001694 |           | -11.8454 | 0.915983 | -3.43108 | 0.001694 |           | -11.8454 | 0.915983 | -3.45682 | 0.001694 |           | -11.8454 | 0.915983 | -3.4465  |
| 60% | 0.001676 |           | -11.8673 | 0.915983 | -3.41449 | 0.001669 |           | -11.8741 | 0.916445 | -3.43032 | 0.001676 |           | -11.8673 | 0.915983 | -3.4116  |
| 70% | 0.001652 |           | -11.8957 | 0.916445 | -3.69506 | 0.001646 |           | -11.9028 | 0.916445 | -3.75283 | 0.001652 |           | -11.8957 | 0.916445 | -3.6524  |
| 80% | 0.001594 |           | -11.966  | 0.916445 | -5.40017 | 0.001594 |           | -11.966  | 0.916445 | -5.35094 | 0.0016   |           | -11.9591 | 0.916445 | -5.24913 |
| 90% | 0.001372 |           | -12.2669 | 0.916445 | -6.51926 | 0.00138  |           | -12.255  | 0.916445 | -6.43531 | 0.001384 |           | -12.249  | 0.916445 | -6.37474 |

Table 5.5: Output of the three samples of Woodchips at 2.5 K/min

|     | AVERAGE WC 2.5K |       |           |       |          |       |          |       |          |       |
|-----|-----------------|-------|-----------|-------|----------|-------|----------|-------|----------|-------|
|     | 1/T             | STDEV | Kissinger | STDEV | KAS      | STDEV | FWO      | STDEV | Friedman | STDEV |
| 10% | 0.001863        | 0%    | 13.69472  | 0%    | -11.6553 | 0%    | 0.916291 | 0%    | -4.60061 | 1%    |
| 20% | 0.0018          | 0%    | 1/Tm      | STDEV | -11.7239 | 0%    | 0.916445 | 0%    | -4.16038 | 0%    |
| 30% | 0.001752        | 0%    | 0.00168   | 0%    | -11.7782 | 0%    | 0.915983 | 0%    | -3.91849 | 0%    |
| 40% | 0.001719        | 0%    |           |       | -11.8154 | 0%    | 0.916445 | 0%    | -3.64408 | 0%    |
| 50% | 0.001694        | 0%    |           |       | -11.8454 | 0%    | 0.915983 | 0%    | -3.4448  | 0%    |
| 60% | 0.001673        | 0%    |           |       | -11.8696 | 0%    | 0.916137 | 0%    | -3.4188  | 0%    |
| 70% | 0.00165         | 0%    |           |       | -11.898  | 0%    | 0.916445 | 0%    | -3.7001  | 1%    |
| 80% | 0.001596        | 0%    |           |       | -11.9637 | 0%    | 0.916445 | 0%    | -5.33341 | 1%    |
| 90% | 0.001379        | 0%    |           |       | -12.257  | 0%    | 0.916445 | 0%    | -6.44311 | 1%    |

The data from all heating rates at each conversion are grouped in a table from which the graphs are plotted (see Table 5.6):

Table 5.6: Gather of the values for Woodchips

| Conversion [%] | Heating Rate [K/min] | Kissinger             |             | KAS                    |              | FWO             |             | Friedman        |             |
|----------------|----------------------|-----------------------|-------------|------------------------|--------------|-----------------|-------------|-----------------|-------------|
|                |                      | $Y[\ln(\beta/T_m^2)]$ | $X [1/T_m]$ | $Y[\ln(\beta/Ta_i^2)]$ | $X [1/Ta_i]$ | $Y[\ln(\beta)]$ | $X [1/T]$   | $Y[\ln(da/dt)]$ | $X [1/T]$   |
| 10%            | 1                    | 12.72930793           | 0.00172134  | -12.53629773           | 0.001895735  | 0               | 0.001895735 | -5.531016941    | 0.001895735 |
|                | 2.5                  | 13.69471772           | 0.001679579 | -11.65528842           | 0.001862589  | 0.916290708     | 0.001862589 | -4.600610366    | 0.001862589 |
|                | 5                    | 14.42170087           | 0.001651528 | -10.99182848           | 0.001835425  | 1.609130173     | 0.001835425 | -3.922478414    | 0.001835425 |
| 20%            | 1                    |                       |             | -12.6088976            | 0.001828154  | 0               | 0.001828154 | -5.0636488      | 0.001828154 |
|                | 2.5                  |                       |             | -11.72389382           | 0.001799639  | 0.916444566     | 0.001799639 | -4.160381018    | 0.001799639 |
|                | 5                    |                       |             | -11.05944128           | 0.001774279  | 1.609284031     | 0.001774279 | -3.463636373    | 0.001774279 |
| 30%            | 1                    |                       |             | -12.65587357           | 0.001785714  | 0               | 0.001785714 | -4.765826567    | 0.001785714 |
|                | 2.5                  |                       |             | -11.7782104            | 0.001751826  | 0.915982992     | 0.001751826 | -3.918485104    | 0.001751826 |
|                | 5                    |                       |             | -11.11005204           | 0.001729944  | 1.609284031     | 0.001729944 | -3.281603731    | 0.001729944 |
| 40%            | 1                    |                       |             | -12.6941934            | 0.001751826  | 0               | 0.001751826 | -4.47833586     | 0.001751826 |
|                | 2.5                  |                       |             | -11.81535167           | 0.001719197  | 0.916444566     | 0.001719197 | -3.644083783    | 0.001719197 |
|                | 5                    |                       |             | -11.1522434            | 0.001693959  | 1.609130173     | 0.001693959 | -3.000825561    | 0.001693959 |
| 50%            | 1                    |                       |             | -12.7218337            | 0.001727785  | 0               | 0.001727785 | -4.342159231    | 0.001727785 |
|                | 2.5                  |                       |             | -11.84539058           | 0.001693959  | 0.915982992     | 0.001693959 | -3.444799709    | 0.001693959 |
|                | 5                    |                       |             | -11.18093145           | 0.001669449  | 1.609591747     | 0.001669449 | -2.772104249    | 0.001669449 |
| 60%            | 1                    |                       |             | -12.74663958           | 0.001706485  | 0               | 0.001706485 | -4.387852884    | 0.001706485 |
|                | 2.5                  |                       |             | -11.869554             | 0.00167349   | 0.91613685      | 0.00167349  | -3.418803474    | 0.00167349  |
|                | 5                    |                       |             | -11.20489903           | 0.001649564  | 1.609591747     | 0.001649564 | -2.7223355      | 0.001649564 |
| 70%            | 1                    |                       |             | -12.78327468           | 0.001675511  | 0               | 0.001675511 | -4.966970922    | 0.001675511 |
|                | 2.5                  |                       |             | -11.89804621           | 0.001649564  | 0.916444566     | 0.001649564 | -3.700096526    | 0.001649564 |
|                | 5                    |                       |             | -11.23344288           | 0.001626314  | 1.609437889     | 0.001626314 | -2.961522575    | 0.001626314 |
| 80%            | 1                    |                       |             | -12.93019309           | 0.001556859  | 0               | 0.001556859 | -6.856113942    | 0.001556859 |
|                | 2.5                  |                       |             | -11.96367367           | 0.001596314  | 0.916444566     | 0.001596314 | -5.333412171    | 0.001596314 |
|                | 5                    |                       |             | -11.28660414           | 0.001583531  | 1.609591747     | 0.001583531 | -4.312153726    | 0.001583531 |
| 90%            | 1                    |                       |             | -13.47341234           | 0.001187009  | 0               | 0.001187009 | -8.463841949    | 0.001187009 |
|                | 2.5                  |                       |             | -12.25695769           | 0.00137859   | 0.916444566     | 0.00137859  | -6.443107569    | 0.00137859  |
|                | 5                    |                       |             | -11.55214572           | 0.001386859  | 1.609284031     | 0.001386859 | -5.642034624    | 0.001386859 |

Each of the methods is plotted in Figure 5.10, Figure 5.11, Figure 5.12 and Figure 5.13 are obtained. The important feature is the gradient and the intercept with the Y-axis, represented in Table 5.7. At first glance, the methods do not give very straight lines when the conversion is high. In terms of analytical analysis, the regression value is lower, and the values calculated might not be as reliable. This would agree with what was explained in Sections 5.2.3.2, 5.2.3.3 and 5.2.3.4, where it was mentioned that the methods do not work at high conversion values.

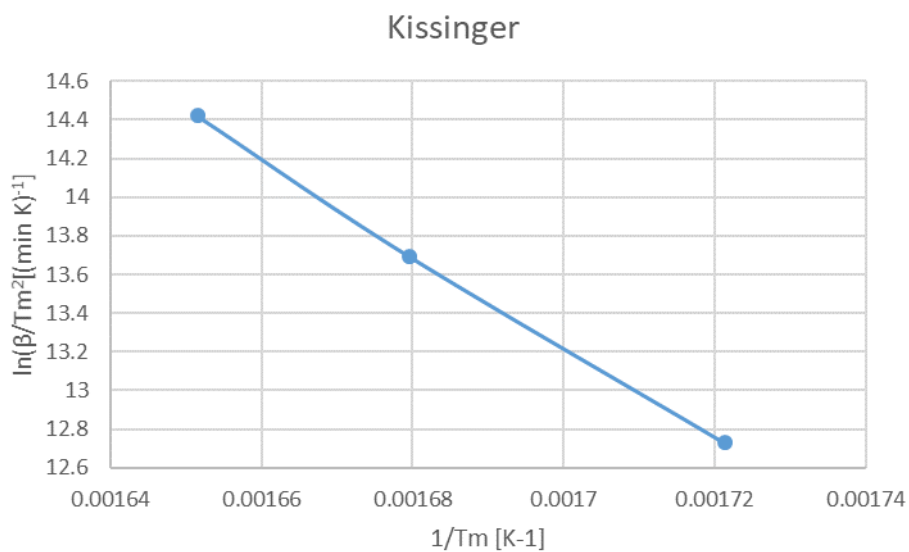


Figure 5.10: Kissinger method for Woodchips

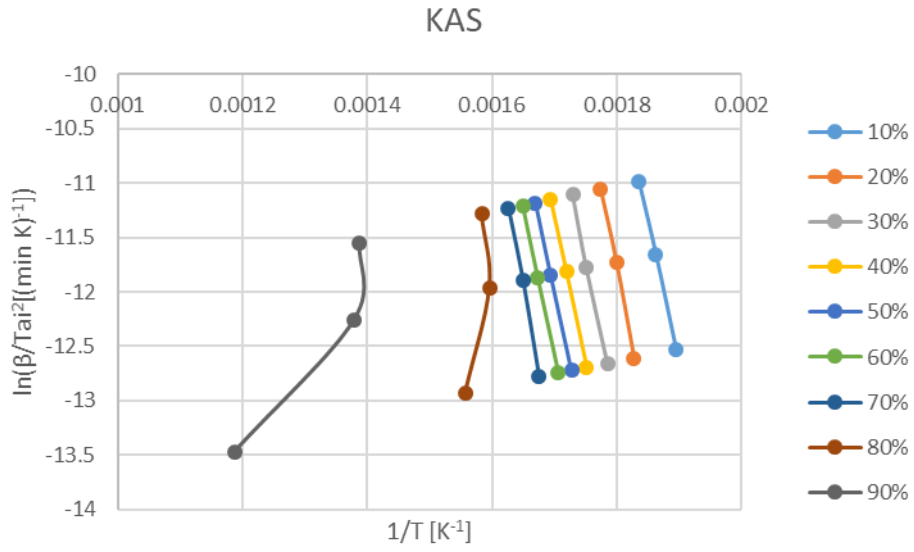


Figure 5.11: KAS method for Woodchips

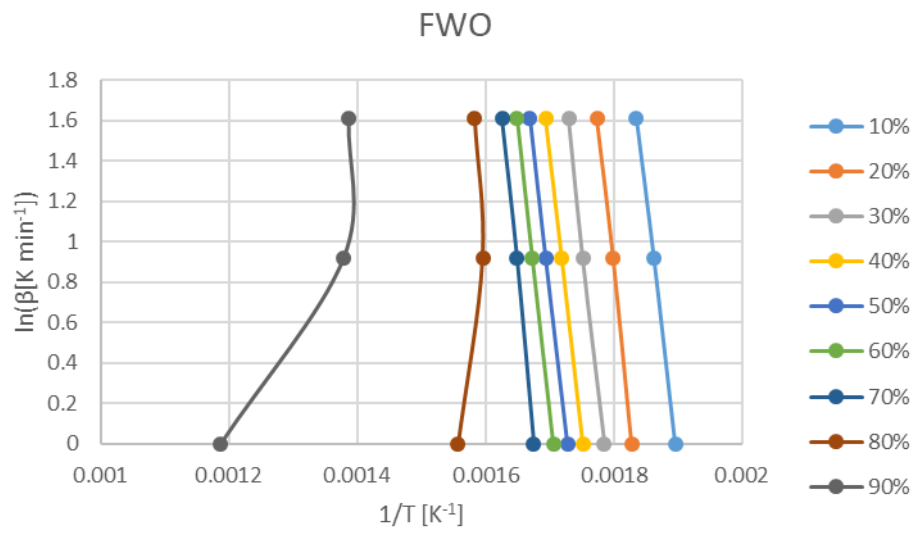


Figure 5.12: FWO method for Woodchips

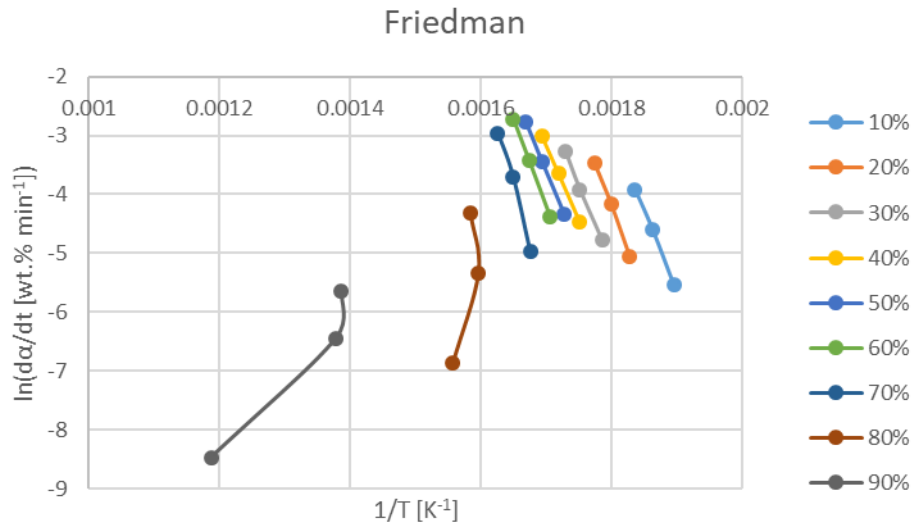


Figure 5.13: Friedman method for Woodchips

Table 5.7: Slope and Y-axis interception for woodchips

|     | Kissinger |          |          | KAS      |          |          | FWO      |          |          | Friedman |          |          |
|-----|-----------|----------|----------|----------|----------|----------|----------|----------|----------|----------|----------|----------|
|     | m         | n        | R        | m        | n        | R        | m        | n        | R        | m        | n        | R        |
| 10% | -24155.2  | 54.29622 | 0.998993 | -25644.1 | 36.08775 | 0.999427 | -26716   | 50.65594 | 0.99948  | -26721.9 | 45.14056 | 0.998904 |
| 20% |           |          |          | -28807.5 | 40.07606 | 0.997679 | -29917.9 | 54.71476 | 0.997862 | -29739.8 | 49.32296 | 0.998353 |
| 30% |           |          |          | -27561.2 | 36.54476 | 0.997925 | -28698.6 | 51.23147 | 0.998071 | -26474.8 | 42.49649 | 0.998239 |
| 40% |           |          |          | -26660.3 | 34.01279 | 0.999951 | -27820.9 | 48.73997 | 0.999958 | -25534.7 | 40.25428 | 0.999999 |
| 50% |           |          |          | -26383.7 | 32.85872 | 0.999839 | -27560.6 | 47.61402 | 0.999848 | -26890.7 | 42.1155  | 0.99991  |
| 60% |           |          |          | -27055.3 | 33.41819 | 0.999848 | -28246.8 | 48.19807 | 0.999855 | -29267.3 | 45.5573  | 0.999994 |
| 70% |           |          |          | -31553.3 | 40.10605 | 0.997464 | -32764.8 | 54.91902 | 0.997663 | -40919.4 | 63.65977 | 0.985833 |
| 80% |           |          |          | 30152.38 | -59.6678 | 0.539998 | 28882.41 | -44.7605 | 0.518633 | 47244.03 | -80.0942 | 0.551933 |
| 90% |           |          |          | 8119.291 | -23.1246 | 0.892241 | 6555.967 | -7.79549 | 0.843316 | 12484.4  | -23.2977 | 0.94235  |

## 5.4 Results

When the slope and the Y-axis intercept are calculated for the different samples, the reaction orders do not influence these calculations. It influences the results for the pre-exponential factor, through the integral term  $\{g(\alpha)\}$  in KAS (5.2.3.2) and FWO (5.2.3.3), and through the mechanistic term  $\{f(\alpha)\}$  in Friedman (5.2.3.4). It is once again, an iterative process between the results and the validation (5.5) to select and calculate the best reaction order. Firstly, a single-step reaction order for the three feedstocks was supposed, and reaction order 1 was used to calculate the pre-exponential factor. According to these two conditions (number of steps and reaction order), the following results were obtained (Table 5.8, Table 5.9 and Table 5.10):

Table 5.8: Results for Woodchips at reaction order 1

|         | Kissinger   |                                     |                          | KAS         |                                     |                          | FWO         |                                     |                          | Friedman    |                                     |                          | AVERAGE     |        |                                     |                          |       |
|---------|-------------|-------------------------------------|--------------------------|-------------|-------------------------------------|--------------------------|-------------|-------------------------------------|--------------------------|-------------|-------------------------------------|--------------------------|-------------|--------|-------------------------------------|--------------------------|-------|
|         | Ea [kJ/mol] | A <sub>0</sub> [min <sup>-1</sup> ] | g(A <sub>0</sub> ) [min] | Ea [kJ/mol] | A <sub>0</sub> [min <sup>-1</sup> ] | g(A <sub>0</sub> ) [min] | Ea [kJ/mol] | A <sub>0</sub> [min <sup>-1</sup> ] | g(A <sub>0</sub> ) [min] | Ea [kJ/mol] | A <sub>0</sub> [min <sup>-1</sup> ] | g(A <sub>0</sub> ) [min] | Ea [kJ/mol] | STDEV  | A <sub>0</sub> [min <sup>-1</sup> ] | g(A <sub>0</sub> ) [min] | STDEV |
| 10%     | 200.8265    | 9.2E+27                             | 27.96356                 | 233.7304    | 1.11E+22                            | 22.04514                 | 230.3272    | 2.51E+21                            | 21.40003                 | 220.989     | 1.01E+20                            | 20.00575                 | 221.4683    | 6%     | 7.14E+22                            | 22.85362                 | 13%   |
| 20%     |             |                                     |                          | 231.5307    | 6.27E+20                            | 20.79698                 | 228.7225    | 1.62E+20                            | 20.20936                 | 241.0371    | 1.54E+21                            | 21.18863                 | 225.5292    | 7%     | 3.46E+22                            | 22.53963                 | 14%   |
| 30%     |             |                                     |                          | 247.2136    | 6.09E+21                            | 21.78449                 | 243.906     | 1.47E+21                            | 21.16779                 | 241.3444    | 5.08E+20                            | 20.70544                 | 233.3226    | 8%     | 8.04E+22                            | 22.90532                 | 13%   |
| 40%     |             |                                     |                          | 218.342     | 5.69E+18                            | 18.75543                 | 216.6527    | 1.83E+18                            | 18.26258                 | 208.3202    | 2.58E+17                            | 17.41085                 | 211.0353    | 3%     | 3.96E+20                            | 20.59811                 | 21%   |
| 50%     |             |                                     |                          | 217.6535    | 2.84E+18                            | 18.45283                 | 216.1623    | 9.5E+17                             | 17.97785                 | 216.1262    | 9.11E+17                            | 17.95932                 | 212.6921    | 3%     | 3.88E+20                            | 20.58839                 | 21%   |
| 60%     |             |                                     |                          | 208.3183    | 2.92E+17                            | 17.46576                 | 207.4144    | 1.1E+17                             | 17.03948                 | 220.8498    | 1.75E+18                            | 18.24371                 | 209.3522    | 3%     | 1.51E+20                            | 20.17813                 | 22%   |
| 70%     |             |                                     |                          | 260.0968    | 7.5E+21                             | 21.87515                 | 256.7782    | 1.87E+21                            | 21.273                   | 326.0744    | 1.16E+27                            | 27.06575                 | 260.944     | 17%    | 3.5E+24                             | 24.54436                 | 12%   |
| 80%     |             |                                     |                          | -234.621    | 1                                   | 0                        | -213.125    | 1                                   | 0                        | -466.945    | 3.01E-41                            | -40.5211                 | -178.466    | -135%  | 0.000725                            | -3.13939                 | -778% |
| 90%     |             |                                     |                          | -73.742     | 1                                   | 0                        | -58.0154    | 1                                   | 0                        | -110.276    | 2.1E-10                             | -9.67822                 | -10.3016    | -1197% | 37267.79                            | 4.571334                 | 308%  |
| AVERAGE | 200.8265    | 9.2E+27                             | 27.96356                 | 145.3914    | 2.81E+21                            | 15.6862                  | 147.647     | 6.69E+20                            | 15.2589                  | 121.9467    | 1.29E+26                            | 10.26445                 | 224.9062    | 7%     | 1.07E+22                            | 22.02965                 | 7%    |

Table 5.9: Results for Wheat Straw at reaction order 1

|         | Kissinger      |                      |                |  | KAS            |                      |                | FWO            |                      |                | Friedman       |                      |                | AVERAGE        |       |                      |                         |       |
|---------|----------------|----------------------|----------------|--|----------------|----------------------|----------------|----------------|----------------------|----------------|----------------|----------------------|----------------|----------------|-------|----------------------|-------------------------|-------|
|         | $E_a$ [kJ/mol] | $A_0$ [ $min^{-1}$ ] | $g(A_0)$ [min] |  | $E_a$ [kJ/mol] | $A_0$ [ $min^{-1}$ ] | $g(A_0)$ [min] | $E_a$ [kJ/mol] | $A_0$ [ $min^{-1}$ ] | $g(A_0)$ [min] | $E_a$ [kJ/mol] | $A_0$ [ $min^{-1}$ ] | $g(A_0)$ [min] | $E_a$ [kJ/mol] | STDEV | $A_0$ [ $min^{-1}$ ] | $g(A_0)$ [ $min^{-1}$ ] | STDEV |
| 10%     | 120.714        | 5.63E+20             | 20.75083       |  | 218.7153       | 1.14E+21             | 21.05671       | 215.8929       | 2.83E+20             | 20.45117       | 213.1892       | 4.43E+19             | 19.64649       | 192.1279       | 21%   | 2.99E+20             | 20.4763                 | 3%    |
| 20%     |                |                      |                |  | 217.2129       | 4.29E+19             | 19.63272       | 215.0289       | 1.23E+19             | 19.09119       | 220.9892       | 2.89E+19             | 19.4615        | 193.4862       | 22%   | 5.42E+19             | 19.73406                | 3%    |
| 30%     |                |                      |                |  | 231.2005       | 3.25E+20             | 20.51252       | 228.5859       | 8.78E+19             | 19.94342       | 232.2016       | 1.31E+20             | 20.11891       | 203.1755       | 23%   | 2.14E+20             | 20.33142                | 2%    |
| 40%     |                |                      |                |  | 222.3084       | 2.25E+19             | 19.35159       | 220.3266       | 6.83E+18             | 18.83436       | 222.4816       | 8.63E+18             | 18.93588       | 196.4577       | 22%   | 2.94E+19             | 19.46816                | 4%    |
| 50%     |                |                      |                |  | 230.3346       | 7.27E+19             | 19.86137       | 228.1187       | 2.13E+19             | 19.32918       | 236.8518       | 1.07E+20             | 20.02894       | 204.0048       | 24%   | 9.83E+19             | 19.99258                | 3%    |
| 60%     |                |                      |                |  | 237.6184       | 2.07E+20             | 20.31564       | 235.1776       | 5.88E+19             | 19.7694        | 265.3689       | 2.12E+22             | 22.32639       | 214.7197       | 26%   | 6.17E+20             | 20.79056                | 5%    |
| 70%     |                |                      |                |  | 307.7849       | 1.68E+26             | 26.22557       | 302.0672       | 2.99E+25             | 25.47592       | 428.9098       | 1.02E+36             | 36.00796       | 289.869        | 38%   | 1.3E+27              | 27.11507                | 20%   |
| 80%     |                |                      |                |  | -291.289       | 1                    | 0              | -266.743       | 1                    | 0              | -434.692       | 6.53E-38             | -37.1848       | -218.002       | -94%  | 7.79E-05             | -4.10848                | -508% |
| 90%     |                |                      |                |  | -70.4069       | 1                    | 0              | -54.5018       | 1                    | 0              | -110.278       | 3.21E-10             | -9.49401       | -28.6182       | -310% | 651.9361             | 2.814205                | 393%  |
| AVERAGE | 120.714        | 5.63E+20             | 20.75083       |  | 144.8311       | 1.87E+25             | 16.32846       | 147.1059       | 3.32E+24             | 15.87718       | 141.6691       | 1.13E+35             | 12.20526       | 213.4058       | 15%   | 1.36E+20             | 20.13218                | 2%    |

Table 5.10: Results for RDF at reaction order 1 and single-step mechanism

|         | Kissinger      |                      |                |  | KAS            |                      |                | FWO            |                      |                | Friedman       |                      |                | AVERAGE        |       |                      |                         |       |
|---------|----------------|----------------------|----------------|--|----------------|----------------------|----------------|----------------|----------------------|----------------|----------------|----------------------|----------------|----------------|-------|----------------------|-------------------------|-------|
|         | $E_a$ [kJ/mol] | $A_0$ [ $min^{-1}$ ] | $g(A_0)$ [min] |  | $E_a$ [kJ/mol] | $A_0$ [ $min^{-1}$ ] | $g(A_0)$ [min] | $E_a$ [kJ/mol] | $A_0$ [ $min^{-1}$ ] | $g(A_0)$ [min] | $E_a$ [kJ/mol] | $A_0$ [ $min^{-1}$ ] | $g(A_0)$ [min] | $E_a$ [kJ/mol] | STDEV | $A_0$ [ $min^{-1}$ ] | $g(A_0)$ [ $min^{-1}$ ] | STDEV |
| 10%     | 119.5856       | 5.51E+18             | 18.74132       |  | 160.0864       | 4.61E+13             | 13.66403       | 160.7287       | 2.41E+13             | 13.3818        | 167.9237       | 1.64E+14             | 14.21454       | 152.0811       | 13%   | 1E+15                | 15.00042                | 15%   |
| 20%     |                |                      |                |  | 205.0974       | 2.69E+17             | 17.42969       | 204.0099       | 9.67E+16             | 16.98521       | 205.5963       | 8.47E+16             | 16.9281        | 183.5723       | 20%   | 3.32E+17             | 17.52108                | 4%    |
| 30%     |                |                      |                |  | 191.7281       | 3.88E+15             | 15.5892        | 191.657        | 1.72E+15             | 15.23458       | 210.1509       | 3.91E+16             | 16.59236       | 178.2804       | 19%   | 3.46E+16             | 16.53936                | 8%    |
| 40%     |                |                      |                |  | 221.5202       | 9.35E+16             | 16.97061       | 220.6162       | 3.54E+16             | 16.54946       | 209.4627       | 7.46E+14             | 14.87253       | 192.7962       | 22%   | 6.07E+16             | 16.78348                | 8%    |
| 50%     |                |                      |                |  | 253.8686       | 1.82E+18             | 18.25921       | 252.2189       | 6.18E+17             | 17.79129       | 278.4862       | 2.03E+19             | 19.30683       | 226.0398       | 28%   | 3.35E+18             | 18.52466                | 3%    |
| 60%     |                |                      |                |  | 278.8235       | 4.29E+19             | 19.63292       | 276.2941       | 1.3E+19              | 19.11238       | 277.3924       | 9.21E+18             | 18.96431       | 238.0239       | 29%   | 1.3E+19              | 19.11273                | 2%    |
| 70%     |                |                      |                |  | 282.2618       | 4.32E+19             | 19.63535       | 279.743        | 1.31E+19             | 19.11794       | 298.9213       | 2.73E+20             | 20.43562       | 245.1279       | 30%   | 3.04E+19             | 19.48256                | 3%    |
| 80%     |                |                      |                |  | 300.3678       | 5.69E+20             | 20.75509       | 297.1307       | 1.58E+20             | 20.1978        | 349.1826       | 6.7E+23              | 23.82635       | 266.5667       | 33%   | 7.59E+20             | 20.88014                | 9%    |
| 90%     |                |                      |                |  | -104.867       | 1                    | 0              | -86.8618       | 1                    | 0              | -194.904       | 2.65E-15             | -14.576        | -66.7618       | -172% | 10.99812             | 1.041319                | 1136% |
| AVERAGE | 119.5856       | 5.51E+18             | 18.74132       |  | 198.7652       | 7.3E+19              | 15.77068       | 199.5041       | 2.05E+19             | 15.3745        | 200.2458       | 7.45E+22             | 14.50718       | 210.311        | 17%   | 9.56E+17             | 17.98055                | 10%   |

There are several aspects to help to understand these tables:

- For each method, the columns are the activation energy ( $E_a$  [kJ/mol]), pre-exponential factor ( $A_0$  [ $min^{-1}$ ]) and the logarithm of this pre-exponential factor ( $log(A_0)$ )
- The values in red were giving negative numbers and, consequently, the calculation of its logarithm was impossible. A negative value for the pre-exponential factor is invalid and was substituted by 1 to obtain a value
- The Kissinger method only calculates a value for the whole range of conversion values, so that value that appears on the conversion value of 10% is used at any conversion value
- The average columns calculate the average values of activation energy and the logarithm of the pre-exponential factor and the typical deviation within. The bottom row shows the average values of the average at each conversion and the standard deviation among the average values. Each of these columns takes into account the Kissinger value.
- The logarithm (with base 10) of the pre-exponential factor is calculated as a better way to compare values. Typically, the pre-exponential factor varies in magnitude orders for any kinetic study within pyrolysis [11, 37, 42, 58, 71, 72]. To calculate the average value, a variation of one order of magnitude would make the whole result unreliable. For example, if there were 9 results with a value of  $10^{23}$  and one result with the value  $10^{25}$ , the average would be  $10^{24}$  in terms of magnitude order; using the logarithm, the final value would be  $10^{23.2}$ , closer to reality and most results.

Graphs comparing the values were produced, to understand and compare the variation of activation energy and pre-exponential factor. The activation energy and logarithm of the pre-exponential factor are compared along with the conversion range in Figure 5.14 and Figure 5.15 for woodchips; Figure 5.16 and Figure 5.17 for wheat Straw; Figure 5.18 and Figure 5.19 for RDF. The activation energies and pre-exponential factors at high conversion values are not represented in these graphs because they altered the graph too much as outliers. Kissinger is represented with a line because there is a single value calculated for all conversion values.

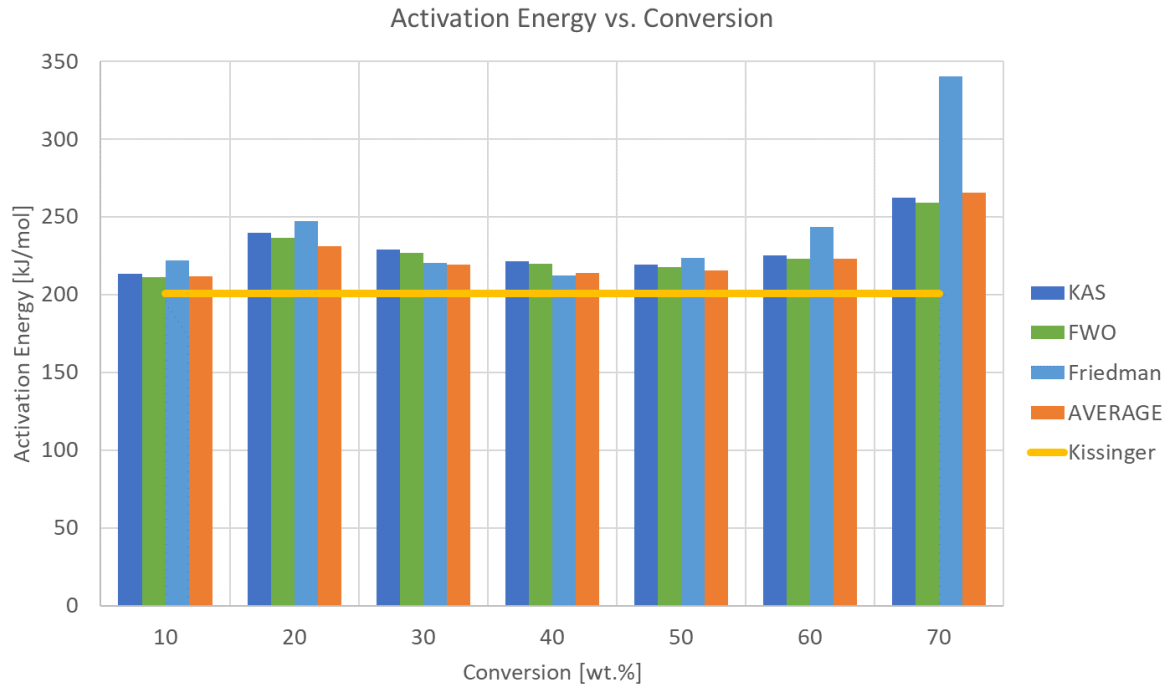


Figure 5.14: Activation energy for Woodchips

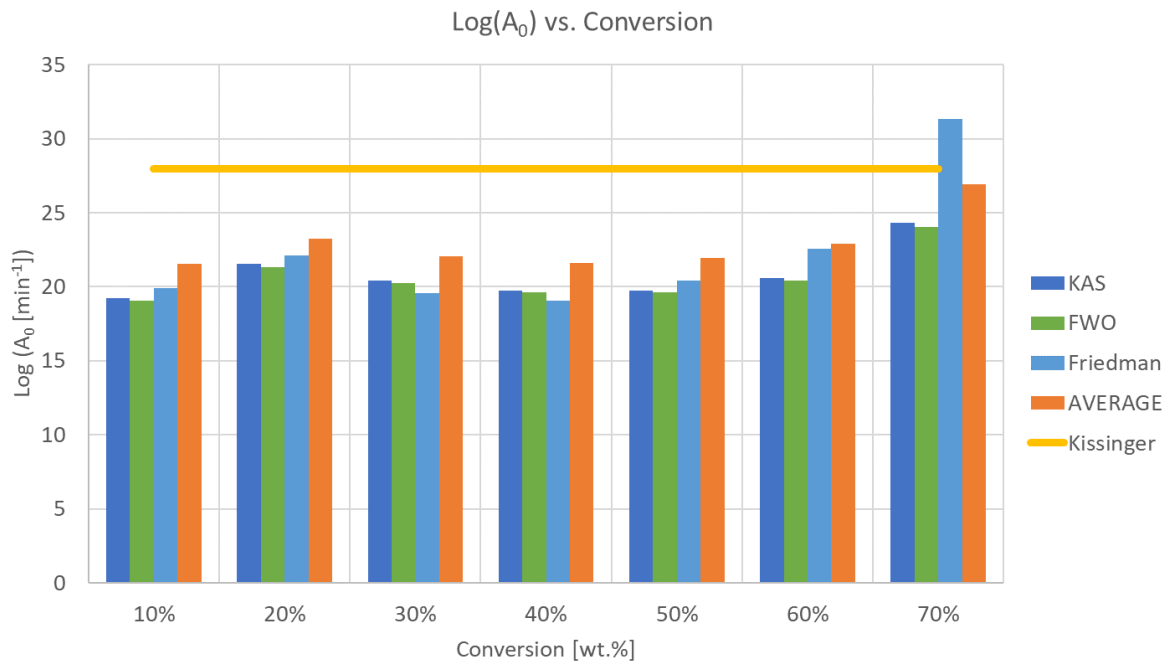


Figure 5.15: Logarithm of the pre-exponential factor for Woodchips



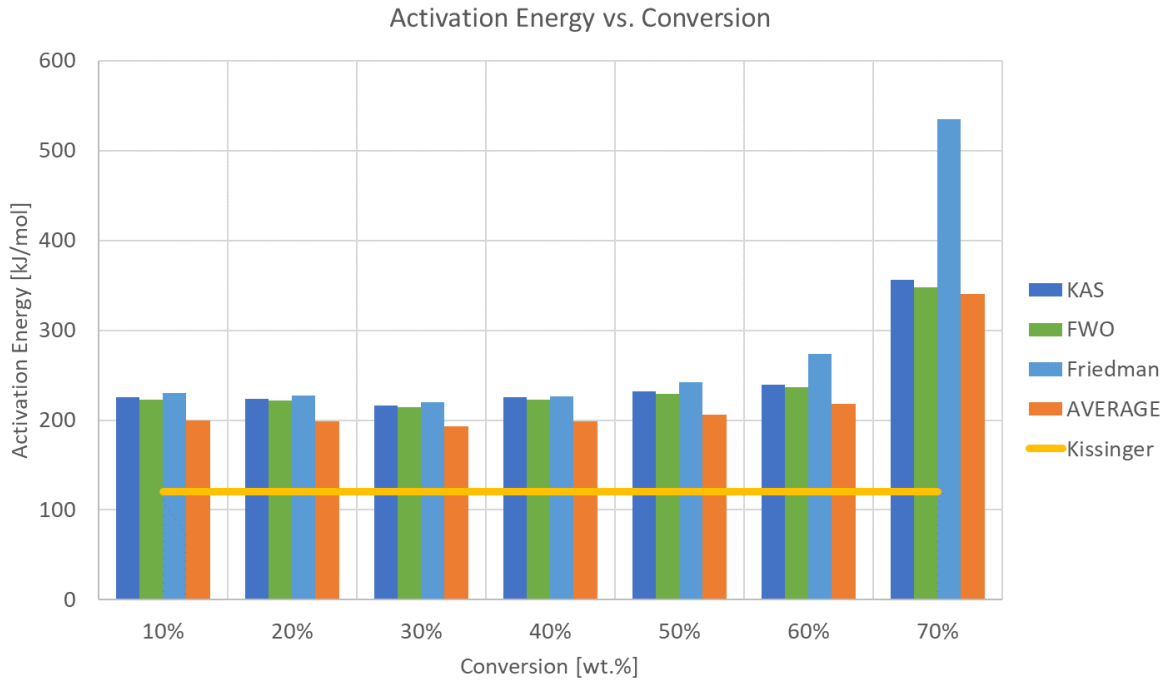


Figure 5.16: Activation Energy for Wheat Straw

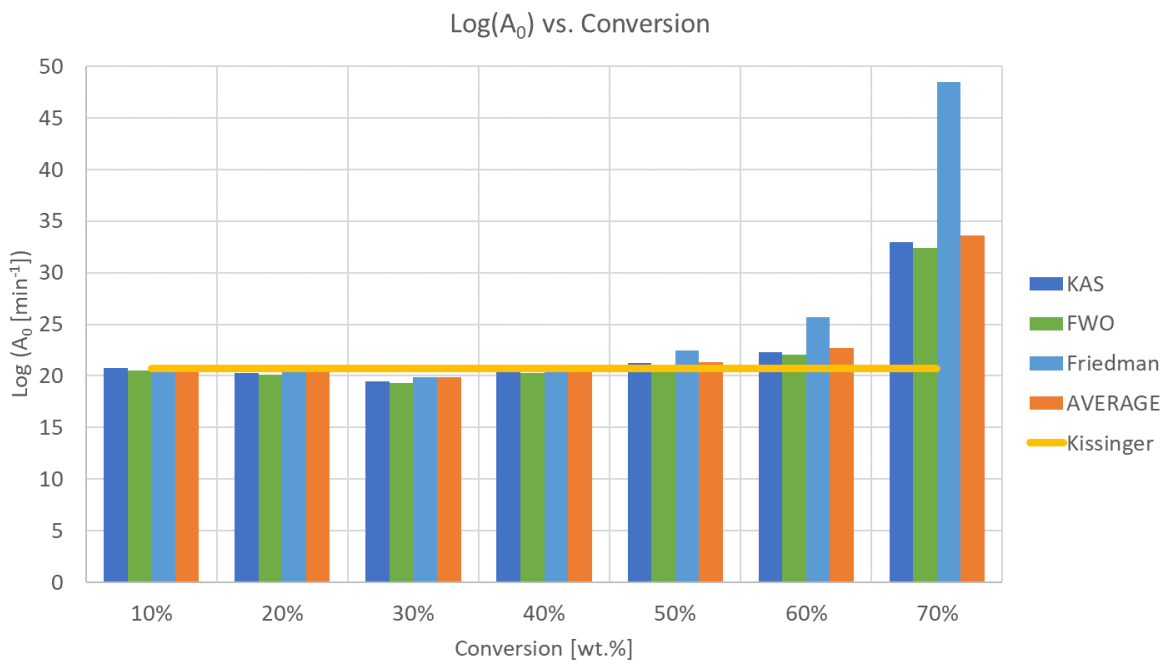


Figure 5.17: Logarithm of the pre-exponential factor for Wheat Straw

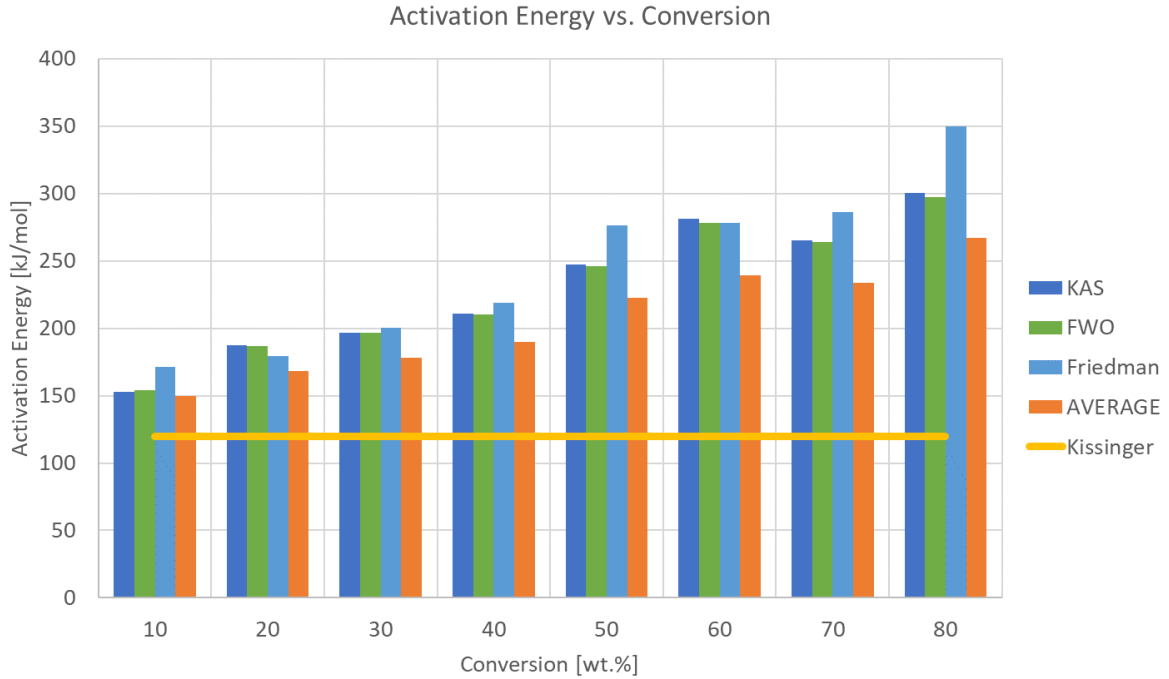


Figure 5.18: Activation energy for RDF

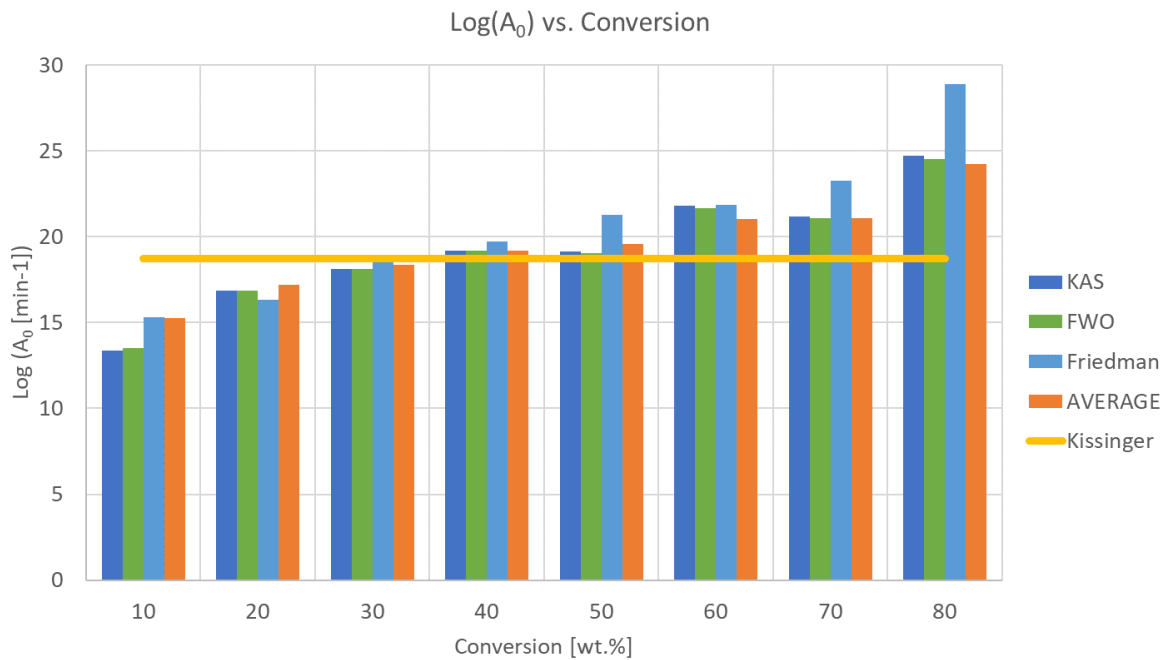


Figure 5.19: Logarithm of the pre-exponential factor for RDF

Overall, we see a good agreement between KAS, FWO and Friedman, although, at high conversion values, Friedman predicts a significantly higher value. It is observed that the average value does not agree with the other three methods; this is due to the influence of Kissinger values on each conversion value.

Previous studies [11, 42, 64] addressed the variability of the activation energy and pre-exponential factor with the conversion values. Çepelioğullar et al. [42] supported the approach of Vyazovkin and Dollimore [64], which attributed the fluctuating values of the parameters to a change

in the limiting reaction. This approach suggests shifts in the values from high to low activation energy. Cortés and Bridgwater [11] attributed the variability to the multiple reactions taking place during pyrolysis, but there is not a trend. Contrary to [42] and [64], the activation energy for RDF increases with the temperature. This higher activation energy with conversion could be the result of higher temperatures, which could lead to more energy available to surpass the activation energy barrier for the reaction to occur. In this research, the variability of the parameters with the conversion is attributed to multiple reactions occurring simultaneously in pyrolysis without any clear trend when conversion (and temperature) increase. Consequently, kinetic parameters depend on the conversion because it determines the reactions occurring and the apparent activation energy and pre-exponential factor.

## 5.5 Model adjustment

It is essential to check how the new data fits the original TGA curve to validate the appropriateness of this methodology. With that purpose, the original values of the TGA are compared to the model values. These values are the time, temperature and the calculated conversion. To calculate the value from each model, the kinetic constant is calculated with the temperature at each point according to the Arrhenius expression in Equation 5.8. The activation energy and pre-exponential factor was an average between the values (excluding the calculations at very high conversion) and using Kissinger once, instead of for each conversion value, which is less realistic. During the calculation of average values for activation energy and pre-exponential factor, some of the values were excluded due to a significant variation compared to the average. For instance, the value of the pre-exponential factor logarithm for wheat straw at 70% differs significantly from the others. These values or outliers that deviated significantly from the average were not considered in the calculations. The final conversion is calculated re-organising the terms from Equation 5.30 for reaction order 1 and calculating the final conversion (Equation 5.42). Using this method, Figure 5.20, Figure 5.21 and Figure 5.22 are obtained for woodchips, wheat straw and RDF, respectively.

$$\alpha_f = 1 - (1 - \alpha_i) \cdot e^{(-k \cdot \Delta t)}$$

*Equation 5.42: Final conversion for reaction order 1*

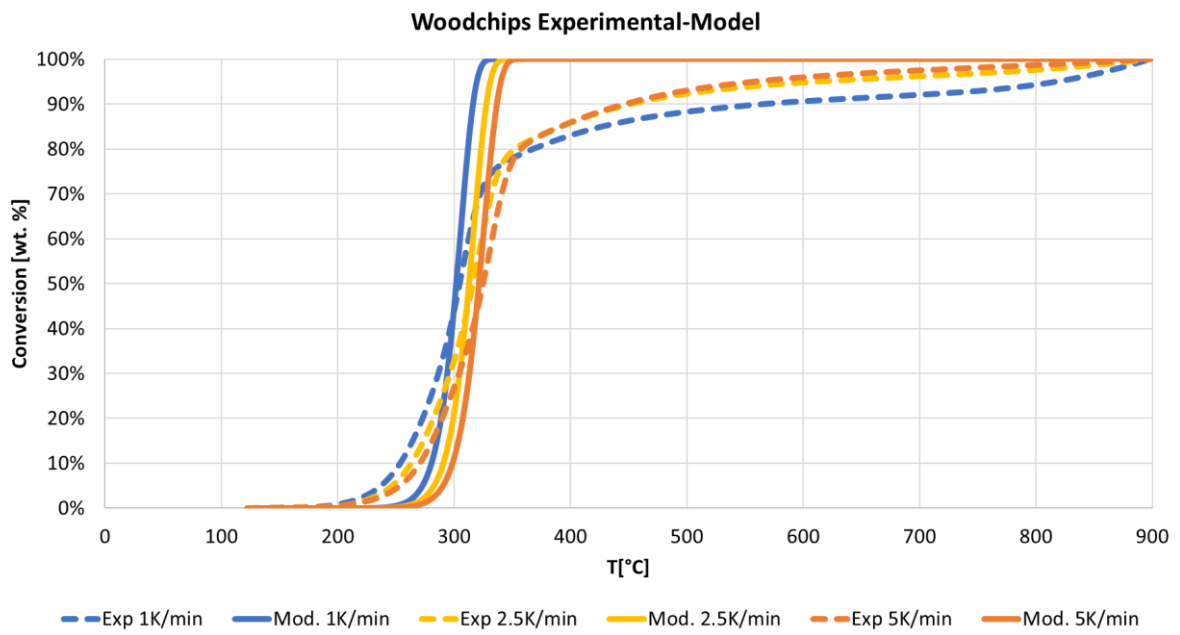


Figure 5.20: comparison Woodchips experimental-model

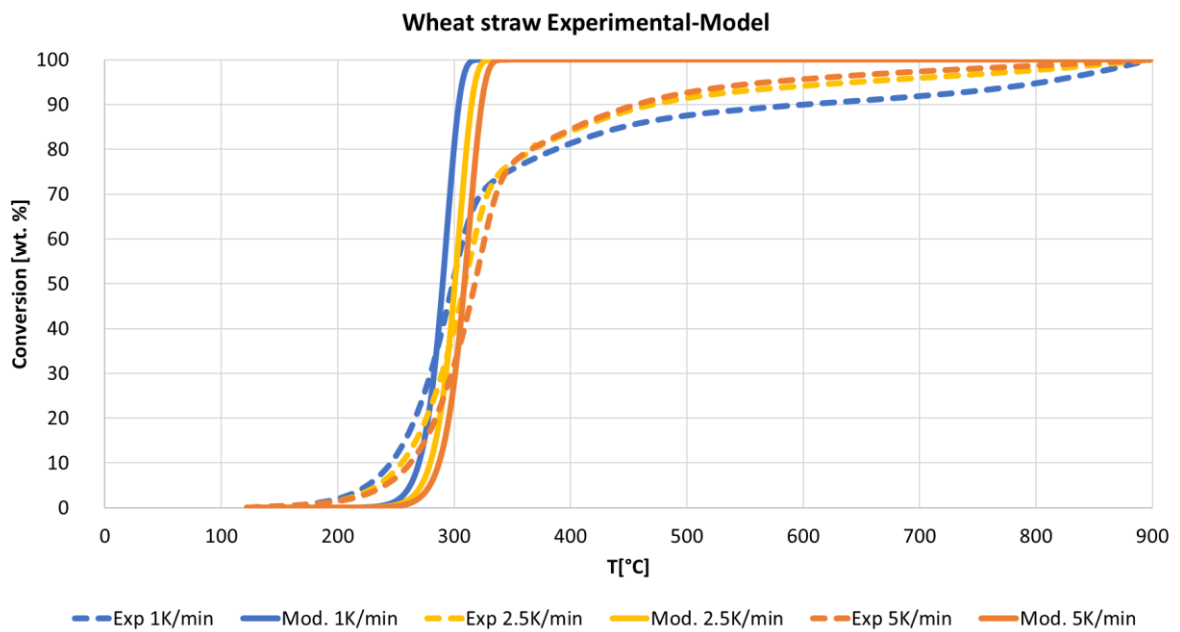


Figure 5.21: comparison Wheat Straw experimental-model

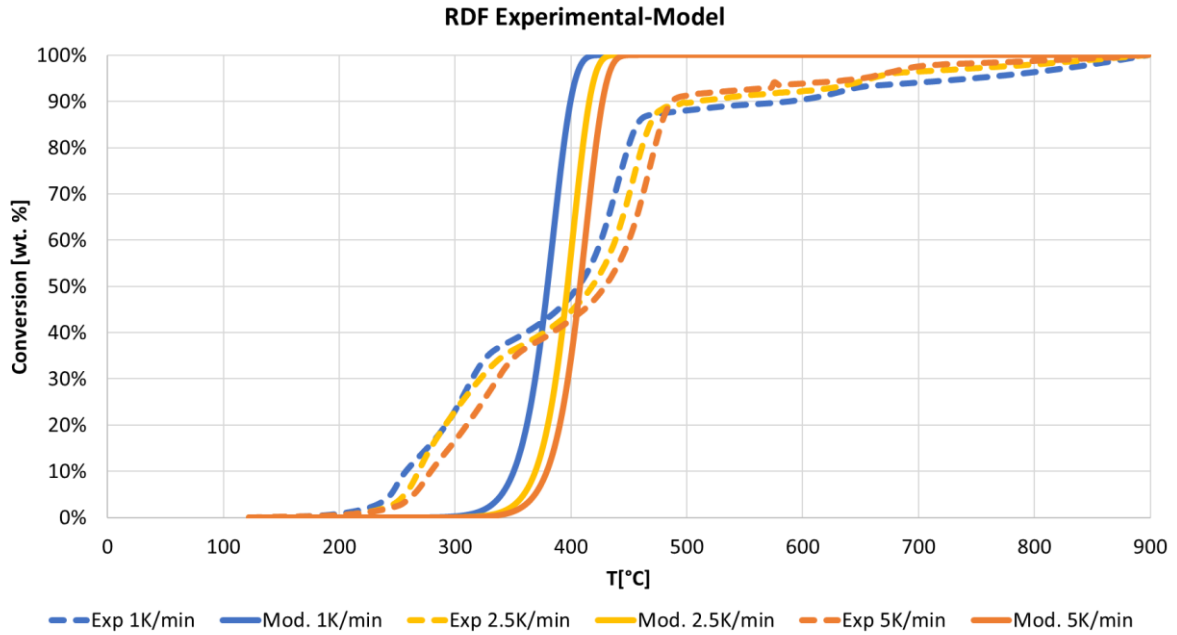


Figure 5.22: comparison RDF experimental-model

These three Figures show that the model does not precisely match the experimental data. In order to create a method that can analytically measure how accurate the model, calculations were needed instead of visual analysis of each reaction order. With that purpose, some extra columns were added; in each extra column, the absolute difference between the conversion value for the experimental and the model is calculated. There is an extra cell where the total error for each heating rate is calculated and a final cell where these errors are summed. The formula is represented in Equation 5.43. The total error for each feedstock with reaction order 1 is shown in Table 5.11. These values are the summaries of absolute conversion differences, so they are dimensionless. It is a method to compare values with other reaction orders. The lowest value that can be achieved is 0, which would mean that the model adjusts perfectly to the curves of the experiment.

$$Total\ error = \sum_{i=1}^{3\ (heating\ rates)} \sum_{t=0}^{t_{final}} |\alpha_{model} - \alpha_{experimental}|$$

Equation 5.43: Total error Model-Experimental

Table 5.11: Total error for first reaction order

| WoodChips | Wheat Straw | RDF    |
|-----------|-------------|--------|
| 90.63     | 99.69       | 114.49 |

These values were used to find the reaction order most similar to the experimental values. The table is the first approximation, and the values are compared to other reaction orders to determine whether they are high or low. Kissinger method (5.2.3.1) is not affected by a change in the reaction order, although it affects KAS (5.2.3.2), FWO (5.2.3.3) through the integral term  $\{g(\alpha)\}$  (Equation 5.30) and Friedman (5.2.3.4) through the mechanistic term  $\{f(\alpha)\}$  (Equation 5.26). The results for the pre-exponential factor change for some methods, but the pathway to calculate the new conversion value changes, because, instead of using Equation 5.42, Equation 5.44 is used when the reaction order is different from 1 and the controlling step is the chemical reaction.

$$\alpha_f = 1 - [1 - k \cdot \Delta t \cdot (n - 1) + (1 - \alpha_i)^{1-n}]^{\frac{1}{1-n}}$$

Equation 5.44: Final conversion when reaction order is different from 1

Simultaneously, a second step for the decomposition of RDF is implemented. Figure 5.18 shows a continuous increase of the activation energy values and Figure 5.9 gives two different peaks, which suggests a second step for the pyrolysis of RDF. The two steps can be attributed to the lignocellulosic and the plastics fractions, respectively. The limit to switch from one step to the other could be established as a temperature or as a conversion value. A temperature limit would more accurately imitate the decomposition of RDF because plastics will only decompose if the degradation temperature is achieved. A limit based on conversion value would ensure that all the lignocellulosic fraction degrades before the plastic fraction. A limit based on the conversion could lead to a decomposition of the plastics without reaching the degradation temperature, only because the conversion of the lignocellulosic fraction is completed. It would require dividing the feedstock into the different materials to analyse each individually instead of taking the RDF as a whole, which is the purpose of this project.

To establish the limit of the kinetic parameters switching towards the plastic fraction, the temperature selected is 375 °C. This value agrees with the curve from TGA (Figure 5.9) and literature [42, 68, 73] where the pyrolysis of cellulose and hemicellulose is completed. Within the experiments, 375 °C corresponds to a 40 wt.% conversion value, and the most significant change in the activation energy in Figure 5.18 occurs between 40 and 50 wt.% conversion values. As a result, the activation energies and pre-exponential values of RDF from conversion values up to 40 wt.% are attributed to the first step of the reaction; the decomposition of cellulose and hemicellulose. Pre-exponential factors and activation energies from higher conversion values correspond to the decomposition of plastics.

As a preliminary study, the reaction orders for all reactions are changed to a value of 2. Additionally, the second step for RDF is implemented when the temperature reaches a value of 375°C. It is a preliminary study because the only objective is to compare if the error value can be lower than the value obtained with reaction order 1. The result is shown in Table 5.12. For woodchips and wheat straw, the error is reduced by approximately 20%. The reduction of error for RDF is higher, probably due to the implementation of a second reaction step rather than the change in the reaction order. This results in a better approximation of the model to the real conversion of RDF during pyrolysis. A better approximation leads to more accurate results when RDF is pyrolysed.

Table 5.12: Error for second reaction order

| WoodChips | Wheat Straw | RDF   |
|-----------|-------------|-------|
| 70.36     | 81.79       | 80.30 |

The tool “Solver” is used for each feedstock to minimise the error. The parameter error is the summary of absolute differences of conversion values between the model and the experiment. This tool is used for each feedstock and the temperature limit when the kinetic constant of RDF changes from cellulose and hemicellulose towards plastics. The final results of the kinetic model for kinetic constants are shown in Table 5.13. The optimum temperature to change the activation energies and pre-exponential factors for RDF was found to be at 350 °C. The final error for each feedstock is shown in Table 5.14.

Table 5.13: Optimum values for the different feedstocks

|              | $E_a$ [kJ/mol] | $A_0$ [min <sup>-1</sup> ] | log ( $A_0$ ) | Reaction order |
|--------------|----------------|----------------------------|---------------|----------------|
| RDF (Step 1) | 210.00         | 1.06E+20                   | 20.02         | 37.19          |
| RDF (Step 2) | 281.37         | 8.81E+21                   | 21.94         | 6.97           |
| WS           | 226.90         | 1.07E+21                   | 21.03         | 7.66           |
| WC           | 218.48         | 2.88E+20                   | 20.46         | 7.06           |

The activation energy and pre-exponential factors are calculated from experimental data, and the reaction order optimised to obtain the minimum error. The values are high when comparing the data with literature and a previous study completed by Bryant [62]. The activation energy and pre-exponential factor are studied individually for each feedstock:

- **RDF:** the activation energy and pre-exponential factor obtained in the previous study of this specific RDF had ranges of 138-162 kJ/mol and  $10^{10}$ - $10^{20}$  min<sup>-1</sup> [62], whereas in literature the ranges were broader with 116-146 kJ/mol and  $10^9$ - $10^{22}$  min<sup>-1</sup> [42, 45, 71, 74]. Overall, the values for the model are higher than previously reported, especially for the activation energy, which does not fall within the range. One of the reasons is the variability of the feedstock. In the case of the pre-exponential factor, there is an additional reason, which is the optimisation of the reaction order, whose increase involves an increase in the value of the pre-exponential factor. In comparison with the work completed previously with the same feedstock, the two key aspects to consider and explain the variation are the amount of sample in the crucible, significantly lower in the previous work [62], and the division into two steps.
- **Wheat Straw:** the trend is similar for wheat straw, whose activation energy and pre-exponential factor ranges were 217-223 kJ/mol and  $10^{16}$ - $10^{19}$  min<sup>-1</sup> for the same feedstock [62] and 44-211 kJ/mol and  $10^6$ - $10^{12}$  min<sup>-1</sup> in the literature [47, 75]. The values to be used in the model are higher than previous ranges but closer than for RDF. The same happens with the pre-exponential factor, especially when it is compared to the work where the same feedstock has been analysed [62]. The possible reason for high values is the change in sample in the crucible or the fact that the data is analysed on a dry basis.
- **Woodchips:** the last feedstock gave ranges for activation energy and pre-exponential factor of 218-229 kJ/mol and  $10^{15}$ - $10^{21}$  min<sup>-1</sup> for the same feedstock [62], whereas in the literature the values were 157-230 kJ/mol and  $10^{11}$ - $10^{17}$  min<sup>-1</sup> [68, 76]. The value of the activation energy falls within the range in the literature, although it is towards the upper range. However, the value of the pre-exponential factor agrees with the previous study of the same feedstock [62].

Table 5.14: Error for optimum reaction orders

|           |             |       |
|-----------|-------------|-------|
| Woodchips | Wheat Straw | RDF   |
| 28.57     | 28.55       | 39.17 |

Compared to the initial error values (with reaction order 1), they are significantly reduced to approximately a third of the initial value. With these new conditions, the figures are re-plotted, and the result is shown in Figure 5.23, Figure 5.24 and Figure 5.25 for woodchips, wheat straw and RDF. A better fit to the experimental values is observed compared to the initial version. It is easily observed why the error for RDF is higher than the others. To change the shape of the curve, a modification to

the activation energy would be needed with the reaction order, but it would not agree with any of the methods currently studied. In addition to all the data for activation energy and pre-exponential factor, there is another assumption, and it is that there is no reaction until the temperature is higher than 150 °C. In the data from TGA, the only mass reduction until that temperature is due to the evaporation of water.

*Assumption 15: No chemical reaction until the temperature is higher than 150 °C*

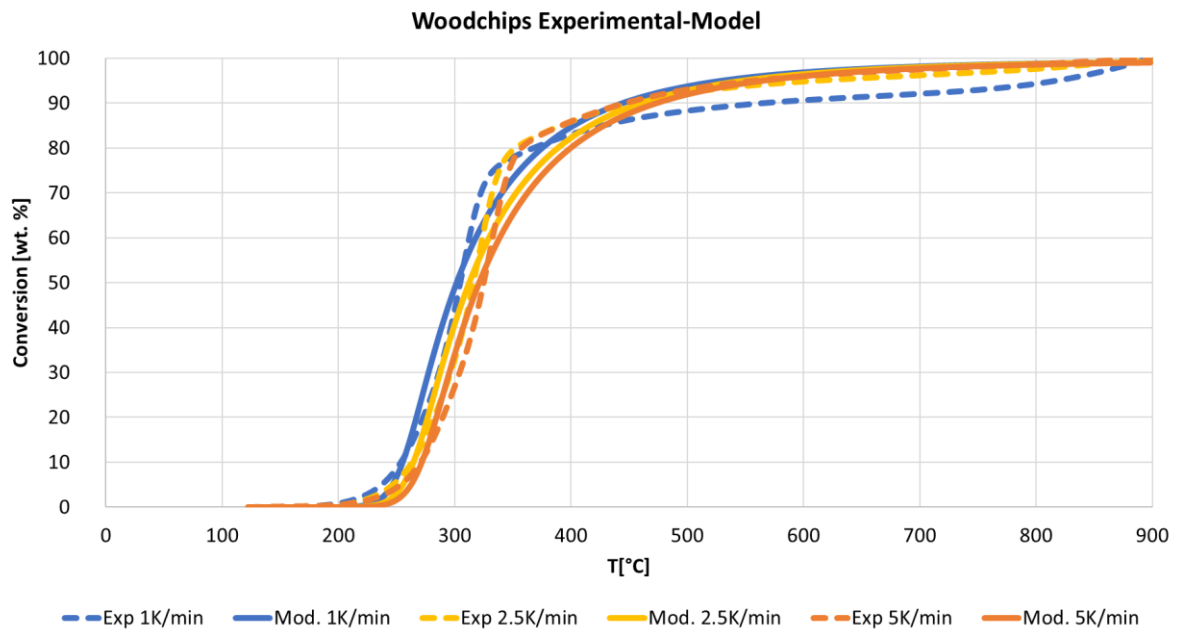


Figure 5.23: Optimum experimental-model for Woodchips

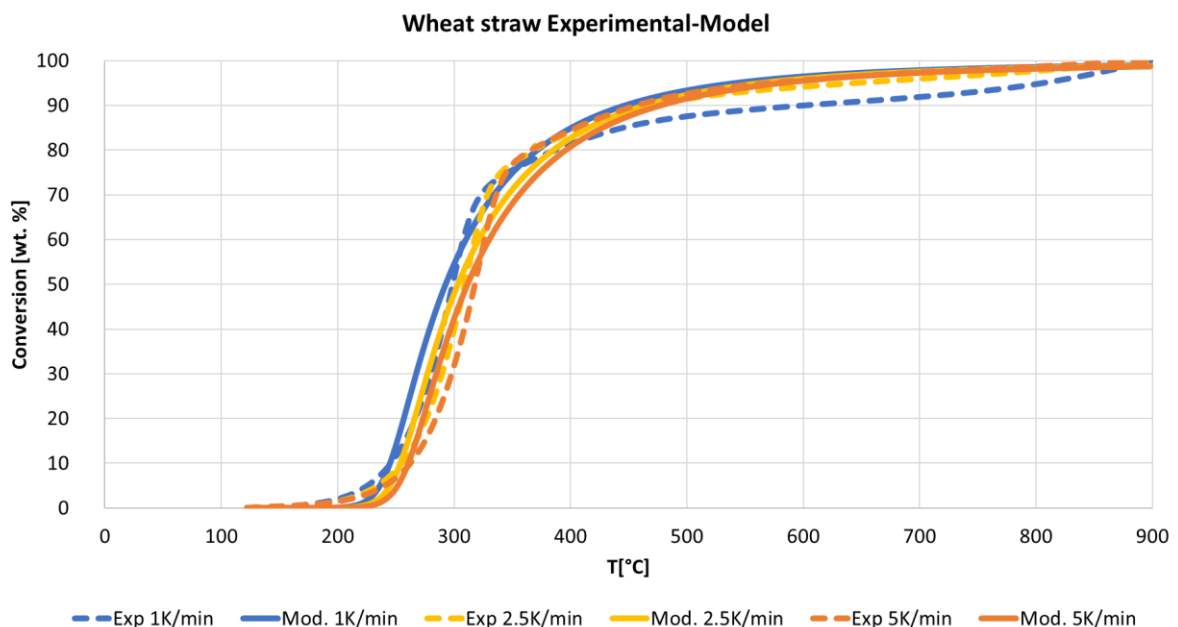


Figure 5.24: Optimum experimental-model for Wheat Straw



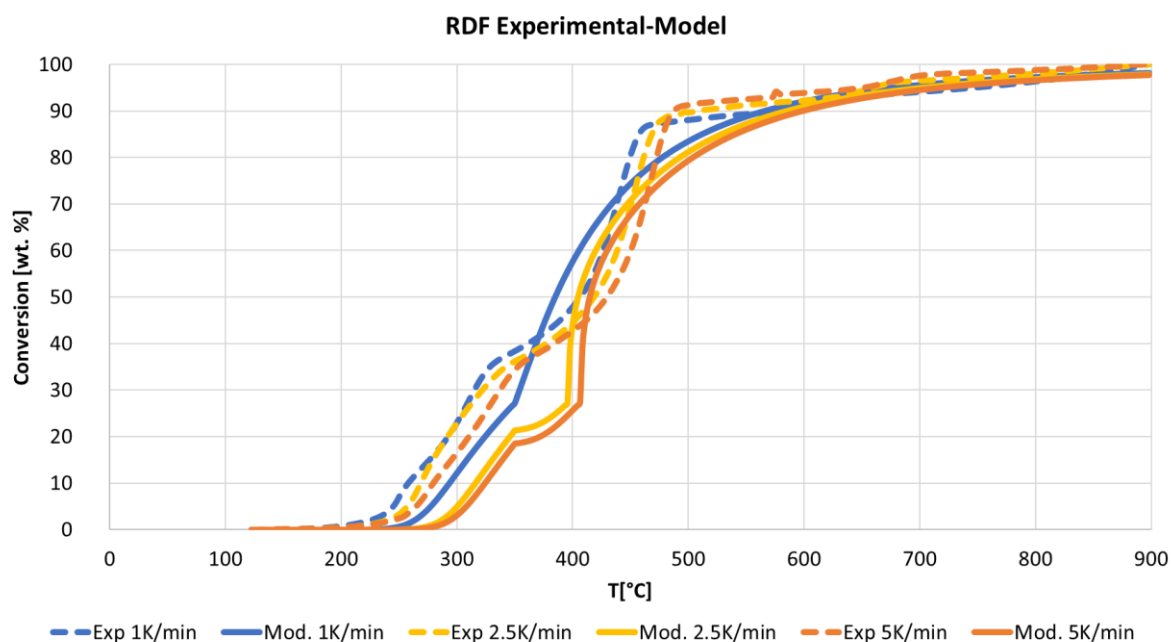


Figure 5.25: Optimum experimental-model for RDF

It is observed that the curves tend to match the experimental data. The apparent values for the reaction orders are high when they are compared with the more common values within chemistry (whose maximum typical values are usually around 4). The lines representing the conversion with the temperature are curves, and that leads to higher reaction orders better fitting the behaviour, using non-linear equations. Besides the curves, it is observed how conversion does not finish at a specific temperature, but the feedstock continues decomposing. This final decomposition is due to lignin, and it contributes to higher orders. An alternative to avoid the high reaction orders is to calculate the activation energy and pre-exponential factor for the degradation of lignin. It was not completed because the data could not be analysed at high conversion values; some of the results gave negative activation energies or pre-exponential factors whose logarithm was negative. To find more data to model lignin decomposition, a trial for Woodchips is shown with calculations and analysis each 5% conversion; the results are represented in Table 5.15, and the activation energy and pre-exponential factor are compared along with the conversion values in Figure 5.26 and Figure 5.27. In this case, the study was not on a dry basis, and the first value is lower than usual. In comparison, there is no more than a value for the decomposition of lignin because the ones next to it have invalid values (negative activation energies and pre-exponential factors) as it happened previously. The mechanism is studied as a single step reaction for the lignocellulosic biomass, and the high orders are retained for a better approximation.

Table 5.15: Kinetic parameters for Woodchips every 5% conversion

|      | Kissinger   |                                     |  | KAS         |                                     |  | FWO         |                                     |  | Friedman    |                                     |  | AVERAGE     |            |                         |                              |            |
|------|-------------|-------------------------------------|--|-------------|-------------------------------------|--|-------------|-------------------------------------|--|-------------|-------------------------------------|--|-------------|------------|-------------------------|------------------------------|------------|
|      | Ea [kJ/mol] | A <sub>0</sub> [min <sup>-1</sup> ] | g(A <sub>0</sub> [min <sup>-1</sup> ]) | Ea [kJ/mol] | A <sub>0</sub> [min <sup>-1</sup> ] | g(A <sub>0</sub> [min <sup>-1</sup> ]) | Ea [kJ/mol] | A <sub>0</sub> [min <sup>-1</sup> ] | g(A <sub>0</sub> [min <sup>-1</sup> ]) | Ea [kJ/mol] | A <sub>0</sub> [min <sup>-1</sup> ] | g(A <sub>0</sub> [min <sup>-1</sup> ]) | Ea [kJ/mol] | STDEV. [%] | A0 [min <sup>-1</sup> ] | log(A0 [min <sup>-1</sup> ]) | STDEV. [%] |
| 5%   | 200.8265    | 9.2E+27                             | 27.96356                               | 52.93592    | 402571.6                            |  | 55.88602    | 774630.6                            | 5.889095                               | 58.68981    | 839133.3                            | 5.923831                               | 92.08455    | 68%        | 1.81E+13                | 13.25883                     | 78%        |
| 10%  |             |                                     |  | 211.2735    | 6.21E+19                            | 19.79335                               | 208.956     | 1.71E+19                            | 19.23182                               | 201.6354    | 1.23E+18                            | 18.09131                               | 205.6728    | 2%         | 1.86E+21                | 21.27001                     | 18%        |
| 15%  |             |                                     |  | 211.2735    | 9.58E+19                            | 19.98158                               | 208.956     | 2.63E+19                            | 19.42004                               | 201.6354    | 1.31E+18                            | 18.11613                               | 205.6728    | 2%         | 2.35E+21                | 21.37033                     | 18%        |
| 20%  |             |                                     |  | 210.0016    | 5.56E+18                            | 18.74507                               | 208.2327    | 1.73E+18                            | 18.23809                               | 219.6119    | 1.56E+19                            | 19.19241                               | 209.6682    | 3%         | 1.08E+21                | 21.03478                     | 19%        |
| 25%  |             |                                     |  | 209.2165    | 2.77E+18                            | 18.44307                               | 207.6297    | 8.98E+17                            | 17.95333                               | 214.9893    | 3.31E+18                            | 18.52048                               | 208.1655    | 2%         | 5.25E+20                | 20.72011                     | 20%        |
| 30%  |             |                                     |  | 164.2426    | 6.1E+13                             | 13.78524                               | 165.0768    | 3.31E+13                            | 13.51963                               | 172.0826    | 1.62E+14                            | 14.21003                               | 175.5571    | 8%         | 2.34E+17                | 17.36962                     | 35%        |
| 35%  |             |                                     |  | 221.1111    | 1.53E+19                            | 19.18481                               | 219.1761    | 4.69E+18                            | 18.67101                               | 207.149     | 2.72E+17                            | 17.43493                               | 212.0657    | 4%         | 6.51E+20                | 20.81358                     | 20%        |
| 40%  |             |                                     |  | 200.7987    | 1.48E+17                            | 17.16998                               | 199.9521    | 5.57E+16                            | 16.74602                               | 192.293     | 9.87E+15                            | 15.99431                               | 198.4676    | 2%         | 2.94E+19                | 19.46847                     | 25%        |
| 45%  |             |                                     |  | 212.7467    | 1.46E+18                            | 18.16374                               | 211.3953    | 5E+17                               | 17.69867                               | 200.0298    | 4.28E+16                            | 16.63125                               | 206.2496    | 3%         | 1.3E+20                 | 20.1143                      | 23%        |
| 50%  |             |                                     |  | 208.9396    | 5.3E+17                             | 17.72413                               | 207.8517    | 1.91E+17                            | 17.28136                               | 201.5513    | 5.22E+16                            | 16.71758                               | 204.7923    | 2%         | 8.35E+19                | 19.92166                     | 23%        |
| 55%  |             |                                     |  | 196.6734    | 3.5E+16                             | 16.54428                               | 196.2472    | 1.44E+16                            | 16.15793                               | 198.8509    | 2.76E+16                            | 16.44142                               | 198.1495    | 1%         | 1.89E+19                | 19.2768                      | 26%        |
| 60%  |             |                                     |  | 199.6343    | 5.46E+16                            | 16.73742                               | 199.1302    | 2.21E+16                            | 16.34463                               | 203.857     | 6.58E+16                            | 16.81811                               | 200.862     | 1%         | 2.92E+19                | 19.46593                     | 25%        |
| 65%  |             |                                     |  | 208.7839    | 3.09E+17                            | 17.48935                               | 207.8895    | 1.16E+17                            | 17.06412                               | 218.4452    | 1.03E+18                            | 18.01448                               | 208.9862    | 3%         | 1.36E+20                | 20.13288                     | 23%        |
| 70%  |             |                                     |  | 213.0103    | 6.23E+17                            | 17.79437                               | 211.9771    | 2.28E+17                            | 17.35841                               | 230.2122    | 8.41E+18                            | 18.92489                               | 214.0065    | 5%         | 3.24E+20                | 20.51031                     | 21%        |
| 75%  |             |                                     |  | 216.6601    | 1.04E+18                            | 18.01583                               | 215.5263    | 3.74E+17                            | 17.57255                               | 243.1487    | 6.79E+19                            | 19.8321                                | 219.0404    | 7%         | 7.01E+20                | 20.84601                     | 20%        |
| 80%  |             |                                     |  | 240.2603    | 7.28E+19                            | 19.86185                               | 238.0988    | 2.2E+19                             | 19.3429                                | 304.4422    | 3.52E+24                            | 24.54623                               | 245.9069    | 15%        | 8.48E+22                | 22.92863                     | 15%        |
| 85%  |             |                                     |  | -411.127    | 1                                   | 0                                      | -380.654    | 1                                   | 0                                      | -390.678    | 1.03E-34                            | -33.9881                               | -245.408    | -105%      | 0.031179                | -1.50614                     | -1458%     |
| 90%  |             |                                     |  | 462.3525    | 4.46E+34                            | 34.64937                               | 450.4646    | 4.73E+33                            | 33.67441                               | 479.7034    | 2.67E+34                            | 34.42668                               | 398.3367    | 29%        | 4.77E+32                | 32.67851                     | 8%         |
| 95%  |             |                                     |  | -207.056    | 1                                   | 0                                      | -184.255    | 1                                   | 0                                      | -245.879    | 8.22E-19                            | -18.0849                               | -109.091    | -165%      | 294.8955                | 2.469668                     | 667%       |
| AVG. | 200.8265    | 9.2E+27                             | 27.96356                               | 198.5976    | 9.17E+17                            | 17.96227                               | 160.3967    | 6.03E+16                            | 16.7806                                | 204.289     | 1.63E+17                            | 17.21309                               | 191.0274    | 9%         | 9.55E+19                | 19.97988                     | 85%        |

Activation Energy vs. Conversion

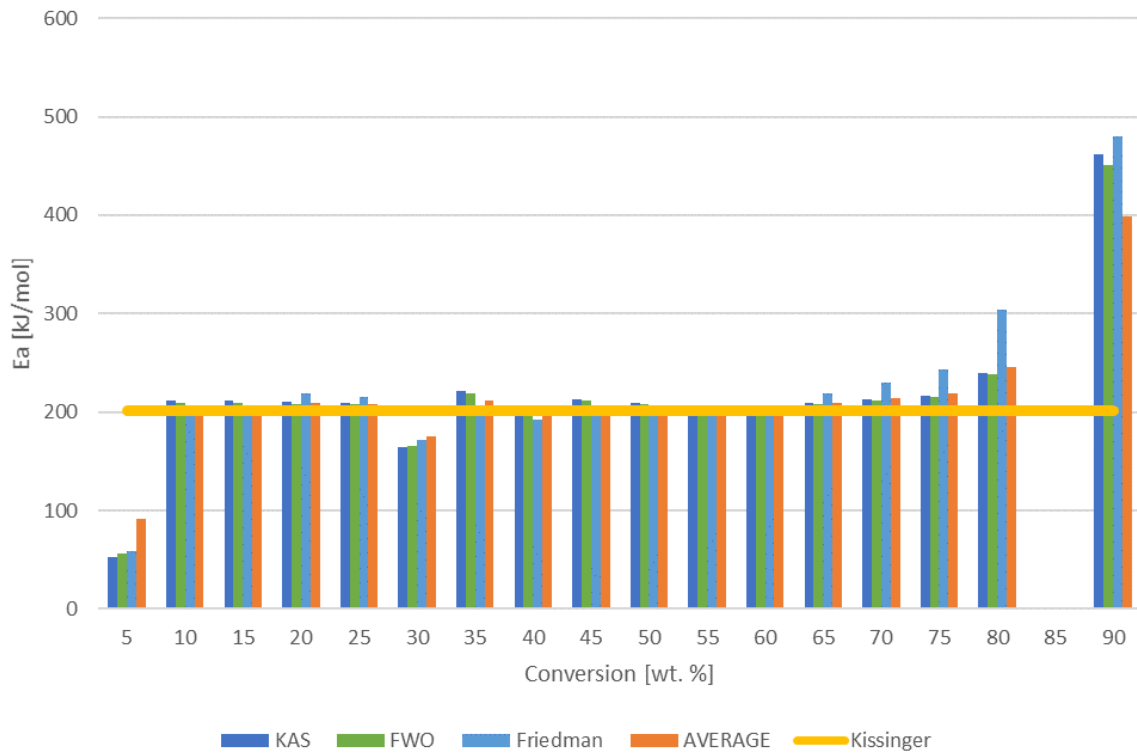


Figure 5.26: Activation energy for Woodchips every 5% conversion

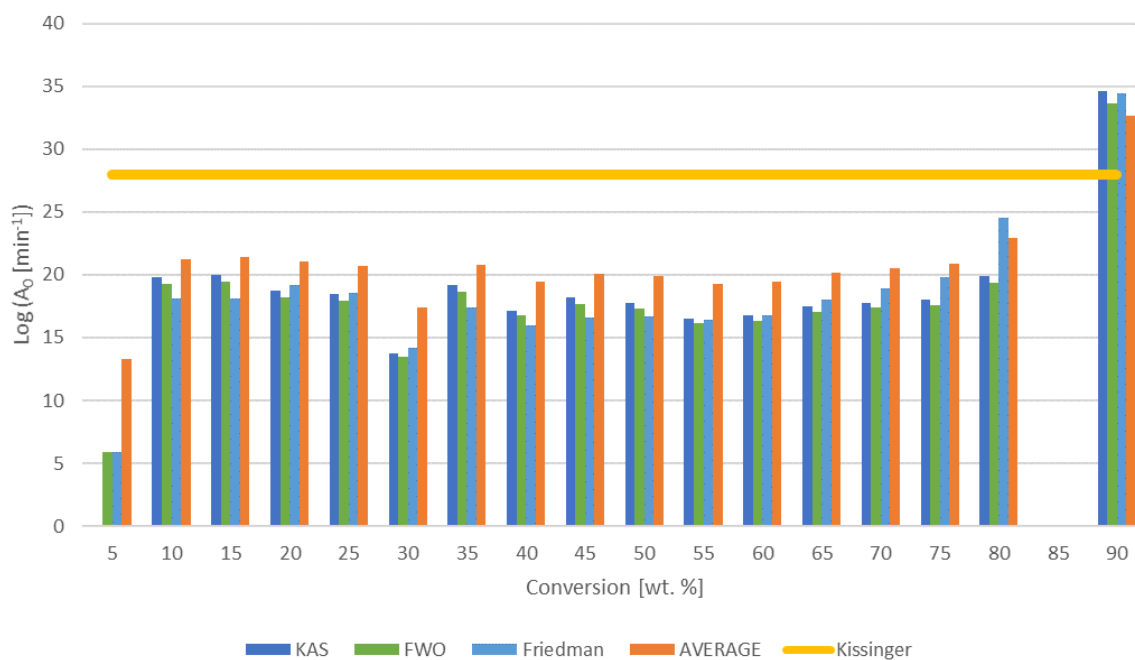


Figure 5.27: Pre-exponential factor for Woodchips every 5% conversion

## 5.6 Analysis of the vapours

It is mentioned that pyrolysis involves hundreds of reactions with thousands of components [1-4]. The production of vapours is an essential aspect of the model because the properties change from one produced gas to another. Ideally, the vapours should be quantified within the experiments to determine the quantity and the moment each is produced. During the experiments, the TGA is coupled to a Mass Spectrometer (MS) to analyse the exit gases. The analysis is used to find a kinetic constant for the formation of gases and predict the exact gas composition in the reactor.

In the literature [36, 45, 54, 70, 77-84] the TGA is coupled with MS and FTIR to measure and quantify certain gases produced during pyrolysis. Basu [7] mentions hydrogen, steam, methane, carbon dioxide, carbon monoxide, acetylene, ethylene and ethane as the most common vapours produced during pyrolysis. In the studies, the last three components are usually omitted to simplify the calculations.

In addition to the components mentioned by Basu [7], nitrogen should be taken into account because it is used as the carrier gas in the TGA. The NIST Chemistry Webbook [85] was consulted to find the most appropriate channels for each component in the MS. For each component, a graph similar to those in Figure 5.28 and Figure 5.29 is obtained. The examples shown are for ethane and hydrogen.

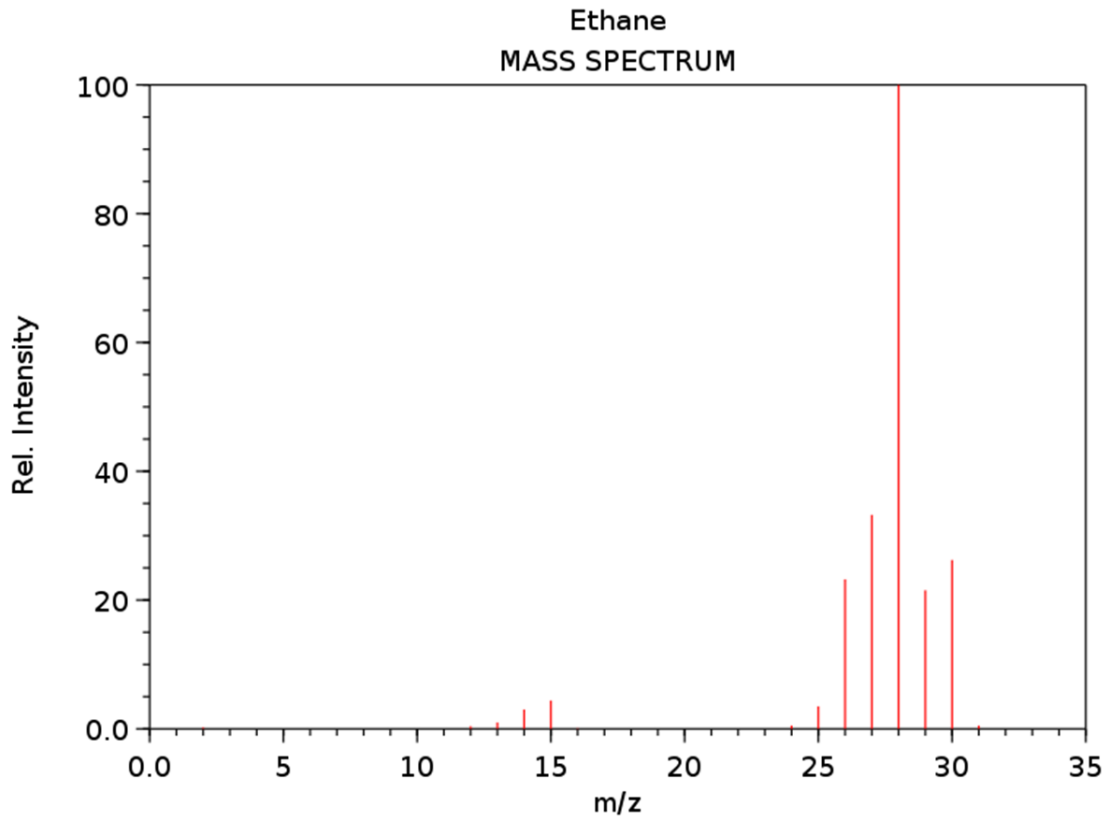


Figure 5.28: Mass spectrum for Ethane (from [85])

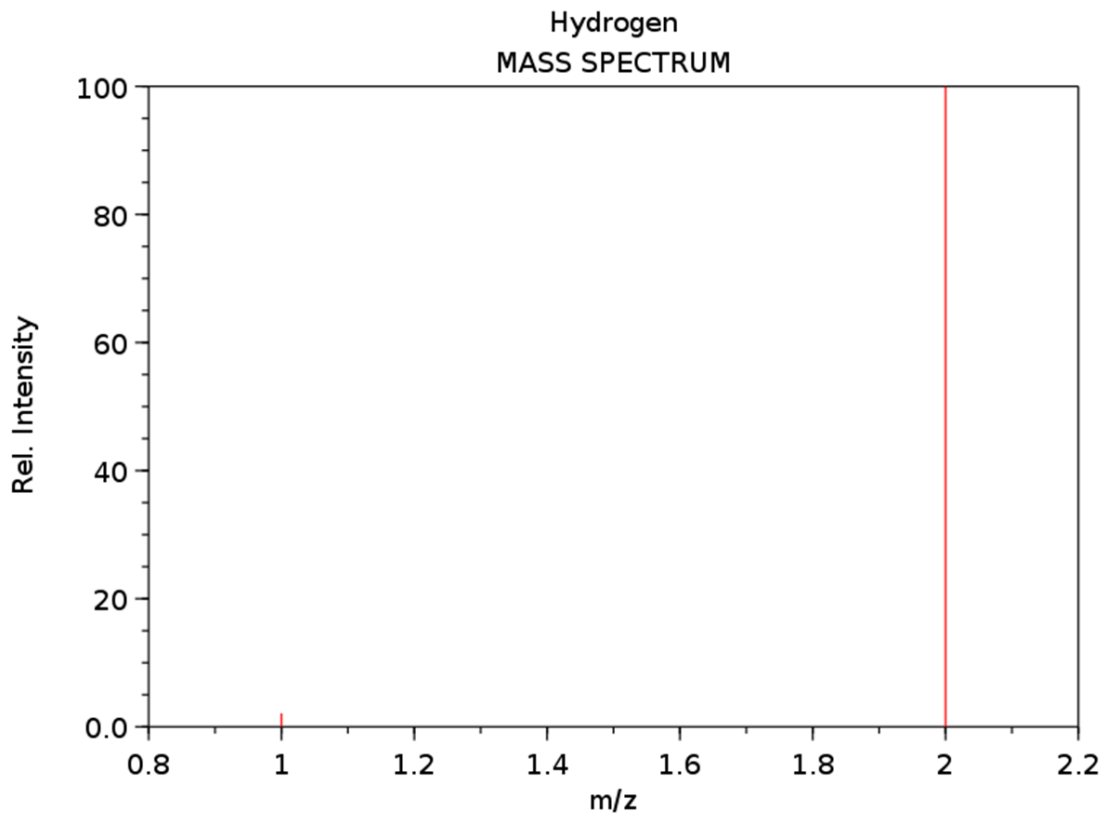


Figure 5.29: Mass spectrum for Hydrogen (from [85])

It is observed that a single component can have many different channels for analysis (ethane), whereas others only have few (hydrogen). To see the channels overlap between components and select the best channels to measure the vapours, Table 5.16 was generated. The m/z columns are the channels of the MS for each component, and the relative intensity is the strength of the signal at each channel. The colour of each m/z is a key to show how many times that value is used for the known components. The colour follows the path green → yellow → orange → red; the closer to red, the more times the number appears in the table. The numbers in green are unique in the table and can be used to measure that specific element if the signal is high enough. The signals in yellow are repeated once, which means that in total, it appears twice on the table. The number of repetition is two for orange, and the numbers which appear in red are repeated four times (there is no number repeated three times). This classification is used to select the channels through which each of the vapours are measured. The selection is a compromise between avoiding repetition (green colour preferred), high intensity of the vapour to measure and, if repeated, low intensity of the other components' signals.

Table 5.16: Channels in the MS per component

| Name            | Formula                       | Signal 1 |                    | Signal 2 |                    | Signal 3 |                    | Signal 4 |                    | Signal 5 |                    | Signal 6 |                    | Signal 7 |                    | Signal 8 |                    |
|-----------------|-------------------------------|----------|--------------------|----------|--------------------|----------|--------------------|----------|--------------------|----------|--------------------|----------|--------------------|----------|--------------------|----------|--------------------|
|                 |                               | m/z      | Relative intensity | m/z      | Relative intensity | m/z      | Relative intensity | m/z      | Relative intensity | m/z      | Relative intensity | m/z      | Relative intensity | m/z      | Relative intensity | m/z      | Relative intensity |
| Nitrogen        | N <sub>2</sub>                | 28       | 100                | 14       | 15                 |          |                    |          |                    |          |                    |          |                    |          |                    |          |                    |
| Hydrogen        | H <sub>2</sub>                | 2        | 100                | 1        | 2.5                |          |                    |          |                    |          |                    |          |                    |          |                    |          |                    |
| Water/Steam     | H <sub>2</sub> O              | 18       | 100                | 19       | 21                 |          |                    |          |                    |          |                    |          |                    |          |                    |          |                    |
| Methane         | CH <sub>4</sub>               | 16       | 100                | 15       | 90                 | 14       | 20                 | 13       | 10                 | 12       | 5                  |          |                    |          |                    |          |                    |
| Carbon dioxide  | CO <sub>2</sub>               | 44       | 100                | 28       | 10                 | 16       | 10                 | 10       | 10                 |          |                    |          |                    |          |                    |          |                    |
| Carbon monoxide | CO                            | 28       | 100                | 12       | 5                  | 16       | 2.5                |          |                    |          |                    |          |                    |          |                    |          |                    |
| Acetylene       | C <sub>2</sub> H <sub>2</sub> | 26       | 100                | 25       | 20                 | 24       | 5                  | 27       | 2.5                | 13       | 2.5                |          |                    |          |                    |          |                    |
| Ethylene        | C <sub>2</sub> H <sub>4</sub> | 28       | 100                | 27       | 62.5               | 26       | 55                 | 25       | 7.5                | 24       | 2.5                |          |                    |          |                    |          |                    |
| Ethane          | C <sub>2</sub> H <sub>6</sub> | 28       | 100                | 27       | 35                 | 30       | 27.5               | 26       | 25                 | 29       | 22.5               | 25       | 5                  | 15       | 5                  | 14       | 2.5                |

The channels selected and measured are 2, 14, 15, 18, 26, 27, 28, 30 and 44. The following equations show the channel and the intensity of each component with percentages. The percentages are the intensity of the component, which are multiplying.

$$2 = 100\% \cdot H_2$$

Equation 5.45: Signal 2 from MS

$$14 = 15\% \cdot N_2 + 20\% \cdot CH_4 + 2.5\% \cdot C_2H_6$$

Equation 5.46: Signal 14 from MS

$$15 = 90\% \cdot CH_4 + 5\% \cdot C_2H_6$$

Equation 5.47: Signal 15 from MS

$$18 = 100\% \cdot H_2O$$

Equation 5.48: Signal 18 from MS

$$26 = 100\% \cdot C_2H_2 + 55\% \cdot C_2H_4 + 25\% \cdot C_2H_6 \quad 27 = 2.5\% \cdot C_2H_2 + 62.5\% \cdot C_2H_4 + 35\% \cdot C_2H_6$$

Equation 5.49: Signal 26 from MS

Equation 5.50: Signal 27 from MS

$$28 = 100\% \cdot N_2 + 100\% \cdot CO + 100\% \cdot C_2H_6 + 10\% \cdot CO_2$$

Equation 5.51: Signal 28 from MS

$$30 = 27.5\% \cdot C_2H_6$$

Equation 5.52: Signal 30 from MS

$$44 = 100\% \cdot C_2H_6$$

Equation 5.53: Signal 44 from MS

The measurements are taken at the same time that the experiments are conducted. The measurements were completed three times per feedstock and per heating rate. One example of the data obtained is represented in Figure 5.30:

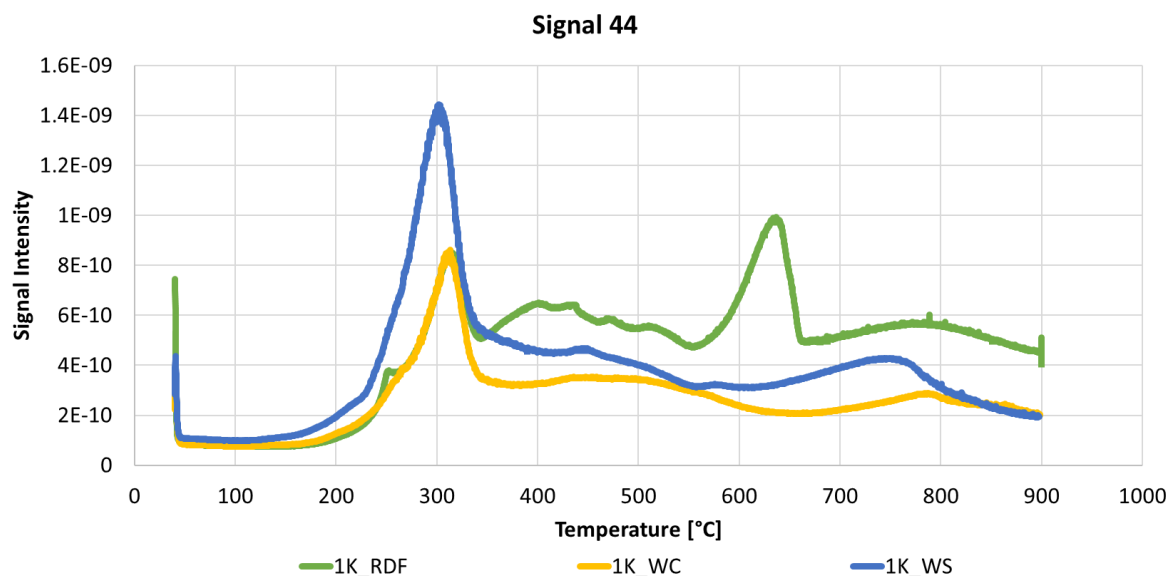


Figure 5.30: MS example for Signal 44

A description of the behaviour of each signal is provided below:

- **2:** there is no significant increase in the signal until 500 °C is reached. The lignocellulosic feedstock has a production peak, whereas the RDF increases the signal gradually with the temperature.
- **14:** a fall appears around 250°C in the lignocellulosic feedstock and increases until reaching almost the initial signal value. At high temperatures (higher than 650°C), the signal decreases gradually. The RDF falls at 450 °C and stays low until the end.
- **15:** there is a fall at 250°C followed by an increase in a wide-peak shape with a maximum of 500 °C. In the case of RDF, the signal remains low until a temperature around 430 °C where a peak appears, which became wider when the heating rate increased.
- **17:** During the measurements, there was an error, and instead of measuring signal 27, the signal 17 was chosen. There is a peak around 140-150 °C, which starts at 80 °C and reaches the initial value around 250 °C. The RDF does not reach a high value, but it has another peak around 400 °C that decreases gradually until the end.
- **18:** there is the typical peak around 100 °C, which is likely to be the water from the feedstock. Another peak is formed around 350 °C. All these peaks are very sensitive to the heating rate because the position varies significantly with the heating rate.
- **26:** there is a constant signal for lignocellulosic materials until the signals fall at 220 °C and increases until reaching values similar to the start. The RDF presents a peak at 450 °C.
- **28:** the signal for RDF decreases in a fall at 250 °C and has a peak at 450 °C. The woody feedstock decreases at 250 °C, but it is mainly constant.
- **30:** at 200 °C there is a fall of the signal. Then the signal increases a maximum around 350 °C and decreases gradually until the end. The RDF shows another peak around 475 °C to decrease again.
- **44:** The lignocellulosic feedstocks present high-intensity peaks at 300 °C compared to the ones showed by the RDF. The RDF has another peak at 650 °C.

From the intensity for each component for each signal, there was an attempt to calculate the quantities of each value following the same procedure as the kinetics. It included subtracting the blank values and establishing the maximum value of each signal within all experiments as the maximum possible. However, the values obtained were not valid because the total fraction of gases gives values

higher than 100%. For that reason, it is concluded that coupling the TGA with an MS only cannot be used to calculate the formation of the vapour quantitatively, although the tendency can be observed. In the literature [45, 78-84] TGA and MS are coupled with another piece of equipment (FTIR) when the method required is quantitative.

Despite this, the model still needs a gas production estimation at each temperature to model properties such as density, viscosity, heating capacity or conductivity. Due to the difficulty and lack of experimental information, the data is found from the literature [45, 78-84]. However, it is mainly the non-condensable fraction that is analysed, which is carbon monoxide (CO), carbon dioxide (CO<sub>2</sub>), methane (CH<sub>4</sub>), hydrogen (H<sub>2</sub>) and water vapour (H<sub>2</sub>O). Therefore, the model is simplified to produce only non-condensable gases inside the reactor for the calculation of properties. In Section 5.7, there is an explanation of how the yields of condensable and non-condensable vapours are calculated.

*Assumption 16: The vapour properties are calculated from the non-condensable fraction and from CO, CO<sub>2</sub>, CH<sub>4</sub>, H<sub>2</sub> and H<sub>2</sub>O, to the carrier gas N<sub>2</sub>*

The method used to calculate the gases produced is a mixture of literature and experimental data. Data from the literature [12, 45, 78-84] is used, analysing the vapours for each study and combining them with the experimental values. A widespread practice in literature is to attribute a channel for each component. For instance, Gómez-Díaz [12] attributed channel 2 directly to hydrogen, 18 to water, 28 for carbon monoxide and 44 for carbon dioxide. It is observed previously (Table 5.16) that some of the MS channels are influenced by many components, such as channel 28 that receives information from carbon dioxide, carbon monoxide, nitrogen, ethylene and ethane. Combining the data from the experiments and the data available, the yields used for the calculation in the model are (Table 5.17 and Table 5.18):

Table 5.17: Gas yields for lignocellulosic biomass

| Lignocellulosic biomass |       |           |       |
|-------------------------|-------|-----------|-------|
|                         | T<500 | 500<T<800 | T>800 |
| CO                      | 25%   | 30%       | 40%   |
| CO <sub>2</sub>         | 25%   | 50%       | 40%   |
| H <sub>2</sub> O        | 40%   | 0%        | 0%    |
| CH <sub>4</sub>         | 10%   | 15%       | 10%   |
| H <sub>2</sub>          | 0%    | 5%        | 10%   |

Table 5.18: Gas yields for RDF

| RDF              |       |           |       |
|------------------|-------|-----------|-------|
|                  | T<500 | 500<T<800 | T>800 |
| CO               | 25%   | 30%       | 30%   |
| CO <sub>2</sub>  | 25%   | 40%       | 30%   |
| H <sub>2</sub> O | 40%   | 0%        | 0%    |
| CH <sub>4</sub>  | 10%   | 20%       | 20%   |
| H <sub>2</sub>   | 0%    | 10%       | 20%   |

The tendency of the tables agrees with the qualitative analysis of the data from the MS, for example, production of hydrogen when temperature surpasses 500 °C and higher production for RDF than for lignocellulosic biomass.

The mass difference due to pyrolysis/ chemical reaction for solids on each of the reactor slices (Sections 7.3.2 and 7.4) is calculated and implemented within the model. The temperature range chosen depends on the average temperature of the slice. It mainly affects the second loop to calculate the temperatures (Figure 4.13), because the properties of the gases change with temperature and when an equilibrium is reached, the composition changes and there is the need of further calculations for the first loop (Section 7.3.2).

## 5.7 Product distribution

With the vapours analysis in Section 5.6, there is an initial insight into the method for calculating the product distribution. With the experiments in Section 5.3, only the solid yield can be calculated. The produced vapours are not differentiated between condensable and non-condensable fraction during the experiments. The yields of the products vary significantly with the feedstock and the conditions according to many studies on pyrolysis [12, 36, 54, 73, 77, 86].

From the experiments using the TGA, the solid yield can be calculated at each temperature. The data from TGA at a heating rate of 1°C/min is studied to do this. This data is valuable because the heating rate is extremely low, and it helps to demonstrate the maximum conversion of solids to products achieved. In other words, the conversion of the solid is 100% for each temperature the TGA achieves with a 1°C/min heating rate. Using Equation 5.54, the normalised weights are calculated and represented in Figure 5.31.

*Assumption 17: The conversion of any of the feedstock studied is 100% at each temperature the TGA achieves with a 1°C/min heating rate*

$$\text{Char Yield}_{\text{Temperature}=T} = \frac{W_T}{W_0}$$

Equation 5.54: Calculation of char yield at each temperature

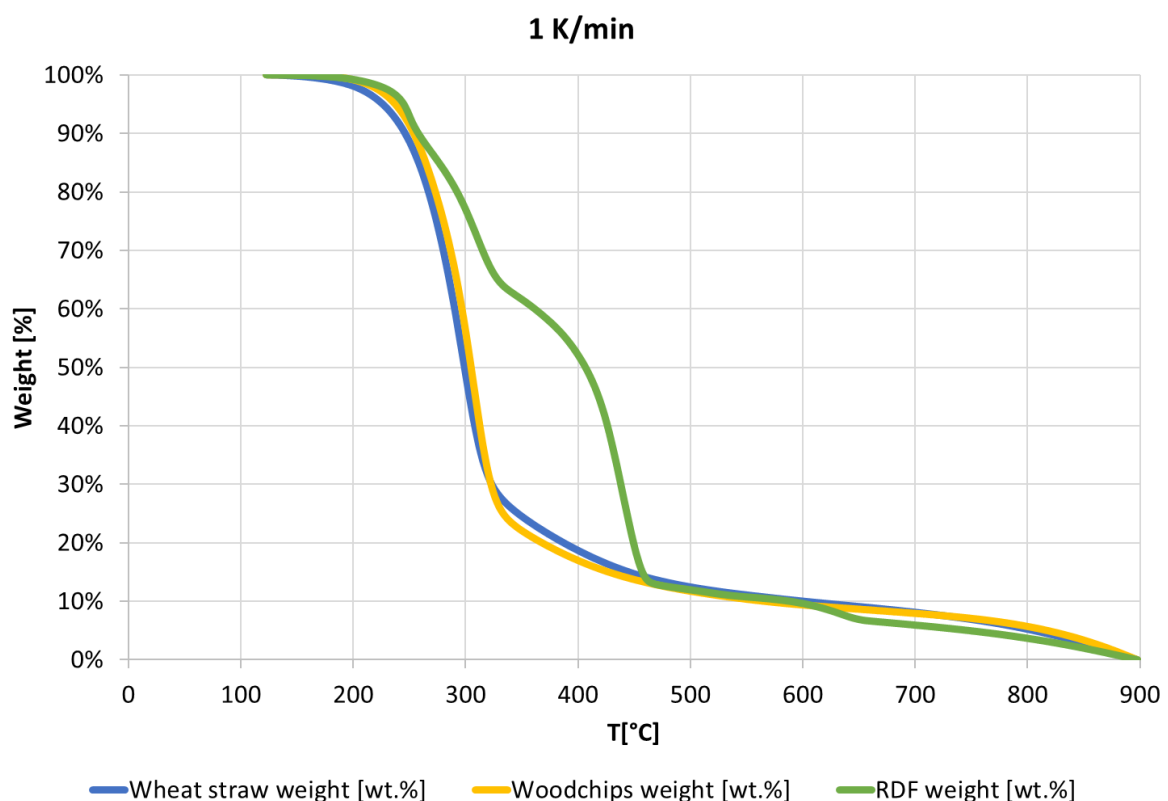


Figure 5.31: Char yield within the temperature range

The char yield is, as anticipated, very high for low temperatures and it reaches a maximum of 40 wt.% char yield at a temperature of approximately 350 °C, which is the overall limit between pyrolysis and torrefaction. It is assumed, that the remaining weight at each temperature is considered as the final char yield at that temperature due to the low heating rate employed. The curve for each



feedstock is adjusted to a 7-degree equation which determines the char yield depending on the temperature. The coefficients for the regression value are shown in Table 5.19. The regression values are over 98% for the three feedstock, so the adjustment and accuracy of the values are high. The numbers indicate the power of the temperature for each coefficient. As an example, Equation 5.55 would be used to adjust the char yield for RDF.

Table 5.19: Coefficients for the char yield of each feedstock

|     | Coefficients (Char vs.T) |           |           |          |           |          |        |      | R <sup>2</sup> |
|-----|--------------------------|-----------|-----------|----------|-----------|----------|--------|------|----------------|
|     | 7                        | 6         | 5         | 4        | 3         | 2        | 1      | 0    |                |
| RDF | 1.72E-19                 | -3.76E-16 | 1.75E-13  | 1.42E-10 | -1.50E-07 | 4.10E-05 | -0.004 | 1.14 | 0.994          |
| WS  | -1.23E-18                | 4.22E-15  | -5.81E-12 | 4.04E-09 | -1.48E-06 | 2.69E-04 | -0.022 | 1.64 | 0.989          |
| WC  | -1.40E-18                | 4.81E-15  | -6.57E-12 | 4.52E-09 | -1.62E-06 | 2.77E-04 | -0.019 | 1.22 | 0.985          |

$$\text{Char yield}(T) = 1.72 \cdot 10^{-19} \cdot T^7 - 3.76 \cdot 10^{-16} \cdot T^6 + 1.75 \cdot 10^{-13} \cdot T^5 + 1.42 \cdot 10^{-10} \cdot T^4 - 1.50 \cdot 10^{-7} \cdot T^3 + 4.10 \cdot 10^{-5} \cdot T^2 - 0.004 \cdot T + 1.14$$

Equation 5.55: Char yield for RDF

This expression will give the value of the char yield per unit of weight. With these equations, the value of the solid product is calculated. Since this model is part of the project GreenCarbon [87], the feedstocks used are utilised by the researcher Filipe Rego at Aston University for pyrolysis in an auger reactor (Sections 1.3 and 11.2.8) [88]. Despite an auger reactor being used for Filipe's study, the model is used to predict the product distribution.

Figure 5.32 represents the yield of the products from wheat straw pyrolysis at a range of temperatures. The organic and aqueous phase constitutes the pyrolysis oil. The other products are char and permanent gases. Once the char yield is removed, the gas and condensable fraction remain and the yields normalised to 100% (see Figure 5.33). The pyrolysis oils are separated into the aqueous and organic phase. These results are obtained from [88], which uses the same feedstocks as this work. The longer residence time is selected to ensure the conversion of the biomass is as high as possible, and there are no unpyrolysed fractions.

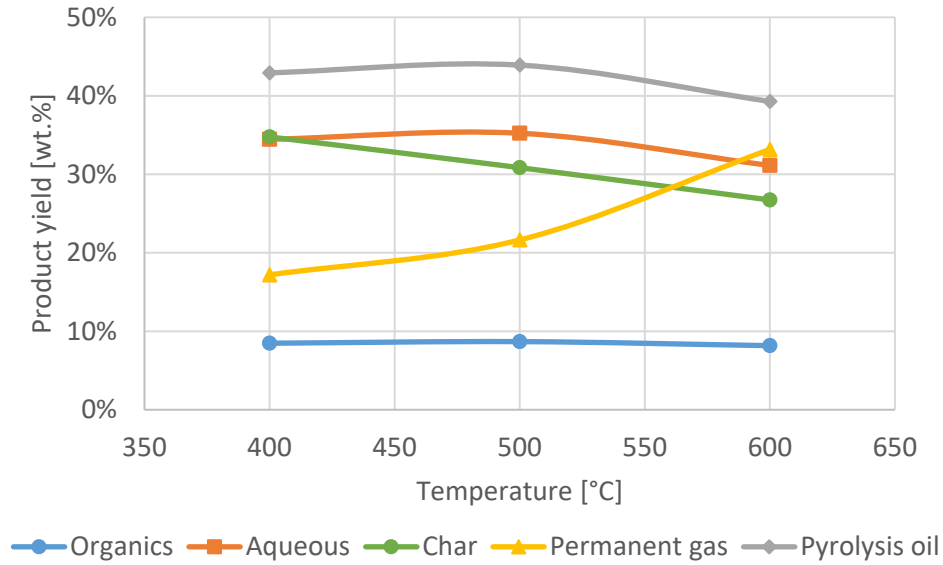


Figure 5.32: Product yields variation with temperature, adapted from [88]

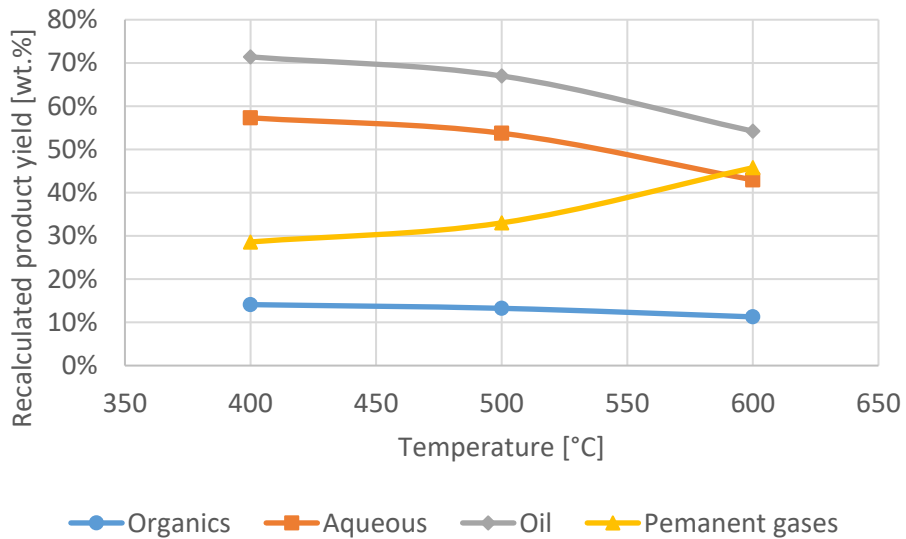


Figure 5.33: Recalculated yields for pyrolysis vapours, adapted from [88]

The data from the graph (Figure 5.33) is adjusted to a third-degree-equation to model the yield of condensable and non-condensable fractions. The adjusting coefficients are shown in Equation 5.56 and Equation 5.57 with perfect regressions ( $R^2=1$ ).

$$Yield_{pyrolysis\ oil} = -4.2 \cdot 10^{-6} \cdot T^2 + 3.31 \cdot 10^{-3} \cdot T + 0.55937$$

Equation 5.56: Yield of pyrolysis oil with temperature

$$Yield_{permanent\ gas} = 4.17 \cdot 10^{-6} \cdot T^2 - 3.31 \cdot 10^{-3} \cdot T + 0.944063$$

Equation 5.57: Yield of permanent gas with temperature

The temperature to which the equations refer is the temperature of solids at the reactor exit because that is the temperature at which pyrolysis occurs on each experiment. The yield is related to the normalised fraction of the vapours. To obtain the actual yield from the biomass, the values need

to be multiplied the opposite of the char yield. The equations are related to the wheat straw, but they are applied to all. The reason is the lack of information for the other feedstocks. Further development of the model should study the expressions for the other feedstocks.

In pyrolysis, it is arguable whether there are three or four products. It depends on how the pyrolysis oil is quantified and if it is separated into an organic and aqueous phase. In this study, it was chosen to measure four products instead of three. The results were analysed to check the evolution of the aqueous and organic phase on a dry basis. The data indicated that the fraction of organics and aqueous phases were not dependant on temperature because in all cases the values were 80 wt.% aqueous phase and 20 wt.% organic phase with less than 5% deviation, which made the correlation aqueous/organic phase very consistent within the pyrolysis oil product.

*Assumption 18: From the vapours generated in pyrolysis, the fraction and evolution of condensable and permanent follow the same equations for all feedstocks. Within the condensable vapours, the fractions organic-aqueous follow the correlation 20/80 wt.%.*

The solid yield is calculated from the TGA experiments. The difference between the mass flow at the entrance and the exit of the reactor is the amount of vapours produced, and the experiments in the auger reactor from Filipe Rego [88] within the GreenCarbon project provides the information to define the fraction of the vapour which is condensable and non-condensable. The solid mass difference, represented by the vapours inside the reactor are modelled as carbon monoxide (CO), carbon dioxide (CO<sub>2</sub>), methane (CH<sub>4</sub>), hydrogen (H<sub>2</sub>) and water vapour (H<sub>2</sub>O) for the calculation of the properties.

*Assumption 19: The fraction of condensable and non-condensable does not vary significantly from auger to rotary reactor*

## 5.8 Reaction heat

The heat of reaction is the amount of energy released or absorbed by the reagents and products when a reaction occurs. It is not a kinetic parameter but thermochemical, yet it is included in this chapter because it is directly correlated to the conversion of the solid and the yield. This variation of energy is usually measured by the reaction temperature, which varies if the control is not efficient.

In the literature, Gómez-Díaz [12] and Anca-Couce [15] expose the difficulty to define pyrolysis as an endothermic or exothermic process, and the lack of consistent heat of reaction values in literature. Gómez-Díaz [12] associates small particles with endothermic reactions and large samples and particle size with exothermic, which could be connected to the interaction of pyrolysis vapours with the solid. Anca-Couce [15] attributes exothermal behaviour when a lidded sample is used, or there is a larger sample of biomass. It is attributed to a higher retention time of volatiles within the biomass, similar to the approach explained by Gómez-Díaz [12]. However, it seems there is a relationship between the component decomposing (cellulose, hemicellulose and lignin).

Both authors [12, 15] agree that Differential Scanning Calorimetry (DSC) is a promising technique to obtain the reaction heat when there is an absence of mass and heat transfer limitations. To calculate the reaction heat, the electrical input to the sample holder is considered, and the radiative heat of this holder is removed before calculating the reaction heat.

The data from the TGA experiments include DSC. The data was manipulated to find the heat of reaction. Some data about the feedstock, such as heat capacity is required for the calculation of the heat according to the method proposed by Rath et al. [89]. Since the heat capacity for the feedstock

can vary, especially for feedstocks such as RDF, the approach changed from trying to calculate the reaction heat to obtain the whole set of heat of reaction values from the literature. For the construction of the model in this work, the heat of pyrolysis for woodchips is 279,637.5 J/kg as an average of the values of Rath et al.[89], for wheat straw it is 360,000 J/kg according to the values of woody biomass from Anca-Couce [15] and 300,000 J/kg for RDF, assumed due to the lack of data in the literature and an average between the others. In this study, the values for pyrolysis of biomass are considered endothermic as calculated more commonly in the literature and also considered constant with temperature. The reason to obtain the values from literature instead of calculating from the TGA experiments is the similar accuracy in both cases. To obtain the values from the experiments, the heat capacity had to be estimated from literature, whereas in the case of reaction heat, the value is directly obtained.

*Assumption 20: The heat of reaction has a single value per feedstock and does not vary with temperature*

This reaction heat is implemented in the model when the solid mass varies. The variation of mass flow multiplied by the reaction heat gives the energy released in that particular slice, which results in an additional source of energy to increase the solids temperature or to achieve a higher temperature in the reactor. This energy released is added to the energy balance of the slice to calculate the new heat to the solid, resulting in an increment of the final temperature (more detailed description in Section 7.3).

## 5.9 References

1. Cortés-Benítez, A.M., *Thermal processing of miscanthus, sugarcane bagasse, sugarcane trash and their acid hydrolysis residues*, in *European Bioenergy Research Institute (EBRI), Engineering and Applied Sciences (EAS)*. 2015, Aston University: Birmingham.
2. White, J.E., W.J. Catallo, and B.L. Legendre, *Biomass pyrolysis kinetics: A comparative critical review with relevant agricultural residue case studies*. *Journal of Analytical and Applied Pyrolysis*, 2011. **91**(1): p. 1-33.
3. Zhu, X.-f. and Q. Lu, *Production of Chemicals from Selective Fast Pyrolysis of Biomass*, in *Biomass*, InTech, Editor. 2010.
4. Peters, J.F., D. Iribarren, and J. Dufour, *Predictive pyrolysis process modelling in Aspen Plus*. 2014.
5. Peters, J.F., et al., *A kinetic reaction model for biomass pyrolysis processes in Aspen Plus*. *Applied Energy*, 2017. **188**: p. 595-603.
6. Peters, J.F., et al., *Experimental validation of a predictive pyrolysis model in Aspen Plus*. 2014.
7. Basu, P., *Biomass gasification, pyrolysis, and torrefaction: practical design and theory*. 2013: London, UK : Elsevier : Academic Press, 2013. Second edition.
8. Diebold, J. and T. Bridgwater, *Overview of Fast Pyrolysis of Biomass for the Production of Liquid Fuels*. 1997. 5-23.
9. Helt, J.E. and R.K. Agrawal, *Production and Characterization of Pyrolysis Liquids from Municipal Solid Waste*. p. 8.
10. Roy, P. and G. Dias, *Prospects for pyrolysis technologies in the bioenergy sector: A review*. *Renewable and Sustainable Energy Reviews*, 2017. **77**: p. 59-69.
11. Cortés, A.M. and A.V. Bridgwater, *Kinetic study of the pyrolysis of miscanthus and its acid hydrolysis residue by thermogravimetric analysis*. *Fuel Processing Technology*, 2015. **138**: p. 184-193.
12. Gómez Díaz, C.J., *Understanding Biomass Pyrolysis Kinetics: Improved Modeling Based on Comprehensive Thermokinetic Analysis*, in *Department of chemical Engineering*. 2006, Universitat Politècnica de Catalunya: Barcelona. p. 223.

13. Antal, M.J., Jr. and G. Varhegyi, *Cellulose Pyrolysis Kinetics: The Current State of Knowledge*. Industrial & Engineering Chemistry Research, 1995. **34**(3): p. 703-717.
14. Di Blasi, C. and M. Lanzetta, *Intrinsic kinetics of isothermal xylan degradation in inert atmosphere*. Journal of Analytical and Applied Pyrolysis, 1997. **40-41**: p. 287-303.
15. Anca-Couce, A., *Reaction mechanisms and multi-scale modelling of lignocellulosic biomass pyrolysis*. Progress in Energy and Combustion Science, 2016. **53**(Supplement C): p. 41-79.
16. Roegiers, J., J.p. Pieters, and F.p. Ronsse, *Heat and mass transfer modelling of auger reactors*, in *Faculteit Bio-ingenieurswetenschappen*. 2016, Universiteit Gent.
17. Patwardhan, P.R., *Understanding the product distribution from biomass fast pyrolysis*, in *Chemical Engineering*. 2010, Iowa State University: Graduate Theses and Dissertation. p. 161.
18. Prakash, N. and T. Karunanithi, *Kinetic modeling in biomass pyrolysis - A review*. J. Appl. Sci. Res., 2008. **4**(12): p. 1627-1636.
19. Broido, A. and M. A. Nelson, *Char yield on pyrolysis of cellulose*. Vol. 24. 1975. 263-268.
20. Milosavljevic, I., V. Oja, and E. Suuberg, *Thermal Effects in Cellulose Pyrolysis: Relationship to Char Formation Processes*. Vol. 35. 1996.
21. Milosavljevic, I. and E.M. Suuberg, *Cellulose Thermal Decomposition Kinetics: Global Mass Loss Kinetics*. Industrial & Engineering Chemistry Research, 1995. **34**(4): p. 1081-1091.
22. Mok, W.S.L. and M.J. Antal, *Effects of pressure on biomass pyrolysis. II. Heats of reaction of cellulose pyrolysis*. Thermochemica Acta, 1983. **68**(2): p. 165-186.
23. Cooley, S. and M.J. Antal, *Kinetics of cellulose pyrolysis in the presence of nitric oxide*. Journal of Analytical and Applied Pyrolysis, 1988. **14**(2): p. 149-161.
24. Shafizadeh, F., et al., *Production of Levoglucosan and Glucose from Pyrolysis of Cellulosic Materials*. Vol. 23. 1979. 3525-3539.
25. Shafizadeh, F., G.D. McGinnis, and C.W. Philpot, *Thermal degradation of xylan and related model compounds*. Carbohydrate Research, 1972. **25**(1): p. 23-33.
26. Koufopoulos, C.A., et al., *Modelling of the pyrolysis of biomass particles. Studies on kinetics, thermal and heat transfer effects*. Vol. 69. 1991. 907-915.
27. Di Blasi, C., *Modeling chemical and physical processes of wood and biomass pyrolysis*. Progress in Energy and Combustion Science, 2008. **34**(1): p. 47-90.
28. Lanzetta, M. and C. Di Blasi, *Pyrolysis kinetics of wheat and corn straw*. Journal of Analytical and Applied Pyrolysis, 1998. **44**(2): p. 181-192.
29. Fantozzi, F., et al., *Rotary Kiln Slow Pyrolysis for Syngas and Char Production From Biomass and Waste — Part II: Introducing Product Yields in the Energy Balance*. Journal of Engineering for Gas Turbines and Power, 2007. **129**(4): p. 908-913.
30. Babler, M.U., et al., *Modelling and pilot plant runs of slow biomass pyrolysis in a rotary kiln*. Applied Energy, 2017. **207**: p. 123-133.
31. Neves, D., et al., *Characterization and prediction of biomass pyrolysis products*. Progress in Energy and Combustion Science, 2011. **37**(5): p. 611-630.
32. Papari, S. and K. Hawboldt, *Development and Validation of a Process Model To Describe Pyrolysis of Forestry Residues in an Auger Reactor*. Energy & Fuels, 2017. **31**(10): p. 10833-10841.
33. Piskorz, J., et al., *Pretreatment of wood and cellulose for production of sugars by fast pyrolysis*. Journal of Analytical and Applied Pyrolysis, 1989. **16**(2): p. 127-142.
34. Banyasz, J.L., et al., *Gas evolution and the mechanism of cellulose pyrolysis*. Fuel, 2001. **80**(12): p. 1757-1763.
35. Banyasz, J.L., et al., *Cellulose pyrolysis: the kinetics of hydroxyacetaldehyde evolution*. Journal of Analytical and Applied Pyrolysis, 2001. **57**(2): p. 223-248.
36. Costa, P.A., et al., *Kinetic Evaluation of the Pyrolysis of Polyethylene Waste*. Energy & Fuels, 2007. **21**(5): p. 2489-2498.
37. Anca-Couce, A., et al., *Kinetic scheme of biomass pyrolysis considering secondary charring reactions*. Energy Conversion and Management, 2014. **87**: p. 687-696.

38. Ranzi, E., et al., *Chemical Kinetics of Biomass Pyrolysis*. Energy & Fuels, 2008. **22**(6): p. 4292-4300.
39. Bridgwater, T. and S. A. Bridge, *A Review of Biomass Pyrolysis and Pyrolysis Technologies*, in *Biomass Pyrolysis Liquids Upgrading and Utilization*, Springer, Editor. 1991, Springer: New York. p. 11-92.
40. Cai, J., et al., *Review of physicochemical properties and analytical characterization of lignocellulosic biomass*. Renewable and Sustainable Energy Reviews, 2017. **76**: p. 309-322.
41. Dhyani, V. and T. Bhaskar, *A comprehensive review on the pyrolysis of lignocellulosic biomass*. Renewable Energy, 2017.
42. Çepelioğullar, Ö., H. Haykırı-Açma, and S. Yaman, *Kinetic modelling of RDF pyrolysis: Model-fitting and model-free approaches*. Waste Management, 2016. **48**: p. 275-284.
43. Çepelioğullar, Ö. and A.E. Pütün, *Products characterization study of a slow pyrolysis of biomass-plastic mixtures in a fixed-bed reactor*. Journal of Analytical and Applied Pyrolysis, 2014. **110**: p. 363-374.
44. Lin, K.-S., et al., *Pyrolysis kinetics of refuse-derived fuel*. Fuel Processing Technology, 1999. **60**(2): p. 103-110.
45. Singh, S., C. Wu, and P.T. Williams, *Pyrolysis of waste materials using TGA-MS and TGA-FTIR as complementary characterisation techniques*. Journal of Analytical and Applied Pyrolysis, 2012. **94**: p. 99-107.
46. Tomasiak, A., *Pyrolysis and Combustion Kinetics of Refuse Derived Fuel and Ash Characterization*. 2017, Instituto Superior Técnico.
47. Cai, J.M. and L.S. Bi, *Kinetic analysis of wheat straw pyrolysis using isoconversional methods*. Journal of Thermal Analysis and Calorimetry, 2009. **98**(1): p. 325.
48. Cai, J., et al., *Processing thermogravimetric analysis data for isoconversional kinetic analysis of lignocellulosic biomass pyrolysis: Case study of corn stalk*. Renewable and Sustainable Energy Reviews, 2018. **82**: p. 2705-2715.
49. Henrich, E., et al., *Combustion and gasification kinetics of pyrolysis chars from waste and biomass*. Journal of Analytical and Applied Pyrolysis, 1998. **49**: p. 221-241.
50. Bradbury, A.G.W., Y. Sakai, and F. Shafizadeh, *A kinetic model for pyrolysis of cellulose*. Journal of Applied Polymer Science, 1979. **23**(11): p. 3271-3280.
51. Branca, C. and C. Di Blasi, *Kinetics of the isothermal degradation of wood in the temperature range 528–708 K*. Journal of Analytical and Applied Pyrolysis, 2003. **67**(2): p. 207-219.
52. Di Blasi, C. and C. Branca, *The Effects of Water Leaching on the Isothermal Degradation Kinetics of Straw*. Vol. 39. 2000.
53. Shafizadeh, F. and P.P.S. Chin, *Thermal Deterioration of Wood*, in *Wood Technology: Chemical Aspects*. 1977, AMERICAN CHEMICAL SOCIETY. p. 57-81.
54. Šimkovic, I., et al., *Thermogravimetric/mass spectrometric characterization of the thermal decomposition of (4-O-methyl-D-glucurono)-D-xylan*. Journal of Applied Polymer Science, 1988. **36**(3): p. 721-728.
55. El-Sayed, S.A. and M.E. Mostafa, *Pyrolysis characteristics and kinetic parameters determination of biomass fuel powders by differential thermal gravimetric analysis (TGA/DTG)*. Energy Conversion and Management, 2014. **85**: p. 165-172.
56. Dhaundiyal, A., et al., *Determination of Kinetic Parameters for the Thermal Decomposition of Parthenium hysterophorus*. Environmental and Climate Technologies, 2018. **22**(1): p. 5-21.
57. Yahya, M.A., Z. Al-Qodah, and C.W.Z. Ngah, *Agricultural bio-waste materials as potential sustainable precursors used for activated carbon production: A review*. Renewable and Sustainable Energy Reviews, 2015. **46**: p. 218-235.
58. Olszewski, M.P., et al., *Pyrolysis Kinetics of Hydrochars Produced from Brewer's Spent Grains*. Catalysts, 2019. **9**(7): p. 625.
59. Álvarez, A., et al., *Determination of kinetic parameters for biomass combustion*. Bioresource Technology, 2016. **216**: p. 36-43.

60. Valdez, P.J. and P.E. Savage, *A reaction network for the hydrothermal liquefaction of Nannochloropsis sp.* Algal Research, 2013. **2**(4): p. 416-425.
61. Hietala, D.C., J.L. Faeth, and P.E. Savage, *A quantitative kinetic model for the fast and isothermal hydrothermal liquefaction of Nannochloropsis sp.* Bioresource Technology, 2016. **214**: p. 102-111.
62. Bryant, C., *Characterisation and Kinetic Study of Pyrolysis Feedstocks from European Project GreenCarbon*, in *European Bioenergy Research Institute (EBRI)*. 2019, Aston University: Birmingham.
63. Coats, A.W. and J.P. Redfern, *Kinetic Parameters from Thermogravimetric Data*. Nature, 1964. **201**(4914): p. 68-69.
64. Vyazovkin, S. and D. Dollimore, *Linear and Nonlinear Procedures in Isoconversional Computations of the Activation Energy of Nonisothermal Reactions in Solids*. Journal of Chemical Information and Computer Sciences, 1996. **36**(1): p. 42-45.
65. Lyon, R.E., *An integral method of nonisothermal kinetic analysis*. Thermochimica Acta, 1997. **297**(1): p. 117-124.
66. Ozawa, T., *A New Method of Analyzing Thermogravimetric Data*. Bulletin of the Chemical Society of Japan, 1965. **38**(11): p. 1881-1886.
67. *Buoyancy Effect of TGA Experiment*. 2013 30th April 2013 [cited 2019 17th June 2019]; Available from: <https://www.cementscience.com/2013/04/buoyancy-effect-of-tga-experiment.html>.
68. Gašparovič, L., Z. Koreňová, and Ľ. Jelemenský, *Kinetic study of wood chips decomposition by TGA*. Chemical Papers, 2010. **64**(2).
69. Cozzani, V., L. Petarca, and L. Tognotti, *Devolatilization and pyrolysis of refuse derived fuels: characterization and kinetic modelling by a thermogravimetric and calorimetric approach*. Fuel, 1995. **74**(6): p. 903-912.
70. Lu, Q., et al., *Influence of pyrolysis temperature and time on the cellulose fast pyrolysis products: Analytical Py-GC/MS study*. Journal of Analytical and Applied Pyrolysis, 2011. **92**(2): p. 430-438.
71. Chhabra, V., Y. Shastri, and S. Bhattacharya, *Kinetics of Pyrolysis of Mixed Municipal Solid Waste-A Review*. Procedia Environmental Sciences, 2016. **35**: p. 513-527.
72. Manyà, J.J., E. Velo, and L. Puigjaner, *Kinetics of Biomass Pyrolysis: a Reformulated Three-Parallel-Reactions Model*. Industrial & Engineering Chemistry Research, 2003. **42**(3): p. 434-441.
73. Cozzani, V., et al., *A Fundamental Study on Conventional Pyrolysis of a Refuse-Derived Fuel*. Industrial & Engineering Chemistry Research, 1995. **34**(6): p. 2006-2020.
74. Seo, M.W., et al., *Pyrolysis characteristics of coal and RDF blends in non-isothermal and isothermal conditions*. Journal of Analytical and Applied Pyrolysis, 2010. **88**(2): p. 160-167.
75. Chen, D., Y. Zheng, and X. Zhu, *In-depth investigation on the pyrolysis kinetics of raw biomass. Part I: Kinetic analysis for the drying and devolatilization stages*. Bioresource Technology, 2013. **131**: p. 40-46.
76. Varma, A.K. and P. Mondal, *Physicochemical characterization and pyrolysis kinetics of wood sawdust*. Energy Sources, Part A: Recovery, Utilization, and Environmental Effects, 2016. **38**(17): p. 2536-2544.
77. Efika, E.C., J.A. Onwudili, and P.T. Williams, *Products from the high temperature pyrolysis of RDF at slow and rapid heating rates*. Journal of Analytical and Applied Pyrolysis, 2015. **112**: p. 14-22.
78. Danon, B., A. de Villiers, and J.F. Görgens, *Elucidation of the different devolatilisation zones of tyre rubber pyrolysis using TGA-MS*. Thermochimica Acta, 2015. **614**: p. 59-61.
79. Gunasee, S.D., et al., *Pyrolysis and combustion of municipal solid wastes: Evaluation of synergistic effects using TGA-MS*. Journal of Analytical and Applied Pyrolysis, 2016. **121**: p. 50-61.

80. Özsin, G. and A.E. Pütün, *Kinetics and evolved gas analysis for pyrolysis of food processing wastes using TGA/MS/FT-IR*. Waste Management, 2017. **64**: p. 315-326.
81. Özsin, G. and A.E. Pütün, *TGA/MS/FT-IR study for kinetic evaluation and evolved gas analysis of a biomass/PVC co-pyrolysis process*. Energy Conversion and Management, 2019. **182**: p. 143-153.
82. Ischia, M., et al., *Pyrolysis study of sewage sludge by TG-MS and TG-GC-MS coupled analyses*. Journal of Thermal Analysis and Calorimetry, 2007. **87**(2): p. 567-574.
83. Lin, X., et al., *Effects of alkali and alkaline earth metals on the co-pyrolysis of cellulose and high density polyethylene using TGA and Py-GC/MS*. Fuel Processing Technology, 2019. **191**: p. 71-78.
84. Sfakiotakis, S. and D. Vamvuka, *Study of co-pyrolysis of olive kernel with waste biomass using TGA/DTG/MS*. Thermochimica Acta, 2018. **670**: p. 44-54.
85. *NIST Chemistry Webook*, ed. N.I.o.S.a. Technology. 2018: U.S. Department of Commerce.
86. Park, J., et al., *Slow pyrolysis of rice straw: analysis of products properties, carbon and energy yields*. Bioresour Technol, 2014. **155**: p. 63-70.
87. GreenCarbon-ETN. *Advanced Carbon Materials from Biowaste: Sustainable Pathways to Drive Innovative Green Technologies*. 2017 2nd November 2018 9th April 2017]; Available from: <http://greencarbon-etn.eu/>.
88. Rego, F., *Intermediate pyrolysis of biomass in a pilot scale continuous screw reactor*, in *EBRI (Energy and Bioproducts Research Institute)*. Forthcoming, Aston University: Aston University.
89. Rath, J., et al., *Heat of wood pyrolysis*. Fuel, 2003. **82**(1): p. 81-91.



## 6 Additional design features

In this chapter, other design aspects of the rotary kiln are introduced and described. The flights mentioned earlier, as a method to enhance heat transfer, are fully described in this chapter. The configuration of the heat source is described in this chapter. Other mechanical aspects of the rotary kiln such as the seals, bearings, feed and collection and construction material are addressed and described in Appendix B, where the process control is also briefly discussed.

### 6.1 Feedstocks

In this project, there are three different feedstocks. They have been selected because they are residues and the material sources are very different. These feedstocks can be utilised for pyrolysis to avoid its disposal or combustion. With disposal, the feedstock degrades with time, releasing the intrinsic carbon in the form of carbon dioxide and other greenhouse gases [1]. For each feedstock, there is a table where several samples are compared through proximate and ultimate analysis (Table 6.1 for RDF, Table 6.2 for wheat straw and Table 6.3 for woodchips).

The proximate analysis measures the moisture, ash content, volatile matter and fixed carbon of the sample. The moisture content is the amount of water in biomass, and it is important in storage, processing and in defining the resultant products. The moisture content is divided into external and inherent. The inherent moisture content is found within the cell walls, whereas the external is the amount above the equilibrium moisture content. The external moisture content is easier to evaporate and is usually removed during storage, whereas the inherent requires a high energy input [2].

Ash content refers to the fraction of residue when the biomass is combusted. In biomass, it generally accounts for the amount of inorganics in the sample, because the primary components are oxides of silica, aluminium, iron, calcium, magnesium, titanium, sodium and potassium [2]. The ash content is a critical parameter because some inorganics like potassium are demonstrated to have a catalytic effect on the cracking of pyrolysis vapours [3, 4]. Ash affects combustion of the biomass or char, where the ash content remains after pyrolysis, because it can produce deposits in the boiler, and can lead to efficiency and deposit problems.

The volatile matter accounts for the condensable vapours and permanent gases when biomass is heated. For a standard calculation of volatile matter, the biomass sample should be heated to a standard temperature at a standard rate. The last part is the fixed carbon, which refers to the solid combustible residue after biomass is heated and volatile matter expelled. It is usually a value calculated by difference, where the moisture, ash content and volatile matter are subtracted to a fraction of biomass represented by the unit [2].

The ultimate analysis shows the content of carbon, hydrogen, nitrogen, sulphur and oxygen. For a better comparison, these results are usually represented on a dry basis or dry ash-free basis. To obtain the elemental composition, the analysis is conducted in elemental analysers which analyses the combustion products of a biomass sample. The oxygen is usually calculated by difference, and other inorganics can be analysed for a more accurate result. Besides this elemental analysis, the ultimate analysis accounts for the High Heating Value (HHV) of the biomass, as a measurement of the energy content. The HHV is the amount of heat available in the biomass, including the heat to evaporate the moisture content and the latent heat of reaction products [2].

#### 6.1.1.1 RDF

RDF stands for Refused Derived Fuel, and the origin is municipal solid waste (MSW), from which the non-combustible substances such as glass or ferrous and non-ferrous metals are removed

[5]. The remaining components of RDF are biodegradable material and plastics. The biodegradable material includes textiles, paper and board, food remnants or other lignocellulosic residues [6, 7].

Worldwide, the production of MSW is approximately 900 million tonnes. The typical disposal of MSW was landfilling or combustion to obtain energy [6]. However, the shortage of available space for landfilling and the environmental pressures to fight climate change are decreasing the acceptance of these uses and pushing to look for new solutions [8-10].

RDF is usually produced with a more uniform particle size distribution and a higher energy density compared to the original MSW. As an example of the composition of RDF, Cozzani et al. [11] analysed RDF, and it was composed mainly by paper and board (65-70 wt.%), with a smaller amount of plastic films (14-16 wt.%) and other materials like textiles (8-12 wt.%). There was also wood and rubber (4-6 wt.%) and non-ferrous metals (0.5-1.5 wt.%) and rigid plastic (1.5-2.5wt.%). The final weight of RDF compared to MSW is 20-40 wt.% (dry basis). Despite all the treatment, RDF is cheaper than conventional fossil fuels, although the heating value is roughly half [5, 7].

Table 6.1 shows the analyses of four samples of RDF from literature. The letters A, B, C and D represent a study from literature. The values are very different because the properties and composition of the waste highly depend on the location of the waste, and on the time the MSW is collected [5, 7]. This table divides the analyses into proximate analysis and ultimate analysis. [2]. The feedstock is supplied by the Dutch company N+P Recycling, with an average diameter of 0.8 cm and maximum length of 5 cm.

Table 6.1: Proximate and ultimate analysis of four samples of RDF feedstock

|   | A [12] | B [13] | C [14] | D [15] |
|---|--------|--------|--------|--------|
| <b>Proximate analysis (wt.%)</b>            |        |        |        |        |
| <b>Volatile matter<sup>1</sup></b>          | 76.9   | 80.4   | 84.7   | 96.6   |
| <b>Fixed carbon<sup>1</sup></b>             | 23.1   | 19.6   | 15.28  | 3.4    |
| <b>Moisture content</b>                     | 0.0    | 4.1    | 7.1    | 2.6    |
| <b>Ash content<sup>2</sup></b>              | 11.4   | 15.5   | 15.6   | 14.8   |
| <b>Ultimate analysis (wt.%)<sup>2</sup></b> |        |        |        |        |
| <b>Carbon</b>                               | 40.8   | 58.5   | 58.0   | 44.0   |
| <b>Hydrogen</b>                             | 6.7    | 21.5   | 7.3    | 6.8    |
| <b>Oxygen</b>                               | 38.9   | 19.5   | 32.8   | 31.1   |
| <b>Nitrogen</b>                             | 0.9    | 0.5    | 1.2    | 1      |
| <b>Sulphur</b>                              | 0.6    | 0.1    | 0.7    | 0.1    |
| <b>Chlorine</b>                             | 0.7    |        |        |        |
| <b>HHV (MJ/kg)</b>                          | 16.4   | 29.0   | 17.7   | 26.9   |

**1: dry ash-free basis**

**2: dry basis**

#### 6.1.1.2 Wheat Straw

This feedstock is the residue of wheat harvesting, a very common cereal worldwide whose consumption in 2019 was 743 million metric tonnes [16]. It is used for feed for animals [17], but it can be part of construction material when mixed with other substances like plastics [18]. It is recognised as a suitable feedstock for renewable energy due to its low cost and high abundance [19]. Overall, the typical composition consists of cellulose is 31.1-44.5 wt.%, for hemicellulose 21.2-21.3 wt.% and lignin 13.2-23.4 wt.% [20, 21]. Table 6.2 shows the proximate and ultimate analysis on five samples of wheat straw, collected from the literature in the studies E, F, G, H and I. This feedstock was provided by an

agricultural company in Belgium through Ghent University, one of the partners of the GreenCarbon project, of which this research is part. The wheat straw is supplied in pellets, with diameters 0.5-0.8 cm and length up to 1.6 cm.

Table 6.2: Proximate and ultimate analysis of five samples of wheat straw feedstock

|   | E [22] | F [19] | G [23] | H [24] | I [25] |
|---|--------|--------|--------|--------|--------|
| <b>Proximate analysis (wt.%)</b>            |        |        |        |        |        |
| Volatile matter <sup>1</sup>                | 81.3   | 84.0   | 79.5   | 83.9   | 80.2   |
| Fixed carbon <sup>1</sup>                   | 18.7   | 16.0   | 20.5   | 16.1   | 19.8   |
| Moisture content                            | 7.2    | 4.6    | 8.7    | 4.1    | 8.2    |
| Ash content <sup>2</sup>                    | 10.3   | 4.9    | 8.4    | 6.6    | 10.3   |
| <b>Ultimate analysis (wt.%)<sup>2</sup></b> |        |        |        |        |        |
| Carbon                                      | 43.6   | 47.2   | 39.1   | 41.4   | 38.2   |
| Hydrogen                                    | 5.9    | 6.0    | 5.3    | 5.6    | 5.2    |
| Oxygen                                      | 39.4   | 46.1   | 53.1   | 53.1   | 39.5   |
| Nitrogen                                    | 0.7    | 0.7    | 0.5    | 0.0    | 0.3    |
| HHV (MJ/kg)                                 | 16.0   | 18.7   | 15.3   | 12.5   | 15     |

**1: dry ash-free basis**

**2: dry basis**

#### 6.1.1.3 Woodchips

Wood is a promising feedstock due to availability and renewability. It is a porous material with structural fibres and characteristic brown colour. Wood is the main component of the stems of trees and other plants. The exploitation of wood should be carefully studied because the trees convert through photosynthesis the carbon dioxide from the atmosphere into oxygen to fight climate change. There are mainly two types of wood, hardwood and softwood. The hardwood is a more durable material with a hard structure composed mainly by cellulose, whereas softwood is softer and more workable without a predominant component [20, 26]. These differences are shown in Table 6.3.

Table 6.3: typical composition for hardwood and softwood [20, 26]

|                      | Softwood | Hardwood |
|----------------------|----------|----------|
| Cellulose (wt.%)     | 47.6     | 45.2     |
| Hemicellulose (wt.%) | 24.4     | 31.3     |
| Lignin (wt.%)        | 28.0     | 21.0     |

Table 6.4 gives an overview of the proximate and ultimate analysis of woodchips, collected from the literature in studies J, K, L, M, and N. The empty cells represent values which were not measured. This feedstock was also obtained from a Belgium company through Ghent University. It is made from residues of different types of wood, although the composition is not specified.

Table 6.4: Proximate and ultimate analysis of five samples of woodchips feedstock

|   | J [27] | K [28] | L [29] | M [30] | N [31] |
|---|--------|--------|--------|--------|--------|
| <b>Proximate analysis (wt.%)</b>            |        |        |        |        |        |
| Volatile matter <sup>1</sup>                | 84.76  | 73.66  | 87.14  | 86.45  | 86.56  |
| Fixed carbon <sup>1</sup>                   | 15.24  | 26.34  | 12.86  | 13.55  | 13.44  |
| Moisture content                            | 0.00   | 0.00   | 9.60   | 3.07   | 0.00   |
| Ash content <sup>2</sup>                    | 2.20   | 5.93   | 4.09   | 3.49   | 0.20   |
| <b>Ultimate analysis (wt.%)<sup>2</sup></b> |        |        |        |        |        |
| Carbon                                      | 49.80  | 48.23  | 45.50  | 46.09  | 50.10  |
| Hydrogen                                    | 6.30   | 6.09   | 6.26   | 6.62   | 6.36   |
| Oxygen                                      | 43.90  | 39.75  | 47.20  | 47.19  | 43.52  |
| Nitrogen                                    |        |        | 1.04   | 0.10   | 0.07   |
| Sulphur                                     |        |        |        |        | <0.05  |
| HHV (MJ/kg)                                 | 17.9   | 19.8   | 15.9   | 18.4   | 20.5   |

### 6.1.2 Repose Angle

Different feedstock properties are required for the calculation of the different aspects of the reactor (Chapters 3, 4 and 5). Some of them, such as the kinetic parameters are calculated from experiments to achieve more accurate results (Chapter 5). Others like the density, calorific value or the thermal conductivity are acquired from literature through an average of the existing values, which are relatively common [11, 25, 32-35]. Other characteristics are less common in literature and may vary along significantly. In this research, the repose angle is a critical parameter for the calculation of the contact areas in Chapter 3, which has a significant impact in Chapter 4. There were no apparent results in the literature for this parameter due to its specific application.

The repose angle is defined as the maximum angle at which a particle of the material can remain without slumping [2]. ASTM standard C144 [36] is used to calculate the repose angle. The method consists of pouring biomass through a funnel, and the biomass particles build a cone naturally. The pouring stops when the particles reach a specific value of the height of diameter of the cone. The diameter of the cone established in this work was 11.5 centimetres. This value was selected because the pouring of biomass was done over the lid of a box to have a reference. The repose angle ( $\phi$ ) is calculated with Equation 6.1 using the height and radius of the cone created by the pile of biomass created when poured through the funnel [2].

$$\phi = \tan^{-1} \left( \frac{\text{Height}}{\text{Radius}} \right)$$

Equation 6.1: repose angle



Figure 6.1: Repose angle experiments for wheat straw

For each feedstock, five experiments were completed (see Figure 6.1). The results of each experiment and the final results are in Table 6.5. These calculated values for the repose angles are used within the model. The cone formed by the pile of solids is influenced by the flowability of the material. Some aspects, such as particle size or moisture content, would influence this flowability [37]. The angles are considered as independent of these two parameters in this study, and potential improvement of this work would correlate these characteristics with the repose angle of the feedstock.

Table 6.5: results of repose angle experiments

|             | 1     | 2     | 3     | 4     | 5     | Average [°]  | Standard deviation [%] |
|-------------|-------|-------|-------|-------|-------|--------------|------------------------|
| RDF         | 43.73 | 41.01 | 41.01 | 41.01 | 43.73 | <b>42.10</b> | 3.16                   |
| Wheat straw | 38.05 | 41.01 | 41.01 | 38.05 | 38.05 | <b>39.23</b> | 3.70                   |
| Woodchips   | 48.50 | 48.50 | 46.33 | 48.81 | 45    | <b>47.43</b> | 3.17                   |

\* All values for the repose angle are expressed in degrees [°] in this table

These repose angles are calculated for the feedstocks within this study. Theoretically, the angle should be the same as long as the feedstocks remain constant and the size of the funnel or the diameter of the pile of biomass should not affect the final result. The amount of biomass or funnel size would change the radius and height of the pile of solids, but the final result would not differ much from the one initially obtained. However, these results would change if any property of the biomass is altered. For instance, the moisture content or particle size could heavily influence the angle of repose [37]. The description of the angle of repose is very rare in literature and the results are very scarce, which would also imply having the same characteristics in terms of moisture content and particle size to make the results comparable.

## 6.2 Flights design and effect

The heat transfer is a critical aspect of pyrolysis and the rotary kilns. Overall, the heat transfer rate can be improved, enhancing some properties such as conductivity of materials, convective heat transfer or emissivity. Additionally, increasing the contact area would also increase the heat transfer rate [38]. One option is to attach extended surfaces, known as fins, flights, dams or bed disturbers, depending on the source [39, 40]. These surfaces are attached by extruding, welding or wrapping. The heat transfer is enhanced by increasing the conductive, convective and radiative area. Despite its

apparent novelty, this mechanism was already used 150 million years ago, during the Jurassic era. The stegosaurus counted on two rows of big bony plates, through which blood flowed. The main aim of these plates was not to protect from predators but cooling down the blood and removing heat. A more modern example would be the flights on an engine block to dispel the heat to the environment, looking carefully, the flights can be observed on motorbikes where the engine is more visible than cars [38].

In the case of rotary kilns, the implementation of flights has an additional advantage. When the feedstock is placed inside the reactor, it reaches the lower part of the kiln, a very hot surface like the wall is put in contact with the raw material at ambient temperature. When heat is transferred to the solid, the construction material cools down and contracts until the material moves ahead. When the cooled fraction of the wall is heated again, it expands again. The continuous exposure of the kiln to cycles of expansion and contraction (thermal stress) shortens the lifetime of the kiln. The addition of flights provides another surface for the solids to obtain heat when it first enters the kiln. Consequently, besides enhancement in the contact areas and the heat transferred, they reduce thermal stress and increase the lifetime of the kiln [41].

### 6.2.1 Types of flights

The architecture and configuration of the flights affect its performance, and there is a wide range of shapes due to the wide range of applications. Flights can be used in any situation where heat exchange is required. For flight design, the only limitation is the imagination of the designer of the equipment [38]. Consequently, all types of flights cannot be described within this work, so it will focus on the most common types for rotary kilns and rotary dryers.

Heat transfer is enhanced due to an increase in the contact area, mostly between the wall and the bed of solids. In the case of rotary kilns, the flights lift the biomass and release it gradually, increasing the gas-solid contact area [42]. Ideally, the solids on the flight should fall gradually as the angular position of the flight increases. Besides the angular position, the falling rate of solids is affected by the holdup (amount of solids on the flights), the repose angle of the feedstock and the shape of the flight [43]. The shape is critical to define the discharging pattern, which is the motivation for the study conducted by Savalagi and Chittappa (2017) [43] where six different types of flights and performance were analysed.

The question would be how to analyse and define a flight. The most common practice is to define the number of segments, the length of each and the angle formed between [44]. Figure 6.2 shows a four-segment flight with the lengths and angles. It is attached to the grey surface, which represents the wall of the reactor. The segments can be added or removed to obtain different configurations, such as the ones from [43] represented in Table 6.6.

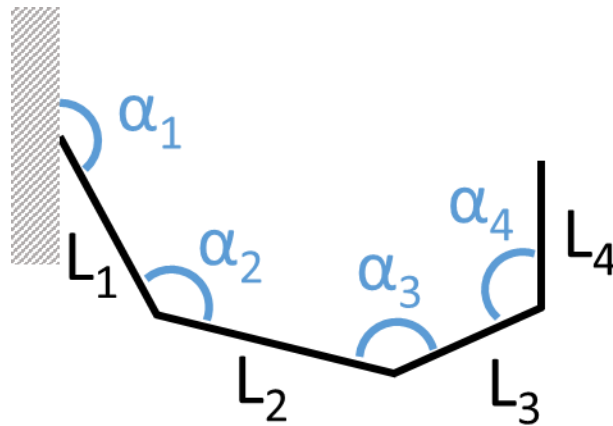


Figure 6.2: Scheme of the flight

Table 6.6: Examples of configurations of flights

| Flights configurations adapted from [43] |          |          |          |          |
|--|----------|----------|----------|----------|
| Flight 1                                 | Flight 2 | Flight 3 | Flight 4 | Flight 5 |
|  |          |          |          |          |

### 6.2.2 Design of a flight

Ideally, the flight should discharge the bed of solids as gradual as possible, to create a continuous curtain of solids showering over the bed, in order to increase the surface area of the solid in the kiln, increasing the contact surface for conduction and convection with the gas, and for radiation with the wall [43].

The parameters from the flight used to calculate the extra surface area caused by the flights are represented in Figure 6.3, adapted from [42]. According to the method to describe flights, a three-segment flight is represented. Each of the symbols is explained within this section and the mathematical explanation.

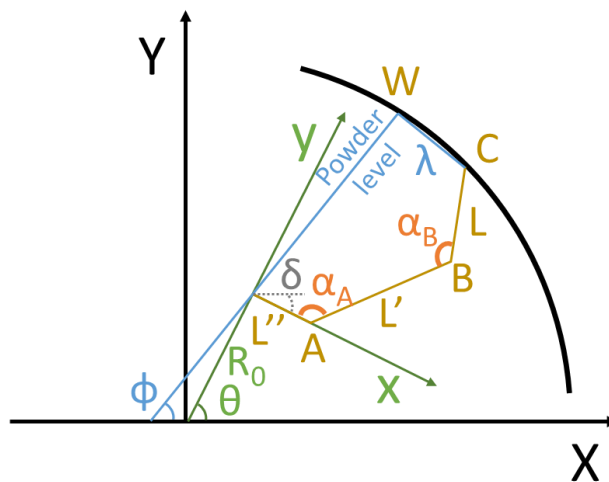


Figure 6.3: Calculation of the volume of feedstock in the flight

The falling solid rate varies with the angular position of the flight ( $\theta$ ), which changes the flight's holdup, defined as the amount of solids held on it. The angular position is established as 0 when the flights are charging with solids, so it is in the middle of the bed of solids, where its height is maximum [42]. The research by Schofield and Glikin (1962) [45] reported the Equation 6.2 linking the dynamic angle of repose ( $\phi$ ) to the dynamic coefficient of friction of the biomass ( $\mu$ ), the angular position, the position of the tip of the flight ( $R_0$ ) and the rotational speed ( $\omega$ ).

$$\tan \phi = \frac{\mu [-] + R_0[m] \cdot \frac{\omega^2 \left[ \frac{(\text{rad/s})^2}{\text{m}^2/\text{s}} \right]}{g} \cdot (\cos \theta - \mu \cdot \sin \theta)[-]}{1 - R_0[m] \cdot \frac{\omega^2 \left[ \frac{(\text{rad/s})^2}{\text{m}^2/\text{s}} \right]}{g} \cdot (\sin \theta - \mu \cdot \cos \theta)[-]}$$

Equation 6.2: Dynamic angle of repose definition

If the dynamic angle of repose of the feedstock has been previously measured or calculated, this formula can be used to obtain the parameter  $R_0$ .

$$\begin{aligned} \tan \phi - \tan \phi \cdot R_0 \cdot \frac{\omega^2}{g} \cdot (\sin \theta - \mu \cdot \cos \theta) &= \mu + R_0 \cdot \frac{\omega^2}{g} \cdot (\cos \theta - \mu \cdot \sin \theta) \\ \tan \phi - \mu &= R_0 \cdot \left[ \frac{\omega^2}{g} \cdot (\cos \theta - \mu \cdot \sin \theta) + \tan \phi \cdot \frac{\omega^2}{g} \cdot (\sin \theta - \mu \cdot \cos \theta) \right] \\ R_0 &= \frac{\tan \phi - \mu}{\frac{\omega^2}{g} \cdot [(\cos \theta - \mu \cdot \sin \theta) + \tan \phi \cdot (\sin \theta - \mu \cdot \cos \theta)]} \end{aligned}$$

The method to calculate the solid contacting inside the kiln is explained in Appendix A, which contains the method from Revol et al. (2001) [42].

### 6.2.3 Analysis

The main aim of the addition of the flights is to increase the contact surface between the solid and the gas inside the reactor. In order to study the effect of each parameter on that surface, a sensitivity analysis was conducted with the parameters previously addressed. There are different parameters which affect the cross-sectional area occupied by the solids, such as the changing falling rate and surface available for the heat transfer. The parameters to be changed are the length ( $L$ ,  $L'$  and  $L''$ ) and angles ( $\alpha_A$  and  $\alpha_B$ ) of the flight. Also, the radius ( $R$ ), angular position ( $\theta$ ), angular velocity ( $\omega$ ), dynamic coefficient of friction ( $\mu$ ) and dynamic angle of repose ( $\phi$ ) also affect the surface occupied by the solid.

The standard parameter values for the sensitivity analysis were those which appear in Table 6.7. These values were estimated for the design of an industrial rotary kiln with a capacity of 3 dry tonnes per hour capacity. During this analysis, one of the main missing points arose.

Table 6.7: Standard values for the sensitivity analysis for the design of the flights

| L [m] | $\alpha_B$ [°] | L' [m] | $\alpha_A$ [°] | L'' [m] | $\phi$ [°] | $\mu$ [-] | $\omega$ [rpm] | $\theta$ [°] | R[m] |
|-------|----------------|--------|----------------|---------|------------|-----------|----------------|--------------|------|
| 0.1   | 120            | 0.4    | 120            | 0.4     | 28.94      | 0.55      | 2              | 26.00        | 1.25 |



The range of values studied was varied as much as possible. However, it was observed that some results were not calculated due to an error in the calculations, such as finding a square root of a negative number. This happens because there are calculations of two second-degree equations, and there might not be an existing solution for some values.

To track the problem, the influence of the parameters on the angle which correlates both sets of coordinates is studied, to see whether the problem with the second-degree equation persists. The standard values are shown in Table 6.8.

*Table 6.8: Standard values for the study of the angle between coordinates*

| R [m] | $R_0$ [m] | $X_c$ [m] | $Y_c$ [m] | $\sigma$ [°] |
|-------|-----------|-----------|-----------|--------------|
| 1.2   | 0.6       | 0.6       | 0.6       | 20           |

The main output of this analysis is the strong influence of radius ( $R$  and  $R_0$ ) on the convergence of the solutions for the second-degree equation. When the radius ( $R$ ) is increased to 1.5, the solution does not converge, and the same happens when the flight radius ( $R_0$ ) is decreased to 0.25 or below.

The analysis of  $R_0$  was completed, and the variability was very high. For instance, it decreased from 2500 to 39 m when the rotational speed increased from 0.25 to 2; or from 101 to 842 m when the angular position increased to 45 °. Figure 6.4 shows the analysis for  $R_0$ , with the radius of the flight on the Y-axis. The percentage of the maximum value for each variable (written in the legend in square brackets) is shown on the X-axis. For instance, the radius at 1 rpm would be where the grey line crosses 50%, which is around 130 m (it is indicated that the maximum for rotational speed is 2 rpm).

Analysing this data, there is much variability in  $R_0$ , and the data is often not valid, such as having a negative radius. Flight radii values larger than kiln diameter are not possible.

### Sensitivity analysis of $R_0$ (position of the tip of the flight) [m]

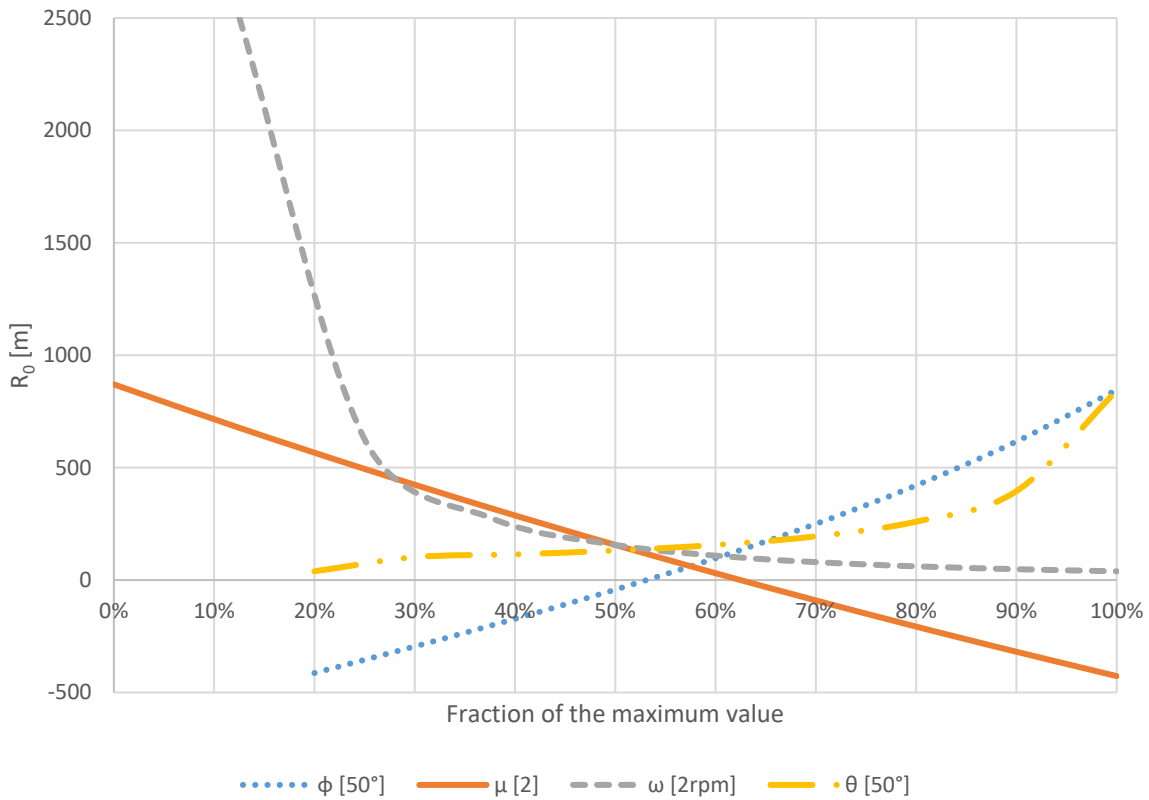


Figure 6.4: Sensitivity analysis of  $R_0$

The main problem for the calculation of the cross-sectional area with the flights is the inability to control the parameter  $R_0$ , which varies greatly according to Figure 6.4. To conduct a sensitivity analysis on the flights, the parameters were amended to achieve a value of 0.8 m, which agrees with the radius of the kiln.

Table 6.9: Standard values for the radius of the flights

| $\phi$ [°] | $\mu$ [-] | $\omega$ [rpm] | $\theta$ [°] |
|------------|-----------|----------------|--------------|
| 29         | 0.55      | 2              | 5            |

After analysis of the parameters affecting flight radius, the sensitivity analysis is conducted. This analysis might appear to be unreliable because the standard values utilised are conditioned by the other sensitivity analysis to make the values converge. However, since it is to study which parameters affect more the final result, the initial values do not have much importance. Figure 6.5 shows the sensitivity analysis results for the parameters affecting the solid surface in the cross-sectional area. The legend defines the X-axis label; next to the name of each parameter in square brackets. The maximum value of the variable is found, and the X-axis value is the percentage of that maximum value.

## Sensitivity analysis of surface of showering solids

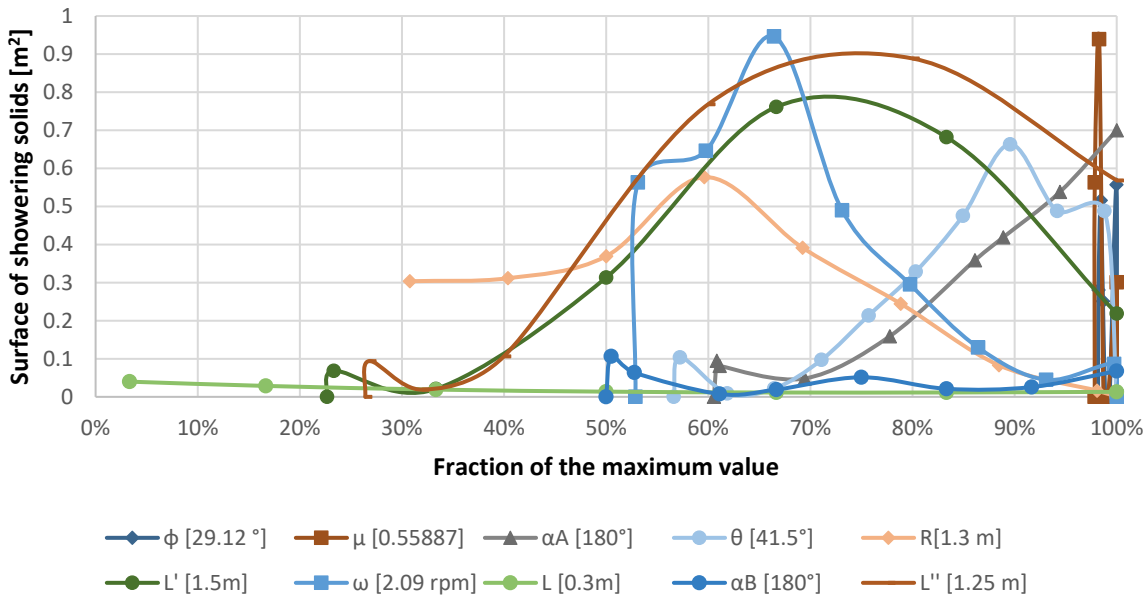


Figure 6.5: Sensitivity analysis for the design of the flights

The maximum values were set for a variety of reasons and depend on the parameter. In the cases of the angles ( $\alpha_A$  and  $\alpha_B$ ) and the lengths of the segments of the flight ( $L$ ,  $L'$  and  $L''$ ), a broader angle than  $180^\circ$  would make more solids fall. Something similar applies to the length of the segments of the flights which are limited by the radius of the rotary kiln (1.25 m as standard value).

For some parameters, the definition is more difficult as the limits of variation are established by a convergence of results, which does not happen in all cases. For instance, the range of angular position studied is very narrow [ $23.5^\circ$ - $41.5^\circ$ ] and for none of the limits does it converge. The difficulties in the design of the flights make the kiln design a challenging task.

This method [42] was chosen due to its “simplicity” and popularity because it is the basis for many other studies [43, 44, 46, 47]. However, there is another disadvantage for this model as well as its difficulty to converge. When a rotary kiln is designed, the solid feeding rate is a key parameter and is crucial to determine other parameters such as length, radius and, consequently the height of the bed of solids (See Chapter 3). None of these appeared in the equations to consider the cross-sectional area occupied by the solids, a key output of this design. At least, the feed rate or the height of the bed (which are interconnected) should appear in the analysis included to determine flights holdup because the flight would not fill in the same way when the filling varies.

### 6.2.4 Influence on the other models

The modelling and optimisation of flights could not be fully realised because equations did not converge. To solve the issue, a generic flight was established, and it was assumed that each flight increased the contact area between the wall and the two components by 10%. To calculate the extra contact surface area, 10% is multiplied by the number of flights and by the filling degree, as shown in the following equations (Equation 6.3 and Equation 6.4). The extra surface between the wall and the gas is calculated in the same way, using 1 minus the filling degree.

*Assumption 21: The temperature of the flight is the same as the wall of the kiln*

$$Flight\ Surface_{Wall \rightarrow Solid} = 10\% \times N_{Flights} \times f \quad Flight\ Surface_{Wall \rightarrow Gas} = 10\% \times N_{Flights} \times (1 - f)$$

Equation 6.3: Surface of the flight wall-solid

Equation 6.4: Surface of the flight wall-gas

It will be assumed that the addition of flights does not affect the bed of solids submodel, which means the residence time and the length of the reactor does not depend on those flights and remains invariable.

*Assumption 22: The length of the bed of solids and the solids residence time are not affected by the flights*

This influence greatly differs from the effect on the heat transfer submodel. The increase of contact surface between the wall and the inside of the reactor enhances the heat transfer. For each slice of the model (Sections 4.5 and 7.3.2), flights increase the contact areas and enhance convection and conduction between the wall and solids, and between the wall and the gases. It is assumed that this extra surface does not affect the calculation of the radiative heat flow. The addition of the flights to the calculation of radiant surface would affect the shape factor, whose calculation is estimated due to the calculation complexity for a three-component system (See Section 4.4.1).

*Assumption 23: The addition of the flights enhances the conductive and convective heat transfer, but it does not affect the radiative heat transfer*

In contrast to the method employed by Revol [42], flights are not considered to increase the area between the gas and the solid by the solids falling rate. This change for a variety of reasons. Firstly, most of the studies and models are designed for rotary driers [42-44, 46, 47] instead of pyrolysis kilns. This aspect has a significant impact because the heating is mostly done by direct contact with the gases inside the reactor. This means that the contact area bed of solids-gases inside the reactor does not gain as much importance as it does when it comes to dryers. It is closely connected to the second reason, which explains the negligibility of the contact area solids-gases. The solids falling that causes more contact area between gases and solids is not considered because the temperatures of the bed of solids and gases in the reactor are very similar and the heat flows due to this extra surface is not that significant (see Figure 7.7). The heat source to increase the temperature of the solids and gases comes mainly from the wall and combustion gases rather than the heat transferred between solids and the gases.

*Assumption 24: The contact area between the solids and gases inside the reactor when the solid is falling from the flights does not affect the heat flows significantly*

### 6.3 Heating method

To achieve the target reaction temperature within the bed of solids, a heat source is needed. Depending on how heat is transferred from the heat source, the processes are divided into direct and indirect heating. The direct heating kilns have overall higher efficiency, although indirect heating might be a better solution. Direct heating kilns burn the organic fraction of the material being processed, whereas further polishing of them is done if an indirect kiln is used.

The *direct heating* consists of direct contact between the heat source and the feedstock. This type of heating is the most common choice for thermal processing due to higher efficiency. The gas produced is a valuable product, and the heat source is a gas, further gas treatment is required. The gases might drag some particles, and the correlation of gas velocity and density with particle density and shape has to be studied to calculate permissible gas velocities. It is mostly used for proppants, minerals, limestone, cement, iron ores and special ceramics and clays. A crucial characteristic of this

study is the inadequacy of this method when the raw material has to be processed in an inert atmosphere [39].

*Indirect heating* is used to process materials in an inert environment, and the material does not contact the process gas. The heating of the material takes place via contact with the hot kiln shell, which is heated from the outside. The efficiency is in general lower than direct heating, although it is crucial if the process requires an inert environment. Not only is it applicable to processes where oxygen is not allowed but with materials which may form an undesirable compound with nitrogen at high temperatures. The indirect heating can provide the needed inert environment for this type of processes. Another advantage is the control of the kiln wall temperature. This heating does not deal with minimum gas production to avoid the drag of particles. The most common applications for indirect heating reactors are carbon black, chemical precipitates, filter cakes and finely ground solids. The high temperatures used in the wall lead to the kilns constructed with resistant alloys, instead of carbon steel [39].

*Assumption 25: As the pyrolysis process needs an inert environment, indirect heating is the option considered.*

### 6.3.1 Configuration

The configuration refers to the direction of the gas compared to the bed of solids within the rotary kiln. The gas refers to the fraction providing heat to the bed of solids to increase the temperature and achieve the pyrolysis temperature. It can either refer to the gases inside the reactor or on the external shell. The gases inside the reactor would account for the condensable and non-condensable fraction of the vapours produced in pyrolysis plus a carrier inert gas (such as nitrogen). These gases account for the condensable and non-condensable fractions. To choose the flow configuration, the material's properties and the overall process requirements are taken into account. Each configuration has its advantages which have to be taken into account within the decision. There are three different configurations, co-current, counter-current and cross-flow. Cross-flow is unique because it is exclusive for the gases in the outer shell and the gases within the kiln are excluded here, whereas the others can be applied for gases inside and outside the kiln [39].

#### 6.3.1.1 Co-current

The co-current configuration is also called parallel. The gas flow has the same direction as the material. It means that the first contact of the coldest material is the hottest gas, which sharply increases the temperature of the material. A profile temperature for the bed of solids and heating gases is represented in Figure 6.6 (adapted from [39]).

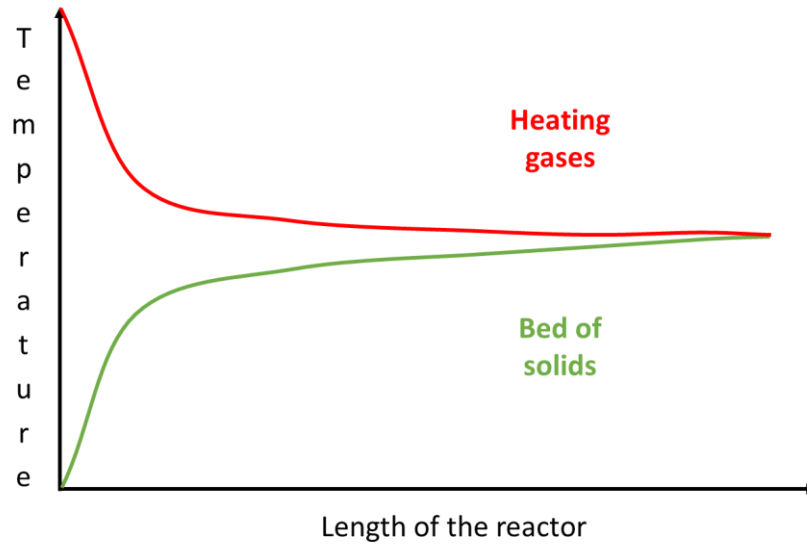


Figure 6.6: Schematic representation of the temperature profile of a co-current reactor

It is more commonly used when the temperature of the material has not to be gradual. This type of configuration is usually found in organic combustion processes due to the lack of a specific end product. Since there is a big temperature change at the beginning, there is very early vaporisation and volatile release [39].

#### 6.3.1.2 Counter-current

Within a counter-current configuration, the gas moves in the opposite direction of the bed of solids. The temperature variation is more gradual than co-current as it is represented in Figure 6.7 where the heating gases are the ones in the outer shell. The coldest material is in contact with the coldest heat source and vice versa. Overall, the counter-current configuration is more efficient in terms of heat transfer. When the kiln is directly heated, the burner is mounted at the end of the thermal processing cycle, and less heat is required, which leads to a lower fuel consumption [39].

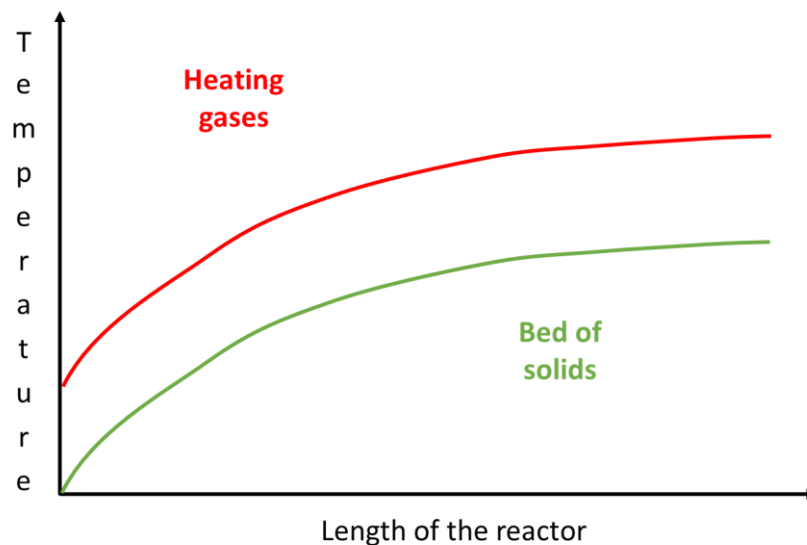


Figure 6.7: Schematic representation of the temperature profile of a counter-current reactor

The initial temperature of the gases is much lower than required in co-current configuration. Furthermore, the temperature of the material and the gas are directly correlated and, overall, the gas

temperature and operating costs are lower. This configuration is a good alternative if a physical or chemical change exists on the material, and the temperature needs a gradual increase to achieve it. For instance, it is the typical configuration in sintering to maintain the phase change under control [39].

#### 6.3.1.3 *Cross-flow*

As it is mentioned previously, the cross-flow heating configuration is applied to the gas in the outer shell. The gas and solid flows are perpendicular to each other. The temperature at which the gases are directed to the kiln is constant. The solids can have constant temperature for an extended time, a feature challenging in other configurations [39].

This configuration allows the processing of material with different heating zones. If the gases are fired in different zones of the reactor, and the gas temperatures are different, the reactor can be divided into zones where the solid temperature could be correlated with the gases, depending on the zone.

### 6.3.2 Heat source

The configuration of the heating is an essential piece of information for the operation of the reactor. Nevertheless, a heating source is needed to make the reactor increase the temperature and conduct pyrolysis. For a pyrolysis reactor, the indirect heating is more promising because the heating gases can be any gases from external pieces of equipment. If the gases used as a heating source were placed inside the reactor, the process would require a further separation of the pyrolysis gases and the heating source [41, 48].

Once the indirect heating is designed and, as explained in Section 7.3.2.1.3, in co-current configuration respect the bed of solids with a flow of combustion gases, the heat source of the combustion gases has to be defined. The combustion gases are the products of the combustion of raw material with air as an oxidising agent to produce mainly carbon dioxide and steam. If the fuel has some impurities, other components may appear such as  $\text{NO}_x$  and  $\text{SO}_x$  [38].

The source of fuel is very variable, and each process has its own choice and customisation for it. Ideally, one of the products should be the fuel for combustion to avoid further consumption of raw materials. Overall, it is the permanent gas the fuel in combustion, although it is subjected to the specific process. For instance, if the permanent gas is the target product like in [49], the fuel for combustion should be different. The fuel can be either the condensable fraction of gases or the char if the gases are the target product. In case that the three products are of interest for further use, the primary raw material (biomass) can become the fuel (besides the feedstock for the process) for combustion and provide energy to the process. If the feedstock is not readily available, then an auxiliary fuel is employed. This auxiliary fuel can be anything that can provide energy to the process [48]. It includes all types of renewable and non-renewable sources of energy, from RDF or MSW whose use is valorisation up to petrol or natural gas with a higher carbon footprint and impact on the environment. As an example, natural gas was burned to warm up the gases to dry the biomass in CENER (see on Section C.2).

#### 6.3.2.1 *Approach within this project*

One of the objectives of this research is to use biomass to reduce emissions of greenhouse gases and reduce climate change. Therefore, the primary fuel for combustion would be one of the products (char, pyrolysis oil or condensable fraction, or permanent gases) to avoid further consumption of raw materials. To consider this, it is important to calculate if the product can provide enough heat for pyrolysis. If all products are developed further, which would be the ideal case, the

fuel to be used should be the feedstock, to avoid further use of other materials and consume exclusively one type of biomass. There are cases where this biomass may be scarce, and there is only feedstock to feed the reactor. In those cases, any other type of biomass should be considered to be used to provide heat for pyrolysis. If none of the above is available, it could be considered to use a non-renewable feedstock such as petrol or natural gas to provide heat to the system although this method would be contrary to the research, which aims to reduce the use of non-renewable materials. The last option would be to use electrical furnaces to increase the temperature of the reactor. This choice may become very costly at an industrial scale. The origin of the electricity may be unknown and contribute to the greenhouse effect.

As a preliminary study to see the potential heat provided by one of the product, the gas was selected as the fuel. It was the selected product to be the fuel because the char is considered a more promising product due to the wide range of uses, and the focus of the GreenCarbon project.

The gas was estimated using the flow of gases at the end of the reactor according to the values given in Section 5.6. From the gases considered in this work (carbon dioxide, carbon monoxide, methane, hydrogen, nitrogen and steam), the carbon monoxide, methane and hydrogen can be used as an energy source to provide energy for pyrolysis, which transform into carbon dioxide and steam with the addition of oxygen. To calculate the energy obtained, the heat of reaction of each specific component is used. It is defined as the energy in heat form released when reactants are converted into products. The calculation is done through the difference of the formation enthalpy of reactants and products, as shown in Figure 6.5. When this heat of reaction applies to combustion, it is called the heat of combustion. It characterises because one of the reagents is oxygen (whose formation enthalpy is 0), and the products are carbon dioxide and steam plus other oxidised contaminants such as SO<sub>x</sub> or NO<sub>x</sub> as the most common examples. The superscript 0 indicates standard value because the value of reaction enthalpy varies with temperature (298.15 K of temperature and 1 atmosphere for pressure) [50].

$$\Delta H_{reaction}^0 = \sum \Delta H_{products}^0 - \sum \Delta H_{reactants}^0$$

Equation 6.5: heat of reaction

The reaction heat is measured in energy per unit mass. Since this measurement is connected to chemical reactions, it is very common to find kJ/mol as the measurement unit, although in this case, the kJ/kg is employed [51]. The potential heat provided by the combustion gases is calculated with Figure 6.6.

$$Heat [W] = \frac{1000}{1} \left[ \frac{W}{kW} \right] \cdot \sum_{i=0}^{CO, H_2, CH_4} \Delta H_{comb,i}^0 \left[ \frac{kJ}{kg} \right] \cdot \dot{m}_i \left[ \frac{kg}{s} \right]$$

Equation 6.6: Heat from the combustion of permanent gases

The heat provided by the gases in the reactor was compared with the potential heat of the permanent gases combustion for a preliminary study. The results (see Table 9.1) suggest that from all the heat obtained with the combustion of the permanent gases, the pyrolysis requires only 50-70% of that heat to be conducted. The remaining 30-50% heat could be used for other parts of the process, such as drying. This is a preliminary study, and there are some assumptions:

- The combustion is considered perfect with no losses
- All the energy can be used to increase the temperature of the solids, but the heat used to increase the temperature of combustion gases which do not oxidise is not calculated



- The design of the oxidiser is not considered in this research. Some aspects to consider in the design of the unit would be:
  - Using one unit to burn any type of fuel with lower efficiency or have a more specific oxidiser with higher efficiency for the selected feedstock.
  - The ash content of the material may be critical in the performance of the unit, melting and reducing the efficiency.

## 6.4 References

1. Basu, P., *Biomass gasification, pyrolysis, and torrefaction: practical design and theory*. 2013: London, UK : Elsevier : Academic Press, 2013. Second edition.
2. Cai, J., et al., *Review of physicochemical properties and analytical characterization of lignocellulosic biomass*. *Renewable and Sustainable Energy Reviews*, 2017. **76**: p. 309-322.
3. Bridgwater, T. and S. A. Bridge, *A Review of Biomass Pyrolysis and Pyrolysis Technologies*, in *Biomass Pyrolysis Liquids Upgrading and Utilization*, Springer, Editor. 1991, Springer: New York. p. 11-92.
4. Bridgwater, A.V., *Review of fast pyrolysis of biomass and product upgrading*. *Biomass and Bioenergy*, 2012. **38**(Supplement C): p. 68-94.
5. Ma, W., et al., *Chlorine characterization and thermal behavior in MSW and RDF*. *Journal of Hazardous Materials*, 2010. **178**(1): p. 489-498.
6. Lin, K.-S., et al., *Pyrolysis kinetics of refuse-derived fuel*. *Fuel Processing Technology*, 1999. **60**(2): p. 103-110.
7. Haykiri-Acma, H., G. Kurt, and S. Yaman, *Properties of Biochars Obtained from RDF by Carbonization: Influences of Devolatilization Severity*. *Waste and Biomass Valorization*, 2017. **8**(3): p. 539-547.
8. Chen, D., et al., *Pyrolysis technologies for municipal solid waste: a review*. *Waste Manag*, 2014. **34**(12): p. 2466-86.
9. Li, A.M., et al., *Experimental studies on municipal solid waste pyrolysis in a laboratory-scale rotary kiln*. *Energy*, 1999. **24**(3): p. 209-218.
10. He, M., et al., *Syngas production from pyrolysis of municipal solid waste (MSW) with dolomite as downstream catalysts*. *Journal of Analytical and Applied Pyrolysis*, 2010. **87**(2): p. 181-187.
11. Cozzani, V., et al., *A Fundamental Study on Conventional Pyrolysis of a Refuse-Derived Fuel*. *Industrial & Engineering Chemistry Research*, 1995. **34**(6): p. 2006-2020.
12. Cozzani, V., L. Petarca, and L. Tognotti, *Devolatilization and pyrolysis of refuse derived fuels: characterization and kinetic modelling by a thermogravimetric and calorimetric approach*. *Fuel*, 1995. **74**(6): p. 903-912.
13. Singh, S., C. Wu, and P.T. Williams, *Pyrolysis of waste materials using TGA-MS and TGA-FTIR as complementary characterisation techniques*. *Journal of Analytical and Applied Pyrolysis*, 2012. **94**: p. 99-107.
14. Çepelioğullar, Ö., H. Haykırı-Açma, and S. Yaman, *Kinetic modelling of RDF pyrolysis: Model-fitting and model-free approaches*. *Waste Management*, 2016. **48**: p. 275-284.
15. Tomasik, A., *Pyrolysis and Combustion Kinetics of Refuse Derived Fuel and Ash Characterization*. 2017, Instituto Superior Técnico.
16. Bryant-Erdmann, S. *Human Wheat Consumption Sets new Record*. 2018 [cited 2020 30th March 2020]; Available from: <https://www.uswheat.org/wheatletter/human-wheat-consumption-sets-new-record/>.
17. Klee G., G., *The wheat straw as an important component of the servings for steers*, in *IPA Quilamapu*. 1983, INIA.
18. Kirkbride-McElroy, A. *Adding Value to Wheat Straw*. [cited 2018 9th March 2018]; Available from: <http://biomassmagazine.com/articles/1367/adding-value-to-wheat-straw>.
19. Greenhalf, C., et al., *Thermochemical characterisation of straws and high yielding perennial grasses*. *Industrial Crops and Products*, 2012. **36**(1): p. 449-459.

20. Dhyani, V. and T. Bhaskar, *A comprehensive review on the pyrolysis of lignocellulosic biomass*. Renewable Energy, 2017.
21. Roßberg, C., *Lignocellulosic material and its role in biorefinery*, in *GreenCarbon Research School 1*, GreenCarbon, Editor. 2017, Fraunhofer Center for Chemical-Biotechnological Processes CBP: University of Ghent.
22. Chen, D., Y. Zheng, and X. Zhu, *In-depth investigation on the pyrolysis kinetics of raw biomass. Part I: Kinetic analysis for the drying and devolatilization stages*. Bioresource Technology, 2013. **131**: p. 40-46.
23. Gómez-Monedero, B., et al., *Pyrolysis of Red Eucalyptus, Camelina Straw, and Wheat Straw in an Ablative Reactor*. Energy & Fuels, 2015. **29**(3): p. 1766-1775.
24. Crombie, K., et al., *The effect of pyrolysis conditions on biochar stability as determined by three methods*. GCB Bioenergy, 2013. **5**(2): p. 122-131.
25. *ECN Phyllis classification*. Phyllis2 2018 [cited 2018 15th May 2018]; Available from: <https://phyllis.nl/Browse/Standard/ECN-Phyllis>.
26. Asmadi, M., H. Kawamoto, and S. Saka, *Characteristics of softwood and hardwood pyrolysis in an ampoule reactor*. Journal of Analytical and Applied Pyrolysis, 2017. **124**(Supplement C): p. 523-535.
27. Babler, M.U., et al., *Modelling and pilot plant runs of slow biomass pyrolysis in a rotary kiln*. Applied Energy, 2017. **207**: p. 123-133.
28. Gašparovič, L., Z. Koreňová, and Ľ. Jelemenský, *Kinetic study of wood chips decomposition by TGA*. Chemical Papers, 2010. **64**(2).
29. Slopiecka, K., P. Bartocci, and F. Fantozzi, *Thermogravimetric analysis and kinetic study of poplar wood pyrolysis*. Applied Energy, 2012. **97**: p. 491-497.
30. Varma, A.K. and P. Mondal, *Physicochemical characterization and pyrolysis kinetics of wood sawdust*. Energy Sources, Part A: Recovery, Utilization, and Environmental Effects, 2016. **38**(17): p. 2536-2544.
31. Tapasvi, D., et al., *Thermal Decomposition Kinetics of Woods with an Emphasis on Torrefaction*. Energy & Fuels, 2013. **27**(10): p. 6134-6145.
32. Gao, L., et al., *Possibility of Refuse Derived Fuel Fire Inception by Spontaneous Ignition*, in *AOFSST Symposium*. 2004, Fire Safety Science Digital Archive.
33. Dupont, C., et al., *Heat capacity measurements of various biomass types and pyrolysis residues*. Vol. 1. 2013.
34. Savage, G.M., *Thermal Conductivity and Specific Heat of Densified Refuse Derived Fuel*. Waste Management & Research, 1989. **7**(1): p. 83-92.
35. Mason, P.E., et al., *Comparative Study of the Thermal Conductivity of Solid Biomass Fuels*. Energy & Fuels, 2016. **30**(3): p. 2158-2163.
36. ASTM, *ASTM C144-18, Standard Specification for Aggregate of for Masonry Mortar*. 2018, ASTM International: West Conshohocken, PA.
37. McGee, E., *AJAX Equipment Ltd. Visit*, C. Day, et al., Editors. 2019: AJAX Equipment Ltd., Milton Works, Mule Street, Bolton, BL2 2AR, United Kingdom.
38. Çengel, Y.A., A.J. Ghajar, and M. Kanoglu, *Heat and mass transfer: fundamentals & applications*. 2015: New York, N.Y.: McGraw-Hill Education, ©2015. 5th ed. in SI units.
39. *The Rotary Kiln Handbook*. 2019: FEECO International.
40. Holman, J.P., *Heat transfer*. 10th ed., International ed. ed. McGraw-Hill series in mechanical engineering. 2010: McGraw-Hill.
41. Stein, P., *Rotary kiln design methodology*, J. López-Ordovás, Editor. 2019: EBRI, Aston University, Birmingham, United Kingdom.
42. Revol, D., C.L. Briens, and J.M. Chabagno, *The design of flights in rotary dryers*. Powder Technology, 2001. **121**(2): p. 230-238.
43. Savalagi, P. and H.C. Chittappa, *Flight Design for Rotary Bagasse Dryer*. International Research Journal of Engineering and Technology (IRJET), 2017. **4**(8): p. 6.

44. Benhsine, I., et al., *Influence of flight shape on discharging profiles of granular material in rotary dryer*. EPJ Web Conf., 2017. **140**: p. 03023.
45. Schofield, F.R. and P.G. Glikin, *Rotary driers and coolers for granular fertilizers*. Chemical Engineering Research and Design, 1962. **40a**: p. 183-190.
46. Sunkara, K.R., et al., *Modeling the discharge characteristics of rectangular flights in a flighted rotary drum*. Powder Technology, 2013. **234**: p. 107-116.
47. Lee, A. and M.E. Sheehan, *Development of a geometric flight unloading model for flighted rotary dryers*. Powder Technology, 2010. **198**(3): p. 395-403.
48. Bridgwater, A.V., *Aspects to consider in the design of a rotary kiln*, J. López-Ordovás, Editor. 2019, Aston University: Energy and Bioproducts Research Institute (EBRI).
49. *Stein's Pyrolysis Video 2013 (SPU Energy Fields)*. 2013, C Meier: Youtube.
50. Singh, N.B., S.S. Das, and A.K. Singh, *Physical chemistry. [electronic resource]*. 2009: New Age International.
51. *Heat of combustion*. Engineering ToolBox 2017 [cited 2020 2nd April 2020]; Available from: [https://www.engineeringtoolbox.com/standard-heat-of-combustion-energy-content-d\\_1987.html](https://www.engineeringtoolbox.com/standard-heat-of-combustion-energy-content-d_1987.html).

## 7 Model integration

### 7.1 Introduction

This chapter explains how the submodels were integrated into the final completed model. The background theory and methods have been described in the previous chapters. Figure 1.12 shows the different submodels and how they interact with each other.

The boxes in grey indicate that the value is taken from a database; there is no calculation or simulation involved. For instance, once the feedstock is selected, the model will automatically give the repose angle, density, calorific value and the thermal conductivity. Each of the values will then feed into a different submodel. The database may contain information produced from experiments or from other models such as kinetic parameters and the expressions to calculate product yields.

The blue boxes and lines denote the parameters the user can introduce as inputs or receive as outputs. The green boxes and lines represent the submodels where the simulations occur. All the parameters in the light green boxes are the outputs of the submodels. There is only one orange box that contains the values for some initial hypotheses and values for some parameters such as the radius, kiln angle, combustion gases flow and rotational speed. These parameters are recalculated along the simulation to optimise the design of the reactor. As it will be explained in 7.5.3, these initial values are not defined arbitrarily but are estimated from previous calculations. Finally, the yellow arrows indicate the flow of information, indicating where the data is produced and where it is used for further calculations.

Within the chapter, the terms model, spreadsheet and algorithm are commonly used to describe the integration of the submodels. They refer to where the equations, expressions and correlations are integrated, and they are defined as follows:

- **Model:** refers to the overall Excel file which contains all the information, formulas and coding.
- **Spreadsheet:** refers to the simple Excel spreadsheet, without coding. When a formula is implemented in the spreadsheet, it does not need any VBA code to run and work.
- **Algorithm:** describes the sections using VBA (Visual Basic Applications), the language code of Excel. When a piece of the work is implemented in the algorithm, it means that coding was required to develop and run it.

As an example to explain the usage of the terms; the heat transfer submodel is included in the **model**, which is then implemented in the **algorithm**. The inputs and results appear in the **spreadsheet**. All of this happens automatically within the overall Excel model file, based on the user inputs.

The inputs have been mentioned previously in Section 1.4. This chapter describes the consequence of each input and the effect on the model.

- **Capacity:** this input indicates the amount of biomass to be processed into the reactor in dry tonnes per hour. The user-defined capacity generates the first approximation for the radius of the reactor. The capacity is needed to calculate residence time, reactor length and the amount of carrier gas in the reactor.

- **Type of feedstock:** three feedstocks are being considered in this project: wheat straw, woodchips, and RDF. The choice of feedstock defines the repose angle and the density for the bed of solids model, which influences the length and the residence time. Also, the choice of feedstock defines the thermal conductivity, heat capacity ( $C_p$ ) and the heat of reaction, which depends on the variation of the conversion and simultaneously affects the heat transfer. For the kinetic model, the feedstock determines the number of reaction steps, and pre-exponential factor, activation energy and reaction order of each. Furthermore, the feedstock determines the equations that correlate the product yields and the reactor temperature. Finally, the feedstock influences the yield of each gas produced.
- **Moisture content:** this characteristic is crucial for calculating the heat demand of the reactor as the amount of heat required varies significantly with moisture content. The vaporisation enthalpy required to remove moisture from the feedstock is high compared with the heat required to increase the temperature of the material.
- **Feedstock shape:** as mentioned in Section 3.5.1, the shape affects the voidage of the bed of solids and, consequently, the contact areas between the solid, gases and the wall. There are two defined shapes, chips and pellets. According to literature, if the shape is defined as chips whose particle size is 15 mm the voidage fraction is 57% [1]; If the shape of the feedstock is pellets, it is associated with a length of 3 mm and a radius of 1.6 mm or 2 mm, the voidage fractions are 38% and 41%, respectively [2]. With this information, for uniform pellets whose length is 3 mm and radius is 2 mm is attributed to a voidage fraction of 40%. The particle size is one of the boundary conditions of the model, and the only two options are the ones defined previously (pellets and chips). The influence of a particle size defined by the user would require a much more detailed model and might not be feasible for this type of work, which requires a variable length, radius and capacity of the reactor, and many simulations of the rotary kiln. Within this work, the shape determines the particle size. All of this would translate into different solids flowability models and heat transfer limitations.
- **Carrier gas:** one of the parameters that can be customised in a rotary kiln is the carrier gas. Some companies prefer to use a carrier gas for the thermochemical decomposition in a rotary kiln [3, 4]. In contrast, in other examples, there is no carrier gas and the gases inside the reactors are the ones produced by the feedstock when it degrades [5, 6]. In this model, the user can decide whether the carrier gas is used and what quantity. If the user wants a carrier gas, the quantity is defined either by the model or by the user. The automatic amount of carrier gas is equivalent to one-third of the capacity of the system. The value of this fraction is not arbitrary, but the most common ratio used in industry [3, 4].

When the carrier gas is not required, the flow of nitrogen is one-thirtieth of the capacity. This fraction was established from a sensitivity analysis once the model had been designed, and it is the lowest limit. If the carrier gas flow is any lower, the model does not converge due to overflow of temperatures. A more detailed description of the overflow of temperatures is found on 7.3.2.1.4.

- **Final temperature or product selection:** the model allows the user to choose between a preferred product and the final temperature. This datum is needed to establish the final solids temperature of the reactor and adjust the flow of combustion gases. The model needs the final target temperature to adjust the combustion gases flow and, with the iterative process, achieve the final conversion. The input is evident when the user defines a final temperature. When a preferred product is selected, the model correlates the product to find an optimum temperature for its production. For the production of char, the temperature should be as low as possible but allowing completion of pyrolysis. For this project, this lower limit for pyrolysis was established as 400 °C (7.5.3) from the experimental work carried out for GreenCarbon by Aston University researcher Filipe Rego [7]. It was found that the maximum pyrolysis oil yield is at a temperature of 500 °C, which is similar to the data from literature [8, 9]. High temperature is needed for increased gas production, and the maximum established in this work is 700 °C. This temperature is estimated, as the maximum in agreement with the literature [8, 10-14].
- **Temperature of the combustion gases:** the final parameter is the temperature at which the combustion gases enter the reactor, which provides the process heat. When defining this parameter, it is essential to consider the co-current configuration of the pyrolysis reactor (explained on 7.3.2.1.3).

## 7.2 Bed of solids

The bed of solids is the first submodel to run. The structure of this model in terms of inputs, calculations and outputs are represented in Figure 7.1. The model extracts some properties from the feedstock selection, properties such as the repose angle and density. The aim is to calculate the radius, length, contact areas, solids residence time, rotational speed and the kiln angle for optimum performance. As a first approximation, the radius is estimated depending on the capacity, and the angle is adjusted to 1°. After several automatic iterative simulations and results, the values are adjusted to achieve a precise conversion of the feedstock. This aspect is explained in detail in 7.5.1.

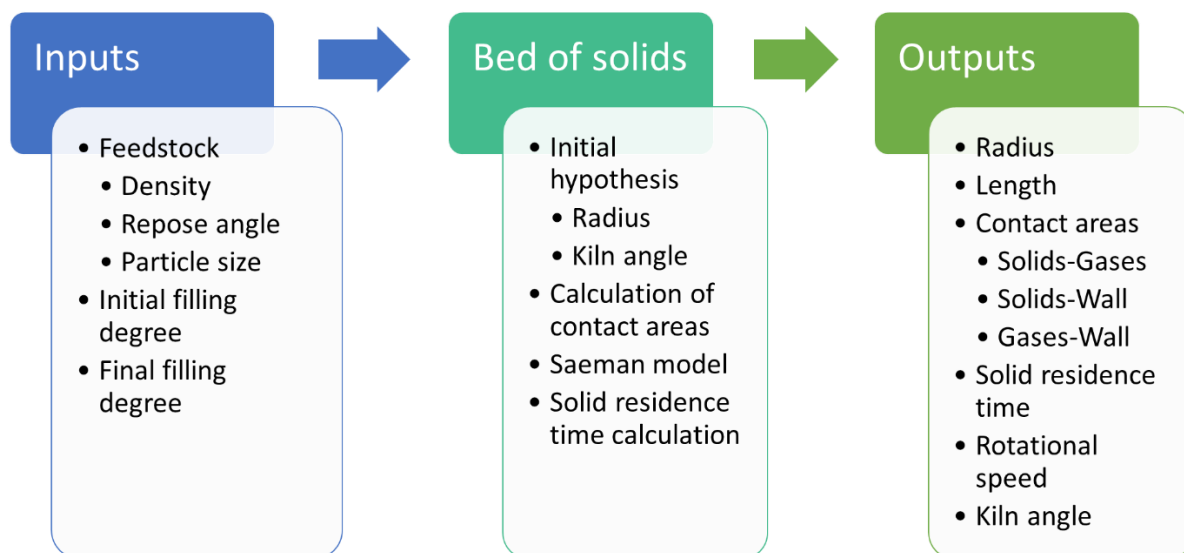


Figure 7.1: Structure of bed of solids submodel

### 7.2.1 Bed motion

One of the objectives of the model is to produce the most homogeneous possible product. After exploring the different types of bed motion on Section 3.1.1.2, a rolling motion was preferred due to its balance of mixing, the portion of the wall covered and constant properties. To achieve rolling motion, the following conditions have to be achieved:

- Froude number (Equation 7.1) should be between a range  $\rightarrow 10^{-4} < Fr < 10^{-2}$

$$Fr = \frac{\omega^2 \cdot R}{g}$$

Equation 7.1: Froude number

- Filling degree should be higher than 10%  $\rightarrow f > 0.1$
- Wall friction coefficient is higher than the critical wall friction coefficient  $\rightarrow \mu_w > \mu_{w,c}$ . This condition is not calculated and it is an assumption of the model.

*Assumption 26: The wall friction coefficient is higher than the critical wall friction coefficient*

To ensure rolling motion, the target Froude number is set the median of the range, which is equivalent to a value of  $10^{-3}$ . The rotational speed ( $\omega$ ) is calculated from an initial estimation of the radius ( $R$ ).

### 7.2.2 Length of the bed of solids

The rotary kiln has aspects influenced by the rotational speed and kiln angle. One of these aspects is the height of the bed of solids, which decreases along reactor length due to the reactor configuration. To calculate the length of the bed of solids, Saeman's model is used and the terms re-organised to calculate the length of the bed of solids according to Equation 7.2.

$$\int_0^{Length} dz = \int_{H_i}^{H_f} \frac{dH}{-\frac{3 \cdot \tan \theta}{4 \cdot \pi \cdot \omega} \cdot Q \cdot [R^2 - (R - H)^2]^{-\frac{3}{2}} + \frac{\tan \beta}{\cos \theta}}$$

Equation 7.2: re-organised Saeman's model

The limits of the integral are the initial and final height of the bed of solids, but only the filling degrees are known. With that purpose, Equation 3.13 correlates the height divided by the radius with the filling degree. The initial and final filling degree is established as 0.15 and 0.1 for the whole study. The limits were estimated according to similar values from the literature [15, 16]. The main aim of the values is to achieve higher heat transfer by radiation, which is more significant with low values of the filling degree (<0.5) [17]. A more significant radiative heat flow is the standard assumption when the target temperatures are high [5, 6].

In some simulations, the value of reactor length became negative without apparent reason. It could be due to the non-ideal behaviour of the bed of solids because Saeman's model required a constant volumetric flow. In contrast, the feedstock is transformed during pyrolysis with density and mass flow varying. The sensitivity analysis of Figure 3.2 was conducted to study the effect of each parameter and ensure a positive length. The method to calculate the integral is automated; otherwise, it would involve the implementation of a MatLab programme adding further complication. The three methods to calculate the integral were the Midpoint, Trapezoid and Simpson rule with 10 and 20 steps to observe the variation between them. The conclusion is that the values do not vary significantly nor with a change in the number of steps (less than a millimetre in more than 20 meters) (Section 3.2).

### 7.2.3 Contact areas

Once the radius, kiln angle, length of the reactor, and filling degrees have been defined, the contact areas can be calculated through trigonometrical calculations described in Section 3.3. The areas and contact areas within the reactor could be calculated following all the steps used in Section 3.3 using radius, the length and finding all the angles and parameters needed. Alternatively, the contact areas divided by the kiln radius and bed of solids length are a function of the average filling degree. The contact areas bed of solids-wall and gases-wall divided by the radius of the reactor and the length of the bed of solids have a linear dependency with the filling degree (Equation 3.22 and Equation 3.23). The contact area between the solids and gases is not linear but represented by a second-degree equation (Equation 3.24). These three equations have alignment to the data higher than 99%, which means that they behave very similar to reality. These equations are used to calculate the contact areas and make the calculations simpler instead of following all steps from Section 3.3.

$$\left(\frac{A}{R \cdot L}\right)_{W-S} = 3.91 \cdot f + 1.24$$

$$\left(\frac{A}{R \cdot L}\right)_{W-G} = -3.91 \cdot f + 5.04$$

Equation 7.3: Wall-solid area as a function of the filling degree

Equation 7.4: Wall-gas area as a function of the filling degree

$$\left(\frac{A}{R \cdot L}\right)_{S-G} = -3.95 \cdot f^2 + 3.83 \cdot f + 1.10$$

Equation 7.5: Solid-Gas area as a function of the filling degree

The conductive heat flow requires the solution of an integral where the contact area goes in the denominator. The equations correlate the areas with the filling degree, which is directly correlated with the height so the area can be related to the height of the bed of solids through a linear expression using the two sets of equation simultaneously and isolating the filling degree. The linear correlations for the areas wall-solids and wall-gases are clear, and the solution to its integration is a logarithm as it is seen on Equation 3.25 and Equation 3.26 for the areas wall-bed of solids and wall-gases inside the reactor, respectively.

When the calculation accounts for the Area between the solids and the gases, the problem becomes more difficult. Firstly, because it is a second-degree equation and the dependency is on height instead of the radius for the integral. For this particular case, Equation 7.6 is developed, and three variations are considered based on a filling degree limits. The steps to find and deduce the term  $A_{gas-solids}(H)$  are explained on Equation 3.28, which results from equalising the filling degree from equations to calculate the contact area gas-solids and the height of the bed of solids when the filling degree is lower than 0.5. Due to this limit on one of the equations used for the deduction, the procedures are different to solve de equation based on the filling degrees, and three cases are studied. Initial and final filling degrees are lower than 0.5, the initial and final filling degree are higher than 0.5, and initial filling degree is higher than 0.5, but the final filling degree is lower than the limit. With those three variations, Equation 7.6 is applied to calculate the denominator of the conductive heat flow. The bold **R** is the value of the radius as a constant for the integral. When it is not bold, it means it is one of the integral limits. As explained on Section 3.5.1, the solutions for the three cases are Equation 3.29 (filling degrees lower than 0.5), Equation 3.30 (filling degrees higher than 0.5), and Equation 3.31 (initial filling degree higher and final filling degree degree lower than 0.5).



$$\int_H^R \frac{dH}{A_{gas-solids}(H)} = \int_H^R \frac{dH}{H \cdot C_1 + C_2} = \frac{\ln\left(\frac{R \cdot C_1 + C_2}{H \cdot C_1 + C_2}\right)}{C_1} = \frac{\ln\left(\frac{R \cdot \frac{m_A}{m_H} \cdot L + (n_A - n_H \cdot \frac{m_A}{m_H}) \cdot R \cdot L}{H \cdot \frac{m_A}{m_H} \cdot L + (n_A - n_H \cdot \frac{m_A}{m_H}) \cdot R \cdot L}\right)}{\frac{m_A}{m_H} \cdot L}$$

Equation 7.6: Integral of gas-solid area with height

### 7.2.4 Residence time

The solids residence time is calculated through the Mean Excursion Time (MET) on Equation 7.7, which is a term that Fantozzi et al. [18] used as an equivalent parameter to the residence time. This method is employed over the conventional  $\left(\frac{Volume}{Volumetric\ flow}\right)$  because it accounts for the length ( $L$ ), the repose angle of the solids ( $\theta$ ), rotational speed ( $\omega$ ), kiln angle ( $\alpha$ ) and the angle of the bed of solids ( $\beta$ ). The formula is represented by Equation 7.7. The residence time of the gases is calculated through the conventional formula  $\left(\frac{Reactor\ length}{Average\ velocity\ of\ gases}\right)$  because the conditions of the kiln do not have a significant effect as the kiln angle and rotational speed are not the driving forces that make the gases to move forward.

$$MET [min] = \tau_R = \frac{L[m] \cdot \theta[rad]}{2 \cdot \pi \cdot \left(\omega[rpm] \cdot \frac{1}{2 \cdot \pi}\right) \left[\frac{rad}{revolutions}\right] \cdot (\tan \alpha + \cos \theta \cdot \tan \beta) \cdot (\cos \beta)^2}$$

Equation 7.7: Mean Excursion Time

### 7.3 Heat transfer

The heat transfer submodel is critical in the development of this work. It simulates the heat flows between the combustion gases, gases inside the reactor and the bed of solids plus the variation of temperature of each component along the reactor. The heat transfer accounts for the losses of the reactor. It adjusts the flow of combustion gases automatically to ensure the bed of solids achieves the target temperature (Figure 7.2).

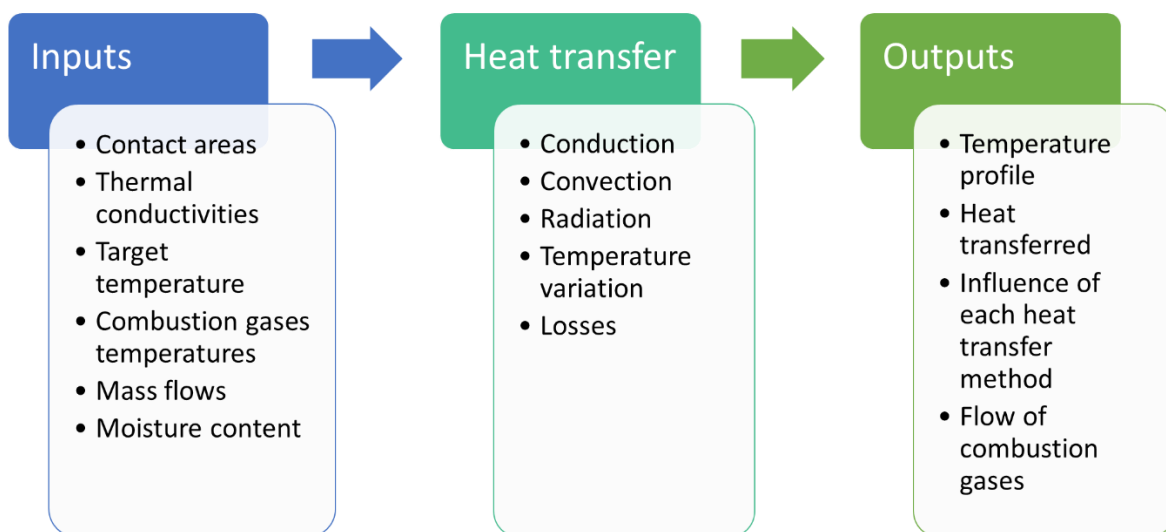


Figure 7.2: Structure of the heat transfer submodel

### 7.3.1 Heat flows

The heat is transferred through the three existing methods, conduction, convection and radiation. All the methods occur between the combustion gases, the bed of solids and gases inside the reactor.

#### 7.3.1.1 Conduction

The conduction occurs when two materials are in contact at different temperatures. When the area is variable, Equation 4.3 is employed. The denominator of this equation is previously calculated in Equation 7.6 for gas and solids contact area and Equation 3.25 and Equation 3.26 for the contact area between the wall and the bed of solids and gases inside the reactor, respectively.

$$Q_x^{cond} [W] = \frac{\lambda \left[ \frac{W}{m \cdot K} \right] \cdot (T_1 - T_2) [K]}{\int_{x_1}^{x_2} \frac{dx}{A(x)} \left[ \frac{m}{m^2} \right]}$$

Equation 7.8: Conductive heat transfer with variable area

The heat transfer submodel combines the contact areas with the voidage and the flights. The effect of each parameter is different depending on the components involved in the area calculation. These parameters do not affect the calculation of the integral because the parameters are considered as constant. The effect of each parameter on the areas are represented in Equation 7.9 for the contact area between the wall and bed of solids, Equation 7.10 for the area between the wall and gases and Equation 7.11 for the area between the bed of solids and gases. The equations take into account the voidage, the efficiency of the flights, the number of flights in the cross-sectional area, and the filling degree ( $f$ ).

$$A'_{wall-solids} = A_{wall-solids} \cdot (1 - voidage) \cdot (1 + Efficiency_{flights} \cdot number_{flights} \cdot f)$$

Equation 7.9: Modified contact area wall-bed of solids

$$A'_{wall-gases} = A_{wall-gases} \cdot (1 + Efficiency_{flights} \cdot number_{flights} \cdot (1 - f))$$

Equation 7.10: Modified contact area wall-gases

$$A'_{gases-solids} = A_{gases-solids} \cdot (1 + voidage)$$

Equation 7.11: Modified contact area gases-bed of solids

Firstly, the contact area between the wall and the bed of solids (Equation 7.9) is affected by the voidage because not all the solids are in contact with the wall. Due to the lack of information to allow the analytical study of the impact of flights on the system (Section 6.2) it was decided to establish a new heat transfer area to account for the flights. The solids do not fill the entire reactor, and that is the reason the total flight area is multiplied by the filling degree, to see the portion of solids affected by this additional heat transfer area.

The contact area between the wall and the gases (Equation 7.10) is affected by the flights and the space available for gas flow ( $1 - filling\ degree$ ). The voidage does not appear because it is considered that the heat transferred from the wall to the gas in the interstices between the solids is negligible compared to the amount on the free surface.

Finally, the contact area between the gas and the solids (Equation 7.11) is affected exclusively by the voidage as the space between the solids is filled with gas. The flights do not affect this area

because it increases the contact area with the wall—the more packed the bed of solids, the lower the voidage. The contact area between the solids and the gases is enhanced by this parameter.

### 7.3.1.2 Convection

Convection is the second heat transfer method and takes place when one of the materials is in movement. It is usually applied to fluids, but in this reactor, there is convection to the solid, which is in motion. Equation 4.5 is applied to a comprehensive system to calculate the convective heat flow. As shown in Section 4.3.1, the difficulty lies in the calculation of the convective heat transfer ( $h$ ) and several methods were explained on Section 4.3.1.2 and 4.3.1.3.

$$Q^{conv}[W] = h \left[ \frac{W}{m^2 \cdot K} \right] \cdot A_s[m^2] \cdot (T_s - T_\infty)[K]$$

Equation 7.12: Convective heat flow

The voidage and the flights affect the convective model in a similar way to conduction (Equation 7.11). At the surface between the gas and the solid, the voidage increases the contact area. The gas velocity is different for the gas in the free space of the kiln compared to the portion in the void space between the solids. The velocity influences the convective heat transfer coefficient and, ideally, a different value should be calculated for each of the zones. This calculation would make the model very complicated, and it is approximated that all gases have the same velocity, which agrees with the previous assumption of the negligible amount of gas in the bed of solids compared to the one flowing on the free space. Furthermore, it is considered the flights do not lift the solids and the area between gas and solids for convection is not increased by this effect.

*Assumption 27: The velocity of the gases does not depend on the gas positioning in the free space or within the space of the bed of solids*

*Assumption 28: The flights do not lift the solids, and no extra area is added due to the effect of solids showering on the free space*

For the convective heat flow from the wall to the bed of solids and the gases, the areas employed are the original plus the area added by the flights. For the gas, the area is from Equation 7.10. The area for the solid is different (Equation 7.13) because the voidage is not considered. The solids have motion, and it is assumed the voidage does not increase the contact area in convection when the particles move along and keep swapping places.

*Assumption 29: The voidage does not affect the contact area between solids and the wall in the convective heat flow*

$$A''_{wall-solids} = A_{wall-solids} \cdot (1 + Efficiency_{flights} \cdot number_{flights} \cdot f)$$

Equation 7.13: Modified area wall- solids for convective heat flow

### 7.3.1.3 Radiation

The last method of heat transfer is radiation. This method is different from the others because it does not need direct contact between the two materials exchanging energy, and it is produced through electromagnetic waves, linked to the internal energy of the particles. The formula employed is Equation 4.21. Section 4.4.1 shows the complexity of the view factor ( $F$ ) and the steps to calculate it are explained.

$$Q_{1 \rightarrow 2}^{rad}[W] = \frac{\sigma \left[ \frac{W}{m^2 \cdot K^4} \right] \cdot (T_1^4 - T_2^4)[K^4]}{\frac{1 - \varepsilon_1[-]}{A_1[m^2] \cdot \varepsilon_1[-]} + \frac{1}{A_1[m^2] \cdot F_{12}[-]} + \frac{1 - \varepsilon_2[-]}{A_2[m^2] \cdot \varepsilon_2[-]}}$$

Equation 7.14: Heat transfer between two grey, diffuse and opaque surfaces

The values of emissivity for the gases inside the reactor, the bed and the wall are 0.5, 0.9 and 0.1, respectively. This parameter is very difficult to correlate due to the lack of information in the literature. The coefficient for the gas was estimated from values in the literature [19]. Ideally, the coefficient for each mixture should be calculated in a similar way to the calorific value (at the end of 7.3.2), identifying each emissivity value and obtaining an average between them. This value is dependent on the composition of the gas. The lack of information within literature makes this tricky. Consequently, a constant value was defined based on an average of those values obtained. A very low emissivity was assumed for the wall to emulate one of the worst-case scenarios and ensure the temperature will be achieved.

### 7.3.2 Approach

The heat flows explained above describe the heat exchange between the three components in the reactor: the bed of solids, the gases inside the reactor, and the wall, whose temperature is considered equivalent to the temperature of the combustion gases.

Within the reactor design, there is the issue of how to calculate the different heat flows where the temperature of each component changes with time. The equations for the heat flows account for a single temperature for each component. In a whole reactor, both input and exit temperatures are important, and the question about which should be considered for calculation will arise. Taking an average temperature for the calculation is inappropriate because the variation is too significant. For instance, the bed of solids increases from 20 to at least 350°C whereas the combustion gases if in counter-current configuration, could decrease in temperature from 1200 to 600 °C. The changes in temperatures alter properties such as the density of the gases or thermal conductivity change, which influence parameters such as Reynolds number or convective heat flow and, eventually, the heat transfer.

Ideally, the heat flows should be calculated at each differential of the length of the reactor where the temperature of each component is constant. To solve this issue, various studies [16, 20] divided the reactor into different parts to study each independently. In this study, a similar perspective is employed. The reactor is divided into slices (or steps), physically identical, and each of them is considered as a CSTR reactor to allow homogeneous properties to calculate the exit temperature of each step. The information each slice needs and the outputs are represented in Figure 4.12, and the algorithm is represented in Figure 4.13. In this way, from the initial 3-D problem, the length is solved by dividing into slices. The remaining 2-D problem is simplified using a CSTR reactor for each step for heat flows calculation, which assumes the properties as constant for each differential of length.

The equations for the heat transferred or absorbed depend on the conductive, convective and radiative heat flows. Within this work, it was assumed that the wall would be the hottest component, followed by the gases inside the reactor, and the bed of solids will be considered as the lowest temperature. Therefore, when the wall interacts with any of the other two components, the wall will be considered as the highest temperature. When the simulation does not follow this direction of heat flow, the heat values will be negative instead of positive. According to this, Equation 7.15, Equation 7.16 and Equation 7.17 show how the heat flows for the calculation of the heat transferred or

absorbed by each component calculated on Watts (W). The only unknown parameter in these equations is  $\eta$ , the coefficient for the losses of the reactor, represented as 25%.

$$Q_{to\ solid} = Q_{wall-solid}^{cond} + Q_{wall-solid}^{conv} + Q_{wall-solid}^{rad} + Q_{gas-solid}^{cond} + Q_{gas-solid}^{conv} + Q_{gas-solid}^{rad}$$

*Equation 7.15: heat transferred to the bed of solids*

$$Q_{to\ gas} = Q_{wall-gas}^{cond} + Q_{wall-gas}^{conv} + Q_{wall-gas}^{rad} - Q_{gas-solid}^{cond} - Q_{gas-solid}^{conv} - Q_{gas-solid}^{rad}$$

*Equation 7.16: Heat transferred to the gases inside the reactor*

$$Q_{from\ wall} = (Q_{wall-solid}^{cond} + Q_{wall-solid}^{conv} + Q_{wall-solid}^{rad} + Q_{wall-gas}^{cond} + Q_{wall-gas}^{conv} + Q_{wall-gas}^{rad}) \cdot (1 + \eta)$$

*Equation 7.17: Heat transferred from the wall*

These heat flows are used to calculate the exit temperatures, and the method is different for each of the components. The general expression to calculate the temperatures is in Equation 4.40. This expression should be customised for each component and condition. For instance, the mass flow for the solids and gases varies when there is a reaction and with moisture content. For each expression, the mass flow, the heat absorbed or transferred, the calorific heat and one of the temperatures is known, so there is a single temperature to solve (highlighted in green) in Equation 7.18 and Equation 7.19 for the combustion gases, Equation 7.20 for the bed of solids and Equation 7.21 for the gases. The expressions used are energy balances for each of the components. For the combustion gases, the expression changes if the configuration is co- or counter-current. After the balance of each component, there is a brief description.

$$Q_{from\ wall} = \dot{m}_{comb} \cdot C_{p\ comb} \cdot (T_{in\ comb} - T_{out\ comb})$$

*Equation 7.18: Energy balance for the combustion gases in co-current configuration*

$$Q_{from\ wall} = \dot{m}_{comb} \cdot C_{p\ comb} \cdot (T_{out\ comb} - T_{in\ comb})$$

*Equation 7.19: Energy balance for the combustion gases in counter-current configuration*

There is no difference on the input and exit flow of combustion gases because it is constant along the reactor since it does not interact with the bed of solids or gases inside the reactor and is only used to heat the reactor. The mass flow of the combustion gases multiplies the calorific capacity and the variation of the temperatures.

In the co-current configuration, the combustion gases enter in the same direction as the other components at a known temperature. This temperature begins high and decreases along the reactor. In a counter-current configuration, the combustion gases flow in the opposite direction to the other components. Depending on the configuration, different target temperatures (in and out) are used to calculate each energy balance. This difference is based on the entry and exit point of the components for each configuration. When it is co-current, the gases enter at a known temperature and decrease along the reactor, and the exit temperature is the unknown variable.

In the counter-current case, the calculation is more complicated. The temperature of the combustion gas varies similarly to the temperature of the solids and vapours, which increase along the reactor length. To simulate the process, it is not possible to simulate the solids, gases inside the reactor and combustion gases from the entrance towards the end simultaneously, because the temperatures of a bed of solids and gases inside the reactor are calculated forward. It would require the backwards calculation of the temperature of the combustion gases, without knowing the temperature of the components with which it is interacting. To solve this problem, a temperature

difference between the combustion gases and components inside the reactor is estimated (with a value of 100°C), and all three are calculated.

$$Q_{to\ solid} = \dot{m}_{solids}^{out} \cdot T_{solids}^{out} \cdot \left( C_{p\ solids}^{out} + C_{p\ H_2O}^{out} \cdot MC_{solids}^{out} \right) - \dot{m}_{solids}^{in} \cdot T_{solids}^{in} \cdot \left( C_{p\ solids}^{in} + C_{p\ H_2O}^{in} \cdot MC_{solids}^{in} \right) - \left( \dot{m}_{solids}^{in} \cdot MC_{solids}^{in} - \dot{m}_{solids}^{out} \cdot MC_{solids}^{out} \right) \cdot \Delta H_{vap} + \left( \dot{m}_{solids}^{in} - \dot{m}_{solids}^{out} \right) \cdot \Delta H_{reaction}$$

Equation 7.20: Energy balance for the bed of solids

Equation 7.20 is used to calculate the heat flow towards or from the bed of solids. The negative or positive number determines the direction of the heat flows. The objective is to find the temperature at which the bed of solids exits the step. This temperature is lower if the heat is partially used to evaporate the water ( $\Delta H_{vap}$ ), and it increases if the reaction heat ( $\Delta H_{reaction}$ ) has a positive value when it is exothermic.

The expression for the heat transferred to the bed of solids is very different from the expression for the combustion gases. For the bed of solids, the flow is not constant, and the mass flow and moisture content ( $MC$ ) vary. The energy balance in the bed of solids takes into account the existing energy and the calorific capacity of the solids plus the moisture content. The mass flow does not directly account for the moisture content because the solid mass flow is measured in dry tonnes per hour. Besides the mass flow of solids with the calorific value and the moisture content, the difference of mass flow (without the moisture content) multiplied by the reaction heat provides more energy if the reaction is exothermic and absorbs part of the energy provided when endothermic.

The other factor is the heat of vaporisation, which accounts for the water evaporated in that step. In the algorithm, the calculation of the final moisture content is completed with a conditional algorithm (function *if* in VBA) and measured as an independent mass flow instead of a percentage. The model considers that the evaporation starts when the input temperature of the solids is higher than 105 °C. Once the temperature is reached, all the heat targets the evaporation of water. The model considers four cases:

- The input temperature of the solids to the step is lower than 105 °C. The heat is transferred to the solids and moisture content, and the exit temperature involves the solids and the moisture content.
- The temperature is higher than 105 °C, moisture content higher than null and the heat transferred to the solid is lower than that needed to evaporate all the water. All heat to the solid goes towards the evaporation of water.
- The heat transferred to the solids is equal or higher than the amount needed to evaporate all the water. The value of the moisture content is set to null, and the remaining heat is used to increase the bed temperature.
- The last case is where the moisture content is already null. In this case, the moisture content stays as zero, and the temperature is calculated.

$$\begin{aligned}
Q_{to\ gas} = & \dot{m}_{gas}^{out} \cdot T_{gas}^{out} \cdot C_{p\ gas}^{out} - \dot{m}_{gas}^{in} \cdot T_{gas}^{in} \cdot C_{p\ gas}^{in} - (\dot{m}_{solids}^{in} \cdot MC_{solids}^{in} - \dot{m}_{solids}^{out} \cdot MC_{solids}^{out}) \\
& \cdot \left( \frac{T_{solids}^{out} + T_{solids}^{in}}{2} \right) \cdot \left( \frac{C_{p\ H_2O}^{out} + C_{p\ H_2O}^{in}}{2} \right) - (\dot{m}_{solids}^{in} - \dot{m}_{solids}^{out}) \cdot \left( \frac{T_{solids}^{out} + T_{solids}^{in}}{2} \right) \\
& \cdot \left( \frac{C_{p\ vol.}^{out} + C_{p\ vol.}^{in}}{2} \right)
\end{aligned}$$

Equation 7.21: Energy balance for the gases inside the reactor

The signs define the direction of this energy balance. A negative sign precedes all the inputs for this energy balance, and the only output has a positive sign on the front.

The energy balance for the gases (Equation 7.21) is the only one which depends directly on the temperature of the other components (bed of solids). The inputs of this energy balance are the gases from the previous step, the portion of the solids that degrades or the water evaporated. The only output is the flow of gases, together with the calorific value and the exit temperature. The moisture content and the pyrolysis gases are separated because they are calculated separately.

The calorific value is difficult to calculate because it is a varying mixture of gases that changes along the reactor. To calculate, the variation of the mass flow is attributed to different gases (see Sections 7.4 and 5.6), and the fraction of each is calculated (Equation 7.22). Then, the calorific value of each gas is multiplied by its fraction and summed (Equation 7.23).

$$x_i = \frac{\dot{m}_i}{\sum_{CO_2, CO, CH_4, H_2, H_2O, N_2} \dot{m}_i} \quad C_{p\ gases} = \sum_{CO_2, CO, CH_4, H_2, H_2O, N_2} C_{p_i} \cdot x_i$$

Equation 7.22: mass fraction of gases

Equation 7.23: Calorific value of the mixture of gases

The variation of the heat capacity with the temperature of the gases is shown in Figure 7.3. The data for the calorific values of each gas and its variation with the temperature are taken from the appendices of Çengel et al. [19]. The dependency of the temperature is linear, with regression values higher than 90%. When the calculation refers to a range of temperatures, heat capacities at the initial and final temperature are calculated, and the average value taken for the calculations.

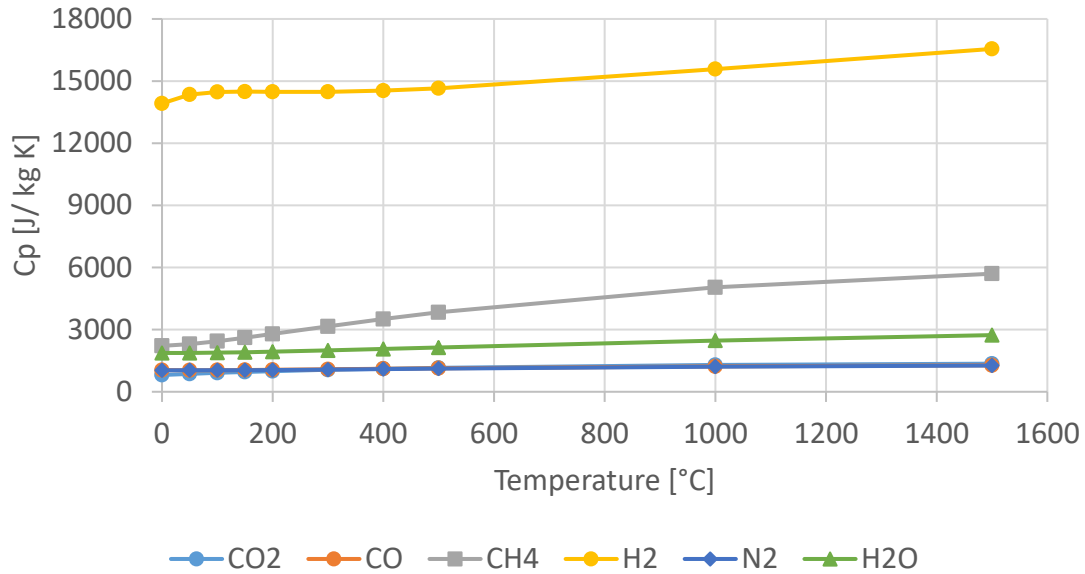


Figure 7.3: Variation of the calorific value of the gases with temperature, data from [19]

### 7.3.2.1 Troubleshooting

#### 7.3.2.1.1 Convergence

To begin the algorithm obtains all constants, values and inputs, which are required to solve each step in the spreadsheet. Among these inputs, the entry temperatures are included. Initially, the exit temperatures are defined as one degree higher than entry temperature for the solids and gases inside the reactor and, in co-current configuration, one degree lower for the combustion gases. With the average values of temperatures, the algorithm calculates the heat flows and the new exit temperatures. The new temperatures are checked automatically to ensure valid values to avoid inconsistent results. For example, the temperature of the gases and solids inside the reactor should be lower than the wall. If the solid temperature is higher than the wall, the exit temperature of solids is automatically reduced to one degree lower than the wall.

The exit temperatures are re-calculated with the new values, which may vary the average temperature and, consequently, the heat flows. There is a counter for the number of times the value is recalculated. The values stop when the temperatures converge or when the iterations counter reaches a value of 32,500; this is near the limit of the integer range on VBA programming (up to 32,767). This iteration limit prevents the model from being stuck on the same step repeatedly. Furthermore, 32,500 repetitions of the same process should lead to a convergence of the temperatures due to the high number of iterations.

The other method to stop the iterations is converging values which happen when Equation 7.24 is accomplished. This equation summates the square of the temperature differences of the three materials (coefficient  $i$ ) between the input and exit temperature within the step. The square is to make all values positive and have a more significant perspective. The summation of the temperature differences must be lower than one, which means that every single difference should be lower than one or the value will not be achieved.

$$\left( \Delta T = \sum_{i=0}^{wall,solid,gases} (T_{i_n} - T_{i_{n-1}})^2 \right) < 1$$

Equation 7.24: Limit of variation of temperature



This convergence is part of the first loop from Figure 4.13. Before moving ahead to the next step, the temperatures are checked once more in detail. Firstly, the number of iterations is consulted; without convergence, the results could be misleading. For the solids, if the iterations limit is reached and the exit temperature is either lower than the input temperature or higher than the wall, the exit temperature is modified. If the temperature of the wall and solid at the entrance is similar (temperature difference less than 3 °C) the temperature difference between the wall and the bed of solids is reduced to 1 at the exit. It would mean there is a problem with the difference in-out, and the temperature is increased by 2°C in that case. For the gases, the considerations and results are the same. When the algorithm converges, and the temperatures are still invalid (temperature of the gases or solids higher than the walls), the highest component exit temperature is defined as having the same value as the wall.

In the second loop from Figure 4.13, the properties, calculated by the spreadsheet, such as viscosity, mass flows (which change with kinetics for the bed of solids and the gases inside the reactor), heat capacities and the dimensionless numbers, are re-calculated and the first loop is reapplied. The difference in temperature is the same as in loop 1; the only difference is the iteration limits, which is 100 for second loop instead of 32,500 (first loop). This difference is based mainly on the fact that during simulations, the computer overwrites the values and the computer keeps changing between two values, so having 32,500 iterations would only increase the time rather than accuracy.

This would be the convergence for a single step, and the results are the inputs for the following slices of the reactor. The number of divisions for the reactor was initially 25 because, in other studies, a similar number was chosen [3, 16]. In the beginning, it was intended that the implementation was in Excel without further coding. However, the computer highlighted the existence of circular references, and it converged for the first steps, but when it reached step 13 the whole file collapsed. Excel did not have enough power to deal with the amount of information. When it recalculated any of the parameters, the computer tried to recalculate all the linked variables at once. Furthermore, the computer needed to follow the logical path for the loops, to reduce the capacity demand and to calculate sensible results. In order to make the computer follow the algorithm and conditions in the correct sequence, a VBA code was created.

Once the algorithm was implemented, the convergence did not happen quickly, and some adjustments were needed. The non-converging behaviour of the model could imply failure in the model because the variables sometimes overflow. The overflow occurs when the value of a variable exceeds its limit. The variables connected with temperature were defined as *single*, whose range is  $[-3.4 \times 10^{38} - 3.4 \times 10^{38}]$ , with a precision of  $1.4 \times 10^{-45}$ . Such a wide range implied the possibility to have very high values, but they were needed to account for the heat transferred by radiation, whose order of magnitude could be  $((10^3)^4 = 10^{12}) (T [K]^4)$ .

One of the most critical steps is when evaporation finishes and produces a divergence in the model due to overflow with 25 steps. The steps were tracked to find the problem, and the result is shown in Figure 7.4. This graphic represents the auxiliary temperatures (*AuxT*) with which the exit temperatures are compared for each of the three components; the summation of the square of their difference should be lower than 1 (Equation 7.24). Ideally, the green and blue lines should lead to converging values as per the purple line, which converges. Instead, the tendency is the opposite, and the difference is higher. The tracking stopped at step 21 because there was enough evidence to see the divergence. The result of Equation 7.24 is represented in Figure 7.5. It is clear that the variation of temperatures increases.

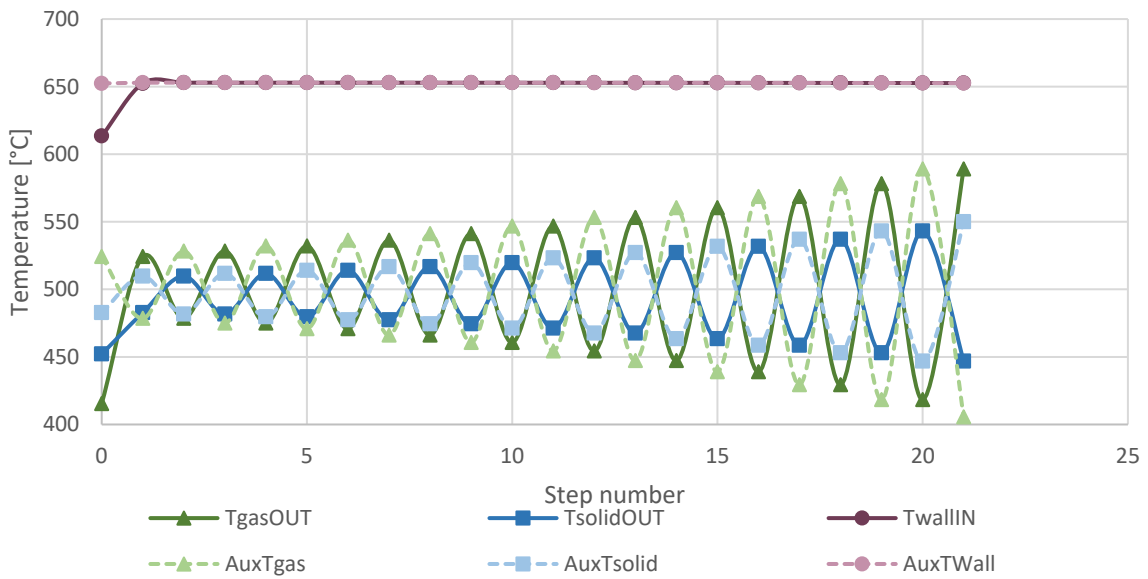


Figure 7.4: tracking of temperatures on step after evaporation

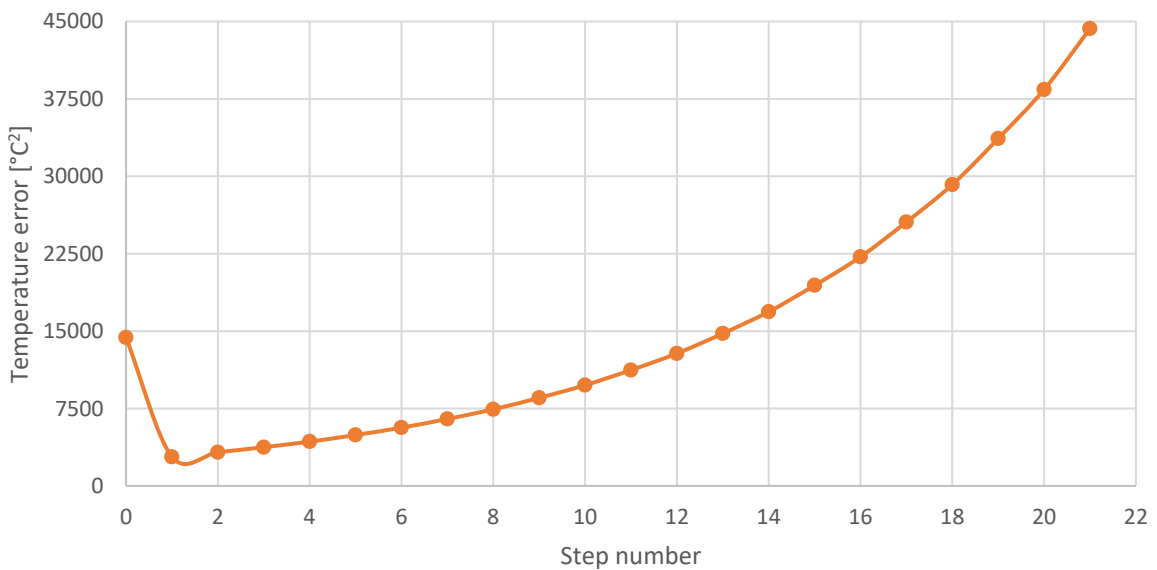


Figure 7.5: Square temperature difference

The origin of the problem was not found, but a potential cause could be the big difference between the entry and the exit temperature. It can lead to more significant differences and heat flows, which makes the calculation of other high numbers more likely. A solution could be to have a lower temperature difference between the entry and exit for each reactor slice. In practice, this statement means increasing the number of steps. With 100 steps, the problem did not appear again. This was the chosen solution for the divergence of data, increasing the number of steps, which narrows the increase of temperature in that step and leads to more convergent values.

#### 7.3.2.1.2 Heat source

A surrounding flow of combustion gases around the reactor is not the only method to heat the rotary kiln. During the chapter, the flow of combustion gases has been mentioned because it is

considered the best choice for this specific research. In Appendix C, there are some examples where the heat source is a pre-heated thermal fluid. This thermal fluid is characterised by thermal stability and operational consistency. There is a significant disadvantage with thermal fluids, which is the operational range, whose maximum is generally around 320 °C. Thermal fluids degrade, change behaviour and properties when the temperature is higher than this limit [3, 4]. It may reduce the efficiency of the whole process because the thermal fluid has to be heated up, and this extra step involves another process operation, whose efficiency is not 100%.

For these reasons, combustion gases were chosen to heat the reactor. The feedstock for combustion is the gases from the reactor. The cell in the model  $Q_w/H$  indicates the portion of energy demanded from the wall (heat source for the solids and gases inside the reactor), and the heat produced by the combustion of the gases. This portion is usually 20-30wt.% of the total energy obtained from the combustion of the gases. The remaining energy can be used in other units, such as the dryer if required.

#### 7.3.2.1.3 Flow of combustion gases

It is fundamental to recall the specific objective of this submodel, which is to simulate a reactor where the bed of solids achieves the desired temperature. The heat source to increase the temperature is the combustion gases. The system is influenced by the co-current or counter-current configuration.

Once the reactor simulation is complete, the final temperature of the solids is compared with the target value. Due to the complex calculation, there is a margin in the temperature of 5°C. This means that the model takes as valid a temperature whose value is either 5°C higher or lower than the target one. The small variation in the final temperature of the solids is established because achieving a temperature of precisely 500 °C in such a complex simulation is not feasible. The composition of the combustion gases is supposed to be 50 wt. % of carbon dioxide (CO<sub>2</sub>) and 50 wt.% steam (H<sub>2</sub>O), as it came from complete and perfect combustion, although the composition can be modified in the model. To modify and define the flow of combustion gases, the configuration needs consideration:

- **Counter-current:** counter-current configuration consists of the solids and gases flowing in opposite directions. It is known for being optimum for heat transfer [21, 22]. This applies to the log mean temperature difference method (See Equation 4.37). For the simulation, the file needs to run the model from the beginning towards the end, and it includes the heat transferred by the combustion gases. In this configuration, combustion gases flow in the opposite direction to the reactants. The ideal case would be for the combustion gases to flow from the end to the beginning with the solids and reaction gases in the opposite direction. The two directions within the reactor create the need to simulate the combustion gases and the components inside the reactor differently. To run the simulation, the combustion gases, flow of solids and pyrolysis vapours should be running in the same direction. To use most of the energy of the combustion gases, it is estimated that the exit temperatures of the gases are 100 °C lower than the target temperature. In general, the most significant contribution to the heat flows is the convective heat transfer, followed by radiation.

Figure 7.6 shows the simulation of a rotary kiln of 3 tonnes per hour, where the final temperature is 500 °C when the combustion gases' exit temperature is 400°C. The temperatures are represented by continuous lines, and the fraction of heat flows by dotted lines. The evolution of the temperatures is very smooth, and convection has a significant influence at the beginning, with radiation becoming more significant along the reactor. When the temperature of the bed at the end of the reactor is not high enough, the flow of combustion gases decreases by 1% (x 0.99).

On the contrary, it is increased by 1% (x 1.01) when the temperature is too high. The reason to decrease combustion gases flow to increase the temperature is the higher combustion gases entry temperature for each step, which induces a larger temperature gap between the components and higher heat flows. In this case, the resulting flow of combustion gases is 3 kg/s (10.8 t/h).

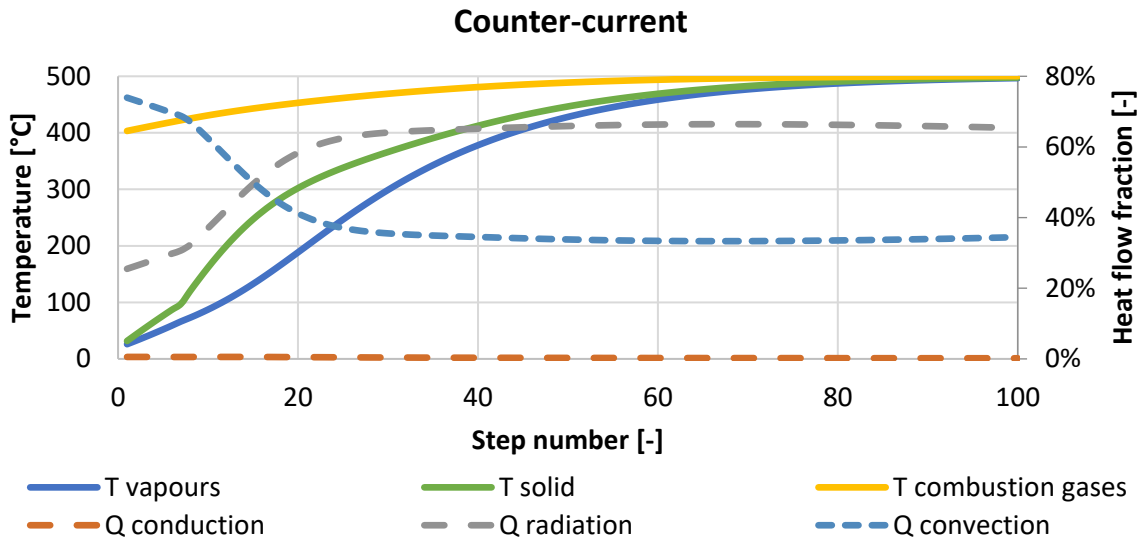


Figure 7.6: temperature profile and heat flow proportions on counter-current configuration

- Co-current:** the case of the co-current configuration is more straightforward from a simulation point of view because the gas and solids are flowing in the same direction. The simulation requires fewer assumptions and is more accurate because the streams move in the same direction. The entry temperature of the reactor gases comes directly from the combustion gases, so the temperature estimation is more accurate. Overall, the initial temperature is 1,200 °C for the combustion gases, very high compared to the ambient temperature (20°C) of the carrier gas and the bed of solids. The same comparison for a fraction of heat flows and the temperature of each component can be seen in Figure 7.7.

There are several points to highlight; firstly, the significant influence of radiation, accounting for 75% of the total heat flow. Another is the high temperature of the combustion gases and its large difference to the bed of solids. A critical aspect to consider is the time taken to reach the target temperature; in both configurations, the length of the reactor and the number of steps are identical, but the point where the user-defined reaction temperature and final temperature are achieved plus the overall temperature profile is very different. Unlike the counter-current configuration, the combustion mass flow is increased when the temperature of the bed is low and is reduced when the final temperature of the bed is too high. The combustion flow needed to achieve 500°C in a co-current configuration is 0.375 kg/s (1.35 t/h).

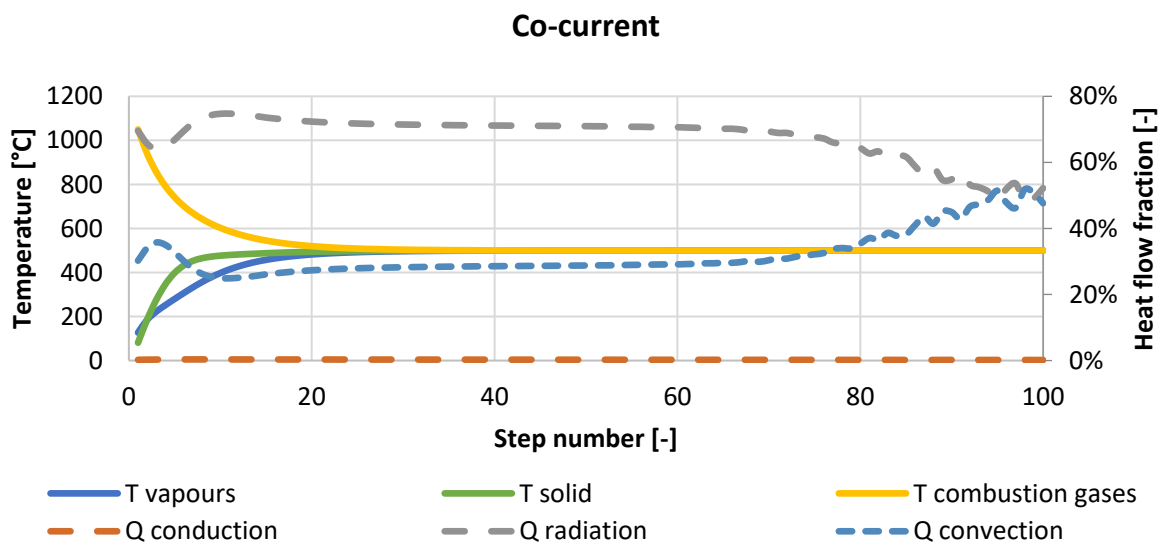


Figure 7.7: temperature profile and heat flows proportions on co-current configuration

There is a big difference between the co-current and counter-current configuration for gas flow and temperature profiles. Both reactors are identical, and the only change is the configuration. For the solids, a mass flow of 3t/h the counter-current configuration needs 10.8 t/h of combustion gases and the co-current 1.35 t/h when the target temperature is 500°C. The energy usage for each is different; in the counter-current configuration, the combustion gas temperature is reduced until it is approximately the same target temperature as for solids before entering the reactor. To achieve this temperature, much heat from the combustion gases has to be used. The large heat content within the combustion gases could lead to a surplus of energy and provide excess heat in the process due to the high combustion gas flow. In the co-current configuration, the combustion gas retains some heat when it exits reactor, and it can be utilised elsewhere within the plant providing energy integration options.

The large combustion gases flow needed for counter-current configuration originated from the combustion of the permanent gases produced in the reactor whose yield is around 30-40 wt.%. It would mean that a 3 t/h input capacity would produce around 1 t/h of gas, and the need for the counter-current configuration is 10.8 t/h, more than ten times the flow of permanent gases produced. The co-current configuration needs, approximately, slightly higher than one-third of the pyrolysis vapours, and it would be feasible if oxygen is used to combust the pyrolysis gases. Nevertheless, there is some energy left from the combustion gases to use in other parts of the plant, such as the dryer.

Besides the flow of combustion gases, the kinetics gain importance in the configuration discussion. It is well known that the reaction rate is higher with increasing temperature because the kinetic constant evolves according to the Arrhenius expression (Equation 5.8). Due to this, it is clear that the preference is for co-current configuration. This arrangement achieves the final temperature faster than the counter-current configuration. It means that for the co-current configuration, the bed of solids remains longer at the final temperature and favours a higher conversion in the reactor with either shorter reactor lengths or solids residence time.

#### 7.3.2.1.4 Flow of carrier gas

Another aspect to consider in the design of a rotary kiln is the carrier gas. This aspect heavily influences the heat transfer model because it implies the presence of gas at the beginning of the reactor. The carrier gas provides an atmosphere for the reactor and reaction. In the absence of carrier gas, the atmosphere is composed of the moisture content evaporated from the biomass and the

pyrolysis vapours produced. Ideally, the model should give the user the choice of using carrier gas or not inside the reactor, and introduce the flow manually, or give a recommendation if it is needed.

According to the industrial experience gained during the project [3, 5, 6, 23], the nitrogen flow into the reactor is one-third of the solids mass flow as a rule of thumb. This principle was applied until all the models were integrated. When the carrier gas flow was modified, the model collapsed due to an overflow of the variables. This was due to a large amount of heat being transferred to a small mass flow of carrier gas, which leads to a dramatic temperature increase and the collapse of the next iteration. The model was pushed to the limit and, when no carrier gas is required, the model will automatically establish a value thirty times lower than the solids mass flow, because otherwise, it collapses. Conversely, an increase in the flow of carrier gas does not make the model collapse but modifies the flow of combustion gases. This is one of the boundary conditions of this project; the gas flow cannot be lower than one-thirtieth of the mass solids flow.

To adapt the model to a zero flow of carrier gas, a solution would be to tell the model that the reactor only includes solids and the combustion gases, until a certain amount of gases is produced, either by the evaporation of moisture content or the degradation of the solid.

#### 7.3.2.1.5 Particle size

One of the most challenging parameters to include in the model was the particle size. This parameter has a unique influence, so a section is included in the heat transfer chapter to explain it (Section 3.5.1). The only parameter affected by the particle size is the voidage. This could lead to a more in-depth discussion about the effect of particle size on heat transfer. The model assumes the heat transfer reaches equilibrium for every single step. If the model is not considered steady-state but transient, this might not be fully accomplished. For a more in-depth study and higher accuracy, CFD would be needed for the simulation, a situation that is not feasible within the scope of this project.

As a further development of this model to estimate the temperature of the particle if the process was to be considered transient, is by applying a coefficient multiplying the heat to solid (Equation 7.20). This coefficient ( $<1$ ) reduces the heat transfer and lowers the exit temperature approaching a more realistic condition if the transient state is considered. This coefficient should be applied to the heat from wall to solids and the reactor gases, to avoid inconsistencies in the model.

For total accuracy, the use of CFD is indispensable, but its complexity makes its implementation in the current model impossible. The model already takes some time to calculate all the parameters without considering the fluid dynamics.

## 7.4 Kinetic model

The kinetics are mostly integrated into the spreadsheet rather than the algorithm. In the chapter where the kinetic model is described (Chapter 5), the dependency of the kinetic constant on the temperature with an Arrhenius expression (Equation 5.8) is explained. This aspect was challenging to implement in the algorithm because there are three feedstocks with different mechanisms, the number of steps in the reaction, and pre-exponential and activation energy values for each step. These are defined in an auxiliary column on the spreadsheet whose values depend on the feedstock. This column contains the coefficients to calculate the char yield as a function of the temperature.

The raw materials used in this project are lignocellulosic biomass and RDF, which consists of cellulose, hemicellulose and lignin, and other components. According to the literature [24], cellulose does not start decomposing below 180 °C, so an initial reaction temperature is needed. This initial temperature is the minimum temperature the bed of solids needs to reach to start reacting. Otherwise, it would be considered as degradation, rather than reaction. The minimum temperature is

rounded to 200 °C, and the average bed temperature is used for the calculation of the kinetic constant. This last statement may lead to some inaccuracies. With a co-current configuration, the temperature of the bed increases rapidly, and the reaction temperature and final temperature are reached during the early steps. The number of steps for which there is a big difference in temperature (larger than 20°C) and reaction is negligible in comparison with the total (around 15%). The kinetic constant calculation accounts for the step number of the reaction. The solution to this issue is explained below with the calculation of the exit conversion.

Once the kinetic constant is calculated when a specific temperature is achieved, the model considers the reaction order and the residence time for that step. The main challenge is the difference in the number of steps dependant on the feedstock, which changes the reaction order ( $n$ ), pre-exponential factor ( $k_0$ ) and activation energy ( $E_a$ ). To solve, the model accounts for a limit (350°C) for which the second steps in the reactions are more significant. From the three feedstocks, only the RDF had a second reaction step. To make the implementation easier, a second step was implemented for all the feedstocks. The key is the identical value of the parameters for the lignocellulosic feedstock (whose decomposition is represented in a single step) and the change for the RDF. In the case of RDF, the values of activation energy and pre-exponential factor to calculate the kinetic constant change when temperature surpasses 350°C and before.

With the pre-exponential factor and the activation energy, the kinetic constant is calculated. The critical aspect for the model is the conversion of the feedstock into products. Equation 7.25 and Equation 7.26 show the method to calculate the conversion for each step. The letter  $\alpha$  is the value of the conversion (Equation 5.25), and it refers to the conversion at the entrance of the step ( $\alpha_{in}$ ) and the exit ( $\alpha_{out}$ ). The initial conversion of the reactor is 0, and at the end, it must be approximately 95 wt.% (more information on section 7.5.1). The influencing factors are the kinetic constant ( $k$ ) and the residence time for each step ( $\tau$ ). The difference between the expressions when the reaction order is one or more is due to Equation 7.27, where the reaction order affects the path to solve the integral. In this equation, the residence time is defined as the difference between the time the feedstock enters and exits that particular step.

$$\alpha_{out} = 1 - (1 - \alpha_{in}) \cdot e^{(-k \cdot \tau)}$$

*Equation 7.25: conversion out with first reaction order*

$$\alpha_{out} = 1 - [k \cdot \tau \cdot (n - 1) + (1 - \alpha_{in})^{1-n}]^{\frac{1}{1-n}}$$

*Equation 7.26: conversion out with reaction order different from one*

$$\int_{\alpha_{in}}^{\alpha_{out}} \frac{d\alpha}{(1 - \alpha)^n} = \int_{t_{in}}^{t_{out}} \frac{dt}{k}$$

*Equation 7.27: variation of conversion with the time*

During the conversion of the biomass, gases are released and modify the gas composition and hence the properties that affect reactor performance, such as velocity, heat capacity or viscosity. The mass flow of solids is measured in dry tonnes per hour, and the production of gases through evaporation and feedstock degradation is measured differently within the model. The heat transfer submodel and reactor slices include the variation of moisture content within the feedstock. This moisture content is expressed in weight percentage of the dry feedstock. Nevertheless, there are two series of extra rows where the flow of gas is indicated, in and out, for the components mentioned previously and water. The difference between the entrance and exit for the specific slice is calculated for each component. In the case of water, there are two streams, the evaporation that is calculated by mass flow in and out that comes from moisture content, and the flow produced from pyrolysis.

To calculate the gases produced the information from Table 5.17 and Table 5.18. The gases produced from the degradation of biomass are calculated to find the exit flows of each gas of an individual step. The difference between the input and output of gases is written in a series of rows, which calculates the amount of gas that is produced from the solid to calculate its composition. These values are employed for the calculation of the gas properties, and amend the gas phase from the reactor.

## 7.5 Integration of the submodels

The three parts of the model (bed of solids, heat transfer and kinetics) are integrated into the primary model, and they complement each other to simulate the behaviour of a rotary kiln. It works for the specific design capacity and calculates the temperature profile and final conversion with a target final temperature. The model runs a reactor and automatically adjusts the combustion gases flow to reach the final temperature at the end of the reactor. Some aspects must be tested to ensure the adequate performance of the reactor and to find the limits.

As a first approach, the influence of the flow of combustion gases on the conversion and final bed temperature was studied. The initial conditions in Table 7.1, and Figure 7.8 shows the result of this first analysis. Since the layout of the combustion flow is co-current, the temperature of the bed of solids increases with the flow of combustion gases. A higher temperature at the end means that the solid degrades more due to a larger kinetic constant and reaches a higher conversion. This first approach prompted a query because all values are valid for a simulation of the process, but in case something changed, it would be difficult to relate and compare the values obtained. For instance, the model could design a reactor with the same length that can be used for two different capacities and conversion values would be different. The same situation would occur when the capacity is constant, but the final temperature changes. It is clear the need for a criterion to compare the mechanical design of different reactors.

Table 7.1: Initial conditions

|                               |           |
|-------------------------------|-----------|
| <b>Solids input</b>           | 3 t/h     |
| <b>Carrier gas input</b>      | 1 t/h     |
| <b>Moisture content</b>       | 10 wt.%   |
| <b>Feedstock</b>              | Woodchips |
| <b>Radius</b>                 | 1.25 m    |
| <b>Length</b>                 | 7.87 m    |
| <b>Kiln Angle</b>             | 1 °       |
| <b>Rotational Speed</b>       | 1.9 rpm   |
| <b>Initial filling degree</b> | 15%       |
| <b>Final filling degree</b>   | 10%       |

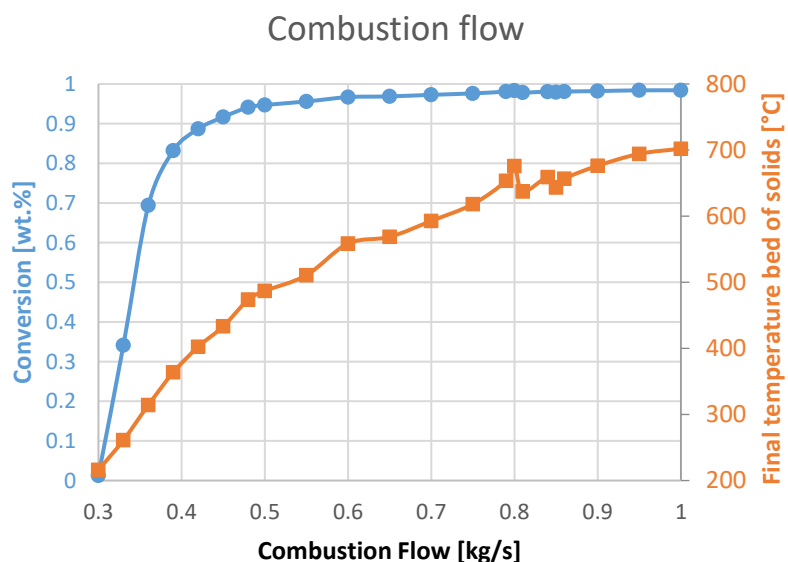


Figure 7.8: Variation of final temperature and conversion with flow of combustion gases

The criterion to obtain comparable values of mechanical specifications of the reactor is the conversion to achieve a value of 95 wt.%. It is very ambitious to obtain an exact value of conversion



(similar to the target temperature). Instead, the conversion should belong to the range [94.51-95.49] wt.% whose rounded value is 95 wt.%. The conversion value assigned as an objective is not arbitrary, it is deduced from Figure 7.8 and the impossibility of reaching full conversion but the feasibility of reaching the value established. The target value is high enough to ensure biomass is highly converted.

### 7.5.1 Target conversion

Several parameters can influence the final conversion, either directly or indirectly. Some affect other variables such as the length of the reactor, which inherently affects the residence time. There are some parameters, which need others' modification to be studied. For instance, an amendment in the radius of the reactor involves a modification in the rotational speed to ensure a Froude number value of  $10^{-3}$  (Equation 3.1). The four studied parameters are the initial filling degree, rotational speed (whose study keeps Froude number within the rolling motion range [ $10^{-2}$ - $10^{-4}$ ]), radius, and kiln angle. To study the parameters, the methodology is similar to others used previously in this work such as Figure 3.2 where the maximum value is shown in the legend within square brackets and the X-axis is the normalised value of the represented parameters. Figure 7.9 shows the results of this analysis for the four parameters. Next to the legend, there is a value between square brackets, which represents the maximum value that the parameter has been assigned. The percentages along the X-axis are the fraction of that maximum value. The standard values for the other experiments are from Table 7.1. The flow of combustion gases is re-calculated for each simulation, and it is not constant, but the final temperature does not change and is fixed at 500 °C.

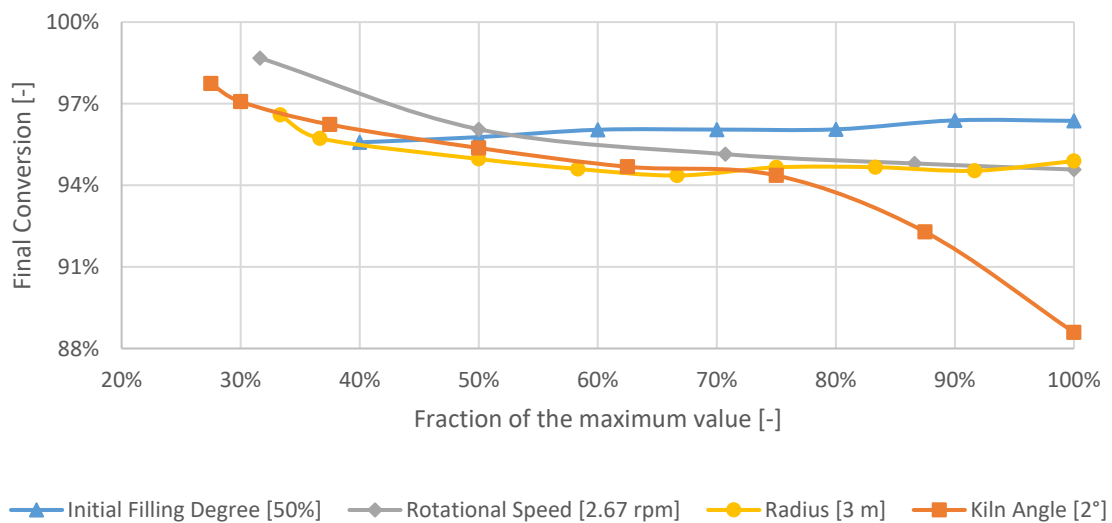


Figure 7.9: Sensitivity Analysis for the conversion

The **initial filling degree** does not affect the conversion significantly. The variation in conversion is around 1% and increases when the initial filling degree rises.

A more filled reactor would require a higher power demand to rotate it. The reason to have a higher conversion at larger filling degrees is an increase of the residence time through the angle of the bed of solids, besides a longer length of the bed of solids. The capacity is constant, but there is more material inside the reactor, which means that it stays longer inside. The reason behind such a small variation is probably due to heat transfer limitations that the maximum-minimum distance (MMD) increases and it takes more time to reach the final temperature.

The link of **rotational speed** with conversion is mainly through the connection with the residence time and the length of the bed of solids (Equation 3.2). The rotational speed influences both the length of the bed of solids and the residence time. A higher rotational speed makes the bed of solids and the residence time shorter because solids move faster towards the end of the reactor. This parameter is more significant than the initial filling degree because it reduces from 99% to 95% when rotation increases from 0.85 to 2.7 rpm. The modification of this parameter involves the amendment of the Fourier number, and the rolling motion can be compromised.

The third parameter that can be modified is the **radius**. Its amendment influences the rotational speed to adjust to a Fourier value of  $10^{-3}$ . The influence is lower than the rotational speed, and it can be freely amended to obtain a higher or lower conversion value. The variation is more significant than others because the conversion range is [94.9%-97%] within this study.

The **kiln angle** is the final parameter studied. It is the most influential parameter on the conversion because it has a high effect on the residence time and the length of the bed of solids. When the reactor angle has increased the length of the bed and the residence time is drastically reduced, which gives a range of conversion values of [88.6-96%]. One of the issues with the angle is the difficulty to achieve the final temperature when the angle is increased because the length of the reactor can become very short. Very low values mean having a length of 2.1 meters and 2 minutes residence time for 3 tonnes per hour reactor when the angle is  $2.5^\circ$ , which seems too low compared to the other results.

The two selected parameters to achieve the conversion value are kiln angle due to its strong influence, and the radius due to its simplicity and the potential effect on the movement of the bed. When the conversion is low, a smaller value for the angle or the radius is needed. The actual values are multiplied by 0.99 and replaced in the spreadsheet to recalculate necessary parameters. If the conversion needs to be decreased, a value of 1.01 is used to increase the value of the variables multiplies the radius and kiln angle. The model checks that the values for the length and the residence time of solids are positive. One of the potential reasons for a negative value is the combination of sines, cosines and other trigonometric functions and its high variability which, combined with sums and subtractions, could give a negative number for the bed of solids or residence time. This aspect is accounted for in the model. If the value is not correct, it returns to the former value. It varies the radius exclusively and, if it remains negative, returns to the former value of the radius and modifies the kiln angle. If the values are still not valid for the positive length of the bed of solids and residence times, 1.005 and 0.995, respectively substitute the variation coefficients 1.01 and 0.99. For each simulation and variation of the radius and/or kiln angle, the simulation to adjust the combustion gases flow and analysis of final conversion value are conducted.

## 7.5.2 Convergence and consistency

Within the algorithm for heat transfer (7.3.2.1.1), there were several parameters to control, measure, and mitigate the divergence of the calculations. There is a counter up to 32,500 iterations for loop 1 (Figure 4.13) and a second counter up to 100 for the second loop. The difference between the input and output of a single step was established as  $2^\circ\text{C}$  if the bed or gases were surpassing the wall temperature. The second counter has a much lower value to determine divergence. During the simulations, it could be observed that the model swapped between two values in a single cell, especially when it is related to the evaporation of water. Initially, the value was the same as the first loop but was reduced to 100 to reduce the simulation time.

When the model is running, there is a set of cells which indicate the number of iterations for loop 1 and 2, and temperature difference between entry and exit for each component. The model

counts the number of times the value 32,500, 100 and 2 or -2 appear in the cells. These counters allow the user to observe the consistency of the model and the results obtained. Examples of convergence are shown in the results chapter 9. As a general rule, the lower the numbers, the more consistent the results.

During the simulation, a group of cells shows the conversion, combustion gases flow and char yield from the previous convergent set of values. This helps the user understand how close the model is to 95 wt.% conversion and for testing of the model for the boundary conditions.

### 7.5.3 Boundary condition and initialising the model

With all previous steps implemented in the model, it calculates the outputs automatically. The model is tested under different conditions to detect the limits where the results do not converge. The two parameters studied were the final temperature and solids input capacity.

The study of these two variables demonstrates the boundary conditions of the model. In the results (Chapter 9), it is seen how the model easily deals with capacities higher than 100 kg/h. That would be one of the boundary conditions of the model although it is still capable of design reactors down to 40 kg/h with less than ten divergent steps in the reactor for the first and second loop. It could be advised that flows lower than 40 kg/h are not reliable.

The other parameter is the final temperature. The algorithm and the model were designed for a reactor with 3 t/h capacity and a final temperature of 500°C as average temperature for pyrolysis. For higher temperatures, the target conversion is easily achieved, although there is a limitation. On the equation to calculate the yield of pyrolysis oils (Equation 5.56), one of the solutions for the third-degree equation is 782 °C. A higher temperature would give a negative value of pyrolysis oil, which would not happen in reality.

To ensure a proper operation, the upper limit of the model is established as 700 °C and avoid values with negative yields. Furthermore, a very high temperature can lead to a very short reactor and residence time. An example would be a 5.7-metre reactor whose solids residence time is 2.7 minutes for a capacity of 3 tonnes per hour, achieving a conversion of 98 wt.%. In these cases, the calculations, especially for the flow of combustion gases, are not consistent. The residence time of the solid is so short that the heat flows and combustion gases flows are very different due to time restrictions to achieve the final temperature. If the feedstock remained for longer inside the reactor, the final conversion is higher than the objective of 95 wt.%.

Unlike the capacity, which is reduced to 10 kg/h despite the divergence of the steps, the solution is not always found when temperature decreases. It is found that the lowest temperature limit for the design is 400 °C. The trial with 350°C for 3 t/h resulted in a length of 238 m and solid residence time of 2 months, but the conversion value was below 94 wt.%. The reason for this is that a low temperature that slows down the degradation, and the resulting kinetic constants are too low to transform the biomass within the model. Therefore, when the temperature is high, the design needs shorter lengths and solids residence time, whereas longer solids residence times and lengths are sought with lower temperatures.

There is also a need for initialising and restarting the model. If two sets of conditions are very different, the model may collapse. For instance, if the model is used to calculate a 3 t/h reactor, the flow of combustion gases could be adequate for such a flow but high enough to make others collapse. If the capacity is changed to 100 kg/h, the model likely collapses due to having a combustion gas flow for a capacity thirty times higher than the actual. The calculation of the radius can be tricky because each simulation can take a long time, and the angle and radius be very different depending on the

initial value. This means that if the new calculation starts with a value for the angle and capacity depending on a former run of the model, the final value of the angle and the radius may become unrealistic. Values from previous simulations should be cleared before starting a new simulation and provide the model with values that will not make it collapse.

To avoid divergence and collapse of the model, a function to establish an initial estimation of the radius and the flow of combustion gases is created. These functions aim to initialise the model giving initial values that are close to the target when the user decides to restart the model for a new calculation once the results have been obtained. These functions act as an initial estimation, but the model overwrites the values during the automatic process. To create the functions, the data from radius and flow of combustion gases flow (for a final temperature of 500 °C) are collected and represented against the capacities. Both correlations are shown in Figure 7.10. The blue axis and line are connected to the data for radius, whose variation with capacity follows a power function, and the expression for its initial estimation is Equation 7.28.

For the combustion gases, the flow variation is linear, represented by the orange line and axis, and Equation 7.29. The linear behaviour seems appropriate because the combustion gases are used as a heat source, and if the solids feed rate is doubled, the amount of heat needed to increase its temperature to the same temperature should be approximately twice the original value. This value of combustion flow gases is used when the model restarts to give an initial estimation of the flow of combustion gases needed to reach a temperature of 500 °C based on the capacity. This estimation is needed to avoid divergence and overflow of the model if the flow of combustion gases is too high for the capacity estimated. From an initial temperature of 500 °C, the model recalculates the flow of combustion gases to achieve the target temperature. The other value that is restarted with the radius and the flow of combustion gases is the kiln angle. It is restarted to 1° as a starting point for the calculations because it simplified the calculations and gave consistent results.

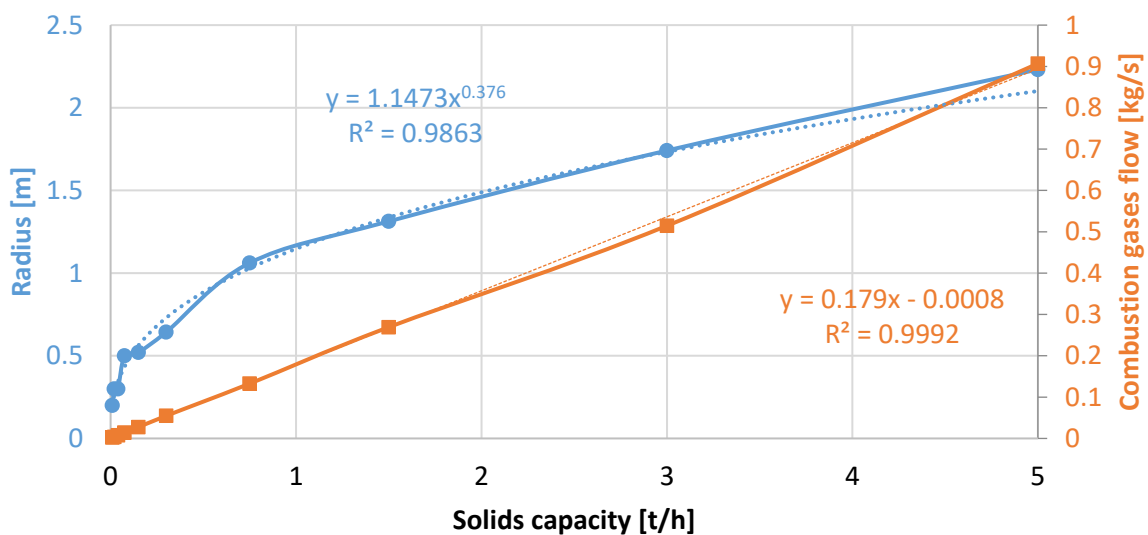


Figure 7.10: Radius and combustion gases flow dependency with solids input

$$R_0[m] = 1.1473 \cdot \left( \dot{m}_{solids} \left[ \frac{t}{h} \right] \right)^{0.376}$$

Equation 7.28: Initial radius

$$\dot{m}_0^{comb} \left[ \frac{kg}{s} \right] = 0.179 \cdot \dot{m}_{solids} \left[ \frac{t}{h} \right] - 0.0008$$

Equation 7.29: initial combustion gases flow

## 7.6 Outputs

The outputs from the model are represented in a different tab, where they are divided into several sections (see Figure 9.4 for the user interface). Firstly, the reactor section gives all the mechanical specifications with the radius, diameter and kiln angle. The flights' section gives the number of flights. The products give both the yields and the flow of every product (char, condensable vapours and non-condensable vapours). The yields are calculated on a dry basis to show the proportion of biomass transformed into each product. The total flow of each product is calculated on a wet basis.

The section for the process details the residence time of solids and vapours, rotational speed, final temperature of the wall, bed of solids and vapours, the heat needed, combustion gas flow and composition, the configuration of combustion gases and voidage. The process section contains a cell in which the heat provided by the combustion gases (combustion enthalpy of the gases multiplied by the flow) is divided by the summation of combustion enthalpies of the non-condensable gases multiplied by the flow of each, to see if the pyrolysis can be autothermal (This aspect is extensively explained on Section 6.3.2.1). There are three more cells where the number of divergences is shown to see how consistent the model is. There is a graph to show the temperature profile of solids, reactor gases and wall, together with the feedstock conversion and the char yield. An example of the graph is given in Figure 7.11, created for 3t/h woodchips with 10% moisture content and a final temperature of 500 °C. It could seem there is a position on the reactor where the char yield decreases. The reason is that the conversion on those positions is lower than the target, with values from 70-80%. The conversion into char implies further devolatilisation of the feedstock with lower solid mass flow but increasing conversion.

The outputs from the final model give a reactor based on the inputs from the user. This model could obtain different values if the initial conditions and approximations (7.5.3) were different. This means that this is not the only solution and, although infinite solutions exist, this model is capable of designing any reactor automatically when inputs are given, which is the innovative factor of this work.

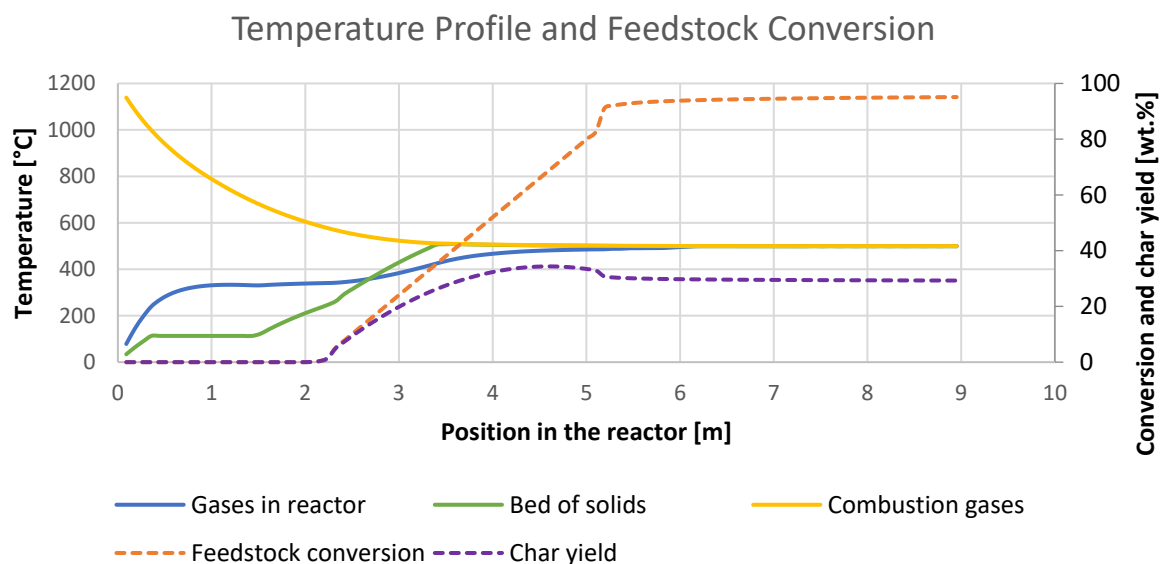


Figure 7.11: Graph from outputs

## 7.7 Adaptability to other processes

This model is designed for the thermochemical process of pyrolysis in a rotary kiln for which there is a wide variety of applications. This model is mainly fixed for pyrolysis, but it can be adapted to other processes if some parameters are changed. There are two processes to which this model could be adapted: torrefaction and drying. This part describes how this model could be adapted.

- **Torrefaction:** the torrefaction process could be simplified as pyrolysis at a lower temperature to degrade the feedstock into a torrefied product. The adaptation of the current model to torrefaction could be easily made if it is supposed that the kinetics for both processes are identical, a fact that seems reasonable because both processes are characterised by a lack of oxygen with increasing solid temperature. The main modification would be the target conversion because torrefaction does not remove all volatiles from the feedstock. In torrefaction, the term Anhydrous Weight Loss (AWL) is generally employed to describe how much the feedstock devolatilised and it is the opposite of char yield. This AWL usually has a value around 25-35wt.% (dry basis), which means that the torrefied product is 65-75 wt.%. Since it is approximately double the average value of char, a conversion of 50 wt.% would be suggested instead of 95 wt.%. The rest of the algorithm would be very similar.
- **Drying:** drying is a process whose objective is to achieve a target moisture content. According to this model, there is no kinetics for drying, and it is treated as an equilibrium process. A further study of drying kinetics would be needed to study the moisture release rate for a more accurate model. The mass and energy balance would change because air is typically used for drying and it is generally in direct contact with the feedstock, unlike pyrolysis where the heat source was indirect. This would change to a more simplistic model where only solids and air would influence the performance of the reactor, and the term of the wall would not be needed.
- **Others:** the rotary kiln can be used for other processes such as gasification or combustion, and the model would require further modification in these cases. Firstly and most importantly, the kinetics change and a completely new study with new kinetics should be implemented. The contact between the heat source and the feedstock is direct, and the heat transfer submodel should be modified with that purpose. If there were a flame at the end of the reactor, the contact surfaces and heat flows would drastically change. Each case should be studied separately to see how to adapt the model to the process needs.
- **Existing pyrolysis processes:** lastly, the model can be used for the simulation of an existing pyrolysis reactor, instead of designing a new one. Although it is not meant to be used with that purpose, the model can be re-adapted, and parameters can be changed to skip some calculations and simulate a process. For instance, the length is calculated using Saeman's model within the model, which is not needed to if the reactor is already built. This aspect could be applied to other results such as the solids residence time, or flow of combustion gases. This aspect would be useful to validate the model and see the differences with reality but also to test the performance of an existing reactor under different conditions.

## 7.8 References

1. Babler, M.U., et al., *Modelling and pilot plant runs of slow biomass pyrolysis in a rotary kiln*. Applied Energy, 2017. **207**: p. 123-133.
2. Rolland, M., et al., *Predicting average void fraction and void fraction uncertainty in fixed beds of poly-lobed particles*. Industrial and engineering chemistry research, 2019. **58**(9): p. 3902-3911.
3. Funcia-Muguerza, I., *Presentation of CENER*, J. López-Ordovás, Editor. 2018, CENER: CENER, Aoiz, Spain.

4. Hagenbeek, R., *Visit to a torrefaction production centre*, J. López-Ordovás, Editor. 2018, Torr-Coal: Dilsen-Stokkem, Belgium.
5. Day, C., *Description of an industrial rotary kiln*, J. López-Ordovás, Editor. 2019: EBRI, Aston University.
6. Stein, P., *Rotary kiln design methodology*, J. López-Ordovás, Editor. 2019: EBRI, Aston University, Birmingham, United Kingdom.
7. Rego, F., *Intermediate pyrolysis of biomass in a pilot scale continuous screw reactor*, in *EBRI (Energy and Bioproducts Research Institute)*. Forthcoming, Aston University: Aston University.
8. Basu, P., *Biomass gasification, pyrolysis, and torrefaction: practical design and theory*. 2013: London, UK : Elsevier : Academic Press, 2013. Second edition.
9. Bridgwater, A.V., *Fast pyrolysis of biomass : a handbook*. 1999: Newbury : CPL Press, ©1999.
10. Bridgwater, A.V., *Review of fast pyrolysis of biomass and product upgrading*. Biomass and Bioenergy, 2012. **38**(Supplement C): p. 68-94.
11. Di Stasi, C., et al., *Physically activated wheat straw-derived biochar for biomass pyrolysis vapors upgrading with high resistance against coke deactivation*. Fuel, 2019. **255**: p. 115807.
12. Bahng, M.-K., et al., *Current technologies for analysis of biomass thermochemical processing: A review*. Analytica Chimica Acta, 2009. **651**(2): p. 117-138.
13. Manyà, J.J., *Pyrolysis for Biochar Purposes: A Review to Establish Current Knowledge Gaps and Research Needs*. Environmental Science & Technology, 2012. **46**(15): p. 7939-7954.
14. Meier, D., et al., *State-of-the-art of fast pyrolysis in IEA bioenergy member countries*. Renewable and Sustainable Energy Reviews, 2013. **20**: p. 619-641.
15. Boateng, A.A., *Rotary kilns: transport phenomena and transport processes*. 2008: Amsterdam ; Boston : Elsevier/Butterworth-Heinemann, ©2008.
16. Maione, R., *Modélisation d'un système de pyrogazéification de la biomasse*. 2017.
17. Boateng, A.A., *Additional information for the design of rotary kilns*, J. López-Ordovás, Editor. 2019.
18. Fantozzi, F., et al., *Rotary Kiln Slow Pyrolysis for Syngas and Char Production From Biomass and Waste—Part I: Working Envelope of the Reactor*. Vol. 129. 2007. 901-907.
19. Çengel, Y.A., A.J. Ghajar, and M. Kanoglu, *Heat and mass transfer: fundamentals & applications*. 2015: New York, N.Y.: McGraw-Hill Education, ©2015. 5th ed. in SI units.
20. Ronsse, F., *Modelling Heat and Mass Transfer in Fluidised Bed Coating Processing*, in *Applied Biological Sciences*. 2006, University of Ghent: Ghent, Belgium. p. 349.
21. Bachmann, H.J., et al., *Toward the Standardization of Biochar Analysis: The COST Action TD1107 Interlaboratory Comparison*. Journal of Agricultural and Food Chemistry, 2016. **64**(2): p. 513-527.
22. Kern, D., *Procesos de transferencia de calor*. 1965, México: CECSA.
23. *Torr-Coal*. 2018 [25th June 2019]; Available from: <http://www.torrcoal.com/>.
24. Bryant, C., *Characterisation and Kinetic Study of Pyrolysis Feedstocks from European Project GreenCarbon*, in *European Bioenergy Research Institute (EBRI)*. 2019, Aston University: Birmingham.

## 8 Industrial application

Rotating reactors have been used for many years as part of industries such as the cement industry, for calcination or drying [1]. Rotary kilns in research are at demo- or pilot-scale size, at dry biomass input capacity of tens to hundreds of kilograms per hour, whereas at an industrial scale would be over a dry tonne per hour of input capacity [2-4]. The lack of rotary kilns in research and its description as a standard technology means that industry possesses much of the technology and know-how of the rotary kiln.

Due to the limited amount of information within the literature, the best practice to learn about the design of rotary kilns are visits to industry professionals working with this technology to share knowledge, thoughts and opinions. If possible, this rotary kiln should be used for pyrolysis or at least, torrefaction. The absence of oxygen is crucial in this work; pyrolysis and torrefaction are the only processes where the lack of oxygen is a significant design factor. Rotary kilns for pyrolysis are not common within the industry and research institutes; whereas rotary kilns for torrefaction are more commonplace. The only difference is the reaction temperature, but in terms of general design such as preventing oxygen from getting into the reactor, feeding and collection systems, the operation and design parameters are very similar. Some important aspects, such as the possible pre- and post-treatment steps, are comparable and observed during site visits to analyse alternatives for the pre-treatment of the feedstock and processing steps of the products.

As part of the project, there were visits to six different companies, which formed part of the industrial secondment requirement of the GreenCarbon project. The companies Torr<sup>®</sup>Coal (The Netherlands) and CENER (Spain) have a rotary kiln which is used for torrefaction at industrial and demonstration-scale. Stein Pyrolysis Ltd. is one of the designers of rotary kilns for pyrolysis, which designed the reactor for Biomass Power Projects (BPP). The three sites of Veolia aimed to classify the Municipal Solid Waste and recover energy from it when possible. Finally, Ajax Equipment Ltd. designs screws which can be used as a reactor or as an external part of the reactor, for feeding, collection or moving the solids through the plant. Appendix C has further description of each of the visits.

### 8.1 Knowledge from the industrial experience

A significant amount of time was invested in industrial experience during the development of this research, nearly 300 hours. The industrial experience gave to this work crucial pieces of information that, aligned and analysed together, pushed the work forward towards the final result. They provided real experience, validation and provided insight into similar and different approaches to problems. It helped to understand aspects for the full process design, an industrial point of view to the problem and a real perspective of the use of biomass. The most significant aspects are summarised as follows:

- An industrial rotary kiln for torrefaction with a capacity of 9 t/h has a diameter of 2 m, and the length is 30 m, and it could be used as an initial estimation for the dimensions of an industrial-scale rotary kiln.
- The heat source for the rotary kiln can vary between systems. The use of a thermal fluid should be considered so as the combustion gases surrounding the reactor.
- The variability of the feedstock is large, and the pre-treatment steps ensure absolute magnitudes and properties at the entrance of the reactor.
- One of the most critical pieces of information from industry is the approach to start the design of the rotary kiln. The division of the reactor into several reactors was a turning point in the research.



- Only the transport of material through screws should be carefully considered in the design of the plant. Each piece of equipment has to be thoroughly designed for the correct performance of the whole system.
- The pre- and post-treatment steps should be considered for each specific process. For instance, the plants of Torr<sup>®</sup>Coal and CENER are designed for torrefaction, yet the steps before and after the reactor are different.
- Pyrolysis can target production of any of the three products, even the gas, which is usually employed to produce energy for the process.
- The effect of kiln angle, rotational speed and gravity is not the only method to push the solids through the reactor.
- There are many processes and separation processes that can be done automatically, such as the separation of ferrous and non-ferrous materials.
- During the process design, the start-up and shutdown need extra safety measures. For instance, there is a cyclone which is by-passed in Torr<sup>®</sup>Coal during the start-up to avoid any equipment damage due to former particles inside the reactor.
- The measurement of parameters is typically by correlation, such as the filling degree being measured with the current needed to rotate the reactor in CENER. There is always a parameter with which it can be correlated.
- The solutions for seals, bearings, thrust rollers, thermal expansions and all mechanical pieces from Appendix B are only limited by the imagination of the designer.
- A common biomass input in industry is 3 dry tonnes per hour. It is very rare to find higher capacities than 5 tonnes per hour.

## 8.2 Pre- and Post-treatment processes

Typically, processes treating biomass involve pre- and post-treatment steps for a variety of reasons. The pre-treatment of biomass aims to achieve a more homogeneous feedstock, and sometimes it requires the partial destruction of the lignocellulosic structure [5]. The products could require post-treatment processes for purification or adjusting properties for the customer and final use. The steps for pre- and post-treatment should be customised on each plant design based on the final use of the products and the raw material. The post-treatment processes are initially used to purify the products, but they are eventually used for its upgrading. These upgrades are to improve specific product characteristics depending on the final use. For instance, a low pH pyrolysis oil could lead to corrosion of vessels and pipework, or the existence of chlorine or alkali metals could cause poisoning of a catalyst used for pyrolysis oil upgrading [6].

### 8.2.1 Pre-treatment

Biomass origin can be vast, so as the properties (composition, density, particle size, moisture content and others). The pre-treatment aims to tailor the biomass properties to support and enhance the performance of the system and, especially, the pyrolysis reactor. The pre-treatment steps are divided into four categories: physical, thermal, chemical or biological. Different pre-treatment steps can have the same objective; for instance, the vibratory sieve shaker [7] and washing [8] aim to reduce the ash content. Each system can contain as many pre-treatment steps as required, and none are required if the quality of the raw material is high. Another opportunity is the combination or repetition of several methods for further improvement. This combination and repetition could incur higher capital and operational cost, a key aspect to be considered.

### 8.2.1.1 Physical pre-treatment

Physical pre-treatment involves processes where the biomass or its properties are transformed by the action of physical forces. The most common steps are milling or grinding and extrusion. This section would account for the screening or separation of materials using one of the properties (size, optical properties or magnetic behaviour).

- **Milling:** milling aims to reduce the particle size of the feedstock. The literature uses particle size reduction with different words such as grinding or shredding, whose main objective is always to reduce the particle size. More specifically, the term chipping is employed with the same purpose for herbaceous biomass such as straw, and chopping is employed for woody biomass [2, 9]. Mainly, there are two types of chippers, disk and drum with the different cutting device. Disc chipper has a rotating disk to which the cutting blades are attached, and it is very common on the paper industry. Drum chippers usually control the amount of oversized chips and are more flexible for the type of feedstock [10]. A reduction in particle size aids biomass flow and feeding into the reactors. It enhances the pyrolysis because the temperature gradients within the particle are reduced and leads to a more homogeneous product. However, this reduction is costly and could increase the operational costs of the plant significantly [5].
- **Extrusion:** it is a method to produce biomass pellets under high pressure. Overall, it shapes the biomass as cylinders, and this process increases the volumetric energy density but also reduces the moisture content due to the pressure applied [5]. It may look like this process is contrary to milling because the particle size increases with extrusion. Very small particle size can affect the flowability negatively (see 12C.3.3 for more information about solids handling), so it cannot be transported through the system. In such a case pelletizing is a solution to consider despite the increase in energy demand and operational cost of the plant [11].
- **Vibratory sieve shaker:** the basis of this process is the sieve shaking which separates dirty biomass and fine residues, which go through a screen and are collected. The soil particles are treated as ash content, and this method leads to its reduction. The ash content can be reduced up to by 48 wt.% when the moisture content was 10 wt.%. This removal is reduced to 13.29 wt.% when the moisture content was 30 wt.% for pinewood [7]. It is industrially used in VEOLIA for the separation of glass from the stream as seen on Section C.3.1.
- **Mixer:** The effect of the rotation of a concrete mixer leads to collision of woodchips with each other. These collisions remove the soil particles from the surface of the woodchips. The soil particles are treated as ash content, and this method leads to its reduction. The removal of ash content is over 40 wt.% when the moisture content of pinewood is 10 wt.%, and it is reduced to 8.6 wt.% with 30 wt.% moisture content [7].
- **Hammermill:** the principle is milling the woodchips with hammers (similar to the facilities of VEOLIA on C.3.1). A side-effect is the separation of soil particles from the surface of the biomass. A screen can be installed to remove smaller particles than a specified size. For pinewood treatment, the ash removal was higher than 50 wt.% independently of the moisture content [7].
- **Debarking:** when particles are overall fixed size (trunks), and before milling, there is a possibility to remove the most external layer of biomass called debarking, which is around 8 wt.% of the weight of the biomass. Debarking aims to avoid contamination due to ash-rich compounds (silica and calcium compounds and dirt) on feedstock surface [10].
- **Screening:** this step aims to separate the particles by size through a screen. A common practice is to recirculate the particles with the larger size before the milling step to achieve a smaller particle size and reduce the size of all particles, so the production of residues is lower [10].

- **Others:** there are other separation methods to remove other fractions of the materials. For instance, the ferrous and non-ferrous metal fractions can be separately removed as seen in C.3.1 with magnetic flaps and an Eddy separator with an inverted magnet, respectively. In this chapter, it is observed that people are sometimes used manual separation of materials.

#### 8.2.1.2 Thermal pre-treatment

Thermal pre-treatment steps are processes which require any heating and/or increment of the temperature of the medium and/or biomass to be conducted. The most common process is drying although there are less common methods such as steam explosion, ultrasound and microwave irradiation.

- **Drying:** The main objective is the reduction or removal of the moisture content. Overall, one of the products of pyrolysis is valorised to provide heat to the system. The remaining heat after pyrolysis is usually used in the dryer, due to its high-energy demand [4, 12]. The main advantage is the improvement in the performance of the pyrolysis process, although the disadvantage is a high energy consumption [5]. The most common technique is a rotary dryer (used by CENER on 12C.2), which combines reliability and flexibility during operation. It is very versatile for feedstock processing, but the moisture is difficult to control, combined with larger dimensions than the other types of dryers. Flash dryers use a stream of heated air to enhance heat and mass transfer and remove the moisture content. It requires high installation costs and fine particle sizes, but they are more compact than rotary dryer and temperatures and retention times are lower. Other types are belt dryers (used by Torr<sup>®</sup>Coal on Section C.1) where biomass is spread on a moving perforated conveyor, and the air is blowing through the belt and feedstock material. The belt dryers are versatile on the type of feedstock. A fluidised-bed can also be used to dry the feedstock [10].
- **Torrefaction:** it is the degradation of biomass in the absence of oxygen at a lower temperature than pyrolysis, which means a range (200-310 °C) [13]. The primary purpose of torrefaction is to remove the moisture content and degrade the hemicellulose partially and, with a lesser extent, cellulose [14-16]. The advantages of torrefied biomass is a higher energy density, improved grindability, hydrophobic, lower risk of biological degradation and better flowability for the feeding into the reactor. Torrefaction affects the product properties, like a lower acidity and higher energy density but also yields of pyrolysis oils in the pyrolysis of hardwood and switch-grass pellets [17]. The disadvantage is the need for high temperature (200-300°C) for a pre-treatment step. It can be argued whether torrefaction is a thermal or a chemical process because it involves chemical reactions.
- **Steam explosion (SE):** it is a similar treatment to the activation of char with steam [18], where the material is exposed to saturated steam at high pressure (1.5-5 MPa) and temperature (150-260°C). It is carried out in a closed vessel for seconds to minutes. The process is followed by rapid depressurisation which causes the biomass structure to 'explode' due to the high pressure of the steam. Mainly, SE breaks the carbohydrate linkages and alters the physical properties of biomass. This pre-treatment reduces the hemicellulose in the feedstock, leading to a decrease in the production of acetic acid and stabilisation of pyrolysis oils [5]. The reduction of hemicellulose may be caused by the dilution of hemicellulose into the steam due to the temperatures employed, which are close to the degradation temperature of the hemicellulose (200-380 °C) [15, 19].
- **Ultrasound irradiation:** ultrasounds usually enhance anaerobic digestion and biomass production from sludge. When used for to biomass, it can accelerate enzymatic hydrolysis, leading to the production of sugars for cavitation effects, which leads to the movement of enzyme molecules and opening the surface of substrates [5].

- **Microwave irradiation:** as developing new technology, microwave irradiation has been used to replace traditional heating of biomass. One of the unique features of microwaves is the ability to generate hot spots in the biomass [20]. It requires further study, although some studies showed higher pyrolysis oil and char yields when biomass was previously dried in a microwave oven instead of the conventional [5, 21].

#### 8.2.1.3 Chemical pre-treatment

Chemical pre-treatments include all those processes where feedstock is mixed with another substance to produce a chemical reaction and transformation in the composition or structure of the material. The aim is to amend the presence of inorganic minerals (ash content), present in the form of metal salts that may affect pyrolysis and its mechanism [5]. For instance, potassium is known as a catalyst for the pyrolysis of biomass [6]. The most common processes are water washing, acid washing and the use of ionic liquids.

- **Water washing:** the water is used to wash the biomass, which reduces the dirt and minerals on the surface of biomass particles. The minerals in the structure of the biomass remain in the matrix [5]. In a study from Di Blasi [22], water washing increased the pyrolysis oil yield and decreased the production of char. This effect may be a consequence of higher moisture content within the feedstock. Typically the minerals whose content is reduced are potassium, sulphur and chlorine [23]. The reduction of ash content is higher than 36 wt.% if the medium is water [8]. The main drawback is the need for drying after and the subsequent energy demand.
- **Acid washing:** it is the same process as water washing but using acids. The acids employed are usually strong acids such as nitric, phosphoric or hydrofluoric acid and they reduce the ash content further than water. Sometimes, the acid can have a further effect than the removal of the ash content. For instance, phosphoric acid is applied for higher production of levoglucosan in pyrolysis oils, and sulphuric acid is a frequent pre-treatment step to extract lignin from biomass in the production of paper [5]. The study [24] washed the biomass with deionised water and hydrochloric acid. The acid removed 99% of the ash content (whose final content was lower than 0.01wt.%), whereas the deionised water reduced the ash content down to 1.3 wt.% although there is no further study to see if the acid washing affected any property of the biomass in the study [24].
- **Ionic liquids:** The ionic liquids combine an organic cation and inorganic anion, which are liquids at room temperatures. The main characteristics are low vapour pressure, chemical stability and non-flammability. In the pre-treatment of biomass, it changes the structure of cellulose and removes the ash content, producing a higher thermal resistance [5].

#### 8.2.1.4 Biological pre-treatment

Biological pre-treatment processes are slower, but the energy demand is lower, and hence so is the carbon and environmental footprint. The main processes considered are fungal, microbial and enzymes pre-treatments [5].

- **Fungal:** some white-rot fungi selectively decompose the lignin component during pyrolysis. A consequence is the possibility to reduce the pyrolysis temperature by 1-35 °C to achieve the same conversion of the feedstock. The use of fungus also reduces SO<sub>x</sub> emissions because the sulphur content decreased by 30-45% [5].
- **Microbial:** certain microbes degrade cellulose and hemicellulose components for the production of biogas. It is a cheap process, although it can take several hours or days to increase the methane yield by 25 wt.% maximum [5].

- **Enzymes:** the hydrolysis of lignin is enhanced by enzymes, and the main effect is a higher production of aromatic phenols and hydrocarbons when biomass is afterwards, pyrolysed. The porosity of the char increases when enzymes are used on the pre-treatment step [5].

## 8.2.2 Post-treatment

The post-treatment processes are used to separate the products and upgrade their target properties. The classification for the post-treatment processes is based on the product to improve, and hence, the categories are char, pyrolysis oil and permanent gases. Some of the processes involve more than one product or even three. For instance, the cyclone involves the three components, but it is described in 8.2.2.1 with the char to avoid repetition. Compared to the pre-treatment (8.2.1), the technical information from industry, the post-treatment steps is more limited. Some of the treatment steps are used at laboratory scale and needs transference to industrial scale.

### 8.2.2.1 Char

As the only solid product at the end of the reactor, char is usually separated by gravity from the condensable and permanent vapours. Some small particles are dragged by the vapours and need separation. Char has pyrophoric behaviour when it is hot, which means that it suffers from auto-ignition. All of this leads to post-treatment for the correct transport of the product. Some further improvement of the char, such as activation to achieve a higher surface area is not described within this work.

- **Washing:** similar to the pre-treatment step, washing is an alternative for the solid product. It is especially interesting when the original feedstock is MSW (Municipal Solid Waste) because it possesses the ability to separate the char from the metals (ferrous and non-ferrous) and the inert material as salts. Inert materials and metals are separated in a further step, and the salts are separated from the aqueous stream afterwards [25].
- **Cyclone:** the cyclone aims to remove the remaining char particles in the vapours (condensable and permanent) [25, 26]. Depending on the process, particles from the cyclone are collected due to a high added value [27], whereas in other systems they are recirculated to the char stream and mixed for further processing [26].
- **Cooling:** it is a crucial step to prevent spontaneous ignition when char contacts air (pyrophoric when it is fresh) if the temperature of the char is high [26, 28]. The most common method is injecting cold water in the equipment which transports the char. It can be in a screw [26] as seen for previous technologies [2, 29] or in a fluidised bed [25].
- **Briquetting:** it is a step which makes the handling of the char easier and cleaner [30]. It is better for the production of energy because the char fines have an ash content in a range 10-30 wt.%, unlike the briquettes which have around 5 wt.%. This is due to dirt such as sand, which appears on the surface. Furthermore, it is required for some uses such as household fuel and the commercialisation of the char. For the briquetting process, a mixture of water and a binder (usually starch, molasses or tar and pitch from the char production) is added to the char fines, and another piece of equipment shapes the char to lumps, balls, cakes or other shapes. This equipment is usually described as rollers that press the char to the specified shape. Finally, the briquettes are dried to remove the moisture content and strengthen the products [31]. The term briquetting could be equivalent to pelletizing, which would agree with the plants studied in Appendix C associated with torrefaction. The principle is to agglomerate the char from the reactor into a shape for a higher energy density and easier handling and transport [2, 4, 27, 29, 32].

### 8.2.2.2 Pyrolysis oils

The pyrolysis oils are the condensable fraction of the vapours. One of the main aims of the oils is to use them as transport fuels, and most post-treatment processes focus on that use. Compared to conventional fuels, the pyrolysis oil has a high oxygen content, high solids content, high viscosity and chemical instability [6]. To upgrade it to conventional transport fuel, it needs full deoxygenation and conventional refining [6]. Unlike the gas and char, this section approaches the post-treatment once the pyrolysis oils are separated from the other products and can be decoupled from the pyrolysis process.

- **Hot-vapour filtration:** the filtration is a physical treatment which aims to reduce the ash and alkali content. The hot-vapour filtration aims to reduce the ash and alkali content to lower values than 0.01% and 10ppm, respectively. Therefore, the amount of char is lower although it keeps the catalytic effect and may lead to the vapours cracking, reducing the yield of pyrolysis oil, reducing viscosity and the average molecular weight of the liquid product. The analogy of this process in gasification would be the use of hot gas filters. Due to the physico-chemical nature of the liquid, the filtration with liquids is very complex and usually requires very high-pressure drops and self-cleaning filters if the target particle size is 5 $\mu$ m [6].
- **Solvent addition:** the addition of polar solvents (the most common one is methanol) makes the viscosity twenty times less than the oil without additives [6]. This is a very interesting application because one of the main drawbacks of pyrolysis oil is the high viscosity compared to conventional fuels such as diesel [13].
- **Emulsions:** to replace the conventional fuels, the pyrolysis oil should blend with hydrocarbon fuels to increase its proportion gradually until they can become a completely independent fuel. They are not miscible, and the only solution is the formation of emulsions to avoid engine modification and employ the pyrolysis oil as a fuel [6].
- **Hydrotreating:** aims to remove the oxygen by a catalytic reaction with hydrogen. Overall, the process is conducted at high pressure (up to 20 MPa) and moderate temperature (up to 400°C). The product is a substance similar to naphtha, which requires orthodox refining that can be conducted in a conventional refinery. A typical yield from biomass to naphtha would be 25 wt.% in weight [6].
- **Zeolite cracking:** the aim is the removal of oxygen. To achieve this, all oxygen is firstly transformed into CO<sub>2</sub>, which the zeolite rejects. The versatility of zeolites is one of the advantages because it can operate on the liquid or vapours, and upgrade either the liquids or re-vaporised liquids [6].
- **Aqueous phase processing:** unlike hydrocarbons, a fraction of pyrolysis oil is soluble in water, and most of the soluble substances are the oxygenated hydrocarbons [6].

### 8.2.2.3 Permanent gases

The permanent gases are the remaining stream after the char is separated by gravity and the pyrolysis oils are separated by temperature difference. The most common practice is the combustion of permanent gases to provide energy for the process. The exception to this practice is when the gases are the main product of the system (like in C.3.2) [12].

- **Condenser/absorber:** direct cooling is usually conducted through spray towers [33] or scrubbers [25]. The principle is to use an immiscible hydrocarbon solvent to reduce the temperature of the vapours (condensable and non-condensable fraction) and condense the condensable fraction. The use of an immiscible solvent (highly refined, non-stabilised aromatic-free paraffinic) makes its separation easier. An indirect cooling system is more common at laboratory scale, using Graham (co-current single tube-shell), coil (single counter-current tube-shell), Allihn (cooling jacket) or spiral condenser [34]. At laboratory scale, it is possible to decrease the temperature of the vapours through a combination of a cold-water condenser (5°C) and dry ice condensers (-70°C). These cooling systems are indirect contact and need cleaning after each experiment because there is a condensation of pyrolysis oils on the wall, and the efficiency decreases. Besides cooling methods, the cold-water and dry ice condensers act as separation method between the pyrolysis oils and the permanent gases because the fraction that condensates is separated by gravity and collected in flasks [35].
- **Filter:** the aim of the filter is to remove the solid particles and ash content in the gases. The gas stream goes through filters with hydrogen sulphide, hydrochloric acid or activated carbon to reduce the ash content [25, 36]. An alternative is to use a ceramic filter, which could cause a pressure drop to separate the char from the vapours stream [34]. The last filter used at industrial scale is the bag filter to remove the remaining particles, and it is a filter medium bag at the end of the duct [37]. At a smaller scale, an alternative is to use a cotton wool filter, which will absorb the aerosols from the permanent gases, purifying this stream [35].
- **Electrostatic Precipitator (ESP):** the ESP aims to remove possible aerosols in the flow of permanent gases [38, 39]. It consists of an electrode energised at a specific voltage, creating a magnetic field and remove the remaining drops and emulsions of bio-oil in the gases [40].
- **Polishing:** one of the last steps of the cleaning of the gases is the polishing, to ensure the emissions of their combustion accomplish the current emission limits or the limits to be connected to the gas grid for the production of energy. One of the methods is the addition of ammonia to reduce potential emissions of NO<sub>x</sub> [27, 41].

### 8.3 References

1. Boateng, A.A., *Rotary kilns: transport phenomena and transport processes*. 2008: Amsterdam ; Boston : Elsevier/Butterworth-Heinemann, ©2008.
2. Funcia-Muguerza, I., *Presentation of CENER*, J. López-Ordovás, Editor. 2018, CENER: CENER, Aoiz, Spain.
3. Bradfield, F.L., *Examination of the Thermal Properties of Municipal Solid Waste and the Scalability of its Pyrolysis*, in *Faculty of Engineering*. 2014, Stellenbosch University: South Africa.
4. Day, C., *Description of an industrial rotary kiln*, J. López-Ordovás, Editor. 2019: EBRI, Aston University.
5. Kan, T., V. Strezov, and T.J. Evans, *Lignocellulosic biomass pyrolysis: A review of product properties and effects of pyrolysis parameters*. *Renewable and Sustainable Energy Reviews*, 2016. **57**: p. 1126-1140.
6. Bridgwater, A.V., *Review of fast pyrolysis of biomass and product upgrading*. *Biomass and Bioenergy*, 2012. **38**(Supplement C): p. 68-94.
7. Pradhan, U., *Physical treatments for reducing biomass ash and effect of ash content on pyrolysis products*, in *Biosystems Engineering*. 2015, Auburn University: Auburn, Alabama.
8. Onwudili, J.A. and J.E. Eke, *Effects of ash removal by agitated aqueous washing and sedimentation on the physico-chemical characteristics and fast pyrolysis of trommel fines*. *Journal of the Energy Institute*, 2019.
9. López-Ordovás, J., et al., *Integrated rotary kiln pilot-scale plant for beechwood torrefaction*. Forthcoming.

10. Olszewski, M.P., *The techno-economics of biocarbon production processes*, in *Faculty of Energy and Fuels*. 2016, AGH University of Science and Technology: Kraków, Poland.
11. *Green-Charcoal*, in *Innovation Towards Sustainable Development*. 2004, Pro Natura International: Paris.
12. Day, C., *Basic project configuration for pyrolysis to syngas at 700 degrees in a rotary retort*, in *Research interests - the full scale projects issues - keyword summary*, B.P.P. Ltd, Editor. 2017, Aston University: Aston University.
13. Basu, P., *Biomass gasification, pyrolysis, and torrefaction: practical design and theory*. 2013: London, UK : Elsevier : Academic Press, 2013. Second edition.
14. Kolokolova, O., et al. *Torrefaction and Pyrolysis of biomass waste in continuous reactors*. in *13th International Conference on Environmental Science and Technology*. 2013. Athens: Global Nest, Secretariat.
15. Gašparovič, L., Z. Koreňová, and Ľ. Jelemenský, *Kinetic study of wood chips decomposition by TGA*. *Chemical Papers*, 2010. **64**(2).
16. Chen, D., Y. Zheng, and X. Zhu, *In-depth investigation on the pyrolysis kinetics of raw biomass. Part I: Kinetic analysis for the drying and devolatilization stages*. *Bioresource Technology*, 2013. **131**: p. 40-46.
17. Boateng, A.A. and C.A. Mullen, *Fast pyrolysis of biomass thermally pretreated by torrefaction*. *Journal of Analytical and Applied Pyrolysis*, 2013. **100**: p. 95-102.
18. Tadda, M.A., et al., *A review on activated carbon: process, application and prospects*. *Journal of Advanced Civil Engineering Practice and Research*, 2016. **2**(1).
19. Bryant, C., *Characterisation and Kinetic Study of Pyrolysis Feedstocks from European Project GreenCarbon*, in *European Bioenergy Research Institute (EBRI)*. 2019, Aston University: Birmingham.
20. Remón, J., et al., *Production of bio-fuels and chemicals by microwave-assisted, catalytic, hydrothermal liquefaction (MAC-HTL) of a mixture of pine and spruce biomass*. *Green Chemistry*, 2019. **21**(2): p. 284-299.
21. Wang, X., et al., *The Influence of Microwave Drying on Biomass Pyrolysis*. *Energy & Fuels*, 2008. **22**(1): p. 67-74.
22. Di Blasi, C. and C. Branca, *The Effects of Water Leaching on the Isothermal Degradation Kinetics of Straw*. Vol. 39. 2000.
23. Deng, L., T. Zhang, and D. Che, *Effect of water washing on fuel properties, pyrolysis and combustion characteristics, and ash fusibility of biomass*. *Fuel Processing Technology*, 2013. **106**: p. 712-720.
24. Mayer, Z.A., A. Apfelbacher, and A. Hornung, *A comparative study on the pyrolysis of metal- and ash-enriched wood and the combustion properties of the gained char*. *Journal of Analytical and Applied Pyrolysis*, 2012. **96**: p. 196-202.
25. Malkow, T., *Novel and innovative pyrolysis and gasification technologies for energy efficient and environmentally sound MSW disposal*. *Waste Management*, 2004. **24**(1): p. 53-79.
26. Roegiers, J., J.p. Pieters, and F.p. Ronsse, *Heat and mass transfer modelling of auger reactors*, in *Faculteit Bio-ingenieurswetenschappen*. 2016, Universiteit Gent.
27. Stein, P., *Rotary kiln design methodology*, J. López-Ordovás, Editor. 2019: EBRI, Aston University, Birmingham, United Kingdom.
28. Chong, K., *Fast Pyrolysis of Biomass*, in *GreenCarbon Research School*, GreenCarbon, Editor. 2017, European Bioenergy Research Institute (EBRI), Aston University: University of Ghent.
29. Hagenbeek, R., *Visit to a torrefaction production centre*, J. López-Ordovás, Editor. 2018, Torr-Coal: Dilsen-Stokkem, Belgium.
30. *From biomass to activated carbon (and everything in between)*, F. international, Editor., FEECO international.
31. Stassen, H.E., *Current Issues in Charcoal Production and Use*, in *Biomass Power for the World*, C.P.T.F. Group, Editor. 2015, Pan Stanford Publishing: New York. p. 760.



32. Garcia-Perez, M., T. Lewis, and C.E. Kruger, *Methods for Producing Biochar and Advanced Biofuels in Washington State Part 1: Literature Review of Pyrolysis Reactors*, in *Ecology Publication*. 2011, Washington State University: Pullman, WA. p. 137 pp.
33. Kern, S., et al., *Rotary kiln pyrolysis of straw and fermentation residues in a 3MW pilot plant – Influence of pyrolysis temperature on pyrolysis product performance*. *Journal of Analytical and Applied Pyrolysis*, 2012. **97**: p. 1-10.
34. Papari, S. and K. Hawboldt, *A review on condensing system for biomass pyrolysis process*. *Fuel Processing Technology*, 2018. **180**: p. 1-13.
35. Yang, Y., et al., *Slow pyrolysis of organic fraction of municipal solid waste (OFMSW): Characterisation of products and screening of the aqueous liquid product for anaerobic digestion*. *Applied Energy*, 2018. **213**: p. 158-168.
36. Pundlik, W., et al., *Acid Demineralization and Characterization of Carbon Black Obtained From Pyrolysis of Waste Tyre Using Thermal Shock Process*. *International Journal of Research in Chemistry and Environment (IJRCE)*, 2013. **3**(1): p. 208-212.
37. Zobel, S. and T. Gries, *9 - The use of nonwovens as filtration materials*, in *Applications of Nonwovens in Technical Textiles*, R.A. Chapman, Editor. 2010, Woodhead Publishing. p. 160-183.
38. Yang, Y., *Energy Production from Biomass and Waste Derived Intermediate Pyrolysis Oils*, in *European Bioenergy Research Institute (EBRI)*. 2014, Aston University: Birmingham. p. 185.
39. Peters, J.F., et al., *Experimental validation of a predictive pyrolysis model in Aspen Plus*. 2014.
40. Mochizuki, T., M. Toba, and Y. Yoshimura, *Effect of Electrostatic Precipitator on Collection Efficiency of Bio-oil in Fast Pyrolysis of Biomass*. *Journal of the Japan Petroleum Institute*, 2013. **56**(6): p. 401-405.
41. Prithiraj, S. and S. Kauchali, *Yields from pyrolysis of refinery residue using a batch process*. *South African Journal of Chemical Engineering*, 2017. **24**: p. 95-115.

## 9 Results and discussion

The result of this research is primarily the model created for the design of the rotary kiln for pyrolysis. In this chapter, some of the data produced by the model are shown. Additionally, the user interfaces of the model are revealed: the inputs, outputs, the screen displayed when the model is working and when the model finishes. Furthermore, some aspects of validation are explained, and examples of how the model can be used are provided.

### 9.1 Scenario analysis

Several reactors were designed to test the model and check the efficiency and correct performance under a range of conditions. The parameters that have been varied are the solid feed rate and target temperature. As expected, the radius increases with biomass input, as do the length of the reactor and solids residence time. The value for the kiln angle depends on the starting value of the radius for the whole design, and there is no clear tendency when capacity varies. When the target temperature is changed, the length and kiln angle follow different trends. With lower temperatures, the length is longer and kiln angle lower, caused by the need for longer solid residence times for the conversion of the biomass. Contrary to this, the kiln angle is higher and length shorter when the temperature increases to avoid conversion values greater than 95 wt.%. These variations (higher kiln angle and shorter length) cause the reduction of solids residence time within the reactor to avoid further reaction of the solids.

An example of the information provided for each scenario analysis is given in Table 9.1. The data in blue are the model inputs or data which is pre-defined inside the model. For instance, the number of flights, the losses, or the initial and final filling degrees is defined within the model. The meaning each parameter is explained below.

Table 9.1: Table for Scenario analysis

|                       |                            |                              |                            |                        |                       |                        |
|-----------------------|----------------------------|------------------------------|----------------------------|------------------------|-----------------------|------------------------|
| Capacity [t/h]        | Moisture Content [-]       | Temperature Objective [°C]   | Feedstock                  | Nitrogen Flow [t/h]    | IN Filling degree [-] | OUT Filling degree [-] |
| 3                     | 10%                        | 500                          | Woodchips                  | 1                      | 15%                   | 10%                    |
| Rotational [rpm]      | Combustion gas flow [kg/s] | T comb [°C]                  | T solid [°C]               | T gas [°C]             | T IN Comb [°C]        | T ambient [°C]         |
| 0.69                  | 0.53                       | 501.48                       | 500.19                     | 498.74                 | 1200                  | 20                     |
| Char yield [-]        | Condensable yield [-]      | Permanent yield [-]          | Char flow [t/h]            | Condensable flow [t/h] | Permanent flow [t/h]  | Conv. OUT [-]          |
| 29.16%                | 47.44%                     | 23.39%                       | 0.87                       | 1.72                   | 0.70                  | 95.41%                 |
| Radius [m]            | Length [m]                 | Kiln Angle [°]               | Solid Residence Time [min] | Extra area flights [-] | N flights [-]         |                        |
| 1.88                  | 8.62                       | 1.083                        | 62.30                      | 10%                    | 5                     |                        |
| Start Reaction T [°C] | Limit 32501 [-]            | Counter limit iterations [-] | Froude number [-]          | Qw/H [-]               | Losses [-]            |                        |
| 200                   | 2                          | 2                            | 1E-03                      | 27.19%                 | 25%                   |                        |

- **Capacity:** it indicates the solids feed rate to the model. It is measured in dry tonnes per hour.
- **Moisture content:** the moisture content in the solid feed as a weight percentage.

- **Temperature objective:** to start the reactor design, a target reaction temperature is set for the solids. This temperature has an impact on the estimation of combustion gas flow which provides the process heat. The temperature is selected directly by the user or is implied by the user selecting the desired end-product. The units are °C.
- **Feedstock:** The user can choose from the three types of feedstock (RDF, woodchips and wheat straw).
- **Nitrogen flow:** The flow of nitrogen is a key parameter, and it is indicated in this cell, which shows the amount in tonnes per hour.
- **IN Filling degree:** This term indicates the initial filling degree and relates to the portion (in percentage) of the cross-sectional area of the kiln filled by solids. The value is constant for all calculations (15%) and stored inside the spreadsheet.
- **OUT Filling degree:** As above but related to the reactor exit. The value is set to 10%, which does not change.
- **Rotational:** Is the rotational speed of the reactor, calculated within the model and shown in revolutions per minute (rpm).
- **Combustion gas flow:** the heat source for the reactor are the combustion gases, whose flow in kg/h is calculated to increase the temperature of the bed of solids to the target temperature.
- **T comb:** it is the temperature of the combustion gases at the exit of the reactor, shown in °C.
- **T solid:** This key parameter stops one of the loops within the algorithm for the heat transfer submodel. It is the calculated temperature of the bed of solids at the end of the reactor. It is measured in °C, and it has to be the same as the target temperature with a variation of  $\pm 5$  °C.
- **T gas:** the gases inside the reactor are modelled according to the information provided in the kinetic chapter (Section 5.6) and temperatures calculated. This is the temperature of the mixture of gases inside the reactor, measured in °C.
- **T IN Comb:** this term is the temperature of the combustion gases when they enter the reactor and are shown in °C. In the co-current configuration, it is one of the values established within the model. In counter-current, it is estimated from the calculations of the reactor.
- **T ambient:** The solids and gases entering the reactor need an initial value of temperature (°C) to calculate the next step. This is the ambient temperature in °C.
- **Char yield:** is the fraction of biomass transformed into char, with a conversion of 95 wt.%. It is indicated in dry basis.
- **Condensable yield:** from the vapours in pyrolysis, this value indicates the fraction of the initial biomass transformed into pyrolysis oil.
- **Permanent yield:** the fraction of permanent gases transformed from biomass is shown with this value on a dry basis.
- **Char flow:** the char flow at the exit of the reactor is indicated and measured in tonnes per hour.
- **Condensable flow:** the flow in wet tonnes per of the condensable liquids. The model assumes that all the water is included in this flow.
- **Permanent flow:** indicates the flow of permanent gases at the exit of the reactor in tonnes per hour.
- **Conv. OUT:** the conversion degree is the factor which stops the model when a specific value is achieved with the correct solids temperature; it is shown as a percentage and indicated with this value.
- **Radius:** one of the mechanical specifications, the radius of the kiln for the processing of the biomass, measured in metres.
- **Length:** it represents the length of the reactor, which coincides with the length of the bed of solids calculated by the Saeman's model. It is indicated in metres.

- **Kiln Angle:** one of the characteristics of the rotary kilns is the angle at which the reactor is inclined. It is another of the mechanical specifications and measured in degrees (°).
- **Solid Residence time:** the time that the bed of solids remains inside the reactor is key for the transformation of the feedstock into the product, and it is indicated in minutes.
- **Extra area flights:** one of the assumptions within this project is that the flights add extra contact area, which is shown as a percentage.
- **N flights:** is the number of flights with the same cross-sectional surface.
- **Start Reaction T:** pyrolysis does not happen at all ranges of temperatures; the value at which it starts according to the experiments and literature is around 200 °C.
- **Limit 32501:** related to model consistency this value is the number of steps at which the limit of 32,501 iterations has been achieved for the current calculation.
- **Counter limit iterations:** if there is no better solution, the increase and decrease of temperature is established with a value of  $\pm 2^{\circ}\text{C}$ , depending on the component. This value measures the amount of time the value was employed.
- **Froude number:** to achieve rolling motion, the value of the Froude dimensionless number has to be within the range  $[10^{-2}-10^{-4}]$ . It is displayed to ensure the rolling motion of the bed.
- **Qw/H:** The heat to conduct the process is obtained from the combustion of the permanent gases. This cell gives a preliminary percentage of the heat needed from the wall to heat the biomass compared to the total heat obtained from the combustion of permanent gases.
- **Losses:** is a fixed parameter within the model, and it means the percentage of heat lost from the wall towards inside the reactor.

The analysis of the different scenarios is used to check the performance of the model. Simultaneously, the boundary conditions are established to know the situations where the model collapses during the calculations. The reasons behind the model difficulties are analysed in Section 7.5.3. The boundary conditions and limitations of the model are primarily related to the solids capacity, process temperature and flow of nitrogen carrier gas. In Section 11.2, potential solutions to remove the assumptions through the amendment of the model or by further research are addressed. Some assumptions create limitations within the model, such as particle shape and size or flight configuration.

## 9.2 User interfaces

There are four main user interfaces: The user input interface (Figure 9.1), the simulation interface (Figure 9.2), the interface when the simulation is completed (Figure 9.3) and the outputs interface (Figure 9.4). The screenshots are taken from the conditions in Figure 9.1.

The input interface allows the user to select the biomass capacity and the feedstock type for the reactor design. Some choices are selected from a drop-down list. The temperature for the process is typed by the user or by the user's choice of the preferred product; the model defines the temperature at which that product yield is maximum. The carrier gas flow is defined in the input interface; the user can define this, or a default value is used by the model. The shape of the feedstock is chosen between chips and pellets, and the moisture content indicated. The last choice is the temperature at which the combustion gases (heat source) enter the reactor, or the model uses the predetermined default value (1200 °C). When the user has introduced all data, the grey button "Let's design it" should be clicked for the file to start working.

|                |           |     |
|----------------|-----------|-----|
| Input capacity | 3         | t/h |
| Feedstock      | Woodchips | -   |

|                  |       |     |
|------------------|-------|-----|
| Feedstock shape  | Chips | -   |
| Moisture content | 10%   | wt. |

Choose between defining a final temperature or a targeted product: Final temperature

Final temperature 500 °C

Do you want nitrogen as carrier gas? Yes

Do you want to type the quantity or do you prefer the model to predict it? Decided by the model

The model will calculate the nitrogen flow for the reactor 1 t/h

Choose between Cocurrent and Countercurrent configuration of the combustion gases to heat the reactor: Cocurrent -

Do you want to indicate the temperature at which the combustion gases will enter into the reactor? No

The reactor will estimate it

Let's design it!

Figure 9.1: Inputs interface

The design can take several hours, and the model automatically changes to another tab called test, shown in Figure 9.2. The model is intended to work on its own without further user interaction. The user can view how far the process has progressed by viewing the cell highlighted in blue. This cell shows the conversion (value over 1) from the former successful iteration (target temperature achieved). The estimations for the radius, kiln angle and length are located under the cells *Prev R*, *Prev angle* and *Prev Length*, respectively on the left of that blue cell. The conversion from the previous iteration is the value in blue. The closer it is to the range [94.51%-95.49%], the less time it should take to reach the conversion value and finish the simulations. The other crucial number is to its left, which shows how many times the radius and the kiln angle were modified. This amendment is after the convergence to the target temperature of the bed of solids. These cells appear as “Calculating” when the model starts working. The other important counter is the number below the cell *Iter. Flow* (in the upper left corner of the second picture in Figure 9.2), which is the number of times the process readjusted the flow of combustion gases with the current configuration kiln angle-radius.

| G Comb [kg/s]               | T objective [C] | T in Comb [C]   | T out Com [C] | Tsout [C] | TGout [C] | Water OU   | Conv.       | OUT        | Char Yield | Solid Yield | Iterations | Counter 1 | Limit 325C | Counter 11  | Layout    | Iter. Flow | IterationK | Step processing | Char flow  | Oil flow  |
|-----------------------------|-----------------|-----------------|---------------|-----------|-----------|------------|-------------|------------|------------|-------------|------------|-----------|------------|-------------|-----------|------------|------------|-----------------|------------|-----------|
| 0.52697229                  | 500             | 1200            | 501.484       | 500.185   | 498.74    | 0          | 95%         | 29%        | 31%        | 0           | 0          | 0         | 2          | 2           | Cocurrent | 1          | 100        | 100             | 0.87489    | 1.72328   |
| Length                      | IN Filling      | Deg OUT Filling | De Kiln angle | Radius    | RT        | Moisture   | Mass flow   | Rotational | Froude nu  | Q to solid  | Q to Gas   | Q from W  | H comb     | N (Gs+Qg)/h | Qw/H      | Adjust Ang | Conv. OUT  | Comb gas        | Char yield | Oil yield |
| 8.6204694                   | 0.15            | 0.1             | 1.08286       | 1.87771   | 62.3033   | 10%        | 3           | 0.69023    | 1.00E-03   | 651452      | 2395995    | 0%        | 27%        | 1           | 95.4114%  | 0.52697    | 29%        | 47%             |            |           |
| Standard flow Input G [t/h] | N Void fraction | Initial Rac     | Slope         | Intercept | Prev R    | Prev angle | Prev Length |            |            |             |            |           |            |             |           | LAST CONV  | 7          | 0.9325412       | 0.01243    | 0.36914   |
| 0.53630945                  | 1               | 57%             | 1.79184       | 0.26307   | 0.10672   | 1.87771    | 1.08286     | 8.62047    |            |             |            |           |            |             |           |            |            |                 |            |           |

| Iter. Flow | IterationK | Step processing | Char flow | Oil flow   |           |
|------------|------------|-----------------|-----------|------------|-----------|
| 1          |            | 100             | 0.87489   | 1.72328    |           |
| Qw/H       | Adjust Ang | Conv. OUT       | Comb gas  | Char yield | Oil yield |
| 27%        | 1          | 95.4114%        | 0.52697   | 29%        | 47%       |
| LAST CONV  | 7          | 0.9325412       | 0.01243   | 0.36914    |           |

Figure 9.2: Interface during simulation

When the simulation is completed, the pop-up window appears (Figure 9.3) on the Excel screen, and the Excel icon on the toolbar starts flashing orange when the design has finished.

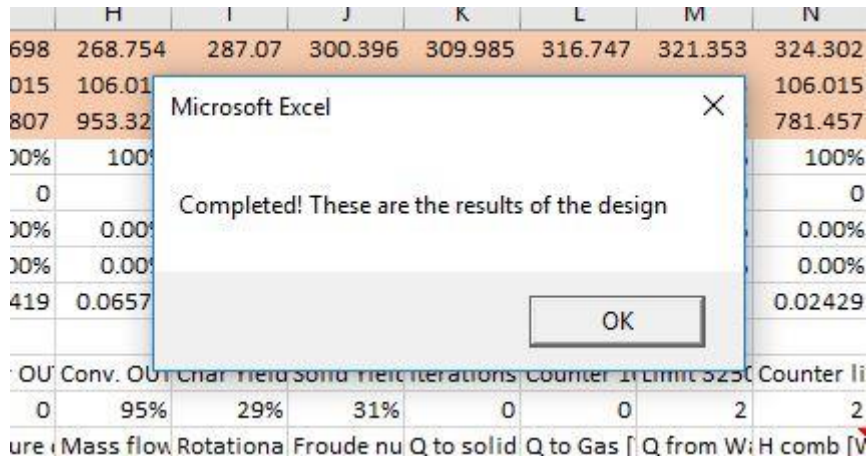


Figure 9.3: Interface when the simulation is completed

The last interface the user faces is the results interface (Figure 9.4), where all the information is displayed. It details mechanical specifications such as the length, diameter and kiln angle of the reactor and the number of flights. The “Products” table displays the yields on a dry basis and the flows on a wet basis. Additionally, the final conversion value is shown together with solid particle size. Several operational parameters are shown in the “Process” table, such as the solids residence time, rotational speed and the final temperatures are displayed. Some details of the combustion gases such as the composition and the configuration in the reactor are also shown. The heat required divided by the combustion heat is the fraction of heat the process needs based on the combustion of the permanent gases. The last table “Convergence” shows model consistency; each iteration could have a maximum value of 100 (one per step), and the other cell can have a maximum of 300 (three per reactor slice): the lower these values, the smaller the number of divergences and more consistency of the results. To restart the model, the user must press the **RESTART!** button. It contains algorithms to estimate values of radius and combustion flow to avoid overflow of the model. A sharp change in the conditions could lead to an overflow and collapse of the model.

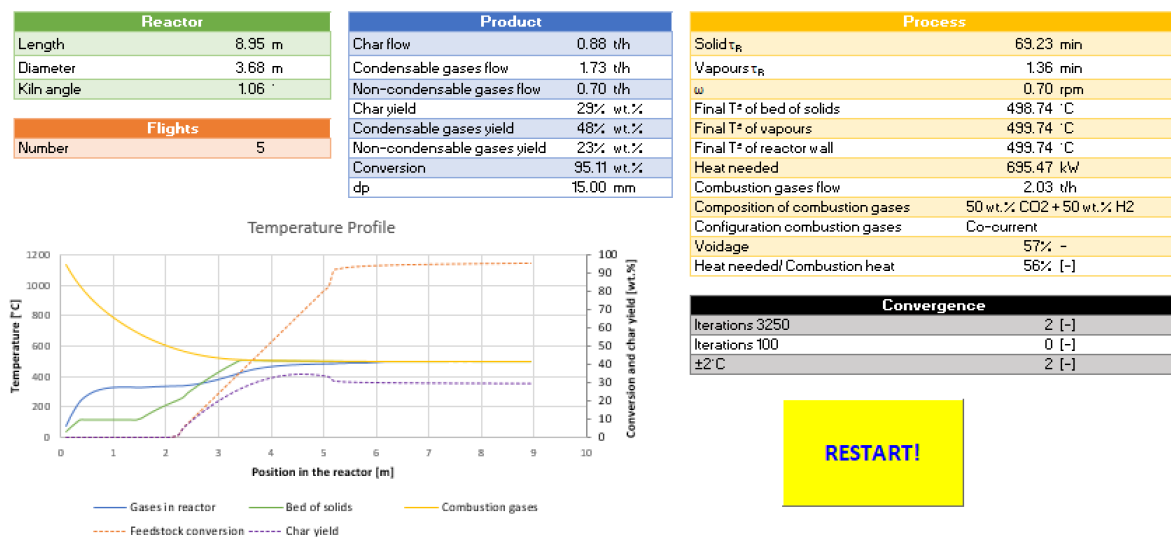


Figure 9.4: Outputs interface validation

### 9.3 Validation of the model

Validation is a crucial aspect to test the model and its similarity to reality. In any research which involves process modelling, validation is used to test model and data reliability. This was the

initial aim of this research, but the use of rotary kilns in research is scarce, and the information from industry is even more limited. For this reason, within this research project, a typical validation process where the results are compared with reality was not possible.

Ideally, to validate the model all the information from the reactor should be considered, such as the filling degree, feedstock, temperature profile of solids and gases, residence time and the radius and reactor length. This information is not always measured and available, and the validation may not be as accurate as desirable. The indispensable aspects to consider a validation successful would be the profile temperature, product yields and distribution, filling degree, and residence time. Studying how these aspects match reality ensures a successful study of the validation. From all the elements, the filling degree may be the most difficult to measure, although a very accurate measurement is not needed because some other aspects such as the length are determined in an actual reactor. The aim of having a filling degree estimation is desired to ensure that the heat is transferred similarly to this model.

Although information from real processes is not collected and compared with the model, the model has been partially validated, so there is a level of confidence in the results. Also, some of the calculations are analysed to see how they could agree with reality. The model was discussed with various industrial stakeholders throughout development, to validate according to industrial best practice as far as possible.

### 9.3.1 Stein Pyrolysis Ltd.

During the meetings with Stein Pyrolysis (extensively described in Section C.3.2), the methodology developed was discussed to ensure the calculations were following the steps a kiln designer usually follows. The formulas used for heat transfer were validated by experts at Stein Pyrolysis (see Chapter 4 and Section 7.3), explaining that they had been employed for the design of rotary kilns within industry, which were working according to the calculations. This step is especially important to ensure the heat flows are correct, and the temperature for each slice and component is similar to reality.

This company had expertise in the design of rotary kilns, and the approach was from a mechanical point of view to ensure the heat was well distributed, instead of a chemical engineering point of view where the reaction rates are the critical step.

### 9.3.2 Auto validation with the model

Another less conventional method for the validation of a process is the critical analysis of the results, using engineering common sense and how they match reality. This method is less conventional, but it serves to see the tendency and if the model follows the right path from a logical point of view.

There are two aspects to analyse, the evolution of the radius and the flow of combustion gas with the biomass input capacity and process temperature. For instance, if the flow rate of biomass is twice as large, the heat requirement and flow of combustion gases are expected to be something around twice the initial value. In addition, the radius is likely increased when the biomass flow increases, although the tendency is not linearly proportional as with the combustion gases flow.

Figure 7.10 in Section 7.5.3 shows the correlation of combustion gas flow and radius with capacity when the target temperature is 500 °C, and it is used to give an initial estimation of the flow of combustion gases and radius within the model. Table 9.2 shows the evolution of radius and combustion gas flow with biomass capacity. The final row called coefficient is the division of the flow of combustion gases by the biomass capacity to see how proportional this correlation is. The resulting

values are very similar, and the standard deviation is lower than 5.6% and mainly produced from the estimation where biomass capacity is 0.01 t/h (10 kg/h), for which the model did not converge consistently. It should be considered that the values of solids temperature are not precisely the same and there may be a difference up to 10 °C (from 495 to 505 °C) and that could be the reason for the variation. The heat losses are also included in this flow of combustion gases. As anticipated, the results show a more significant need for combustion gas flow with larger capacity, as well as the need for a larger reactor (radius) when capacity increases. The only exception is the constant value of the radius between 40 and 20 kg/h, caused by very similar starting values for the radius. However, the lengths of the beds of solids are 2 and 1.35 meters, respectively, which corresponds to bigger reactors for larger capacities. Similarly, the heat demand is higher when the biomass capacity increases.

Table 9.2: Relation radius and flow of combustion gases with biomass capacity

|  |      |      |      |      |      |      |      |      |       |       |
|--|------|------|------|------|------|------|------|------|-------|-------|
| <b>Radius [m]</b>                      | 2.23 | 1.74 | 1.31 | 1.06 | 0.64 | 0.52 | 0.50 | 0.30 | 0.30  | 0.20  |
| <b>Flow of combustion gases (kg/s)</b> | 0.91 | 0.51 | 0.27 | 0.13 | 0.05 | 0.03 | 0.01 | 0.01 | 0.004 | 0.002 |
| <b>Biomass capacity (t/h)</b>          | 5.00 | 3.00 | 1.50 | 0.75 | 0.30 | 0.15 | 0.08 | 0.04 | 0.02  | 0.01  |
| <b>Coefficient</b>                     | 0.18 | 0.17 | 0.18 | 0.18 | 0.18 | 0.18 | 0.19 | 0.19 | 0.19  | 0.21  |

The other aspect which could provide a source of validation is the final temperature of the solids and the flow of combustion gases required. In Table 9.3, the values of combustion gas flow for 3 tonnes per hour reactors in a co-current configuration are shown. The estimation of the gas flow increases with the temperature due to the higher heat demand to achieve higher temperatures. This analysis agrees with the higher heat required to reach a higher temperature.

Table 9.3: evolution of flow of combustion gases with solids temperature

|  |      |      |      |      |
|--|------|------|------|------|
| <b>Temperature solid [°C]</b>          | 709  | 499  | 398  | 351  |
| <b>Flow of combustion gases [kg/s]</b> | 0.97 | 0.51 | 0.46 | 0.42 |

### 9.3.3 Validation outcomes

The model agrees with what it anticipated when temperature and/or biomass capacity increase. This is not an accurate method of validation because there may be many misleading pieces of information that lead to wrong results and designs. However, this analysis does make the model more reliable, and it shows that the model follows what is expected, but it highlights the need for further validation with real data to test its accuracy.

## 9.4 Case study

A small case study compares the reactor design for the three feedstock to illustrate how this model could be utilised. Three sets of conditions are studied for each feedstock: 3 t/h and 500 °C, 1.5 t/h and 500°C and 3 t/h and 400 °C. The results are shown in Table 9.4.

Table 9.4: Case study



| Feedstock               | Wood chips | Wheat straw | RDF    | Wood chips | Wheat straw | RDF   | Wood chips | Wheat straw | RDF   |
|-------------------------|------------|-------------|--------|------------|-------------|-------|------------|-------------|-------|
| Capacity [t/h]          | 3          | 3           | 3      | 1.5        | 1.5         | 1.5   | 3          | 3           | 3     |
| Target Temperature [°C] | 500        | 500         | 500    | 500        | 500         | 500   | 400        | 400         | 400   |
| Radius [m]              | 1.74       | 1.72        | 1.34   | 1.31       | 1.27        | 1.21  | 1.38       | 1.36        | 1.35  |
| Length [m]              | 8.31       | 10.85       | 156.60 | 6.50       | 8.98        | 10.89 | 70.89      | 208.65      | 57.80 |
| Kiln angle [°]          | 1.16       | 0.99        | 0.79   | 1.14       | 0.95        | 0.90  | 0.92       | 0.79        | 0.78  |
| Conversion [wt.%]       | 95.4%      | 94.6%       | 94.8%  | 95.4%      | 94.6%       | 87.5% | 95.2%      | 95.3%       | 80.6% |
| Limit 32500 [-]         | 2          | 2           | 98     | 2          | 2           | 26    | 40         | 2           | 17    |
| Limit ±2°C [-]          | 2          | 2           | 15     | 2          | 2           | 3     | 2          | 0           | 3     |

The results are represented in Figure 9.5, Figure 9.6 and Figure 9.7. Figure 9.5, shows the radius and the length; Figure 9.6 indicates the kiln angle and conversion; Figure 9.7 gives an idea of how consistent each set of results is. To read the graphs easily, the left Y-axis is blue, and the corresponding data is blue on the graph. Similarly, the right Y-axis has a green colour. The shape of each set of conditions is unique. The square marker and continuous line are used for 3 t/h and 500 °C; the triangle marker and dotted line are for 3 t/h capacity, and target temperature 400 °C; A circle-shaped marker and discontinuous line corresponds to a 1.5 t/h capacity and 500 °C as the target temperature.

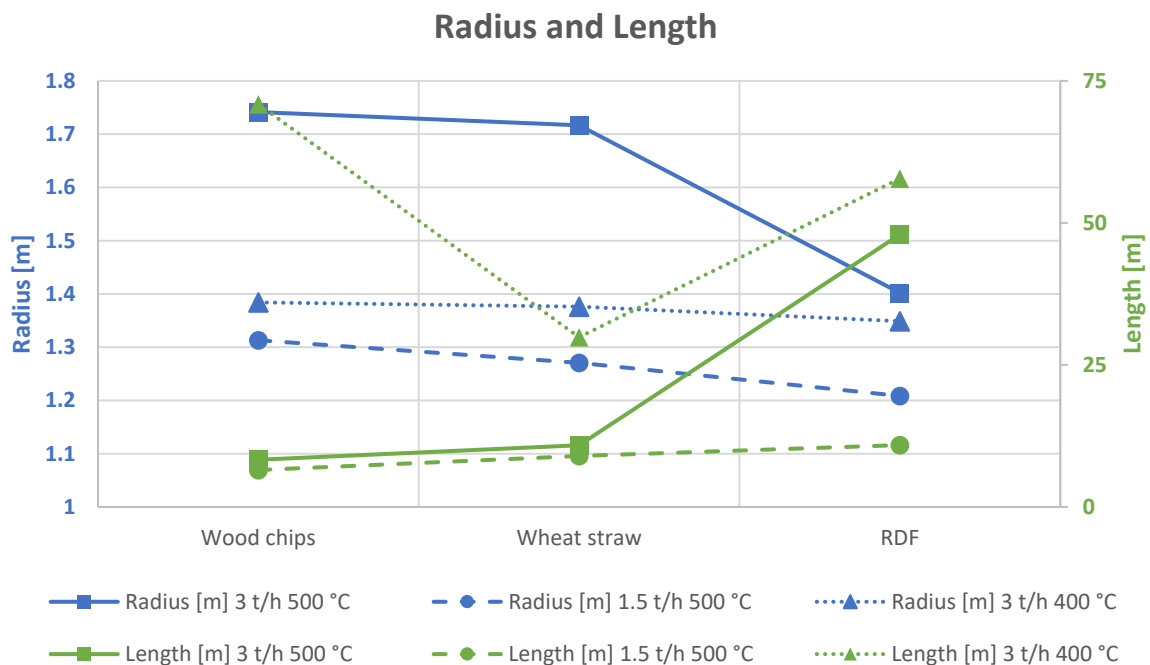


Figure 9.5: Radius and Length of the case study

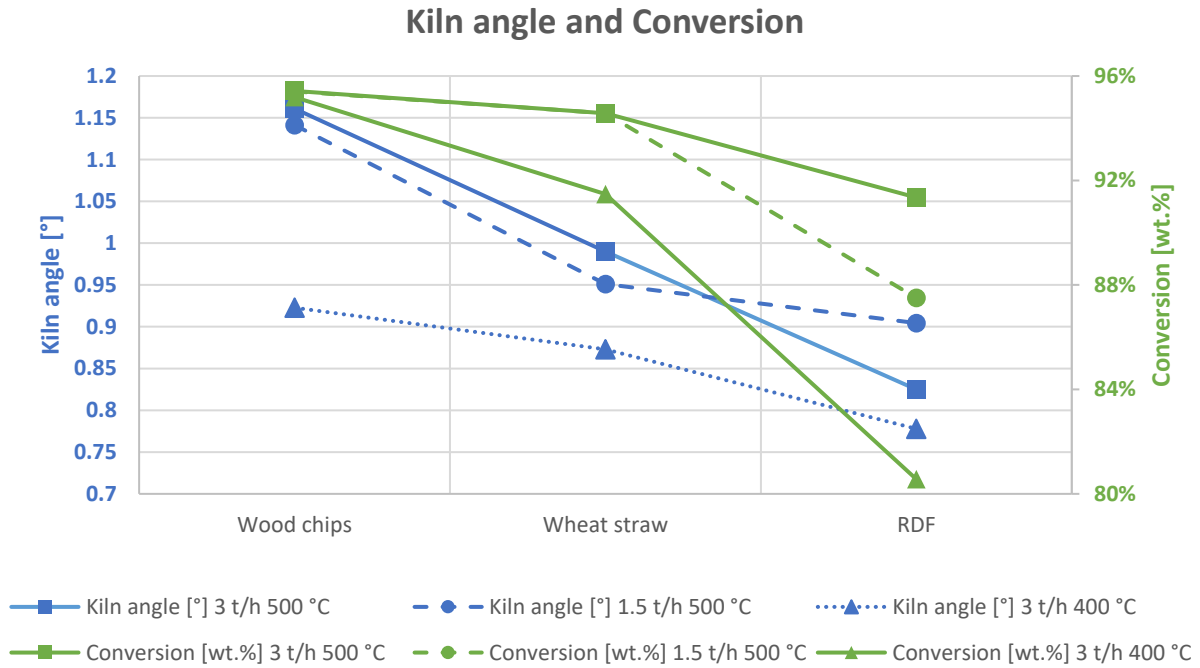


Figure 9.6: kiln angle and conversion of the case study

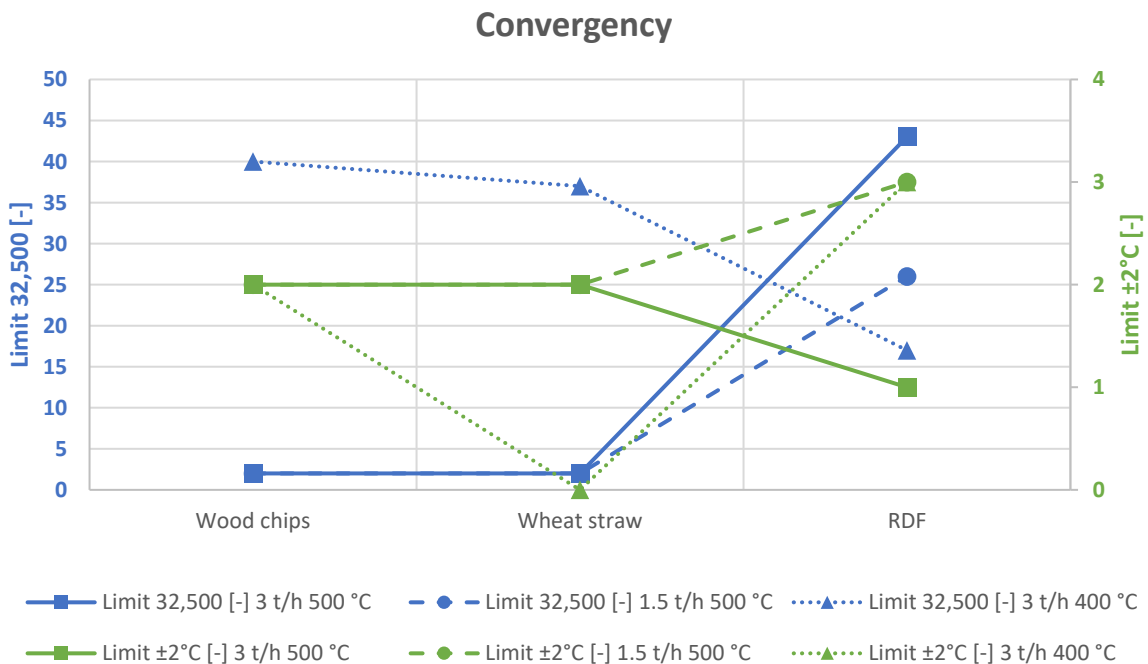


Figure 9.7: Convergence of the case study

Firstly, it should be noted that the simulations with RDF only achieved target conversion when the capacity was 3 t/h and the target temperature 500 °C. For that reason, the length, kiln angle and radius of RDF when the conditions are different should not be compared to the others.

As anticipated, the length of the reactor increases when the temperature decreases, although no apparent trend is observed between the feedstocks. The RDF simulation with conversion value lower than the target occurred due to an overflow in the model. Before substituting the data, it was observed how the length of the reactor was significantly higher than the others, using values of 200 meters or even longer. Therefore, RDF needs longer reactors to be converted into char. The kiln angle and radius are modified to make the reactor longer and increase the solids residence time to achieve a higher conversion.

The reactor length is found similar to the values from the industrial experience (Appendix C). The results of the simulation show the impact of temperature on reactor length, and some values could be questioned. When the temperature decreases to 400 °C, the reactor length changes from approximately 10 m to more than 70 meters and a value of 200 meters appear. However, according to Perry [1] (which shows several examples of lengths and radii of rotary kilns), the ratio length-diameter of the 70-metre-reactor would be 25.68, which is similar to the information provided by the book, whose average is 26.63. However, the 200-metre reactor would have a ratio of 76.71, three times higher than the average, and much higher than the maximum value found on Perry [1], calculated as 42.6, which suggests a possible error or overestimation in the simulation and results. To measure the accuracy of this calculation and the reliability of this model, validation (Section 9.3) would show how accurate and reliable this model is.

One remarkable aspect is the comparison of convergence values between the simulations. Except for the wood chips with 3 t/h and 400 °C, most of the values are low for wood chips and wheat straw. RDF convergence is worse and takes longer to achieve the conversion value. The reason for poorer convergence is not apparent because the algorithm is the same for the three feedstocks, although the need for longer reactors is attributed to longer residence time and worse kinetic parameters. It is observed (Section 5.4 and Table 5.13) how the activation energy for the second step of RDF is significantly higher (25%) than the others. The higher activation energy is likely to be a critical parameter (more influential than pre-exponential factor), and the reason why RDF generally takes longer to be converted into char. Consequently, RDF requires longer reactors and residence time to be pyrolysed. The convergence of the model decreases when temperature and capacity decrease, being the reduction of target temperature more critical than the capacity.

## 9.5 Limitations

This research aimed to design a model which could automatically design a rotary kiln. Several assumptions had to be made to design a model capable of simulating a reactor and obtaining valid specifications. The model works consistently on a range of operational conditions. However, it is recognised that it is not perfect, and some aspects could be improved (see Section 11.2).

In Section 7.5.3, the limitation of temperature and the need for restarting the model was addressed. A very high temperature may need a very short reactor which would achieve the conversion in a very short time. The effect of a low temperature would be the opposite, a very low conversion value with a very long reactor. The operating temperature range at which the model operates is [400-600 °C].

The capacity range is different from the temperature because it relates more to consistency than achieving the conversion value. The model is very consistent when the reactor capacity is 3 t/h, but the number of steps which do not converge increases when the capacity decreases. The capacity operating range for which this model achieves consistent results is 100 kg/h - 5 t/h, although the model achieves a solution down to 10kg/h, but with lower reliability and consistency.

The feedstock was studied in Section 9.4, and the behaviour of woodchips and wheat straw was very similar. The RDF caused problems, but it may still be successful although with lower reliability than the other feedstocks. Additionally, it should be considered that the properties (density, kinetic parameters and calorific value) of the RDF for which the plant is designed are probably different from the one within this model.

During the design of the model, it was concluded that the co-current configuration of combustion gases was more effective than counter-current. Co-current configuration is used in this design, and the option for counter-current is not implemented; although the option is mentioned as a future model development.

The moisture content has not been tested in this model, and there is no apparent upper or lower limit, although it should be studied further.

The last parameter is the nitrogen flow, used to create an inert atmosphere. The main problem with a low nitrogen flow is overflow of the model and its consequent collapse. A higher flow rate than the design value (a third of the solid feeding rate) has not been studied although presumably, the effect would be an increase in combustion gases flow. As studied, the minimum flow is one-thirtieth of the solid flow rate. Otherwise, the significant heat flow input into the nitrogen makes the model overflow and collapse.

There can be two reasons why the model is not successful, inconsistent results or overflow. The division of the reactor in slices intended to reduce the dimensions of heat transfer calculation, and obtain more consistent results due to the smaller size of the reactor to calculate. The division into 100 slices is not practical for very long reactors. The idea was to reduce temperature difference between components, and the input and output of each component on each slice. If these differences are low, the model converges smoothly and consistently. However, when the length of a reactor is 200 meters or more, each slice is 2 meters, and the interaction between components can potentially cause an overflow of the variables due to the big temperature difference and big numbers involved on those calculations. Similarly, the values converge quickly if component temperatures are similar because the variation is lower and the chance of having diverging values decreases.

## 9.6 References

1. Perry, R.H. and D.W. Green, *Perry's chemical engineers' handbook*. 2008: New York : McGraw-Hill, ©2008. 8th ed. / prepared by a staff of specialists under the editorial direction of editor-in-chief, Don W. Green, late editor, Robert H. Perry.

## 10 Conclusions

This study aimed to create an innovative modelling methodology for the design of a slow pyrolysis reactor. The objective was to analyse the char production methods by slow pyrolysis and create a model which automatically designs a pyrolysis reactor based on user inputs.

The key outcomes of this research are a thorough review of the slow pyrolysis technologies, the model which automatically designs a pyrolysis reactor, and a methodology to design such a reactor, which is essential for the development of this work.

Slow pyrolysis is mostly known for the use of small, unsophisticated systems to produce char. The review of technologies helps to uncover all the different methods to produce char and the differences between these methods. The classification and assessment resulted in the rotary kiln as the most promising technology for this study. The grading method is a valuable tool to find the most suitable technology, although it needs to be adapted for each analysis.

The design of any of these technologies needs to consider three essential aspects: the bed of solids, heat transfer and pyrolysis kinetics. The lack of a methodology in literature which integrates these aspects is the main research gaps identified for slow pyrolysis. During the development of the model, each section was analysed individually. Different pieces of information from the literature and industry were adapted to the current study by the creation of an innovative integrated model.

The division of the reactor into slices was a common methodology used in industrial reactor design, identified by close collaboration with industrial partners. This method was transferred to academia within this work and facilitated the implementation of a sophisticated heat transfer algorithm. The algorithm was independently developed using the basics of heat transfer, but several approximations were made to estimate necessary parameters, such as the view factors in radiation for complex three-component-systems. For the kinetics, the activation energy and pre-exponential factor were calculated for each feedstock. Additionally, a method for the optimisation of the reaction orders was developed and implemented. This method allowed the calculation of different reaction orders and found the most suitable solution.

A comprehensive and thorough methodology was developed within this work for the design of a rotary kiln. This methodology included assumptions to achieve a compromise between accuracy and computational time and power. It analyses the three parts that form the model: bed of solids, heat transfer and kinetics. Additionally, this research provides a full description of each part and the methodology used and how to integrate the solutions into one.

The model is simple but thoroughly developed to account for all the processes occurring during pyrolysis. Users can investigate custom reactor designs, as they can specify a number of key variables such as feedstock and scale. It is a very powerful tool that can be used in industry or by potential investors to obtain a first approximation of the dimensions of a pyrolysis reactor. It is beneficial in research because it shows a methodology for the design of reactors and a method to combine all the theory. Another use of the model in industry and research is to conduct experiments in a rotary kiln as a first approximation because they would be fast, low risk and low cost. It is acknowledged that the reactor model is not perfect, and some parts could be improved as addressed in Section 11.2, but it provides a valuable step forward in the development of slow pyrolysis reactor design.

From this research, it could be concluded that the creation of a model for the design of a pyrolysis reactor is a very complex task. It can be as complicated as the researcher needs, but it will also increase the computational power requirement. The contrary would result in an oversimplified

model that would not match the reality. The balance between an accurate and consistent but straightforward model was one of the challenges in this research. It was overcome through the division of the reactor into slices, which makes each step simpler to solve; and through integrated models to solve each slice, which accounts for heat flows, gas properties and solids conversion into pyrolysis products.

## 11 Next steps and future implementation

This chapter explains aspects where the model could be improved by further development or additional in-depth study. Potential solutions for these aspects are presented and discussed.

### 11.1 Validation

The most critical step to further develop this work is with additional validation of the constructed model. The use of rotary kilns in research is limited, and few examples are found [1-3]. Information about these reactors could not be accessed for validation during the development of this work due to the lack of viable information. The data from rotary kilns in industry is more extensive but unavailable due to confidentiality issues.

Validation is a crucial aspect in all models to reality-check the model behaviour. It is a significant gap in this research which could not be completed due to the lack of resources, despite the efforts made to contact industry. It should be the first consideration if there is further research in this area.

### 11.2 Model improvements

There are several assumptions and calculations which can be improved if the model was developed further.

#### 11.2.1 Flow of nitrogen

One of the assumptions was a set minimum flow of nitrogen; set at a value of one-thirtieth of the solids flow. If the flow of solids is three tonnes per hour, the minimum nitrogen flow is 100 kg per hour, which is a significant expenditure of nitrogen. The model failed with lower values of nitrogen flow.

To solve this problem, there could be a conditional algorithm which instructs the model to calculate only the solids and combustion gas heat flow when the flow of gases inside the reactor is lower than the value of one-thirtieth. This condition would be removed once the amount of gases inside the reactor reaches one-thirtieth of the solids input, and this condition should be applied to every heat flow calculation.

Alternatively, a solution would be to divide the reactor into more slices, as the divergence currently occurs when there were 25 reactor slices. This solution is riskier because it may not converge even with the changes and would require more calculations for the model, which could increase the calculation time significantly.

#### 11.2.2 Vapours inside the reactor

The gases inside the reactor are modelled as a mixture of nitrogen, steam, hydrogen, methane and carbon monoxide to obtain the properties such as viscosity, density or thermal conductivity. The range of vapours produced in pyrolysis is much more extensive, and for a more accurate model, the components should be identified and modelled. The calorific capacity, thermal conductivity, density and viscosity and their evolution with temperature should be studied and implemented.

#### 11.2.3 CFD modelling

One of the most challenging aspects to estimate is how the particles increase in temperature and the existence of any temperature gradients. Computational Fluid Dynamics (CFD) would be needed to assess how efficient and uniform the heating of the particle. Overall, CFD requires high computational power and long-running times to simulate the evolution of a particle. This technology could be used to study how the pyrolysis gases are released.

To avoid full implementation of CFD within the model, there could be a coefficient which represents the heating efficiency of a particle, estimating the fraction of heat transferred that reaches the centre of the particle or apply that coefficient to the total variation of temperature. This coefficient could be correlated to the particle size, and the model could calculate the factor in each specific case depending on the particle size.

#### 11.2.4 Voidage

Another aspect closely related to particle size is the voidage of the rotating bed of solids. The voidage of the bed is an aspect scarcely studied in the literature. In this research, the particle shape relates to particle size and a voidage value. A study of the influence of both aspects would increase the accuracy of the model. An idea for further development would be an equation where the particle size and shape are involved, and the result is the voidage. It needs to be highlighted that the value of the voidage is for a rotating bed of solids instead of a fixed bed of solids, which is more common in literature.

#### 11.2.5 The behaviour of the solids

The behaviour of the solids inside the reactor could be improved through further study. This work includes Saeman's model to calculate the length of the bed of solids. One of the assumptions for this model is a constant volumetric flow of solids, which is not accomplished within the work. Furthermore, the evolution of the conductivity, density and the other properties of the solids should be considered.

An alternative is the use of an internal configuration to control the bed length and the residence time of the solids. The internal configuration could refer to the use of an internal screw in the reactor to push the biomass and control the residence time, or the use of tailor-made flights with the same purpose.

#### 11.2.6 Flights design

The thorough design of the flights was not conducted successfully, and an assumption of extra area per flight was made at the end. Further study of the flights and implementation within the model would be necessary to develop this model further and to calculate extra conduction area from wall to solid and the gas, in addition to the extra convection area between the bed and the gases by the showering of solid particles.

#### 11.2.7 Heat losses

The term heat losses indicate the fraction of heat transmitted by the wall that is lost due to transmission to the atmosphere. In this work, it is quantified as 25%, which means that wall losses are a quarter of the energy transmitted to the reactor. The most important aspect of improving here is the concept, which indicates the percentage of heat transmitted. It would mean that if there is a system with three components at the same temperature, even if this temperature is as high as 800 °C, the system would not lose any temperature due to heat losses because there is no heat transmitted within.

A possible solution would be to have a losses coefficient for each step and component, which depends on the temperature. This coefficient subtracts its percentage to the total amount of energy, measured mainly in temperature, and the new exit temperature is re-calculated. In this way, the losses would correlate to the energy (and temperature) of the component rather than heat transmitted. If the reactor is well isolated, this coefficient could be exclusively applied to the combustion gases.



### 11.2.8 Product distribution

The char yield is estimated for each feedstock and calculated from experiments conducted. The area for further development is the vapour fraction, which is divided into condensable and non-condensable and whose results from wheat straw (feedstock used within this research) experiments from Rego [4] are applied to all feedstocks. The fraction of condensable and non-condensable should be studied for each feedstock. If there were more than three results (temperatures), the model could be more accurate in the calculations. Furthermore, if it was possible, the condensable fraction should be divided into the organics and aqueous phase, which follows a constant 20/80 proportion in this work.

Ideally, the experiments to determine the product distribution should be conducted in a rotary kiln to obtain more similar results. This would compare the performance and pyrolysis behaviour of a rotary kiln and a screw reactor for the same feedstock.

### 11.2.9 Product properties

The last suggestion would be an addition to this project. The model predicts the behaviour and performance of the reactor for the pyrolysis of biomass, calculating the product distribution and flows. This model would gain value with an estimation of the product properties, based on the process temperature, nitrogen flow, and some initial feedstock characteristics such as the type of feedstock, and some analysis such as ash content or particle size. From that data, the model could estimate the properties (HHV, surface area and others) based on previous experiments. Alternatively, it may be better to have a database where the model chooses the most similar characteristics of the products when the inputs are given.

### 11.2.10 Simulation time

Despite all the potential aspects to improve the model, it still takes hours to design the reactor due to the calculation complexity and all the iterations and conditions. The time required for the design is a compromise between the accuracy of the calculations and the time it takes. It is essential to highlight that during the reactor design, the reactor is simulated many times; for every iteration the combustion flow is re-calculated, and this is done every time the kiln angle and radius are adjusted to achieve the conversion value (95 wt.%).

### 11.2.11 Optimisation

This project aims to design a reactor specified by user inputs, and there are infinite combinations to accomplish this requirement. Another potential improvement for further development of this model would be the criteria to optimise the reactor. This criteria depends on the individual user and can account for many different options. Optimising the reactor can relate to reducing the reactor volume, which would decrease the capital cost (CAPEX), and it could be achieved through the amendment of the angle. Another option would be to reduce the energy provided by the combustion gases flow, which could be by enhancement of contact area, more flights attach or better insulation to reduce the heat losses.

### 11.2.12 Adaptability to other thermochemical processes

As described in Section 7.7, the rotary kiln is a technology used in other fields for drying, calcination or torrefaction. Depending on the use, this model can be adapted to perform similar calculations but applied to other processes. Each case should be studied separately because the procedures and amendments would change, depending on the process.

### 11.3 Future implementation

This model aims to give the real specifications of a rotary kiln and how it should behave with the given inputs. Once the validation is completed, it can be studied how this model represents reality. There are aspects which cannot be omitted, such as the techno-economic assessment (TEA) of this process. This research represents the reactor performance, but the economics of the system should be carefully considered before the construction of the plant. Within this TEA, the capital and operational costs are included, and some aspects like the logistic costs, related mainly to the transport of the biomass are studied. All these factors should be carefully considered before the construction of the kiln.

### 11.4 Dissemination

This research as a whole and some sections have been presented in different conferences, schools and other events for further dissemination. The international conferences where this research has been presented are:

- 12<sup>th</sup> ECCRIA - The European Conference on Fuel and Energy Research and its Applications; 5<sup>th</sup> - 7<sup>th</sup> September 2018; Cardiff University, United Kingdom.
- 27<sup>th</sup> European Biomass Conference & Exhibition (EUBCE 2019); 27<sup>th</sup> - 30<sup>th</sup> May 2018; Lisbon Congress Centre (CCL), Lisbon, Portugal.
- 36<sup>th</sup> Chemical Engineering National Conference (XXXVIJNIQ); 4<sup>th</sup> – 6<sup>th</sup> September 2019; Engineering and Architecture School (EINA), University of Zaragoza, Zaragoza, Spain.
- Biochar II Conference: Production, Characterisation and Applications; 15<sup>th</sup> – 20<sup>th</sup> September 2019; Grand Hotel San Michele, Cetraro, Italy.
- 23<sup>rd</sup> edition of the International Conference on Analytical and Applied Pyrolysis (PYRO 2020); Postponed to 29<sup>th</sup> November -4<sup>th</sup> December due to COVID 19; Het Pand, Ghent, Belgium.

Furthermore, there are some articles at the preparation stage for publication in scientific journals:

- López-Ordovás, J., Bridgwater, A.V., Chong, K. (Forthcoming). "Construction of a model for the design of rotary kilns for the pyrolysis of biomass." This article would give an overview of the whole PhD, trying to sum up all the thesis in a single article for the description of the model and to address the main components.
- López-Ordovás, J., Bridgwater, A.V., Chong, K. (Forthcoming). "Char fuel production in developed countries - a comparative study of the current slow pyrolysis technologies." This article would be based on the chapter where all the slow pyrolysis technologies are compared for the production in a developed country
- López-Ordovás, J., Bryant, C., Bridgwater, A.V., Chong, K. (Forthcoming). "Pyrolysis kinetic study of wheat straw, woodchips and RDF - GreenCarbon project." The study of the kinetic parameters is one of the most promising outputs of this project. Not only the kinetics parameters are found but a method to find the optimum reaction order is created.
- López-Ordovás, J., et al. (Forthcoming). "Integrated rotary kiln pilot-scale plant for beechwood torrefaction." This article describes the work conducted in CENER, with the experiments in a pilot-scale rotary kiln for torrefaction.

## 11.5 References

1. Mašek, O., et al., *Consistency of biochar properties over time and production scales: A characterisation of standard materials*. Journal of Analytical and Applied Pyrolysis, 2018. **132**: p. 200-210.
2. Bradfield, F.L., *Examination of the Thermal Properties of Municipal Solid Waste and the Scalability of its Pyrolysis*, in *Faculty of Engineering*. 2014, Stellenbosch University: South Africa.
3. Chiaramonti, D. *Slow Pyrolysis for Biochar Production and Carbon Sequestration*. in *European Biomass Conference & Exhibition (EUBCE)*. 2019. Lisbon.
4. Rego, F., *Intermediate pyrolysis of biomass in a pilot scale continuous screw reactor*, in *EBRI (Energy and Bioproducts Research Institute)*. Forthcoming, Aston University: Aston University.

## 12 Appendices

### Appendix A. Mathematical design of a flight

The method for calculation of the surface of the solid on contacting gas inside the kiln is based on two sets of Cartesian coordinates. The origin of the set  $[x, y]$  is the tip of the flight, establishing the x-axis along its last segment (represented in green on Figure 6.3). For the set  $[X, Y]$  (in black) the origin is the drum axis, the centre of the kiln. Both sets of coordinates are correlated to calculate the solids falling from the lower case set to the capital set of coordinates.

The flights are three-segmented, and they are defined based on its coordinates, defined by the points they link, defined in Table 12.1. Simultaneously, the length of each segment and the angle they form define the coordinates of the points, given in Table 12.2 .

Table 12.1: Definition of the segments of the flight

| Segment 1 | Segment 2                       | Segment 3   |
|-----------|---------------------------------|---|
| $y_1 = 0$ | $y_2 = a_2 + b_2 \cdot x$       | $y_3 = a_3 + b_3 \cdot x$                         |
|           | $a_2 = x_A \cdot \tan \alpha_A$ | $a_3 = y_B + x_B \cdot \tan(\alpha_A + \alpha_B)$ |
|           | $b_2 = -\tan \alpha_A$          | $b_3 = -\tan(\alpha_A + \alpha_B)$                |
| $x < x_A$ | $x_A < x < x_B$                 | $x_B < x < x_C$                                   |

Table 12.2: Coordinates of the points

| Point A     | Point B                              | Point C   |
|-------------|--------------------------------------|---|
| $x_A = L''$ | $x_B = x_A - L' \cdot \cos \alpha_A$ | $x_C = x_B + L \cdot \cos(\alpha_A + \alpha_B)$ |
| $y_A = 0$   | $y_B = L' \cdot \sin \alpha_A$       | $y_C = y_B - L \cdot \sin(\alpha_A + \alpha_B)$ |

The position of the last point must satisfy the following equations because the flight is located on the wall of a drum with a radius R. The coordinates  $X_C$  and  $Y_C$  are defined as follow.

$$X_C^2 + Y_C^2 = R^2$$

$$X_C = X_0 + x_C \cdot \cos \delta - y_C \cdot \sin \delta = R_0 \cdot \cos \theta + x_C \cdot \cos \delta - y_C \cdot \sin \delta$$

$$Y_C = Y_0 + y_C \cdot \cos \delta - x_C \cdot \sin \delta = R_0 \cdot \sin \theta + y_C \cdot \cos \delta - x_C \cdot \sin \delta$$

Substituting  $X_C$  and  $Y_C$  on the equation with the radius of the kiln, the angle which correlates the two sets of coordinates ( $\delta$ ) can be calculated according to this mathematical demonstration for any angular position ( $\theta$ ):

$$R^2 = R_0^2 + x_C^2 + y_C^2 + \cos \delta \cdot (2 \cdot R_0 \cdot x_C \cdot \cos \theta + 2 \cdot R_0 \cdot y_C \cdot \sin \theta) + \sin \delta \cdot (2 \cdot R_0 \cdot x_C \cdot \sin \theta - 2 \cdot R_0 \cdot y_C \cdot \cos \theta)$$

$$M = N \cdot \cos \delta + P \cdot \sin \delta$$

$$M = R^2 - R_0^2 - x_C^2 - y_C^2$$

$$N = 2 \cdot R_0 \cdot x_C \cdot \cos \theta + 2 \cdot R_0 \cdot y_C \cdot \sin \theta$$

$$\begin{aligned}
P &= 2 \cdot R_0 \cdot x_C \cdot \sin \theta - 2 \cdot R_0 \cdot y_C \cdot \cos \theta \\
t &= \sin \delta \\
\sqrt{1 - t^2} &= \cos \delta \\
M - P \cdot t &= N \cdot \sqrt{1 - t^2} \\
M^2 - 2 \cdot M \cdot P \cdot t + t^2 \cdot P^2 &= (1 - t^2) \cdot N^2 \\
(N^2 + P^2) \cdot t^2 + (-2 \cdot M \cdot P) \cdot t + (M^2 - N^2) &= 0 \\
\delta &= \arcsin t
\end{aligned}$$

To calculate the solids falling rate, the powder level line is a crucial factor and it is given by:

$$y = x \cdot \tan \gamma = x \cdot \tan(\phi - \delta)$$

The intersection with the second and third segment of the flight has the following abscissas and ordinates:

$$\begin{aligned}
x_2 &= \frac{a_2}{\tan \gamma - b_2} & y_2 &= a_2 + b_2 \cdot x \\
x_3 &= \frac{a_3}{\tan \gamma - b_3} & y_3 &= a_3 + b_3 \cdot x
\end{aligned}$$

The abscissa of the intersection of the solid level line with the drum wall is calculated through the following second-degree equation, whose coefficients are listed below:

$$x_W = \frac{-B_W \pm \sqrt{B_W^2 - 4 \cdot A_W \cdot C_W}}{2 \cdot A_W}$$

$$A_W = 1 + (\tan \gamma)^2 \quad B_W = 2 \cdot X_0 \cdot (\cos \delta - \tan \gamma \cdot \sin \delta) \quad C_W = R_0^2 - R^2$$

The equation for the ordinate is:

$$y_W = x_W \cdot \tan \gamma$$

Up to this point, all coordinates, angles and segments have been defined and it is the moment to explain the cross-sectional area occupied by solid powder. There are four different cases and scenarios to analyse and calculate the cross-sectional area:

The first case is the one where the powder reaches the wall, which occurs when:

$$\gamma > A \cdot \tan \left( \frac{y_C}{x_C} \right)$$

And the cross-sectional area of the powder of the solid is calculated with the following equation, having  $\beta$  as corresponds.

$$S = \frac{R^2}{2} \cdot (\beta - \sin \beta) + \frac{1}{2} \cdot |x_A \cdot y_B + x_B \cdot y_C - x_C \cdot y_B + x_C \cdot y_W - x_W \cdot y_C|$$

$$\beta = 2 \cdot A \cdot \sin \left[ \frac{\sqrt{(x_C - x_W)^2 + (y_C - y_W)^2}}{2 \cdot R} \right]$$

On the second case the solid on the flight does not reach the wall but it does reach the third segment, the one closest to the wall when the two conditions are achieved:

$$\gamma > A \cdot \tan\left(\frac{y_C}{x_C}\right)$$

$$\sqrt{(x_3 - x_C)^2 + (y_3 - y_C)^2} < L$$

According to these conditions, the cross-sectional occupied by the powder is calculated through the formula:

$$S = \frac{1}{2} \cdot |x_A \cdot y_B + x_B \cdot y_3 - x_3 \cdot y_B|$$

The solids only reach the second segment of the flight when the conditions achieved are:

$$\gamma > A \cdot \tan\left(\frac{y_C}{x_C}\right)$$

$$\sqrt{(x_2 - x_B)^2 + (y_2 - y_B)^2} < L'$$

$$y_2 > 0$$

The added surface by the flight is then:

$$S = \frac{1}{2} \cdot |x_A \cdot y_2|$$

The last case scenario is the one where the flight is empty, occurring when:

$$y_2 < 0$$

Consequently, the surface occupied by the solids would be null.

## Appendix B. Mechanical features

This appendix contains a description of mechanical aspects of the rotary kiln which are usually overlooked. Among the aspects studied, seals, bearings, drive assembly and construction materials are studied. Related to the plant, the measurement and control of process parameters are studied, so as the transport of material along a plant.

### B.1. Sealing

The main objectives of sealing are to prevent the process gases escaping and air from getting into the reactor. It connects the static case of the kiln with the rotating reactor. It is especially important to prevent air from getting into a pyrolysis reactor because of explosion risk. Sealing helps with temperature control because air can produce some non-controlled exothermic reactions and choosing the right seal is critical. If there are no reactions, a leak could cause the temperature to drop due to a lower air temperature compared to the one inside the reactor and, if the leak is severe, it may disrupt the process. Since most of the kilns work at negative pressure, it is more likely that air leaks in. It is a difficult engineering task because the seal is required between a moving and a stationary part. This stationary part is usually called breeching and it is the most common leak point [1, 2]. The seals are designed to isolate the reactor, and they are not expected to handle material flow issues [2]. For the design of the seal, the aspects to consider are:

- **Operating temperature:** is a crucial factor affecting the lifetime of the seal. Degradation is reduced if the operating condition is closer to the design temperature [3].
- **Seal torque:** the torque refers to the force required overcome the friction to rotate on the seal. Different design, components, lubricants, temperatures, rotational speed affect the seal torque [3].
- **Internal pressure:** during the design of elastomeric seals, the internal pressure is considered zero. One advantage is the satisfactory performance up to 0.20 bar. A higher pressure forces the lip of the seal against the shaft and increases the friction. With hours of operation, the pressure excess could lead to a failure due to the deformation of the seal [3].
- **Shaft speed:** an increase in the shaft speed raises the force needed to rotate the shaft, the friction and the temperature achieved from this friction. This increase in temperature could harden the sealing material and reduce sealing capacity [3].
- **Lubrication:** there is a film of oil on which the seal runs, preventing the sealing lip from hardening and cracking produced by the friction-generated heat. This lubricant has to agree with the working temperatures and prevent chemical reaction between the rubber used for sealing and the lubricant [3].
- **Shaft finish:** the roughness of the shaft to rotate the reactor is tailored. Higher roughness could penetrate the film of lubricant, which would accelerate lip wear due to the leakage. A smoother shaft could allow lubricant leaks, producing excessive friction heat and hardening the seal [3].
- **Shaft to kiln eccentricity:** alignment between the rotating centre of the shaft which produces the rotation of the kiln and the kiln is essential to avoid greater sealing on one side than the other [3].
- **Dynamic shaft runout:** the shaft must rotate around its centre, otherwise the lip of the seal would be moving back and forth and would produce leakage [3].
- **Pressure:** a higher pressure than the design produces more friction between the shaft and the sealing, increasing the heating and wear [3].
- **Kiln:** the resulting roughness of the inner kiln is important because it interacts with the sealing and a too coarse ending can cause a leak path by itself or a sharp edge may produce damage on other materials [3].

The standard sealing method for rotary kilns and dryers are leaf seals according to FEECO [1]. There are alternative methods such as the clipper split seals, oil seals, flexilip, pro-tech and v-seals [3]. Most of the designs have to be customised for each specific process, varying with the operating temperatures, pressures, components involved, gradient temperatures and aim of the process [4]. The most common reasons for failure are abrasion or contamination, expansion and contraction of the shell, excessive runout, low maintenance or overflow of the product [2].

#### B.1.1. Leaf Seals

This type of seal is composed of many sprung steel leaves, bolted to the breeching, and the elastic part of each leaf is pushing against the wear plate of the rotating kiln, keeping the pressure inside the kiln to create a good seal with the mounting flange. A good analogy to understand this system is a fanned-out deck of cards where an end is bolted to the breeching and the other is pushing the reactor to avoid any gas from escaping [1]. A representative scheme is shown on Figure 12.1.



*Figure 12.1: Leaf sealing from [1]*

A variation of this method is the double-leaf seal and it could be potentially used for pyrolysis because it is employed where keeping the atmosphere inside the rotary kiln is critical, aided by better sealing. There are two layers of leaves on the top of each other and, additionally, there is a purge gas introduced between them, pushing outward so in case there was a leak, the gases may go out but no oxygen would flow in [1].

It is one of the critical parts of a rotary kiln, especially for pyrolysis where air must be kept outside the kiln. A leak of air entering to the reactor would mix with the reactor gases, which could lead to very exothermic reactions, and towards an increase of temperature, loss of temperature control and inconsistencies in the process, or even an explosion if it is not controlled in time [1].

#### B.1.2. Clipper Split

The name is given due to the outer rubber case and the elastomeric sealing ring. The main advantage is that the sealing does not corrode or rust and forms a gasket-type seal between the



housing and the outer cylinder. The replacement of the ring is not very difficult and is very brief compared to other technologies. Due to the non-metallic design, there is no metal shaving of the kiln when installing the seals. The composite may degrade when the temperature or pressures of the reactor are very different from ambient [4]. A scheme of the process is found in Figure 12.2.



*Figure 12.2: Clipper split sealing, from [3]*

### B.1.3. Oil

Oil seals refer to the structures such as Figure 12.3 because it provides an additional case for the outer diameter of the kiln. It is intended that the metal outer diameter covers the construction of the external shell of the kiln. The number of rings can be adapted to one or two, depending on the requirement.



*Figure 12.3: oil sealing, from [3]*

### B.1.4. Flexilip

The technology from Figure 12.4 provides further protection of the material when the operating conditions surpasses the capacity of elastomeric materials. In situations where high speed or high pressure are used and there is a need for chemical resistance or low torsion, this technology provides an excellent solution [3].



*Figure 12.4: Flexilip sealing [3]*

#### **B.1.5. ProTech**

A ProTech sealing system is represented in Figure 12.5. It is a system to improve the mean time between failures, especially interesting when this parameter is critical. The technology is based on non-contact between the seal and substances inside the kiln using two elastomeric rings which aim to hinder contact, and all lubricant is fully dedicated to sealing. However, it is more complex and the investment needed is higher [3].



*Figure 12.5: ProTech sealing [3]*

#### **B.1.6. V-shaped**

This type of seals can be used as a primary seal or as an extra measure to protect an existing system. It is an economical method when the surfaces of the kiln and the seal can be in contact and the kiln rotating. Figure 12.6 shows a drawing of the V-shaped; the wall could accommodate on the V-shaped part to seal the content of the reactor [3]. It can be combined with other technologies to ensure a better sealing. For instance, combined with a graphite ring between the two materials could produce a better isolation of the kiln content [5].



*Figure 12.6: V-shaped sealing [3]*

## B.2. Bearings

The bearings are the pieces of equipment used to support the reactor and minimise the loss of power and friction associated with the rotating motion of the kiln. The start-up of the process is especially important in the design of the bearing because the starting friction is twice the running friction. When a bearing has to be designed, the size, load to be received and lifetime are specified. The aspects to consider are fatigue loading, friction, heat, corrosion resistance, material properties, lubrication, tolerances, assembly and cost. To accomplish all the specifications, the bearing is divided into four essential parts, the outer ring, the inner ring, rolling element and the separator. In many cases, the bearings are manufactured with a closure envelope to protect them from dirt, but there is extra-difficulty to lubricate if it is fully covered and it has to be done in the factory [6].

In addition to the bearings, it is essential to estimate the number of piers to support the load of the whole kiln. The number required is usually two or three depending on the dimension and the ratio  $L/D$ , although no apparent limit is established in the literature [7]. During operation, the bearings need lubrication to distribute and dissipate heat, prevent corrosion of the bearing surfaces and provide a lubricant film between the sliding and rolling surfaces [6].

Most of the types of bearings are single-row, which could withstand a small misalignment. To deal with higher values, there is a possibility to use double-row bearings, which can carry heavier radial and thrust loads. The main types are ball bearings, helical rollers, spherical-roller thrust bearing, needle bearing and tapered roller bearing [6].

### B.2.1. Ball-bearing

The ball bearing is a type of bearing where the rolling element are balls, and arranged according to the separator distribution and covered with the outer ring. It is the most basic design of a bearing and it has several variations, such as adding an extra-row, which depending on its position, it would produce self-alignment, or having an angular contact to have a shaft inclined on it. Figure 12.7 provides a representation of a ball bearing to see in detail the components and structure [6].



*Figure 12.7: ball bearing scheme, from [6]*

#### **B.2.2. Straight roller bearings**

The main characteristic is the capacity to carry a greater radial load due to a greater contact area, but the geometry between the raceways and rollers cannot deal with any misalignment of the rollers could be deformed and move. The separators are very heavy and the rolling elements are short straight cylinders [6].

#### **B.2.3. Helical roller**

The rolling elements in this bearing are rectangular material wound into rollers, hardened and ground. This process provides flexibility to take misalignment. The main characteristic is the ability to take the case and potentially the shaft as the inner and outer shell respectively if space is limited [6].

#### **B.2.4. Spherical-roller thrust bearing**

The use of inclined spheres as rolling element helps the bearing to deal with misalignment, and it supports a heavier load. This occurs because contact area between the elements and raceways (inner and outer rings) rises when the load increases due to an increase in pressure [6].

#### **B.2.5. Needle bearing**

This bearing is characterised by limited radial space to deal with high load capacity. It is a characteristic type of bearing where the rings are not indispensable and may be removed due to the long cylinders being part of the design [6].

#### **B.2.6. Tapered roller bearing**

This system counts on the advantages of the ball and straight roller bearings because it deals with radial and thrust loads, and a combination of both. One of the most important parts is the design of the inclined cylinders (rolling element) as they have the same axis as the bearing [6].

### B.3. Drive assembly

As deduced from the name, rotary kilns are continually turning, via a component called the drive assembly. The difference between the options is the required horsepower for the process and move the reactor, dependent on its size [8]. There are mainly four available arrangements: chain and sprocket, gear drive, friction drive and direct drive [1].

#### B.3.1. Chain & Sprocket

This option is very similar to the one used in a bicycle (as it is seen in Figure 12.8). A large sprocket wraps around the kiln with a chain that goes to the reducer and motor. This motor drives a gear box, spinning a small sprocket attached to the large sprocket wrapping around the rotary drum through a chain [1].



*Figure 12.8: Chain & Sprocket, from [9]*

This technology is generally used for small reactors, up to 75 horsepower, although it is very competitive for smaller works, being cost-effective and easy to run [8].

### B.4. Gear Drive

This arrangement is called a gear and pinion configuration [8]. It is similar to the chain and sprocket (B.3.1). The difference is the sprocket around the kiln, which is replaced by gear around the drum. There is a small gear drive, meshed with one around the kiln. This small gear is the one which rotates [1].



Figure 12.9: Gear and pinion schemes, from [10]

It is more costly compared to the chain and sprocket, but it is suitable for applications above 75 horsepower and requires lower maintenance [1]. This method is usually employed to rotate the inner and outer kiln and outer kiln and could be a better solution in systems where the rotary kiln is single and there is no surrounding outer kiln. It is more common in the cement industry or for drying [2, 11, 12]. It is one of the most straightforward configurations and depending on the layout of the toothed wheels and the geometry, they are divided into spur, helical, bevel and worms gears [6].

#### B.4.1. Friction Drive

The method consists of four trunnion wheels, two of them connected by one shaft, which drives the wheels. These wheels are driven by a shaft mounted reducer and motor arrangement [1].



Figure 12.10: Friction Drive mechanism, from [13]

This configuration is used in applications with low horsepower required. The rotated kilns have a diameter of 1.8 m (6') or smaller [1]. This mechanism is used by some rotary dryers, such as the one in BIO2C in CENER [14] and others [8, 11].

#### B.4.2. Direct Drive

This last arrangement uses a shaft, mounted to a solid plate, used as the discharge end on the outlet of the kiln. The connection between shaft, drive motor and reducer is with a coupling or a mounting arrangement. It is used with motors up to 75 horsepower, attributed to small and medium-sized drums [1, 8].

## B.5. Construction materials

The housing materials surround the reactor cylinder. Further considerations are related to the thermal expansion, which could be critical on the reactor design. [3]. Typically, the direct-fired kiln wall is carbon steel (with refractory lining) and the indirectly-heated reactors must have a more heat-resistant alloy to resist higher temperatures [1]. The consideration of the materials can be crucial; for instance the thermal expansion of aluminium is almost double that of steel. When the reactor goes through thermal cycles, a steel case can lose the required pressure if the housing is made of aluminium [3]. The refractory is described for the outer shell as a method to minimise losses [15]. Carbon steel, low-alloy steel and stainless steel are more usually considered for the construction of the inner kiln, where the biomass degrades through pyrolysis [1].

### B.5.1. Refractory

The refractory is a crucial part in a direct-fired kilns, it keeps the heat inside the reactor, for heat retention, and protects the outer shell from high temperatures inside. It is an essential feature in the reactor and there are several options available. In principle, it is not a material recommended for indirectly-fired kilns because it adds another layer from the heat source to the material. However, it might be a good choice for the outer shell, to decrease heat losses. The refractories are divided into two types: castable and brick, and the type chosen depends on the temperature, material chemistry and how abrasive the feedstock and products are. In terms of price, brick installation is higher although the acquisition cost is similar for both [1].

The refractory is a key element to operate efficiently and, more important, control the temperature inside the kiln. The material degrades overtime, causing a loss in its efficiency and, consequently, the kilns. Even a small damage can cause a material trap or cold spot, leading to inconsistencies in the process and heat distortion. The main source of degradation of the refractory is the continuous dilatation when heated and contraction when cooling. This process receives the name of thermal cycles, and it can be applied to any material, and gains importance in pyrolysis when the feedstock is driven into the reactor and cools down the wall. Because it is rotating, the point where the feedstock falls is a function of time and the cooling is produced on different parts. Some chemicals may also damage the refractory; For example chlorides attack aggressively the refractory, resulting in excessive wear. The refractory can be designed in advance to deal with these substances. Consequently, a reuse of a rotary kiln can also lead to failure because the design is not as customised as it should be and certain substances can be released [1].

The refractory has two different layers, a working and insulating layer. The working layer is the one in contact with the feedstock. This working layer deals with the high temperatures from the kiln and with the abrasive behaviour of the material although it loses insulating capabilities when it is denser. Next is the insulating layer, which is to keep the high temperatures within, to avoid high temperatures reaching the shell and causing damage or heat loss from the reactor [1]. The material is typically the same for both layers (brick or castable) although its chemistry is different. The working layer is usually stronger, more conductive and with higher density. The insulating layer requires a lower conductivity and can be softer and lighter. The thickness of each layer varies with the material processed and temperature requirements of the kiln [1].

Occasionally, the number of layers is different from the general case. If the processing temperatures are low or the efficiency losses not as important, only the working layer is used. When temperatures are very high, or the efficiency is very critical, an extra layer of baked ceramic fibre is used; it is similar to the fiberglass insulation from houses but denser [1].

### B.5.2. Carbon steel

It is the most common material in process plants because is ductile, weldable, cheap and versatile. However, corrosion resistance is limited and it is mostly used for organic chemicals or neutral and basic aqueous solutions. Extra-thickness is added (corrosion allowance) to solve the issue of corrosion and to give a desired lifetime. Other techniques to hinder and minimise corrosion are painting, spraying with aluminium and/or wrapping with aluminium foil [16].

### B.5.3. Low-Alloy steels

One or more alloying agents are combined with the carbon steel to improve the resistance to corrosion and mechanical properties. Overall, the addition of small amounts of alloying materials enhances the resistance to corrosion to atmospheric environments but it is less effective against liquid corrosives, to the point that the resistance is similar to the carbon steel with solutions. The extra-mechanical strength permits the designer to add a thicker wall. As an example of a typical low-alloy grade, the AISI (American Iron and Steel Institute) 4340 has 0.40% Carbon, 0.70% Manganese, 1.85% Nickel, 0.80% Chromium and 0.25% Molybdenum combined with carbon steel. Each of the elements has a different purpose. Nickel improves properties at low temperature and corrosion. Chromium makes the alloy harder and more resistive to abrasion, corrosion and oxidation. Molybdenum is used to increase strength at higher temperatures than ambient [16].

### B.5.4. Stainless Steel

There are many types of stainless steels, whose basis is iron with a small of chromium (12-30%) and nickel (0-22%). There are minor amounts of other elements such as carbon, niobium, copper, molybdenum, selenium, tantalum and titanium. They are characterised for a higher resistance to heat and corrosion, they are not contaminating and the shape can be easily customised. The stainless steel is divided into four groups: martensitic, ferritic, austenitic and duplex [16].

- **Martensitic:** the main additive is chromium with a range of 12-20% content plus smaller amounts of carbon plus other components. These elements focus more on increasing the strength of the alloy, because it is only feasible for mildly corrosive environments. These materials are in general susceptible to embrittlement caused by hydrogen in hardened condition [16].
- **Ferritic:** the chromium content is within a range of 15-30% and the carbon content is around 0.1%. The chromium is added to enhance the resistance to corrosion. This type of steel increases the strength by cold working and it is reduced by heat treatment. It is ductile and the resistance to corrosion is rated good overall although some reducing acids such as chlorhydric acid may corrode it. It deals with mildly corrosive solutions and oxidising media without further damage to the surface. One alloy of this type is the one used in nitric acid plants, because it is very resistant to oxidation if the temperature is lower than 800 °C [16].
- **Austenitic:** it is characterised for having the highest resistance to corrosion of the stainless steel. The content of nickel is 6-22% and in chromium is 16-26% with lower carbon content than 0.03% to hinder precipitation of carbide (e.g. chromium carbide). These alloys are tough and ductile, although its manufacturing is difficult because rigid machines, heavy cuts and low speeds are crucial to obtain the material. To avoid the precipitation of carbides when welding, some stabilizers (titanium, niobium or tantalum) are added to the alloy. For further corrosion resistance, nickel can be added, which creates an oxide film on the surface of the alloy, although if the medium is reductive, it may lead to a stress-corrosion cracking if this oxide film is removed [16].



- **Duplex:** the name comes from the combination of an austenitic and a ferritic phase. The chromium content is either 18%, 22% or 25% in this type of alloy. As a consequence, the general resistance of the alloy increases. The stress-corrosion resistance increases compared to austenitic although the general corrosion resistance is similar. Due to the mixture of alloys, the strength is significantly higher, and it can be even used in offshore oil platforms for the strength and corrosion resistance. At higher temperatures than 474 °C, the material suffers from embrittlement [16].

## B.6. Other mechanical elements

Besides all the elements described previously, there are other elements necessary in the kiln.

- **Riding rings:** This element is used to distribute the weight of the kiln, and gives integrity and strength to the shell. It gives surface extra on which the reactor is supported [1].
- **Thrust rollers:** The thrust rollers pushes against the riding rings, to avoid movement or drift from the drum [1]. There could be some confusion due to the apparent similarity of this element with bearings. The bearings sit on the thrust rollers, which avoid further movement of the outer kiln when the reactor (internal kiln) is rotating [7].
- **Trunnion wheels:** These wheels are used as the support for the rotating kiln, to ensure that the rotation is smooth and concentric. The base of the wheels is steel with sealed roller bearings. The purpose of this element is to bear the weight of the drum. The description is similar to the purpose of the riding rings. The difference is that the riding rings distribute the weight of the kiln on the trunnion wheels, which are the actual elements supporting the kiln [1].

## B.7. Measure and Control of process parameters

Many parameters that can be measured in a rotary pyrolysis reactor. Starting from the material within the kiln and the heat source, a set of mass/volumetric flows, temperatures, velocities or sample analysis could be measured for the walls of the reactor, combustion gases, the vapours inside the kiln and the bed of solids. The sample analysis measure properties such as conductivity, conversion or viscosity if it is a fluid. In the process the rotational speed can be controlled and varied to adjust specific parameters once the reactor is constructed or the feeding rate modified [1].

Before, the measurements of temperatures were conducted through thermocouples in direct contact with the kiln with the use of bushing and riders. With the new technologies, the use of Bluetooth for wireless measurements and tracking of temperatures is very common [7]. The direct measurement (direct contact) of temperature had the drawback of being affected by the external environment, leading to a large detection error besides the difficulty to adapt the system to a rotating kiln. The major benefits of wireless measurements are accurate repeatability and lower maintenance compared to wired solutions. Wireless technology is currently widespread in the industry [1, 17-19]. Besides the temperature, wireless technology is applied to humidity, carbon dioxide, carbon monoxide, hydrogen sulphide, voltage, pressure and differential air pressure. These properties can be monitored, and further applications can be used for detection such as motion, voltage or moisture detection [17]. As it is seen from the information below, some properties can be used to measure others. For instance, the use of the filling degree can be measured through the measurement of current intensity and the correlation between them [20]. The equipment utilised for the measurement of the kiln properties should be customised for optimum performance.

### B.7.1. FEECO

FEECO [1] follows several data points, and adjust process variables in real-time if needed. The gathered data includes:

- Drum Slope
- Rotational Speed

- Emissions
- Feed and product rates (*tracked in real-time*)
- Temperature
  - Feed
  - Internal
  - Product
  - Exhaust Gas
- Heater Amps (*tracked in real-time*)
- Outlet Gas Parameters
- Residence Time
- Samples
  - Feed
  - Product
  - Internal Kiln
- Steam Flow
- System Pressures (*tracked in real-time*)
- Gas Sampling for carbon monoxide, nitrogen compounds and others related to combustion (*tracked in real-time*)

### B.7.2. University of Edinburgh

The rotary kiln at the University of Edinburgh controls the external temperature of the wall of the reactor through a 3-section heating and the wall temperature is controlled through 3 thermocouples. As an innovative point, the temperatures of the bed of solids and gases are monitored through four thermocouples along the kiln. The rotation of the kiln and feeding rate is also controlled. The kiln angle can be manually modified slightly to vary the conditions of the reactor [21].

To measure the flow of gases and liquids there are several options. Differential pressure sensors with orifice plates are a simple and low-cost option and, besides knowing the composition of the vapour, a long straight pipe is needed. For unknown gas mixtures, thermal mass flow meters can be used but they are very sensitive tools to high temperatures and condensation. Another option would be Doppler flow meters, which are external to the pipes and do not need to deal with process conditions; they require a long section of unobstructed straight pipe and they are costly. Coriolis flow meters are robust and flexible but expensive [21].

### B.7.3. Torr®Coal

The rotary kiln from Torr®Coal (Section C.1) is used for torrefaction instead of pyrolysis. The methods to measure and control the process can be extrapolated to a pyrolysis because the only difference is the condensable vapours not being condensed but burned to obtain energy.

The temperature of the wall of the rotating kiln is measured through 4 thermocouples along the inner kiln. The temperature of the bed of solids can be controlled but the technology used is confidential.

The other measurement and control methods for the process are not disclosed within this work.

### B.7.4. CENER

Despite being used for torrefaction, the rotary kiln in CENER [14] (Section C.2) measures different magnitudes within the process:

- The rotational speed is controlled through the frequency with Hz (Hertz), which can be directly related to the actual rotation speed if the pulley ratio is known.
- The moisture content is measured before feeding the reactor through two measurements of each feeding unit (big bag), and the dryer performance is adjusted according to these results.
- The volumetric filling was controlled by the amps. The amps are the intensity needed to rotate the reactor, crucial on achieving a good performance in any reactor.

- The temperature of the wall of the reactor is controlled through thermocouples. There is one at the entrance and one at the exit to measure the feedstock and product temperature, respectively, and four along the kiln to measure the wall temperature.
- The temperature inside the reactor is controlled by the entrance temperature of the thermal fluid which heats the reactor, because it remains almost constant along the process due to its high heating value.
- The solids mass flow is measured at the entrance and the exit, together with the volumetric flow of the torrefaction gases and some parameters such as the thermal fluid temperature can be adjusted to match the desired product temperature and gas production.
- The other properties of the materials are measured when a sample is taken and analysed, which is usually completed after experiments.

## B.8. Transport of material

The handling of solids is the largest industrial activity in the world with a larger volume than 16 billion tonnes per year and it is present in all industries. Handling is a vast term because it includes storage, feeding, conveying, mixing and milling [22]. One of the essential elements that is often overlooked is the transport of materials within a system. The most common practice to move solids is to use gravity. It is mostly employed in hoppers to move solids down. There are some cases where the solids cannot move by the force of gravity and need an external force. This is found when the equipment is at the same height, or the solids needs to travel upwards. In these exceptions, two systems are commonly used, the screw and a basket conveyor. Screws (Figure 12.11) are commonly used for feeding and collection for pyrolysis even at laboratory scale and to cool the char or torrefied material from the reactor (see Section C.2) [23]. The use of screws could crush the biomass or char particles, creating a dusty environment that could lead to a potential risk of explosion. The other method to transport the material is the basket conveyor (see on Figure 12.12), which consists of a series of baskets attached to a conveyor moving and dropping the material on the next step or piece of equipment. The disadvantage is that only half of the volume of the basket conveyor is used because the baskets have to return to collect more solids [20]. The main difference is the shape of the casing, circular for the screw and squared for the basket conveyor.



Figure 12.11: screw transport mechanism from CENER [24]

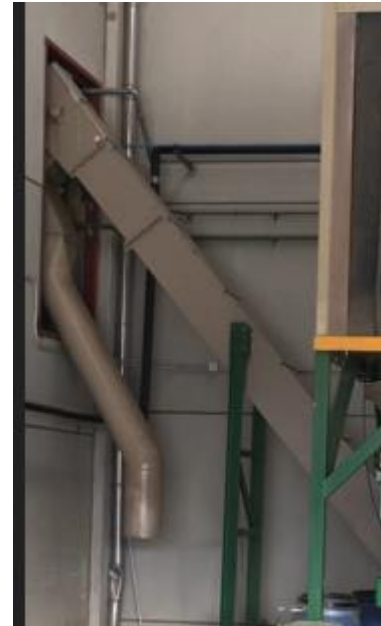


Figure 12.12: Basket conveyor from CENER [24]

For gases, pressure differences are employed to move the gases between equipment. A fan can be used to create this pressure difference. Finally, liquids are moved and separated by gravity when it is possible and sometimes, a pump is used to increase the pressure. At laboratory scale, these processes are usually conducted manually and the information at industrial scale is more limited because manual operation is avoided at larger scale to reduce risks and human error [25].

### B.9. Feeding and collection

The most common method to feed material into the reactor is by feed screw and/or chute, made from a heat-resistant alloy. In solids processing, the main objective is to keep the solids moving without agglomeration, arching or bird nesting. For rotary kilns, the design for the feeding screw needs customisation depending on the solids and their characteristics such as bulk density, wall friction, shear strength, permeability, particle size, presence of lumps or moisture content [26]. Another possibility is to use a conveyor to drop the biomass inside the kiln if the material is granular [7].

The collection refers to the last part of the kiln, where the products exit is known as discharge breeching or product discharge area. In a direct heated kiln, it is used to mount the kiln burner if the configuration is counter-current [1]. The methods are the same as for feeding, using a screw or a conveyor [15]. Instead of piling char until reaching the height of the collecting system (a screw for example), there could be long straight flights to lift the char and place in a tube opened on the upper part where the collecting system would be located to start transporting the biomass.

### B.10. Piping

The connection between the reactor and the process need to cope with the thermal expansion of the reactor. The construction materials of the reactor have overall low elastic deformation limits, which means that, when they are deformed, it is usually plastic and it does not come back to its original shape. For that reason, the thermal expansion should be carefully considered even if the longitudinal expansion is less than 10 centimetres for a 3 t/h reactor according to [15]. The failure to estimate or overlook the thermal expansion could lead to a failure or breakdown of the reactor [27].

There are two types of expansion, longitudinal and axial. The longitudinal expansion is the extra length produced in the reactor as a consequence of the increase of temperature. To deal with longitudinal expansion, one of the ends of the reactor is fixed hindering movement and expansion through flanges, whereas the implementation of bellows on the other end absorbs the thermal expansion. For the axial expansion is divided into two parts, along the reactor and on each of the ends. Along the reactor, the axial expansion is considered on the construction when a clearance is left between the kiln and the sliding joint. Using this method, the reactor will sit on the joint when it is expanded without modifying further the alignments with the other components. Regarding the ends of the reactor, dished ends are used because this geometry can deal with a small variation of diameter [15, 25].

### B.10.1. Flanges

The fixed end of the reactor is constructed with a flange. It is a widespread method to join pipes. To select the flanges, the connection types, operational pressure and temperature and materials are considered [28]. The types of flanges are:

- **Threaded:** known as screwed flanges, this type has a thread inside the hole which fits the pipe connection. It is simple but it is not recommended for processes where the temperature or pressure is different from ambient because it can cause leaks [28].
- **Socket-Weld:** it is described as a female socket where the pipe is fitted, and welded. The most common application are low pressure and temperatures [28].
- **Slip-On:** this flange is placed on the pipe with the matching diameter and welded from inside and outside. These flanges are typically made of forged construction and provided with the equipment [28].
- **Lap Joint:** the stub end and a loose backing flange composes this flange. The stub end is welded to the pipe to allow the backing flange to move freely. It is a method used for dismantling and it is small in comparison to the other types [28].
- **Weld Neck:** it is the most common type of flange because it is welded to the pipe made it feasible for high pressure and temperature applications [28].
- **Blind:** it is the end of a pipe because it is employed to terminate the pipe and isolate the system. It has a blank disk in the hole [28].

### B.10.2. Bellows

The longitudinal expansion is usually compensated with the use of bellows on the no-fixed end of the reactor. Additionally, the reactor sits on sliding joints which move according to the thermal expansion and align with the thrust rollers. As shown in Figure 12.13, the bellows consist of two flanges joined with a section that deals with the thermal expansion. The aim is to prevent damage to the equipment from thermal expansion, vibration, pressure or other mechanical forces. In the case of **metallic bellows**, this section is corrugated metal. The material of the metals could be from stainless steel to high-grade nickel alloys. The **rubber expansion joints** use a flexible section, made of natural or synthetic elastomers with metallic reinforcements to relieve stress on the pipe due to thermal changes. This type of joint can absorb lateral, torsional and angular movements to prevent damage to the equipment. The final type of bellows is the **Teflon expansion joint**, which uses Teflon on the section, material with a low reactivity and ideal for very corrosive materials. The system is not appropriate for the use at high temperatures [29].



Figure 12.13: bellow joint, from [29]

## B.11. References

1. *The Rotary Kiln Handbook*. 2019: FEECO International.
2. *What Kiln Parts Do You Need Serviced?* 2020 [cited 2020 1st April 2020]; Available from: <https://www.industrialkiln.com/parts/kiln/>.
3. *Rotary Seal Design Guide*, in *Rotary Seals*. 2018, Parker Hannifin Corporation, Engineered Materials Group, North America.
4. Jukui, H., et al., *Rotary sealing structure of tundish baking device*, in *Espacenet*, M.M.E.T.B.C. Ltd, Editor. 2014: China. p. 5.
5. Peizhe, G., *Rotary kiln graphite sealing block*, in *Espacenet*. 2014: China.
6. Shigley, J.E. and C.R. Mischke, *Mechanical engineering design*. Sixth edition ed. 2001: McGraw Hill.
7. Boateng, A.A., *Additional information for the design of rotary kilns*, J. López-Ordovás, Editor. 2019.
8. *The Rotary Dryer Handbook*. 2019: FEECO International.
9. *Cogs vector bicycle sprocket*. [cited 2020 12th June 2020]; Available from: <https://ya-webdesign.com/image/cogs-vector-bicycle-sprocket/995173.html>.
10. Mistry, J. *Gear and pinion*. Available from: <https://in.pinterest.com/akshaypulley/>.
11. *FLSmidth group*. 2020 [cited 2020 1st April 2020]; Available from: <https://www.flsmidth.com>.
12. *Metso Group*. 2020 [cited 2020 1st April 2020]; Available from: <https://www.metso.com>.
13. *Friction Drive picture*. [cited 2020 12th June 2020]; Available from: [https://commons.wikimedia.org/wiki/File:Friction\\_Drive\\_With\\_Variable\\_Load\\_Torque\\_-\\_Mechanisms\\_-\\_Kolkata\\_2010-07-02\\_6447.JPG](https://commons.wikimedia.org/wiki/File:Friction_Drive_With_Variable_Load_Torque_-_Mechanisms_-_Kolkata_2010-07-02_6447.JPG).
14. CENER, *Biorefinery and Bioenergy Centre (BIO2C); Pretreatment Unit*, in <http://www.cener.com/areas-de-investigacion/biomasa/centro-biorrefineria-y-bioenergia/>, N.R.E.C. (CENER), Editor. 2019, CENER: Pamplona, Spain.
15. Stein, P., *Rotary kiln design methodology*, J. López-Ordovás, Editor. 2019: EBRI, Aston University, Birmingham, United Kingdom.
16. Perry, R.H. and D.W. Green, *Perry's chemical engineers' handbook*. 2008: New York : McGraw-Hill, ©2008. 8th ed. / prepared by a staff of specialists under the editorial direction of editor-in-chief, Don W. Green, late editor, Robert H. Perry.
17. *Wireless Sensor Types*. [Web page] 2020 [cited 2020 1st April 2020]; Available from: <https://wireless-sensors.co.uk/wireless-sensors>.
18. *Wireless Technology Improves Cement Rotary Kiln Temperature Readings*, Honeywell, Editor. 2008, 2008 Honeywell International Inc.: Automatic & Control Solutions; Process Solutions; Honeywell; 2500 W. Union hills Dr.; Phoenix, AZ 85027.

19. *Contact Monitoring of Temperature in Kaolin Rotary Kiln*. 2017 27th April 2017 [cited 2020 1st April 2020]; Available from: <http://www.yhcalciner.com/kiln/Contact-Monitoring-of-Temperature-in-Rotary-Kiln.html>.
20. Funcia-Muguerza, I., *Presentation of CENER*, J. López-Ordovás, Editor. 2018, CENER: CENER, Aoiz, Spain.
21. Roy-Poirier, A., *Coproduction of biofuels and biochar by slow pyrolysis in a rotary kiln*, in *School of Engineering*. 2016, University of Edinburgh: Edinburgh.
22. McGee, E., *AJAX Equipment Ltd. Visit*, C. Day, et al., Editors. 2019: AJAX Equipment Ltd., Milton Works, Mule Street, Bolton, BL2 2AR, United Kingdom.
23. Yang, Y., et al., *Combined heat and power from the intermediate pyrolysis of biomass materials: performance, economics and environmental impact*. *Applied Energy*, 2017. **191**: p. 639-652.
24. *National Renewable Energy Centre*. 2019 [cited 2019 11th June 2019]; Webpage of the Research Centre]. Available from: <http://www.cener.com/en/>.
25. Day, C., *Description of an industrial rotary kiln*, J. López-Ordovás, Editor. 2019: EBRI, Aston University.
26. *AJAX Ltd*. 2019 [cited 2019 4th November 2019]; Available from: <http://www.ajax.co.uk/>.
27. Bridgwater, A.V., *Aspects to consider in the design of a rotary kiln*, J. López-Ordovás, Editor. 2019, Aston University: Energy and Bioproducts Research Institute (EBRI).
28. *Pipe Flanges - A complete Guide for Engineer*. HarHat Engineer 2020 [cited 2020 1st April 2020]; Available from: <https://hardhatengineer.com/types-flanges-used-piping/>.
29. Sölken, W. *Expansion Joints (Bellows) in Piping Systems*. 2008 [cited 2020 1st April 2020]; Available from: [http://www.wermac.org/specials/expansion\\_joint.html](http://www.wermac.org/specials/expansion_joint.html).

## Appendix C. Industrial experience

This appendix describes the visits conducted during the development of this research, which accounts for nearly 300 hours. The visits were done to Torr<sup>®</sup>Coal (The Netherlands) by initiative of the student, and CENER (Spain) through the BRISK2 project [1]. The visits to the Veolia plants, Ajax Equipment Ltd. and Stein Pyrolysis Ltd. were in United Kingdom and conducted in conjunction with the company Biomass Power Projects (BPP), as part of the secondment from GreenCarbon project.

### C.1. Torr<sup>®</sup>Coal

Torr<sup>®</sup>Coal is a Dutch company which uses the agro-residues to produce high-value bio-coal [2]. Bio-coal is the torrefied product from agro-residues. Torr<sup>®</sup>Coal normally processes woodchips within a temperature range 280-310°C, which means that the process is torrefaction instead of pyrolysis. The input capacity is 76,000 dry annual tonnes of woodchips (equivalent to 9.5 tonnes per hour), to produce 35,000 tonnes of torrefied biomass. A scheme of the process is presented in Figure 12.14. The information from this section is obtained at [3].

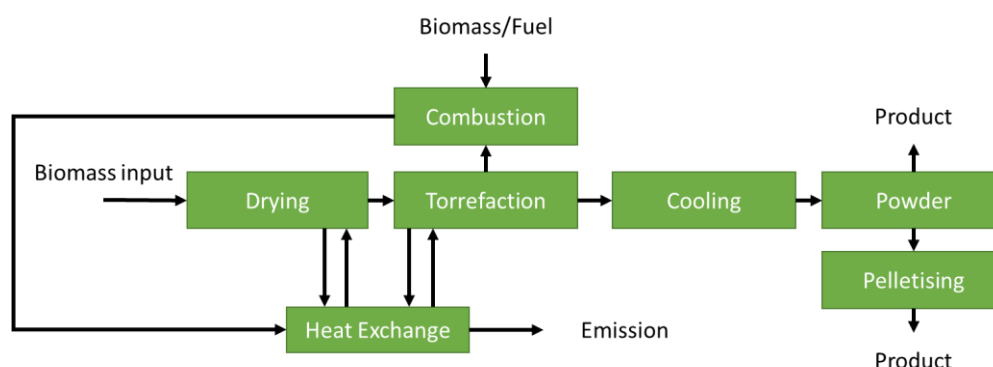


Figure 12.14: Scheme of the plant

The biomass is fed to a drier where moisture content is reduced to below 5wt.% before moving to the reactor where torrefaction occurs. The gases produced from torrefaction are burned and the released heat is employed to provide heat to the reactor and the drier. Due to the auto-ignition feature of the product, the torrefied material needs cooling before the storage and/or pelletising, depending on the needs of the customer [2].

#### C.1.1. Business driving forces

The company participates in the Dutch policy to be a coal-free country by 2050, and reducing the carbon consumption by 2025 by 95 wt.%. Torrefied biomass is a promising replacement for coal, as long as the biomass is not grown on land required for food agriculture. Torr<sup>®</sup>Coal actively considers this aspect of purchasing biomass and selling their product.

#### C.1.2. Facilities

The main office of the company is located in Sittard, The Netherlands. The production centre is located in Belgium, in the district of Dilsen-Stokkem. One of the reasons is to keep office-based staff away from the production site, where operational risk is higher. Figure 12.15 shows the production centre.





Figure 12.15: View of Google maps of Torr®Coal Production Centre

- *The rotary kiln*

This rotary kiln is designed to achieve temperatures up to 700 °C although the range employed is 280-310°C. One unusual aspect of its performance is the feedstock, because instead of RDF, for which the plant was designed, the primary feedstock is woodchips. The feedstock properties analysed at the entrance of the reactor are the moisture content and the particle size. The system does not have a chipper or chopper to reduce the particle size because it does not need further reduction to accomplish the reactor requirements. The reason behind a maximum of 5 wt.% moisture content is a much higher energy demand in the reactor and the need for longer residence time to deal with a higher moisture content. Furthermore, the gases at the exit will probably be different with a higher moisture content.

The average solid yield is 65 wt.%, with the remaining 35 wt.% as torrefaction gases. To ensure excellent performance, the temperature of the gases is measured and controlled via four thermocouples; the solid temperature is measured but the technology used remains confidential for Torr®Coal. The diameter of the reactor is 2.3 m and the length 30 m. The solids residence time is approximately an hour, with a rotational speed of a revolution per minute.

- *The process*

The biomass is received and stored outside. The bacteria in the pile of biomass increases the temperature and partial drying occurs. The rain will only increase the superficial moisture content and is easily removed. The moisture content of the feedstock fed to the system is within a range of 40-45 wt.% moisture content.

The drier system is a conveyor belt which moves the previously warmed air to improve the heat transfer. The drying temperature is 90 °C to avoid further removal of volatiles from the feedstock, and drop the moisture content from 40-45 wt.% to 5 wt.%.

Before the screw feeder, there are several valves to control the feed input and prevent oxygen from entering the reactor. After the reactor, the gases and the solid are separated by gravity. The gas moves upwards and the solid falls downwards.

The gas streams go through a cyclone to remove the remaining solid particles and are recirculated to the solid stream. The solid-free gases move to a combustion chamber where they are

burnt to provide energy to the plant, prioritised to the dryer and the torrefier. The exit temperature of the gases from the combustion chamber is 1,000°C.

The combustion gases pass through a heat exchanger and are cooled by synthetic oil before being released to the atmosphere. This synthetic oil is used in a closed-loop, and it is chosen to maintain thermochemical properties when it is exposed to many temperature changes. The dryer uses the oil to warm the air for the biomass dryer and it flows around the torrefier to increase the temperature of the solid and maintain control of the process temperature.

The solid stream, including the particles from the cyclone, moves to a cooling screw that reduce the temperature. According to Torr<sup>®</sup>Coal experiments, the temperature of the solids stream needs to be under 70°C to hinder its pyrophoric behaviour when it is exposed to air. As a safety measure, the temperature of the torrefied product at the end of the cooling screw is 45°C.

The main objective of torrefaction is to obtain a better product for energy production. In addition to structural transformation, torrefaction improves the grindability of the material. According to Hagenbeek [3], torrefaction removes lignin from the structure, without which the material becomes brittle. This is contrary to literature [4-6], which indicates that hemicellulose and, to a lesser extent, cellulose, are the components removed during torrefaction.

Before storage, the solid product is crushed and milled. Crushing randomly breaks down the particle, resulting in a very heterogeneous particle size distribution whereas milling produces a powdery product to be stored in bags or a post-treatment can be applied such as pelletisation.

- *The plant as a whole*

Based on empirical results, the process is autothermal if the initial moisture content is under 45 wt.%. The energy obtained from the combustion of the gases is high enough to heat the rotary kiln and reduce the moisture content of the biomass in the dryer to 5 wt.%. The process needs some extra energy when the moisture content reaches 50 wt.%, which only happens on cold and rainy days in winter. Extra heat is also required for the start-up of the plant. The fuel used to provide this extra heat is propane.

One of the differential characteristics of Torr<sup>®</sup>Coal torrefied products is the certificate from the Belgian government for the product quality mainly for energy production and stability. Based on this, the criteria for a high-quality torrefied product is to increase the temperature over 280°C and a high heating value of the feedstock larger than 20MJ/kg. The torrefied product used to be gasified by a company called Torr<sup>®</sup>Gas, which eventually became part of Torr<sup>®</sup>Coal.

Any rejected products was used for the smoking zone outside the plant (Figure 12.16), to retain most of the residues from cigarettes and reduce the waste production.



Figure 12.16: Smoking area

### C.1.3. Torrefaction market

The market for torrefaction is still small and the technology needs dissemination. One of the advantages of torrefaction against pyrolysis is the operating prices. When the temperature increases from 300 °C to 700°C, the price is four times higher. Once the value of the products from this process increases, the plants will be able to run for 8,000 hours per year, as per the initial, instead of three days per week which is the current situation. It is important to disseminate this process to focus more on renewable energy.

### C.2. CENER

Part of this research was partially completed at the National Renewable Energy Centre (CENER) [7] as part of the Biofuels Research Infrastructure project (BRISK2) [1], managed by KTH Royal Institute of Technology [8]. CENER is a research institute which develops innovative solutions and acts as technical support to companies and institutions within six areas: wind, solar thermal and photovoltaic, biomass, energy efficiency and generation in buildings, and energy grid integration. If it is not indicated, the information in this section is from [9] and, to a lesser extent, from [7, 10].

CENER has a smaller rotary kiln than Torr®Coal, with an input biomass capacity of 500 kg/h (dry basis) and a range of working temperatures 240-310°C. The purpose of this reactor is experimental rather than industrial production, so it is designed to deal with a wide variety of biomass feedstocks. The input capacity and performance can be adapted to the need of each experiment in a range of 200-500 kg/h. The scheme of the process is represented in Figure 12.17. Despite the continuous design intention, it is possible to work in batches and do some intermediate storage, such

as the big bags after the drier. The red marks are the points of the system where a sample is extracted and analysed.

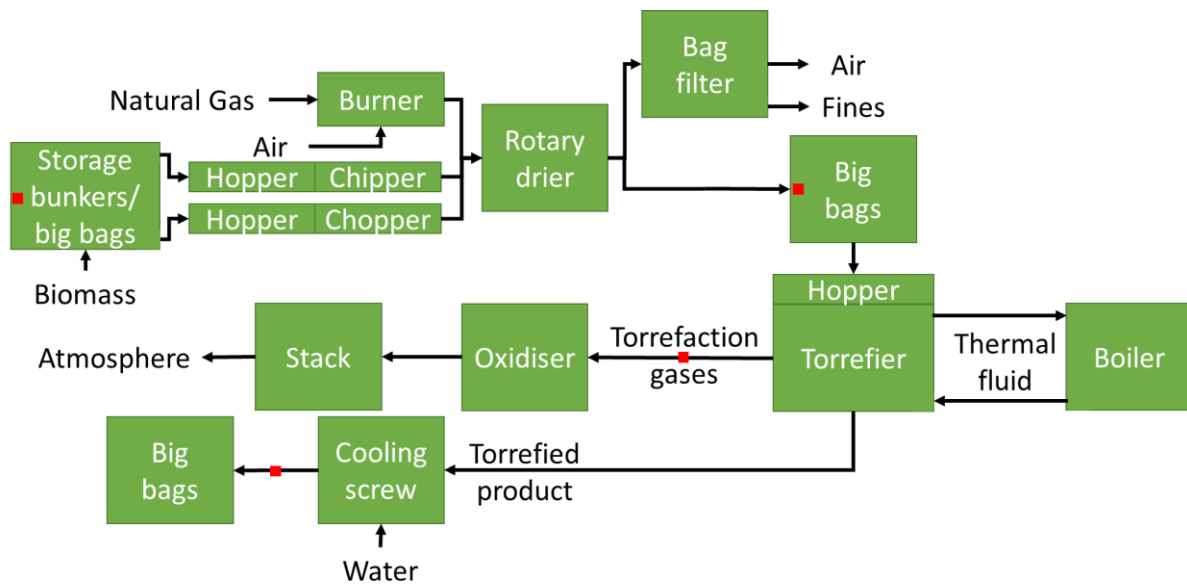


Figure 12.17: Flow diagram of the process in CENER

From bunkers, where the biomass is stored or from big bags, it is moved to a chopper or chipper, depending on the biomass and fed to the rotary drier together with pre-warmed air. The air goes through the sleeve filters to remove the fines before its release. The dried product can be stored or to a cooling screw before feeding the hopper before the torrefier. The solid stream from the torrefier is driven to a cooling screw to mix the torrefied product with water and reduce its temperature. The gases from torrefaction are oxidised before their release to the atmosphere. The cooling screw after drying and torrefaction is due to the pyrophoric nature of biomass and its torrefied product.

### C.2.1. Facilities

- *Storage and size reduction*

The biomass is stored in silos or big bags, with a volume of 1 m<sup>3</sup> and, as a thumb rule, 300 kg per bag, but the weight depends on the feedstock density. This biomass has to be pre-treated to achieve a particle size of approximately 9 mm and a moisture content lower than 15 wt.%.

The first step of the biomass is size reduction. With that purpose, the biomass is fed to the corresponding hopper of the chopper or the chipper, depending on its nature. The biomass coming in from farms, consisting of straw in general (herbaceous biomass), was driven through the chipper. The lignocellulosic biomass goes through the chopper (woody biomass). The size reduction is conducted for a better performance of the reactor and to increase the heat transfer efficiency.

- *Drying and bag filter*

One of the main feedstock properties to control in torrefaction or pyrolysis is the moisture content at the entrance of the reactor. The dryer partially removes moisture content to a value lower than 15 wt.%. To ensure this final moisture content, the filling degree, rotational speed and gas suction are controlled. Natural gas is combusted with air and the resulting gases are used to dry the biomass, using direct contact between these gases and the biomass. In an industrial system, this step should be optimised, using the energy of torrefaction gases and avoiding the use of non-renewable fuels such as

natural gas. The filling degree is measured and controlled with the current intensity. The moisture content is analysed at the end of the drier, taking two samples per big bag (at the middle of filling and at the end) and varying the parameters accordingly to adjust the moisture content; an increase in gas suction and rotational speed will involve a lower moisture content reduction because the contact time between gases and solids would be lower. The drier (Figure 12.18) is supported on two sets of wheels which control the rotational speed of the kiln.



Figure 12.18: Biomass Dryer

In Torr<sup>®</sup>Coal, the moisture content could vary depending on the season. However, the variation in this plant is broad with a 40 wt.% difference between winter and summer the minimum temperature on winter would be around -5°C and the maximum temperature in summer is 33 °C. The gases from the drier go through bag filters to collect and remove the particulates.

- *Torrefaction*

Torrefaction is the primary purpose of the plant and is conducted in a rotary kiln. The unique feature of the reactor is the gas extraction point in the middle of its length as shown in Figure 12.19, which causes counter-current gas flow to the solid at the end of the reactor and co-current at the beginning. Typically, rotary kilns have extraction either at the beginning or at the end of the reactor. The volume of the reactor is 1.8 m<sup>3</sup> and the input capacity between 200-500 kg/h. The inert atmosphere is caused by a continuous flow of nitrogen, equivalent to one-third of the solids mass flow (dry basis). The internal configuration of the reactor was confidential for CENER and could not be released and published.

A thermocouple at the entrance and exit measure the solid temperatures, and four along the reactor measure the rotating wall temperature. As a safety measure, there is a slight overpressure in the reactor.

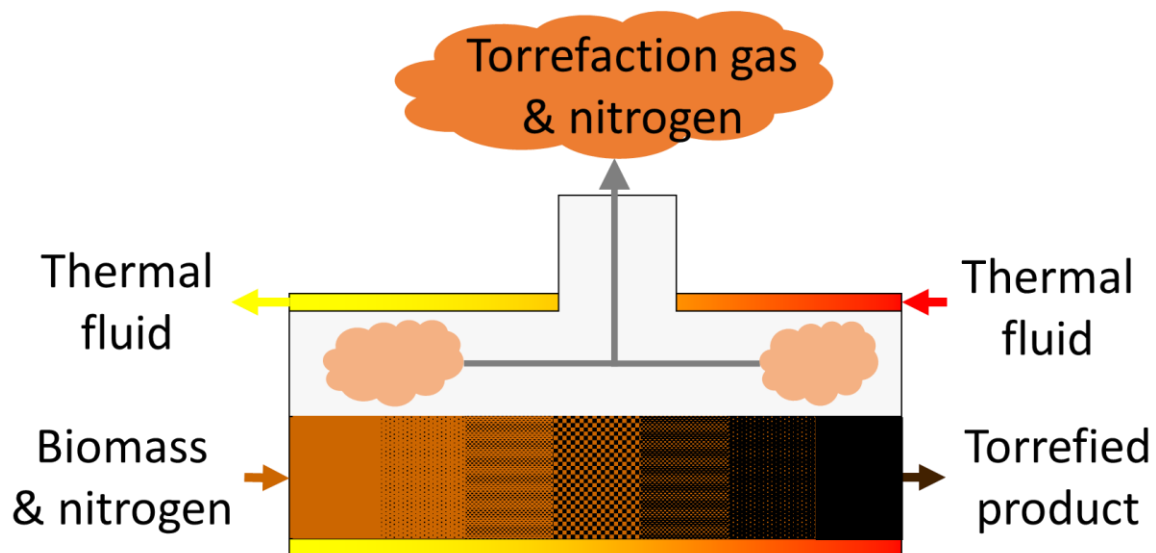


Figure 12.19: Scheme of the torrefier

A thermal fluid surrounds the reactor and increases the temperature of the bed of solids. The reason for the use of a thermal fluid was the requirement to control the temperature in the reactor. The thermal liquid has a very high calorific value and its temperature varies slightly along the reactor, establishing a constant wall temperature. The configuration is counter-current but as observed in the experiments and results (C.2.4), the temperature variation of the liquid is minimal.

- *Solid and Gaseous Product*

Torrefaction gases and nitrogen are extracted from the middle of the reactor (Figure 12.19). A fan, whose maximum torrefaction gas flow is 120 Nm<sup>3</sup>/h, extracts the gases by pressure difference and controls the volumetric flow. A higher flow would lead to operational and safety issues and the fan could break down. This is the main reason why the experiments are simulated before the experiments as the fan causes operational limitations. It means that even if the torrefier is capable of dealing with 500 °C and 310 °C, the flow of torrefaction gases produced might be too high for the process. For instance, 300 kg/h at 280 °C would produce 120 Nm<sup>3</sup>/h. The gases are moved to an oxidiser where they are burnt to be released as flue gases to minimise air pollution.

The solid product moves independently of the torrefaction gases. If the torrefied material contacts air when it exits the reactor, there is a risk of auto-ignition. To avoid this, a flow of 20 kg/h of water is injected into the transport screw used to move the material. The water is not absorbed by the torrefied product due to its hydrophobic nature [11].

### C.2.2. AWL

The most common objective of torrefaction is to increase the energy density and, consequently, the Low Heating Value (LHV). This is achieved through the removal of moisture content and partially hemicellulose and, to a lesser extent, cellulose [4-6, 12]. The LHV is directly correlated with the Average Weight Loss (AWL). Consequently, it is reasonable that this is the targeted property of the process, because it can predict the LHV of the product.

As deduced from its name, AWL indicates the weight loss during torrefaction; so it is the portion of the initial weight that volatilises and is transformed into gases. This weight loss includes moisture content and the partial degradation of other components (cellulose and hemicellulose). The method to calculate AWL is represented in Equation 12.1. The water flow subtracted is the flow used

to cool down the torrefied product. Therefore, the solid yield can be deduced from the AWL from Equation 12.2:

$$AWL[\text{wt. \%}] = \frac{\text{weight of the big bag [kg]} - \text{water flow} \left[ \frac{\text{kg}}{\text{h}} \right] \times t [\text{h}]}{\text{biomass feeding rate} \left[ \frac{\text{kg}}{\text{h}} \right] \times t [\text{h}] \times (1 - \text{moisture content [\text{wt. \%}]})}$$

*Equation 12.1: AWL equation*

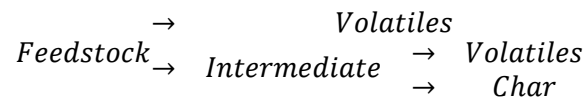
$$\text{Solid yield [\text{wt. \%}]} = 100 - AWL [\text{wt. \%}]$$

*Equation 12.2: Solid yield equation*

The AWL and the LHV of the solid product follow the same tendency, which means that the higher the AWL, the higher the LHV. It is crucial to consider that a higher AWL implies a lower production of solid product if the feed rate remains constant and the target AWL should be a compromise between the LHV and the production rate.

### C.2.3. Experimental Design

Before the experiments at CENER, a simulation tool is used to estimate the results and avoid damage to the system. The model combined a heat transfer method and a kinetic method, which was based on the model developed by Di Blasi and Lanzetta [13], using an isothermal method instead of isoconversional as used in this research (see Section 5.2.1). The mechanism scheme proposed by Di Blasi and Lanzetta is represented in Equation 12.3. Before the design of the simulation tool, experiments with TGA and DSC were completed to find the kinetic parameters and the heat of reactions (reaction enthalpies).



*Equation 12.3: Di Blasi and Lanzetta mechanism*

Within the model, characteristics such as the gas velocity, heat transfer coefficient and entrance and exit temperatures were calculated for each differential of length. The mass and energy balances have to be closed for each differential of length and the whole reactor. A scheme about the inputs, and the outputs of the model are represented in Figure 12.20.

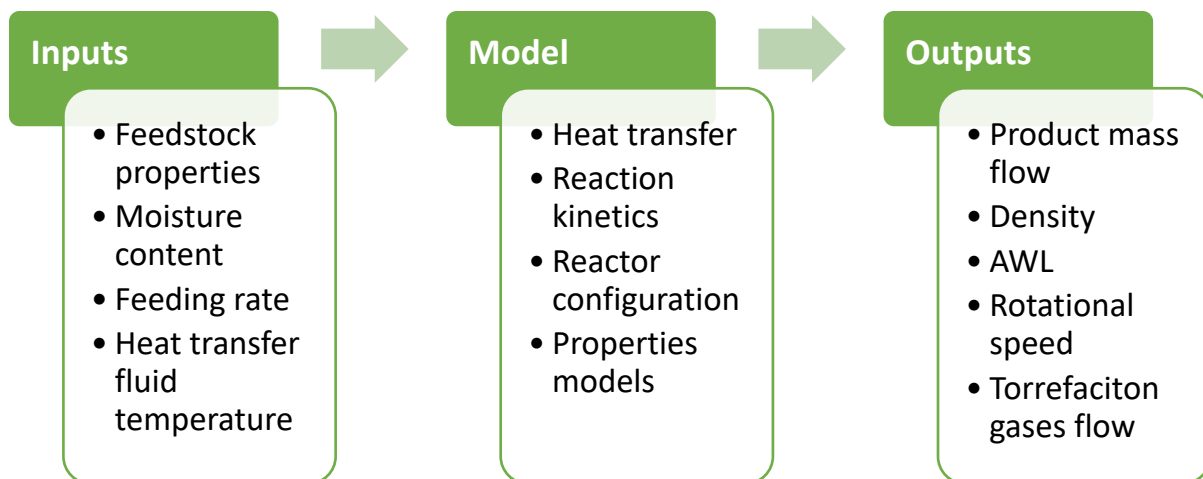


Figure 12.20: Scheme of the model used in CENER

Some descriptive aspects of the model employed in CENER are as follows:

- To simulate the flow model, several perfectly mixed reactors in series are considered. The inputs for one stage are the outputs from the previous one.
- The heat transfer coefficient is based on biomass physical properties (particle size, density, flow and others), through a submodel developed by CENER. The filling degree and temperatures of the wall are established and defined within to achieve an efficient heat transfer.
- One assumption is that negligible temperature gradients occur inside the particle, and the biomass particles are considered isothermal.
- Another aspect is the negligible heat flow between the gas and the solid.
- Mass and energy balance equations are solved for each stage.

- *Limitations*

The reason to simulate the experiments is not only to predict the results but ensuring excellent system performance. As mentioned previously, the system has certain restrictions with the solid feeding rate of the reactor and the range of reaction temperatures. The range of solids feeding rate and reaction temperature cannot be combined freely; There is an additional restriction which makes simulation necessary, which is the flow of torrefaction gases towards extracted by a fan. Consequently, the simulation needs to be precise for the torrefaction gases production to avoid any damage to the equipment.

Therefore, there is a list of several system limitations plus the target of adequate performance of the system:

- The reaction temperature should be higher than 240°C but lower than 310°C
- The feeding rate of solids should be within a range of 200 to 500 kg/h
- The volumetric flow of torrefaction gases produced should be lower than 120 Nm<sup>3</sup>/h
- The AWL should have a value within the range 25-35 wt.%. This is the target value of AWL which is a good compromise between torrefied product and LHV
- Another limitation would be the moisture content, but it is controlled during the drying step to ensure a moisture content lower than 15 wt.%

The parameters that can be modified to achieve an adequate AWL and avoid exceeding the torrefaction gas production limit are the reaction temperature and solids feeding rate. The influence



of the reaction temperature and the solids feeding rate on the torrefier performance is based on feasibility of the heat to reaching all the particles.

○ Influence of the reaction temperature

The temperature directly influences the AWL and torrefaction gas production. An increase in temperature will increase the AWL, although it increases the volume of torrefaction gases, which could lead to an excessive flow for the fan. A higher reaction temperature produces a higher heat flow, and consequently, the heat reaches all particles earlier, producing higher reaction rates.

Decreasing the temperature is an appropriate method to decrease the production of torrefaction gases; however, the AWL is decreased and might become too low for the process. This is due to a lower temperature difference and a lower heat flow, which makes the particles to reach the reaction temperature later, with slower reaction rates.

○ Influence of solids feeding rate

The feeding rate has a more complex influence than the reaction temperature on the process. When the feeding rate is decreased the AWL increases and the production of torrefaction gases increases. More gases are released because more heat reaches the particle and can release the intrinsic gases from torrefaction and the residence time increases.

The most interesting relationship occurs with an increase in the solids feeding rate. A higher feeding rate means more solids for the same heat flow, and, consequently, the AWL would decrease because the heat cannot reach all particles. The torrefaction gases may increase as well. This happens because, increasing the solids feeding rate, means increasing the total input of moisture content, which is evaporated during torrefaction. In this sense, either increasing or decreasing the solids feeding rate could raise the amount of gases produced. Which factor has the most significant influence, the increment of the total water evaporated or the gases released has not been studied.

Some examples of the possible results are shown in Table 12.3.

Table 12.3: Experimental Design Table

|         |                                     |      |      |      |      |      |      |      |
|---------|-------------------------------------|------|------|------|------|------|------|------|
| INPUTS  | Temperature [°C]                    | 240  | 240  | 260  | 280  | 260  | 280  | 280  |
|         | Volumetric flow [m <sup>3</sup> /h] | 350  | 400  | 400  | 400  | 450  | 450  | 425  |
| OUTPUTS | Gases produced [Nm <sup>3</sup> /h] | 85   | 90   | 101  | 122  | 99   | 111  | 116  |
|         | AWL [wt.%]                          | 13.1 | 11.5 | 14.6 | 20.4 | 11.2 | 14.2 | 17.1 |

#### C.2.4. Experiments

After simulating several conditions, the two most promising combinations of feed rate-temperature were 300 kg/h-260°C and 300 kg/h-280°C. With the simulation of these data, the expected AWLs were 25 wt.% and 35 wt.%, respectively. The steady-state is estimated to be reached approximately after an hour when the parameters are changed. The leading indicator of steady-state is the flow of torrefaction gases, which should remain constant. Each of the experiments lasted for an hour and fifteen minutes. The results of the experiments and the comparison with the model are shown in Table 12.4.

Table 12.4: Results of the experiments

| Experiment 1: 300 kg/h and 260 °C<br>Experiment 2: 300 kg/h and 280 °C |                              | Experiment number |      |            |       |
|--|------------------------------|-------------------|------|------------|-------|
|  |                              | 1                 |      | 2          |       |
|  |                              | Model             | Exp. | Model      | Exp.  |
| Thermal fluid  | Outlet T [°C]                | 260               | 260  | 280        | 279.5 |
|  | Thermal fluid heat [kW]      | 66                | 58   | 70         | 73    |
| Biomass  | Type                         | Beech wood        |      | Beech wood |       |
|  | Mass flow [kg/h]             | 300               | 300  | 300        | 300   |
|  | Density [kg/m <sup>3</sup> ] | 310               | 310  | 310        | 310   |
|  | Moisture content [wt.%]      | 9.9               | 9.9  | 9.9        | 9.9   |
| Torrefied product  | Mass flow [kg/h]             | 218               | 227  | 199        | 198   |
|  | Density [kg/m <sup>3</sup> ] | 325               | 330  | 345        | 355   |
|  | Exit T [°C]                  | 243               | 234  | 252        | 251   |
|  | AWL [wt.%] (d.a.f.*)         | 19.4              | 15.9 | 26.8       | 26.6  |
| Torrefaction Gases   | Exit T [°C]                  | 219               | 224  | 229        | 225   |
|  | Flow [Nm <sup>3</sup> /h]    | 92                | 91   | 111        | 99    |

\*d.a.f.: dry ash free basis

In Table 12.4, the data in the *Biomass* section are the inputs from the user. In *Torrefied product* and *Gases* section, a good comparison between the model and reality can be observed. In the first experiment, conducted at 260 °C, the results varied around 5%, except the torrefaction gas flow, whose variation was negligible. The AWL varied around 20% in this experiment, which is a notable change. The reason for such high variation is because the experimental temperature of the product is lower than expected, but the mass flow is higher, so even if these variations are small, they drive the variation in the same direction, decreasing the experimental AWL.

The second experiment, conducted at 280 °C, provided results more similar to those from the model. In some cases, the variation was negligible and only for the final density (3%), and gas flow (10%) was the variation noticeable. The reason for a less efficient approximation in the first experiment is a closer operation to the working temperature limit of the reactor (240-310 °C). From the results, it is observed that a single increase of 20 °C in the simulation leads to an increase of almost 7.4 wt. % (dry ash-free) in the AWL during the simulation. In the experiments, the variations were 17 °C and 10.7 wt. %.

### C.3. Secondment in BPP

The GreenCarbon project has collaboration with the company biomass Power Projects Ltd (BPP). This company have expertise in developing industrial-scale biomass power plants, with a typical solid throughput of 3 t/h. Recent projects include pyrolysis to gas technologies to provide clients with the opportunity of benefiting from UK financial incentives for the production of energy [14]. BPP made a connection with several companies which added value to the research conducted at Aston University, providing a real industrial environment and expertise on a wide range of fields.

#### C.3.1. Veolia

Veolia is a multinational company with more than 171,000 employees worldwide (14,000 in the UK). The main areas of impact are waste, water and energy management solutions, aiming for a sustainable development, towards a circular economy and the preservation of scarce raw materials.

It has many plants around the UK in a wide variety of sectors: energy recovery, integrated waste management, materials recovery, composting, reuse and recycling and waste transfer. Information of three types were obtained from the visits and are presented as follows [15].

- *Veolia Avonmouth Recycling and Recovery Centre*

This centre processes waste wood and commercial solid waste and supply wood chips to local biomass power stations and RDF cubes-- the plants' process around 50,000 tonnes per year of each feedstock. The information in this section is adapted from the report written by Yang Yang from the visit to the facilities [16].

The origin of the wood used in this centre is waste from diverse areas, some of them can be packaging such as crates and pallets, construction material or consequence of municipal waste such as furniture. To separate ferrous metal a magnetic separator is employed; and the non-ferrous metals are removed with a metal finder with compressed air guns which eject the non-ferrous metal after being detected by the IR (infrared) based metal finder. A 45 t/h hammer mill shredder reduces the size of the particles, which are separated in a trommel screen. Overall, 10-15wt.% of the particles have a particle size lower than 5 mm, and the rest are considered chips up to a particle size of 60 mm, if the size is bigger is returned to the shredder. Within the waste wood, there are different types of qualities; for instance, Grade A waste wood refers to the material used for packaging, such as crates and pallets; Contrary to it, Grade C waste wood has contaminants of paint and coating. The price depends on the grade and the most common buyers are from biomass power stations. A scheme of the flowsheet of the feedstock is shown in Figure 12.21.

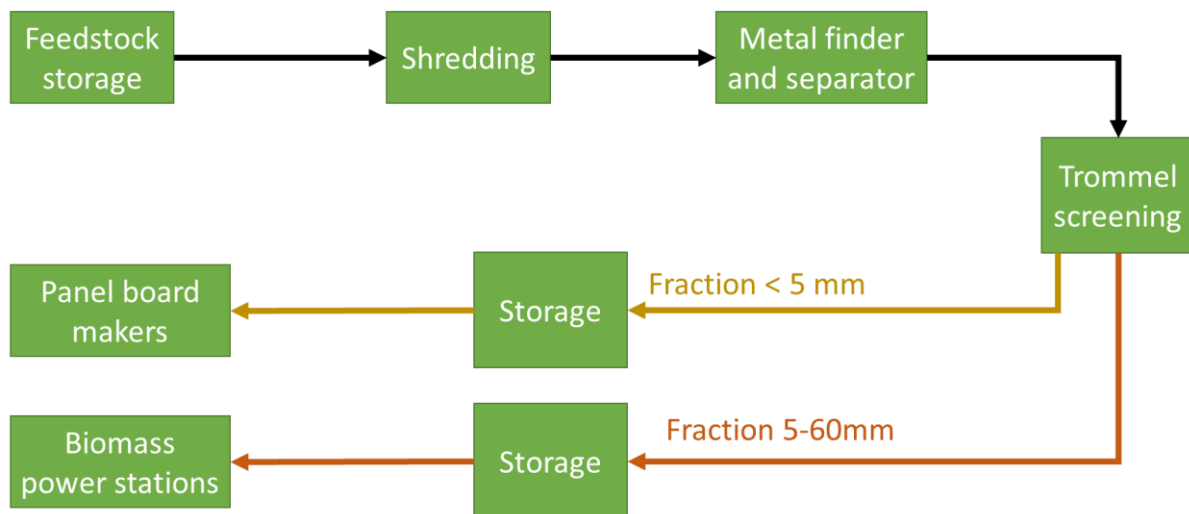


Figure 12.21: Process flowsheet for waste wood processing

Besides the wood, this centre also processes commercial waste from local businesses, whose most common materials are plastic packaging, metals, paper and cardboard, and food waste. Figure 12.22 shows that the first step is a low-speed blade shredder because the storage is in cubes. The main aim of processing the waste is to transform it into RDF, from which the metals have been removed. After removing the ferrous and non-ferrous metals separately, the baling compactor increases the density of the cubes, which is around 1.10 kg/m<sup>3</sup> compared with 0.25 kg/m<sup>3</sup> when it arrives at the plant.

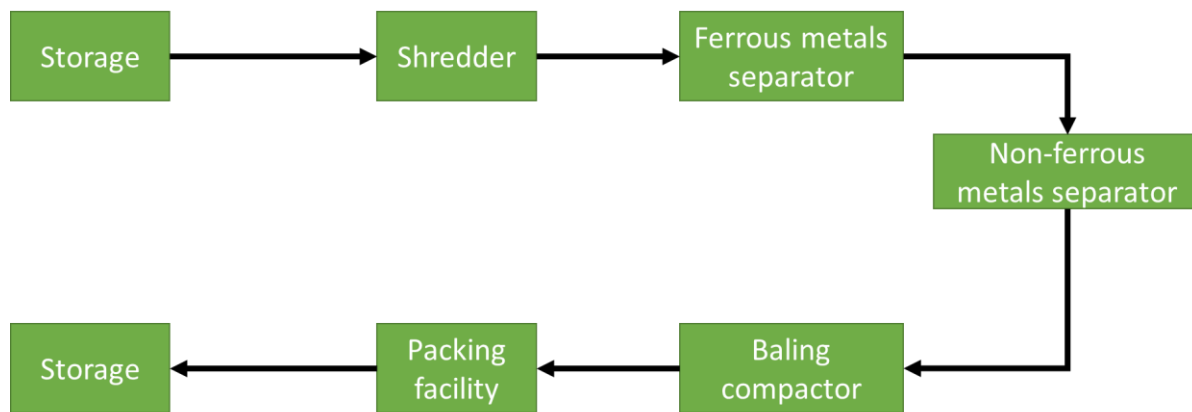


Figure 12.22: Process flowsheet for commercial waste processing

From this experience, specific ideas for pre- and post-treatment methods are acquired for both lignocellulosic material such as wood waste, and more heterogeneous mixture such as commercial waste.

- *Veolia Energy Recovery Facility*

The main aim of it is to produce energy out of non-recyclable waste from households. It is located in Tyseley Energy Park and the capacity is about 350,000 ton/year of waste which is led to two boilers. The plant produces 25 MWe of electricity and powers about 40,000 homes in Birmingham. The plant includes a clinical waste treatment plant, with a capacity of 5,000 ton/year, considerably lower than the non-recyclable waste's section. In both cases, the process used to produce energy is combustion (incineration) [17].

The production of waste in the UK in 2014 was 26,000,000 tons, from which 41 wt.% is recycled/reused/composted, 25 wt.% is landfilled and only 14 wt.% is used for energy production. It is easily deduced that the Veolia plant cannot deal with the total waste used for energy production. Despite supposing to find only non-recyclable materials, some plastics and metals can be mixed within. Combustion is known for the flexibility on the feedstock; however, some materials can be problematic for the plant, e.g. metals can melt, plastics produce chlorine, etc.

The waste is delivered to the bunker by lorries where it is moved and mixed by two cranes located on top. The waste falls by gravity feed shot, pushed with a ramp feeder, to feed one of the Steinmüller boilers. Two are situated in parallel to process the waste. Within each reactor, the grate is divided into several zones (3 vertical radiant passes and 1 horizontal convective pass). The end of the grate is used for cooling. The processing temperature for the household and clinical waste is 1,000 °C with an excess of oxygen within of 6-7%. There are specific post-treatment steps for the flue gas:

- The flue gas from the boilers is used to produce steam at 450 °C and 40 bar.
- Ammonia is added to the flue gas to reduce NO<sub>x</sub> emissions, with the Selective Non-Catalytic Reduction (SNCR) process.
- Hydrochloric acid (HCl) and sulphur oxides (SO<sub>x</sub>) and powder activated carbon are used to remove dioxins and heavy metals from the flue gas.
- Dust, fly ash and adsorbents are removed by bag filters. The clean flue gas is sent to the stack, before which a portion is analysed to determine the characteristics and ensure the law enforcement, in terms of dust, SO<sub>2</sub>, NO<sub>x</sub>, HCl, Total Organic Carbon (TOC), CO and H<sub>2</sub>O concentrations.

The solid residue is mostly stored underground in former salt mining sites, or landfilled. The ash from the boilers is quenched. Some of its applications are aggregate in concrete, in roads and car parks or embankments. The steam goes to an Allen turbine connected to a generator where electricity is produced. The steam is cooled down and reused in a closed-loop for energy production.

- *Veolia Material Recovery Facility*

The last type of plant from Veolia is an example of a facility for the recovery of the material, whose capacity is about 50,000 wet ton/ year. This plant is located in Cannock and the primary source of waste is the area of Birmingham.

The main aim of the facility is to separate the waste into five streams: glass, ferrous metal, non-ferrous metal, plastics and residual stream. In this way, the recyclables can be sent for recycling and the residuals for energy production. The received clinical waste is processed in an autoclave, shredded, compressed and sent to the Veolia plant described above (Veolia Energy Recovery Facility) to produce energy in the incinerator. Figure 12.23 shows a schematic of the solids flow within the plant.

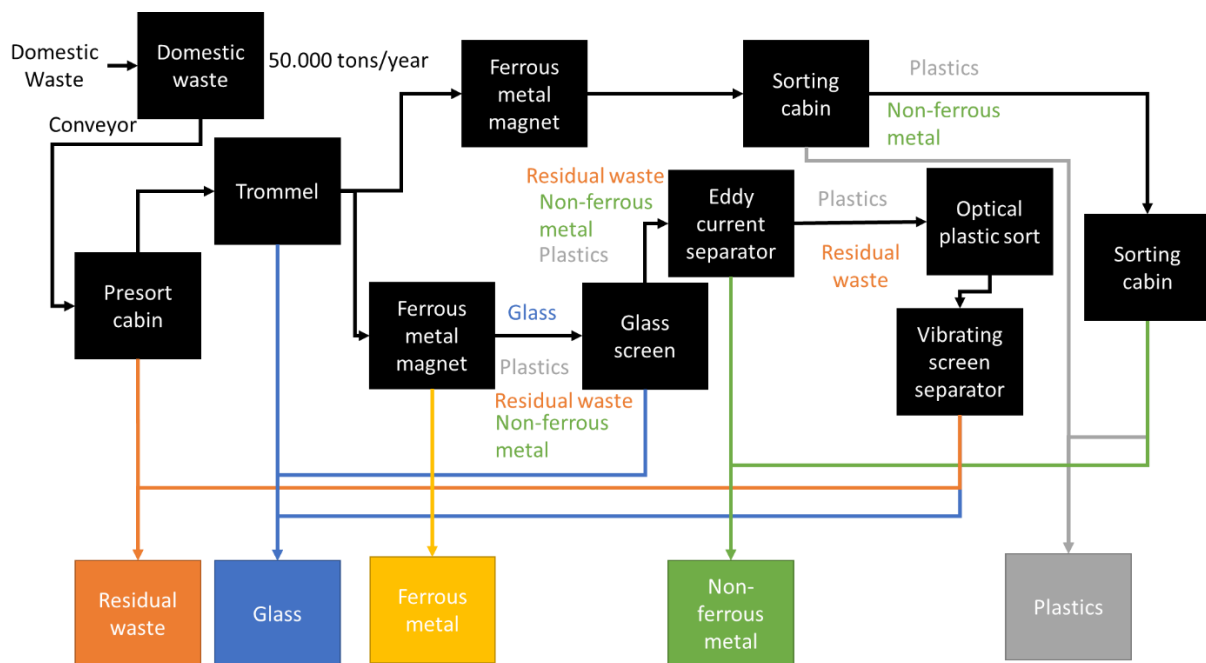


Figure 12.23: Plant flow diagram of the waste streams

The waste is transported to a conveyor belt with shovel excavator from the tipping hall where it is received. The first conveyor belt has sensors to measure the height of the waste to estimate the incoming volume. It is preferred overweighting the waste due to the conveyor angle and vibrations caused during its movement.

Paper and bags are preliminarily separated in a cabinet. Some non-recyclable wastes such as kitchen pans are removed from this stream manually. The stream containing glass enters a trommel which crushes it and the fraction under 10 mm is removed from the bottom through a screen. The ferrous portion is separated from the non-ferrous with a conveyor with magnetic flaps. The Eddy current separator leads the input stream to a fall with two directions. An inverted magnet makes the pieces to fall into one or another. It is used to separate aluminium objects from other non-ferrous materials.

An IR sensor detects low-density plastics in the main waste stream, and are separated by an air-blower. The stream that the air-blower creates is only about 60% plastics since other materials are separated. Mixing this stream with another from the facility increases the plastic content to 80%. The remaining portion of glass in the waste stream is removed by vibrating screen, which is combined with the trommel screen.

After all these steps, the waste flow is reduced by 90 wt.%, and is sent to the facility described in Veolia energy Recovery Facility to produce energy. The composition is around 40 wt.% of paper and cardboard, which is equivalent to 2,000 annual tons and some plastic films and bottles and cans. There is some on-going research in the industry to separate the recyclable components from this stream.

The waste streams are usually baled to be transported to other facilities. For instance, the bales with plastic waste are sent to another Veolia plant facility to separate the plastics into different types. The most valuable products are the non-ferrous metals, although they only comprise 3 to 5 wt.% of the wastes, and are sent to Germany to be melted and reused.

### C.3.2. Stein Pyrolysis Ltd.

Stein Pyrolysis Ltd. is a company which designs rotary kilns to convert waste into bioproducts/biofuels to generate electricity and/or heating. The biofuels are produced from a wide variety of feedstocks: municipal solid waste (MSW), industrial waste, sewage-sludge, woodchips, rejected crops and tyres. The process usually starts with moisture content and particle size reduction down to 5 wt.% and 15 mm, respectively. Fuel is fed through a hopper and compressed by a piston against a closed gate valve to remove air. A screw breaks the pellets and feeds them into a rotary kiln. The pyrolysis hinders the transformation of chlorine into dioxins due to the lack of air. The products are extracted with a screw and separated by gravity. The char (a by-product in this specific process) goes down and is led to a burner to provide energy for the pyrolysis process, and the ash content is melted, and vitrified slag is collected at the bottom of the second converter and used as aggregate. The gas is quenched to separate the heavy metals in the form of sludge, and remaining gas is scrubbed clean to remove the remaining pollutants, tars and oils from the gas. The tars and oils are recycled back to the process to transform them into gas. The heat of the process is the recovery in a unit to make steam or hot water for domestic or industrial use. The remaining syngas is employed can be used in standard gas boiler, gas engine or gas turbine for the production of electrical or heat power [18]. The information for this section is obtained from [19].

In a pyrolysis plant, all components are essential. The pyrolysis reactor is crucial for the performance of the whole system. One of the projects of BPP was to design, build and run a pyrolysis plant of Municipal Solid Waste (MSW). The reactor was a rotary kiln and it was designed by Peter Stein, part of Stein Pyrolysis Ltd.

A background in mechanical and electrical engineering influenced the approach to design a rotary kiln for this company. During the meetings with the company, they focused on the reduction of thermal stress to lengthen the reactor lifetime (up to 15 years), instead of focusing on pyrolysis as a chemical reaction. One of the main concerns in the design was the leak of oxygen inside the reactor as a safety hazard. Mainly, the aim was to produce a mixture of hydrogen and methane using waste as the raw material. The use of a rotary kiln over a screw was the lower abrasion and stress on reactors 'material.

The approach of the company was different from the one from this work. In most of the cases, a kiln was given to the company and the aim was to improve the efficiency and performance. Some retorts were also designed from scratch such as the one for BPP. The aimed characteristic of the

performance of the kiln was consistency and accuracy, mainly subjected to thermodynamics. The equations used within this work for the heat transfer to the bed of solids were validated by the company as a successful kilns designers. Although the results are not compared to the previously designed reactors. This topic is further discussed in Section 9.4. These equations would change if the kiln is fired to increase the temperature instead of heated by gases flowing around the reactor.

The whole design of a rotary kiln implies many different aspects and characteristics to consider and the description and discussion of each are deeply explained in Chapter 6 and Appendix B. From a starting design, Stein Pyrolysis Ltd. used the following:

- To deal with the longitudinal expansion, one of the reactor ends is fixed, while the other sits on wheels and absorb the expansion when the reactor expands and grows. The diameter thermal expansion is solved with dished ends which allows thermal expansion. Another option is the use of bellows and/or sliding joints.
- To place the solid inside the reactor, the design of the flights aims to minimise the solids in contact with the wall, which would cause thermal stress on each rotation and shorten the reactor lifetime. According to Peter [19], the shorter length and larger radius would be equivalent to lengthen the lifetime, because the portion of wall thermally stressed by the solids would be lower although some heat transfer restrictions could appear.
- The heat should be distributed as uniformly as possible. Ideally the flow of the combustion gases to increase the wall temperature should be in spiral instead of parallel to the reactor to achieve more uniform heating.
- The reactor relies on clearances to deal with the expansion of length and diameter. Despite the low thermal expansion (75 mm in a 3 t/h reactor), the construction material has not got plastic behaviour and could break.
- Overall, Stein Pyrolysis Ltd. used low filling degrees (<20%) to make convection and radiation more significant within the process, and the conduction more negligible.
- In the designs, the objective is to keep all air out and extract the vapours from pyrolysis as soon as possible. This fast extraction without any carrier gas could lead to corrosion of the seals if the material is rubber, and the importance of materials like Viton is demonstrated. Simultaneously, it has to deal with the motion of the kiln and the thermal expansion.
- It is important to highlight that the design aimed for the production of gas and the solid carbon was a waste product, used to produce energy and obtain combustion gases at a temperature of 1000°C to heat the reactor. The process ran according to the standards as long as the heating value of the feedstock was higher than 18 MJ/kg and moisture content lower than 5 wt.%. Otherwise, the energy demand for moisture evaporation would be too high and the energy content of the char too low to produce energy for the process and an auxiliary fuel would be needed. In the case of higher moisture content, half of the length of the reactor would be used only to dry the feedstock.
- Through the design of the flights, the thermal stress is reduced and residence time is controlled, due to its innovative shape, which moves the feedstock a specified length on each rotation.
- Feeding and collection are by a screw and refrigerated with external water stream to avoid further degradation and partial starting of pyrolysis reactor.
- As rules-of-thumb for reactors whose capacities are 3 t/h, the solid residence time is around 45 minutes, the diameter-length ratio is found in the range (1-2.2), and the rotational speed is within the range (4-12).
- To design the reactor and calculate the heat flows, the reactor is divided into identical slices and the equations are applied individually to each step.

- For the gases, the main post-treatment steps were cyclone where small solid particles, with high value in the market, were separated. The non-condensable fraction is separated from the condensables by a quench to reduce the temperature down to 80 °C, and two absorbers.
- According to the company, to initiate the design of a reactor, only the very basic information such as temperatures should be considered. It should become more involved with the progress of the project as a design methodology.
- The flow of the gases around the reactor should be laminar to make the heat transfer as smooth as possible and achieve a more homogeneous heating.
- The rotational speed is the last parameter to be adjusted. This is different from the approach on this work which used the Froude number to achieve rolling motion. This reactor used the flights to push the solid forward.
- The energy demand from the pyrolysis reactor compared to the energy produced by the combustion of the char is around 20%. The rest of the heat could be used in other units in the system such as the dryer.
- Direct heating of the reactor through direct firing would add complexity to control the temperatures, and it would make the process more expensive.
- If the vapours inside the reactor were extracted from the feed entrance, there might be condensation problems due to contact of hot vapours with cold feedstock, and that is why a co-current approach is employed.
- The pyrolysis of plastics may lead to the production of chlorines, which could lead to a pollution problem.
- When designing a kiln, a higher capacity means more stability and more balance, coupled with a more linear estimation compared to lower capacities (<500 kg/h).

### C.3.3. AJAX Equipment Ltd.

Within a pyrolysis reactor, the solids handling is an essential design consideration. Besides the bed of solids behaviour within the reactor, the biomass has to be fed, and the solid product has to be collected, all without allowing air to enter (to ensure proper pyrolysis and to avoid self-ignition before cooling). The most common practice for solids handling is screw conveyors, although other systems such as paddle mixers are considered. The information is obtained from [20] and [21].

Companies such as AJAX Equipment Ltd. works on customised screws for the processing of solids, the largest industrial activity in the world with an estimated volume higher than 16 billion annual tonnes, included in most industries such as food, pharma, mining, steel or cement. The average range of capacities for the screw designs is between 200 kg/h and 1.5 ton/h. Although biomass is not the main area of expertise for this company, they have built biomass handling screws; For instance, a moving paddle reactor for torrefaction or pyrolysis for Cornell University. The screws are sometimes slightly heated up to 80 °C, but jackets with hot oil can be applied to heat the reactor up to 320 °C if a higher or lower temperature is required, then it is necessary to have internal heating or cooling methods.

The solid handling design requires the feedstock to undergo testing to prevent problems such as arching, stable rathole, birdnesting or hang-up. In the case of char, it can agglomerate and produce lumps, and it can contain unpyrolysed materials. The main aim of solids handling is to maintain adequate flow and avoid problems such as agglomeration. A secondary objective is to design the screw to minimise dust formation, and its casing and seals minimise dust and explosions. The aspects that can affect the flowability of the solids are:

- **Bulk density:** it is the driving force for gravity flow



- **Hausner ratio:** which correlates the tapped and poured bulk densities
- **Wall Friction:** opposes slip on contact surfaces
- **Shear strength:** which avoids the deformation for flowing
- **Permeability:** to know how gas can get through the bulk solid
- **Particle size:** because fine powders can arch or agglomerate
- **Presence of lumps:** which could cause jams. To unjam hoppers, some people use vibration techniques, but it should not happen with an appropriate design
- **Moisture content:** the particles behave differently with different moisture content values
- **Equipment factors:** like the shape of the hopper, outlet size and others affect the behaviour of solids or how the solid is fed. It can be by conveyors instead of the typical hoppers moved by gravity

Screws are the most common method to transport solids due to its reliability to control the flow and wide range of design capacities. According to the Managing Director [21], there is no upper limit for the input capacity of the materials, and the most common industrial input is 3 tonnes per hour and it is infrequent to find a plant with higher feeding than 5 tonnes per hour.

The screw is not the only part which is designed to process the solids. Another critical part of the equipment which supports the movement of solids is the hopper to where biomass is stored. The main parameters to design the hoppers are the shape of the material, the size and its density, in loose and compacted conditions. The shear strength is critical for the angle of the hopper and its friction with the wall, which can determine whether the solids flow for precise angles and shapes of the equipment. The configuration of the hoppers can be conical, squared or a hybrid. In recent experiments, another configuration with diverging ends is being studied for material that may interlock and cause birdnesting.

#### C.4. References

1. *BRISK2: Biofuel Research Infrastructure*. BRISK2 project webpage 2018 [cited 2018 7th December 2018]; Available from: <https://www.brisk2.eu/>.
2. *Torr-Coal*. 2018 25th June 2019]; Available from: <http://www.torrcoal.com/>.
3. Hagenbeek, R., *Visit to a torrefaction production centre*, J. López-Ordovás, Editor. 2018, Torr-Coal: Dilsen-Stokkem, Belgium.
4. Kolokolova, O., et al. *Torrefaction and Pyrolysis of biomass waste in continuous reactors*. in *13th International Conference on Environmental Science and Technology*. 2013. Athens: Global Nest, Secretariat.
5. Gašparovič, L., Z. Koreňová, and Ľ. Jelemenský, *Kinetic study of wood chips decomposition by TGA*. Chemical Papers, 2010. **64**(2).
6. Chen, D., Y. Zheng, and X. Zhu, *In-depth investigation on the pyrolysis kinetics of raw biomass. Part I: Kinetic analysis for the drying and devolatilization stages*. Bioresource Technology, 2013. **131**: p. 40-46.
7. *National Renewable Energy Centre*. 2019 [cited 2019 11th June 2019]; Webpage of the Research Centre]. Available from: <http://www.cener.com/en/>.
8. *KTH: Royal Institute of Technology*. Department of Chemical Engineering July 2019]; Available from: <https://www.kth.se/ket/process-technology/research-1.294587>.
9. Funcia-Muguerza, I., *Presentation of CENER*, J. López-Ordovás, Editor. 2018, CENER: CENER, Aoiz, Spain.
10. CENER, *Biorefinery and Bioenergy Centre (BIO2C); Pretreatment Unit*, in <http://www.cener.com/areas-de-investigacion/biomasa/centro-biorrefineria-y-bioenergia/>, N.R.E.C. (CENER), Editor. 2019, CENER: Pamplona, Spain.

11. Basu, P., *Biomass gasification, pyrolysis, and torrefaction: practical design and theory*. 2013: London, UK : Elsevier : Academic Press, 2013. Second edition.
12. López-Ordovás, J., et al., *Integrated rotary kiln pilot-scale plant for beechwood torrefaction*. Forthcoming.
13. Di Blasi, C. and M. Lanzetta, *Intrinsic kinetics of isothermal xylan degradation in inert atmosphere*. *Journal of Analytical and Applied Pyrolysis*, 1997. **40-41**: p. 287-303.
14. GreenCarbon-ETN. *Advanced Carbon Materials from Biowaste: Sustainable Pathways to Drive Innovative Green Technologies*. 2017 2nd November 2018 9th April 2017]; Available from: <http://greencarbon-etn.eu/>.
15. *Veolia webpage*. 2018 29th August 2019]; Available from: <https://www.veolia.co.uk/about-us/group-overview>.
16. Yang, Y., *Veolia Avonmouth Plant Visit*. 2017, Aston University: EBRI.
17. Rego, F. and J. López-Ordovás, *Visit to the Veolia Energy Recovery Facility (ERF)*. 2018, Aston University: EBRI.
18. *Stein's Pyrolysis Video 2013 (SPU Energy Fields)*. 2013, C Meier: Youtube.
19. Stein, P., *Rotary kiln design methodology*, J. López-Ordovás, Editor. 2019: EBRI, Aston University, Birmingham, United Kingdom.
20. *AJAX Ltd*. 2019 [cited 2019 4th November 2019]; Available from: <http://www.ajax.co.uk/>.
21. McGee, E., *AJAX Equipment Ltd. Visit*, C. Day, et al., Editors. 2019: AJAX Equipment Ltd., Milton Works, Mule Street, Bolton, BL2 2AR, United Kingdom.